Universidade de Aveiro Departamento de Química
2015

Inês Dias Lamego

Estudo da resposta metabólica de células de osteossarcoma a agentes anticancerígenos convencionais e novos por metabolómica de RMN

Evaluation of the metabolomic response of osteosarcoma cells to conventional and new anticancer drugs by NMR metabolomics

Universidade de Aveiro Departamento de Química
2015

Inês Dias Lamego

Estudo da resposta metabólica de células de osteossarcoma a agentes anticancerígenos convencionais e novos por metabolómica de RMN

Evaluation of the metabolomic response of osteosarcoma cells to conventional and new anticancer drugs by NMR metabolomics

Tese apresentada à Universidade de Aveiro para cumprimento dos requisitos necessários à obtenção do grau de Doutor em Química, realizada sob a orientação científica da Doutora Ana Maria Pissarra Coelho Gil, Professora Associada com Agregação do Departamento de Química da Universidade de Aveiro, da Doutora Maria Paula Matos Marques, Professora Auxiliar da Faculdade de Ciências e Tecnologia da Universidade de Coimbra e da Doutora Iola Melissa Fernandes Duarte, Investigadora Auxiliar do Departamento de Química da Universidade de Aveiro.

Apoio financeiro da Fundação para a Ciência e Tecnologia (FCT) – bolsa de Investigação FCT SFRH/BD/63916/2009 financiada pelo Programa Operacional Potencial Humano (POPH) e Fundo Europeu de Desenvolvimento Regional (FEDER) e Programa Operacional Factores de Competitividade (COMPETE) – FCT/PTDC/SAU-BEB-66896/2006, CICECO-FCOMP-01-0124-FEDER-037271, PEst-OE/QUI/UI0070/2014, PEst-C/CTM/LA0011/2013; da Universidade de Aveiro – Centro de Investigação em Materiais Cerâmicos e Compósitos (CICECO); da empresa Bruker BioSpin GmbH. Agradecemos ainda à Rede Nacional de RMN (RNRMN), suportada com fundos da FCT, e ao CRMN – Centre de RMN à Très Hauts Champs, CNRS/ENS Lyon, França.

À vida.

O júri

Presidente

Professor Doutor Paulo Jorge dos Santos Gonçalves Ferreira
Professor Catedrático do Departamento de Electrónica, Telecomunicações e Informática da Universidade de Aveiro

Professor Doutor Carlos Frederico de Gusmão Campos Geraldes
Professor Catedrático do Departamento Ciências da Vida da Faculdade de Ciências e Tecnologia da Universidade de Coimbra

Doutor Miguel Augusto Rico Botas Castanho
Professor Catedrático, Faculdade de Medicina da Universidade de Lisboa

Doutora Carmen Diniz Pereira
Professora Auxiliar, Faculdade de Farmácia da Universidade do Porto

Doutor Brian James Goodfelow
Professor Auxiliar do Departamento de Química da Universidade de Aveiro

Doutora Helena Cristina Correia de Oliveira
Bolseira de Pós-Doutoramento do Departamento de Biologia da Universidade de Aveiro

Orientadora

Doutora Ana Maria Pissarra Coelho Gil
Professora Associada com Agregação do Departamento de Química, Laboratório Associado CICECO da Universidade de Aveiro

Co-Orientadora

Doutora Maria Paula Matos Marques
Professora Auxiliar do Departamento Ciências da Vida da Faculdade de Ciências e Tecnologia da Universidade de Coimbra

Agradecimentos

O meu primeiro agradecimento é dirigido à Drª Ana M. Gil e à Drª Iola F. Duarte, orientadora e co-orientadora desta tese, respectivamente. Agradeço-vos o conhecimento que me transmitiram e a oportunidade de realizar este trabalho de investigação na área da metabolómica de RMN, cujas potencialidades, confesso, me conquistaram.

Em segundo lugar quero deixar um profundo agradecimento à Drª Maria Paula M. Marques, também co-orientadora desta tese. Nunca esquecerei os nossos lanches de final de tarde na Unidade, nem os minutos que sempre arranjava para vermos este ou aquele resultado, nem o sorriso generoso com que sempre partilhou comigo o tanto que sabe. Na sua pessoa, não posso deixar de agradecer também a todos com quem me cruzei na Unidade desde o início desta maratona. Agradeço em especial à Ana Lúcia e ao Dr. Luís, pela amizade, pela permanente disponibilidade no laboratório e pelas noites em que, tão generosamente, me abriram as portas de vossa casa (obrigada também à D. Isabel!).

Agradeço à Rede Nacional de RMN, à FCT, ao CICECO, ao Departamento de Biologia na pessoa da Drª Helena Oliveira, à Universidade de Aveiro e à Unidade de I&D Química Física Molecular (Universidade de Coimbra), pelos meios necessários à realização deste trabalho.

Um obrigado aos meus amigos "socialistas" oliveirenses. Não por serem socialistas, claro, mas por tantas vezes serem o "escape" que eu precisei ao longo destes anos, e por sempre ter encontrado na vossa companhia, entre uma e outra piada, uma palavra de conforto e um mimo ao ego.

Agradeço, do fundo do meu coração, aos tant@s e sincer@s amig@s que fiz na UA ao longo destes anos. Não podendo referir o nome de todos, agradeço em especial (e sem qualquer ordem de importância) à Cláudia, às 3 Joanas, à Sílvia, à Susana, ao João e ao Gonçalo. A cumplicidade, os sorrisos, os nervos e até as lágrimas que partilhámos desenharam uma amizade que levo comigo, muito além das fronteiras físicas deste espaço e tempo. Vocês foram a cafeína sem a qual cada passo teria sido bem mais difícil. Obrigada.

Por último, mas nunca em último: a minha família. Agradeço aos meus padrinhos (tia Bela e tio Bide), pelo abraço forte, garante de que sempre lá estarão para mim. Agradeço à Lina e ao Xano, meus sogros, pela alegria, pelo acreditar, pela companhia, por toda a ajuda e por todo o carinho. Agradeço à Mónica e ao Jota, que são meus irmãos sem o serem e com quem sei poder contar até à 25ª hora do dia. Agradeço à minha mãe, a minha Zinha, porque além de ser a pessoa mais generosa que conheço é também aquela que, sem cobranças, mais acredita em mim e incondicionalmente me ama. Agradeço à minha mais fiel companheira, a Minie, por sorrir com cada kilo que tem a mais cada vez que me vê. E termino. Termino com um obrigado em que cada letra é pulsada com o coração: ao Ricardo, meu marido. Obrigada pelos abraços apertados nos momentos de desânimo, pelas palavras mais realistas em outros momentos de desânimo e pelas gargalhadas em momentos de muito cansaço. Obrigada por teres, com as tuas, agarrado as minhas mãos ao leme quando me apeteceu desistir e por teres feito tudo o que estava ao teu alcance para que eu nunca perdesse o norte nesta viagem. Isto é também teu.

Palavras-chave

Osteossarcoma, células MG-63, osteoblastos, cisplatina (cDDP), doxorrubicina (DOX), metotrexato (MTX), Pd_2Spm, cancro, quimioterapia, metabolómica, espectroscopia de ressonância magnética nuclear (RMN), alta resolução e rotação segundo o ângulo mágico (HRMAS), análise multivariada.

Resumo

Este trabalho teve como principal objetivo estudar os efeitos metabólicos de alguns fármacos (três fármacos convencionais e um em desenvolvimento) em células de osteossarcoma (OS) e osteoblastos, através da medição de alterações dos perfis metabólicos celulares por metabolómica usando espectroscopia de Ressonância Magnética Nuclear (RMN).

O Capítulo 1 apresenta um enquadramento teórico deste trabalho, começando por identificar as principais características metabólicas que descrevem o cancro em geral, assim como as famílias e mecanismos de ação dos fármacos usados no seu tratamento. São ainda apresentados os fármacos usados atualmente na quimioterapia do OS, bem como o complexo de Paládio (II) com espermina, Pd_2Spm, com potencial atividade anticancerígena. Seguidamente, é explicada a estratégia da metabolómica celular e apresentado o estado da arte de estudos metabolómicos do efeito de agentes anticancerígenos em células. No Capítulo 2, apresentam-se os princípios das técnicas analíticas usadas neste trabalho, nomeadamente ensaios biológicos, espectroscopia de RMN e análise multivariada e estatística dos resultados. Os detalhes e procedimentos experimentais relativos aos métodos usados são descritos no Capítulo 3.

O estudo da reprodutibilidade analítica e biológica do perfil metabólico de células MG-63 medido por RMN de alta resolução e rotação segundo o ângulo mágico (HRMAS) é apresentado no Capítulo 4. Avalia-se o impacto de vários fatores (integridade celular, velocidade de rotação da amostra, temperatura, duração e parâmetros de aquisição) nas características e qualidade do espectro de RMN HRMAS de ^1H, definindo-se então os parâmetros de aquisição dos espectros a adquirir subsequentemente. Avaliam-se também os efeitos do nº de passagens celulares e do tempo de armazenamento no perfil metabólico de células MG-63.

O Capítulo 5 descreve o impacto metabólico de fármacos convencionais usados atualmente na quimioterapia do OS, estudado por metabolómica por RMN de células lisadas e análise de extratos celulares aquosos. Os resultados mostram que as células MG-63 tratadas com cisplatina (cDDP) sofrem um aumento dramático do teor de lípidos, alterações dos níveis de constituintes dos fosfolípidos (compostos de colina) e de indicadores de degradação do DNA, associados a fenómenos de apoptose. Nas células expostas a doxorrubicina (DOX) ou a metotrexato (MTX) foram identificadas alterações metabólicas mais ténues, com a quase total ausência de alterações no teor de lípidos. Foram também detetadas alterações em metabolitos relacionados com o ciclo de Krebs, stress oxidativo e metabolismo de nucleótidos, interpretadas tentativamente à luz dos mecanismos de ação de cada um dos fármacos. O impacto metabólico da exposição de células MG-63 e osteoblastos a cDDP e ao complexo de Pd_2Spm é apresentado no Capítulo 6. Os resultados mostram que, apesar de ambos os fármacos poderem ligar ao DNA, as alterações metabólicas que decorrem da sua ação são muito distintas, nomeadamente no que respeita às variações nos teores de lípidos (ausentes para Pd_2Spm). Ensaios de medição de apoptose mostraram que, contrariamente ao verificado para células MG-63 expostas a cDDP, a redução do número de células por exposição a Pd_2Spm não se deve a fenómenos de morte celular por apoptose ou necrose. Além disso, este último complexo exerce um efeito mais marcado em osteoblastos do que nas células cancerígenas, o inverso parecendo acontecer com a exposição a cDDP. Contudo, os resultados da exposição de células MG-63 a regimes de tratamento combinado com base em cocktails de cDDP ou Pd_2Spm, descritos no Capítulo 7, mostram que, em combinação, os dois agentes induzem respostas metabólicas semelhantes entre si, decorrentes de mecanismos de sinergia entre fármacos. Finalmente, sumariam-se no Capítulo 8 as conclusões deste trabalho e apontam-se perspetivas de trabalho futuro.

Keywords

Osteosarcoma, MG-63 cells, osteoblasts, cisplatin (cDDP), doxorubicin (DOX), methotrexate (MTX), Pd_2Spm, cancer, chemotherapy, metabolomics, nuclear magnetic resonance (NMR) spectroscopy, high resolution magic angle spinning (HRMAS), multivariate analysis (MVA).

Abstract

The main scope of this work was to evaluate the metabolic effects of anticancer agents (three conventional and one new) in osteosarcoma (OS) cells and osteoblasts, by measuring alterations in the metabolic profile of cells by nuclear magnetic resonance (NMR) spectroscopy metabolomics.

Chapter 1 gives a theoretical framework of this work, beginning with the main metabolic characteristics that globally describe cancer as well as the families and mechanisms of action of drugs used in chemotherapy. The drugs used nowadays to treat OS are also presented, together with the Palladium(II) complex with spermine, Pd_2Spm, potentially active against cancer. Then, the global strategy for cell metabolomics is explained and the state of the art of metabolomic studies that analyze the effect of anticancer agents in cells is presented. In Chapter 2, the fundamentals of the analytical techniques used in this work, namely for biological assays, NMR spectroscopy and multivariate and statistical analysis of the results are described. A detailed description of the experimental procedures adopted throughout this work is given in Chapter 3.

The biological and analytical reproducibility of the metabolic profile of MG-63 cells by high resolution magic angle spinning (HRMAS) NMR is evaluated in Chapter 4. The metabolic impact of several factors (cellular integrity, spinning rate, temperature, time and acquisition parameters) on the ^1H HRMAS NMR spectral profile and quality is analysed, enabling the definition of the best acquisition parameters for further experiments. The metabolic consequences of increasing number of passages in MG-63 cells as well as the duration of storage are also investigated.

Chapter 5 describes the metabolic impact of drugs conventionally used in OS chemotherapy, through NMR metabolomics studies of lysed cells and aqueous extracts analysis. The results show that MG-63 cells treated with cisplatin (cDDP) undergo a strong up-regulation of lipid contents, alterations in phospholipid constituents (choline compounds) and biomarkers of DNA degradation, all associated with cell death by apoptosis. Cells exposed to doxorubicin (DOX) or methotrexate (MTX) showed much slighter metabolic changes, without any relevant alteration in lipid contents. However, metabolic changes associated with altered Krebs cycle, oxidative stress and nucleotides metabolism were detected and were tentatively interpreted at the light of the known mechanisms of action of these drugs. The metabolic impact of the exposure of MG-63 cells and osteoblasts to cDDP and the Pd_2Spm complex is described in Chapter 6. Results show that, despite the ability of the two agents to bind DNA, the metabolic consequences that arise from exposure to them are distinct, namely in what concerns to variation in lipid contents (absent for Pd_2Spm). Apoptosis detection assays showed that, differently from what was seen for MG-63 cells treated with cDDP, the decreased number of living cells upon exposure to Pd_2Spm was not due to cell death by apoptosis or necrosis. Moreover, the latter agent induces more marked alterations in osteoblasts than in cancer cells, while the opposite seemed to occur upon cDDP exposure. Nevertheless, the results from MG-63 cells exposure to combination regimens with cDDP- or Pd_2Spm-based cocktails, described in Chapter 7, revealed that, in combination, the two agents induce similar metabolic responses, arising from synergy mechanisms between the tested drugs.

Finally, the main conclusions of this thesis are summarized in Chapter 8, and future perspectives in the light of this work are presented.

INDEX

List of abbreviations and symbols

(amino acids expressed in 3-letter code)

1D	One dimensional
Abs	Absorbance
ANN	Artificial Neural Networks
cDDP	Cisplatin
CERMAX	Centro de Ressonância Magnética Abel Xavier
Cho	Choline
CLASSY	Cluster Analysis Statistical Spectroscopy
COSY	Correlation spectroscopy
CPMG	Carr-Purcell-Meiboom-Gill
CR	Classification Rate
CV	Cross Validation
d	Doublet
dd	Doublet of Doublets
DMEM	Dulbecco's Modified Eagle's Medium
DMSO	Dimethyl sulfoxide
DNA	Deoxyribonucleic acid
DOX	Doxorubicin
DSS	dimethylsilapentanesulfonic acid
EDTA	Ethylenediaminetetraacetic acid
ERETIC	Electronic Reference To access In vivo Concentrations
F1	1^{st} dimension
F2	2^{nd} dimension
FBS	Fetal Bovine Serum
FID	Free Induction Decay
FN	False Negative
FP	False Positive
FT	Fourier Transformation
GABA	γ-aminobutyrate
GAP	GTPase activating proteins
GPC	Glycerophosphocholine

GSH	Reduced glutathione
GSSH	Oxidized glutathione
h	hours
HBSS	Hanks' Balanced Salt solution
HCA	Hierarchical Cluster Analysis
HDAC	Histone Deacetylase
HMDB	Human Metabolome Database
HOb	Human Osteoblasts
HRMAS	High Resolution Magic Angle Spinning
HSQC	Heteronuclear Single Quantum Coherence
IARC	International Agency for Research on Cancer
IC_{50}	Half inhibitory concentration
INEPT	Insensitive Nuclei Enhanced by Polarization Transfer Sequence
ITQB	Instituto de Tecnologia Química e Biológica
J	Coupling constant
J-res	*J*-resolved
L.f.a.	Lipid fatty acids
LV	Latent Variable
m	multiplet
MCCV	Monte Carlos Cross-Validation
MEM	Minimum Essential Medium
m-Ino	*myo*-Inositol
MLEV-17	Malcom Levitt-17 sequence
MS	Mass Spectrometry
ms	miliseconds
MTT	(3-(4,5-dimethylthiazol-2-yl)-2,5-diphenyltetrazolium bromide
MTX	Methotrexate
MVA	Multivariate Analysis
NADH	Nicotinamide Adenine Dinucleotide (reduced)
NLM	Non-Linear Mapping
NMR	Nuclear Magnetic Spectroscopy
NS	Number of Scans
OPLS-DA	Orthogonal Partial Least Squares-Discriminant Analysis

OS	Osteosarcoma
PBS	Phosphate Buffer Saline
PC	Phosphocholine
PC	Principle Component
PCA	Principle Component Analysis
PE	Phosphoethanolamine
PI	Propidium Iodide
PLS-DA	Partial Least Square-Discriminant Analysis
ppm	Parts per million
PQN	Probabilistic Quotient Normalization
PS	Phosphatidylserine
PTC	Phosphatidylcholine
PUFA	Polyunsaturated Fatty Acid
PULCON	Pulse Length Based Concentrations Determination
Q^2	Goodness of prediction or prediction power
r	Correlation coefficient
R^2_X	Variation explained by the X matrix
R^2_Y	Variation explained by the Y matrix
RG	Receiver Gain
ROC	Receiver Operating Characteristic
RSPA	Recursive Segment-wise Peak Alignment
s	singlet
Sens	Sensitivity
SIMCA	Soft Independent Modelling of Class Analogy
s-Ino	*Scyllo*-Inositol
SOM	Self-Organizing Maps
SOPs	Standard Operating Procedures
Spec	Specificity
SR	Spinning Rate
SRB	Sulforhodamine B
STOCSY	Statistical Total Correlation Spectroscopy
SW	Spectral Window
t	triplet

TCA	Trichloroacetic acid
TD	Size of the FID
TMS	Tetramethylsilane
TN	True Negative
TOCSY	Total Correlation Spectroscopy
TP	True Positive
TPR	True Positive Rate
TSP	3-trimethylsilylpropionic acid
UDP	Uridine Diphosphate
UV	Unit Variance
UXP	UDP/UDP-GNac
Vast	Variable Stability
VEGF	Vascular Endothelial Growth Factor
VIP	Variable Importance for the Projection

1. Introduction

The term cancer designates an extensive group of diseases that can affect any part of the body, also known as malignant tumours or neoplasms. Cancer is generally the result of an accumulation of mutations in oncogenes and tumour suppression genes, the latter encoding regulatory proteins that normally control cell division (Nelson and Cox, 2005).

According to the *World Cancer Report* 2014 of the International Agency for Research on Cancer (IARC), the specialized cancer agency of the World Health Organization (WHO), in 2012 the worldwide burden of cancer increased to 14 million new cases *per* year and is expected to rise to 22 million annually within the next two decades (World Cancer Report, 2014). During the same period, the number of deaths attributed to cancer is expected to rise from 8.2 to 13 million per year. As shown is Figure 1.1, in 2012 the most frequently detected cancers were those of the lung (1.8 million cases), breast (1.7 million) and colorectum (1.4 million), while the most deadly were lung (1.6 million), liver (0.8 million) and stomach (0.7 million) cancers. The cancer statistics based on gender reveal that the overall incidence rate is almost 25% higher in men than in women (World Cancer Report, 2014).

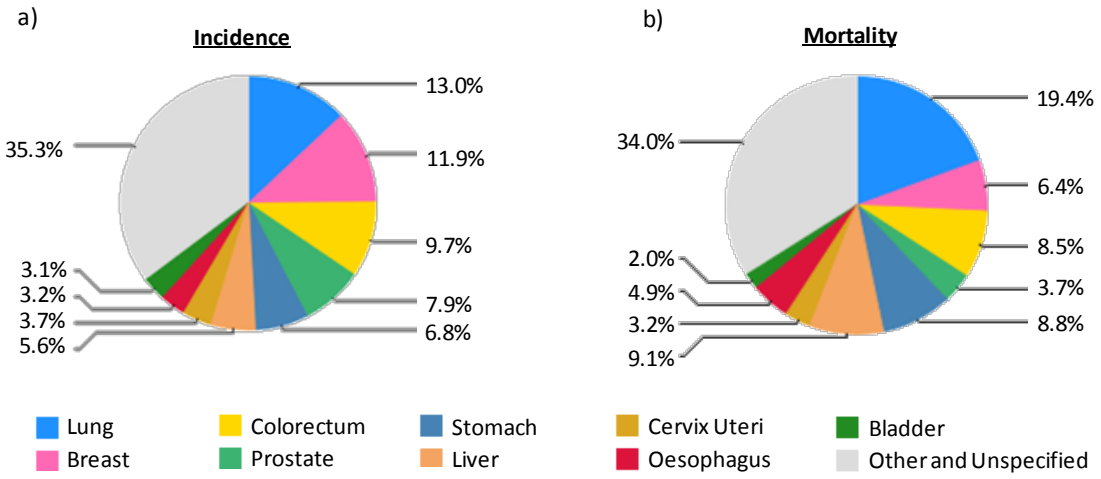

Figure 1.1. Cancer statistics for both genders: a) incidence and b) mortality data for all ages, based on 2012 average population (World Cancer Report, 2014).

Developing countries are noted to be disproportionately affected by cancer, given that more than 60% of the world's total cases are registered in Africa, Asia and Central and South America and 70% of the world's deaths by cancer also occur in these regions, due to the lack of early detection and poor access to treatment. Despite all the investment in investigation and

health care, it is thought that around half of the diagnosed cancers could be avoided if current knowledge was adequately applied (World Cancer Report, 2014).

This chapter begins by reviewing the metabolic alterations that describe carcinogenesis, followed by an overview of anticancer drugs categories and known mechanisms of action. Then, focus is given to osteosarcoma (OS) and to the drugs commonly used for its treatment, including an introduction to a new Pd(II) agent potentially active against OS. Finally, the state of the art regarding the application of metabolomics to assess the impact of drugs on cultured cancer cells.

1.1. Metabolic Hallmarks of Cancer

The transformation of a normal cell into a neoplastic one occurs through a multistage process, from a pre-cancerous lesion to a malignant tumour, as a result of the interaction between individual genetic factors and three categories of external agents: physical carcinogens (*e.g.* ultraviolet and ionizing radiations), chemical carcinogens (*e.g.* tobacco smoke and arsenic) and biological carcinogens (infections from viruses, bacteria or parasites) (World Cancer Report, 2014). Furthermore, the probability of developing cancer dramatically increases with age, probably due to an accumulation of exposure to risk factors in combination with a reduced ability of cellular repair mechanisms upon ageing (World Cancer Report, 2014).

Initial Considerations: the Tumor Microenvironment

Research has shown that the complexity of the tumor microenvironment is at least comparable to that of normal/healthy tissues (Hanahan and Weinberg, 2011). Accordingly, in order to understand the biology of tumours, it is important to consider the different specialized cell types within them (Figure 1.2a), as well as the microenvironment in which the tumorigenesis process takes place (Figure 1.2b).

Cancer cells carrying genetic mutations, both in oncogenes and tumour suppression genes, are responsible for initiating and driving tumorigenesis. These cells form a relatively homogeneous cell population until late stages of tumorigenesis, when increased cell proliferation and genetic instability promote the emergence of distinct subpopulations. Cancer stem cells are rare tumour-initiating cells that share transcriptional characteristics with normal stem cell population. The origin of these cells in solid tumours is not yet clear and may vary between tumour types: they may either originate from normal stem cells or from progenitor cells that

undergo oncogenic transformation. Once primary tumours are formed, cancer stem cells have the ability of self-renewal and generation of further differentiated cells (Hanahan and Weinberg, 2011).

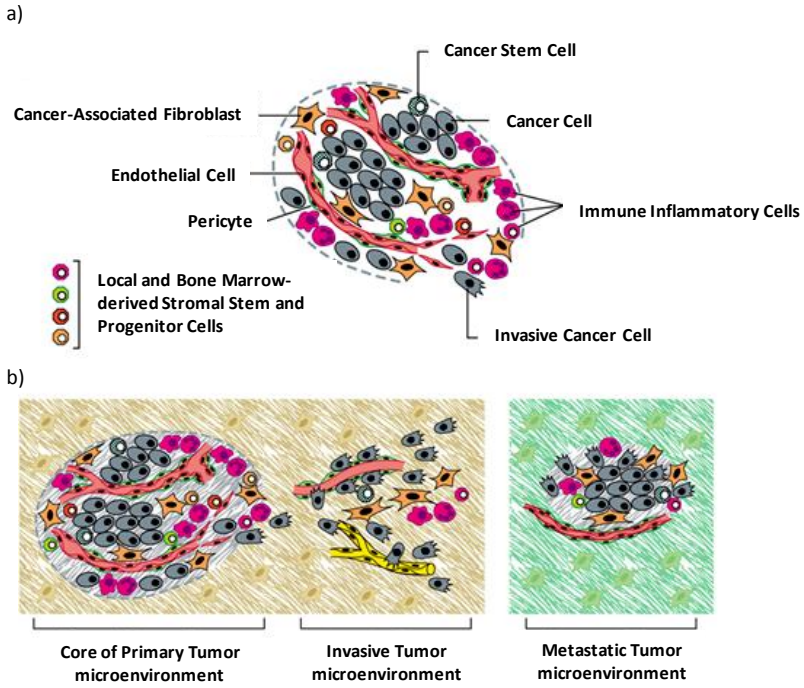

Figure 1.2. Cells in tumour microenvironments: a) assembly of cells that constitute most solid tumors and b) distinct tumour microenvironments (adapted from Hanahan and Weinberg, 2011).

Other types of cells associated to the neoplastic process comprise endothelial cells, pericytes and fibroblasts. Endothelial cells are involved in a series of signal-transduction pathways functionally implicated in developmental and tumour-associated angiogenesis processes. Pericytes are specialized mesenchymal cells with finger-like projections that surround the endothelial tubing of blood vessels. These cells also cooperate with endothelial cells in the synthesis of vascular basement membranes that serve as an anchor for both types of cells, thus displaying a vital role in supporting the tumour endothelium. In contrast to normal wound healing where they appear transiently, tumors can be associated with sites of chronic inflammation where inflammatory cells persist. This has been associated with a series of tissue pathologies apart from neoplasia (*e.g.* fibrosis, aberrant angiogenesis). Inflammatory cells, in turn, are able to release a variety of signalling molecules that act as effectors in fostering tumorigenesis. Fibroblastic cells are responsible for the enhancement of tumour phenotype through the promotion of cancer cell proliferation, angiogenesis, invasion and metastasis. The complete list of contributions from cancer-associated fibroblasts to tumour pathogenesis is far from complete,

but these cells are already known to be undoubtedly associated with the formation of desmoplastic stroma, characteristic of many advanced carcinomas (Hanahan and Weinberg, 2011).

The formation of the tumor complex environment is only made possible through the biological capabilities acquired by cancer cells during the multistep development of human tumors (Hanahan and Weinberg, 2011). These capabilities, also called hallmarks, constitute an organizing principle to rationalize the complexities of neoplastic disease development. The first paper on the subject proposed eight hallmarks of cancer (Hanahan and Weinberg, 2000) and in 2011, the same authors proposed two additional hallmarks (Hanahan and Weinberg, 2011). This will be the basis of the following description of the characteristics of cancer. Cancer hallmarks include sustaining proliferative signalling, evading growth suppressors, resisting cell death, inducing angiogenesis, enabling replicative immortality, activating invasion and metastasis, reprogramming energy metabolism and evading immune destruction (Figure 1.3).

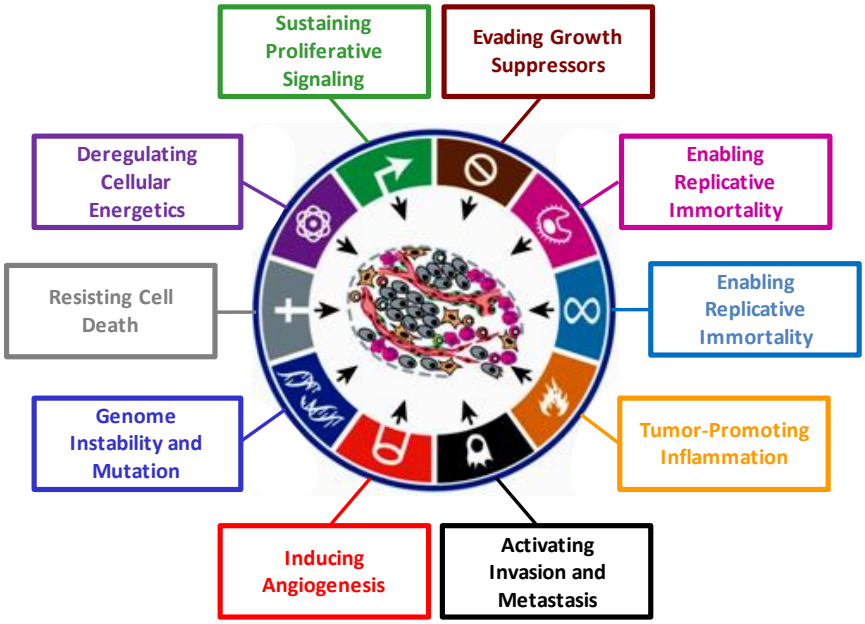

Figure 1.3. The hallmarks of cancer (adapted from Hanahan and Weinberg, 2011).

Sustaining Proliferative Signalling

Cancer cells are able to sustain proliferative signalling in several different ways: by producing growth factor ligands themselves, resulting in self proliferative stimulation; by sending signals that stimulate normal cells within the supporting tumour-associated stroma; by elevating the levels of the signal receptor proteins at the cancer cell surface; or through activation of

components of the signalling pathway, downstream of receptors (Hanahan and Weinberg, 2011). As an example, it is currently known that around 40% of the diagnosed human melanomas acquire mutations that affect the structure of the B-Raf protein, resulting in a constitutive signalling through Raf to the mitogen-activated protein (MAP)-kinase pathway (Davies and Samuels, 2010).

Evading Growth Suppressors

In order to keep growing, cancer cells must circumvent pathways that negatively regulate their proliferation, many of these depending on the action of tumour suppressor genes. Two important tumour suppressors are known to encode the retinoblastoma-associated and TP53 proteins which play important roles in two key complementary cellular regulatory pathways, responsible for cell proliferation or, alternatively, activate senescence and apoptotic programs (Hanahan and Weinberg, 2011). Cancer cells with alterations in the retinoblastoma pathway display continuous cell proliferation. In normal cells, whereas retinoblastoma transduces growth inhibitory signals originating outside the cell, TP53 responds to stress and abnormalities within the cell thus stopping the progression of the cell cycle until their correction, or triggering apoptosis. Changes in TP53 protein in cancer cells lead to a weakening of this monitoring and regulatory system (Olivier *et al*., 2010).

Resisting Cell Death

Tumor cells may adopt several strategies to circumvent apoptosis. One of the most frequent one is the elimination of the TP53 tumor suppressor function, resulting in the loss of one critical damage sensor of the apoptotic pathway (Olivier *et al*., 2010). Additionally, tumors may also increase the expression of antiapoptotic regulators (e.g Bcl-2) by downregulating pro-apoptotic factors (e.g Bax) (Yip and Reed, 2008). Autophagy also mediates tumour cell survival. Autophagy enables the cells to break down cellular organelles (like ribosomes and mitochondria) allowing the resultant catabolites to be recycled for biosynthesis and energy metabolism. Recent studies have shown that nutrient starvation, radiotherapy and specific cytotoxic drugs induce elevated levels of autophagy, which seem to be cytoprotective for cancer cells (White and DiPaola, 2009; Apel *et al*., 2009; Amaravadi and Thompson, 2007; Mathew *et al*., 2007). Necrosis has also shown to have pro-inflammatory and tumour promoting potential. Differently from normal tissues, in which inflammatory cells are recruited to eliminate necrotic debris, in tumour tissues evidences suggest that inflammatory cells are capable of fostering angiogenesis, cancer

cell proliferation and invasiveness. Moreover, in neoplasia, necrotic cells seem to release bioactive factors that stimulate viable cells to proliferate thus promoting tumorigenesis. (Hanahan and Weinberg, 2011; Grivennikov *et al*., 2010).

Inducing Angiogenesis

In healthy tissues, the development of the vasculature occurs during embryogenesis, after which normal vasculature remains quite quiescent. Generally, angiogenesis is only transiently reactivated in situations of wound healing or female reproductive cycling. In the case of tumour tissue, the angiogenesis process remains, inducing a continuous spread out of vessels to sustain neoplastic expansion. Two of the most well-known angiogenesis inducers and inhibitors are the vascular endothelial growth factor A (VEGF-A) (Goel and Mercurio, 2013) and thrombospondin-1 (TSP-1) (Wang *et al*., 1996), respectively. In fact, recent work showed that the expression of the gene that encodes for VEGF can be upregulated both by hypoxia and oncogene signalling (Ferrara, 2009; Mac Gabhann and Popel, 2008). Additionally, pericytes have been found to be associated with the neovasculature of several tumors (Raza *et al*., 2010; Bergers and Song, 2005).

Activating Invasion and Metastasis

The process of invasion and metastasis occurs through multistep biological changes, which begin in local invasion, followed by intravasation by cancer cells into surrounding blood and lymphatic vessels. These are used to drive cancer cells to distant tissues, where they leave the vessels and form small nodules of cancer cells. The final step encompasses the growth of the micrometastatic lesions into macroscopic tumors, through a process named colonization (Hanahan and Weinberg, 2011). Recent research has shown that the ability of cancer cells to invade, resist apoptosis and disseminate is acquired in the context of a regulatory program, refered as epithelial-mesenchymal transition (EMT) (Klymkowsky and Savagner, 2009; Polyak and Weinberg, 2009). This program can be permanently or transiently activated by cancer cells in the course of invasion and metastasis.

Enabling Replicative Immortality

The immortalization of a reduced number of cells that precedes the tumour formation has been associated with their capacity to maintain telomeric DNA in such acceptable length in order to prevent the triggering of senescence and/or apoptosis. This is achieved mainly through the upregulation of telomerase expression, but also via an alternative recombination-based telomere

maintenance mechanism. Multiple evidences suggest that the telomeres that protect the end of chromosomes are key players in cells' ability for unlimited proliferation (Blasco, 2005; Shay and Wright, 2000).

Reprogramming of Energy Metabolism

This issue is a particularly relevant one in relation to the theme of the present thesis. The deregulated cell proliferation that drives tumorigenesis is necessarily accompanied by adjustments in energy metabolism in order to fuel cell growth and division (Hanahan and Weinberg, 2011). Under aerobic conditions, normal cells produce pyruvate from glucose through glycolysis in the cytosol and then convert it to carbon dioxide in the mitochondrial Krebs cycle. This reaction originates NADH that in turn fuels oxidative phosphorylation for ATP production, with reduced production of lactate. Only when submitted to anaerobic conditions do healthy cells produce large amounts of lactate. On the contrary, in cancer cells, increased lactate production occurs regardless of oxygen availability. This metabolic adaptation of cancer cells is known as aerobic glycolysis or Warburg effect (Warburg, 1924; Warburg, 1956) (Figure 1.4).

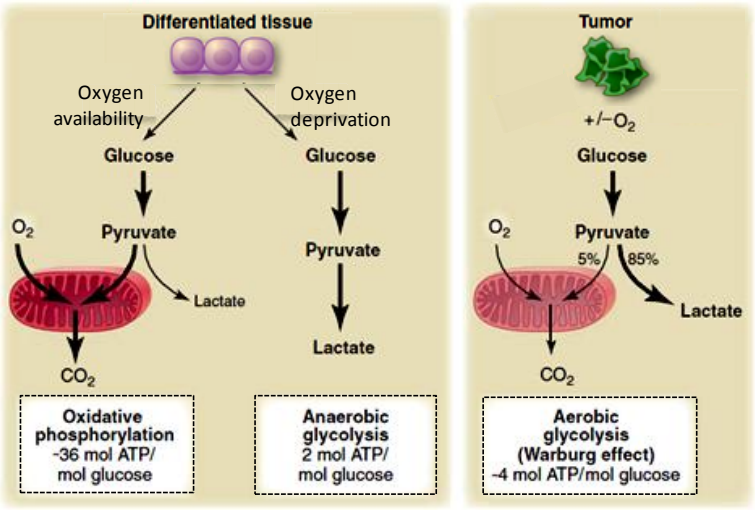

Figure 1.4. Schematic representation of the differences between oxidative phosphorylation, anaerobic glycolysis and Warburg effect (adapted from Heiden *et al*., 2009).

This lower efficiency of ATP production afforded by glycolysis in relation to mitochondrial oxidative phosphorylation in cancer cells is in part compensated by the upregulation of glucose transporters, namely GLUT1, resulting in an increased rate of glucose import into the cytoplasm. These and other glycolytic fuelling adaptations of cancer cells have been related to activated oncogenes, namely RAS and MYC, and tumour mutant suppressors, as TP53 (Jones and Thompson, 2009; DeBerardinis *et al*., 2008). Some of the many recent articles that review the

Warburg effect (Weljie and Jirik, 2010; Heiden *et al*., 2009; Ferreira, 2010; Antone, 2012; Annibaldi and Widmann, 2010) have also highlighted the additional knowledge acquired in recent years on other altered metabolic pathways as a consequence of the hypoxic conditions felt by cancer cells, namely those concerning glutamine metabolism and *de novo* lipid and nucleic acid synthesis.

The role of glutamine in tumorigenesis has been very recently reviewed (Daye and Wellen, 2012; Hensley *et al*., 2013).Glutamine metabolism is crucial for cell proliferation due to the use of this amino acid as a primary carbon source for energy production and biosynthesis, combined with its role in cell signalling and redox homeostasis regulation (Figure 1.5).

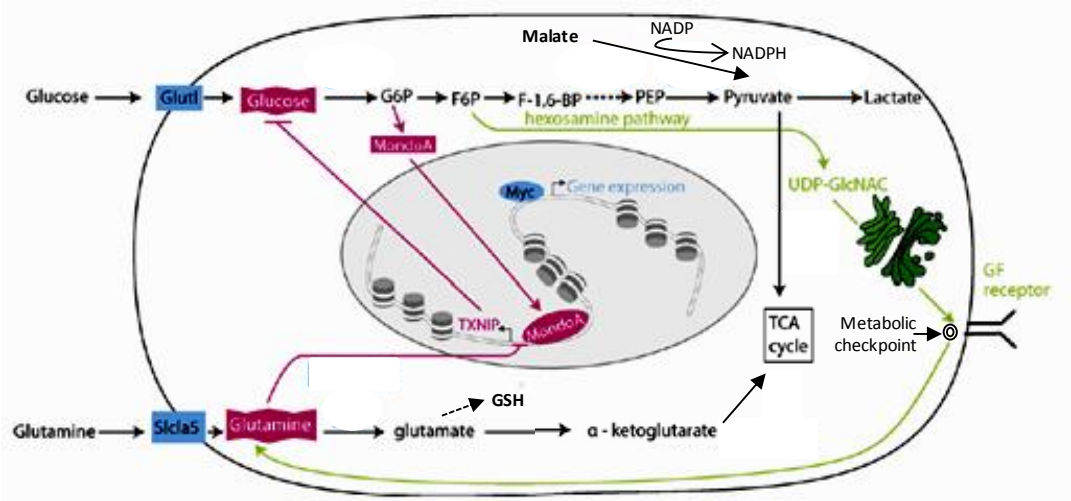

Figure 1.5. Coordination of glucose and glutamine utilization in cancer (adapted from Daye and Wellen, 2012).

The regulation of the redox homeostasis by glutamine is due to its central contribution to glutamate biosynthesis from which, together with cysteine and glycine, a potent endogenous antioxidant is built: glutathione. Moreover, the normalization of the levels of the reduced form of glutathione requires NADPH, which production can be potentiated by the metabolism of glutamine through malic enzyme (Wise and Thompson, 2010). Additionally, recent studies suggest that cells actively regulate the metabolism of glucose and glutamine, depending on their reciprocal availability: glucose availability was shown to modulate the cellular uptake of glutamine through the hexosamine biosynthetic pathway, a branch of glucose metabolism that generates UDP-N-acetyl-glucosamine (UDP-GlcNAc) (Figure 1.5). In short, the glucose flux into the hexosamine biosynthetic pathway to support the glycosylation of surface receptors may serve as metabolic checkpoint, through which cells can control growth-factor-dependent uptake of

glutamine, in a glucose dependent manner (Daye and Wellen, 2012). As a key player in cancer cell proliferation, glutamine metabolism is regulated by oncogenes and tumour suppressors.

Increasing evidence shows that cancer cells possess altered lipid metabolism (Podo, 1999; Fernandis and Wenk, 2009; Santos and Schulze, 2012). Several types of cancer cells present increased rates of *de novo* lipid synthesis in order to fulfil their metabolic requirements. The increased proliferation rate of cancer cells demand increased fatty acid production for the production of phosphoglycerides which, together with cholesterol, can be used to build cell membranes. The mobilization of fatty acids from lipid stores and its degradation in the mitochondria through β-oxidation can provide energy when required. The oncogenic activation of the PI3K/Akt pathway induces the uptake of glucose and its use for lipid synthesis through activation of the transcription factor sterol regulatory element-binding proteins (SREBPs). AMPK is activated in response to low cellular energy levels, preventing lipid synthesis and promoting its β-oxidation. The activation of HIF1 (Hypoxia Inducible Factor 1) by hypoxic conditions of tumour tissues reduces the flux of glucose to acetyl-CoA through mitochondria. The production of α-ketoglutarate from glutamine provides the cytoplasmatic citrate in tumour cells, which can in turn be used to fatty acid synthesis (Figure 1.6) (Santos and Schulze, 2012).

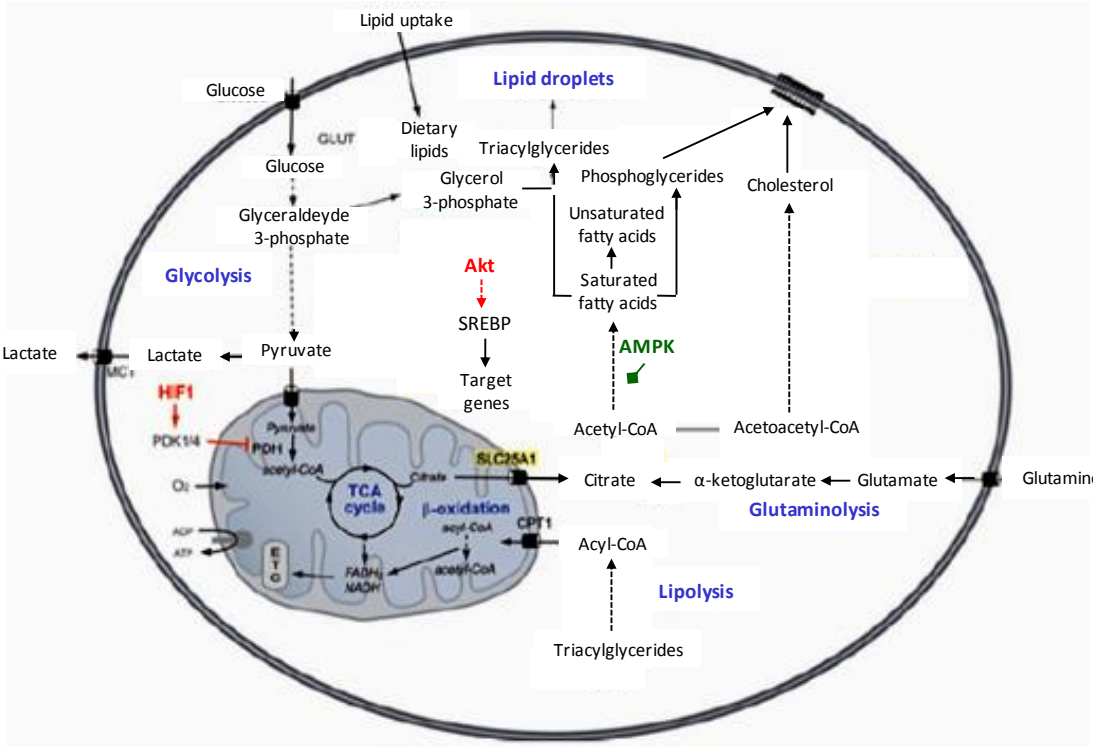

Figure 1.6. Regulation of lipid metabolism by oncogenic signalling pathways (adapted from Santos and Schulze, 2012).

Nucleotide metabolism is also altered in tumour cells, as proven by their larger nucleotide pool (necessary to ensure the proliferative activity), the higher activity of the nucleotide anabolic pathway and its reduced catabolic pathway (Tong *et al*., 2009). The biosynthesis of purines and pyrimidines needs ribose-5-phosphate (R5P), produced from glycolytic intermediates that enter the pentose phosphate pathway (PPP) and nonessential amino acids derived from glucose and glutamine catabolism. In turn, ribose-5-phosphate can be either synthesized from glucose-6-phosphate (through oxidative branch of the PPP) or from fructose-6-phosphate and glyceraldehydes-3-phosphate (GA3P, through non-oxidative branch of PPP). In normal cells, ribose-5-phosphate is preferentially produced *via* PPP, while in tumour cells the non-oxidative pathway constitutes the main source of ribose-5-phosphate production (Boros *et al*., 1998). Besides its role in the stimulation of anaerobic glycolysis, HIF1 is also crucial in this preference for the non-oxidative PPP. Thus, tumour cells possess a complex interplay between glycolysis, glutaminolysis and the *de novo* nucleotides synthesis (Figure 1.7) (Tong *et al*., 2009).

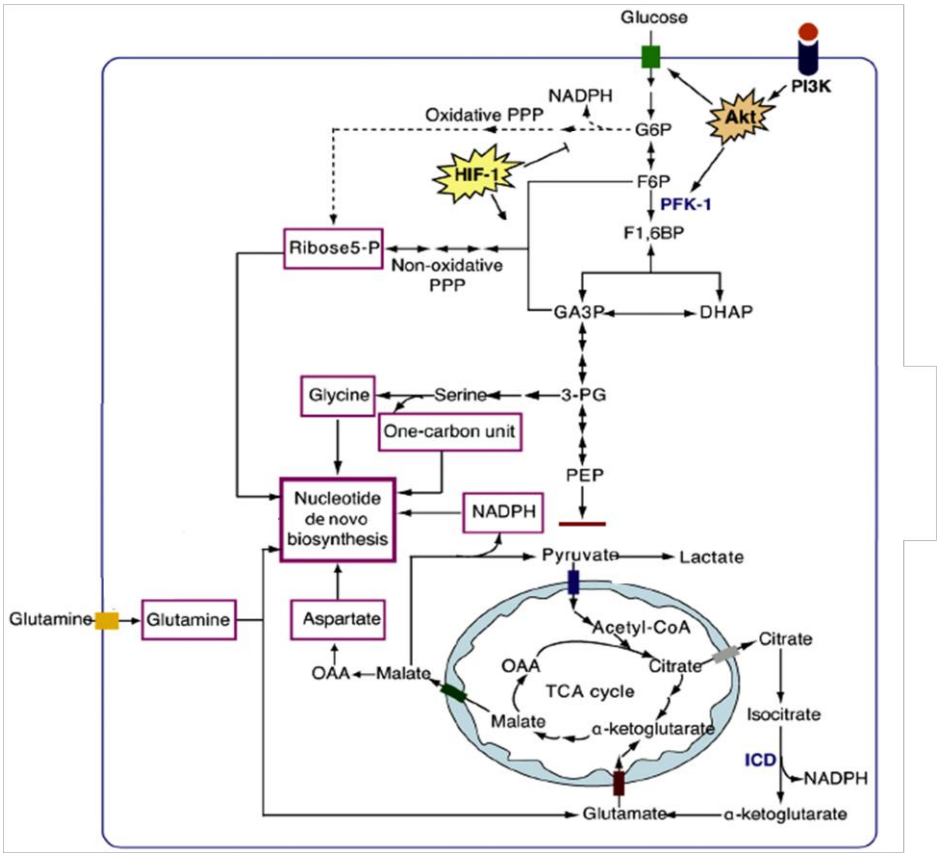

Figure 1.7. Regulation of glycolysis, glutaminolysis and *de novo* nucleotide biosynthesis in tumour cells (adapted from Tong *et al*., 2009).

All the steps in the non-oxidative PPP are reversible, which means that the relative levels of metabolic substrates and products drive the direction of the pathway. Thus, with the purpose of

diverting glycolytic compounds into PPP (through the non-oxidative pathway) tumour cells need to maintain high levels of fructose-6-phosphate and/or GA3P (Tong *et al*., 2009).

Evading Immune Destruction

Increasing evidence suggests that solid tumours somehow evade detection by the immune system, or at least are able to restrict the extent of immunological activity, thereby evading immune destruction (Yang *et al*., 2010; Shields *et al*., 2010). One of the main strategies of tumors to evade eradication seems to lie on the disabling of the components of the immune system that are activated to eliminate them. For instance, cancer cells may stop cytotoxic T lymphocytes and natural killer cells, by secreting TGF-β or other immunosuppressive factors. Other strategies of the tumour tissues to suppress cytotoxic lymphocytes consist of the recruitment of inflammatory cells that are actively immunosuppressive, as regulatory T cells and myeloid-derived suppressor cells (Hanahan and Weinberg, 2011).

The enormous complexity of the tumorigenesis process seems to be far beyond the above briefly referred topics. Several recent papers offer very interesting reviews about general findings on cancer cell metabolism and recent knowledge on cancer cell reprogramming (Locasale and Cantley, 2010; Negrini *et al*., 2010; Cantor and Sabatini, 2012; Dang, 2012; Fiachi and Chiarugi, 2012; Jones and Schulze, 2012; Schulze and Harris, 2012; Ward and Thompson, 2012; Dang, 2013; Wu and Zhao, 2013; Gaude and Frezza, 2014; Phan *et al*., 2014)

1.2. Drugs Used in Cancer Treatment: Families and Mechanisms

The metabolic hallmarks of cancer described in the previous section constitute potential therapeutic targets. Inhibition of cancer specific pathways is prone to limit tumor growth and promote its eventual shrinkage. With this purpose, several drugs have been investigated and taken from *in vitro* testing to clinical trials. This section comprises the description of the agents presently used in anticancer research according to their targets and mechanisms of action and the classes hereby presented reflect those proposed by specific literature (Skeel, 2007).

1.2.1. Alkylating Agents

Alkylating agents are among the first type of drugs used in systemic chemotherapy and include nitrogen mustards (*e.g.* cyclophosphamide and ifosfamide), alkyl sulphonates, aziridines and nitrosoureas (*e.g.* chloroethyl nitrosourea, CENU). The general mode of action of these drugs is based on the formation of an ethyleneimonium intermediate ion which, due its high instability, forms covalent bonds with DNA bases (Warwick, 1963). Bifunctional alkylating agents possess two reactive groups characterized by the presence of a lone pair of electrons on the nitrogen atom, the donation of which gives rise to an unstable ethyleneimonium ion followed by loss of a negatively charged chloride radical. The ethyleneimonium ion may further destabilized to form a carbonium ion, both intermediates being able to sequentially bond to guanine residues within the DNA double helix, yielding either intra- or inter-strand adducts (Figure 1.8) (Airley, 2009).

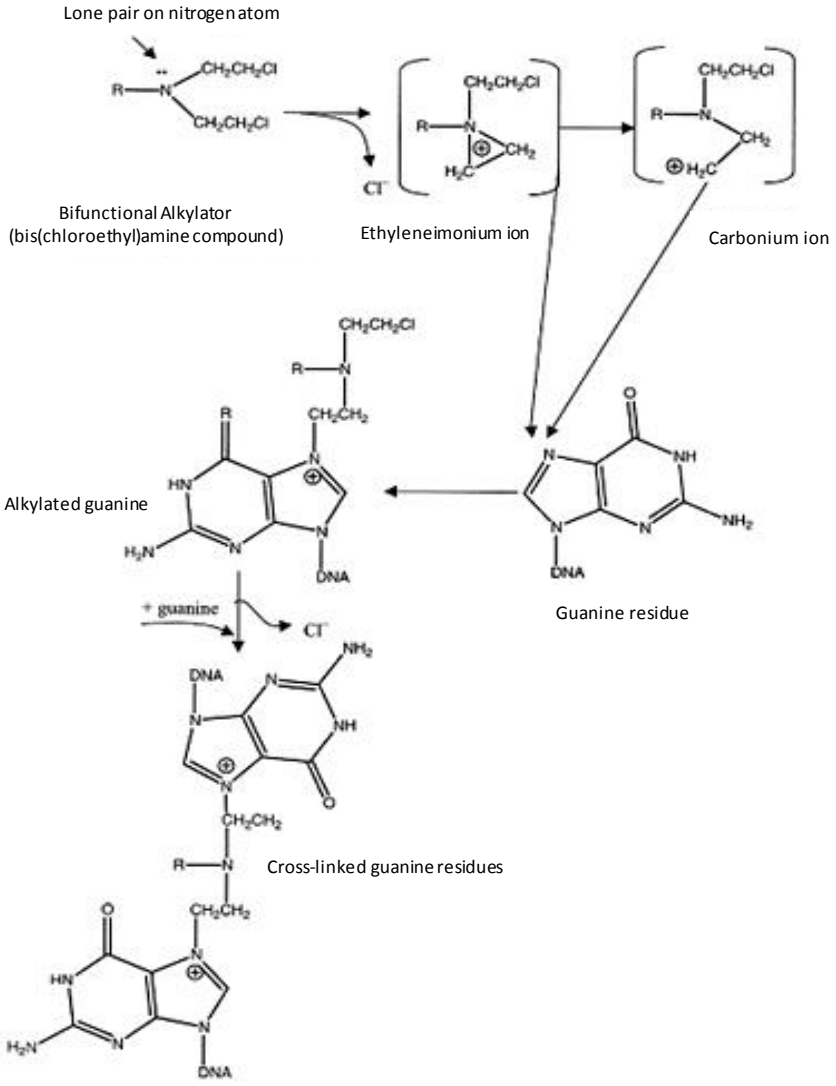

Figure 1.8. General mode of action of alkylating agents (adapted from Airley, 2009).

1.2.2. Metal-based Anticancer Agents

In the case of platinum-containing drugs (cisplatin or cDDP, oxaplatin and carboplatin), the formation of an intermediate occurs when the drug enters the cell, where hydrolysis of the chlorine atoms takes place, due to lower intracellular concentration of Cl^- ions. An unstable aquo intermediate is formed (drug activation step), which then binds to DNA bases (mostly guanine and adenine), through Pt-N^7 bonds (Airley, 2009).

1.2.3. Antimetabolites

Several drugs act by mimicking the structure of natural occurring molecules and, for this reason they are generally designated as antimetabolites (Bardos, 1974). Their designation is based on the type of agent they mimic: 1) inhibitors of purine and pyrimidine biosynthesis: the structure is similar to those of enzymes involved in DNA synthesis; 2) purine analogues: similar to purine free bases, thus being incorporated into nucleotides; 3) nucleosides analogues: comprising a purine or pyrimidine base linked to a deoxyribose sugar that is intracellularly phosphorylated, therefore interfering with DNA elongation; 4) pyrimidine analogues (*e.g.* 5-Fluorouracil); or 5) antifolates (*e.g.* methotrexate), which antagonise folic acid activity. (Airley, 2009)

1.2.4. Antitumor Antibiotics

Anthracyclines (*e.g.* doxorubicin, daunorubicin, epirubicin) are a group of antitumor antibiotics and are among the most potent chemotherapeutic agents (Hortobágyi, 1997). These agents have several modes of actions: 1) intercalation in the DNA double helix, thus disrupting base pairing and base stacking, subsequently interfering with DNA synthesis and replication; 2) production of free radicals through the interaction between anthracyclines and molecular oxygen, thus resulting in the production of peroxides, superoxide and hydroxyl radicals responsible for injury of several cellular components; 3) inhibition of topoisomerase II, yielding a stable DNA-enzyme complex that prevents the rejoining of DNA breaks (Airley, 2009). Antitumour antibiotics that are not anthracyclines include actinomycin-D, bleomycin and mitomycin-C (Airley, 2009).

1.2.5. Mitotic Inhibitors

Mitotic inhibitors alter the dynamics of the mitotic spindle by targeting tubulin, the main structural protein constituent of microtubules. As cell-cycle dependent agents, these drugs act at the M-phase, i.e., when the chromosomes are aligned on the mitotic spindle (Senese *et al*., 2014). Vinca alkaloids (*e.g.* Vincrastine), derived from the plant *Vinca rosea* are an example of these agents, and act by binding to one of the soluble subunits of the tubulin, inducing a conformational change responsible for an increase in the affinity between tubulin filaments. These agents reduce the rate of microtubules growth by stabilising them, hence compromising the dynamics necessary for mitotic spindle formation during metaphase. Taxanes represent another group of mitotic inhibitors, namely the frequently used paclitaxel and docetaxel. Contrary to Vinca alkaloids, these agents promote tubulin polymerisation by binding to a subunit in the inner surface of the microtubule cylinder. This induces a conformational change in the tubulin molecules which promotes its self-assembly and function loss (Airley, 2009).

1.2.6. Hormonal Agents

Breast, prostate, ovary, cervix and testicles carcinomas are examples of hormone-dependent neoplasias. The regulation of growth and differentiation of tissues that suffer the influence of hormones is dependent on their binding to the respective receptor. Estrogens and androgens are examples of hormones, the interaction of which with specific receptors triggers a series of events responsible for cell proliferation (Airley, 2009).

This class of anticancer drugs encompasses four main types of compounds: aromatase inhibitors (*e.g.*Anastrazole), that block the action of aromatase (or estrogen synthase) involved in the final step of estrogen synthesis from androgens; anti-androgens (*e.g.* flutamide), which compete with natural androgens for the binding to androgen receptors; endocrine agents (*e.g.* leuprolide),which modulate the hypothalamus-hypophysis axis in order to inhibit the production of luteinizing hormone (LH) and follicle-stimulating hormone (FSH), responsible for the production of male and female hormones; and estrogen antagonists (*e.g.* tamoxifen) (Airley, 2009).

1.2.7. Antiangiogenic and Antivascular Agents

The growth and survival of solid tumours depend on the correct supply of nutrients through functional vasculature networks (Jain, 2002). Based on this, antiangiogenic and antivascular disrupting agents have emerged as important players in chemotherapy.

Antiangiogenic drugs hinder the process of new blood vessel formation in cancer tissues, thus targeting angiogenesis and blocking the ability of a cancer cells population to proliferate, survive and invade surrounding tissues, either by tumour growth or metastasis (Airley, 2009). Agents like HIF-1 or VEGF (vascular endothelial growth factor) have the ability to promote angiogenesis in hypoxic conditions. In the search for novel antiangiogenic agents, a number of possible sites of pharmacological intervention must be taken into account: using angiostatic agents like endostatin, an inhibition of angiogenesis is supposed to be achieved; targeting growth factors, for example by using growth factor receptor antagonist will suppress their action on endothelial cell growth; matrix metalloproteinase inhibitors will inhibit invasion of surrounding tissues by tumour cells; inhibitors of cell adhesion molecules and cell junctions (integrin inhibitors) will difficult cell survival in a solid tumour (Figure 1.9).

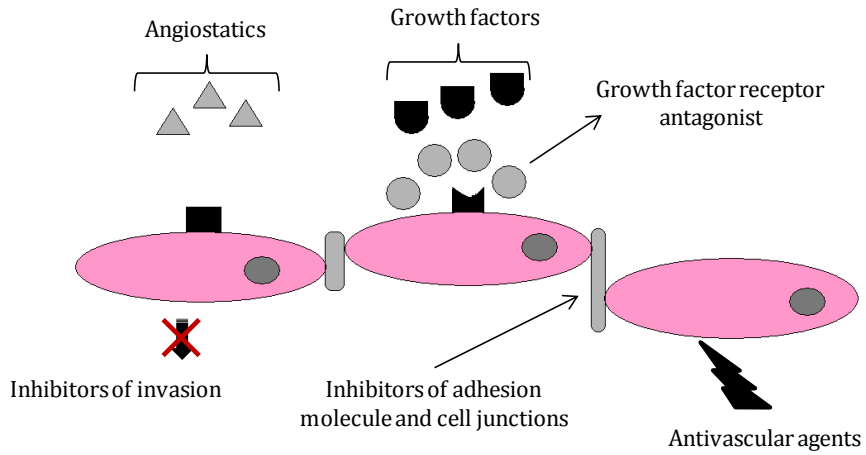

Figure 1.9. Sites of pharmacological intervention when designing angiogenesis inhibitors (adapted from Airley, 2009)

Vascular disrupting agents intend to destroy the structural and functional integrity of existent vasculature (Liu and Deisseroth, 2006). The use of this kind of agents aims at inducing the collapse of existing tumour blood vasculature, leading to ischemia (oxygen privation) and tumour cell death. Vascular disrupting agents act upon endothelial cells in a similar way of that of tubulin binding drugs such as Vinca alkaloids and taxanes. Because tumour vascular endothelium shows differences from normal vasculature (increased rate of endothelium proliferation, lack of

extravascular pericytes and increased fragility due to abnormal basement membrane and thin muscular wall), tubulin-binding vascular disrupting agents can directly target malignant vessels.

1.2.8. Topoisomerase Inhibitors

Topoisomerase I and II have little similarity in terms of amino acid sequence and are different in what concerns molecular mass and function, although both play a very important role in DNA replication and packaging. Topoisomerase I is responsible for a single DNA strand break and enables the unwinding of the broken single strand through the other, in a process that does not depend on ATP, once this enzyme preserves the energy of the phosphodiester linkage break through a covalent link between the phosphate group and the enzyme itself, at the cleavage point. Then it uses this preserved energy to restore the phosphodiester linkage and seal its break to the strand. On the other hand, topoisomerase II induces breaks in the two DNA strands and at the same time, it can twist or unwind them through an ATP-dependent process (Airley, 2009). irinotecan and etoposide are examples of Topoisomerase I and II inhibitors, respectively (Lindskog *et al*., 2004).

1.2.9. Molecularly Targeted

Tumor Hypoxia – HIF-1 Inhibitors

As mentioned before, tumour hypoxia is a phenomenon that is usually associated with solid tumours. Because tumour cells proliferation rate is very high, there is not enough time to correct angiogenesis and some cancer cells even experiment complete anoxia, a condition in which cells are able to survive only for short periods of time. In order to survive this hostile environment, cancer cells undergo a number of adaptive modifications regulated by the transcription factor hypoxia-inducible factor 1 (HIF1) (Semenza, 2003). HIF1 is a complex constituted by two subunits, HIF1α and HIF1β. The first can rapidly be degraded under normal oxygen conditions, whereas HIF-1β exists independently of tissue oxygenation. In hypoxic conditions both subunits are present, and so they complex. The formation of this dimer induces a conformational change that enables this transcription factor to bind hypoxia-response element (an enhancer sequence of DNA localized in the promoter region of hypoxia-inducible genes). This ends by activating genes that

encode for proteins involved in response to hypoxia. HIF1 inhibitors as anticancer drugs, block the adaptive response of cancer tissues to hypoxia, thus contributing for tumour remission (Airley, 2009).

Tyrosine Kinase Inhibitors

Tyrosine kinase is a very important player in malignant progression since the expression of receptors and proteins that result from its activation play a role in many important metabolic pathways related to cancer. Tyrosine kinase catalyses the transfer of a phosphorous group from ATP to a tyrosine residue on effector proteins. This phosphorylation act as a signal that regulates the expression of genes that control among others, cell survival, proliferation and the capacity to metastasize. There are two types of tyrosine kinases: receptor tyrosine kinases, where the enzyme is part of a membrane bound receptor and non receptor tyrosine kinases that frequently lie in the cytoplasm or in the internal surface of the cell (Gottschalk *et al.*, 2004).

Ras Inhibitors

Ras is a 3-member family of proto-oncogenes (H-Ras, N-Ras, K-Ras) that codes for a GTPase located in the inner surface of the plasma membrane, and activates growth factor-mediated signal transduction pathways, responsible for the regulation of cell proliferation and survival. Single point mutations in specific codons of Ras are responsible for its oncogenic transformation and subsequent prevalence of the constitutively active GTP form. For this reason, in tumours that express the Ras oncogene, there is an amplification of the signal transduction pathways that mediates malignant transformation progression (Baines *et al*., 2011). In order to be functional, Ras must undergo post-translational modifications that allow its anchorage to the inner surface of the plasma membrane. Farnesyl transferase is a heterodimeric metalloenzyme that is responsible for this. Due to its crucial importance for Ras activation, Ras farnesyl transferase has become a target in novel anticancer agents development (Airley, 2009).

Heat Shock Protein (HSP) 90 inhibitors

Heat shock proteins (HSP) are a family of proteins produced in response to heat stress, with the particular objective of protecting specific proteins, vulnerable to damage and denaturation in these conditions. HSP90 (90 kDa) has a wide range of binding proteins, but is its action on proteins involved in signal transduction of tumour proliferative and regulatory processes, that attract more interest and promotes many studies on anticancer drug design. HSP90 binding proteins interfere

in processes like: oncogene expression, signal transduction, transcription factor HIF-1 and TP53 (Gomez-Monterrey *et al*., 2012). Therefore, HSP90 inhibitors have multiple modes of action, such as the suppression of growth factor production, inhibition of kinases associated with progression through cell cycle, inhibition of oestrogen-induced cellular proliferation (hormone-dependent cancers) and the induction of apoptosis (Airley, 2009).

Histone Deacetylase (HDAC) inhibitors

DNA packaging into chromosomes depends on the action of histones. Histone deacetylases (HDAC) are enzymes that change chromatic structure and promote altered gene expression in cancer. By removing acetyl groups from lysine residues, HDAC restores positive charge enabling DNA condensation and repressing transcription of specific genes that may inhibit cellular proliferation and tumour growth. In the contrary, inhibition of HDAC leads to an accumulation of hyperacetylated histones, inhibiting tumour growth by activating the transcription of genes responsible for cell cycle arrest, differentiation and/or apoptosis (Atadja, 2011).

Phosphoinositide 3-kinase (PI3K) inhibitors

Phosphoinositide 3-kinases (PI3K) are a family of lipid kinases that catalyse the formation of phosphatidylinositol 3,4-bisphosphate and phosphatidylinositol 3,4,5-triphosphate. These molecules selectively bind many signalling proteins, leading to activation of downstream signalling pathways. The three main classes of members of this family mediate many key cellular processes including growth and survival, cell cycle entry, adhesion and migration. For this reason PI3K looks like an attractive target for novel mechanism-based anticancer treatment (Beloueche-Babari *et al*., 2006).

Choline Kinase inhibitors

Choline kinase catalyses the phosphorylation of choline by ATP in the presence of Mg^{2+}, yielding phosphocholine. This enzyme step commits choline to Kennedy pathway for the biosynthesis of phosphatidylcholine, the major phospholipid constituent of biomembranes. Increased activity of choline kinase has been reported to be associated with an enhanced generation of PC, mostly independently of the rate of net PtdCho biosynthesis. In addition, chemical carcinogens have been shown to cause induction of choline kinase activity, leading to PC accumulation. Recently, increased activity of this enzyme has been shown in human tumour-derived cell lines and in a variety of human tumours compared with their corresponding normal

tissues (Al-Saffar *et al*., 2006). These findings strongly suggest the role of choline kinase as a potential target for the development of anticancer drugs.

PPARγ receptor

The peroxisome proliferator-activated receptor-γ (PPARγ) plays a central role in the process of adipocyte differentiation and is expressed at high levels in each of the major histological types of human liposarcoma. Ligands to the PPARγ nuclear receptor induce terminal adipocyte differentiation of preadipocytes and primary human liposarcoma cells. The induction of adipocyte differentiation by PPARγ ligands results in the expression of adipocyte-specific genes, a rapid accumulation of intracellular triglycerides, and withdrawal from the cell cycle. This induction of terminal differentiation by synthetic ligands to the nuclear receptors that regulate growth and differentiation represents a promising therapy for the treatment of certain malignancies (Chen *et al*., 2002).

1.3. Drugs Commonly used in Osteosarcoma Treatment

This section begins by presenting osteosarcoma (OS) and the current clinical protocols for its treatment as well as new OS treatment strategies and agents. The currently most used drugs for OS treatment (cisplatin, doxorubicin and methotrexate) are addressed later, focusing on their particular mechanisms of action, in the light of the previously defined families of compounds.

1.3.1. Osteosarcoma: Definition and Prevalence

In the human body, new bone is permanently being formed, while old one is dissolved. The interior of most bones is hollow (containing the bone marrow) and their outer part is a network of fibrous tissue called matrix, in which calcium ions are deposited. Osteoblast is the name given to the cells that lay down new bone and osteoclasts are those responsible for dissolving old bone tissue. Figure 1.10a schematically represents the elements that constitute the bone architecture.

Cells from any part of the bone can differentiate into a tumour. Primary bone cancers are called sarcomas and their origin is the bone itself. There are benign (not cancerous) and malignant (cancerous) primary bone tumors, of different types, whose names are based on the area of bone or surrounding tissue that is affected and on the type of cells forming the tumour.

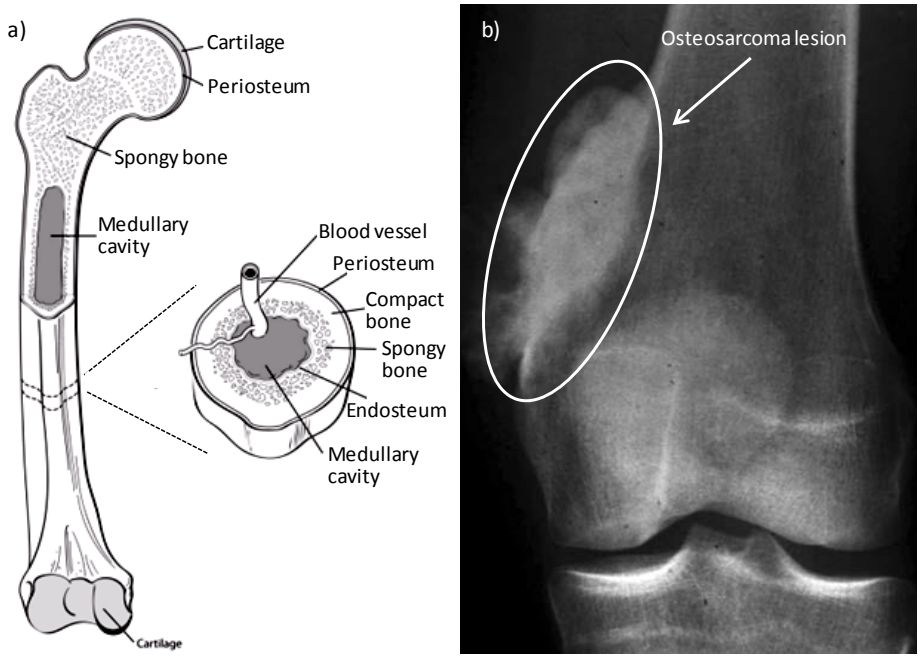

Figure 1.10. a) Schematic representation of the bone constituting elements (adapted from www.cancer.org/cancer/bonecancer) and b) X-ray image of an OS lesion (adapted from Ta *et al*., 2009).

Bone cancers are rare events and, according to the American Cancer Society, they account for less than 0.2% of all diagnosed cancers. In adults, more than 40% of primary bone malignancies are chondrosarcomas, followed by osteosarcoma (28%), chordomas (10%), Ewing tumors (8%) and malignant fibrosarcomas (4%). Osteosarcoma is the most common solid tumour of bone affecting pediatric and adolescent age groups with an incidence of 56%, followed by Ewing tumors (34%) and chondrosarcomas (6%) (www.cancer.org/cancer/bonecancer).

Unlike most other primary tumors of bone, Ewing sarcoma involves a translocation in the eleventh and twenty second chromosomes. The result of that translocation is the protein EWS-FLI1, which has been pointed as an aberrant transcription factor that drives the pathogenesis of this type of tumour (Schwab *et al*., 2012). Ewing sarcomas predominantly occur in the pelvis, the diaphyseal regions of long bones and bones of the chest wall. Chondrosarcoma is a vast group of malignant bone tumors that originate a cartilaginous (chondroid) matrix, often found in bones that elongate due to endochondral ossification. They can emerge as primary or secondary (associated with metastatic phenomena) tumors in benign precursor lesions, they are generally slow growing and seldom metastasize (van Driel and van Leeuwen, 2014). Fibrosarcomas develop more often in soft tissues than in bones, and when in the latter the most affected are those from the legs, arms and jaw. Chordoma usually occurs in the base of the skull and bones of the spine. It is about twice as common in men that in women, it tends to grow slowly and rarely metastasizes,

although it often reappears in the same area if not removed completely. Osteosarcoma (also named osteogenic sarcoma) usually appears between the ages of 10 and 30, it rarely develops in middle-aged people and is more common in male than females. It mostly affects the bones of the arms, legs and pelvis. (www.cancer.org/cancer/bonecancer)

Specifically in relation to OS, it produces osteoid tissue and is characterized by spindle-shaped cells. Osteosarcoma generally presents as a high grade sarcoma and possesses an increased ability to metastasize, especially to the lung (van Driel and van Leeuwen, 2014). Several factors have been identified as contributing to the pathology of OS: mutation in p53 and RB tumour suppressor pathways, teenage growth spurt, Paget's disease, chemical agents (e.g. beryllium), radiation and viruses containing the Src oncogene (Dai *et al*., 2011). Despite being rare, OS has been pointed as the third most common cancer in adolescence with an incidence rate lower than only lymphomas and brain tumors in this age group. Metastatic disease is an important concern in this malignancy: about 10-20% of patients present macroscopic evidence of metastatic disease at the time of OS diagnosis, but around 30-40% patients with localized OS will develop a local or distant relapse. The relapse within 5 years after the initial treatment of OS is rare (between 1-2% of all OS patients), but when occurs is associated with a poor prognosis. The 5 years overall survival for recurrent OS is around 23-29% (Luetke *et al*., 2014).

With regard to OS symptomatology, patients usually refer local pain, localized swelling and limitation of joint movement. Medical evaluation begins with a full clinical history, physical examination and radiographs (Figure 1.10b), the latter being useful to evaluate osseous changes. Magnetic Resonance Imaging (MRI) is used to assess the soft tissue component, its relation to surrounding tissues, vessels and nerves, being essential for safe definitive surgery. The diagnosis of OS must always include a histological verification of biopsies (Ritter and Bielack, 2010).

1.3.2. Clinical Protocols in Osteosarcoma

In osteosarcoma, local therapy alone is often insufficient, since 80-90% of all patients with localized disease develop metastasis (Ritter and Bielack, 2010). For this reason, current treatment modalities comprehend preoperative (also called neoadjuvant) induction therapy, followed by surgical removal of tissue and then postoperative (adjuvant) chemotherapy, resulting in the cure of approximately two-thirds of patients with localized disease (Ritter and Bielack, 2010). The

whole process of chemotherapy usually lasts for 6-8 months. OS was long considered as a radiotherapy-resistant tumour, thus limited knowledge on this field is available. However, recent studies demonstrated that radiotherapy might improve the outcome of patients further treated with multiagent chemotherapy who showed unable to undergo complete resection, a modality that would require additional evaluation in controlled clinical trials (Ritter and Bielack, 2010).

Currently, cisplatin, doxorubicin, high-dose methotrexate and ifosfamide are considered the most active agents (in combined regimens) for OS therapy (Ta *et al*., 2009), but there is still a need for optimizing treatment strategies. In this line, a randomized trial of the European and American Osteosarcoma Study (EURAMOS) group is ongoing since 2001, to optimize treatment schemes for resectable OS based on the histological response to preoperative chemotherapy (http://212.219.75.232/euramos/euramos_i_trial.asp).

EURAMOS 1 is a protocol that joins together four leading groups in the field of osteosarcoma research: the Children's Oncology Group (COG), the Cooperative Osteosarcoma Study Group (COSS), the European Osteosarcoma Intergroup (EOI) and the Scandinavian Sarcoma Group (SSG). Focusing on a low incidence disease, the collaboration between these groups broadens the sharing of knowledge between healthcare professionals and enables the evaluation of a higher number of patients. This study includes all patients with resectable high grade OS, with either localized and primarily metastasized tumours. All registered patients are exposed to a three drug treatment that consists of two cycles of cisplatin and doxorubicin, together with four cycles of methotrexate. Once the patients have recovered from chemotherapy, they undergo surgical removal of the tumour. If postoperative tumour biopsies still reveal malignance traces, adjuvant chemotherapy, α-interferon or ifosfamide combined with etoposide, being added to the previously referred therapeutic regimen, is applied for a new cycle of treatment. Accordingly, the study also intended to understand the differences in regard to disease outcome resulting from the use of α-interferon and ifosfamide/etoposide (Figure 1.11).

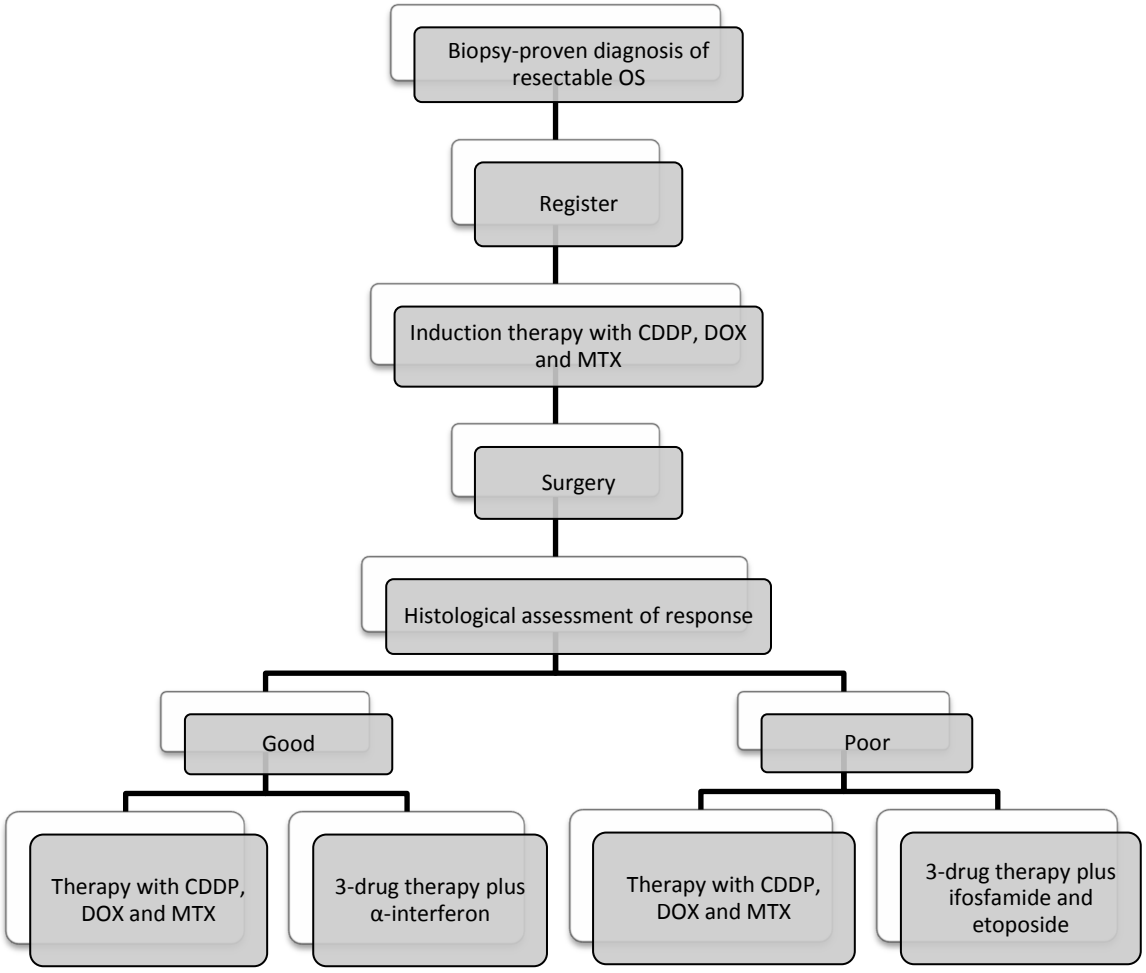

Figure 1.11. Strategy flowchart adopted in EURAMOS protocol trial (adapted from http://212.219.75.232/euramos/ euramos_i_trial.asp)

The scheduled treatment dates adopted in the EURAMOS protocol trial is depicted in Figure 1.12. Prior to surgical removal of the tumour the patients are submitted to two cycles of chemical treatment (5 weeks each), each constituted by one administration of cisplatin and doxorubicin and (during the first week) and two administrations of methotrexate (in weeks 4 and 5).

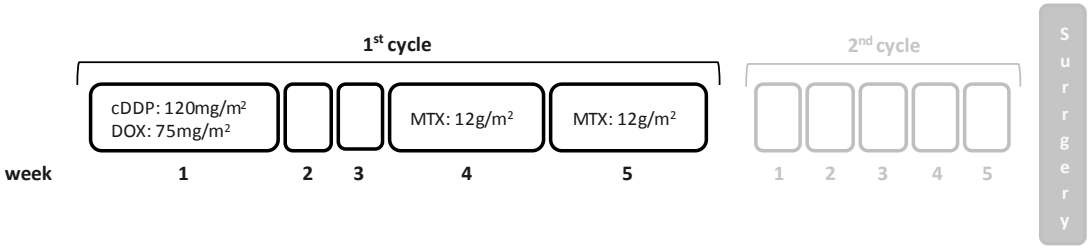

Figure 1.12. Scheduled treatment dates adopted in the EURAMOS protocol trial (adapted from http://212.219.75.232/euramos/ euramos_i_trial.asp).

Despite the findings achieved so far and the current attempt to optimize the dosing regimen of these drugs through the large scale EURAMOS protocol, the search for more effective agents and treatment modalities against OS continues. Table 1.1 lists some of the emerging strategies, molecular targets and respective drugs which have recently being studied for the treatment of OS. As shown, strategies under investigation include overcoming drug resistance (e.g. inhibiting drug efflux), inhibition of signalling receptors and transduction (e.g. mTOR pathway), inhibition of osteoclasts-mediated bone destruction and inhibition of angiogenesis (Luetke *et al*., 2014).

Table 1.1. Novel strategies and molecular targets for OS treatment (adapted from Luetke *et al*., 2014).

	Strategy/Molecular target	Drug
Novel delivery mechanisms	*Overcoming drug resistance*	
	○ Inhibition of cellular DNA synthesis and cell growth	SLIT™ cDDP Gemcitabine
	○ Induction of apoptosis and cell cycle arrest	Docetaxel
	○ Novel antifolates	Trimetrexate (RCF independent)
	○ Inhibition of drug efflux	Curcumin
	Inhibition of signaling receptors and transduction	
	○ IGF/IGF-1R pathway	Robatumumab, Figitumab, Cixutumumab
	○ mTOR pathway	Ridaforolimus, Everolimus
	○ Src pathway	Sorafenib, Dasatinib, Saracatinib
	○ HER2 overexpression	Trastuzumab
Altering the tumor microenvironment	*Inhibition of osteoclasts-mediated bone destruction*	
	○ Biphosphonates	Zoledronic acid, Pamidronate
	○ RANKL inhibitors	Denosumab
	Inhibition of angiogenesis	
	○ VEGF inhibitors	Bevacizumab
	○ Collagen XVIII-α 1	Endostar

SLIT: sustain lipid inhalation targeting (aerosolizes liposomal formulation), RCF: reduced folate carrier, IGF-1R: insulin-like growth factor 1, mTOR: mammalian target of rapamycin, Src: membrane-associated tyrosine kinase, HER2: human epidermal growth factor receptor 2, RANKL: receptor activator of nuclear factor-κB ligand.

The effect of interferon and ifosfamide/etoposide administration is beyond the scope of this thesis which is focused on the metabolic effects of the drugs conventionally used in OS treatment - cisplatin, doxorubicin and methotrexate - alone or in combination.

1.3.3. Cisplatin (cDDP), Doxorubicin (DOX) and Methotrexate (MTX)

Cisplatin, doxorubicin and methotrexate are the most effective known agents in OS treatment (Ta *et al*., 2009). This motivated their choice for single- and drug-combination

experiments in a cell culture model of OS (MG-63 cell line, available in a laboratory of the group) adopted in this work, in order to investigate the metabolic impact of drugs in the biochemistry of OS tissues. Therefore, a deeper explanation on their modes of action is presented below.

Cisplatin, cDDP

Cisplatin, *cis-diamminedichloroplatinum (II)*, is a metal-based agent widely used in chemotherapy of solid tumors and haematological malignancies (Tsang *et al*., 2009). It is administered to cancer patients intravenously as a saline solution (sodium chloride). Once in the bloodstream, it remains intact due to the relatively high concentration of chloride ions (~100 mM). After entering the cell, either by passive diffusion or active transport (*e.g.* CTR1 receptor), cDDP molecule is hydrolysed, the chloride ligand being replaced by water (due to the much lower intracellular concentration of chloride ions relative to the extracellular medium), yielding an unstable, positively charged, species. This activated drug is prone to interact with a number of possible targets: DNA, RNA and sulfur-containing compounds as metallothionein and glutathione, the former (DNA) being cisplatin's main pharmacological target (Figure 1.13) (Tsang *et al*., 2009).

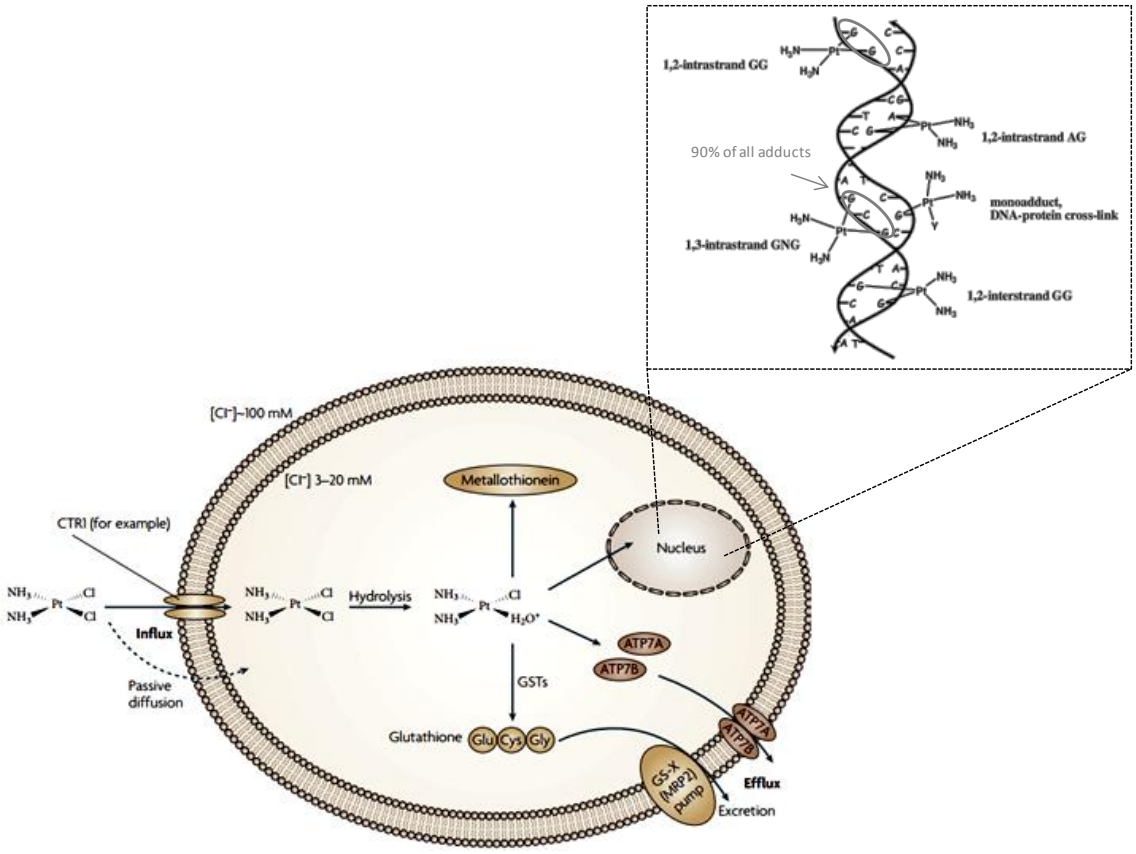

Figure 1.13. Mechanism of action of cisplatin (adapted from Kelland, 2007 and Pizarro and Sadler, 2009).

Cisplatin coordinates to DNA mainly through the N^7 atoms of the purine bases (guanine and adenine) within the double helix (Pizarro and Sadler, 2009). Different types of cDDP-DNA adducts can be formed, but the most frequent are those in which the metal coordinates to two adjacent purine moieties of the DNA strand (1,2-intrastrand). Although adducts involving one guanine and one adenine can also be found, the purine base guanine is the most frequently involved, accounting for around 90% of all adducts (inset of Figure 1.13), due to the formation of a favouring H-bond interaction between the purine carbonyl and the drug's amine groups. These drug-DNA adducts (mostly 1,2-intrastrand, Figure 1.13) are responsible for disrupting of base pairing and base-stacking, causing the DNA helix to become kinked and affecting replication and transcription processes (by blocking the action of DNA polymerase), as well as mechanisms of DNA repair. This interferes with the normal functions of the cell and ultimately conducts to cell death (by apoptosis) (Gibson, 2009).

Doxorubicin, DOX

Doxorubicin is an anthracycline and is one the most potent antineoplastic agent of the antitumour antibiotics class (Tacar *et al*., 2013). Due to its mode of action, DOX shares some characteristic features with metal-based agents. It exerts both antimitotic and cytotoxic activities through several mechanisms: formation of DNA adducts *via* intercalation between base pairs, and inhibition of topoisomerase II by stabilization of the DNA-topoisomerase II complex, thus preventing the DNA double helix from being resealed.

The resulting DNA damage induces cytochrome c release in mitochondria, which activates caspases-mediated apoptosis. In cases of acquired resistance, P-glycoprotein inhibits DOX effect by performing drug efflux, together with blocking of cytochrome c release by Bcl-2 and Bcl-xL and XIAP inhibition of the triggering of caspase pathway – Figure 1.14 (Kim *et al*., 2009).

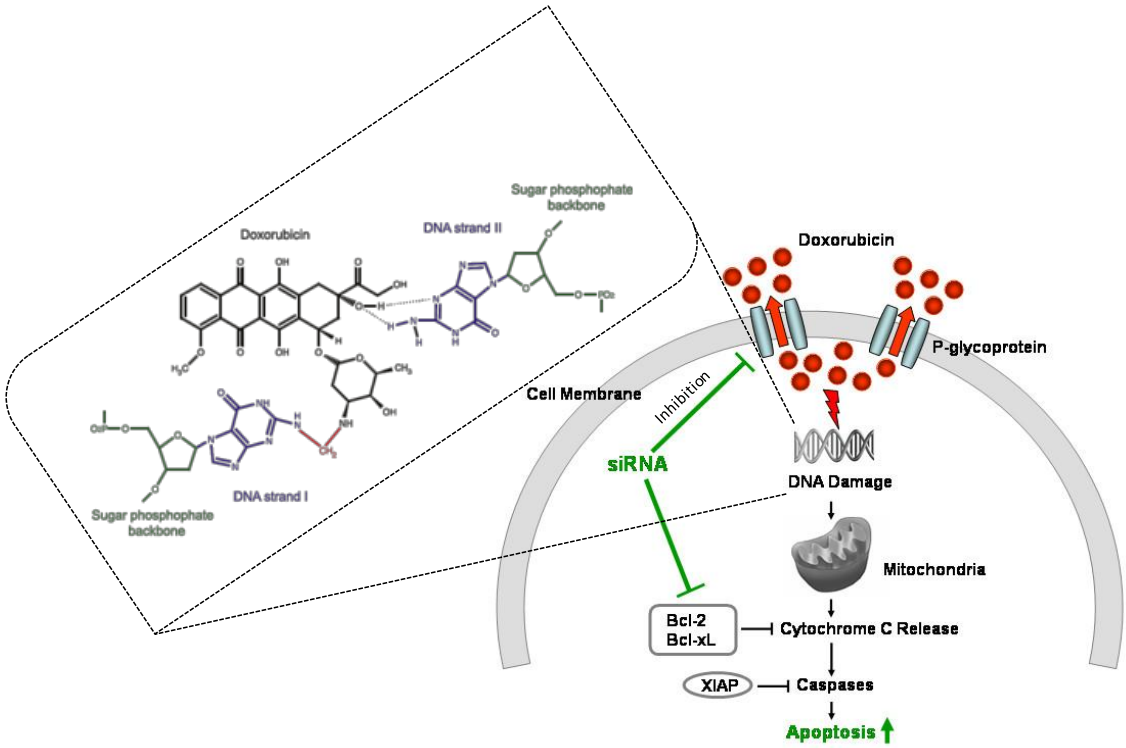

Figure 1.14. Mechanism of action of doxorubicin (adapted from Kim *et al*., 2009 and Yang *et* al., 2014).

Methotrexate, MTX

Methotrexate (MTX) is an antimetabolite - a folate analogue that competitively inhibits the enzyme dihydrofolate reductase (Tian *et al*., 2007). MTX enters the cells *via* the reduced folate carrier 1 (RFC1) and effluxes through the ABC B1 and ABC C1-4 proteins, members of the P-glycoprotein family. Once inside the cell, MTX is polyglutamated (addition of multiple glutamic acid residues through an enzymatic process) by the enzyme folypolyglutamate synthase (FPGS). This enzyme, in turn, can be reversed by γ-glutamyl hydrolase (GGH) that catalyses the removal of the γ-linked polyglutamates, thus facilitating the MTX efflux from the cell. Polyglutamated MTX (MTX-PG) has several important functions: it retains MTX intracellularly; inhibits dihydrofolate reductase (DHFR) that reduces dihydrofolate to tetrahydrofolate; and inhibits thymidilate synthetase (TYMS) which converts deoxyuridylate to the deoxythymidylate in the *de novo* pyrimidine biosynthetic pathway (Figure 1.15) (Assaraf, 2007).

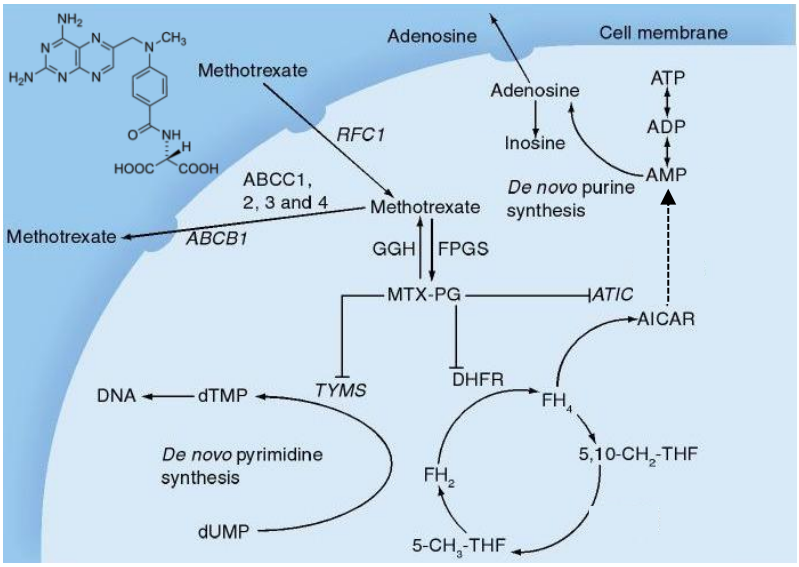

Figure 1.15. Mechanism of action of methotrexate (adapted from Nagy *et al*., 2010).

1.4. A Palladium (II) Complex Potentially Active Against Osteosarcoma: Pd_2Spm

The use of systemic chemotherapy protocols have improved the long-term survival from 20% to 70% for patients with localized OS disease, but this survival rate has remained essentially unchanged over the past 20 years (O'Day and Gorlick, 2009). In order to improve event-free and overall patient survival, EURAMOS 1 (presented in section 1.3.2) implemented a clinical trial for evaluating the benefit of adding ifosfamide plus etoposide to postoperative cDDP+DOX+MTX chemotherapy schemes in poor responders (>10% viable tumour), or pegylated (with attached polyethylene glycol polymer chains) IFN-α to the same postoperative chemotherapy regimen in good responders (<10% viable tumour). Nevertheless, the prognosis is still poor for patients with metastatic disease (O'Day and Gorlick, 2009).

The discovery of the antitumor activity of cDDP fostered the investigation on metal-based anticancer agents. Over the last decades, the rational design of this type of complexes has involved the following metal centers: platinum (both Pt(II) and Pt(IV)), ruthenium (Ru(II) and Ru(III)), titanium (Ti(IV)) and gold (Au(I) and Au(III)) (Muhammad and Guo, 2014). Multinuclear Pt(II) chelates, in particular, have been found to display a unique, non-conventional mode of DNA binding through long range cross-linking interactions not occurring with classical non-multinuclear Pt(II) drugs (as cDDP or Carboplatin), leading to an increased cytotoxic activity as compared to cDDP and its analogues. Pt(IV) prodrugs, in turn, have been investigated as a promising strategy to

reduce drug toxicity and overcome drug resistance, as they can be activated inside tumour cells (by Pt(IV) to Pt(II) reduction) (Muhammad and Guo, 2014).

The considerable similarity between the coordination chemistry of Pd(II) and Pt(II) (both metals being in the same group, X (ten), of the periodic table), promoted the investigation on the potential antitumor properties of Pd(II) complexes. The present work may add to these research studies on Pd(II) agents as an alternative to Pt(II) ones, with improved properties: as to selectivity, cytotoxic capacity and acquired resistance phenomena.

Several Pd(II) complexes have been reported to display favorable cytotoxicity at pH 6.8 (common pH value in tumour cells) (Ray *et al*., 2007). Nevertheless, these compounds are about 10^5 times more reactive than Pt(II) analogues, due to the rapid hydrolysis in solution of the leaving group within the complex. This well known higher chemical lability typical of Pd(II) relative to Pt(II) compounds may prevent the complex from reaching its pharmacological target in its activated state (Butour *et al*., 1997). In order to overcome this limitation, several Pd(II)-based coordination compounds have been designed, using distinct ligands (usually bulky groups with a view to attain a slower kinetics of hydrolysis): *trans*-Pd(II) complexes, Pd(II) compounds containing bidentate nitrogen ligands, Pd(II) complexes bearing phosphine or mixed donor atom ligands and multinuclear Pd(II)-polyamine chelates (Abu-Sarrah *et al*., 2008; Marques, 2013). The latter include the Pd(II)-polyamine complex, Pd_2Spm tested in this work (*Spm* spermine, $H_2N(CH_2)_3NH(CH_2)_4NH(CH_2)_3NH_2$) (Figure 1.16).

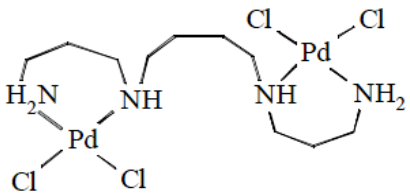

Figure 1.16. Chemical structure of Pd_2Spm.

Polynuclear polyamine complexes have attracted special attention in the last twenty years, due to their ability to form long-distance interstrand adducts with DNA, which often circumvent cDDP resistance. In particular, linear aliphatic polyamines possess a high conformational freedom and have suitable flexibility and polidenticity that favor their interaction with metal ions through coordination (such as Pt(II) and Pd(II)) as well as with biological molecules (*e.g.* DNA) *via* hydrophobic interactions. Biogenic amines, namely the linear tetramine spermine, are physiological polycations, crucial for cell growth and differentiation. The dinuclear Pd_2Spm chelate

was first synthesized and assessed as to its antitumor properties against human breast and leukemia cancer cells (MDA-MB-468 and HL-60, respectively) by Navarro-Ranninger and coworkers (Navarro-Ranninger *et al*., 1993).

In ovarian cells, Pd_2Spm cytotoxic ability was found to be lower than cDDP but higher than that of its Pt(II) analogue. Moreover, this compound was found to be more effective against a cDDP-resistant cell line than its Pt(II) counterpart (Tummala *et al*., 2010). In addition when comparing the activities of Pd_2Spm and cDDP in human breast cancer cells, Pd_2Spm showed to be more effective against an estrogen-independent (ER(-)) cell line, while cisplatin was more effective towards the estrogen-dependent (ER(+)) one (Fiuza *et al*., 2011). This same study claimed that, similarly to cDDP, the Pd(II) spermine complex triggers phosphorylation of H2AX and greatly influences cell morphology by severely affecting the cytoskeleton.

Regarding the effect of a Pd(II) for Pt(II) substitution on the antitumor activity of this type of polyamine complexes, the Pd(II) agents showed an improved time- and dose-dependent cytotoxicity on HSC-3 human oral cancer when compared to their Pt(II) analogues (Soares *et al*., 2007). Strong interaction with DNA was clearly evidenced by atomic force microscopy techniques, which detected the formation of stable adducts or aggregates between Pd_2Spm and DNA (Corduneanu *et al*., 2010).

The above described results justify the choice of Pd_2Spm as a promising prospective anticancer agent towards OS, and fostered the present study on its metabolic impact in both osteoblasts and osteosarcoma human cells.

1.5. Cell Metabolomics

This section describes the concepts underlying metabolomics, as well as the analytical and bioinformatic tools that are generally applied to study the metabolome and pursuit the definition of a metabolic signature for a given perturbation. Then, the state of the art on the application of metabolomics to anticancer drug testing in cells is presented.

1.5.1. Principles and General Applications

Metabolites are low molecular weight molecules (<1 kDa) that act as carriers, substrates or products in cellular biochemical pathways. As final end products of biological cascades in the cells,

they reflect upstream alterations in genes and proteins (Figure 1.17). Moreover, given the high interdependence of all levels of biological organisation, perturbations in metabolism can generate upstream consequences. Therefore, the measurement of metabolite levels in cells, tissues or biofluids represents a valuable approach to understand the overall status of the organism. Metabolomics (or metabonomics) is an approach that enables the comprehensive detection and characterisation of changes in the global metabolic profiles induced by those pathophysiological stimuli, thus constituting a crucial complementary approach to the other "omic" sciences (Goodacre, 2005).

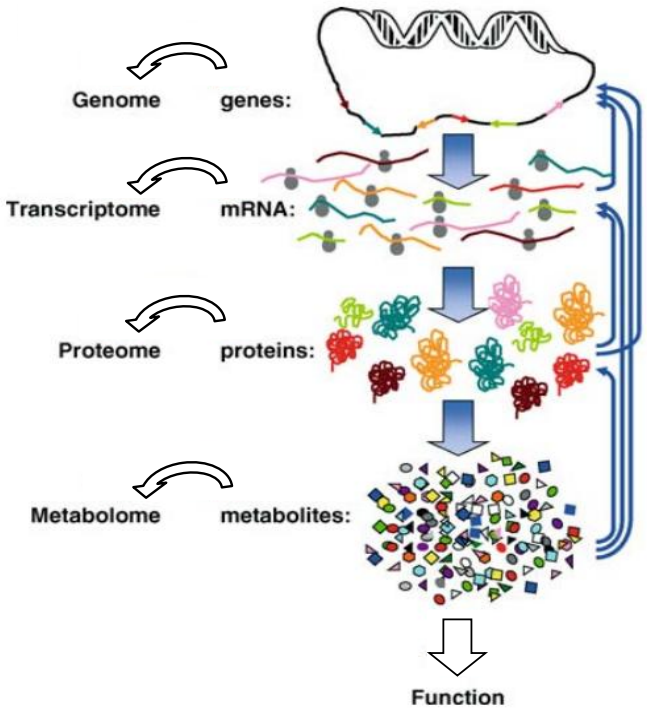

Figure 1.17. Schematic representation of the organization and interactions between different levels within a cell (adapted from Goodacre, 2005).

Originally, the term metabolomics has been used to express the detection and quantitation of metabolites comprising the metabolome of living cells, whereas metabonomics has been regarded as the study of dynamic metabolic changes that take place in response to a perturbation. Indeed, metabonomics has formally emerged in 1999, as an appealing approach to perform the quantitative measurement of the multivariate metabolic responses of multicellular systems to pathophysiological stimuli or genetic modification (Nicholson *et al*., 1999). Nowadays, the two terms are used interchangeably and as the term metabolomics is more frequently referred in the literature, it will be used throughout this thesis.

One of the most important features of metabolomic studies is that, in contrast to classical biochemical approaches that search for a limited and pre-defined number of compounds, they comprise the analysis of a large range of metabolites (frequently around hundreds). Being essentially untargeted, metabolomics allows the detection of unpredicted findings, offering a more complete overall picture of the global dynamics of cellular metabolism.

As schematically depicted in Figure 1.18, the general strategy followed in metabolomic studies begins with sample collection (Figure 1.18a) and analysis by high throughput techniques (mainly NMR spectroscopy and hyphenated MS) (Figure 1.18b and 1.18c), alone or in combination (Pan and Raftery, 2007), the assignment of the obtained spectral data (Figure 1.18b and 1.18c), application of bioinformatic tools (particularly Multivariate Analysis, MVA) (Figure 1.18d) to maximize relevant information recovery from the complex datasets analysed, and ends with the biochemical interpretation (Figure 1.18e) of the metabolic changes detected.

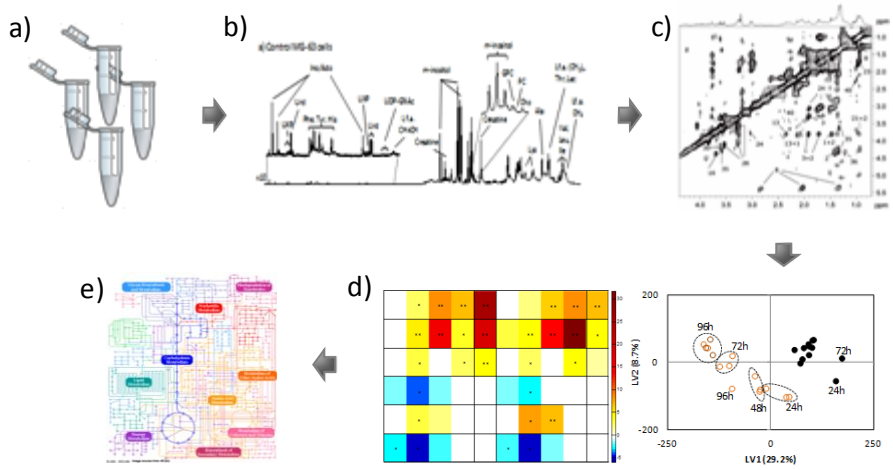

Figure 1.18. Typical metabolomics workflow: a) sample collection and b) analysis using one or more high-throughput analytical techniques, c) signals assignment, d) chemometric and bioinformatic tools and e) biochemical interpretation of results.

The most frequently used analytical techniques in metabolomics are Nuclear Magnetic Resonance (NMR) spectroscopy and Liquid or Gas Chromatography Mass Spectrometry (LC- or GC-MS). Other approaches such as Fourier Transform Infra-Red (FTIR) spectroscopy and arrayed electrochemical detection have also been applied in some studies (Lindon *et al*., 2007; Jobard *et al*., 2010).

High-resolution NMR spectroscopy, particularly of ^{1}H nucleus (high sensitivity and natural abundance) (Figure 1.18b), constitutes one of the most used techniques in metabolomic studies, once it enables a wide range of metabolites (e.g. amino acids, sugars, lipid moieties, organic acids,

nucleosides) to be detected simultaneously and without any special sample preparation, in very distinct complex biological matrices such as biofluids, tissues and cells, in a non-destructive manner. The non-invasive nature of NMR gains special importance when considering the translation from the *ex vivo* or *in vitro* biomarkers to clinical applications. Moreover, NMR enables automated analysis of large sample numbers with high analytical reproducibility. Nonetheless, NMR has an inherent low sensitivity with typical limits of detection falling in the sub-millimolar range, although the advent of very high field magnets and cryoprobes has allowed these limits to be pushed to the micro to nanomolar range (Lindon *et al*., 2007). The leading role of NMR in the field of metabolomics has been extensively reviewed in human disease diagnosis (Emwas *et al*., 2013; Duarte *et al*., 2014; Gebregiworgis and Powers, 2012), namely in cancer (Spratlin *et al*., 2009; Serkova and Glunde, 2009) and drug discovery (Chiaradonna *et al*., 2012; Holzgrabe, 2010; Powers, 2009).

NMR metabolomic studies have greatly benefited from the development of High Resolution Magic Angle Spinning (HRMAS), as it allows the direct analysis of semi-solid samples (like tissues and cells), thus avoiding the use of extraction procedures. This technique is based on the rapid sample spinning at an angle of 54.7º relative to the applied magnetic field, in order to average out the anisotropic effects that broaden the lines thus, improving spectral resolution. Coupled to the relatively high spinning rates (4-6 kHz), the provision of a deuterium (^{2}H) lock signal (which compensates for variations in the magnetic field across time) yields remarkably high-resolution spectra, resulting in much higher and sharper peaks (Lindon *et al*., 2009). Thus, with HRMAS well resolved spectra can be obtained from reduced amounts of intact tissue or cell pellet. HRMAS has been widely used as tool for the metabolic characterization of cancer (Moestue *et al*., 2011; DeFeo and Cheng, 2010; Sitter *et al*., 2009).

Regarding MS metabolomics, it is important to review the principles of the technique. MS is based on the determination of the mass-to-charge ratio (*m/*z) of charged compounds: molecules, clusters of molecules, complexes or fragments (Lei *et al.,* 2011). Briefly, a mass spectrometer is composed of: an ion source, a mass analyser, a detector and a data system. After ionization, analytes are transferred to the high vacuum of the mass spectrometer, they are then separated according to *m/z* in the mass analyser and the ion current is measured in the detector. Finally, the signals are transmitted to the data system which gives a plot of ion abundance against *m/z*, corresponding to the mass spectrum of that analysed sample. Mass Spectrometry coupled to chromatographic separation apparatus (GC or LC) has also been largely used as a metabolic

profiling tool (Lei *et al.,* 2011). Inherently more sensitive that NMR, MS is able to detect many compounds that escape NMR analysis. Nevertheless, chromatographically-hyphenated MS analysis is necessarily guided for specific classes of substances, thereby requiring different separation procedures. Moreover, MS methods can be quite challenging in term of reproducibility and metabolite identification. Despite these difficulties, GC- and LC-MS have been increasingly used in mammalian metabolomic studies: disease diagnosis (Buzatto *et al*., 2014; Gowda *et al*., 2008), cancer research (Liesenfeld *et al*., 2013) and drug discovery (Buck *et al*., 2014; Drexler *et al*., 2011). The complementarity between NMR and MS relies on the fact that the untargeted analysis performed by the former can be used to more efficiently target (in terms of families of compounds of interest) the MS analysis more sensitive (Johnson and Gonzalez, 2012).

Obtained whether by NMR or MS methods, metabolomic analysis encompasses highly complex datasets that require subsequent multivariate analysis (as described in section 2.3.2), to maximize information recovery and, eventually, biomarker identification (Trygg *et al*., 2007).

1.5.2. Anticancer Drug Testing in Cells through Metabolomics: State of the Art

In vitro models allow experimental variables to be simplified in order to study biochemical disorders that occur in specific tissues or organs under well-controlled and easily assessed conditions. Moreover, cell culture applications are free from additional confounding factors that typically affect animal models and, especially, human subjects (*e.g.* age, gender, global health and environmental exposure), potentially providing more readily interpretable results (Cuperlovic-Culf *et al.,* 2010). On the other hand, cell culture systems may be over-simplistic and lead to misleading results, as when individual cell types are cultured *in vitro*, the crosstalk between multiple tissue cells is absent, and the information on the dynamic processes that modulate *in vivo* biochemistry may be lost. In spite of these limitations, cell culture studies are an indispensable tool in several areas of research, like drug testing, playing a crucial role in verifying hypothesis about biochemical processes or mechanisms of action at the molecular level (Astashkina *et al.,* 2012). In regard to cell metabolomics, there are many possible valuable applications like: analysis of cellular phenotype, which enables molecular comparison of disease subtypes and identification of potential disease markers of therapeutic targets; systems biology, whereby metabolic networks can be accessed through metabolomics alone or in combination with other omics data; time-course assessment of metabolic pathways; toxicology and drug

testing studies, to understand both the metabolism of the drug (pharmacokinetics) and the consequences of drug administration on the models organism or cells (pharmacodynamics) (Cuperlovic-Culf *et al.,* 2010). The alterations to the metabolic profile of cells have been studied in samples of different natures: cell extracts (Martineau *et al.,* 2011) obtained with different extraction solvents like trichloroacetic acid (Lane *et al.,* 2007; Fan *et al.,* 2005), perchloric acid (Moreno *et al.,* 1998; Santini *et al.,* 2004; Santini *et al.,* 2006) and methanol and/or chloroform (Teng *et al.,* 2009); cell suspensions (Ferreti *et al.,* 2002; Santini *et al.,* 2001; Rosi *et al.,* 2004); intact or lysed cell pellets analysed by HRMAS (Morvan *et al.,* 2013; Pan *et al.,* 2013; Borel *et al.,* 2007).

In the field of oncological research, cell metabolomics has been increasingly used to study the metabolic singularities of cancer cell lines from different origins, knowledge that is often used as basis for the development of novel drugs (Halama, 2014). As shown in Figure 1.19 NMR in particular has been largely applied to study the pharmacodynamic behaviour of both conventional and emerging drugs and to get further insights into their modes of action, perturbed biochemical pathways and resistance phenomena (Merz and Serkova, 2009; Powers, 2009; Rodriguez *et al*., 2008; Garcia-Alvarez *et al.,* 2011).

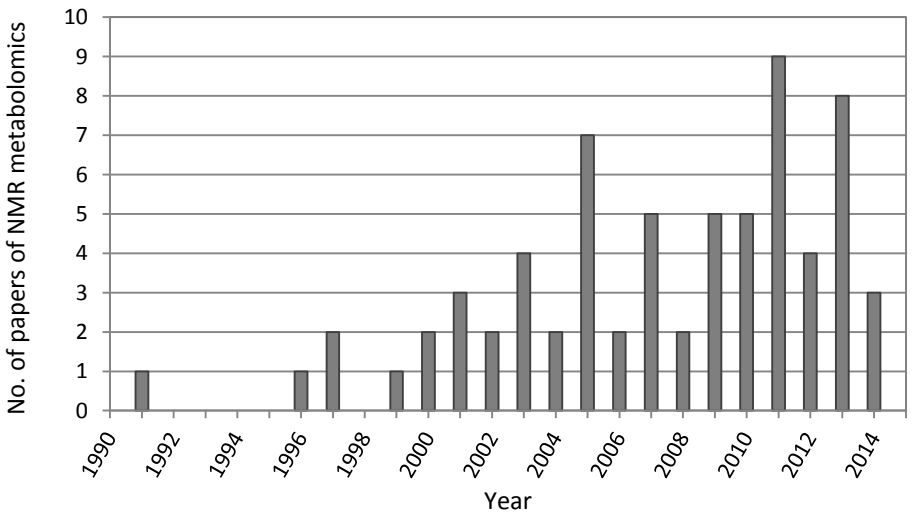

Figure 1.19. Number of studies on NMR metabolomics of cultured mammalian cells for anticancer drug testing (source www.webofknowledge.com, until 20th November 2014).

The following section will briefly review the state of the art on anticancer drug testing performed by NMR metabolomics of cultured cells, the approach employed in this thesis. Table 1.2 lists the studies performed on cultured cell by NMR metabolomics, according to the families defined above (section 1.2) in this chapter. Given the high number of such studies, the

subsequent discussion focuses only on a selection of more recent and/or complete NMR studies. In the following section, a brief review of MS metabolomics cell studies will be presented.

Table 1.2. Overview of literature on NMR metabolomics of cultured mammalian cells for anticancer drug testing.

Class	Type	Agent	Tested cells	Reference
Alkylating Agents	Nitrosourea	CENU	Melanoma: B16	Morvan *et al.*, 2003
			Melanoma: B16 Lung cancer: 3LL	Morvan *et al.*, 2007
			Osteosarcoma: 143B Hepatocarcinoma: HepG2	Loiseau *et al.*, 2009
		Lomustine	Glioma: 18 cell lines	El-Deredy *et al.*, 1997
		Temozolomide	Brain cancer: SF188	Mancuso *et al.*, 2005
		Fotemustine	Hepatocarcinoma: HepG2 Osteosarcoma: 143B	Bayet-Robert *et al.*, 2010
	Chloroethyl-urea	ICEU	Colon cancer: CT-26	Borel *et al.*, 2007
Metal-based	Metal salt	Cisplatin	Lung cancer: A549	Huang *et al.*, 2003
			Neuroblastoma: SH-SY5Y, SK-N-BE (2), SK-N-FI, SK-N-AS, IMR-32	Lindskog *et al.*, 2004
			Osteosarcoma: MG-63	Duarte *et al.*, 2010
			Glioma: BT4C	Mirbahai *et al.*, 2011
			Brain cancer: BT4C, U87-MG, DAOY, PFSK-1, ST-PNET	Pan *et al.*, 2011
			Lung cancer: A549	Duarte *et al.*, 2013
			Neuroectodermal tumor: DAYO, PESK-1	Pan *et al.*, 2013
			Pluripotent stem cells	Stechow *et al.*, 2013
			Normal liver: L02	Liu *et al.*, 2014
			Osteosarcoma: MG-63	Lamego *et al.*, 2014
Antimetabolites	Pyrimidine analogs	5-Fluoruracil	Breast cancer: DU4475	Cooper *et al.*, 2001
	Antifolate	Methotrexate	Breast cancer: MB231, MB435, MCF-7	Sterin *et al.*, 2001
			Osteosarcoma: MG-63	Lamego *et al.*, 2014
	Nucleoside analog	Gencitabine	Pancreatic cancer: PK9	Ohmine *et al.*, 2012
Antitumor antibiotics		Doxorucibin	Leukemia: K562	Le Moyec *et al.*, 1996
			Leukemia: Jurkat T cell	Blankenberg *et al.*, 1997
			Leukemia: L1210 Colorectal cancer: SW620	Ronen *et al.*, 1999
			Leukemia: K562	Le Moyec *et al.*, 2000
			Breast cancer: MCF-7 Colorectal cancer: LoVo	Santini *et al.*, 2001
			Breast cancer: MB231, MB435, MCF-7	Sterin *et al.*, 2001
			Leukemia: HL60	Rainaldi *et al.*, 2008
			Melanoma: B16	Triba *et al.*, 2010
			Osteosarcoma: MG-63	Lamego *et al.*, 2014
Mitotic inhibitors		Paclitaxel	Leukemia: K562	Le Moyec *et al.*, 1996
			Breast cancer: MCF-7, MDA-MB-231, MDA-MB-435	Sterin *et al.*, 2001
			Leukemia: K562	Brisdelli *et al.*, 2003 Knijn *et al.*, 2005
			Breast cancer: MCF-7, BT-20	Musacchio *et al.*, 2009

Table 1.2 (cont.). Overview of literature on NMR metabolomics of cultured mammalian cells for anticancer drug testing.

Class	Type	Agent	Tested cells	Reference
Mitotic inhibitors		Docetaxel	Breast cancer: MCF-7, MDA-MB-231	Morse *et al.*, 2007
			Breast cancer: MCF-7	Bayet-Robert *et al.*, 2010
			Breast cancer: MCF-7, MDA-MB-231	Bayet-Robert *et al.*, 2013
		Vinblastine	Renal cell carcinoma: KTCTL-26, KTCTL-2	Lutz *et al.*, 2005
Hormonal agents	Corticosteroid	Dexamethasone	Thymoma cells: WEHI7.2	Lutz *et al.*, 2002
			Adenocarcinoma: HeLa Leukemia: CCRF-CEM Ovarian carcinoma: SKOV-3	Tiziani *et al.*, 2011
	Estrogen antagonist	Tamoxifen	Endometrial cells: Ishikawa	Griffin *et al.*, 2003
Inhibitors of Topoisomerase		Irinotecan Etoposide	Neuroblastoma: SH-SY5Y, SK-N-BE (2), SK-N-FI, SK-N-AS, IMR-32	Lindskog *et al.*, 2004
Molecularly targeted	HIF1 inhibitors	PX-478	Colon cancer: HT29	Jordan *et al.*, 2005
	Tyrosine kinase inhibitors	Imatinib	Leukemia: BCR-ABL(+), BCR-ABL(-)	Gottschalk *et al.*, 2004
			Leukemia: CML	Boros *et al.*, 2005
			Leukemia: BCR-ABL(+),K562	Klawitter *et al.*, 2009
			Leukemia: LAMA-84, K562	Klawitter *et al.*, 2009 Kominsky *et al.*, 2009
			Leukemia: Myl	Dewar *et al.*, 2010
		PD166866	Fibroblasts: 3T6	Piccioni *et al.*, 2007
		AG957	Leukemia: K562	Knijn *et al.*, 2005
	Ras inhibitors	U0126	Breast cancer: MDA-MB-231, MCF-7, Hs578T Colon carcinoma: HCT116	Beloueche-Babari *et al.*,2005
	HSP90 inhibitors	17AAG	Colorectal cancer: HCT116, HT29, SW620	Chung *et al.*, 2003
			Prostate cancer: PC3, LNCaP	Lodi *et al.*, 2011
			Breast cancer: MCF-7	Lodi *et al.*, 2011
	HDAC inhibitors	Phenylacetate	Prostate cancer: DU145	Milkevitch *et al.*, 2005
		Phenylbutyrate		Milkevitch *et al.*, 2005 Milkevitch *et al.*, 2007
		LAQ824	Colorectal cancer: HT29	Chung *et al.*, 2008
		SAHA		
		Trichostatin	Primary hepatocytes	Ellis *et al.*, 2010
			Lung cancer: H460	Amoêdo *et al.*, 2011
	PI3K inhibitors	LY24002	Breast cancer: MDA-MB-231, MCF-7, Hs578T	Beloueche-Babari *et al.*, 2006
			Prostate cancer: PC3, LNCaP	Lodi *et al.*, 2011a
			Breast cancer: MCF-7	Lodi *et al.*, 2011b
	Choline kinase inhibitors	MN58b	Breast cancer: MDA-MB-231 Colon cancer: HT29	Al-Saffar *et al.*, 2006
	PPARγ inhibitors	Thiazolidenedione	Liposarcoma: 3T3F442A	Chen *et al.*, 2002
	Hexokinase inhibitor	Lonidamine	Breast cancer: MDA-MB-231, MDA-MB-245, MCF-7	Mardor *et al.*, 2000
	2,5-lipoxygenases inhibitor	MT30, CAPE	Glioblastoma: A172, Hs683, U373	Morin *et al.*, 2013

Table 1.2 (cont.). Overview of literature on NMR metabolomics of cultured mammalian cells for anticancer drug testing.

Class	Type	Agent	Tested cells	Reference
	Pyruvate dehydrogenase kinase	Dichloroacetate	Breast cancer: MDA-MB-231, MCF-7	Lefort *et al.*, 2014
	Xanthine dehydrogenase inhibitor	Allopurinol	Breast cancer: MDA-MB-231, MCF-7	Lefort *et al.*, 2014
	Calcium channel blockers	Diltiazem	Renal carcinoma: KTCTL-2, KTCTL-26	Lutz *et al.*, 2005
Other agents		BEZ	Leukemia: HL-60, KG1a and K562	Tiziani *et al.*, 2009
		MPA	Leukemia: HL-60, KG1a and K562	Tiziani *et al.*, 2009
		Silica nanoparticles	Adenocarcinoma: HeLa	Feng *et al.*, 2013
		Ascididemin	Breast cancer: MCF-7	Morvan *et al.*, 2013
		Gold Nanorods	Lung cancer: A549	Zhang *et al.*, 2013
		Metformin	Breast Cancer: MCF-7, MDA-MB-231, BT-474	Corominas-Faja *et al.*, 2012
		Methyltrienolone	Prostate cancer: LnCAP	MacKinnon *et al.*, 2012
		2-deoxyglucose	Breast cancer: MCF-7	Kaplan *et al.*, 1991
		Resveratrol	Hepatoblastoma: HepG2	Massimi *et al.*, 2012
		Sodium butyrate and Trichostatin	Lung cancer: H460	Amoêdo *et al.*, 2011
		2,3,7,8-tetrachlorodibenzo-p-dioxin	Hepatoblastoma: HepG2	Jennen *et al.*, 2011 Ruiz-Aracama *et al.*, 2011
		Bezielle	Breast cancer: SKBR3, BT474	Klawitter *et al.*, 2011
		Marine natural products	Breast cancer: MCF-7	Bayet-Robert *et al.*, 2010

CENU: chloroethyl nitrosourea, ICEU: N-(4-iodophenyl)-N'-(2-chloroethyl) urea, SAHA: suberoylanilide hydroxamic acid, BEZ: bezafibrate, MPA: medroxyprogesterone acetate.

Alkylating Agents

Chloroethyl nitrosourea, CENU, used in the treatment of melanoma and glioma, is among the alkylating agents whose effects have been studied by NMR metabolic profiling, both *in vitro*, using cultured cells, and *ex vivo* using animal models. In particular, this drug has been found to induce significant alterations in phospholipids metabolism in different cell types, as viewed by ^{1}H HRMAS NMR of intact cell pellets. In B16 melanoma cells (Morvan *et al*., 2003), CENU treatment induced a down-regulation of phosphocholine (PC), attributed to altered CDP-Cho pathway and increased phospholipase A activity, and a dramatic rise in phosphoethanolamine (PE) contents. Comparison between B16 melanoma and 3LL pulmonary carcinoma animal models (Morvan *et al*., 2007) confirmed the previous phosphoethanolamine (PE) results and clarified that, although some differences were observed in the metabolic profile of the untreated tumour types, the most significant metabolic features of CENU-treatment were common to both. Additional results

witnessed the activation of pathways implicated in energy production and down-regulation of nucleotide *de novo* synthesis.

Human glioma cells treated with temozolomide and analysed by ^{31}P NMR spectroscopy showed decreased PC levels in relation to those of GPC and diphosphodiester (Mancuso *et al*., 2005). Treated cells also exhibited a marked reduction in aerobic metabolism and TCA cycle and were associated with mitochondrial dysfunction-mediated apoptosis.

Together with other complementary methods, NMR also revealed the effects of CENU on the bioenergetic metabolism of two cell lines differing in their oxidative phosphorylation (OXPHOS) background, the most differentiated one (with the least impaired OXPHOS background) being able to escape drug-induced death (Loiseau *et al*., 2009). This survival advantage of differentiated cells resulted in high lactate/pyruvate ratios (biochemical markers of respiratory chain deficiencies) although no significant lactate variations were measured. Thus, mitochondrial OXPHOX background seems to play a crucial role in cells response to chemotherapy.

HRMAS NMR was also used to evaluate the metabolic impact of fotemustine (an alkylating agent that damages DNA) in hepatocarcinoma and osteosarcoma cells (Bayet-Robert *et al*., 2010). An increase in PC levels was measured in both cell lines upon treatment, what was associated with the activation of choline-kinase or the stimulation of ATP biosynthesis (since ATP is required as cofactor of the previous reaction). However, several metabolites were found to vary differently between the tested cell lines: Glu increased in osteosarcoma cells and decreased in hepatocarcinoma and lipids, which accumulate in treated osteosarcoma cells, didn't change in hepatocarcinoma cells. This study highlighted the potential of HRMAS NMR metabolomics in unveiling specificities of the metabolic response of different cell lines to treatment, by bringing insights into drugs mode of action and tumour cell adaptation to treatment (Bayet-Robert *et al*., 2010).

Metal-Based Anticancer Agents

The first study in which NMR metabolomics was used to evaluate the metabolic response of cancer cells to cDDP dates of 2003 (Huang *et al*., 2003). In this study, an increase in the mean chain length of fatty acids (given by CH_2/CH_3) was detected in lung cancer cells treated with cDDP, as well as a decrease of the choline compounds/CH_3 and ethanolamine/creatine. Moreover, ^{31}P NMR showed a decrease of phosphomonoesters and ATP levels with treatment. These cDDP-

induced alterations were associated with perturbations in the composition and properties of the membrane phospholipids, giving rise to changes in the plasma membrane fluidity. This study (Huang *et al*., 2003) also evaluated the response of cDDP-resistant lung cancer cells, which changes were found to be opposite from those refered above.

The metabolic response of MG-63 cells to cDDP-treatment was evaluated by NMR, in a work of our own and part of this thesis (Duarte *et al*, 2010; Lamego *et al*., 2014). The results revealed significant changes in lipids, choline and choline-containing compounds, what was associated with the occurrence of apoptosis and perturbations in the lipid metabolism regulation. Decreases in Glu and Tau were measured upon cDDP-exposure, possibly reflecting oxidative stress and activation of DNA-related defense mechanisms, respectively. The cDDP-induced decreases in *m*- and *s*-Inositol were interpreted as indicators of cellular stress response mechanisms activation and the decreases in Ino/Ado were seen as reflecting reduced DNA synthesis. This work (Duarte *et al*, 2010) resulted of this thesis and will be presented in detail in subsequent chapters.

Recent studies have evaluated the effects of cDDP over neuroectodermal tumour cells (Pan *et al*., 2013). Results from HRMAS analysis showed increases in saturated and unsaturated lipids that were associated with accumulation of lipid droplets prior to DNA fragmentation and apoptosis. Analysis of lipidic extracts revealed that the main responsible for the elevation of unsaturated lipid moieties was mainly due to oleic and linoneic acids accumulation. In lung cancer cells (Duarte *et al*., 2013), increased lipid contents (particularly unsaturated triglycerides) as well as increased nucleotide sugars (particularly UDP-GlcNAc) were pointed as markers of cDDP exposure, together with an increase of sorbitol and decreased niacinamide and several amino acids (Gln, Ala, Lys, Met, Phe, Tyr and citrulline). Similarly, cDDP treatment of brain tumour cells induced augments of UDP-GlcNAc but also of UDP-GalNAc together with higher levels of lipids, both associated with evolving cell death (Pan *et al*., 2011).

Antimetabolites

As shown by ^{1}H NMR of mammary carcinoma cell suspensions, treatment with 5-Fu is associated with a global increase of mobile lipids (ML) (Cooper *et al*., 2001). Cells respond to treatment increasing mobile lipid acyl chains levels and glycerol contents as well as raising choline and decreasing PC levels. Since naturally involved in the regulation of the above metabolites, phospholipase A1 and A2 activities are thought to be potentiated by 5-Fu exposure inducing an accumulation of ML that in turn seems to be a general response to cytotoxic insults.

Global changes in phospholipids were also detected by *in vivo* and *ex vivo* (extracts) analysis of a mouse mammary carcinoma model treated with 5-Fu (Street *et al*., 1997). ^{31}P NMR metabolic profile data indicated a drop in PC levels after exposure to the drug that was reflected in a consistent increase of PME/PC ratio. The later is even pointed in the literature as good indicator of tumour response to this particular therapy. But other choline compounds seem to be altered after 5-Fu treatment, namely GPC, and also PE and GPE. In what concerns to tumour bioenergetics, exposure to 5-Fu induces considerable changes in important energy charge indices as NTP/Pi and PCr/Pi ratios, results that *in vivo* reflected improved tumour flow on cancerous tissues after treatment.

Recently, a ^{1}H HRMAS NMR study evaluated the response of MG-63 osteosarcoma cells to MTX-treatment (Lamego *et al*., 2014). This work is part of this thesis and will be explored in detail in chapter 5. In short, decreased PC levels were the most significant change upon MTX-exposure, which, together with the absence of alterations in lipids, was tentatively interpreted as evidencing no membrane degradation, decreased phosphatidylcholine (PTC) synthesis and inhibition of *de novo* synthesis of lipids.

Antitumor Antibiotics

Due to its mode of action, doxorubicin shares some characteristics with alkylating agents as shown by comparison of ^{31}P NMR data of colorectal carcinoma cells treated with doxorubicin or with one alkylating agent (Ronen *et al*., 1999). The overall results were not drug specific, showing increased glycolytic intermediates independently on the DNA damaging agent used, what foresees an inhibition of the glycolytic pathway by the two agents.

The overall pathways involved in doxorubicin induced apoptosis seem to relate with lipids metabolism, namely with membrane lipids according to the ^{1}H NMR data of treated T-Jurkat cells suspensions, which revealed a reduction of Cho/CH_3 and an increase in CH_2/CH_3 that positively relates with the fraction of the apoptotic cells (Blankenberg *et al*., 1997). Moreover, CH_3 moieties were not significantly altered with doxorubicin treatment what, on one hand means that this particular portion of fatty acid chains does not seem to be greatly affected by exposure to this drug and, on the other hand, that the dynamic changes of the membrane may be largely attributed to loss of choline compounds by the lipid bilayer.

^{1}H NMR of leukemia cells treated with doxorubicin revealed a drop in GSH levels, what can be attributed to cells response mechanism of doxorubicin to generate free oxygen radicals. Another important decrease that was supposed to relate with oxidative stress, occurred in Tau that among others has antioxidant properties. Interestingly, Tau levels increased in cells that were submitted to a necrotic stimulus what, keeping in mind that the necrotic phenomenon is characterized by swelling of cells, point Tau – important in osmoregulatory processes – as possible biomarker to distinguish between the two types of cell death (Rainaldi *et al*., 2008).

In a recent study, part of the work presented in this thesis, the metabolic response of MG-63 osteosarcoma cells to DOX exposure was investigated (Lamego *et al*., 2014). In summary, the results suggested significant membrane degradation, decreased membrane synthesis and apparent inhibition of *de novo* lipid synthesis in treated cells. Moreover, a link between UDP-GlcNAc and the active pathways of membrane degradation and energy metabolism was found in the metabolic information recovered from DOX-treated cells.

Doxorubicin chemotherapy treatments also face the problem of resistance. Some ^{1}H NMR evidences show that resistance may be associated with membrane lipids metabolism and the capacity to adapt to oxidative stress. The comparison between K562 human leukemia cells and their resistant counterparts (both treated with doxorubicin) revealed higher Cho/CH_3 ratios and loss of fatty acid signals (lower CH_2/CH_3). Measurements on Gln levels showed a drop for this metabolite that was associated with a higher turnover of it through Gln-Glu-GSH, supporting the hypothesis that cells capacity to face oxidative stress represents a survival advantage and may underlie a mechanism that contributes to resistance (Moyec *et al*., 1996).

Mitotic Inhibitors

Used for the treatment of mammary and ovary carcinoma and Kaposi sarcoma, Paclitaxel acts by blocking the microtubules dynamics, inducing a 2 step formation of ^{1}H NMR visible mobile lipids along with ongoing apoptosis (Brisdelli *et al*., 2003). Besides mobile lipids formation, this drug seems to induce early accumulation of PC that may be attributed to alterations in phospholipids metabolism. Once no significant changes in GSH or *m*-Inositol are known, no important alterations in oxidative mechanisms or osmoregulation processes are supposed to be associated with Taxol treatment (Knijn *et al*., 2005).

Docetaxel is approved for the treatment of breast and prostate cancers as well as small-cell carcinoma of the lung (Morse *et al*., 2007). This drug has increased affinity for tubulin and higher

antitumour activity than that of Paclitaxel. ^{31}P MRS of extracts of breast cancer cell lines treated with docetaxel revealed important changes in choline compounds (Morse *et al*., 2007). The detected drop in PC and rise in GPC were also confirmed through *in vivo* and *ex vivo* analysis and are coincident with mitotic catastrophe. Complementary *in vitro* NMR tests with cell lines with different grades of differentiation show that this drug-induced changes in Cho metabolites get more pronounced as cancer get more aggressive. Breast cancer cells were tested in their response to the mitotic inhibitor docetaxel (Bayet-Robert *et al*., 2010). HRMAS results revealed that after 48 hours drug-treatment, cells decreased GSH and taurine levels possibly as a consequence of activation of drug efflux detoxification processes. The decrease of PC together with increments of cytidine diphosphocholine (CTP) in response to treatment suggested activation of PC:CTP cytidylyltransferase, which activity is closely related to cell cycle and cytoskeletal organization. Drug-induced increase of poli-unsaturated fatty acids (PUFA), was interpreted as reflecting decreased β-oxidation or lower rates of membrane formation.

Vinblastine, a Vinca alkaloid, was used to unveil metabolic changes induced by treatment that could be associated with mitotic inhibitors resistance (Lutz *et al*., 2005). ^{1}H and ^{31}P MRS data of human renal cell carcinoma (RCC) line and its vinblastine resistant variant were acquired and the comparison of the results revealed significant changes in phosphate metabolites and in cells' energetic state (. Results showed that increased GPC and also GPC/PC ratios in response to VBL treatment. Contrarily to KTCTL-2 cells were no alterations were detected, resistant cells also suffered a drop in Pi concentration and an increase of PCr levels that together, indicate increased energy requirements by these cells, what was attributed to P-170 glycoprotein activity.

Hormonal Agents

Tamoxifen is currently used for the treatment of both early and advanced ER(+)breast cancer in pre- and post-menopausal women (Griffin *et al*., 2003). Acting as an antagonist in breast tissue, tamoxifen also acts as a partial agonist on the endometrium, what has been linked to the occurrence of endometrial carcinoma in some women. The ^{1}H HRMAS NMR metabolic characterisation of endometrial adenocarcinoma cells response to tamoxifen, demonstrated that this agent induces significant and time-dependent increases in nucleotides levels (namely uridine and adenosine), suggesting that tamoxifen affects RNA transcription and also interferes with the intracellular contents of Ethanolamine and *m*-Inositol, constituents of cellular membranes, what may reflect phosphoglyceride mobilisation and cell membrane synthesis (Griffin *et al*., 2003).

Dexamethasone is a potent synthetic member of the glucocorticoid class of steroid drugs, which presents anti-inflammatory and immunosuppressant properties (Lutz *et al*., 2002). Glucocorticoids have been used for more than 2 decades to treat leukemia and lymphoma however, a considerable number of patients that suffer from these pathologies are resistant to glucocorticoids. Some evidences show that increased antioxidant defence contributes to cells increased resistance to dexamethasone. The ^{31}P NMR analysis of extracts of dexamethasone-treated thymoma cells, which present increasing antioxidant capacity, revealed significant alterations in phosphate metabolism (Lutz *et al*., 2002). The ratio of Cho containing phospholipids to ethanolamine containing phospholipids was generally reduced in steroid-resistant cells. PE and its derivatives contained higher amounts of PUFA than the Cho containing analogs. Considering that PUFA are readily oxidized by reactive oxygen species, this increased amount of PE can lead to higher antioxidant defences and may thus contribute to the steroid resistance in this cells. Resistance to steroids therapy also seem to have to do with decreased ATP and energetic status and increased concentrations of hexose and triose phosphates.

Inhibitors of Topoisomerase

Etoposide and irinotecan are topoisomerase I and II inhibitors, respectively. The metabolic effects of these two agents were investigated on neuroblastoma cell lines with various drug sensitivities (Lindskog *et al*., 2004). The global ^{1}H MRS metabolic changes induced by treatment showed, for both drugs, important changes in lipids metabolism. After chemotherapy, neuroblastoma cells showed time-dependent changes in response to irinotecan treatment particularly in Cho and CH_2 resonances. A positive correlation was found between CH_2/Cho ratio and the extent of cell death after cytotoxic treatment (Lindskog *et al*., 2004).

Molecularly Targeted

PX-478 is an HIF inhibitor whose effects on metabolic profile of HT-29 cell line were decreased glucose consumption and lactate production (Jordan *et al*., 2005). ^{1}H and ^{31}P MRS studies on an animal model of the same cells, gave further information on metabolic changes induced by this agent. Decreased PC and GPC were responsible for a drop of the total choline resonance and PE and glycerophosphoethanolamine (GPE) were also proved to decrease with treatment. Beyond membrane lipids alterations a significant decrease was also observed in *m*-inositol levels. Thus, these metabolites may have potential as ^{1}H or ^{31}P MRS-visible biomarkers of drug response *in vivo* or *ex vivo* markers of response (Jordan *et al*., 2005).

Imatinib is an anticancer drug used in the treatment of chronic myelogenous leukemia (CML), gastrointestinal stromal tumours and some other diseases. NMR has been used to elucidate about the metabolic changes induced by imatinib treatment on leukemia cells. Once again, the main observed changes linked to glycolytic activity and lipids metabolism (Kominsky *et al*., 2009; Klawitter *et al*., 2009; Gottschalk *et al*., 2004). Imatinib treatment seems to induce a decrease in glucose uptake and metabolism and the use of labelled glucose in the media helped the detection of a decreased lactate production also. Some evidences also suggest an increase on Glu production after exposure, and the analysis of labelled experiments point glucose as one of its precursors. Lipids and specially membrane lipids seem to be greatly affected by imatinib treatment. Decreases in PC and phosphatidylcholine (PTC) and increments on GPC levels result in an overall decline of phosphomonoesters/phosphodiesters ratio and are thought to be due to inhibition of cell proliferation and differentiation processes, as well as cellular membrane dysfunctions related to apoptotic events. Increased PUFA and CH_2/CH_3 resonances after imatinib treatment were associated with ongoing cell death and together with the alterations on Cho compounds, probably result from either activated PTC catabolism or inactivated PTC anabolism (Kominsky *et al*., 2009; Klawitter *et al*., 2009; Gottschalk *et al*., 2004).

^{1}H and ^{31}P NMR of prostatic carcinoma cells showed a very significant time course accumulation of lipids in phenylacetate- (PA) or phenylbutyrate-treated (PB) cells (Milkevitch *et al*., 2005). Besides the observed general lipids accumulation, total choline, whose levels did not change significantly in controls, suffered important increases in treated cells. Although no significant changes were seen in phosphomonoesters, GPC contents increased markedly in exposed cells. These total choline and GPC increments after PA or PB exposure were attributed to the activation of phospholipase A2, since fatty acids and GPC are released by the consecutive action of this enzyme and lysophospholipase on phospholipids (Milkevitch *et al*., 2005).

^{31}P NMR spectroscopy was used to unveil some of the metabolic markers of breast cancer cell lines response to PIK3 inhibitors: LY294002 and wortmannin (Beloueche-Babari *et al*., 2006). The results from LY294002-treatment showed a consistent drop of PC, accompanied by a decrease of PC/GPC in all tested breast cancer cells, whether intact or extracts. Treatment with wortmannin resulted in a reduction of PC contents and changes of GPC and GPE levels (although not statistically relevant). The consistent drop of PC observed for both treatments suggest PC as a common metabolic marker of PI3K inhibition, what in turn relates PC production with a common metabolic target of these two inhibitors of PI3K pathway.

The use of MS metabolomics of cultured mammalian cells for anticancer drug testing has gained importance in the last few years (Figure 1.20) although a lower number of papers have been published compared to NMR metabolomics. This possibly relates to the more complex sample preparation for MS analysis, which implies extraction procedures and requires a more complex and time consuming optimisation of experimental acquisition parameters. Additionally, MS has usually been employed in a targeted manner, thus comprising very few untargeted studies, due to the additional complexity of the resulting data and, hence, its interpretation.

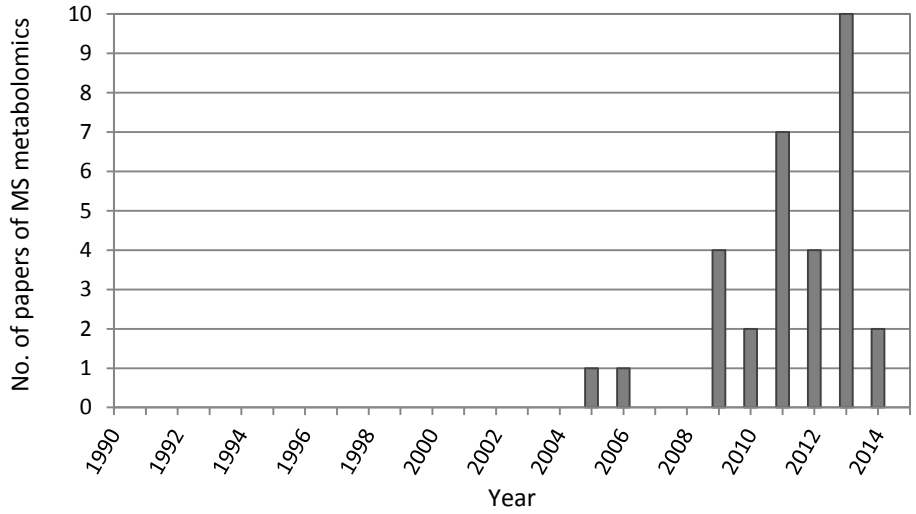

Figure 1.20. Number of studies on MS metabolomics of cultured mammalian cells for anticancer drug testing (source www.webofknowledge.com, until 20th November 2014).

A list of the available MS metabolomics studies of cultured mammalian cells for anticancer drug testing, divided according to the different classes of chemotherapy agents is presented in Table 1.3. Since the emphasis of this thesis is on NMR, an overview of the knowledge produced in this area through MS metabolomics will be presented only for studies in which either cell lines (MG-63) or drugs (cDDP, DOX or MTX) tested in this thesis were investigated.

Table 1.3. Overview of literature on MS metabolomics of cultured mammalian cells for anticancer drug testing.

Class	Type	Agent	Tested cells	Reference
Metal-based	Metal salt	Cisplatin	Pluripotent stem cells	Stechow *et al.*, 2013
Antimetabolites	Pyrimidine analogs	5-Fluoruracil	Colorectal cancer: HCT116	Uehara *et al.*, 2009
			Leukemia: Jurkat	Miura *et al.*, 2010
			Hepatoblastoma: HepG2 Embryonic kidney: HEK293	Halama *et al.*, 2013
			Gastric cancer: MNK45	Sasada *et al.*, 2013
		Gemcitabine	Colorectal cancer: HCT116	Uehara *et al.*, 2009
	Antifolate	Methotrexate	Melanoma: Hela	Myint *et al.*, 2009
			Colorectal cancer: HTC116	Uehara *et al.*, 2009
			Leukemia: Jurkat	Miura *et al.*, 2010

Table 1.3 (cont.). Overview of literature on MS metabolomics of cultured mammalian cells for anticancer drug testing.

Class	Type	Agent	Tested cells	Reference
Antitumor antibiotics		Doxorubicin	Breast cancer: MCF-7	Cao *et al.*, 2013
			Hypopharyngeal tumor: FaDu	Kotze *et al.*, 2013
Hormonal agents	Androgen agonist	R1881	Prostate cancer: RWPE, PC3, DU145, VCaP, LNCaP	Putluri *et al.*, 2011
	Steroid hormone	Dehydroepiandrosterone	Hepatoblastoma: SK-Hep-1	Cheng *et al.*, 2011
Inhibitors of Topoisomerase		Etoposide	Hepatoblastoma: HepG2 Embryonic kidney: HEK293	Halama *et al.*, 2013
		ARQ501	Primary hepatocytes	Miao *et al.*, 2009
Molecularly targeted	Tyrosine kinase inhibitors	Imatinib	Leukemia: CML	Boros *et al.*, 2005
	Protease inhibitors	Indinavir	Cervical cancer: C33A	Kim *et al.*, 2014
		Lopinavir		
	HSP90 inhibitors	Celasterol	Adenocarcinoma: HeLa	Hu *et al.*, 2013
	PI3K inhibitors	LY24002	Glioblastoma: U87MG	Pandher *et al.*, 2009
	PAF inhibitor	Gossypol	Ovarian cancer: SKOV-3	Wang *et al.*, 2013
Other agents		PNU-91325, rosiglitazone, pioglitazone	Hepatoblastoma: HepG2	Harrigan *et al.*, 2006
		Lovastatin	Breast cancer: MDA-MB-231, MDA-MB-468	Klawitter *et al.*, 2010
		Dehydroepiandrosterone	Hepatoblastoma: SK-Hep-1	Cheng *et al.*, 2011
		Docosahaexanoic acid	Pancreatic cancer: PaCa-44	D'Alessandro *et al.*, 2011
		Bezielle	Breast cancer: SKBR3, BT474	Klawitter *et al.*, 2011
		$GdCl_3$	Adenocarcinoma: HeLa	Long *et al.*, 2011
		2,3,7,8-tetrachlorodibenzo-p-dioxin	Hepatoblastoma: HepG2	Jennen *et al.*, 2011 Ruiz-Aracama *et al.*, 2011
		Metformin	Breast cancer: MCF-7, BT-474, MDA-MB-231	Corominas-Fajas *et al.*, 2012
		Phenolic compounds	Colorectal cancer: HT29, SW480	Fernández-Arroyo *et al.*, 2012
			Colorectal cancer: HT29	Ibañez *et al.*, 2012
			Leukemia: K562	Valdes *et al.*, 2012
		Perfluorooctanoic acid	Normal liver: L02	Peng *et al.*, 2013
		EPA	Lung cancer: A549, H596	Pirman *et al.*, 2013
		Flavonoid derivative	Hepatoblastoma: HepG2	Gao *et al.*, 2014

YNB, Yunnan Baiyao, EPA: eicosapentaenoic acid.

The metabolic response of pluripotent stem cells to cDDP treatment was investigated by integrated MS metabolomics and transcriptomics (Stechow *et al*., 2013). The results revealed changes in metabolites involved in Met degradation pathways, polyamine synthesis and catabolism, urea cycle, Pro and Arg metabolism as well as nucleotide metabolism in cDDP-treated cells.

Concerning the metabolic effects of antimetabolites administration, LC/MS analysis of colorectal cells treated with MTX revealed a decrease of dTDP and increases in 5'phosphoribosylglycinamide (GAR), 5'phosphorobosyl-5-amino-4-imidazolecarboxamide (AICAR) and dUMP (substrates or products of the enzymes that catalyse purine and thymidine biosynthesis, inhibited by MTX) (Uehara *et al*., 2009). 5'-phosphoribosyl-4-(N-succinocarboxamide)-5-aminoimidazole (SAICAR) was also found to increase with MTX as well as UTP (Myint *et al*., 2009). When administered to leukemia cells, MTX was also found to down-regulate UDP-GlcNAc biosynthesis (Miura *et al*., 2010).

Recent work investigated the metabolic consequences of the antitumor antibiotics DOX on breast cancer cells by MS metabolomics (Cao *et al*., 2013). The results showed that DOX promoted a down-regulation of proteins biosynthesis, purines, pyrimidines and glutathione as well as a decreased rate of glycolysis, which in turn enhanced glycerol metabolism (Cao *et al*., 2013). This increased glycerol metabolism and decreased glutathione biosynthesis suggested a drug-induced generation of reactive oxygen species (ROS) and a weakened ability of treated cells to balance ROS, respectively. In hypopharyngeal tumour cells (Kotze *et al*., 2013), cholesterol and diacylglycerols were pointed as drug-response markers and when high dose DOX is administered Gln alterations also became relevant.

1.6. Aims and Outline of this Work

The general aim of this thesis was to characterize, interpret and compare the metabolic response of osteosarcoma cells to selected conventional anticancer drugs and to a new palladium complex, in order to achieve a better understanding of the drugs mechanisms of action and, subsequently, effects arising from drug combination protocols. In this line, the specific aims were:

- To optimize cell culturing and sampling conditions for NMR spectroscopy and to evaluate the influence of different experimental procedures on the cell's spectral profiles.
- To characterize in detail the metabolome (inventory of endogenous metabolites involved in cells biochemical pathways) of human osteosarcoma MG-63 cells and to characterise their metabolic response to three drugs conventionally used in the treatment of OS: cisplatin, doxorubicin and methotrexate.
- To characterise the metabolic profile of human osteoblast (HOb) cells and establish the differences in relation to that of previously characterized MG-63 OS cells metabolome.

– To evaluate the metabolic response of MG-63 cells to Pd_2Spm, potentially active against OS, in relation to the metabolic perturbation induced by cisplatin and to comprehensively understand the metabolic impact of each of these two drugs in HOb cells, concluding about the possible advantages of using the new Pd(II) agent.

– To understand the metabolic impact of conventionally used drug combination regimens (cisplatin, doxorubicin, methotrexate) on MG-63 OS cells in relation to that induced by combination regimens including Pd(II) drug (Pd_2Spm, doxorubicin, methotrexate).

2. Analytical Methods

2.1. Biological Assays

2.1.1. Trypan Blue, Sulforhodamine B (SRB) and 3-(4,5-dimethylthiazol-2-yl)-2,5-diphenyltetrazolium bromide (MTT) Assays

Trypan blue, SRB and MTT assays were used throughout this work to evaluate cell integrity and density (Trypan Blue and SRB) and cell viability (MTT). The principles and methodologies of each of these methods are described below.

The Trypan Blue Assay

The Trypan blue dye (chemical structure shown in Figure 2.1) exclusion colorimetric test is a standard cellular biology method for quantifying living (morphologically intact) cells. This method is based on a simple principle: living cells possess intact cell membranes that exclude the Trypan blue dye (the same principle applying to Eosin and propidium iodide dyes, mostly used to stain proteins and DNA, respectively), whereas the cells with a compromised/damaged membrane appear blue-coloured under the light microscope (Strober, 2001). This assay was applied to assess the extent of cell death at each time point of the experiments performed for NMR, allowing plots of number of cells as a function of time to be built. Additionally, this quantification, performed prior to NMR data acquisition, was used to confirm that the samples analysed had indeed been exposed to the chosen drug concentration since, at the time point for which IC_{50} was determined, a reduction of 50% in the number of living cells was expected (excluding possible experimental errors).

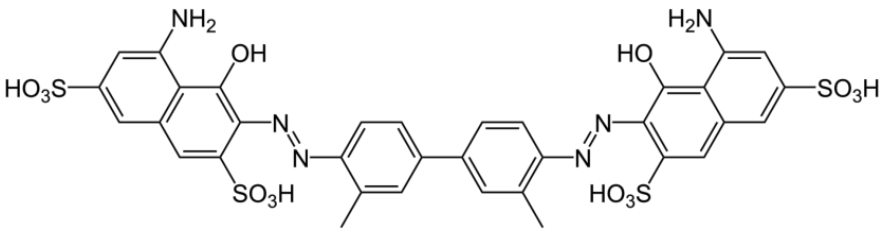

Figure 2.1. Chemical structure of Trypan blue dye.

The SRB Assay

The SRB dye (sulforhodamine B, chemical structure shown in Figure 2.2) assay was first described by Skehan and co-workers in 1989 (Skehan *et al*., 1989), in the course of an anticancer drug discovery program carried out by the National Cancer Institute, USA. This assay is based on the capacity of the sulforhodamine B dye to bind electrostatically (depending on pH) to protein basic amino acid residues. SRB links to proteins of trichloroacetic (TCA)-fixed cells under mild acidic conditions and can be solubilised by weak bases as Tris (tris-hydroxymethyl-aminomethane), prior to optical density measurement (Voigt *et al*., 2005). A very important advantage of this method is the fact that the colorimetric end point is non-destructive and indefinitely stable, which allows samples to be analysed, by spectrophotometry at 540 nm, days after the experiment.

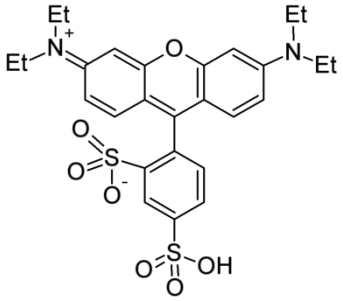

Figure 2.2. Chemical structure of SRB fluorescent dye.

Compared to the MTT assay, the SRB method shows a better linearity with cell number, higher sensitivity and the corresponding staining is cell-line independent. Furthermore, as opposed to MTT, SRB has been successfully used in freshly lysed cells (hence, easily stained) preserving cell debris unstained, thus providing a reliable way of measuring sensitivity to drugs (Keepers *et al*., 1991).

In the present work, the SRB assay was used for IC_{50} determination of the effect of Pd_2Spm on MG-63 cells, as well as for obtaining the 12 days growth curve of osteoblasts.

The MTT Assay

The MTT (3-(4,5-dimethylthiazol-2-yl)-2,5-diphenyltetrazolium bromide, chemical structure shown in Figure 2.4) assay, established by Mossmann in 1983, (Mossmann, 1983) is based on the reduction of the water soluble yellow tetrazolium salt (MTT) to insoluble violet formazan crystals

via cleavage of the tetrazolium ring by mitochondrial NADH-dependent dehydrogenases of metabolically active cells (Figure 2.3). This process can be followed spectrophotometrically, as formazan is a coloured product (maximum absorbance at 570 nm), that accumulates inside the viable cells, since cell membranes are impermeable to it. The amount of formazan produced is assumed to be directly proportional to the number of viable cells (Berridge *et al*., 1993).

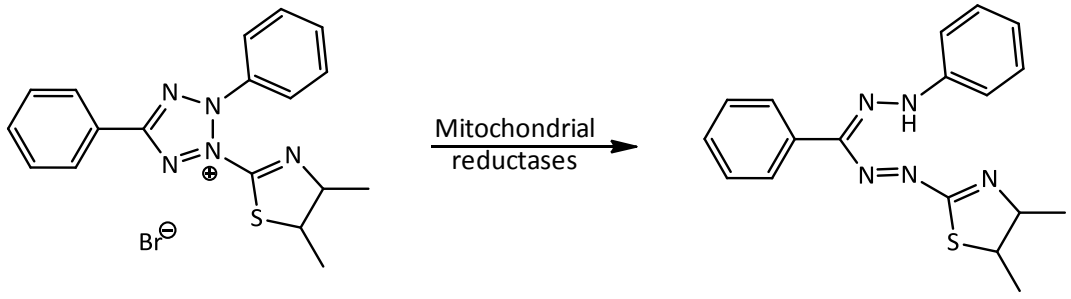

Figure 2.3. Reduction of MTT to formazan crystals by mitochondrial NADH-dependent dehydrogenases of metabolically active cells.

The MTT assay is generally accepted as a reliable, rapid and inexpensive method to assess cell viability (Kepp *et al*., 2011). In this work, this method was used to determine IC_{50} values for each of the tested drugs, with the exception of Pd_2Spm.

2.1.2. Fluorescein Isothiocyanate (FITC) Annexin V/Propidium Iodide (PI) Assay for Apoptosis Detection

Apoptosis is a normal physiological process, crucial for the maintenance of tissue homeostasis. This process relates to programmed cell death and is characterised by a number of morphological features including disassembling of cytoskeleton and nuclear envelope, fragmentation of nuclear DNA and alteration of cell surface, so that dying cells shrink and condense, becoming rapidly phagocytosed (Alberts *et al*., 2002). Cellular events involving the plasmatic membrane constitute the earliest features of the process. In apoptotic cells, the membrane phospholipid phosphatidylserine (PS) is translocated from the inner to the outer membrane layer, thus exposing PS to the external cellular environment (Kerr *et al*., 1972).

Annexin V is a 36 kDa Ca^{2+}-dependent phospholipid-binding protein with high affinity for PS, thus binding to it in apoptotic cells (Vermes *et al*., 1995). Annexin can also be conjugated to the fluorochrome FITC (fluorescein isothiocyanate) while keeping its affinity for PS, therefore being

very useful as a sensitive fluorescent probe for flow cytometry analysis of cell cultures. Since PS externalisation is one of the first events of apoptosis, FITC-Annexin V staining identifies cells in early apoptotic stages. In addition, experiments based on nuclear changes (such as DNA fragmentation and loss of nuclear membrane integrity) can be used as markers of late apoptosis or necrotic processes. Hence, staining with FITC-Annexin V is commonly used in combination with a vital dye such as propidium iodide (PI) to allow different stages of apoptosis to be identified simultaneously: viable cells with intact cell membranes exclude PI, whereas cells with damaged membranes are permeable to it. Consequently, viable cells appear negative for both FITC-Annexin V and PI, cells in early apoptosis are positive for FITC Annexin V and negative for PI, and cells already undergoing late apoptosis are both FITC-Annexin V and PI positive (Figure 2.4).

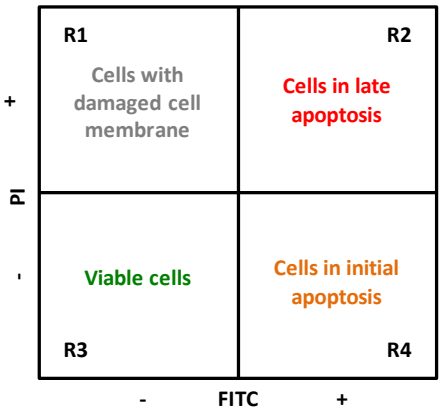

Figure 2.4. Schematic representation of the information obtained with the FITC-Annexin V/PI apoptosis detection method.

Cells in the R1 quadrant display no apoptosis-related damaged cell membranes (FITC-Annexin V(-)/PI (+)) with PI labelling arising from cells mechanically damaged during the assay; cells in the R2 quadrant are undergoing late apoptosis (FITC-Annexin V(+)/PI (+)); cells in the R3 quadrant are viable (FITC-Annexin V (-)/PI (-)) and, finally, cells allocated to the R4 quadrant are undergoing initial apoptosis (FITC-Annexin V (+)/PI (-)).

2.2. Nuclear Magnetic Resonance (NMR) Spectroscopy

2.2.1. Principles of NMR Spectroscopy

NMR spectroscopy has emerged in the early 1940s (Becker, 1993) and since then, this technique has suffered tremendous improvements, having nowadays a leading role in most scientific fields.

Atomic nuclei have characteristic proton/neutron compositions which, in some nuclei, induce the property known as spin, perceived as a rotational motion of the nucleus. The nuclear spin generates a magnetic dipole along the nucleus rotation axis, corresponding to a magnetic moment, **μ**, associated to the spin angular moment, **P**, and the spin quantum number **I**. Only the nuclei with non-zero values of **I** (**I** assuming either integer or half-integer values) are detectable by NMR, e.g.: ^{1}H, ^{9}F, ^{13}C, ^{15}N and ^{31}P with *I*=1/2; ^{2}H, ^{14}N with *I*=1 and ^{17}O with *I*=5/2. For nuclei with *I*≠0, **I** and **μ** relate to each other by the expression $\boldsymbol{\mu} = \gamma.\mathbf{I}$, where γ is the gyromagnetic ratio, which relates to the sensitivity of each particular nucleus (γ=2.675 x 10^{-8} rad.$T^{-1}s^{-1}$, for ^{1}H). For nuclei with *I*=1/2, the presence of an external magnetic field $\mathbf{B_0}$ induces two possible spin orientations that correspond to different energy levels. The number of possible spin orientations is given by the magnetic quantum number $\boldsymbol{m_I}$ described by the equation $\boldsymbol{m_I}=2\mathbf{I}+1$. For a nucleus with I=1/2, spin orientations may be either parallel (lower energy, α) or antiparallel (higher energy, β) and the energy difference (**△E**) between α and β states is given by $\triangle\mathbf{E}=\gamma.\hbar.\mathbf{B_0}$, where ħ is the Planck's constant (h) divided by 2π. The external magnetic field $\mathbf{B_0}$ induces a torque (momentum that causes rotation about an axis) on the nuclei, leading the spins to precess around the direction of the applied $\mathbf{B_0}$ (Figure 2.5a). This is called Larmor precession and it occurs at a frequency named Larmor frequency, expressed as linear or angular frequencies: ν_0 ($\nu_0=-\gamma.\mathbf{B_0}/2\pi$ in Hz) or $\boldsymbol{\omega_0}$ ($\boldsymbol{\omega_0}=-\gamma.\mathbf{B_0}$ in rad.s^{-1}) (Lindon *et al*., 2000).

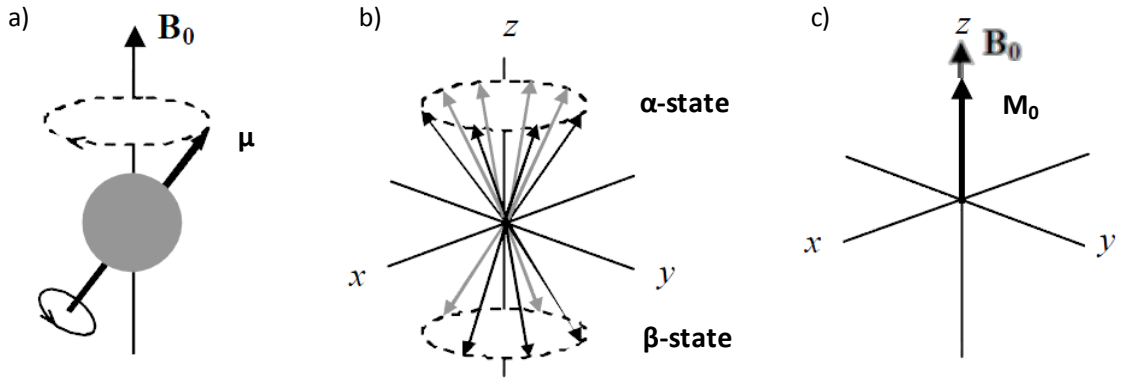

Figure 2.5. a) Precession of an individual magnetic moment **μ** around the external magnetic field $\mathbf{B_0}$, b) precession of magnetic moments in the α and β spin states and c) resulting magnetic moment $\mathbf{M_0}$ reflecting the excess of spin population in the α state (adapted from Claridge, 1999).

The Boltzmann equation (Eq. 2.1) describes the distribution of the spins by the two energy levels (considering, for instance, the case of protons), in which *N* refers to the number of spins in each spin state, **△E** is the difference between the energetic states, *k* is the Boltzmann constant and T the absolute temperature. Accordingly, in the presence of $\mathbf{B_0}$ and at thermal equilibrium,

there will be an excess of spins in the α state, thus creating a bulk magnetization $\mathbf{M_0}$, parallel to $\mathbf{B_0}$ (Reynolds, 2000).

$$\frac{N_\alpha}{N_\beta} = e^{\frac{\Delta E}{kT}} \qquad \text{|Eq. 2.1|}$$

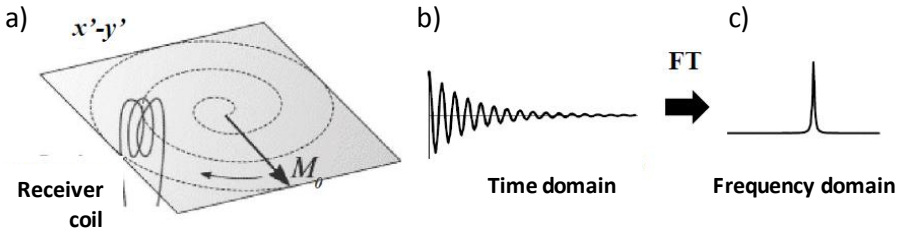

Figure 2.6. a) scheme of the magnetization vector $\mathbf{M_0}$ precessing on the x'-y' plane around the z axis, cutting the receiver coil aligned with the same plane, b) time domain signal or free induction decay (FID) and c) frequency domain signal of the FID after applying the Fourier transformation (FT) (adapted from Keller, 1988 and Keeler, 2002).

The detection of the NMR signal (Figure 2.6) involves the application of a radiofrequency (RF) pulse for a established period of time, commonly of the order of μs (Keller, 1988). The RF is then transmitted through a coil that surrounds the sample, which induces a magnetic field $\mathbf{B_1}$ in the transverse plain, perpendicular to $\mathbf{B_0}$, and made to oscillate at the Larmor frequency. To facilitate the visualisation of the rotating fields and precessing vectors, a reference rotating frame (x', y', z'=z) spinning at the Larmor frequency around z is used, rather than the static laboratory frame (x, y, z). The applied RF pulse (usually corresponding to a 90˚ radiation pulse) causes the net magnetization $\mathbf{M_0}$ to flip from the z axis to the x'-y' plane. After the pulse, the magnetization vector is reestablished, in a way that the transverse magnetization gradually disappears towards z, ending at its starting $\mathbf{M_0}$ value, through a process called relaxation. To detect the NMR signal, the receiver reads the signal in the x'-y' plane which is crossed by the magnetization vector $\mathbf{M_0}$, thus originating a current that is amplified and recorded, known as Free Induction Decay (FID). This is a time domain signal (*f(t)*), subsequently transformed into a frequency domain (*f(w)*), i.e. the NMR spectrum, by applying a Fourier transformation (FT, Eq. 2.2).

$$f(w) = \int_{-\infty}^{+\infty} f(t)\, e^{-iwt} dt \qquad \text{|Eq. 2.2|}$$

Relaxation

The relaxation process occurs through two main mechanisms, named spin-lattice and spin-spin relaxation, also known as longitudinal and transverse relaxation, respectively. These processes are characterized by time constants named relaxation times T_1 and T_2, respectively. T_1 describes the exponential decay of the net magnetization in the z axis whereas T_2 accounts for the relaxation process in the x'-y' plane. The spin-lattice relaxation refers to the exchange of magnetization with the surroundings and the z component of magnetization (M_z) is expressed in terms of T_1 according to Eq. 2.3. The spin-spin relaxation relates to a spin-spin exchange process, resulting from differences in magnetic field that are experienced by the spins, due to sample heterogeneities or intra- and inter-molecular interactions. Described in terms of T_2 by Equations 2.4 and 2.5, these differences cause the spanning out of the magnetization component in the x'-y' plane, so that ultimately no net magnetization exists in this plane (Jacobsen *et al*., 2007).

$$M_z = M_0 \times (1 - e^{-t/T_1}) \qquad |\text{Eq. 2.3}|$$

$$M_x = M_0 \times sin(2\pi w_0 t) e^{-t/T_2} \qquad |\text{Eq. 2.4}|$$

$$M_y = -M_0 \times cos(2\pi w_0 t) e^{-t/T_2} \qquad |\text{Eq. 2.5}|$$

Finally, it is important to note that T_2 relates to the width at half height of the NMR signals ($\triangle \nu_{1/2}$), according to a relationship of proportionality between $\triangle \nu_{1/2}$, and $1/\pi.T_2^*$ (Claridge *et al*., 1999). Therefore, large and slowly diffusing molecules are characterized by short T_2 values and thus, give rise to broad NMR resonances. Indeed, both T_1 and T_2 values are related to molecular mobility, as illustrated in Figure 2.6. For nonviscous liquids, containing fast diffusing molecules, therefore with short correlation time, τ_C, T_1 and T_2 are identical (initial phase of curve shown in Figure 2.7) (Harris *et al*., 1987). As mobility decreases (τ_C increases), T_1 goes through a minimum (at $\tau_C^2 = \nu_0^{-1}$, where ν_0 is the resonance frequency) determined by field strength (see different red lines in Figure 2.7) from which it increases, while T_2 continues to decrease (Figure 2.7). T_2 eventually reaches a minimum limiting value when the sample is in the solid state.

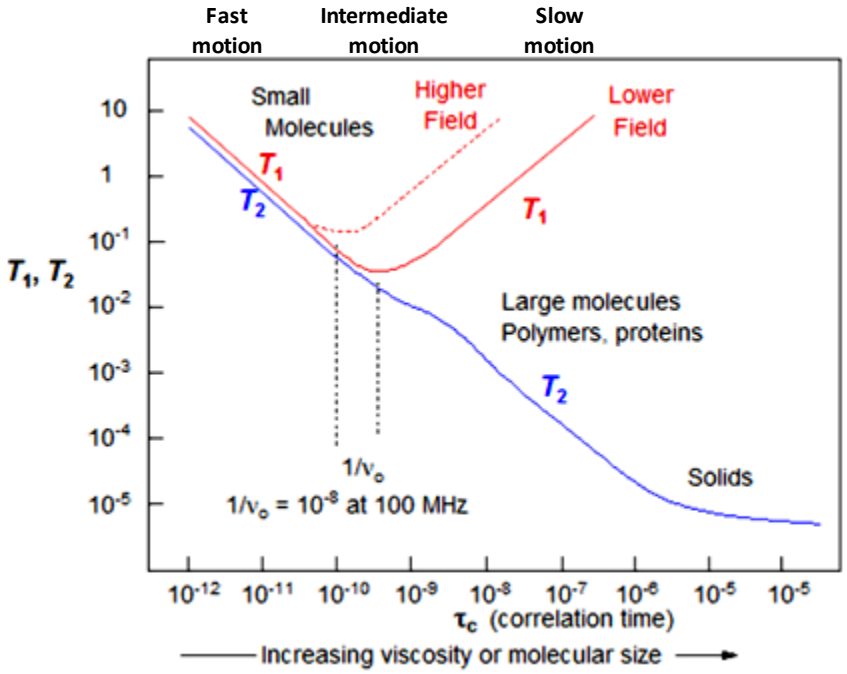

Figure 2.7. Schematic representation of the dependence of T_1 and T_2 on the molecular tumbling rates, expressed by the correlation time, τ_C (adapted from Harris, 1987).

Chemical Shift and Scalar Coupling

Each nucleus is surrounded by electrons that create a local magnetic field, that either opposes or reinforces the applied magnetic field ($\mathbf{B_0}$). The local field may act as a shield and causes each nucleus to experience different effective magnetic fields ($\mathbf{B_{eff}}$) (Lindon *et al.*, 2000). Thus, the effective magnetic field experienced by the nucleus results from the addition of $\mathbf{B_0}$ and the local magnetic field produced by the surrounding electrons (Eq. 2.6, where σ is the shielding constant, which may adopt either positive or negative values).

$$B_{eff} = B_0 \times (1 - \sigma) \qquad |\text{Eq. 2.6}|$$

The chemical environment that surrounds the nucleus (determined by the neighboring atoms and chemical bonds) determines the frequency ($\boldsymbol{\nu}$) at which each nucleus resonates, resulting in absorption peaks at singular positions in the NMR spectrum. The position of each NMR resonance is measured by its resonance frequency, which is proportional to the magnetic field strength and depends directly on the operating frequency of the spectrometer ($\boldsymbol{\nu_{ref}}$). The resultant dimensionless value is called chemical shift ($\boldsymbol{\delta}$) and is expressed in parts per million

(ppm) (Eq.2.7). This results in a chemical shift scale that is independent of the frequency of the NMR spectrometer used (Lindon *et al*., 2000; Jacobsen, 2007).

$$\delta = 10^6 \times (\frac{\nu - \nu_{ref}}{\nu_{ref}}) \qquad |\text{Eq. 2.7}|$$

The frequencies of the methyl groups bound to the silicon atom of chemically stable compounds such as dimethylsilapentanesulfonic acids (DSS), tetramethylsilane (TMS) or trimethylsilyl propionate (TSP) are usually used as reference for ^{1}H and ^{13}C ppm calibration (Santini *et al*., 2001). Nevertheless, TSP has been found to be sensitive to intermolecular interactions in cellular samples (and, in general, in complex mixtures) and for that reason, in this work chemical shifts were internally referenced to alanine signal at δ 1.48 (Duarte *et al*., 2010; Duarte *et al*., 2013). Typical ranges of chemical shift values for ^{1}H and ^{13}C nuclei in common functional groups are listed in table 2.1.

Table 2.1. ^{1}H and ^{13}C chemical shifts of common functional groups (adapted from Fan *et al*., 1996).

^{1}H chemical shifts		**^{13}C chemical shifts**	
Chemical group	**δ (ppm)**	**Chemical group**	**δ (ppm)**
C-CH_3	0.7-1.1	-CH_3 (methyl)	8-30
=C-CH_3	1.5-1.8	-CH_2 (methylene)	14-55
$COCH_3$ (acetyl)	2.0-2.5	-CH- (methane)	22-60
N-CH_3	2.5-3.3	-C- (quaternary)	30-40
O-CH_3	3.3-4.3	CH_2=C-R	100-150
CO-CH_2-C	1.3-2.5	C=C-C=C-R	110-150
O-CH_2-C	4.0-5.0	Heteroaromatic ring	100-165
C-CH-OH	3.3-4.0	C-OH (alcohol)	44-85
C-CH-O-ester	4.2-5.3	C-O-C (ester)	55-85
=CH-C (olefinic)	5.5-8.5	R-COOH (saturated)	165-188
Aromatic ring	6.0-9.0	R-C=C-COOH	158-174
-CHO (aldehyde)	9.0-10.2	R-COOR' (saturated)	158-178
-COOH	10.5-13.5	R-C=C-COOR'	152-172
C-OH (alcohol)	1.5-6.0	R-CHO (saturated)	196-220
C-OH (phenol)	6.5-18.5	R-C=C-CHO	176-195
Primary amines	1.1-1.8	Saturated ketones	195-220
Secondary amines	1.2-2.1	C-N-R_2	20-70
CO-NH	5.0-6.5	R-CO-NH_2	150-178

Nuclei interact with their neighboring nuclei through a mechanism known as spin-spin coupling, scalar coupling or *J*-coupling, which occurs *via* electrons of the chemical bonds (Harris, 1987). The interaction between neighboring spins of nuclei A and X induces a shift in their energy levels that is dependent on their quantum numbers m_A and m_X and their coupling constant J_{AX} (parameter that reflects the strength of the interaction). This through-bond nuclear interaction results in the splitting of the NMR signal into a multiplicity given by 2*nI*+1, where *n* corresponds to the number of neighbor equivalent nuclei (Lindon *et al*., 2000; Jacobsen, 2007).

Quantitation in NMR

In ^{1}H NMR spectra, the area under a signal is directly proportional to the number of nuclei giving rise to it. NMR spectroscopy is, therefore, a quantitative technique, as long as spectral acquisition is performed under quantitative conditions. Such conditions are fulfilled if inter-scan delays are at least 5 times the longest T_1, thus ensuring near complete relaxation of all spins (Jacobsen *et al*., 2007). In such conditions, the concentration of a given compound may be calculated using Eq. 2.8 which expresses that the concentration of a certain compound B (C_B) may be determined given the concentration of a reference compound A (C_A), the integral of the reference signal (A_A) and that of the compound signal to be quantified (A_B), as well as considering the number of protons giving rise to the reference peak (n_A) and to the signal to be quantified (n_B).

$$\frac{C_A}{C_B} = \frac{A_A \times n_B}{A_B \times n_A} \qquad |\text{Eq. 2.8}|$$

However, the quantitative analysis in complex mixtures, such as cell samples or other biological samples, is often hampered by the broadening of resonances which may result from interactions within sample components and between these and the reference compound. This effect will compromise area assessment as faithfully reflecting concentrations. In order to overcome these limitations, alternative approaches have been considered in complex misture analysis (mostly in a metabolomics context). The Electronic Reference To acess In vivo Concentrations (ERETIC) method (Barantin *et al*., 1997) is able to create a reference signal that can be either generated during acquisition or synthetically produced in the postprocessing and has been used to determine absolute concentrations on biological samples analysed by liquid state NMR (Akoka *et al*., 1999) or HRMAS (Albers *et al*., 2009). Other possibility is the use of the PULCON principle (PUlse length based CONcentrations determination), which requires no particular hardware or software (Wider and Dreier 2006) and has very recently been used for quantification of phosphorilated compounds in breast tumor tissue samples by ^{31}P HRMAS (Esmaeili *et al*., 2014). PULCON consists of the determination of the concentration of metabolites present in the samples using as external reference, the spectrum of a standard compound with known concentration, obtained under identical experimental conditions (Esmaeili *et al*., 2014).

2.2.2. One-Dimensional (1D) and Two-Dimensional (2D) NMR Spectroscopy

^{1}H is the most extensively used nucleus in metabolomic studies, due to its high sensitivity and natural abundance. The assignment of ^{1}H NMR spectra of complex mixtures is a lengthy but necessary procedure, which usually requires several 1D and 2D NMR methods. In 1D NMR, experiments usually require a preparation step in which spins reach equilibrium (during a relaxation delay d1) and the application of an RF pulse, followed by signal acquisition. Three types of 1D ^{1}H NMR experiments are commonly used for the study of complex mixtures: the standard NMR experiments (e.g. using the *noesypr1d* pulse sequence, Bruker library), that consist of a preparation step with water presaturation, followed by a 90˚ pulse, and are used to detect signals from all type of molecules, and other two experiments which intend to selectively detect signals from small or macromolecules, respectively. These are named Carr-Purcell-Meiboom-Gill (CPMG) or T_2-edited experiments and diffusion-edited experiments, respectively, and the corresponding pulse programs are shown in Figure 2.8. CPMG experiments (e.g. using the *cpmgpr1d* pulse program, Bruker library) improve the visibility of narrow signals arising from small molecules, making use of a spin echo sequence followed by a delay during which the magnetization decreases exponentially with the ratio between τ/T_2. This means that the magnetization from macromolecules (with lower T_2 relaxation times) decreases faster than small molecules (higher T_2 relaxation times), thus the inclusion of an inter-pulse delay period τ (refered as to d20 in Figure 2.8b) results in the attenuation of the broad signals. On the other hand, diffusion-edited experiments (e.g. using the *ledbpgp2s1dpr* pulse program, Bruker library) are performed to more accurately detect signals arising from large and slowly diffusing macromolecules with low T_2 values. In this experiment, after an initial 90˚pulse magnetization is diphased through the application of gradients. Then, a new gradient is applied to allow the molecules to diffuse and, once diffusion depends on the size of the molecule, the position of larger molecules will remain almost unaffected in contrast to small ones. At this time, a new gradient (opposite to the initial) is applied, to refocus the magnetization of macromolecules and attenuate the resonances from smaller ones (Lindon *et al*., 2004; Duarte *et al*., 2009).

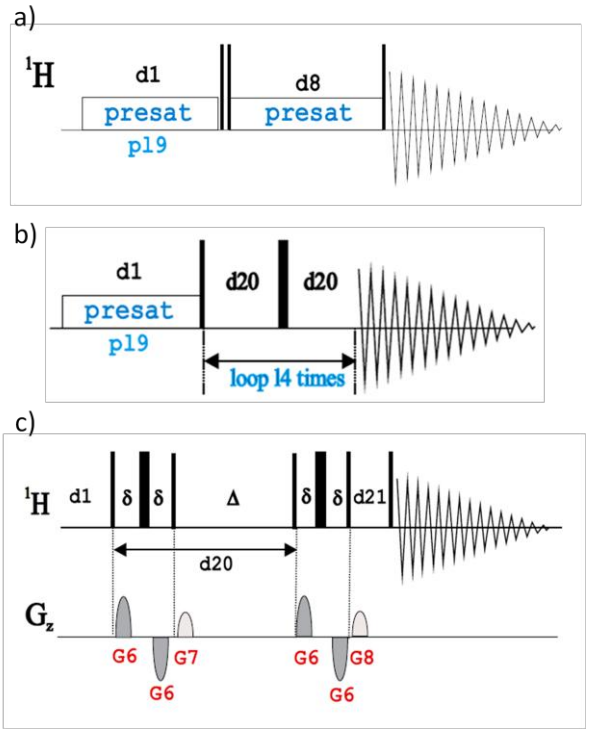

Figure 2.8. Pulse sequences of typical 1D experiments: a) standard 1D, b) CPMG and c) diffusion-edited (adapted from the Bruker Avance 1D/2D manual, Bruker 2003).

The initial steps in the signal assignment process rely on the comparison between chemical shifts, signal multiplicity and coupling constants measured in the 1D spectra and similar data available in the literature (Ulrich *et al.*, 2008; Wishart *et al.*, 2013), as well as with spectra of reference compounds. The 1D spectra of complex mixtures typically comprise hundreds of well resolved signals, which correspond to a wide range of low molecular weight molecules, often superimposed with broad resonances arising from larger molecules, such as lipids and proteins. 2D NMR methods are a valuable tool to deal with this sample complexity and enable the construction of a significantly more complete list of assigned metabolites. All 2D NMR experiments possess the same generic format, consisting in four steps: preparation, evolution (t_1) mixing and detection (t_2) periods. Briefly, the preparation step encompasses a relaxation time that allows spins to reach equilibrium, followed by a 90˚ pulse that brings the magnetization to the x'-y' plane. During the evolution step, a series of pulses is applied to force the energy transfer between nuclei, thus establishing the second dimension. According to the specificities of the pulse sequence chosen, additional pulses may be applied prior to signal detection (Claridge, 1999).

Relying on inter-nuclei interactions, two types of 2D experiments are usually used in the context of mixture analysis: homonuclear and heteronuclear correlation experiments. In the context of metabolomic studies, correlation spectroscopy (COSY) and total correlation

spectroscopy (TOCSY) are two possible experiments of homonuclear proton correlation, that give rise to spectra where peaks that are seen outside the diagonal line, represent ^{1}H-^{1}H spin coupling connectivities, facilitating the assignment of different spin systems and compounds. Another valuable 2D experiment, also a ^{1}H-^{1}H experiment is *J*-resolved (*J*-res), that attenuates peaks from macromolecules and yields information on the multiplicity and coupling patterns of resonances. Heteronuclear single quantum coherence (HSQC) is a heteronuclear experiment which usually correlates the proton and the ^{13}C (Lindon *et al.*, 2004; Duarte *et al.*, 2009). Regarding homonuclear experiments, 2D COSY gives coupling information over two or three bonds while TOCSY spectra provide information on coupled protons that belong to the same spin-system, which can be up to five bonds apart. Therefore, TOCSY experiment enables the identification of all resonances within a spin-system, assuming a crucial importance for metabolite assignment. In the TOCSY experiment, the evolution step is followed by a spin-lock sequence during the mixing time (Malcolm Levitt-17 sequence, MLEV-17) which allows the coherence transfer between all coupled nuclei from a spin-system. The general scheme of the TOCSY sequence is shown in Figure 2.9.

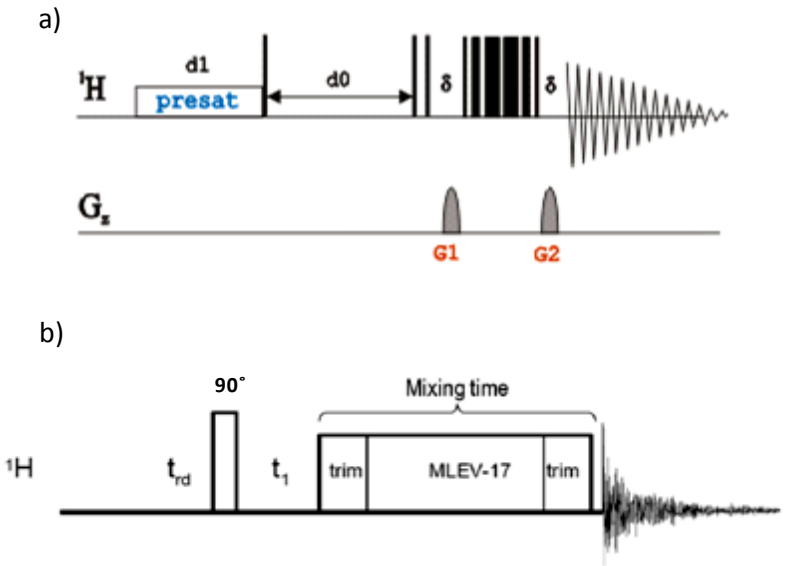

Figure 2.9. a) COSY and b) TOCSY pulse sequence (adapted from the Bruker Avance 1D/2D manual, Bruker 2003).

The heteronuclear correlation HSQC experiments give information on the chemical shift of ^{13}C scalar coupled with ^{1}H chemical shift of the directly connected proton. As shown in Figure 2.10, this experiment starts with a 90˚ pulse for proton magnetization, then an insensitive nuclei enhanced by polarization transfer sequence (INEPT) transfers the magnetization from the ^{1}H to the bounded ^{13}C, recovering the magnetization from ^{13}C to the ^{1}H.

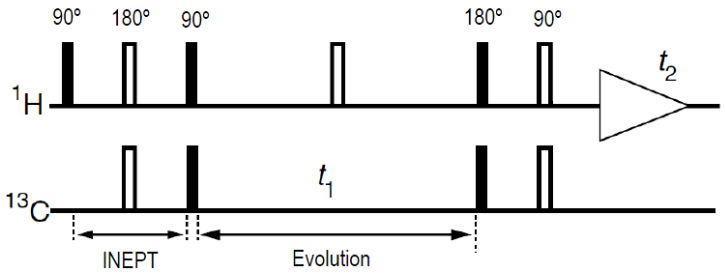

Figure 2.10. HSQC pulse sequence (adapted from Keeler, 2002).

In *J*-res experiments, information about multiplicity is contained in the F1 dimension and scalar couplings are shown in F2 dimension. This aids in the identification of non-overlapped multiplets, allowing the coupling constants (*J*) to be determined. The pulse sequence starts with a 90˚ pulse to create magnetization, followed by a 180˚ pulse by the midpoint of the evolution time to refocus the proton shifts (but not scalar couplings) that appear in the F1 dimension (Figure 2.11a). At this time, the interpretation of the spectra is more complicated, since F2 contains information about both chemical shift and coupling constants. To make spectral interpretation easier by only retaining chemical shift information in F2, a "tilting" of the multiplets through a 45˚ angle is performed (Figure 2.11b).

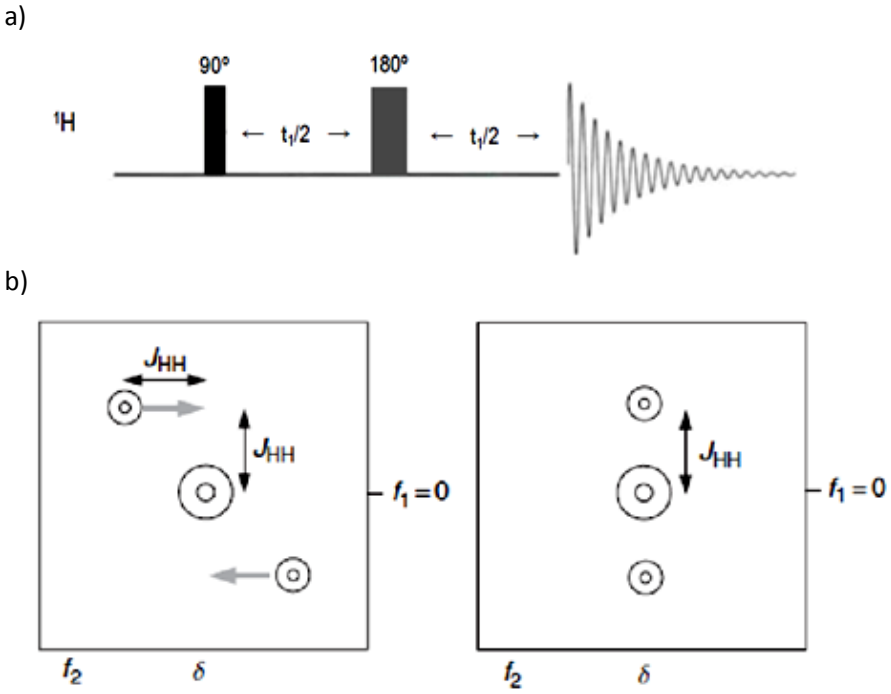

Figure 2.11. *J*-res pulse sequence. (adapted from Claridge, 1999)

In more recent years, cryogenic probes have contributed to the improvement of spectral resolution and sensitivity (Lindon *et al*., 2007). These probes possess a way of cooling down the

detector coil and preamplifier (and not the sample) to around 20K, which leads to an improvement in spectral signal to noise ratio of more than five times, thanks to a reduction in the electronics' thermal noise of the spectrometer; this in turn leads to a reduction in spectral acquisition times (of about 25 times) (Lindon *et al*., 2007).

2.2.3. High Resolution Magic Angle Spinning (HRMAS) NMR Spectroscopy

For a nucleus with spin I, the nuclear energy state is dominated by the Zeeman interaction with the external magnetic field $\mathbf{B_0}$ (described by an Hamiltonian term $\hat{H}_z$), the chemical shift interaction ($\hat{H}_{CS}$) and the scalar spin-spin interaction ($\hat{H}_{SC}$), which result in a total Hamiltonian expression defined by these three Hamiltonian operators ($\hat{H}$). Due to the rapid tumbling of the molecules in liquid state, these interactions are isotropic, thus resulting in discrete average values for chemical shifts and coupling constants. In solid state NMR, additional mechanisms have to be taken into consideration, namely, the anisotropy of the chemical shift interaction ($\hat{H}_{CS}$), dipole-dipole interactions ($\hat{H}_D$) and quadrupolar interactions ($\hat{H}_Q$), the later occurring only in nuclei with spin I>1/2, due to the interaction of the nuclear electric quadrupole moment with the non spherically symmetrical electric field around the nucleus. Therefore, the interactions felt by a nucleus in solid state are described by the Hamiltonian expression that comprises these operators, as well as those referred above for liquid state NMR. These solid state anisotropic interactions are due to the restricted motion of the molecules and lead to the broadening of spectral lines (Fyfe, 1983).

The NMR spectra of semi-solid samples such as tissues or cells are also influenced by line broadening caused by anisotropic interactions (mainly chemical shift anisotropy and dipolar interactions) and sample heterogeneity. This limitation has been largely overcome through high-resolution magic angle spinning (HRMAS) NMR, which enables the acquisition of well resolved spectra of small amounts of semi-solid samples (Claridge, 1999). Figure 2.12a shows the zirconia rotors in which samples are packed for analysis in a HRMAS probe (Figure 2.12b). This technique is based on the rapid spinning of the sample (usually around 4-6 kHz), at an angle of 54.7˚ relative to the applied magnetic field $\mathbf{B_0}$ (Figure 2.12c), in order to average out the anisotropic effects that broaden the lines, thus improving spectral resolution. This happens because the dipolar couplings are proportional to the factor $r^{-3}(3\cos^2\theta-1)$ (where r is the internuclear separation) which becomes zero for $\theta = 54.7^\circ$ (Claridge, 1999). Therefore, the effect of sample rotation is to average out the

effect of chemical shift anisotropy and anisotropy of dipolar interactions, and provided that the spinning rate is high enough, single values of chemical shifts are obtained, mimicking the isotropic values observed in solution state.

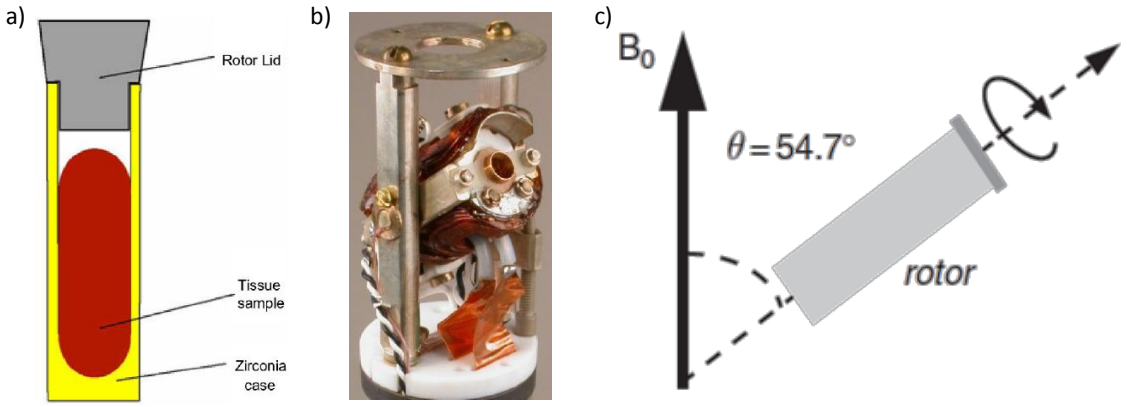

Figure 2.12. HRMAS NMR related apparatus: (a) representation of a zirconia 4 mm rotor, (b) the sample compartment of a 4 mm HRMAS NMR probe, showing a gradient coil at the magic angle, c) representation of sample rotation at the magic angle (adapted from Lindon *et al*., 2009 and Claridge, 1999).

Figure 2.13 clearly demonstrates the spectral improvements produced by Magic Angle Spinning (MAS) in a ^{1}H NMR spectra of an intact piece of liver tissue.

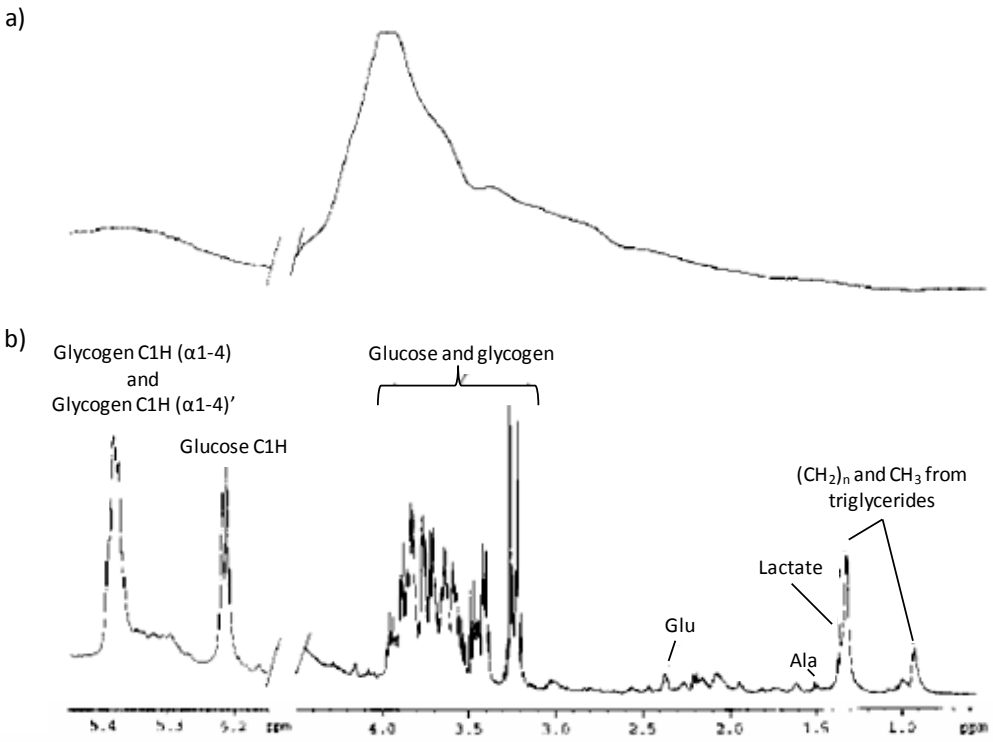

Figure 2.13. 600 MHz CPMG ^{1}H NMR spectra of control liver acquired either a) in static conditions and b) at a spinning rate of 6.2 kHz (adapted from Bollard *et al*., 2000).

Coupled to relatively high spinning rates, the use of a deuterium (^{2}H) lock signal (which compensates for variations in the magnetic field across time) yields remarkable high-resolution spectra, resulting in much higher and sharper peaks (Lindon *et al*., 2009). Moreover, HRMAS probes are configured with a Z-gradient aligned along the magic angle, enabling the access of a wide variety of NMR experimental techniques including gradient enhanced solvent suppression and artifact free 2D homonuclear and heteronuclear experiments. Disposable rotor inserts are available for easy sample preparation and/or safety issues, namely when dealing with toxic samples (*e.g.* samples exposed to toxic agents), as drug-exposed samples used in some of the studies described ahead in this thesis.

2.3. Data Pre-Processing and Analysis

The metabolomic analysis of biologic samples (cells, tissues or biofluids) encompasses the manipulation of complex datasets, usually with several hundreds of variables. In order to extract meaningful biological information from the NMR spectra of complex mixtures, appropriate data pre-processing procedures and statistical/multivariate methods must be applied. Prior to statistical or multivariate analysis, important pre-processing steps include alignment, normalization and scaling procedures. Conventional univariate statistical methods such as Student's *t*-test, Wilcoxon, Mann-Whitney test or ANOVA, which perform the analysis of one variable at a time, are unpractical as a first approach to extract this kind of information from such complex datasets. On the other hand, Multivariate Analysis (MVA) has the ability of dealing with all the variables in one single analysis with the additional advantage of allowing the construction of predictive models. Thus, MVA is a method of excellence to extract relevant information from the whole data set, and is usually complemented by univariate analysis to extract statistical meaning of those suggested variations. Finally, the validation of the MVA results is of paramount importance to ensure the reliability of MVA models (Kjeldahl and Bro, 2010). In the following sections these steps are described in detail.

2.3.1. Data Pre-Processing

Metabolomics data is usually translated into two-dimensional matrices of intensities, where each line corresponds to a different observation or object (sample, time point, etc.) and each

column represents a variable which in the case of NMR metabolomics, corresponds to a chemical shift.

The alignment or bucketing of shifted signals is usually a first pre-processing procedure, particularly in samples like urine, which may vary significantly in terms of pH or ionic strengh. Indeed, changes in NMR peak chemical shifts are frequently found in sample spectra due to slight changes in pH, temperature or salt concentration, constituting one of the first issues to be tackled in order to be able to adequately compare different spectra. In the case of cellular samples, minor variations in peaks position are detected (lower than 0.5Hz or 0.001 ppm) with the exception of peaks of the amino acid histidine (due to ionization of its NH group of the imidazole ring with a pKa close to 6, leading to the instability of the bonds of the ring and the formation of tautomeric species). In order to correct these minor chemical shift deviations between samples, spectral alignment may be performed, as in this work, using the algorithm recursive segment-wise peak alignment (RSPA) (Veselkov *et al*., 2009). Other alignment algorithms are available such as interval correlated shifting (icoshift) (Savorani *et al*., 2010), fast iterative warping algorithm (Alm *et al*., 2009) and hierarchical cluster-based peak alignment (CluPA) (Vu *et al*., 2011). Spectral bucketing, also known as binning, can also be applied to tackle chemical shift variations in peaks (Lindon *et al*., 2007; Smolinska *et al*., 2012). This procedure consists of dividing de spectrum in fixed or variable widths, which can vary from 0.005 to 0.04 ppm. Despite being helpful in eliminating differences in peak positions, with a consequent reduction in the complexity of the matrix, bucketing entails some loss of spectral resolution.

Normalization is required in order to account for differences in concentration or total amount of different samples. Normalization of the data is, thus, a crucial pre-processing step in metabolomic studies since it aims to reduce these differences so that all samples become comparable in terms of absolute intensities, and only profile changes or relative intensity ones are detected. This step assumes particular relevance in cell culture studies where drugs cytotoxicity is evaluated since, for increased times of exposure, the number of cells in treated groups is half or less than that of control groups. Normalization is applied to each spectrum (corresponding to a row in the data matrix) typically by dividing each point by a constant, which can be determined in several different manners. A commonly used way of determining this normalization factor is to divide each variable by the total integrated intensity (total area) of its spectrum (Veselkov *et al*., 2011). However the metabolic profile of MG-63 cells is dominated by broad and intense resonances attributed to lipid fatty acid acyl chains which gain even more importance when cells

are exposed to certain drugs. In this and other similar cases, the normalization to total area particularly affects the normalization of low intensity signals: the richer the spectrum in lipid signals, the higher is the total area and so, the less importance is attributed to small resonances after normalization. Therefore, to overcome this, an alternative normalization method was applied throughout this work: probabilistic quotient normalization (PQN) (Dieterle *et al*., 2006). This method uses a spectrum or set of spectra (for instance, the spectra of control samples when studying drug-induced effects) as reference to calculate the most probable dilution coefficient of the whole set of samples, thus reducing the contribution of exceptionally concentrated compounds. For that, the method calculates the quotient between each variable (point) of each spectrum and the median value of the given control group. Then, the median value of all quotients – also referred as the most probable quotient – is chosen and used as normalization factor for each sample (Dieterle *et al*., 2006).

Data scaling constitutes another important pre-processing step, where each variable is divided by a scaling factor. In projection based methods, compounds present in higher concentrations are given higher importance and can dominate the projections, hindering potentially valuable changes in metabolites present in lower concentrations (Smolinska *et al*., 2012; Xia *et al*., 2013). There are several ways in which data scaling may be performed (Ebbels *et* al., 2011; Craig *et* al., 2006; van den Berg *et* al., 2006; Worley *et al*., 2013; Smolinska *et al*., 2012; van der Berg *et al*., 2006), the main comprising: 1) mean centering, that compensates for differences between low- and high-concentrated compounds, by converting all values to vary around zero instead of around the mean of the compound level; 2) Unit Variance, also known as auto-scaling, which applies mean centering (subtraction of sample mean value) and divides each variable by its standard deviation; 3) Pareto scaling, with which after mean centering each variable is divided by the square root of its standard variation; 4) range scaling, in which mean centered data are divided by the difference between the minimal and the maximal concentration of a metabolite (influenced by outliers); 5) Vast (VAriable STability) scaling, consisting of an auto-scaling divided by the coefficient of variation of that variable; and 6) level scaling which addresses relative responses by using the mean as scaling factor. In this thesis, mean centering, Unit Variance and Pareto scaling were applied to the spectral data. Unit Variance was the scaling method chosen as it attributes equal importance to all metabolites, independently of their concentrations, thus enabling low concentrated compounds to be identified as varying

importantly with drug exposure. Nevertheless, mean centering was also occasionally used to unveil time course trajectories of samples.

2.3.2. Multivariate Analysis (MVA) Methods

In order to handle the complex data obtained in metabolomic studies and obtain reliable models that may successfully classify each sample and identify relevant profile differences between sample groups, multivariate statistical methods (chemometrics) are needed. Indeed, MVA is an indispensable tool in metabolomics, since it enables the observation and analysis of several statistical variables at a time, searching for consistent patterns of variation that may account for samples' grouping and biomarker identification (Madsen *et al*., 2010). MVA comprehends both unsupervised and supervised approaches, differing in the quantity and type of information that is provided about the samples. In unsupervised methods, computations are performed without any information on sample classes, for instance control *vs* drug-treated, maximizing the main sources of variations and enabling a blind identification of outliers, trends (for instance, temporal ones) or grouping tendencies. Principal Component Analysis (PCA) is the most extensively used unsupervised method in metabolomic studies and will be described in detail below. There are many other unsupervised methods available such as Hierarchical Cluster Analysis (HCA), K-means, Self-Organizing Maps (SOM) and Non-Linear Mapping (NLM) (Lindon *et al*., 2007; Smolinska *et al*., 2012). On the other hand, supervised methods require *a priori* information on samples grouping, computing models with the objective of maximizing differences between the established classes. Thus, they are crucial in metabolomic studies since enable, besides classification, sample prediction. Partial Least Squares-Discriminant Analysis (PLS-DA) and its orthogonal variation (OPLS-DA) are some of the most used supervised methods and will be described in detail in this chapter. Nonetheless, other supervised methods exist such as Soft Independent Modeling of Class Analogy (SIMCA), Artificial Neural Networks (ANN) or canonical correlation. (Lindon *et al*., 2007; Smolinska *et al*., 2012)

2.3.2.1. Principal Components Analysis (PCA)

PCA calculates linear combinations of the original variables producing much fewer and more informative factors called Principal Components (PCs), which describe decreasing amounts

of data variance (Trygg *et al*., 2007). PCs are orthogonal to each other and are linear combinations of the variables contained in the original matrix **X** according to Equation 2.9, where the matrix of projections of **X** is designated by **T**, corresponding to the scores, **P** is the loadings matrix and **E** is the residual matrix.

$$X = TP^T + E \qquad |\text{Eq. 2.9}|$$

The projection of observations/samples into this low-dimension model plane formed by the PCs is visualized as a scores plot, where each point corresponds to a sample spectrum, enabling the identification of groups, trends and outliers through the analysis of their relative position in the plot – similar observations appear close in the scores plane. Figure 2.14 shows a global scheme of the general computation of a PCA model from the original dataset is shown. As can be seen, the multidimensional matrix **X** is projected into a two-dimensional space in which the main variation of the matrix is contained is the two first calculated components (or PCs). The scores plot, by means of relative position of the observations, translates the most relevant original information into similarities or differences between samples and finally, the loadings plot explains which variables are responsible for those similarities/differences between the observations (Trygg *et al*., 2007).

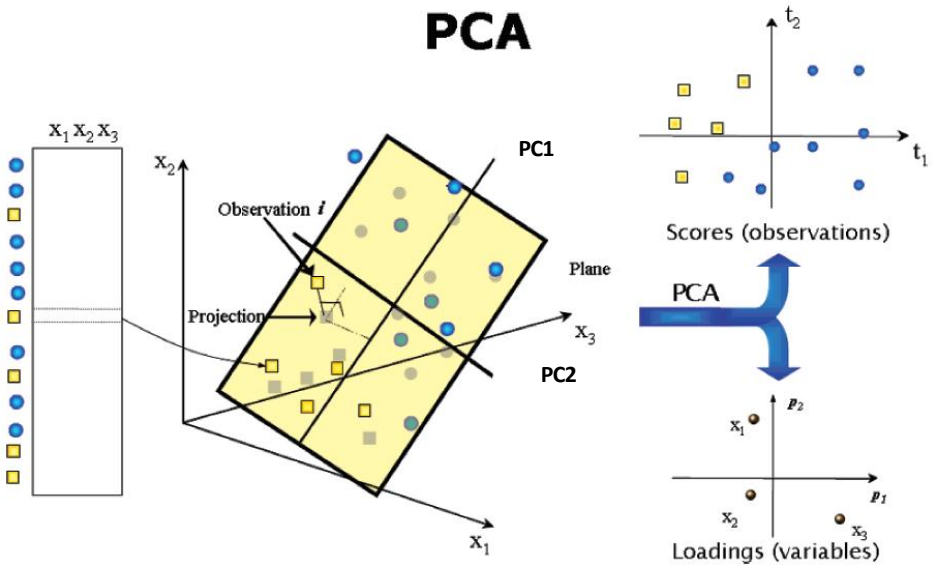

Figure 2.14. Scheme of the construction of a projection-based PCA model (adapted from Trygg *et al*., 2007).

The loadings plot describes the influence of the variables (e.g. chemical shift, intensity) in that model plane, and the relation among them. The direction of the distribution of the

observations in the scores plot corresponds to that of the loadings plot, and *vice versa* (Trygg *et al*., 2007; Lindon *et al*., 2007).

2.3.2.2. Partial Least Squares and Orthogonal Partial Least Squares – Discriminant Analysis (PLS-DA and OPLS-DA)

Once the overall tendencies are revealed by unsupervised approaches, supervised methods may be applied to the data in order to maximize grouping, thus optimizing the recovery of information that explains it. Supervised methods make use of *a priori* knowledge to find out patterns and rules that enable the prediction of new data. PLS and OPLS are examples of supervised methods commonly used in metabolomics studies and can be used Discriminant Analysis (DA) with the objective of establishing an optimal position to trace a discriminant surface that best separates classes. (Trygg *et al*., 2007; Wiklund *et al*., 2008) PLS-DA is a regression method which intends to find out the relationship between two data matrices referred to as **X** (e.g. NMR data) and **Y** (information about sample membership, i.e. controls *vs* drug-treated). Like PCA, PLS-DA is a projection-based approach that assumes that data variations can be reduced in low dimension spaces called latent variables (LVs), which constitute linear combinations of the original variables. The first calculated LV in a PLS-DA contains the highest amount of variation between classes which, in turn, may not correspond to the highest source of variation within the dataset. (Trygg *et al*., 2007; Lindon *et al*., 2007; Smolinska *et al*., 2012) The model can then be expressed in terms of **X** and **Y**, as given in Equations 2.9 and 2.10, where **T** represents the scores common to **X** and **Y** matrices, respectively, **P** and **C** the respective loading matrices and **E** and **F** the respective residual information in the two matrices.

$$Y = TC^T + F \qquad |\text{Eq. 2.10}|$$

The PLS-DA model can also be given by Eq. 2.11, in which **Y** matrix is expressed in terms of **X**, where **b** represents the regression coefficients of each variable and **r** the residual information of the matrix.

$$Y = Xb + r \qquad |\text{Eq. 2.11}|$$

The orthogonal transformation of PLS-DA, OPLS-DA, intends to separate the systematic variation of **X** matrix into two parts: one linearly related to **Y** and one orthogonal (unrelated) to **Y**.

This division of **X** matrix facilitates the model interpretation. The OPLS-DA model contains two modeled variations: the response-orthogonal ($\mathbf{T_oP^T_o}$) and the response-predictive ($\mathbf{T_pP^T_p}$), as given by Eq. 2.12. For the modeling of **Y**, only the Y-predictive variation ($\mathbf{U_pQ'_p}$) is considered (Eq. 2.13) (Lindon *et al*., 2007; Smolinska *et al*., 2012).

$$\text{Model of X: } X = T_oP^T_o + T_pP^T_p + E \qquad |\text{Eq. 2.12}|$$

$$\text{Model of Y: } Y = T_pC^T_p + F \qquad |\text{Eq. 2.13}|$$

For comparable number of LVs, OPLS-DA and PLS-DA possess comparable predictive powers. OPLS has advantages over PLS-DA in what refers to interpretability, since orthogonal modelling filters out irrelevant variations; nevertheless it does not replace PLS-DA (Smolinska *et al*., 2012).

2.3.2.3. Statistical Total Correlation Spectroscopy (STOCSY)

Statistical Total Correlation Spectroscopy (STOCSY) is a very useful approach for peak assignment and determination of metabolic correlations (Cloarec *et al*., 2005). In this work this method was used to achieve both objectives. STOCSY is based on correlation properties inside the matrix **C** (correlations between peak intensities), enabling the identification of positive correlations between peaks that arise from a particular spin system. STOCSY has also been used to identify molecules involved in the same metabolic pathways, based on their biological covariance, resulting in different colorations for positive and negative correlated molecules, corresponding to variations in the same and opposite directions respectively. STOCSY computations are based on Eq. 2.14, where **X1** and **X2** refer to the autoscaled data matrices (Cloarec *et al*., 2005).

$$C = \frac{1}{n-1} X_1^T X_2 \qquad |\text{Eq. 2.14}|$$

STOCSY was developed to increase the information recovery from complex 1D NMR spectra, but can also be applied to 2D data and to homo or heteronuclear comparisons within the spectral data. Recent developments combine STOCSY and HCA in an approach designated by CLASSY (Cluster Analysis Statistical Spectroscopy), with some advantages over conventional STOCSY, namely increased accuracy with which the correlations between peaks of the same molecule are determined. Correlations between datasets acquired through two different

experimental techniques (e.g. NMR and MS) can also be determined by heterospectroscopic STOCSY (Smolinska *et al*., 2012).

2.3.2.4. Validation of MVA Models

The study of biological samples through metabolomics implies the existence of many more variables (*e.g.* chemical shift in NMR or *m/z* in MS) than samples, which increase the possibility of finding a model that fits the data showing an apparently good separation of sample groups in the multivariate space. Although the apparent geometrical grouping obtained in supervised models' scores plots, these can fail to extract differences between groups (Westerhuis *et al*., 2008). For this reason, validation emerges as one of the most valuable tools in metabolomics studies, since it enables the determination of robustness of the model and its predictive ability. In typical metabolomic studies which analyse for instance control *vs* drug-treated cells, the whole dataset must be divided into a training dataset, that will be used to develop and test the model and a second validation dataset, in which model accuracy will be tested, i.e., check if the model classifies a new sample in the correct group. This is called external validation, which is now considered as the best means to establish a reliable predictive performance of the model (Smolinska *et al*., 2012).

The reduced number of biological samples commonly available forces the use of the whole sample groups as training set and, in these cases, Cross Validation (CV) can be used to prove how well a model works for the prediction of new samples. CV is thus a reliable approach to evaluate the model predictive power, which consists of an initial division of the data into a number of groups with which training models are built, leaving just one group to be used for the prediction test (Westerhuis *et al*., 2008). Permutation tests constitute another way of performing model validation, through which is tested if a given model is significantly different from a null hypothesis model (randomly obtained). Permutation tests imply that sample grouping information is randomly permuted as model is recomputed. This enables the robustness of the model to be determined (Westerhuis *et al*., 2008). The robustness of a model can also be evaluated through parameters obtained through confusion matrices: classification rate (CR), sensitivity and specificity. Confusion matrices are composed by false positives (FP), false negatives (FN), true positives (TP) and true negatives (TN) as shown in Figure 2.15a. The CR refers to the percentage of samples that were correctly classified in the model, sensitivity (also referred to as true positive

rate, TPR) indicates the number of true positives as a percentage of all positives, 1-specificity (or false positive rate, FPR) refers to the number of false positives as a percentage of all negatives, calculated according Eq. 2.14 to 2.17, respectively.

$$CR = \frac{TP+TN}{TP+TN+FP+FN} \quad |\text{Eq. 2.14}|$$

$$Sensitivity\ (TPR) = \frac{TP}{TP+FP} \quad |\text{Eq. 2.15}|$$

$$1 - Specificity\ (FPR) = \frac{FP}{TN+FN} \quad |\text{Eq. 2.16}|$$

The plot of sensitivity (TPR) *vs* 1-specificity (FPR) results in the Receiver Operating Characteristic (ROC) plot. In this work, ROC plots were built from sensitivity and specificity of the PLS-DA model and calculated through Monte Carlo Cross Validation (MCCV). To perform MCCV, the original dataset is divided into a training and a prediction set, in which the latter is used for class membership prediction. An important feature of MCCV is that it is usually performs at least 500 iterations, and for each the Q^2 value and confusion matrix are determined. Moreover, MCCV can be repeated for permuted classes and if the model is robust enough, a complete separation between true and permuted classes in observed in the ROC plot, as shown is Figure 2.15c (Xu and Liang, 2001; Xia *et al*., 2013).

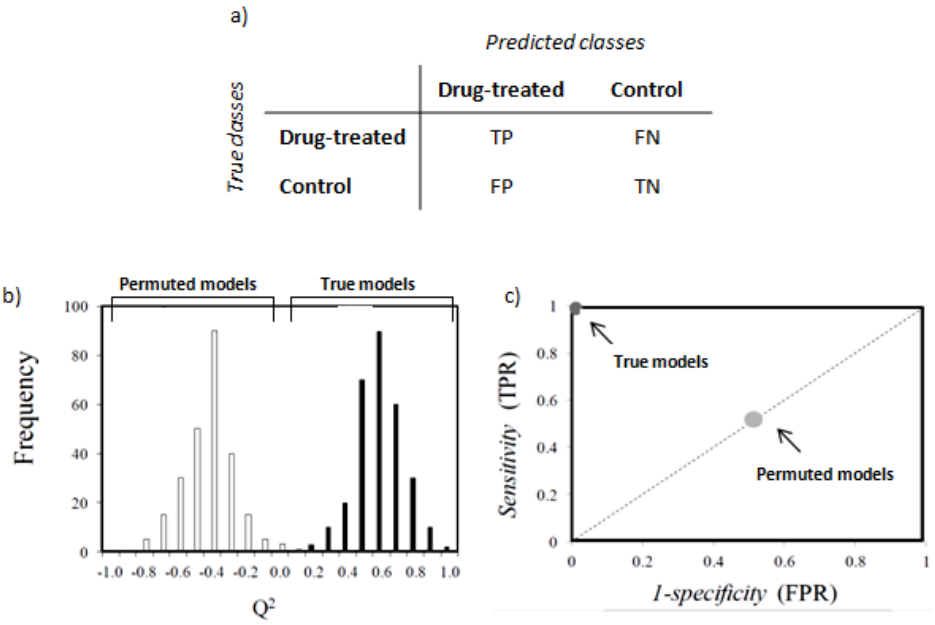

Figure 2.15. Examples of a) confusion matrix obtained for two classes, b) Q^2 distribution of true and permuted models and c) MCCV-obtained representations of ROC space plot (adapted from Diaz, 2014).

PLS-DA computations also provide a parameter that evaluates the discriminant power of the model, called predictive power and given by a Q^2 parameter. For robust models this parameter is closer to 1, meaning that predictive classification almost always matches real classification. Due to variation inherent to each sample (even within the same class) it is very difficult to achieve the ideal Q^2 value of 1. By comparing the Q^2 distribution of the permuted models with original ones, evaluation of the predictive power of the model can be made: minimal overlapping between the Q^2 of true (original) and permuted models indicates a model with an interesting predictive power (Figure 2.15b) (Westerhuis *et al*., 2008).

2.3.3. Statistical Methods

Univariate analysis presents some advantages over multivariate analysis, such as ease of application, ease of interpretation and ease of communication of the results. Nevertheless, single variables and markers do not provide the comprehensive knowledge that metabolomic studies intend to achieve. The analysis of biological phenomena by metabolomics implies a comprehensive characterization of the biological processes, which is translated in a metabolic picture that simultaneously correlate several compounds from the sample under study, what can only be achieved with multivariate analysis. Still, an increasing number of metabolomic studies apply both univariate and multivariate statistical methods. This can be explained by the complementary information that the two approaches provide: on the one hand, MVA looks for the metabolic relationships reflected in metabolites correlation and variation and univariate methods compares individual variations, independently on the whole profile. This means that a particular metabolite variation can be found relevant through MVA and not show individual statistical significant when analysed apart from the rest of the profile, and *vice-versa*. This may be explained by the high complexity of the dataset, with a considerable number of non relevant variables that mask important information (Saccenti *et al*., 2014).

Univariate methods can be parametric or non-parametric, for data that follows a normal distribution or not, respectively. In this work, univariate analysis was used to compare groups of three (sometimes only two) samples and, since no reliable determination can be made on data normality in such a reduced sample group, unpaired t-test (parametric) was used for *p*-value calculations.

3. Experimental Procedures

The present chapter describes the experimental procedures carried out throughout this work, therefore comprising cell culturing, sample preparation for analysis, NMR data acquisition and data analysis.

3.1. Cell Lines and Biological Assays

This section describes the cell growth and drug exposed protocols performed in biological assays with the osteosarcoma MG-63 and osteoblast HOb cell lines.

3.1.1. Cell Lines

Two human (adherent) cell lines were tested throughout this work: the MG-63 cancer cell line and a healthy osteoblast cell line (the HOb cell line). Figure 3.1 shows the microscopic appearance of the corresponding cells in terms of cell size and morphology.

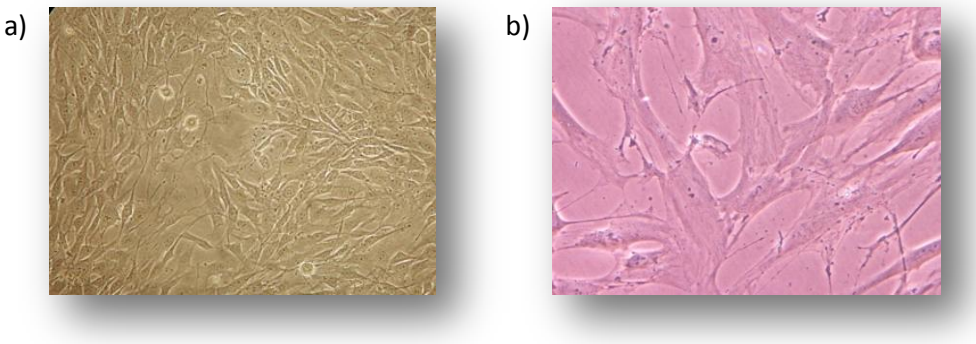

Figure 3.1. Optical microscope photographs (x 200) of the human a) MG-63 and b) HOb cell lines.

A study by Pautke and co-workers (Pautke *et al*., 2004) offers a characterization of three osteosarcoma cell lines (MG-63, Saos-2 and U-2 OS), in comparison to human osteoblasts. Regarding morphology, such results evidenced that the mean size of attached osteosarcoma cells is around 1/6 that of osteoblasts (as clearly evidenced in Figure 3.1) and, unlike osteoblasts, the size of the cancer cells does not vary according to their degree of confluence. Moreover, strictly referring to MG-63 *vs* HOb cells, the former have an oval to spindle-shape, without branching-cell processes while healthy cells are less consistent in shape (although still having a characteristic

morphology, illustrated in Figure 3.1) displaying several elongated and prominent cell branching processes.

The human MG-63 osteosarcoma cells are morphologically classified as fibroblasts (due to their elongated shape) and were established from an osteosarcoma of a 14 year old Caucasian male (Billiau *et al*., 1977; Heremans *et al*., 1978). This cell line has a population doubling time of approximately 24 hours and can be propagated for several tens of passages, with preservation of morphological characteristics and doubling times. These properties explain the common choise of this cells line for model studies in different research contexts. Human osteoblasts have the ability to synthesize bone matrix. The HOb cells used here were isolated from normal adult human bone, cryopreserved at their second passage and may be propagated for at least 10 population doublings (according to the information of the supplier and our own experience).

3.1.2. Cell Culture

The human MG-63 OS cells (kindly provided by the Associate Laboratory IBMC/INEB, Portugal) are adherent and grow in monolayers. Cells were grown in Minimum Essential Medium (MEM, Sigma-Aldrich), supplemented with 10% heat-inactivated fetal bovine serum (FBS, Alfagene), 1 mM sodium pyruvate (Sigma-Aldrich), 1 mM non-essential amino acids (Sigma-Aldrich) and antibiotics (penicillin-streptomycin, Sigma-Aldrich) and maintained under humidified atmosphere, at 5% CO_2 and 37˚C (MCO-19A Incubator, SanyoElectric Co., Ltd.). Due to the high number of cells needed for the NMR experiments (*ca*.10 x 10^6 per sample), cells were grown in 150 cm^2 cultures flasks. When a confluence of *ca* 90% was reached, the cells were washed with phosphate buffered saline (PBS, pH 7.4, Sigma-Aldrich) and harvested with the addition of a 0.05% trypsin/ethylenedieminetetraacetic acid (EDTA, Sigma-Aldrich) solution. After detachment of the cells, trypsin was immediately neutralized by adding twice volume of complete MEM. Cell suspensions were then centrifuged at 1100 rpm for 5 minutes, at 21˚C (MPW-350 Centrifuge), and resuspended in a known volume of MEM, from which 100 µL were taken for cell counting through the Trypan blue assay (either to continue growth or to proceed for drug exposure experiments).

Human osteoblasts (HOb, 406-05a, Sigma-Aldrich), similarly to MG-63, are adherent cells that grow in monolayers. In this work, these cells were cultured in Osteoblast Basal Medium (Sigma-Aldrich) supplemented with Osteoblast Growth Supplement and were maintained under a humidified atmosphere, at 5% CO_2 and 37˚C. Although of larger dimensions than the MG-63 cells,

a good NMR signal-to-noise ratio still required *ca*. 1 x 10^6 cells per sample, and for this reason HOb cells were grown in 150 cm^2 cultures flasks. According to the supplier's instructions, cells were seeded at a 10000 cell/cm^2 density and subdivided at *ca.* 80% confluence. The cells were then washed with Hank's Balanced Salt Solution (HBSS, Sigma-Aldrich) and harvested by addition of a 0.05% trypsin/EDTA solution (just enough to cover the bottom of the flask). Due to the increased sensitivity of these cells, compared to the tumour OS cell line, as soon as cells became round (*i.e.* detached) a trypsin neutralizing solution (5% FBS in HBSS) was added to stop trypsin action. Cells were then centrifuged at 1200 rpm, at 21˚C for 5 minutes and resuspended in a known volume of *Osteoblast Growth Medium*, from which 100 µL were taken for cell counting by Trypan blue assay, either to continue growth or to proceed for drug exposure experiments.

3.1.3. Cytotoxic Evaluation

3.1.3.1. Drug Exposure and IC_{50} Determination

Single Drug Exposure

For single drug exposure experiments, 5x10^6 MG-63 cells were plated in 100 mm diameter Petri dishes, corresponding to a density of approximately 80 000 cells/cm^2, in order to provide sufficiently high cell number for NMR analysis. After waiting for 24 hours for cells to adhere, the assays were initiated (t = 0h) by adding a volume of stock solution of each drug to be tested at its IC_{50} concentration in the Petri dish containing 12 mL of MEM culture medium. All cells were used after 21-30 passages, if not referred otherwise. At each time point, cells were harvested by trypsinisation, washed with PBS pH 7.4 and centrifuged (6 minutes, 1000 rpm, 21˚C). Cells were then added the deuterated solutions for NMR analysis (section 3.2.1.1.) prior to storage at -80˚C until spectroscopic analysis. For each drug, three independent assays were carried out, with duplicates for each condition (time point and drug dosage). cDDP was obtained from Sigma-Aldrich, DOX and MTX from Fisher Scientific and Pd_2Spm was kindly provided by Molecular Physical-Chemistry (QFM) I&D Unit, Faculty of Science and Technology, University of Coimbra. The different single drug exposure studies performed with MG-63 cells are listed in Table 3.1.

Table 3.1: Solutions and time course conditions used in single drug assays in MG-63 cells.

Drug	Solvent	Drug concentration	Time points (h)	Controls group
cDDP (*study 1*)	PBS	30 µM 50 µM	0, 12, 18, 24, 48	PBS (120 µL)
DOX	Mili Q water	3 µM	0, 12, 24, 36, 48	Mili Q water (12 µL)
MTX	DMSO	3 µM	0, 12, 24, 36, 48	DMSO (12 µL)
Pd_2Spm[a]	DMSO (6%) in PBS	12 µM	0, 12, 24, 36, 48	PBS (120 µL)
cDDP (*study 2*)[a, b]	PBS	30 µM	0, 12, 24, 36, 48	PBS (120 µL)

[a] Only two independent assays were considered for analysis.

[b] Performed in parallel with Pd_2Spm assays, as a drug exposure reference.

HOb cells were used for NMR experiments upon exposure to cDDP and Pd_2Spm. In these assays, $1x10^6$ cells were seeded in 100 mm diameter Petri dishes (corresponding to a density of approximately 15 000 cells/cm^2) and, after waiting 24 hours for cells to adhere, experiments were initiated (t = 0h) by adding the appropriate volumes of cDDP or Pd_2Spm stock solutions that led to an IC_{50} concentrations as previously determined for MG-63 cells (Table 3.1). Due to the high costs of the cell culture medium and considering the time-consuming task of growing large numbers of HOb cells due to their long doubling time, experiments with these cells were confined to the time points 0 and 24 hours. After exposure to each drug, cells were harvested by trypsinisation, washed with HBSS and centrifuged at 1200 rpm, at 21˚C for 5 minutes. Cells were then prepared for NMR analysis (section 3.2.1.1.) and stored at -80˚C until spectroscopic acquisition. Two independent assays were carried out, with duplicates for each condition (time point and drug dosage). All cells were used in passages numbers from 4 to 10.

Drug Combination Exposure

Regarding assays of MG-63 cells exposure to drug combinations (drug cocktails), a similar protocol was followed, although dosages had to be adjusted in order to enable a sufficiently high percentage of living cells to be obtained for NMR analysis. In this line and according to the drug concentrations used in clinic (described in the EURAMOS protocol, http://212.219.75.232/ euramos /euramos_i_trial.asp), the IC_{50} concentration of DOX (3 µM) was used as a reference to determine the dosages of cDDP or Pd_2Spm (4.8 µM) and MTX (480 µM) to use in these assays. Regarding the MTX concentration, preliminary tests revealed that a decrease of up to 100 times in concentration, resulted in a similar decrease in proliferation rates of MG-63 cells, thus 4.8 µM was selected to be used in these assays. As a matter of simplicity and due to cell culture limitations, the weeks scale in the EURAMOS protocol was converted into a days scale in cell experiments,

and a single dose of methotrexate was administered to cells. Solutions and time course conditions used are listed in Table 3.2.

Table 3.2: Solutions and time course conditions used in drug combination assays in MG-63 cells.

Drug/ Drug combination	Solvent	Drug concentration	Time points (h)	Controls group
DOX + cDDP	Mili Q water	3 µM	24, 48, 72, 96	PBS
	PBS	4.8 µM		
DOX + Pd_2Spm	Mili Q water	3 µM	24, 48, 72, 96	PBS
	PBS	4.8 µM		
MTX	DMSO	4.8 µM	24*	PBS

* after 72h treatment with DOX+cDDP or DOX+Pd_2Spm.

MG-63 cells were seeded at $5x10^6$ cells *per* dish and after waiting 24h for cells to adhere the experiment was initiated by adding cDDP+DOX or Pd_2Spm+DOX. Then, at 24, 48 and 72 hours duplicates of each condition were collected and handled as previously described. At 72 hours, MTX was added to either cDDP+DOX or Pd_2Spm+DOX exposed cells and after an additional 24 hours period these samples were also collected, so that changes attributed just to MTX action (and not the whole cocktail) could be assessed. Figure 3.2 schematically presents the entire process of drug administration and sample collection.

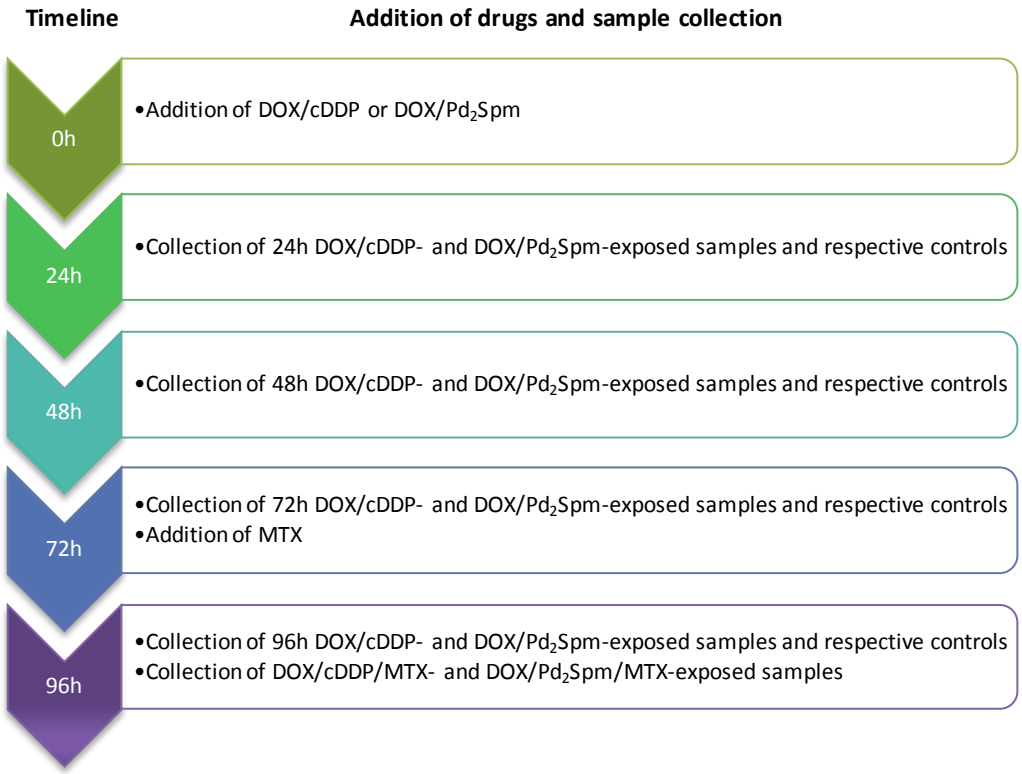

Figure 3.2. Schematic representation of assays of cells exposure to drug combinations.

Duplicates were obtained for each condition (mixed together whenever required to ensure a good signal-to-noise ratio) and 3 independent assays were performed. Similarly to single drug assays, cells were then lysed and stored at -80˚C until NMR analysis.

3.1.3.2. Trypan Blue Assay

The Trypan blue colorimetric assay (Strober, 2001) was used to assess the number of morphologically intact cells (cells with undamaged cell membranes), either for seeding purposes or to determine the extent of cell death at each established time point of drug exposure. For this purpose, after the washing steps, the cells were incubated with a solution of Trypan blue dye (0.4 % *(w/v)* in PBS, Sigma-Aldrich) and then counted by observation under the optical microscope using a Neubauer-counting chamber (Boeco). As a result, the number of cells with intact membranes and, therefore, dye excluding was expressed in terms of mean ± standard deviation.

3.1.3.3. MTT Assay

The MTT assay (Mosmann, 1983) was used to estimate the IC_{50} concentration for cDDP, DOX and MTX. MG-63 cells were plated on 24-well plates at 100000 cells per well. Cells were enabled to adhere for 24 hours, treated with different concentrations of each drug (cDDP: 10, 30 and 50 µM; DOX: 0.1, 1, 3 and 6 µM; MTX: 0.1, 0.5, 1, 3 and 5 µM) and incubated in a humidified atmosphere at 37˚C, 5% CO_2. After 24 hours of drug exposure, cells were washed with 1 mL of PBS, 250 µL of MTT solution (0.5 mg/mL in PBS, Sigma-Aldrich) was added to each well and plates were incubated for 3 hours. The violet MTT formazan precipitate was then solubilised by adding 500 µL of dimethylsulfoxide (DMSO, Sigma-Aldrich) to each well and absorbance was measured at 570 nm on a microplate reader (Biotek µQuant MQX200 UV-Visible Spectrophotometer, *Gen5* software, Biotek). Experiments were performed in triplicate and each of 3 independent assays. Absorbance of control cells was taken as 100% and the values of treated cells were calculated as a percentage of the control. Accordingly, IC_{50} values of 30, 3 and 3 µM were determined for cDDP, DOX and MTX, respectively, at 24 hours of drug exposure.

3.1.3.4. Reversibility Assays

Reversibility assays were performed with a view to understand if cDDP- and Pd_2Spm-induced effects are reverted after drug removal. Upon a 24 hours treatment with either cDDP or Pd_2Spm in the same conditions as previously described for *Single Drug Exposure* (see section 3.1.3.1), the culture medium from control and treated Petri dishes was removed, MG-63 cells were washed with PBS and 12 mL of fresh, drug-free medium was added. After a 3 days recovery period, MG-63 cells were collected and prepared for NMR analysis as described in section 3.2.1.1.

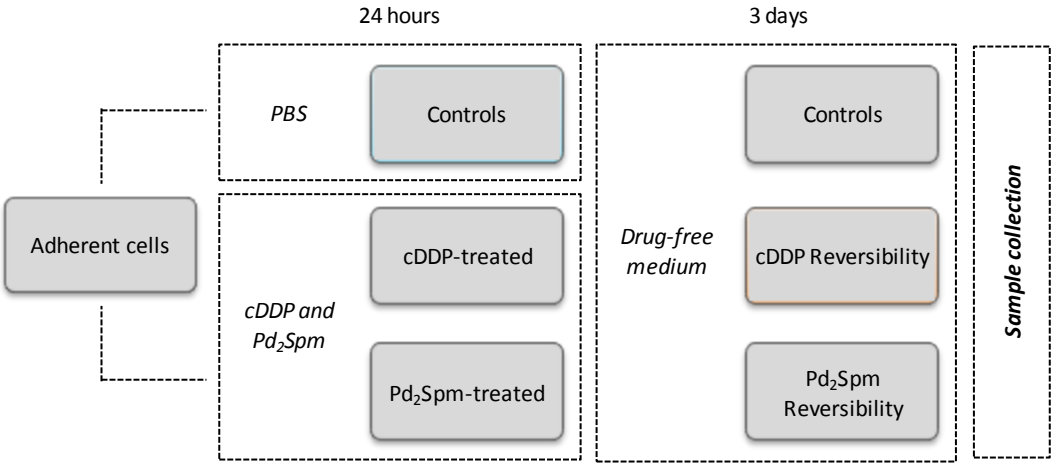

Figure 3.3. Schematic representation of the reversibility assays. PBS: phosphate buffered saline.

Reversibility assays were also performed with HOb cells, following the protocol described for MG-63 cells with HOb cell culture specificities (culture medium, saline solution, cell's seeding density).

3.1.4. Antiproliferative Activity Evaluation: SRB Assay

The colorimetric SRB assay (Skehan *et al.,* 1989) was used to determine the IC_{50} concentration for Pd_2Spm of MG-63 cells, to obtain the growth curves of the HOb cells and to evaluate the influence of drug combination treatment in these cells.

For IC_{50} determination, MG-63 cells were seeded on 24-well plates at 100 000 cells *per* well. After adhering, cells were treated with increasing doses of Pd_2Spm (1, 3, 5, 10, 15, 20 and 30 µM) and incubated in a humidified atmosphere at 37˚C, 5% CO_2. After 12, 24, 36, 48 and 72 hours of drug exposure, cells were washed twice with PBS and once with miliQ water (to remove the salt).

After water removal in the incubator for 10 minutes, the cells were fixed overnight with 2 mL/well of 1% acetic acid in methanol, at -20˚C. The solvent excess was then discarded and the plate was left to dry at room temperature. The same repeated was performed for each plate (corresponding to a different exposure period), after which 1mL of SRB (Sigma-Aldrich) 0.5% in acetic acid (g/v) was added to each well and plate was incubated in the dark for 1 hour, at 37˚C. MG-63 cells were washed with 1% acetic acid solution to remove non-bonded SRB and dried overnight, at room temperature. The amount of SRB bounded to protein of cells was dissolved by adding 2 mL of a 10 mM Tris solution at pH 10, and absorbance was read at 540 nm (Tris solution was used as blank). Cell density was expressed in %, according to Eq 3.1.

$$\text{Cell Density}\ (\%) = \frac{Abs_{treated} - Abs_{0h}}{Abs_{control} - Abs_{0h}} \times 100 \qquad |\text{Eq. 3.1}|$$

Regarding the growth curves, after an initial replication of the HOb cells in *Osteoblast Growth Medium*, osteoblasts growth was also tested in another culture media also commonly used for establishing and growing osteoblast primary cells and/or other osteoblast-like cells. Actually, besides the *Osteoblast Growth Medium* recommend by the cell's supplier, HOb cells can also be cultured in DME/F12 (1:1 mixture of Dulbecco's Modified Eagle's Medium – DMEM – and Ham's F-12 Nutrient Mixture) (Piva *et al*., 2011) or McCoy's medium (Ma *et al*., 2011) (with or without the addition of ascorbic acid, at 30 µg/mL). $10x10^3$ HOb cells/well were seeded in 12-well plates, in triplicate. Due to the marked difference in growth rates in relation to other tested media, *Osteoblast Growth Medium* was chosen to culture HOb cells. For 12 consecutive days, at each 24 hours, one plate of cells was collected and prepared for the SRB assay, as described above for MG-63 cells (saline solution used for HOb cells washing steps was HBSS). As an example, the growth curve of HOb cells in *Osteoblast Growth Medium* is shown in Figure 3.4.

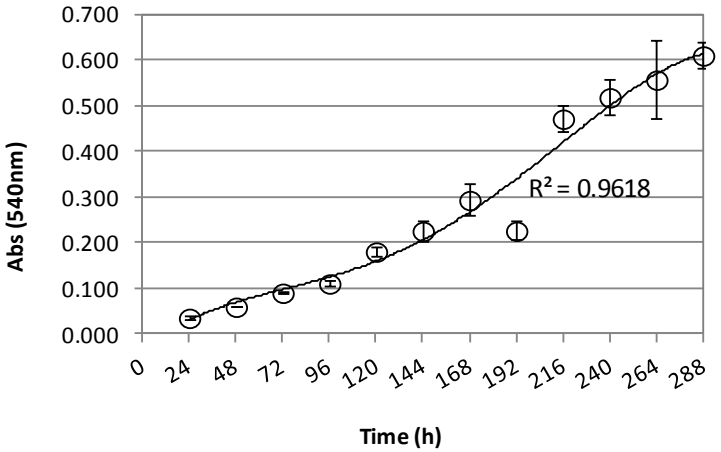

Figure 3.4. Growth curve of HOb cell line, determined by SRB assay during 12 days.

In exponential growth, HOb cells were shown to have a doubling time of around 72 hours (3 days), which is three times longer than that of MG-63 cells (around 24 hours).

3.1.5. Apoptosis Detection Using FITC Annexin V/Propidium Iodide

MG-63 cells were cultured in 6-wells plates and after appropriate growth conditions and exposure to IC_{50} concentrations of either cDDP or Pd_2Spm, each well was washed with 2 mL of PBS. Cells were then detached by the addition of 500 µL trypsin/EDTA solution, after which 1 mL of MEM medium was added to inactivate trypsin. Cells were harvested and counted by the Trypan blue assay. Cell suspensions were centrifuged at 2250 rpm, for 5 minutes at 4˚C, supernatant discarded and 1 mL of PBS added without pellet resuspension. After a second centrifugation, the supernatant was discarded and each pellet was resuspended in 1X Annexin Binding buffer to a suspension of $1x10^6$ cells/mL. 100 µL of each cell suspension was transferred to a 5 mL tube to which 5 µL of FITC Annexin V and 5 µL of Propidium Iodide (PI) were added. After 15 minutes incubation in the dark, at room temperature, 400 µL of 1X Annexin Binding Buffer was added to each tube. The refered buffers and solutions were part of the FITC Annexin V apoptosis detection kit (BD Pharmingen). Samples were then analysed by flow cytometry within 1 hour (maximum). At last 10000 events per sample were acquired and the percentage of cells in each quadrant was estimated according to Eq. 3.2. Three independent assays were performed in triplicate.

$$\text{Cells in each quadrant } (\%) = \frac{\text{no.of cells in each quadrant}}{\text{total no. of cells}} \times 100 \qquad |\text{Eq. 3.2}|$$

3.2. Analysis by NMR Spectroscopy

3.2.1. Cell Sample Preparation for NMR Analysis

3.2.1.1. Preparation of Cells and Cell Extracts

After cell growth and drug exposure procedures, cells were washed with PBS (or with HBSS, for HOb cells), suspended in 1mL PBS/D_2O (0.14 M NaCl, 0.0027 M KCl, 0.0015 M KH_2PO_4, 0.0081 M Na_2HPO_4 in deuterated water, pH 7.4), centrifuged (1000 rpm, 6 min, 21˚C) and resuspended in 35 µL PBS/D_2O, to which 5 µL PBS/D_2O containing TSP 0.25% (for chemical shift referencing) were

added. Whenever needed, in order to have a good signal-to-noise relation in NMR data, duplicates of the same condition were mixed. This procedure was based on that described in (Duarte *et al*., 2009). D_2O was acquired from Cortecnet Europe and D_2O containing 0.75% TSP was obtained from Sigma-Aldrich.

Cell Lysis

To obtain a suspension of lysed cells (both MG-63 and HOb), a three-fold cycle of liquid nitrogen dipping and sonication was applied to the frozen samples prepared previously. Finally, and for the sake of safety, all samples from single drug exposure assays were transferred to a sealed NMR disposable insert (*ca* 35 µL) and stored at -80˚C (Duarte *et al*., 2009). Samples from other experimental sets were stored in eppendorfs and transferred at the moment of analysis to the HRMAS rotors.

Trichloroacetic Acid (TCA) Extraction

TCA extractions followed a previously reported procedure (Huang *et al*., 2003) and was applied to samples treated for 48 hours with sole drugs cDDP, DOX, MTX and Pd_2Spm and drug combinations cDDP+DOX and Pd_2Spm+DOX. The control samples collected at 48 hours from cDDP exposure and combination assays were also extracted. This was a meticulous procedure that involved the recovery of the samples already analysed by HRMAS (around 30 µL of pellet), which resulted in some sample loss and precluded the recovery of the entire set of replicates. Table 3.3 lists the samples that were successfully recovered and extracted.

Table 3.3: TCA samples for ^{1}H NMR analysis.

Sample (year)	Time point	Number of Replicates
Control (2009)	48 hours	1
30 µM cDDP (2009)		2
3 µM DOX (2011)		3
3 µM MTX (2011)		3
12 µM Pd_2Spm (2012)		2
Control (2013)		3
4.8 µM cDDP+3 µM DOX		3
4.8 µM Pd_2Spm+3 µM DOX		3

In order to perform this extraction, 200 µL of TCA 6% (prepared from a commercial solution of TCA 20% (w/v), Fisher Scientific) in distilled water was added to the cell pellet (around 70-100 µL), followed by vigorous shaking in a vortex for 20 seconds and placement in an ice bath for 10 minutes. After this period a new 20 seconds vortex cycle was performed just before a 10 min

centrifugation at 13000 rpm, at room temperature. Proteins were precipitated and the acidic extract was transferred to an eppendorf, an equal volume of distilled water being added. The sample was vortexed again for 60 seconds. After this extraction procedure, samples were dried by evaporation under vacuum and were stored at -80˚C until NMR analysis. Dried TCA extracts were solved in 550 µL of sodium buffer prepared in 100% D_2O, vortexed and 500 µL of each sample was transferred to a NMR tube at the moment of analysis.

3.2.1.2. Study of the Influence of Several Factors on the Spectral Quality

Cells Integrity: Intact vs Lysed Cells

After applying the cell growth protocol described in section 3.1.2., different manipulation and storage procedures were employed, in order to evaluate their consequences on cell integrity and ^{1}H HRMAS NMR spectra. This different handling and storage procedures to which MG-63 cells were submitted are schematically represented in Figure 3.5.

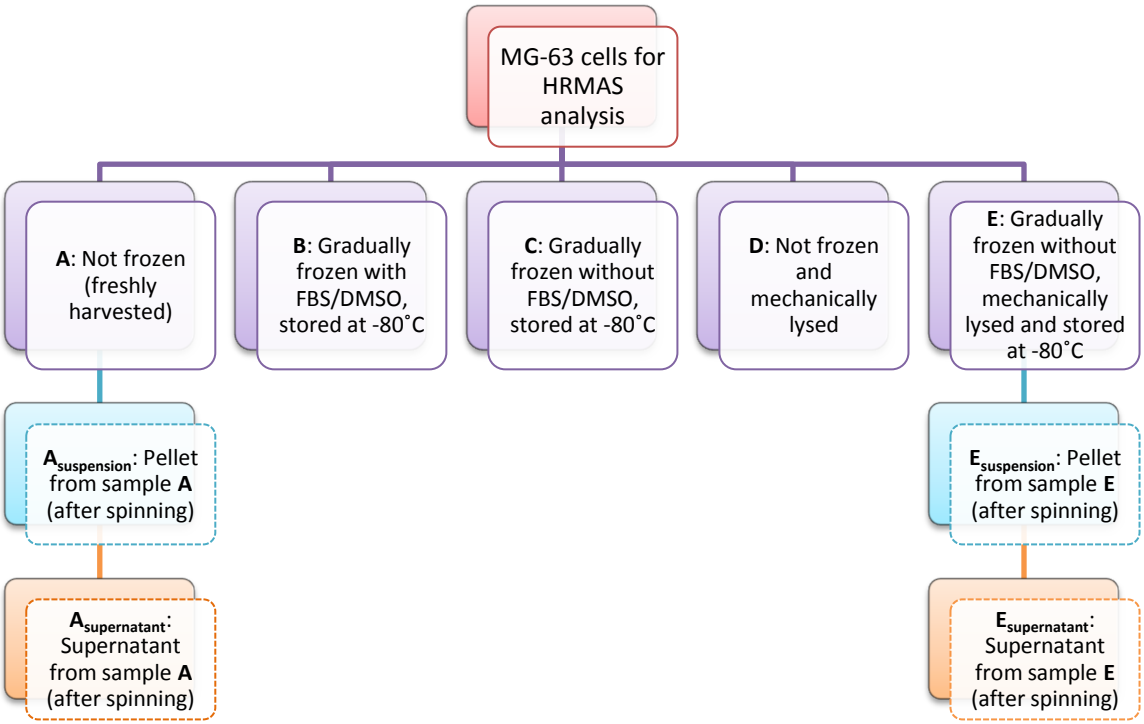

Figure 3.5. Schematic representation of the protocols followed for preparation of cell samples (adapted from Duarte *et al*., 2009). Dashed boxes indicate solution state NMR.

Sample **A** is constituted of MG-63 cells that, upon washing with PBS and PBS/D_2O, were analysed by HRMAS within 2 – 3 hours after harvesting (period during which they were kept

refrigerated at 4˚C), without any freezing process. Samples $\mathbf{A_{suspension}}$ and $\mathbf{A_{supernatant}}$ represent the cell pellet and sample supernatant from **A**, respectively, that were collected after spinning of the sample (HRMAS analysis) and were analysed by solution state ^{1}H NMR. Sample **B** was obtained by suspending the cells in a cryoprotective solution (FBS with 10% DMSO), gradually freezing and storage at -80˚C for *ca.* 1 month (prior to NMR analysis the sample was washed with PBS to remove the cryoprotective agent). Sample **C** resulted from gradually freezing the cell pellets without adding the cryoprotective agent and storing at -80˚C for *ca.* 1 month (cells were thawing immediately prior to analysis). Sample **D** was obtained by mechanical lysis of freshly harvested cells (refrigerated for up to 3 hours) through sonication and dipping into liquid nitrogen. Sample **E** corresponded to cells gradually frozen and kept frozen at -80˚C for *ca.* 1 month, after which lysis protocol was performed. Samples $\mathbf{E_{suspension}}$ and $\mathbf{E_{supernatant}}$ represent the cell pellet and sample supernatant from **E**, respectively, that were collected after spinning of the sample (HRMAS analysis) and were analysed by solution state ^{1}H NMR.

Reproducibility Assays

To evaluate the reproducibility of the cells culture and harvesting procedures, $5x10^{6}$ MG-63 cells were plated in 100 mm diameter Petri dishes. After waiting 24 hours for cells to adhere, the experiment was initiated (t = 0h). At 12, 18, 24 and 48 hours of growth, cells were collected in triplicate, washed with PBS, centrifuged (6 minutes, 1000 rpm, 21˚C), prepared for NMR analysis (as described in section 3.2.1.1.) and stored at -80˚C until HRMAS NMR acquisition. Three independent assays were performed, yielding a total of 9 samples per time point.

Cell Passage Number

In order to understand the influence of the number of cell passages on the metabolic profile of the MG-63 cells, these were continually cultured and divided. When reaching passages 25, 35 and 45, $5x10^{6}$ cells were seeded in 100 mm diameter Petri dishes and harvested 24 hours later. Cells were then prepared for NMR analysis (as described in section 3.2.1.1.) and stored at -80˚C until data acquisition. Only one sample for each chosen passage number was collected, without any further replicates.

The influence of the number of cell passages was also evaluated for MG-63 cells treated with IC_{50} concentrations of cDDP. Accordingly, MG-63 cells with increasing number of passages (#25, #35 and #45) were exposed to 30 µM of CDDP for 24 hours. Only one sample at each chosen passage number was collected (without any further replicates).

Sample Stability During Storage

MG-63 cells at passage number 23 were grown in T-75 cm^2 culture flasks. Once confluence was reached, cells from 10 flasks were harvested, mixed together, washed with PBS and divided into 12 equivalent pools, each of them containing around 8 million cells (determined by the Trypan blue assay). Each cellular pool was prepared for HRMAS NMR analysis and stored at -80˚C until acquisition. The 1st pool was analysed within the next 2 weeks and, whenever possible, a new sample was evaluated every 2 months, the last one being analysed upon 27 months of storage. Problems associated with shimming optimisation during NMR acquisition led to the exclusion of the sample at 20 months of storage.

3.2.2. Glutathione/Drug Competition Assays

Glutathione/drug competition assays were performed with the aim of understand complexation reactions between reduced glutathione (GSH) and metal ions of drugs used in biological assays, Pt(II) and Pd(II) present in cDDP and Pd_2Spm respectively. With this purpose, fresh solutions of GSH (reduced glutathione) and of cDDP or Pd_2Spm in PBS/D_2O(100%) were prepared and mixed: GSH fresh solution was mixed with each of the 2 drug solutions and reaction kinetics was followed for 3 hours by 1D ^{1}H NMR, with one spectrum being registered every 15 minutes. Solutions of GSSG (oxidized form of glutathione) and Pd_2Spm were also prepared and analysed alone by NMR to aid signal assignment. In Table 3.4 the solutions prepared and their purpose are listed.

Table 3.4: Information on solutions prepared for GSH competition assays.

Solution	Concentration	Solvent	Purpose of study
GSH (fresh)	1 mM	PBS in 100% D_2O	Assignment
GSSG (fresh)	1 mM		Assignment
GSH/cDDP	1 mM/0.5 mM		Kinetics
GSH/Pd_2Spm	1 mM/0.5 mM		Kinetics
Pd_2Spm	0.5 mM		Assignment

3.2.3. NMR Data Acquisition and Processing

3.2.3.1. NMR Equipment

The facilities and NMR spectrometers on which NMR experiments were carried out are listed in Table 3.5. All samples (including those contained in rotor inserts) were kept frozen until a few minutes (*ca.* 10 minutes) prior to analysis, just long enough to ensure they were completely thawed when inserted into the probe. Due to time constraints in the NMR spectrometer of University of Aveiro, NMR analysis had to be performed outside, namely at *CRMN* (Lyon, France) and CERMAX (Oeiras, Portugal), the latter being accessed within the Portuguese NMR network.

Table 3.5: Facilities and equipment used to perform the NMR experiments.

NMR facility	Spectrometer and equipment	Assay (year)
CRMN – Centre de RMN à Très Hauts Champs, CNRS/ENS Lyon, France	• SB Bruker Avance II, 700 MHz • 4mm HRMAS probe • T = 277K	cDDP (2009)
CERMAX – Centro de Ressonância Magnética António Xavier – ITQB, Oeiras, Portugal[a]	• Bruker Avance II +, 500 MHz • 4mm HRMAS probe • Room temperature	Reproducibility (2010)
	• Bruker Avance II +, 800 MHz • 4mm HRMAS probe • T = 277K	DOX and MTX (2011)
		Pd_2Spm and cDDP (2012)
Departamento de Química, Universidade de Aveiro, Portugal	• Bruker Avance DRX, 500 MHz • 4mm HRMAS probe • T = 277K	Influence of cell integrity (2009)
		Influence of cell passage no. (2012)
		Stability during storage (2010-2012)
		Influence of acquisition parameters (2011)
		Drug combination assays (2013)
	• Bruker Avance DRX, 500 MHz • TXI probe • T = 277 and 310K	GSH competition assays (2013)
	• Bruker Avance DRX, 500 MHz • 5mm BBI probe • TXI probe • T = 298K	TCA extracts (2013)

[a] Accessed within the Portuguese NMR network (PT NMR).

3.2.3.2. Spectral Acquisition (1D and 2D ^{1}H Experiments)

^{1}H HRMAS NMR experiments employed, as a starting point, the cell analysis acquisition parameters obtained from literature (Santini *et al*., 2004). These were then optimized for the samples to be studied, in order to obtain a good signal-to-noise ratio with short acquisition times (typically around 30 min). A total of 128 scans were acquired for each standard 1D ^{1}H NMR

experiment (*noesypr1d*, Bruker library) with suppression of the water signal by presaturation (power level for presaturation, PL9, 55 dB) during the relaxation delay (D1, 4 s) and mixing time (D8, 100 ms). Experiments were acquired with a spectral window (SW) of 6510.42 Hz and 32 k data points (TD). Receiver gain (RG) was set to 256. The rotor containing the sample was spun at the magic angle (54.7˚ relative to the magnetic field) at a 4 kHz spinning rate. A Bruker cooling unit was used to cool down the bearing air flowing into the probe, in order to enable acquisitions to be performed at the temperature of 277 K.

T_2-edited (Carr-Purcell-Meiboom-Gill, CPMG, *cpmgpr1d*, Bruker library) and diffusion-edited (*ledbpgp2s1dpr* from Bruker library) experiments were also recorded. Details on the 1D pulse programs from Bruker pulse program library can be found in Chapter 2 (for the ^{1}H nucleus) and acquisition parameters are listed in Table 3.6.

Table 3.6: Acquisition parameters used for 1D ^{1}H HRMAS NMR spectra of lysed cells suspension.

Acquisition parameters – 500 MHz (Aveiro)		
Standard (*noesypr1d*)	**CPMG** (*cpmgpr1d*)	**Diffusion-edited** (*ledbpgp2s1dpr*)
NS: 256	**NS:** 256	**NS:** 256
D1: 4s	**D1:** 4s	**D1:** 4s
D8: 100ms	**τ:** 300 μs	**δ:** 2ms
SW: 6510.42Hz	**n:** 150	**△:** 100ms
TD: 32k points	**SW:** 6510.42Hz	**SW:** 6510.42Hz
RG: 256	**TD:** 32k points	**TD:** 32k points
PL9: 55dB	**RG:** 1024	**RG:** 256
	PL9: 55dB	**PL9:** 55dB
Acquisition parameters – 500 MHz (CERMAX)	**Acquisition parameters – 700 MHz (Lyon)**	**Acquisition parameters – 800 MHz (CERMAX, MG/HOb)**
Standard (*noesypr1d*)	**Standard** (*noesypr1d*)	**Standard** (*noesypr1d*)
NS: 256	**NS:** 256	**NS:** 256/512
D1: 4s	**D1:** 2s	**D1:** 4s/2s
D8: 100ms	**D8:** 100ms	**D8:** 100ms
SW: 6510.42Hz	**SW:** 9803.922Hz	**SW:** 9803.922Hz
TD: 32k points	**TD:** 32k points	**TD:** 32k points
RG: 128	**RG:** 512	**RG:** 256/256
PL9: 60dB	**PL9:** 50dB	**PL9:** 50dB

NS: number of scans, D1: relaxation delay, D8: mixing time, SW: size of spectral window, TD: number of data points, RG: receiver gain, PL9: power level for presaturation, τ: echo time, n: number of (τ-180˚-τ) loops, 2nτ: total spin-spin relaxation time, △: diffusion time, δ: gradient duration.

The NMR spectra of TCA extracts were acquired at 298 K, using either a BBI or a TXI probe. A total of 512 scans were acquired for each standard 1D ^{1}H NMR experiment (*noesypr1d* from

Bruker library) with water signal suppression by presaturation (power level for presaturation, PL9, 52 or 45 dB) during the relaxation delay (D1, 4 s) and mixing time (D8, 100 ms). Experiments were acquired with a size of the spectral window (SW) of 6510.42 Hz and 32 k data points (TD). Receiver gain (RG) was set to 256 or 203.

2D total correlation spectroscopy (TOCSY) and heteronuclear single quantum coherence (HSQC) spectra were registered for selected samples to aid spectral assignment. Bruker Avance spectrometers operating at 500 and 800 MHz for ^{1}H observation were used to record the 2D spectra. The acquisition parameters were based on previous studies on cells (Santini *et al.,* 2004) and submitted to further optimization to these particular type of samples. Typically, TOCSY spectra were acquired in phase-sensitive mode using States-TPPI (time proportional phase incrementation) detection using the MLEV-17 pulse sequence (*mlevgsst19* and *dipsi2pphpr* pulse programs from Bruker library) and ^{1}H-^{13}C phase-sensitive (echo/antiecho) HSQC was recorded with inverse detection and carbon decoupling during acquisition (*hsqcetgppr* and *invietgpsi* pulse programs from Bruker library). Both 2D experiments were recorded with a minimum of 56 scans and a relaxation delay time (D1) of 2 s was used. For both TOCSY and HSQC spectra, 2 or 4 k data points were used in the F1 dimension and a minimum of 220 points in the F2 dimension.

3.2.3.3. Spectral Processing and Assignment

All spectra were processed using the Bruker TopSpin 3.2 software (from Bruker BioSpin, Reinstetten, Germany). Standard 1D spectra were Fourier transformed (FT), processed with a line broadening (LB) of 0.3 Hz (or 0.5 Hz for diffusion-edited experiments) and a zero filling factor of 2 (to 64k points), manually phased and baseline corrected. Chemical shifts were referenced internally to the alanine signal at δ 1.48. 3-(trimethylsilyl)propionate sodium salt (TSP) was not used as chemical shift reference once it was found to suffer interactions with sample constituents (proteins for instance) resulting in a line-broadening of its signal. Nevertheless, and once it was added in a known concentration which allowed well resolved signal to be obtained with only few scans (TSP at 0.025% in the sample), TSP was particularly useful for shimming optimization purposes. 2D spectra were Fourier transformed (FT), processed with a line broadening (LB) of 0.3 Hz, manually phased and baseline corrected. Chemical shifts were also referenced to the alanine signal.

In order to aid peak assignment, CPMG and diffusion-edited ^{1}H NMR spectra were acquired as well as 2D experiments (TOCSY and HSQC). Spectral assignments were also aided by the use of several NMR spectra of known standards obtained through Metabolic Profiling Database, Biorefcode (courtesy of NMR Applications, NMR division, Bruker BioSpin, Rheinsteten, Germany), the Human Metabolome Database (HMDB, Wishart *et al*., 2013) and the Biological Magnetic Resonance Data Bank (BMRB, Ulrich *et al*., 2008). Statistical total correlation spectroscopy (STOCSY) analysis was used for assignment purposes as well (properly indicated in assignment tables), with the objective of unveiling whole spin systems.

3.2.3.4. Proton Relaxation Times Measurement

The ^{1}H relaxation times constants T_1 and T_2 were measured for lysed MG-63 cell samples under HRMAS conditions.

For measuring ^{1}H T_1 values a standard inversion-recovery pulse sequence was used, while for the determination of ^{1}H T_2, the CPMG pulse sequence was used. Table 3.7 lists the main acquisition and processing parameters used in these experiments.

Table 3.7: Acquisition and processing parameters used for T_1 and T_2 measurements in lysed MG-63 cells.

T_1 measurement (*t1irpr*)	**T_2 measurement (*t2zgpr*)**
NS: 40	**NS:** 40
D1: 10s	**D1:** 10s
TD[F1]: 26 points	**TD[F1]:** 30 points
TD[F2]: 16384 points	**TD[F2]:** 16384 points
SW[F1]: 1.9995 ppm	**SW[F1]:** 1.9995 ppm
SW[F2]: 13.0174 ppm	**SW[F2]:** 13.0174 ppm
Range of delays: 0.01-20.00	**Range of loops:** 5-8000
Processing parameters	
SI [F1]: 16384 points	**SI [F1]:** 16384 points
SI [F2]: 26 points	**SI [F2]:** 30 points
LB: 0.3 Hz	**LB:** 0.3 Hz

NS: number of scans, D1: relaxation delay, SW: size of spectral window, TD: number of data points.

The determination of ^{1}H T_1 and T_2 values was performed with T_1/T_2 calculation routine of Topspin 3.1, through the construction of exponential graphics, in which each point corresponds to one 1D spectrum, resulting in curves with rates $1/T_1$ and $-1/T_2$, described by Equations 3.3 and

3.4, respectively, where *y* is the integral area of the peak, *t* is the delay (Eq. 3.3) or total echo time (Eq. 3.4) used, *A* is a constant representing the amplitude of the decay.

$$y(t) = y(0) + Ae^{(-\frac{t}{T_1})} \quad |\text{Eq. 3.3}|$$

$$y(t) = Ae^{(-\frac{t}{T_2})} \quad |\text{Eq. 3.4}|$$

3.3. Multivariate and Statistical Analysis of the NMR Data

3.3.1. Data Pre-Processing

1D spectra were aligned using a recursive segment-wise peak alignment (RSPA) algorithm (Veselkov *et al*., 2009) and normalized to probabilistic peak alignment (PQN, Diertle *et al*., 2006) to account for dilution-independent effects on spectral area (MATLAB version 7.12.0, The MathWorks Inc.). Data were then scaled and, although mean centering and Pareto scaling were sometimes used to detect temporal trajectories of samples with treatment, unit variance (UV) was the most used scaling method to extract information on metabolic changes with drug-exposure.

3.3.2. PCA, PLS-DA and STOCSY

PCA, PLS-DA and OPLS-DA were applied to the data in which samples were classified as *Control* or *Drug-treated*, using SIMCA –P 11.5 (Umetrics, Sweden) employing a default seven-fold internal cross validation, from which Q^2 (predictive ability) and R^2 (explained variance) were extracted. Relevant drug-induced metabolic changes were assigned from the weight loadings plots obtained from PLS-DA models. The loadings plots of UV-scaled models were coloured according to the Variable Importance in the Projection (VIP) parameters list automatically calculated by SIMCA-P program for the respective PLS-DA model. All presented MVA models were validated through MCCV (Wiklund *et al.,* 2007; Westerhuis *et al*., 2008), using an in-house software developed by Professor António Barros. STOSCY analysis was performed to aid assignment (properly indicated in assignment tables) and to unveil metabolic correlations between metabolites (conveniently indicated throughout the text whenever used). Since reduced numbers of replicates per sample were available, metabolic correlations were investigated

considering data from both *Control* and *Drug-treated* groups. In fact, STOCSY analysis performed only with the data of one group of samples (either *control* or *drug-treated*) frequently resulted in strong correlations with noise regions and, on the other hand, when considering data from the two groups this issue was eliminated. The inclusion of the data of *controls* does not alter either the recovery of information from drug-induced metabolic correlations or the comparison between different drugs, since the information of *Controls* is very similar regardless of the drug tested and, thus, only drug-induced correlations are obtained.

The magnitude of variation of NMR peaks pointed by MVA as possibly relevant for group separation was evaluated by performing signal integration, using the Amix-Viewer software (Bruker, version 3.9.11). Signal deconvolution was also used for choline region, particularly for GPC and PC peaks, which frequently presented a considerable degree of superimposition.

3.3.3. Statistical Analysis

For each metabolite, the statistical significance of the difference between the means of the two groups (*control* and *drug-treated*) were assessed using the two sample *t*-test. A *p*-value < 0.05, with a confidence level of 95%, was considered statistically significant. Integration results were used to construct time course graphs. Integration values were also used to determine percentages (%) of variation of compounds in drug-treated samples relative to controls and Effect Size (ES) was also calculated with a correction factor for reduced number of samples, according to Eq. 3.5 to 3.9 (Berben *et al*., 2012), where *smd* is the standardized mean difference, s_{pooled} the pooled standard deviation, *df* the degrees of freedom, *SE* the standard error, *J* the correction factor for reduced number of samples, *Mean* the mean of integrals, *n* the number of samples and *SD* the standard deviation. By measuring fold change relative to controls, ES values were performed in complement to % of variation to corroborate (or not) previous *t*-test statistical validation (due to the fragility of performing such statistical validation with just 3 samples per group). ES calculations were used to build heatmaps with MATLAB program (version 7.12.0, The MathWorks Inc.) which enabled the comparison of changes (in relation to control group) along exposure periods and/or among different drugs, helping to unveil common and/or opposite changes through a colourmap, where positive changes appear yellow-red coloured and negative ones are green-blue coloured.

$$ES_{gsmd}=JxES_{smd} \quad |Eq.\ 3.5|$$

$$J=1-(3/(4df-1)) \quad |Eq.\ 3.6|$$

$$ES_{smd}=(Mean_{CTR}-Mean_{Drug})/s_{pooled} \quad |Eq.\ 3.7|$$

$$s_{pooled}=\sqrt{[((n_{CTR}-1)SD^2_{CTR}+(n_{Drug}-1)SD^2_{Drug})/df]} \quad |Eq.\ 3.8|$$

$$df=n_{CTR}+n_{Drug}-2,\ SE_{gsmd}=\sqrt{[J^2x((n_{CTR}+n_{Drug})/(n_{CTR}xn_{Drug})+(ES^2_{smd}/2(n_{CTR}+n_{Drug})))]} \quad |Eq.\ 3.9|$$

A global scheme of the entire process of multivariate and statistical analysis of the NMR data is presented in Figure 3.6.

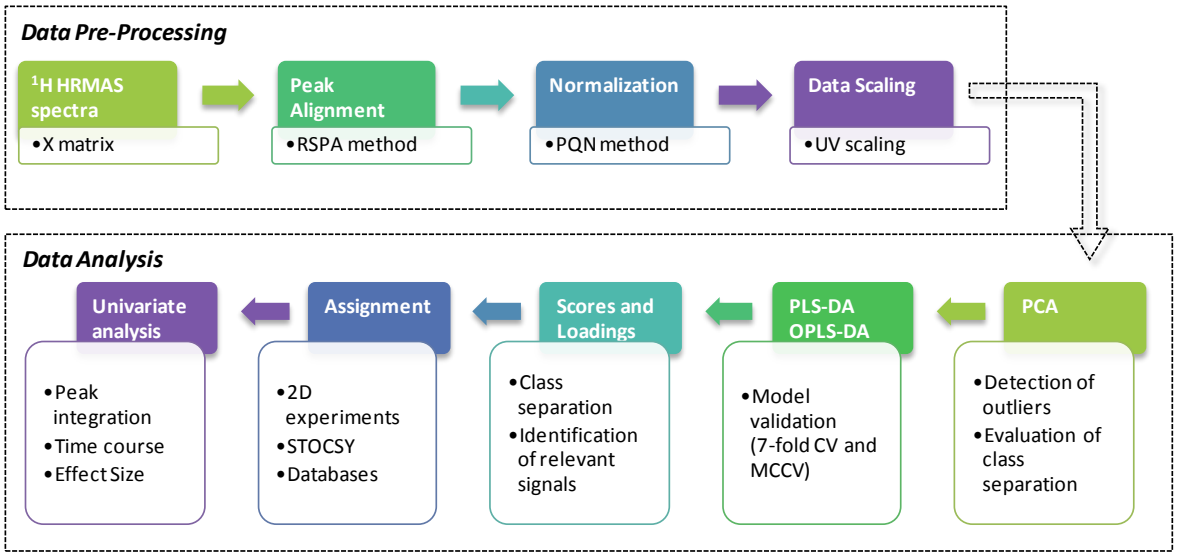

Figure 3.6. Schematic representation of pre-processing and analysis of the ^{1}H HRMAS NMR data. RSPA: recursive segment-wise peak alignment, PQN: probabilistic quotient normalisation, UV: unit variance, CV: cross-validation, MCCV: Monte Carlo cross/validation.

The peak assignment step, which appears at the final stages of the process of multivariate and statistical analysis of the NMR data (indicated in Figure 3.6) was actually performed throughout the entire process of data analysis, since the first analysis of the data is obtained by visual inspection of the spectra and frequently, metabolite variations are newly revealed by multivariate analysis raising the need for additional assignment work.

4. Spectral Assignment and Assessment of Analytical and Biological Reproducibility of the Metabolic Profile of MG-63 Cells: a HRMAS NMR Study

The establishment of Standard Operating Procedures (SOPs) is of crucial importance to produce cell samples that can be replicated in subsequent assays with satisfactory reproducibility, thus enabling robust metabolomics conclusions to be drawn. SOPs are particularly important in cell HRMAS NMR studies, in comparison to liquid state NMR, due to the relative complexity of cell samples handling and NMR acquisition procedures. The present chapter begins by comparing the spectral profiles of intact and lysed cells, prepared by different protocols, in order to define the best sample presentation for more informative spectra to be obtained. This is followed by detailed peak assignment of the ^{1}H HRMAS NMR spectral profile of MG-63 cells. Next, the influence of certain acquisition conditions (spinning rate, sample temperature, acquisition time) and sample relaxation properties on spectral profile is described. Finally, a reproducibility check is performed and the influence of storage conditions evaluated, in order to assess the conditions for best sample quality and spectral reproducibility.

4.1. Spectral Profile of Intact and Lysed MG-63 Cells

Given the value of HRMAS in aiding a global picture of the metabolome of a whole sample to be obtained (enabling both hydrophilic and hydrophobic compounds to be detected in one single experiment) it is important to understand in which state, intact or lysed, would cell samples provide the best quality HRMAS spectra. The results hereby presented are part of our own work published in Duarte *et al*., 2009.

Determination of the number of cells by the Trypan blue assay indicated that protective freezing in FBS/DMSO is as efficient in preserving cell integrity as using freshly harvested cells, kept briefly under refrigeration until analysis. For procedures A and B most cells remained intact, samples obtained through protective freezing presenting the advantage of easiness of storage over longer periods. Samples C, D, and E give information, respectively, on unintentional cell lysis by unprotected freezing and storage at -80 °C, the extent of mechanical lysis using a snap-

freezing/sonication procedure, and the cumulative effects of freezing, storage at -80 °C and mechanical lysis. All of these procedures (C, D and E) produced cells which showed total staining with Trypan blue, indicating total membrane disruption, thus meaning that freezing process is, by itself, enough to promote cell lysis. According to these results, cells cannot be considered intact when analysed after being frozen without a cryoprotective solution.

Figure 4.1 shows the ^{1}H HRMAS NMR spectra of MG-63 cells submitted to different handling conditions. Spectral analysis reveals that although all spectral profiles are dominated by broad lipid resonances, the spectra corresponding to fully lysed cells, samples D and E (Figure 4.1d and 4.1e), show many additional sharp signals arising from metabolites released from the intracellular shell. The spectral profiles of samples A and B (Figure 4.1a and 4.1b), which comprise mainly intact cells, are generally similar, revealing a dominance of lipids content (probably comprising contributions from both membrane/or intracellular lipids), and a lesser number of sharp peaks arising from small cellular metabolites, namely some amino acids. However, the intensities of $N(CH_3)_3^+$ resonances of choline-containing compounds change between samples A and B (Figure 4.1a and 4.1b) with a considerable lower level of PC+GPC (Figure 4.2) in the sample prepared according to protocol B (gradually frozen with cryoprotectant). PC and GPC are membrane breakdown products and their higher contents in samples A (freshly harvested cells suggest higher membrane degradation, compared to sample B. In sample A, this may arise because of the activity of degrading enzymes during the 2-3 hours refrigeration period between harvesting and NMR analysis. Interestingly, choline content is similar for samples A and B. In addition, PTC integrals remain high for samples A and B, reflecting the maintenance of cell integrity for the majority of cells (since PTC integrals were measured in diffusion-edited spectra, not acquired for every sample, PTC integral for sample B is missing). These results show that, despite equivalent results given by the Trypan blue assay of these samples (*ca*. 70-80%), the NMR lipid profiles indicate that cell membranes are less degraded in the case of samples cryoprotected with FBS/DMSO after harvesting (sample B), compared to fresh samples (sample A).

The study of samples C (gradually frozen without cryoprotectant) gives insight on the effect of cell freezing without the use of a cryoprotective agent. The results given by the Trypan blue exclusion assay have shown that cells are cleaved in the process, similarly to samples D and E for which a cell lysis method was intentionally applied. MG-63 cells show a marked increase in choline (Figure 4.2) as a consequence of cell lysis.

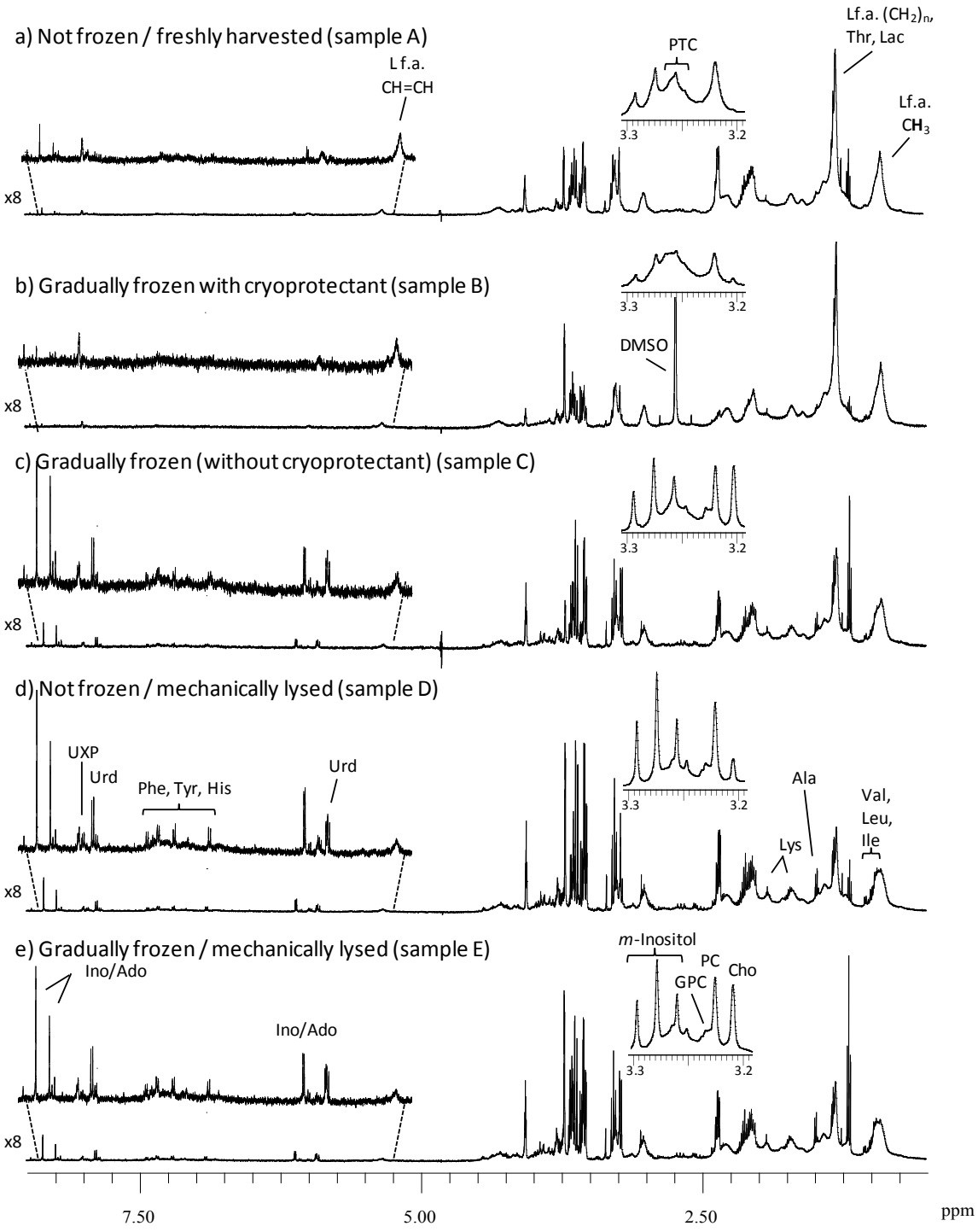

Figure 4.1. 500 MHz ^{1}H HRMAS NMR spectra of MG-63 cells submitted to different conditions: a) sample A, b) sample B, c) sample C, d) sample D and e) sample E. Main assignments are noted.

Moreover, the PC+GPC increase (Figure 4.2) in lysed cells is only noted relative to samples B (suggested to be the less degraded of all), with similar values to those found for sample A. The decrease in PTC is also confirmed. Thus, it seems plausible to suggest that choline and/or PC+GPC to PTC ratios may be used as general indicators of the extension of cell physical breakage. Taking

choline as the final end-product of cell choline-containing lipids, comparison between samples suggests, therefore, that unprotected freezing (sample C) may have a more disruptive effect than intentional mechanical lysis (sample D), with the cumulative effects (sample E) giving the highest cell breakage extension. As noted above, in fresh cells (sample A), where cell breakage occurs to a much lesser extent, and possibly in parallel with membrane enzymatic degradation, GPC and PC contents seem to be better degradation indicators.

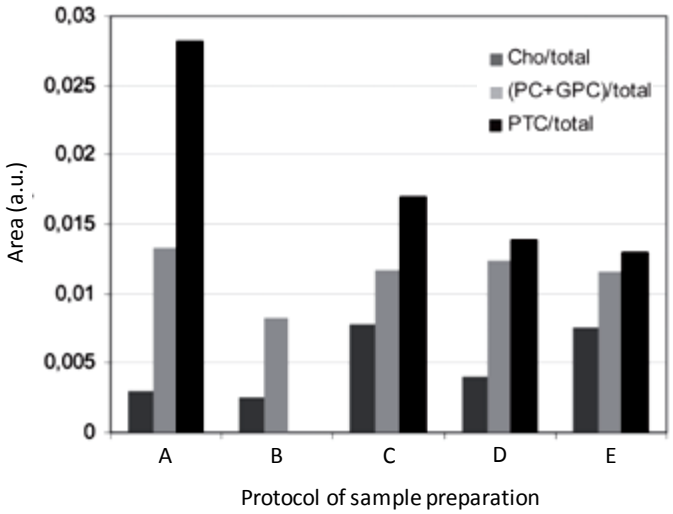

Figure 4.2. Integral values obtained for selected choline-containing compounds (Cho δ 3.20, PC δ 3.22, GPC δ 3.23 and PTC δ 3.26) relative to total spectral area in the standard 1D spectra of MG-63 cells (adapted from Duarte *et al.,* 2009). Since PTC integrals were measured in diffusion-edited spectra, which were not acquired for every sample, PTC integral is missing for sample B.

In an attempt to compare HRMAS and solution-state NMR, which is still generally more readily available than the former, the information provided by both methods on the metabolic profile of intact cells was compared. The spectra of sample A of MG-63 cells by ^{1}H HRMAS and by solution-state ^{1}H NMR of both the cell suspension ($A_{suspension}$) and the supernatant removed after deposition of the cells ($A_{supernatant}$) were obtained (not shown). Spectral analysis shows that, as expected, the lipid profile is improved by the HRMAS technique, compared to the cell suspension spectrum. The lower signal-to-noise ratio of the latter spectrum is due to the enhanced dilution of the sample, being expected to degrade overtime because of cell deposition in the tube. Interestingly, the spectrum obtained for the supernatant of sample A (fresh cells) is very similar to that of the corresponding suspension, indicating that metabolites leaked from the small percentage of broken cells, thus showing that significant metabolite loss may occur when supposedly intact cells pellets are washed and their metabolome analysed.

As shown above, whenever cell metabolome characterization is intended at a fixed point in time, the use of fully lysed cells is recommended since enhanced metabolic information is obtained (with particular improvements in lipids and choline compounds). Moreover, the use of different NMR methods has shown that the corresponding spectra of fully lysed cells (samples E, $E_{suspension}$ and $E_{supernatant}$) are significantly similar, both in terms of resolution and of the metabolic profiles detected, the main difference being that, as expected, lipid signals are enhanced in the HRMAS spectrum (E) and hardly detected in the supernatant measured by solution-state NMR ($E_{supernatant}$). A lipid profile is also observed for the cellular suspension ($E_{suspension}$), but the gradual deposition with time renders this option inadequate for lipid characterization.

These results show that, when dealing with fully lysed samples, particularly in metabolomic studies, great care must be paid to the profile of small metabolites and choline compounds since they are highly sensitive to the sample handling conditions (namely the extent of cell lysis), in order to ensure suitable reproducibility of samples and spectra.

4.2. Spectral Assignment of ^{1}H HRMAS NMR Spectrum of Lysed MG-63 Cells

The typical ^{1}H HRMAS NMR spectrum of lysed MG-63 cells contains several tens of signals arising from numerous metabolites. As shown in Figure 4.3a and listed in Table 4.1, several metabolites have been identified by 1D and 2D NMR, with the assistance of several databases, namely the Human Metabolome Database (HMDB) (Wishart *et al*., 2013), Biological Magnetic Resonance Data Bank (BMRB) (http://www.bmrb.wisc.edu/) and Bruker Biorefcode 2.0.0 (courtesy of Bruker BioSpin Rheinsteten, Germany) as well as comparison with previous reports (Santini *et al*., 2004; Santini *et al*., 2006a; Santini *et al*., 2006b; Santini *et al*., 2006c; Duarte *et al*., 2010). Metabolites identified comprised organic acids (formate and lactate), polyalcohols (*m*- and *s*-inositols), several amino acids (Ala, Arg, Asp/Asn, Gln, Glu, Gly, His, Ile, Leu, Lys, Met, Phe, Pro, Tau, Thr, Tyr, Val), choline and choline-containing compounds (GPC and PC) and phosphoethanolamine (PE), nucleotides and derivatives (Ino/Ado, uridine, UXP, cytidine and several other compounds (N-acetyl moieties, creatine, reduced glutathione (GSH) and hypoxanthine). As shown in Figure 4.3b and 4.3c in CPMG and diffusion-edited experiments (explained in section 2.2.2), respectively, sharp and broad peaks are selected, the latter arising from slowly diffusing molecules like proteins and fatty acyl lipid moieties (lipid fatty acyl moieties, L f.a. CH_3, $(CH_2)_n$, CH_2CH_2CO, CH_2COO, $=CHCH_2CH=$ and $CH=CH$). Since both sharp and main broad

resonances could be successfully assigned in the standard 1D spectrum (Figure 4.3a), only standard 1D noesy experiments were routinely acquired subsequently.

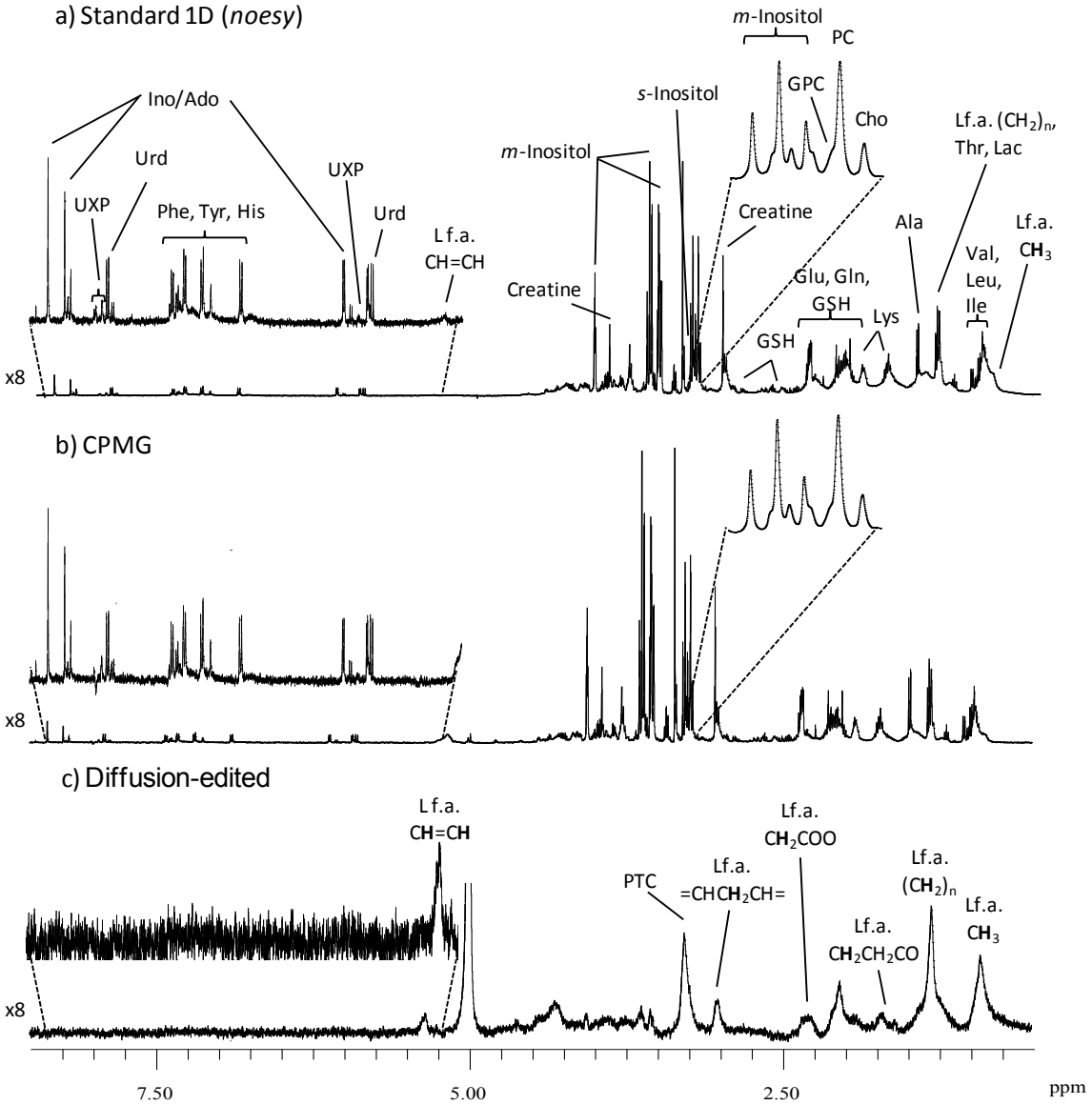

Figure 4.3. Typical 500 MHz 1D ^{1}H HRMAS NMR spectra of MG-63 cells: a) standard 1D, b) CPMG and c) diffusion-edited experiments Insets show expansions of choline compounds (3.2-3.3 ppm) and aromatic (5.2-8.5 ppm) regions. Main assignments are noted.

To aid peak assignment, TOCSY and HSQC experiments were acquired and expansions of the respective spectra are shown in Figure 4.4 TOCSY (Figure 4.4a) experiments are crucial to assign complete spin systems, particularly low intensity signals, not rarely overlapped with other resonances. On the other hand, the assignment of singlet resonances (without scalar correlations that can be assigned through TOCSY experiments) is assisted by HSQC spectra (Figure 4.4b).

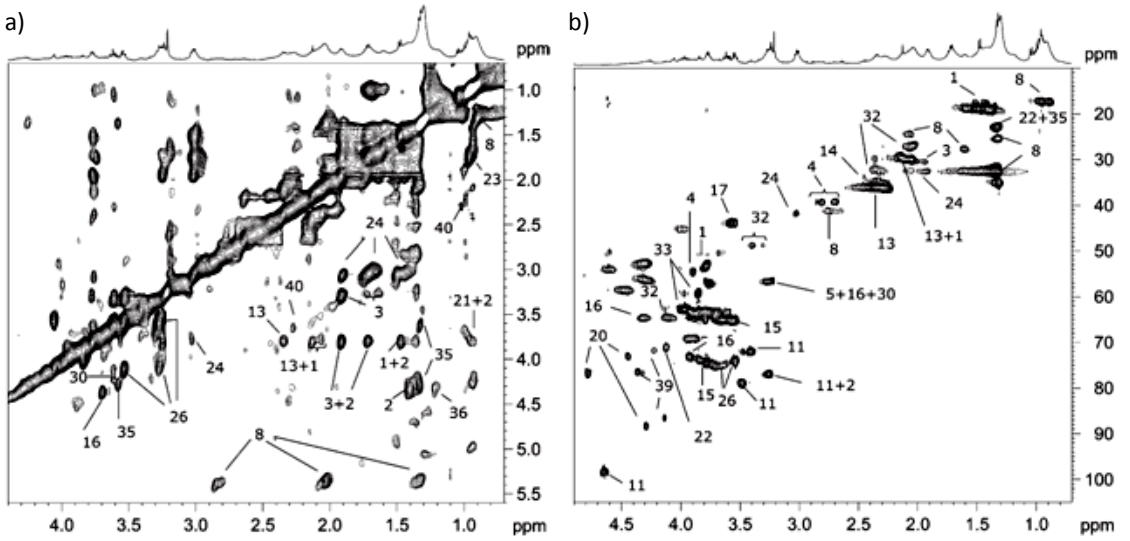

Figure 4.4. Expansions of 0.5-4.5 ppm region of the 500 MHz 2D HRMAS NMR spectra of MG-63 cells: a) TOCSY and b) HSQC experiments. 1: Ala, 2: Ala (bonded), 3: Arg, 4: Asn/Asp, 5: choline, 6: creatine, 7: cytidine, 8: L f.a., 9: formate, 10: fumarate, 11: glucose, 12: GSH, 13: Glu, 14: Gln, 15: glycerol, 16: GPC, 17: Gly, 18: His, 19: hypoxanthine, 20: Ino/Ado, 21: Ile, 22: lactate, 23: Leu, 24: Lys, 25: Met, 26: *m*-Inositol, 27: niacinamide, 28: Phe, 29: PTC, 30: PC, 31: PE, 32: Pro, 33: Ser, 34: Tau, 35: Thr, 36: Thr (bonded), 37: Tyr, 38: uracil, 39: uridine, 40: Val.

In addition, STOCSY analysis enabled the identification of full spin systems, within the resonances not readily assigned by 1D and 2D NMR. The STOCSY recorded in Figure 4.5 showed, for instance, that the triplet at δ 2.30 is strongly and positively correlated with peaks at δ 1.91 (multiplet) and at δ 3.00 (triplet) ($r > 0.8$), thus enabling the assignment of the complete spin system of GABA. Besides being useful for assignment purposes, STOCSY analysis can also be used to identify metabolic relationships between metabolites and thus, when used for assignment, STOCSY results must be carefully analysed by comparison with existing information from literature and databases. All the metabolites assigned through STOCSY are identified in Table 4.1.

Overall, 47 metabolites were identified in the ^{1}H HRMAS NMR spectra of lysed MG-63 cells, most of which having been previously identified in these cells (Santini *et al.,* 2004; Santini *et al.,* 2006a; Santini *et al.,* 2006b; Santini *et al.,* 2006c; Duarte *et al.,* 2009; Duarte *et al.,* 2010). The UDP-GNAc derivatives (UDP-GlcNAc and UDP-GalNAc) are here newly assigned.

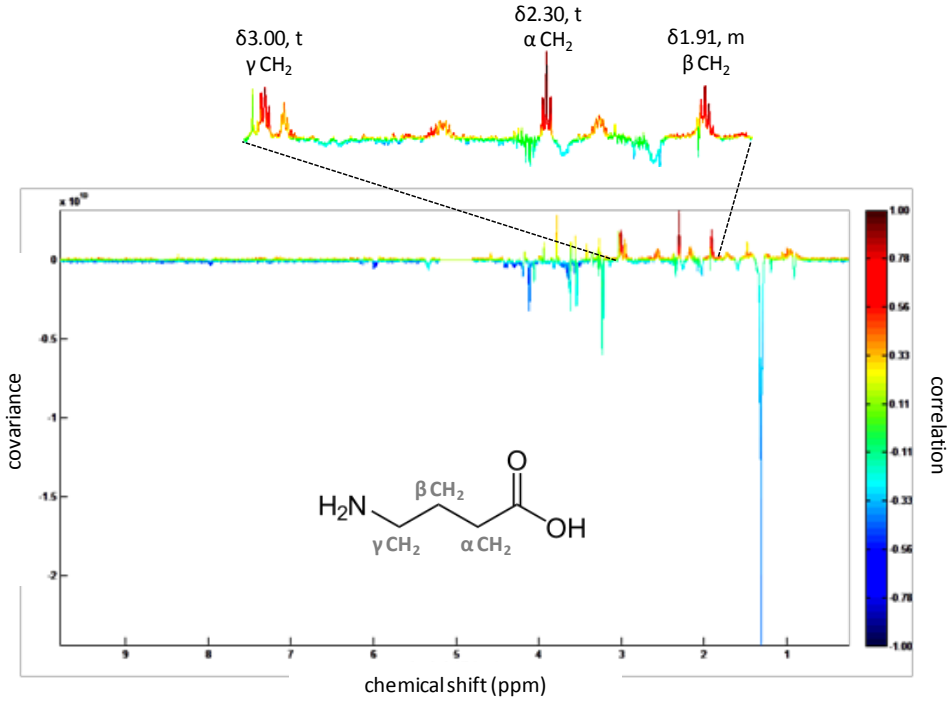

Figure 4.5. STOCSY for the assignment of γ-aminobutyric acid (GABA).

Table 4.1: List of metabolite assignments in $^{1}H/^{13}C$ HRMAS NMR spectra of lysed MG-63 cells. Legend: *s* singlet, *d* doublet, *t* triplet, *q* quartet, *dd* double of doublets, *m* multiplet.

Compound	Assignment	δ ^{1}H ppm (multiplicity)/ δ ^{13}C ppm
Acetate	βCH_3	1.92 (s)
Alanine	βCH_3	1.48 (d)/ 18.76
	αCH	3.78 (q)/ 53.18
Arginine	γCH_2	1.69 (m)
	βCH_2	1.92 (m)
	δCH_2	3.25 (t)
	αCH	3.77 (t)
Aspartate	βCH_3	2.69 (dd)/ 39.12
	$\beta' CH_3$	2.83 (dd)/ 39.12
	αCH	3.89 (dd)/ 54.51
Cholesterol	C18	0.72
Choline	$N(CH_3)_3$	3.21 (s)/ 56.42
	$CH_2(NH)$	3.54
	$CH_2(OH)$	4.08
Creatine	CH_3	3.03 (s)/ 41.75
	CH_2	3.94 (s)/ 59.20
Cytidine		5.91
		6.06 (d)
		7.83 (d)
Ethanol	βCH_3	1.19 (t)/ 17.10
	αCH_2	3.65 (q)/ 57.03
Ethanolamine	$CH_2(NH_2)$	3.13 (t)
	$CH_2(OH)$	3.82 (t)

Table 4.1 (cont.): List of metabolite assignments in $^{1}H/^{13}C$ HRMAS NMR spectra of lysed MG-63 cells. Legend: *s* singlet, *d* doublet, *t* triplet, *q* quartet, *dd* double of doublets, *m* multiplet.

Compound	Assignment	δ ^{1}H ppm (multiplicity)/ δ ^{13}C ppm
Fatty acyl (F.A.) chain peaks	CH_3	0.88-0.95/17.07
	$(CH_2)_n$	1.31/25.32,32.48,34.91
	C**H**$_2$CH$_2$CO	1.59/27.63
	CH=CHC**H**$_2$	2.04/26.91
	CH_2CO	2.26/36.10
	=CHC**H**$_2$CH=	2.83/41.17
	CH=CH	5.33/132.17
Formate	CH	8.46 (s)/ 172.68
γ-Aminobutyric acid[a]	βCH_2	1.91 (m)
	αCH_2	2.30 (t)
	γCH_2	3.00 (t)
Glutamate	$\beta\beta' CH_3$	2.09/29.64
	γCH_2	2.35/35.95
	αCH	3.78 (dd)/ 53.20
Glutamine	βCH_2	2.13/29.58
	γCH_2	2.45/33.70
	αCH	3.76/57.04
Glutathione (reduced)[a]	βCH_2 Glu	2.17/29.34
	γCH Glu	2.56/36.02
	αCH_2 Cys	2.96/26.76
	αCH Glu	3.77/46.52,57.08
	γCH_2 Cys	4.17/57.51
Glycerol	$C1H_2$	3.57/65.11
	$C3H_2$	3.64/65.11
	C2H	3.78/72.52
Glycerol (in lipids)	$C1H_2$	4.09
	$C3H_2$	4.30
	C2H	5.23
Glycerophospho	$N(CH_3)_3$	3.24 (s)/ 56.54
choline (GPC)	γCH_2	3.65/65.02
	$\beta CH/\beta' CH_2(N)$	3.87/69.16
	αCH_2	3.91/73.08
		3.94/69.10
	$\alpha CH_2(P)$	4.33/64.49
Glycine	αCH_2	3.56 (s)/ 43.84
Histidine	C4H, ring	7.27 (s)
Hypoxanthine	C2H	8.19 (s)/ 147.76
	C8H	8.21 (s)/ 144.37
Inosine / Adenosine	C4'H, ribose	4.29/88.28
	C3'H, ribose	4.44/72.95
	C2'H, ribose	4.78 (t)/ 76.69
	C1'H, ribose	6.11 (d)/ 90.92
	C2H, ring	8.23 (s)/ 148.59
	C8H, ring	8.36 (s)/ 142.98
Isoleucine	δCH_3	0.94 (t)/ 17.06
	$\beta' CH_3$	1.01 (d)/ 20.17
	βCH	1.99
	αCH	3.65
Lactate	βCH_3	1.33 (d)/ 22.73
	αCH	4.13 (q)/ 70.92

Table 4.1 (cont.): List of metabolite assignments in $^{1}H/^{13}C$ HRMAS NMR spectra of lysed MG-63 cells. Legend: *s* singlet, *d* doublet, *t* triplet, *q* quartet, *dd* double of doublets, *m* multiplet.

Compound	Assignment	δ ^{1}H ppm (multiplicity)/ δ ^{13}C ppm
Leucine	δCH_3	0.95 (d)/ 25.31
	$\delta' CH_3$	0.97 (d)/ 23.64
	$\gamma CH/\beta CH_2$	1.72/26.88
	αCH	3.76 (t)/ 57.06
Lysine	γCH_2	1.47/25.39
	δCH_2	1.73/28.88
	βCH_2	1.92/32.41
	εCH_2	3.02 (t)/ 41.69
	αCH	3.76 (t)/ 57.07
Methionine	$\varepsilon CH_3/ \beta CH_2$	2.13 (s)/ 16.89
	γCH_2	2.64 (t)/ 29.17
	αCH	3.87 (t)/ 54.40
myo-Inositol	C5H	3.27 (t)/ 74.63
	C1H, C3H	3.54 (dd)/ 74.03
	C4H, C6H	3.62 (t)/ 74.73
	C2H	4.05 (t)/ 74.52
Niacinamide	N5, ring	7.59
	N6, ring	8.71
	N2, ring	8.94
Phenylalanine	βCH	3.15
	$\beta' CH$	3.29
	αCH	3.99 (dd)/ 58.83
	C2H, C6H, ring	7.32/131.83
	C4H, ring	7.37/129.63
	C3H, C5H, ring	7.42/131.78
Phosphatidyl cholines (PTC)	$N(CH_3)_3$	3.27 (s)/ 56.62
Phosphocholine (PC)	$N(CH_3)_3$	3.23 (s)/ 56.53
	$N\text{-}CH_2$	3.61 (s)/ 65.03
	$PO_3\text{-}CH_2$	4.19/62.22
Phosphoethanol amine (PE)	$N\text{-}CH_2$	3.25/42.55
	$PO_3\text{-}CH_2$	3.97/62.81
Proline	γCH_2	2.01/26.89
	βCH	2.07/27.07
	$\beta' CH$	2.35/31.98
	δCH	3.33 (t)/ 48.54
	$\delta' CH$	3.41 (t)/ 48.54
	αCH	4.12 (t)/ 64.48
Scyllo-Inositol	CH	3.34 (s)/ 76.64
Serine	αCH	3.84/59.13
	$\beta\beta' CH$	3.97 (dd)/ 62.78
Succinate	$\alpha, \beta CH_2$	2.41 (s)
Taurine	$S\text{-}CH_2$	3.25 (t)/ 38.37
	$N\text{-}CH_2$	3.42 (t)/ 48.68
Threonine	γCH_3	1.32 (d)/ 22.73
	αCH	3.58 (d)/ 65.12
	βCH	4.26/71.71
Tyrosine	$\beta\beta' CH$	3.05/3.18
	αCH	3.95/59.20
	C3H, C5H, ring	6.89 (d)/ 118.39
	C2H, C6H, ring	7.19 (d)/ 133.39

Table 4.1 (cont.): List of metabolite assignments in $^{1}H/^{13}C$ HRMAS NMR spectra of lysed MG-63 cells. Legend: *s* singlet, *d* doublet, *t* triplet, *q* quartet, *dd* double of doublets, *m* multiplet.

Compound	Assignment	δ ^{1}H ppm (multiplicity)/ δ ^{13}C ppm
UDP/UTP[a]	C1'H, ribose	5.98
	C6H, ring	7.98
UDP-GalNAc[a]		2.08
	C1H, Glc	5.52
UDP-GlcNAc[a]		2.09
	C1H, Gal	5.62
Uracil	C5H, ring	5.80 (d)
	C6H, ring	7.53 (d)
Uridine	C4'H, ribose	4.12/70.93
	C3'H, ribose	4.22 (dd)/ 71.66
	C2'H, ribose	4.34 (dd)/ 76.57
	C1'H, ribose	5.89 (d)/ 91.95
	C5H, ring	5.92 (d)/ 91.77
	C6H, ring	7.87 (d)/ 144.32
Valine	γCH_3	0.99 (d)/ 17.06
	$\gamma' CH_3$	1.05 (d)/ 16.98
	βCH	2.28/27.87
	αCH	3.63 (d)/ 64.98

[a] Metabolites assigned through STOCSY.

4.3. Influence of Acquisition Conditions on the Cell Metabolic Profile

Sample spinning in HRMAS NMR experiments implies a set of direct or indirect consequences on the nature and dynamics of the sample: phase separation inside the rotor that, in turn, induces alterations in metabolites mobility (thus, visibility also) and sample heating that induces also alterations in metabolites' mobility and chemical shift variations, as well as increased enzymatic and chemical activity within the sample. Since some of these effects may irreversibly alter the sample, they must be considered when defining the best experimental conditions. With this in mind, the following studies intended to determine the influence of spinning rate (SR), sample temperature and acquisition time duration on sample and spectral quality. In addition, sample relaxation properties, namely described by T_1 and T_2 relaxation times, were characterised and their impact on spectral characteristics described. The results allowed the best value for each of the referred conditions to be chosen, giving insight into a field with very few reports on literature (Griffin *et al.,* 2002; Griffin *et al.,* 2003; Duarte *et al.,* 2009; Martin-Sitjar *et al.,* 2012).

4.3.1. Spinning Rate (SR)

In order to evaluate the influence of spinning rate on the ^{1}H HRMAS NMR spectra of fully lysed MG-63 cells, a range of rates from 3 to 7 kHz was tested (stable spinning rates were not

achieved for lower SR values) (Figure 4.6). As expected, a considerable increase in signals intensity is observed at higher spinning rates, with the most significant improvement being observed from 3 to 4 kHz. This is particularly seen for peaks arising from amino acids, whose signal intensities suffer a marked increase from 3 to 4 kHz, with very slight increases at higher SR. Besides the effects of higher SR in reducing the dipolar couplings and chemical shift anisotropy, it is also possible that a contribution of some sample heating and possible partial phase separation, leaving polar metabolites such as amino acids in a more liquid-like environment, thus increasing their visibility. A similar tendency was detected for creatine and *m*- and *s*-inositols.

Resonances arising from choline and PC show a considerable increase from 3 to 4 kHz, remaining essentially stable at higher spinning rates in parallel with a slight deviation for lower chemical shifts, probably due to sample heating promoted by spinning. For PC, these results are in partial agreement with those obtained in Martin-Sitjar work (Martin-Sitjar *et al.,* 2012), in which the intensity of PC was found to increase up to 6 kHz.

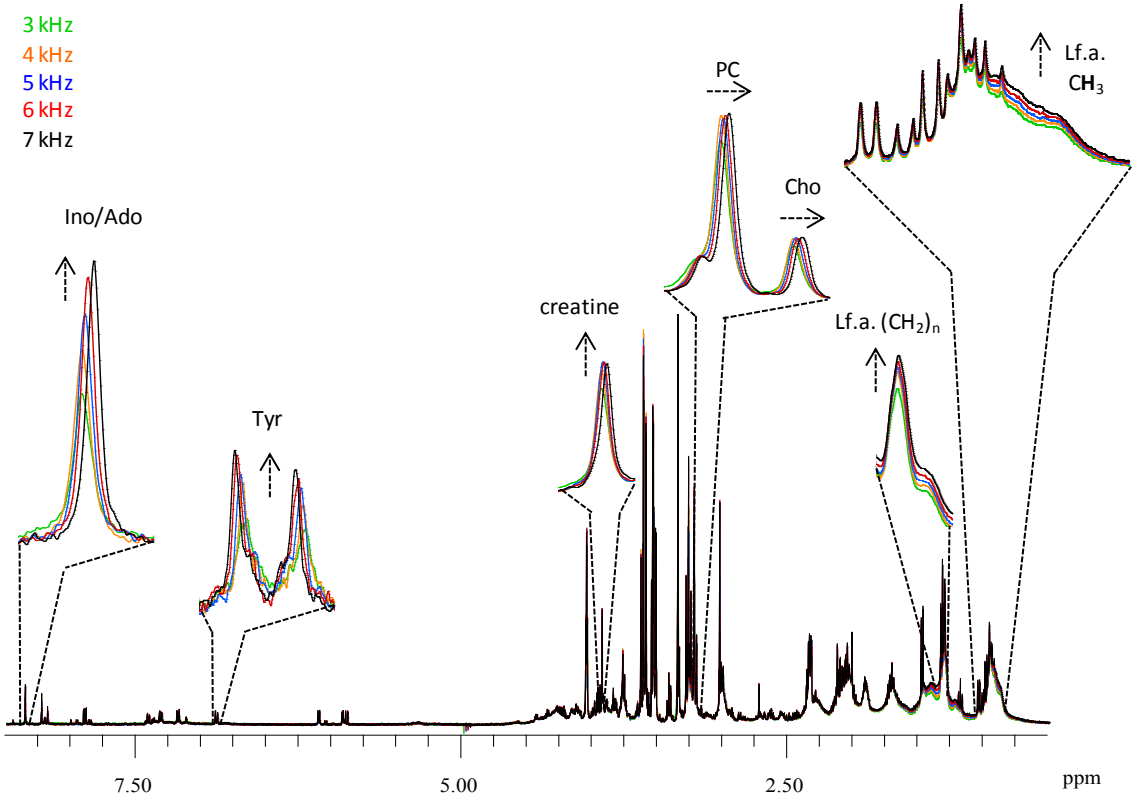

Figure 4.6. 500 MHz ^{1}H HRMAS NMR spectra of MG-63 cells with spinning rates ranging from 3 to 7 kHz (see colour legend in top left of figure). Insets show the main variations and direction of change.

Regarding Ino/Ado and Tyr, increases in signal intensities were detected up to 6 kHz.

Finally, increasing SR (from 3 to 7 kHz) induced an increase in the intensity of resonances from lipids. These results are in agreement with those reported in similar measurements in C6 glioma cells (Martin-Sitjar *et al.,* 2012). Similar determinations in glioma tissue (Griffin *et al.,* 2003) found no alterations in the line width and intensity of lipid signals for SR ranging from 1 to 9 kHz, showing the distinct behaviour of different types of samples.

In order to test the reversibility of the above described changes, a last spectrum was acquired at a spinning rate of 4 kHz. Minor increases of Met, Lys, Gly, Phe and Tyr and decreases of Ino/Ado were observed, with no further variations in other metabolites. This finding shows that sample alterations induced by high SR are not completely reversible, drawing attention for the persistence of phase separation inside the rotor and for eventually occurring enzymatic activity (even after submitting samples to very low storage temperatures). This is not in complete agreement with a literature report on glioma cells (Martin-Sitjar *et al.,* 2012), in which the authors concluded that the metabolite changes induced by increasing spinning rates were essentially reversible.

The effect of sample spinning rate and spectral acquisition duration on the integrity of MG-63 cells, as well as of other two cellular lines were also evaluated (Duarte *et al.,* 2009). Trypan blue results showed that the behaviour of cells spun at 4 kHz for 2 hours is greatly dependent on cell type and, in the particular case of MG-63 cells, this procedure does not affect greatly their integrity. Additionally, the results of HRMAS analysis of neuronal and glial cells revealed that spinning rates ranging from 1 to 6 kHz exerted little effect on either shape or intensity of detected resonances and claim that at the end of experiment (around 40 minutes) cells that stained with Trypan blue increased just 3% (Griffin *et al.,* 2002). These results once again highlight the importance of evaluating the influence of spinning rate for each particular type of cell sample.

According to these results, a spinning rate of 4 kHz was chosen for HRMAS analysis.

4.3.2. Sample Temperature

The following study intended to determine how sample temperature during acquisition influences the global profile of the ^{1}H HRMAS NMR spectra. With that purpose, spectra were recorded at temperatures ranging from 4 to 25˚C (Figure 4.7).

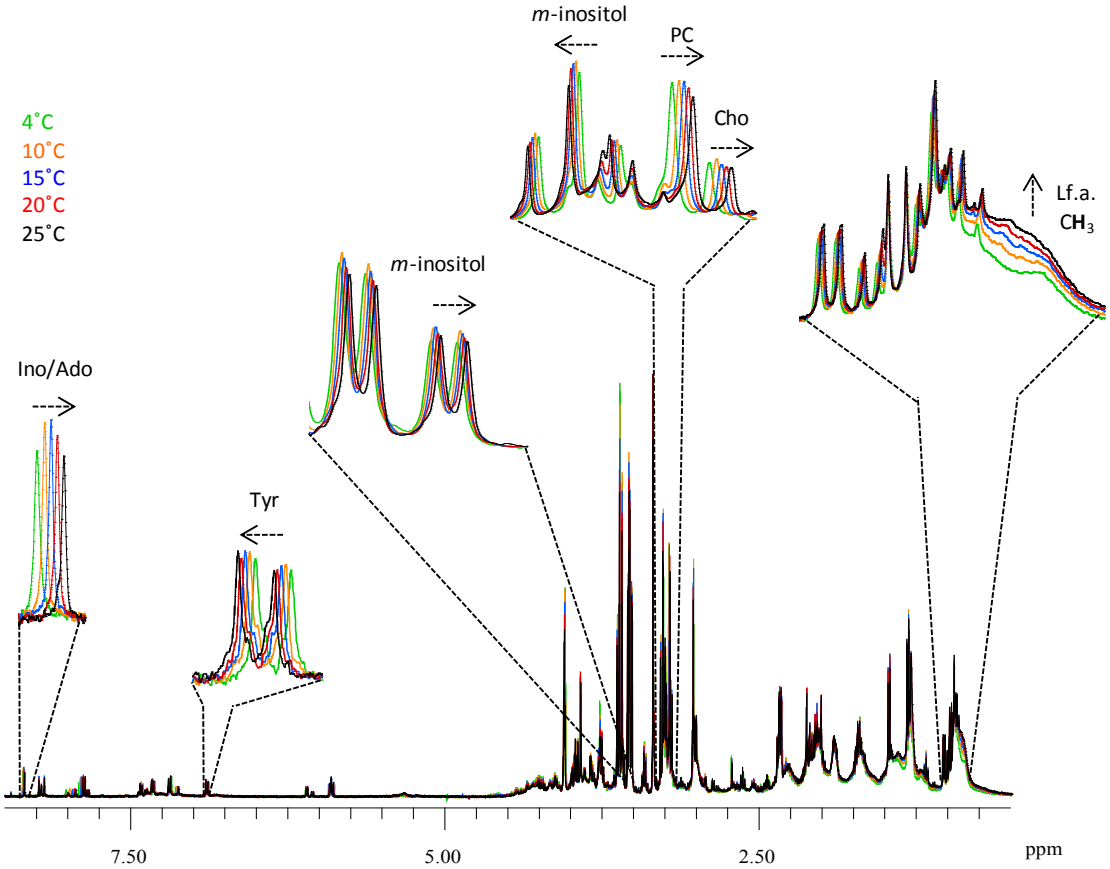

Figure 4.7. 500 MHz ^{1}H HRMAS NMR spectra of MG-63 cells acquired at different temperatures: 4, 10, 15, 20 and 25˚C (see colour legend in top left of figure). Insets show the main changes.

These results show a more marked increase in the resonances of CH_3 and $(CH_2)_n$ of lipids, compared to the results recorded as a function of spinning rate (Figure 4.6). This reflects the large sensitivity of lipids to temperature and their resulting increased molecular mobility. Visual inspection of the spectra in Figure 4.7 reveals no relevant additional changes in metabolites intensity. Therefore, considering the increases in signal intensity previously observed for several metabolites as a function of spinning rate (Figure 4.6), it may be concluded that such changes are mainly due to some sample separation (allocation of polar small molecules to the liquid phase and, hence, more mobile environment), rather than due to sample heating. In addition, for the majority of metabolites, chemical shifts suffer some deviation with temperature, again more markedly than for the spinning-induced effect, for which only choline compound peaks were seen to change in position (Figure 4.6).

Some of the above presented results confirmed earlier HRMAS studies of neuronal and glial cells (Griffin *et al.,* 2002), in which authors concluded that an increase in temperature (ranging from 4 to 27˚C) caused an increases in the intensity of CH_3 and $(CH_2)_n$ signals from lipids (no

further changes in other lipid resonances), while relative intensities for Ala and lactate remained constant. On the other hand, studies of glioma tissue (Griffin *et al.,* 2003), referred no alterations of the lipid signals between 4 and 20˚C, once again highlighting the different dynamic behaviour of lipids in distinct cellular matrixes.

The reversibility of the changes observed with temperature (Figure 4.7) was also evaluated by comparison with a spectrum subsequently acquired back at 4˚C, *ca.* 1h30min after the first spectral acquisition (Figure 4.8). Such comparison evaluates both the effect of sample heating and sample spinning for over one hour.

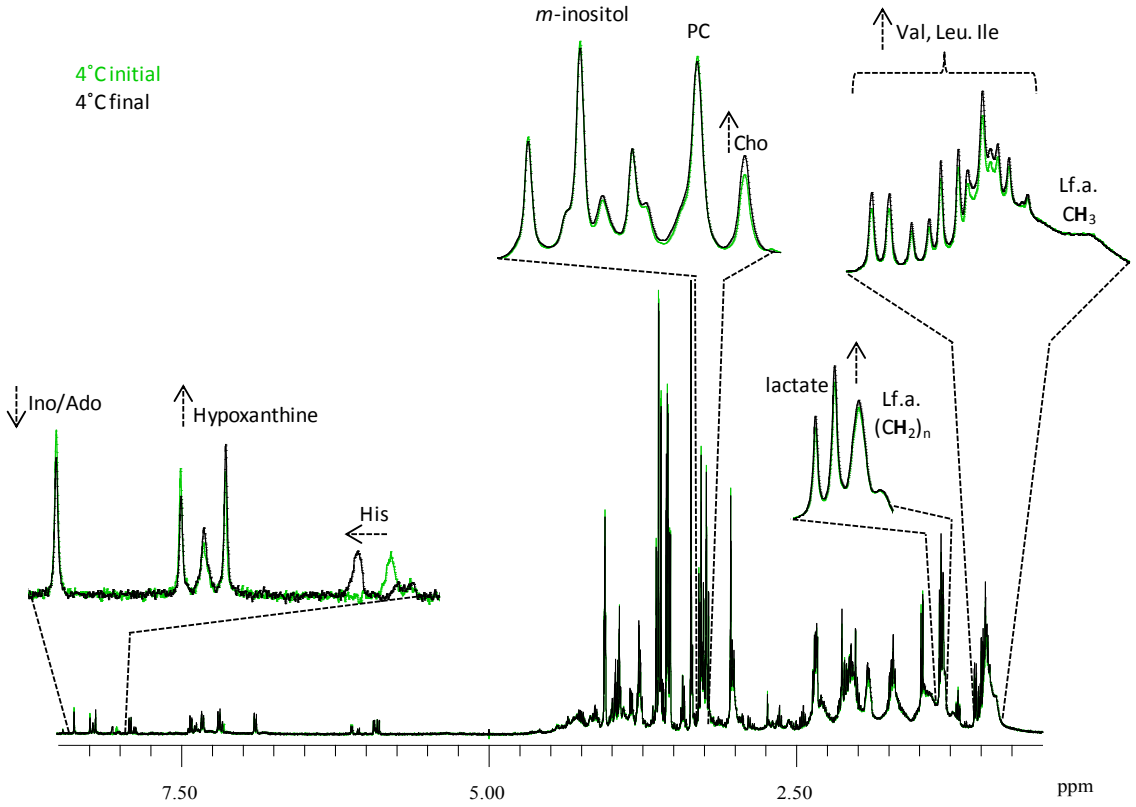

Figure 4.8. 500 MHz ^{1}H HRMAS NMR spectra of MG-63 cells acquired at 4˚C at the beginning (green) and the end (black) of temperature increase assays. Insets show the main changes.

As shown in Figure 4.8, lasting metabolic changes induced by temperature increases are revealed to be tenuous. Only discrete increases of some amino acids (Val, Leu, Ile, Lys, Met, Gly, Tyr and Phe), lactate and $(CH_2)_n$ of lipids are noted in the last spectrum acquired at 4˚C, in comparison to the first spectrum recorded at 4˚C. Increases in choline and hypoxanthine as well as decreases in inosine constitute slightly more pronounced changes. The alterations measured for these compounds probably relate both to phase separation of sample components inside the rotor and alterations to sample composition eventually promoted by some enzymatic activity.

Interestingly, the latter is supported by the fact that an irreversible change seems to occur in the chemical shift of His, shifted for higher ppm values characteristic of lower pH values.

In line with the above presented results, 4˚C was chosen as the most appropriate temperature for HRMAS analysis of cell samples.

4.3.3. Acquisition Duration

Mechanical and sample heating effects have already been demonstrated to be important in determining the exact spectral profile of cell samples. Therefore, the duration of spectral acquisition is a clear important factor to be studied too. In this work, this was evaluated by considering overnight (*ca.* 10 hours) runs, at both 4 and at 22˚C.

Visual comparison of the first and the last spectra of a 10 hours acquisition of MG-63 cells at 4˚C is shown in Figure 4.9.

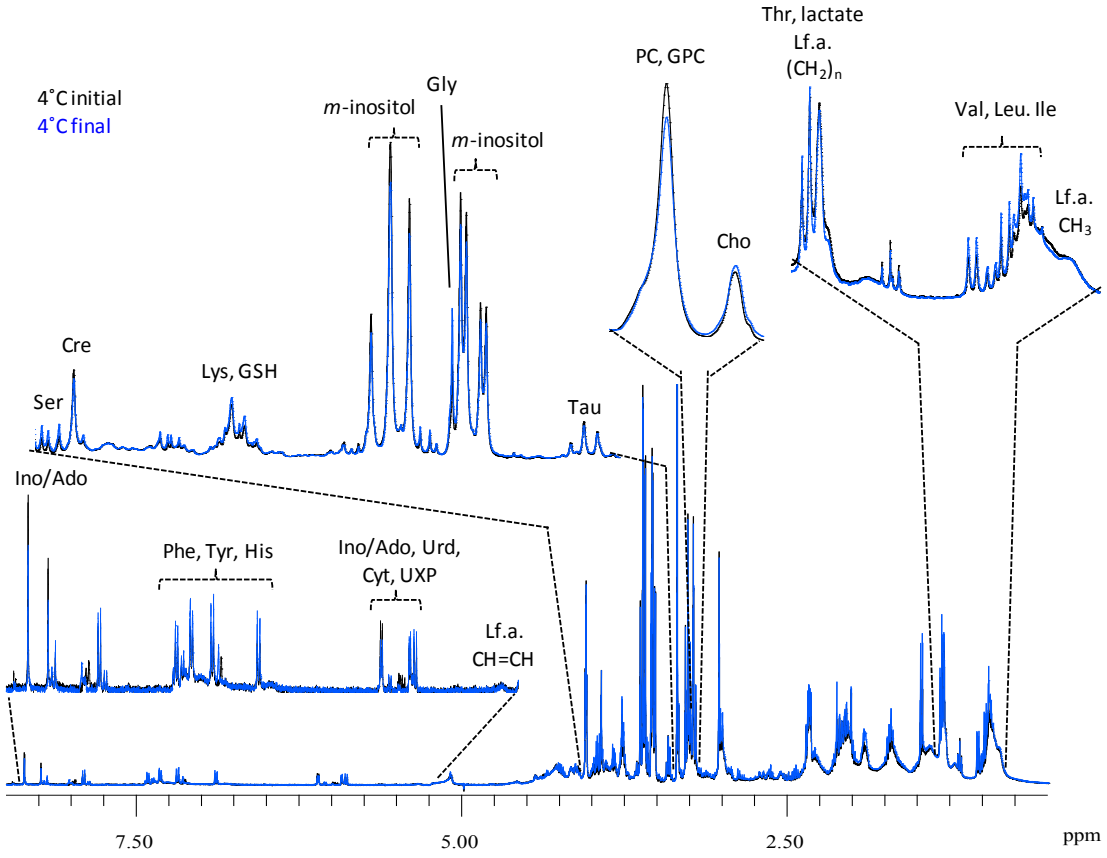

Figure 4.9. 500 MHz ^{1}H HRMAS NMR spectra of MG-63 cells at the beginning (black) and end (blue) of a 10 hours acquisition at 4˚C. Insets show the main changes.

Visual inspection of the spectra in Figure 4.9 shows that 4˚C ensures a high stability of the sample metabolite composition, over the period of 10 hours, with maximum global variations of 10% relatively to the first acquired spectrum. The most significant fluctuations were registered for uridine, hypoxanthine, Phe and Tyr. These are less resolved signals, with lower signal-to-noise ratios, what might contribute to an increased error in signal integration and thus, to the apparent more significant fluctuations registered for those metabolites.

Figure 4.10 shows de initial and final spectra of fully lysed MG-63 cells, during a 10 hours acquisition at 22˚C. A global increase of the intensity of the peaks of amino acids is clearly detected through visual inspection, as well as of uridine, hypoxanthine and choline compounds.

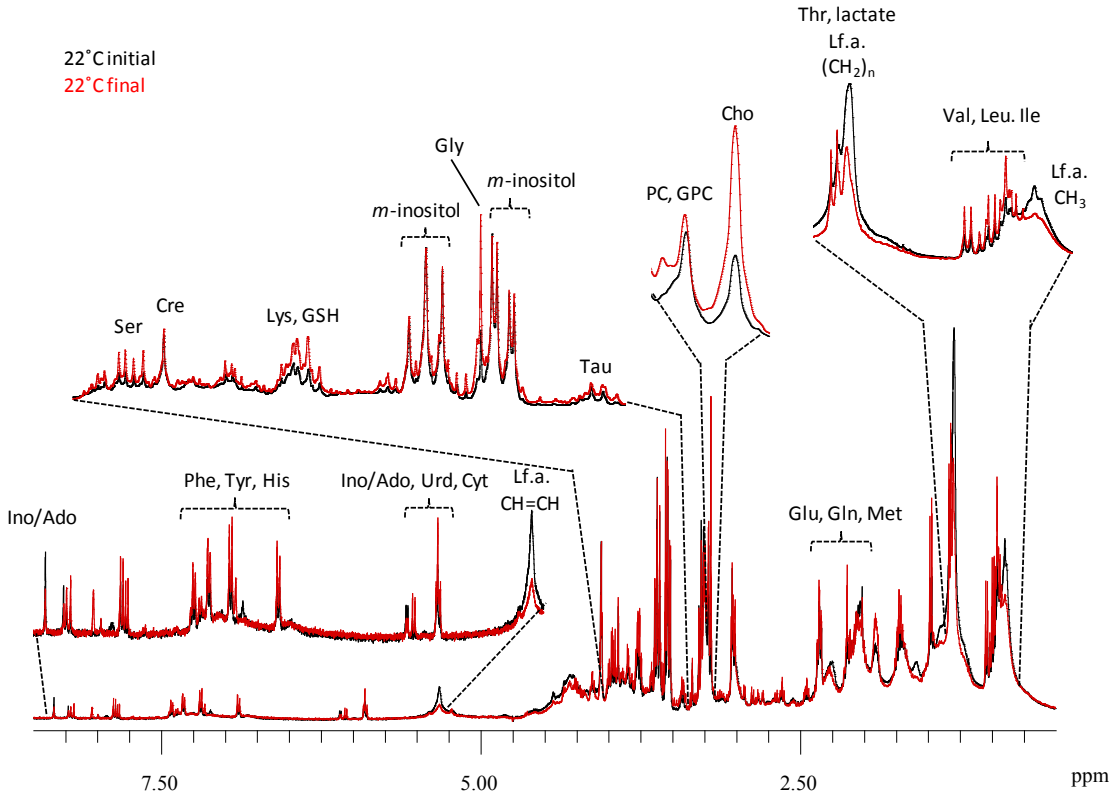

Figure 4.10. 500 MHz ^{1}H HRMAS NMR spectra of MG-63 cells at the beginning (black) and end (red) of a 10 hours acquisition at 22˚C. Insets show the main changes.

When compared to the results of previous section (4.3.2), in which increments of sample temperature were found to increase the intensities of the lipid signals, long term spinning at 22˚C induces distinct metabolic alterations. After *ca*. 10 hours spinning at 22˚C, the sample suffers a marked decrease of lipids, probably associated with their biochemical alteration in the sample since, after long term spinning at 4˚C lipid signals showed to be very stable, thus excluding the mechanical action in the sample, induced by spinning, as responsible for this lipids decrease.

Additionally, dramatic changes in the choline compounds region, as well as clear variations seen in amino acid levels were exclusive of long term spinning at high temperature (22˚C), thus highlighting the danger that spectral acquisition under such conditions represents for sample stability. The strong suggestion of a pH shift upon consecutive increases of sample temperature (section 4.3.2) is once again present. The proton of the NH group of His was also found to shift for higher ppm values, and more pronounced shifts were detected when long term spectral acquisition was performed at 22˚C, showing that temperature induces a crucial influence on sample pH, eventually due to potentiation of enzymatic activity.

PCA of the spectra registered during 10 hours at 4 and 22˚C (Figure 4.11) shows a clear clustering of the spectra acquired at 4˚C, reflecting the high stability of the sample at low temperatures, even for an acquisition of 10 hours (the shifted point refers to the spectrum acquired after 1 hour of experiment, which has slightly broader signals) . On the other hand, at 22˚C samples describe a clear time course trajectory along PC2, reflecting a greater magnitude of metabolites variation when compared to lower acquisition temperatures.

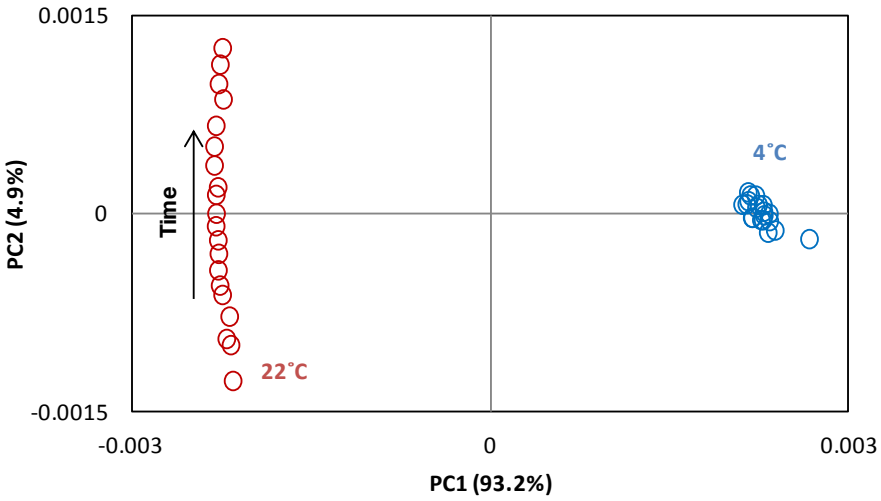

Figure 4.11. PCA scores plot ^{1}H HRMAS NMR spectra of MG-63 cells at 4˚C (blue) and at 22˚C (red), during a 10 hours acquisition time (Ctr scaling, R^2X=0.997 and Q^2=0.992). Arrow indicates time course of samples acquired at 22˚C.

Signal integration of varying peaks was used to construct time course plots corresponding to the 10 hours acquisitions at 4 and 22˚C. The intensity of lipids signals decrease at both temperatures, although more dramatically at the higher temperature (Figure 4.12a). This confirms the opposite effect compared to short-term sample spinning, even at a relative high temperature (25˚C, see Figure 4.7), a possible indication of degradation processes. In what concerns choline

compounds (Figure 4.12b), for acquisitions at 4˚C fluctuations did not reach 10% whereas, at 22˚C, and dispite the small variations of PC, dramatic increases were registered in choline (*ca*. 100%) and GPC (*ca*. 40%). These increases in choline and GPC are most probably associated with their increased mobility as a consequence of the decreased viscosity, which can occur as a consequence of the high temperatures of acquisition (if so, such increasing tendency would have been observed in Figure 4.7) or mechanical action due to long term effect.

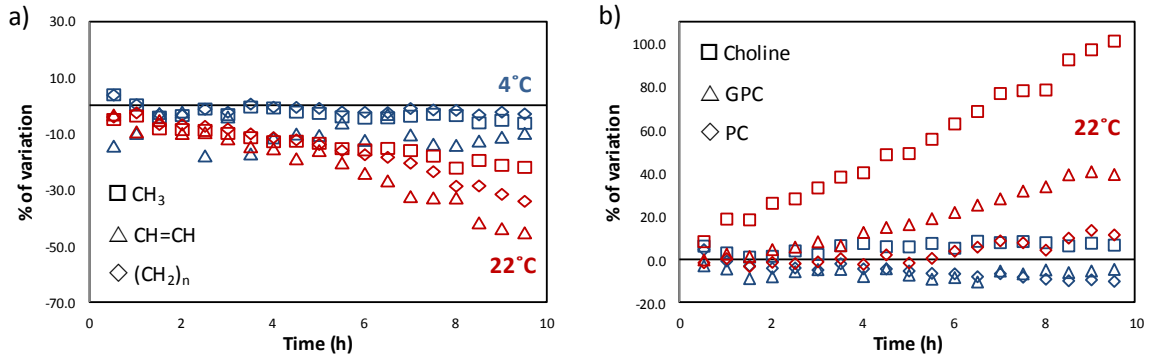

Figure 4.12. Time course variation (in %) of a) lipids and b) choline compounds, during acquisition at 4˚C (blue) and at 22˚C (red) for 10 hours.

The time course of several amino acids is presented in Figure 4.13. As can be seen, both temperatures induce an increase of amino acids with time of acquisition, however, at 22˚C, the changes nearly doubled those measured at 4˚C. Since this increase with time happens for the two tested temperatures, the observed variation is not attributable to a biochemical phenomenon but to an increased visibility of these compounds induced by concomitant phase separation (consequence of sample spinning) and some sample heating. Gly is the amino acid that shows the highest variation (*ca*. 110%), probably due to its small size. Glu levels revealed to be very stable with time, for both temperatures of acquisition.

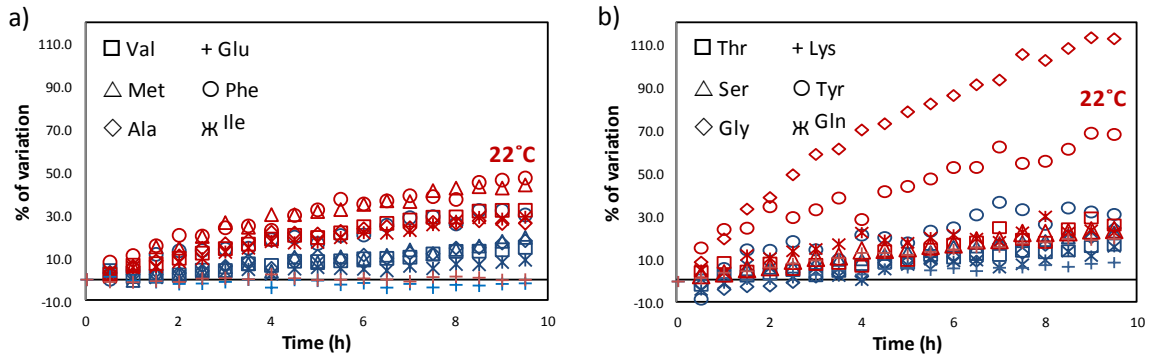

Figure 4.13. Time course variation (in %) of amino acids, during acquisition at 4˚C (blue) and at 22˚C (red) for 10 hours.

Decreases of around 30% were measured for UXP (Figure 4.14a) after 10 hours acquisition at 4˚C however it was not possible to identify this compound in the spectrum acquired at 22˚C. Increases at 4˚C are probably associated with the fact that with sample spinning this compound stays in a more mobile phase thus improving its NMR detection, while for higher temperatures, some biochemical alteration phenomenon must account for its non detection. Regarding Ino/Ado (Figure 4.14a), which revealed to be very stable at 4˚C, a considerable decrease is seen when data acquisition was performed at 22˚C, also suggesting the occurrence of biochemical alteration processes. Uridine (Figure 4.14a) shows considerable increases already at 4˚C, that in turn increase in magnitude when measurements were performed at 22˚C, suggesting that improvements in the mobility are the most important effects accounting for its variations.

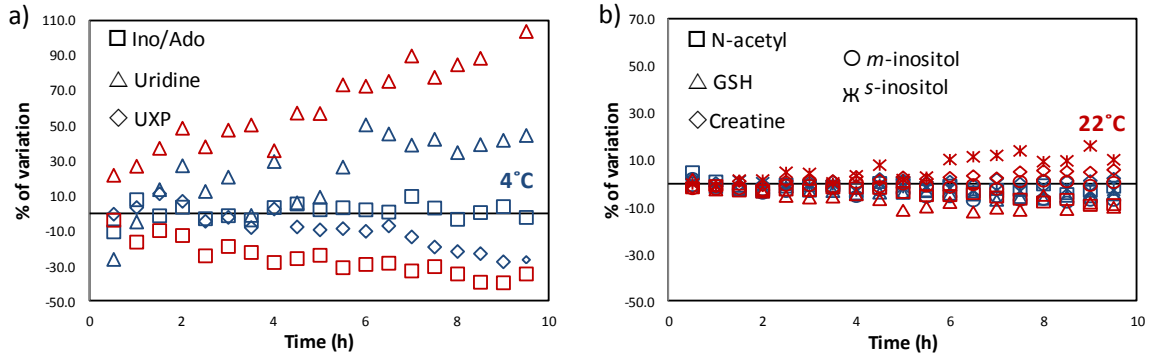

Figure 4.14. Time course variation (in %) of a) nucleotides and derivatives and b) other compounds, during acquisition at 4˚C (blue) and at 22˚C (red) for 10 hours.

Time course variation of other compounds (Figure 4.14b) shows that at both 4 and 22˚C variations in N-acetyl, creatine, *m*- and *s*-inositol do not go beyond 10%, reflecting their relative stability. A similar trend is observed for GSH, but it is interesting to note that, at 22˚C, it decreases more markedly than at 4˚C, possibly suggesting its degradation as consequence of increased stress conditions of samples at higher temperatures (Yamamoto and Ishihara, 1994).

As shown above, an increased stability of sample metabolites is achieved at 4˚C, what fostered its choice for further cell sample analysis.

4.3.4. Sample Relaxation Properties

If metabolite quantitation is intended, then the relation between relation time T_1 properties with the relaxation delay time (D1) needs to be considered. In this case, it is crucial to

guarantee that the time between consecutive scans is long enough to ensure complete relaxation of all nuclei so that quantitative intensities are achieved. This condition is accomplished when a period of, at least, 5 times the longest T_1 (Bharti and Roy, 2012) measured in the sample is respected between scans. In order to determine in which conditions the ^{1}H HRMAS NMR spectra of lysed MG-63 cells may be considered quantitative, a set of experiments were performed with different D1 times, ranging from 2 to 6 seconds (Figure 4.15).

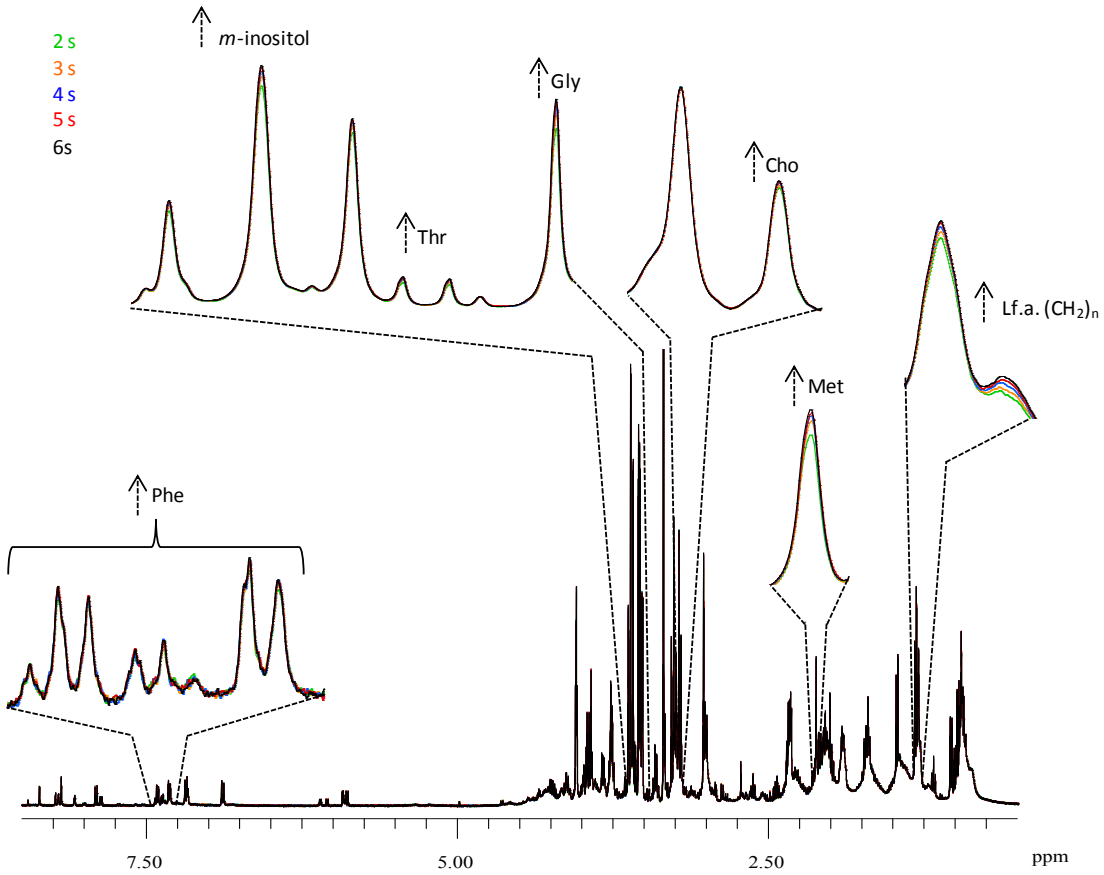

Figure 4.15. 500 MHz ^{1}H HRMAS NMR spectra of MG-63 cells with increasing relaxation delay times, ranging from 2 to 6 s (see colour legend in top left of figure). Insets show the main changes.

Results show no considerable spectral variations with D1 ranging from 2 to 6 seconds for the majority of the detected signals. Only for $(CH_2)_n$ of lipids, choline, *m*-Inositol and amino acids Gly, Met, Thr and Phe a slight increase of signal intensity was detected for increasing D1 times, specially until a relaxation delay of 4 seconds.

Table 4.2, shows the set of T_1 values obtained for all integrable signals. Indeed, these results indicate that a D1 of 4 seconds (as chosen for the spectra in this work) will not allow for the absolute quantitation of choline, some amino acids (Gly, Phe, Tau, Thr and Tyr), Ino/Ado, creatine and *m*- and *s*-Inositol, while providing quantitative measurements for PC, ethanol, lactate

and some amino acids (Ala, Glu, Ser and Val). Regarding lipid resonances (CH3, $(CH_2)_n$ and CH=CH), the apparent short T_1 values (Table 4.2) suggest that these moieties may be quantified with a D1 of 4 seconds, however it is possible that the relaxation times measured correspond to a faster-relaxing sub-population, a second slower-relaxing sub-population justifying the visual dependence of lipid peak intensities on the D1 delay. Gly is the metabolite with the highest T_1, 2.9 seconds, in sample. Since a D1 of 4 seconds is not long enough to ensure complete relaxation of all ^{1}H nuclei, only semi-quantitative information can be extracted from spectral data. To our knowledge, there are no studies in the literature in which T_1 relaxation times are determined in cell samples and, in particular in lysed cell samples.

Table 4.2. Proton longitudinal relaxation times (T_1) measured for peaks identified in 500 MHz ^{1}H HRMAS NMR spectra of lysed MG-63 cells.

Family of compounds	Metabolite (δ, ppm)	T_1 (s)	Standard Deviation
Lipids	Lipids –C**H**$_3$ (δ 0.91)*	0.258	2.037E-02
	Lipids –(C**H**$_2$)$_n$ (δ 1.31)*	0.415	4.412E-02
	Lipids –C**H**=C**H**- (δ 5.33)*	0.315	3.469E-02
Choline compounds	Choline (δ 3.21)**	1.380	3.189E-02
	Phosphocholine (δ 3.23)	0.541	2.238E-02
Amino Acids	Alanine (δ 1.48)	0.442	3.349E-02
	Glutamate (δ 2.35)	0.698	1.800E-02
	Glycine (δ 3.56)**	2.916	1.451E-02
	Phenylalanine (δ 7.32)**	1.157	7.690E-03
	Serine (δ 3.97)	0.605	1.495E-02
	Taurine (δ 3.42)**	1.350	1.899E-02
	Threonine (δ 3.58)**	1.209	1.834E-02
	Tyrosine (δ 6.89)**	0.989	8.267E-03
	Valine (δ 1.04)	0.249	2.247E-02
Nuc. and Deriv.	Inosine/Adenosine (δ 8.36)**	1.483	8.024E-03
Other Metabolites	Acetate(s) (δ 2.02)	0.541	3.147E-02
	Creatine (δ 3.94)**	1.371	2.949E-02
	Ethanol (δ 1.19)	0.551	6.106E-02
	Lactate (δ 4.13)	0.422	3.577E-02
	m-Inositol (δ 4.05)**	1.143	2.487E-02
	s-Inositol (δ 3.34)**	1.317	1.654E-02

* Compounds partially quantifiable with a D1 of 4 seconds. ** Compounds not absolutely quantifiable with a D1 of 4 seconds.

The choice of the appropriate D1 value to be used is performed based on a compromise between two factors: best possible signal intensities of all resonances and the total acquisition time of the spectrum. For maximum intensities of all peaks and, hence, full quantitative conditions, a D1 of *ca*. 15 seconds would have to be considered, thus involving considerably longer acquisition times, compromising sample integrity during acquisition. Therefore, the value of 4 seconds was chosen, with the knowledge that absolute quantitation may only be considered for a subset of compounds, while allowing for relative intensity analysis for all compounds. In metabolomics, the intention is normally to detect profile changes, that is, corresponding relative

intensity changes. Hence, semi-quantitative conditions are usually employed and completely acceptable, whenever absolute quantitation is not specifically aimed for.

In addition to T_1 measurements, transverse relaxation times (T_2) help to evaluate the relative overall molecular mobility of different metabolites in the sample, information which may be valuable in distinguishing different dynamic environments for instance regarding free and macromolecule-bound metabolites. The results of T_2 measurements for all integrable resonances are listed in Table 4.3.

Table 4.3. Proton transverse relaxation times (T_2) measured for peaks identified in 500 MHz ^{1}H HRMAS NMR spectra of lysed MG-63 cells.

Family of compounds	Metabolite (δ, ppm)	T_2 (ms)	Standard Deviation
Lipids	Lipids –C**H**$_3$ (δ 0.91)	35.16	2.061E-02
	Lipids –(C**H**$_2$)$_n$ (δ 1.31)	373.8	1.101E-01
Choline compounds	Choline (δ 3.21)	587.5	2.069E-02
	Phosphocholine (δ 3.23)	242.6	1.942E-02
Amino Acids	Alanine (δ 1.48)	306.8	7.379E-02
	Glutamate (δ 2.35)	322.0	3.250E-02
	Glycine (δ 3.56)	419.8	5.129E-02
	Phenylalanine (δ 7.32)	343.7	4.098E-02
	Serine (δ 3.97)	301.4	5.814E-02
	Taurine (δ 3.42)	597.8	4.934E-02
	Threonine (δ 3.58)	331.5	4.673E-02
	Tyrosine (δ 6.89)	349.2	7.454E-02
	Valine (δ 1.04)	182.3	7.050E-02
Nuc. and Deriv.	Inosine/Adenosine (δ 8.36)	553.9	5.354E-02
Other Metabolites	Acetate(s) (δ 2.02)	179.2	7.662E-02
	Creatine (δ 3.94)	382.6	3.010E-02
	Ethanol (δ 1.19)	924.7	1.223E-01
	Lactate (δ 4.13)	226.0	9.499E-02
	m-Inositol (δ 4.05)	450.2	8.555E-03
	s-Inositol (δ 3.34)	342.1	2.592E-02

T_2 values range from 35 ms for CH_3 of lipids to 925 ms for ethanol. For CH_3 of lipids the determined T_2 is of the order of tens while for all other measured metabolites, including for $(CH_2)_n$ of lipids it is of the order of hundreds, suggesting a lower mobility for the lipid chain terminals, which is difficult to explain, at this stage. Again, the possible multi-exponential behaviour of lipid resonances should be tested for a more complete dynamic characterisation of these compounds. Among the small compounds, Val, acetate and lactate exhibit relatively low T_2 times, showing that these compounds may be possibly adsorbed to macromolecules. The very distinct values found for choline (587 ms) and PC (242 ms) may also reflect different dynamic environments and inter-compound interactions affecting each of these compounds.

4.4. Spectral Profile Reproducibility Check and Influence of Sample Storage

4.4.1. Spectral Profile Reproducibility Check

The reproducibility of the ^{1}H HRMAS NMR profile of lysed MG-63 cells was assessed in order to establish the impact of the practical protocols of cell culture, harvesting and mechanical lysis on the spectral profile of these cells. This knowledge is useful in two ways: firstly, it helps to determine the minimal level of spectral variability inherent to sample preparation above which meaningful variations (e.g. due to drug exposure) may be detected; secondly, it enables the identification of the compounds which are more sensitive to experimental protocol and for which over interpretation of variations should be avoided. Figures 4.16 and 4.17 show the ^{1}H HRMAS NMR spectra of triplicates of each of three independent assays, for lysed MG-63 cells collected at 0 and 48 hours, respectively.

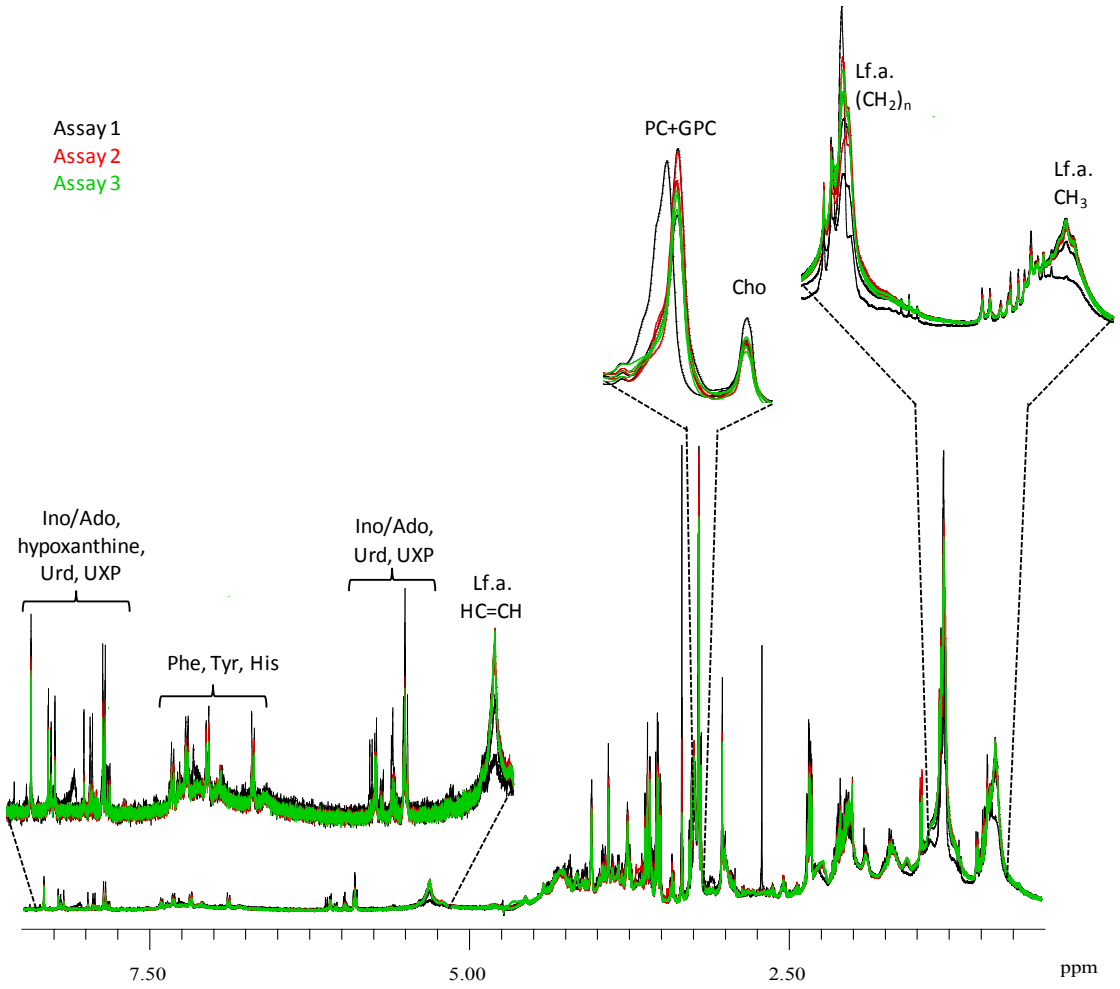

Figure 4.16. 500 MHz ^{1}H HRMAS NMR spectra of lysed MG-63 cells collected at 0 hours, at 22˚C. Different colours correspond to distinct assays (see top left of figure).

All these spectra were recorded at 22˚C, despite the previous choice of 4˚C as the adequate temperature of acquisition. This was so due to lack of refrigerating capability of the instrument used (500 MHz in CERMAX, ITQB, Oeiras, Portugal). This should not, however, hinder any conclusions to be drawn, since all time intervals included in protocol (during which sample degradation may occur), were similar.

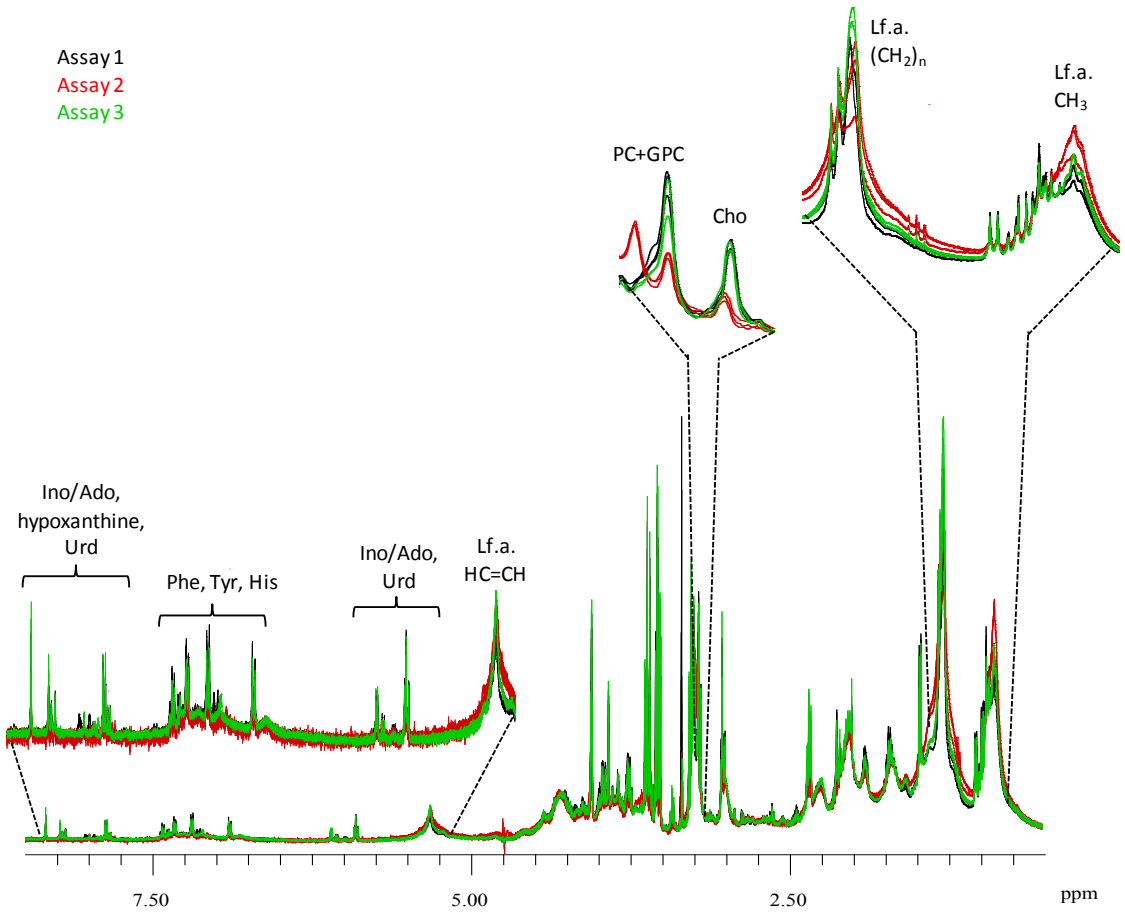

Figure 4.17. 500 MHz ^{1}H HRMAS NMR spectra of lysed MG-63 cells collected at 48 hours, at 22˚C. Different colours correspond to distinct assays (see top left of figure).

Regarding intra-assay comparison of spectra, the highest degree of dispersion between replicates occurred at 0 hours (Figure 4.16) in assay 1, with one replica showing lower lipids signals and a different profile in choline compounds, and at 48 hours (Figure 4.17) in assay 2, with one replica showing lower lipid signals. In relation to inter-assay comparison, spectra show a low dispersion between assays at 0 hours (Figure 4.16, with the already refered exception of one replica) and a low dispersion between assays 1 and 3 at 48 hours (Figure 4.17). At 48 hours, differences are noted in assay 2, namely a global decrease of amino acids, *m*- and *s*-Inositol, creatine, uridine and Ino/Ado, together with a dramatically different profile of the choline compounds region. Regarding other time points (12, 18 and 24 hours), similar changes were

observed in some of the spectra replica. It is difficult to advance a specific explanation for the changes noted, since the same experimental procedures were in principle followed for all 3 assays, but this study shows that small differences may occur and have some impact on the measured cell profile, namely in relation to lipids and choline compounds (eventually due to nuances in the lysis protocol (as shown in section 4.1).

The PCA scores plot of PC1 *vs* PC3 coloured as function of assay (Figure 4.18) enables general differences between spectra to be visualised (similar tendencies were observed in the PCA scores plot of PC1 *vs* PC2, with a slightly higher dispersion between samples). This result shows no clustering of samples according to assay, which indicates a general agreement between assays, with exception of assay 1 (in black in Figure 4.18) for which a large dispersion (not related to time course) is confirmed graphically. In assay 2 (in red in Figure 4.18), samples at 48 hours are separated from the rest of the samples, as again already inferred by visual inspection, this having been attributed to a global decrease of amino acids, *m*- and *s*-Inositol, creatine, uridine and inosine and a singular profile of the choline compounds region. Samples of assay 3 (in green in Figure 4.18) are those with lower dispersion, and for which no clear time course tendency was found.

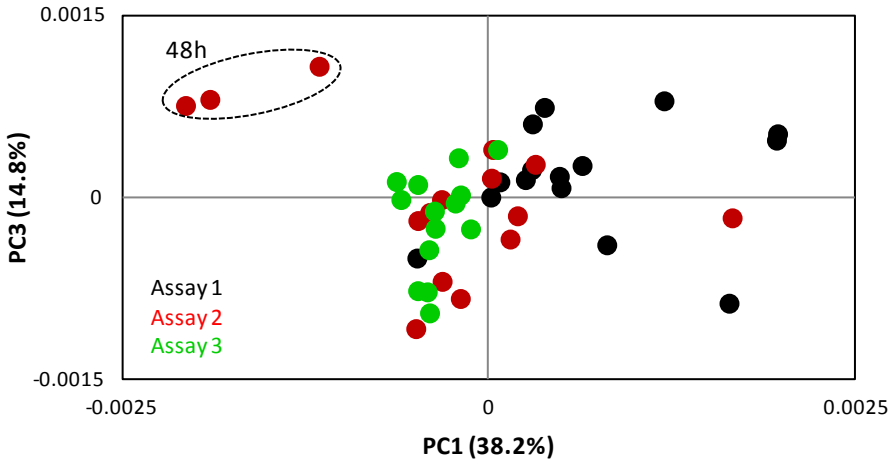

Figure 4.18. PCA scores plot of PC1 *vs* PC3 of reproducibility assays. Ctr scaled model, 5 components, R^2X=0.869 and Q^2=0.740. Different colours correspond to distinct assays.

The analysis of the same PCA scores plot coloured per assay, but comparing PC2 *vs* PC3 (Figure 4.19) shows that even though there are variations between assays, their time course is similar and describable along PC3. This result indicates the advantage of comparing time course

trajectories instead of single points in time. Figure 4.19 also shows that experimentally-induced dispersion leads to shifts along the PC2 axis. In order to get further insight into these differences between samples from assay to assay, several spectral signals were integrated and *p*-values determined.

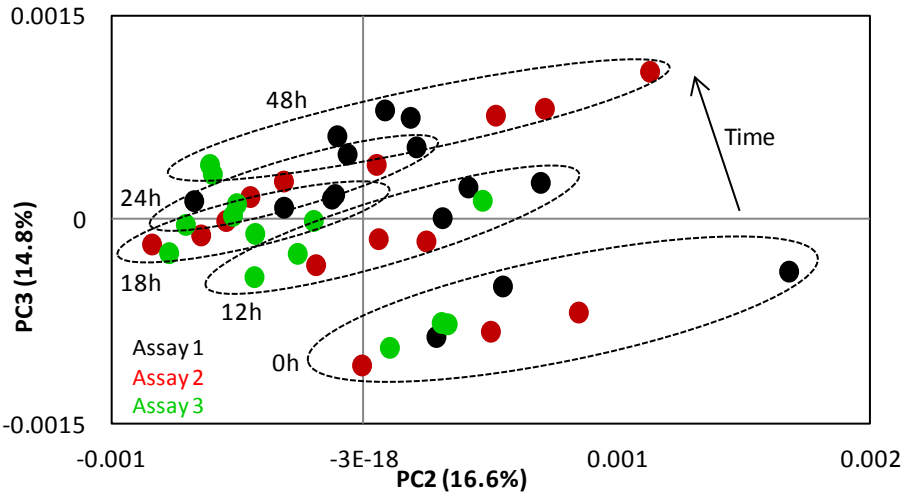

Figure 4.19. PCA scores plot of the PC2 *vs* PC3 of reproducibility assays. Ctr scaled model, 5 components, R^2X=0.869 and Q^2=0.740. Different colours correspond to distinct assays.

Differences in lipid resonances were found to be small but statistically relevant only at 18 and at 48 hours (Figure 4.20) possibly as a consequence of slightly different sample spinning durations due to the sample-dependent need to optimize NMR acquisition (namely for sample shimming). This is consistent with observations previously described in section 4.3.3. Also, since these experiments were performed at room temperature (22˚C), possible slight variations in the time required for complete defrosting and temperature homogenisation within the sample may contribute to the above described changes in lipid resonances. Regarding choline compounds, choline levels (Figure 4.20d) revealed to be very stable from assay to assay, with just one statistically relevant difference at 48 hours between assay 1 and 2. PC and GPC (Figure 4.20e) showed a considerable number of statistically relevant differences. These results once again show how choline compounds (particularly PC and GPC) reflect unintentional differences in the lysis protocol and for this reason, special care have to be given when considering drug-induced changes in this type of compounds.

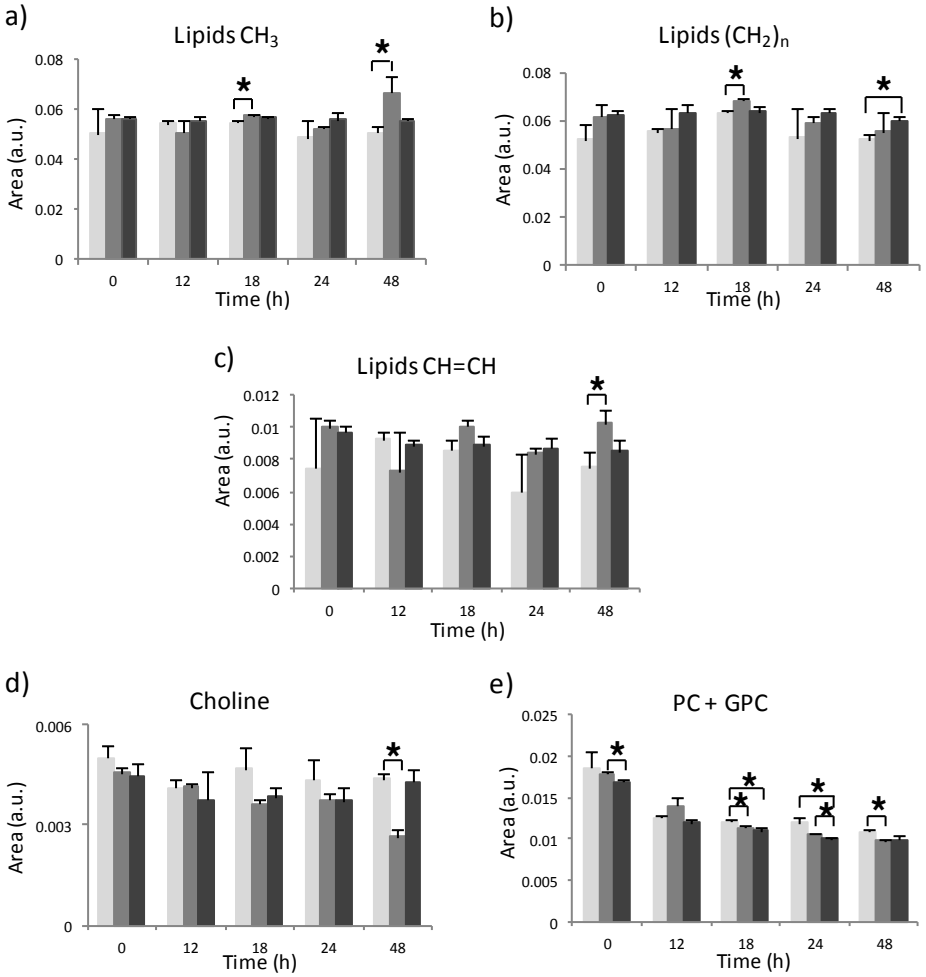

Figure 4.20. Time course integrals of selected lipids and choline compounds signals. (Error bars reflect n=9. Assay 1 (■), assay 2 (■) and assay 3 (■); *p<0.05)

Amino acid analysis (Figure 4.21) reveals significant variations (magnitudes varying from amino acid to amino acid) between assays for Phe, Gly, Leu, Lys, Met, Tyr, Pro and Val. These differences were more frequent at 48 hours but for Gly and Pro additional significant differences were also found for other time points. This probably relates once again to slight differences in the time necessary to optimise spectral acquisition and the temperature of acquisition (which, as shown in section 4.3.2, interferes with amino acids levels).

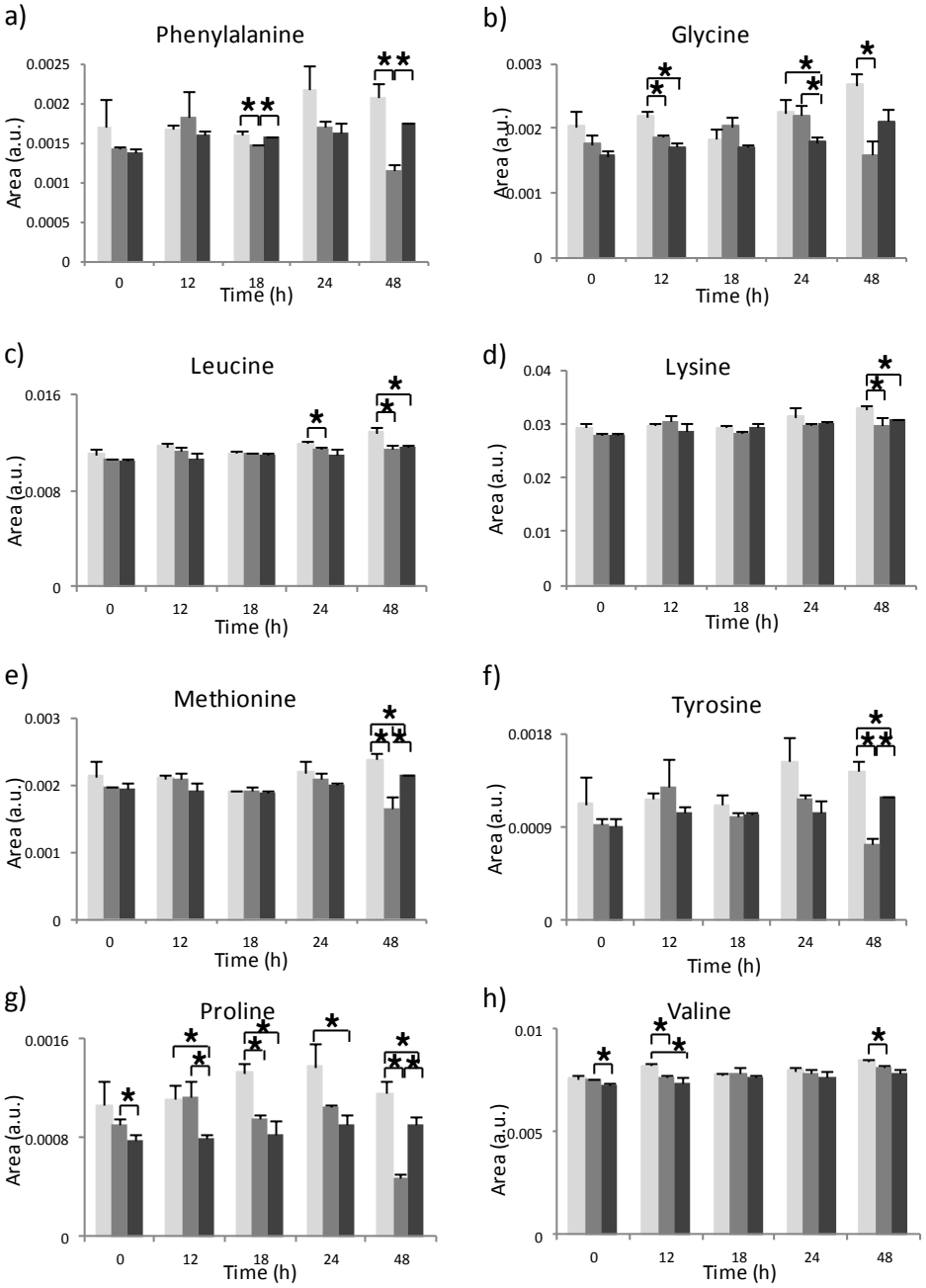

Figure 4.21. Time course integrals of selected amino acids. (Error bars reflect n=9. Assay 1 (■), assay 2 (■) and assay 3 (■); *p<0.05)

For Ino/Ado and uridine (Figure 4.22), statistically relevant differences between assays were measured possibly due to biochemical alterations related to slight differences in temperature and time of spectral acquisition, the latter implying also differences in samples spinning periods (and respective consequences in metabolites visibility by NMR).

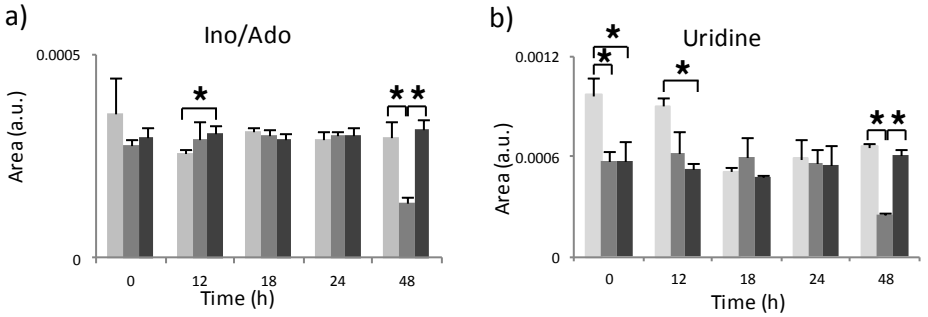

Figure 4.22. Time course integrals of nucleotides and derivatives. (Error bars reflect n=9. Assay 1 (■), assay 2 (■) and assay 3 (■); *p<0.05)

As shown in Figure 4.23, significant differences were also detected for creatine (0 and 48 hours), *m*- and *s*-inositol (18, 24 and 48 hours). Interestingly, despite the global decrease over time, no statistically relevant differences were found in GSH levels between assays (Figure 4.23).

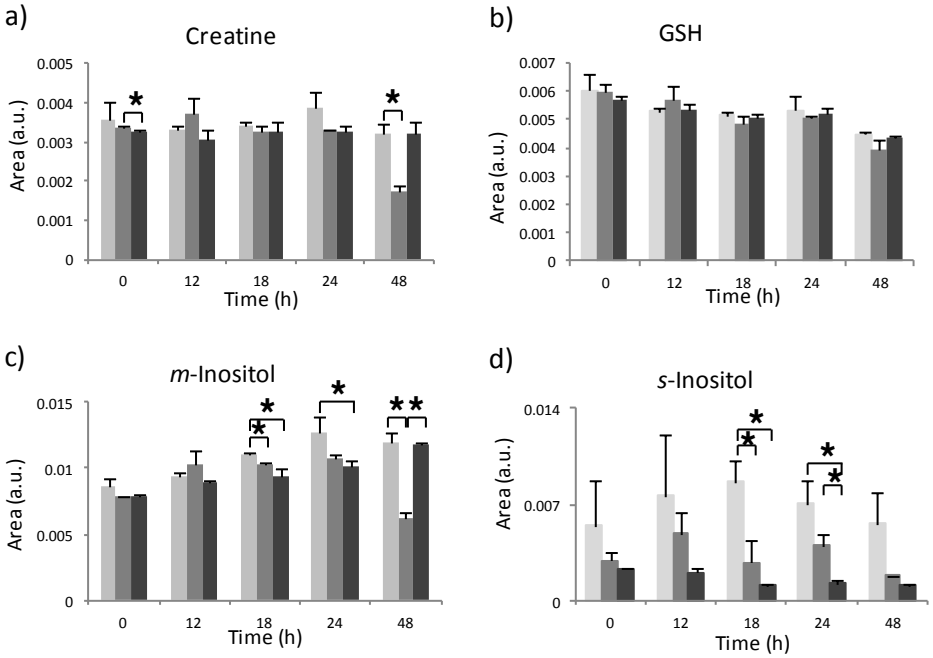

Figure 4.23. Time course integrals of other compounds. (Error bars reflect n=9. Assay 1 (■), assay 2 (■) and assay 3 (■); *p<0.05)

These results show that the whole cell handling procedure results in intra and inter-assay differences between samples that must be taken into consideration when searching for drug- or other perturbation-induced changes.

4.4.2. Cell Passage Number

The influence of cell passage number (designated by #) on the metabolic profile of MG-63 cells is here presented at a very exploratory level (only one replica per condition) and, to our knowledge, for the first time. Figure 4.24 shows the ^{1}H HR MAS NMR spectra of lysed MG-63 cells with increasing number of cell passages.

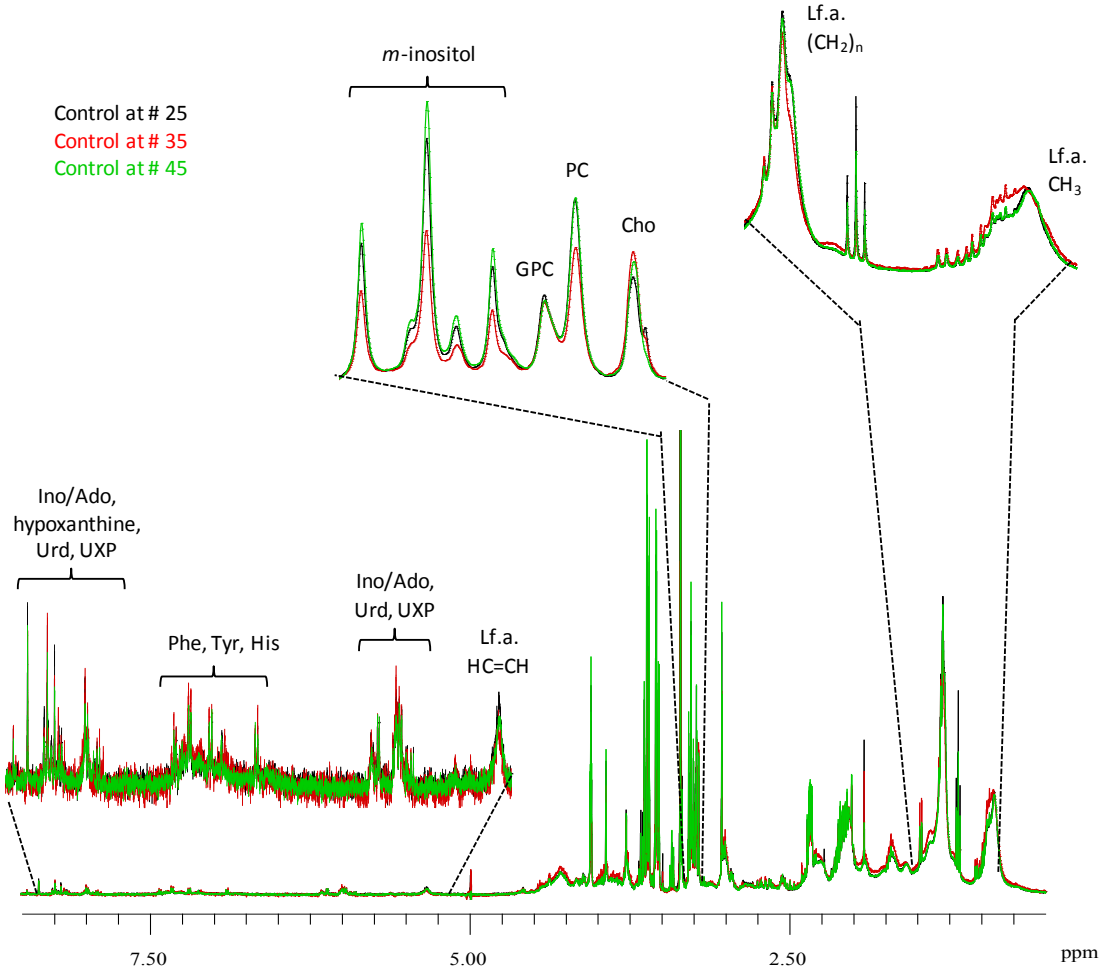

Figure 4.24. 500 MHz ^{1}H HRMAS NMR spectra of MG-63 cells with passage numbers 25, 35 and 45. Different colours correspond to distinct assays (see top left of figure).

Minor changes are addressed when comparing the spectra of MG-63 cells at #25 and at #45. However, when comparing these with the spectrum of MG-63 cells at #35, a considerable number of differences were identified: cells at #35 showed a global increase of the amino acids Val, Leu, Ile, Ala, Lys, Gly and Phe and decrease of Glu and Tau. Slightly decreased $(CH_2)_n$ and CH=CH resonances of lipids and lower creatine, *m*- and *s*-inositol were also seen in #35 cells together with changes in choline:PC ratio. Since very similar profiles were found for cells at #25 and #45 and due to the lack of replicates, it seems apparent that the effect of passage numbers in

not significant (at least in the range considered), the differences seen in the #35 sample being possibly due to effects of the handling protocol (culture, harvesting, mechanical lysis) of those cells.

Besides trying to understand if the number of cell passages influences the profile of control cells, this experiment also searched for differences in the drug-response profile of MG-63 cells with increasing number of passages since, hypothetically, the minor changes detected between cells at #25 and #45 might be determinant in response to drug, resulting in different profiles of treated-cells. Figure 4.25 compares the metabolic profile of MG-63 cells with increasing number of passages exposed to 30 µM cDDP for 24 hours.

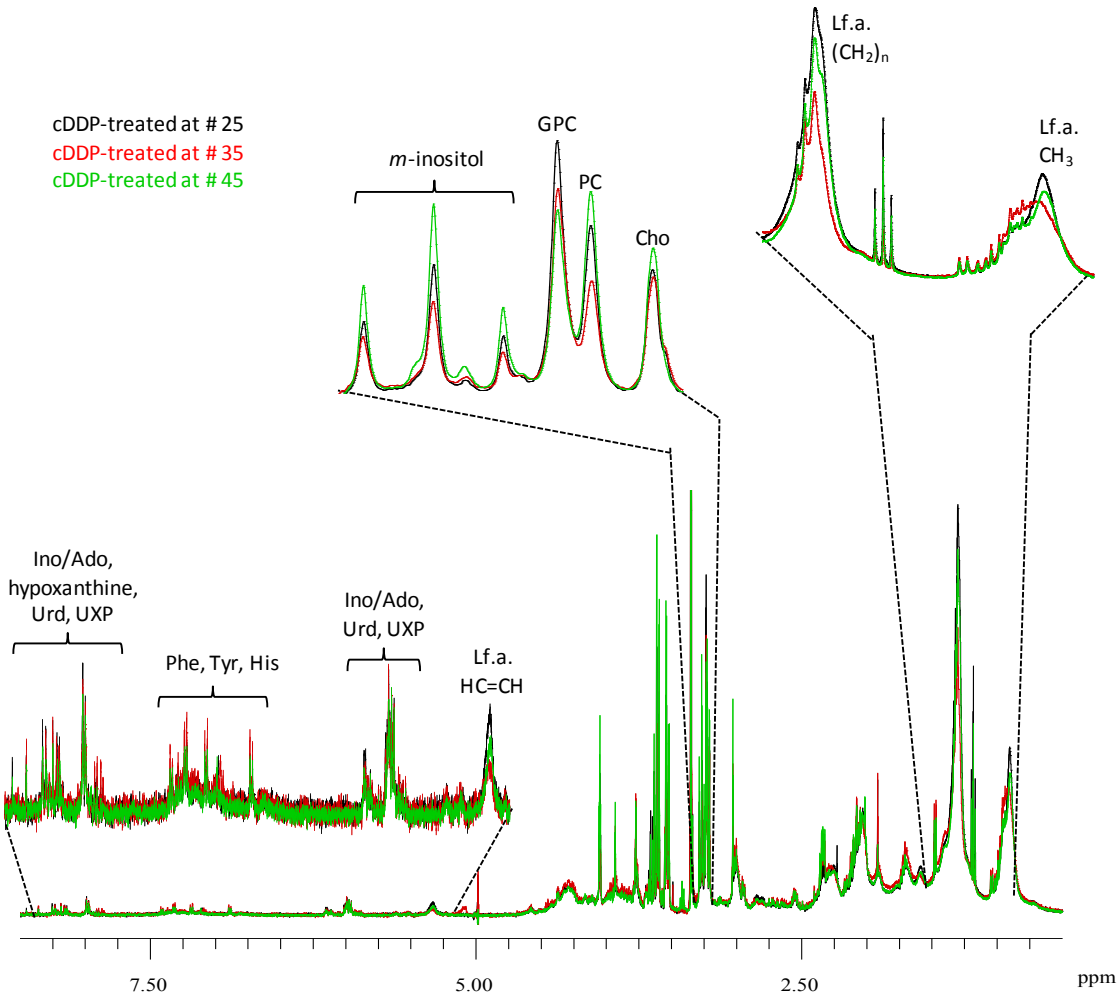

Figure 4.25. 500 MHz ^{1}H HRMAS NMR spectra of cDDP-treated MG-63 cells with passage numbers 25, 35 and 45. Different colours correspond to distinct assays (see top left of figure).

Visual inspection reveals, once again, marked differences in the profile of #35 cells, when compared to #25 and #45, what cannot be dissociated from the different metabolic profile of the respective control cells (already mentioned). However, when comparing the response profile of cells at #25 with that of #45, whose controls were found to be very similar, a considerable number of changes were detected in cells with higher number of passages: increased Glu, Tau, creatine and *m*-inositol together with slight decreased lipids signals and a change in the global profile of the choline-compounds region (induced by a decrease in GPC).

Signals of both control and treated spectra were also integrated and, since some differences were already noted in control conditions, the results expressed as *treated:control ratios* (not shown), in order to aid interpretation. Since this was an exploratory experiment, only one sample *per* condition was obtained (no error bars) thus, when analyzing the calculated ratios, only those showing consistent increasing/decreasing tendencies with number of passages were considered relevant. Slight increasing tendencies were found for PC, Glu, Thr, Tau, *m*-Inositol and creatine while a decreasing tendency for GPC was detected in response to cDDP as the number of cell passages increases.

Despite exploratory, this experiment suggests that the metabolic response of MG-63 cells which differ by several number of passages might be slightly different namely affecting some choline compounds (PC and GPC), amino acids (Glu, Thr and Tau), *m*-Inositol and creatine, and therefore must be considered for cell studies. Further studies would be needed confirm the magnitude of these changes.

4.4.3. Sample Stability During Storage at -80˚C

Beyond the frequent impossibility of immediate analysis, biological samples are often too valuable to be discarded after spectral acquisition. In this line, it is important to know how long cell samples can be stored and still ensure accurate metabolic profile information. To evaluate this, a total of 11 samples were considered for analysis of stability during a 27 months period of storage at -80˚C. Visual comparison of the spectra acquired at increasing times of storage is shown in Figures 4.26 (0.5-4.1 ppm) and 4.27 (5.2-8.5 ppm).

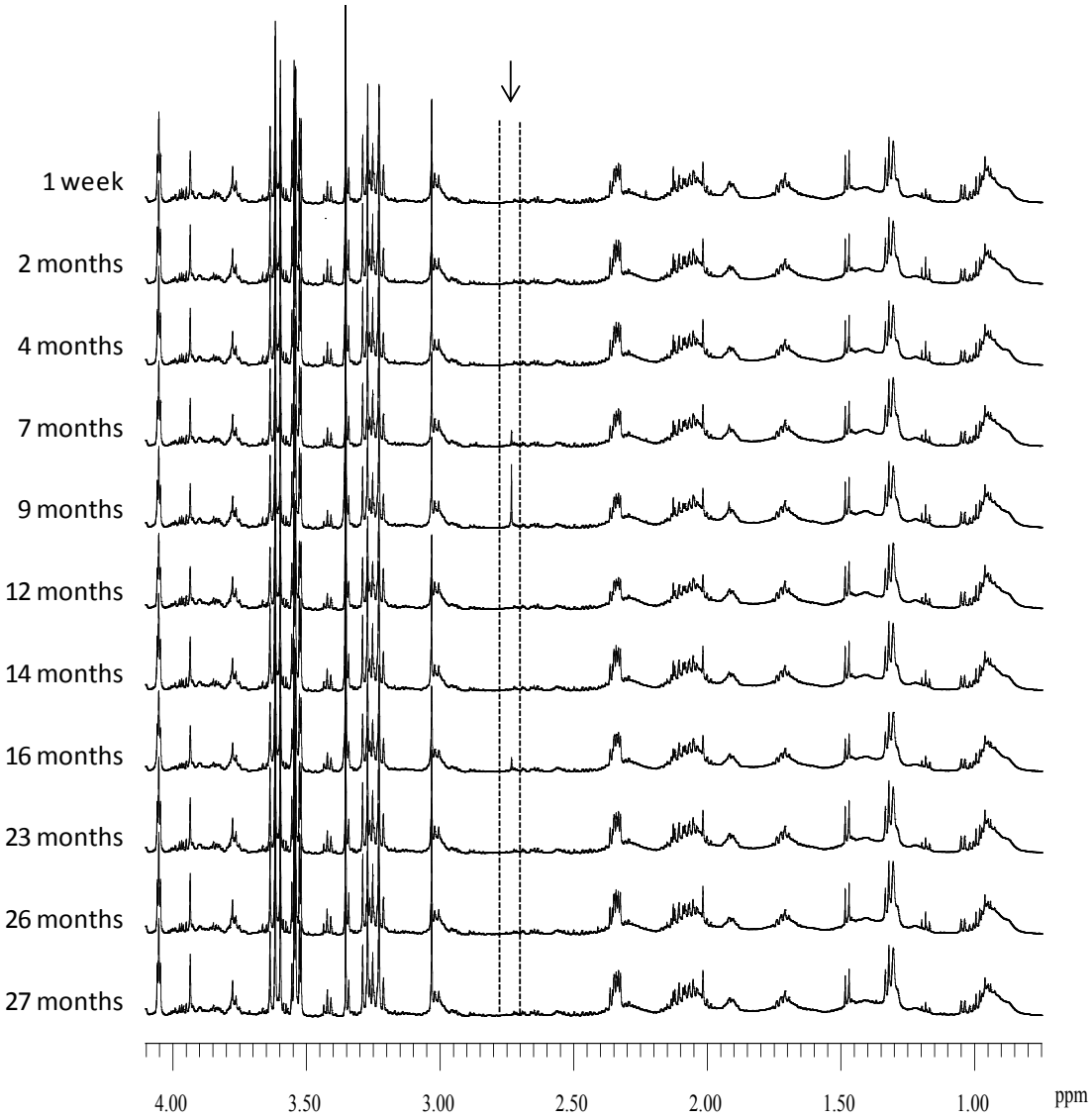

Figure 4.26. 500 MHz ^{1}H HRMAS NMR spectra of MG-63 cells with increasing times of storage, ranging from 1 week to 27 months. 0.5-4.1 ppm region is shown. (Arrow indicates Un. at δ 2.73).

Analysis of the 0.5-4.1 ppm region (Figure 4.26) does not show any clear time course variation of metabolites (either amino acids, lipids or other compounds like *m*-Inositol, creatine or GSH) during the 27 months of storage at -80˚C. Interestingly, a singlet at δ 2.73 is observed occasionally in the spectra of frozen samples, at 7, 9 and 16 months of storage. Since it was not possible to assign the corresponding metabolite and the respective variations do not describe a consistent change over time, it is not possible to advance an interpretation for such signal. Visual inspection of Figure 4.27 (5.2-8.5 ppm region), suggests a slight change in uridine and UXP levels together with random chemical shift fluctuations of the His resonances, thus suggesting slight pH variations of samples in time. No further changes in other metabolites were noted, thus

suggesting that storage at -80˚C is able to preserve cell samples for long periods of storage with minor metabolic consequences.

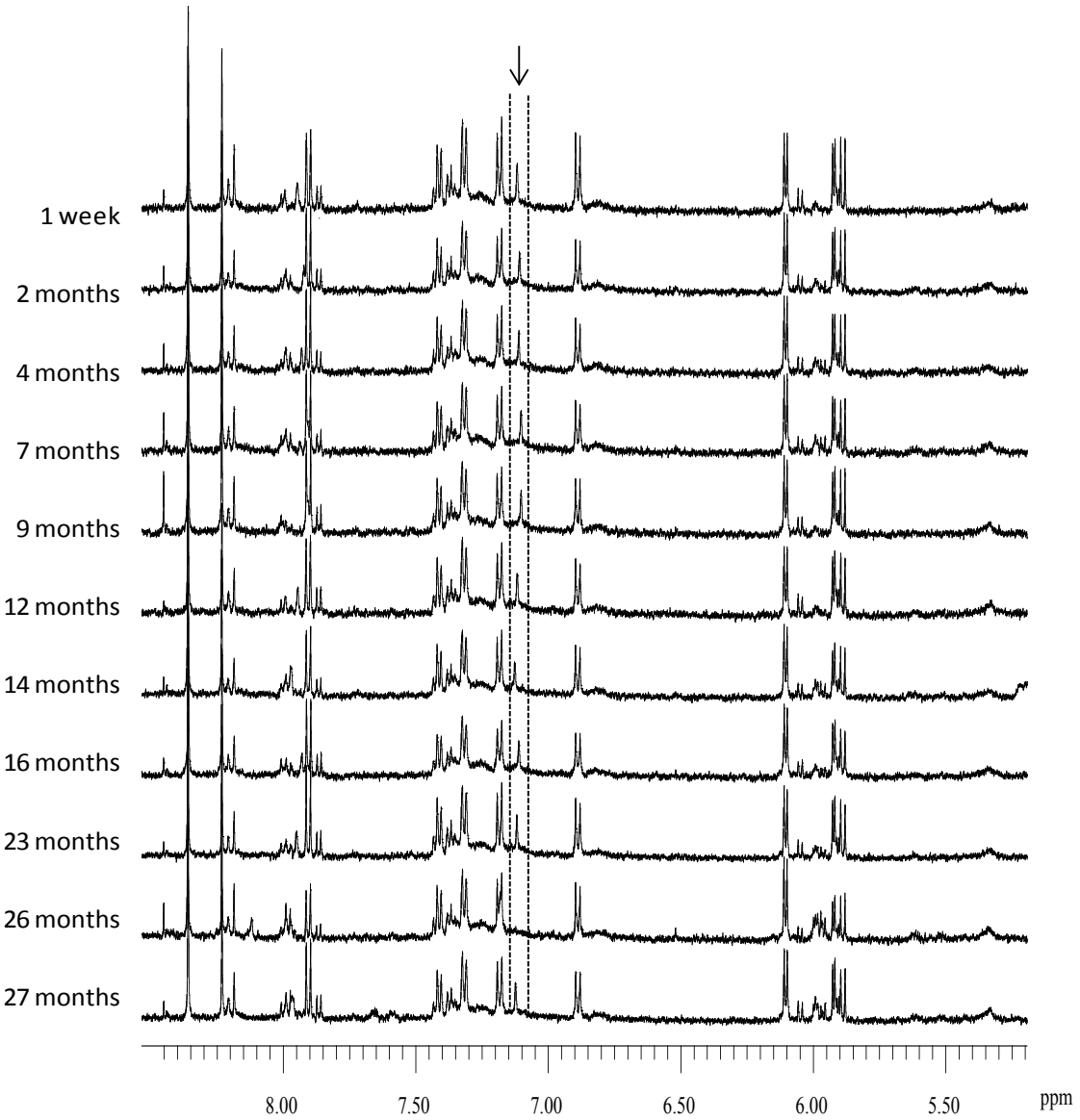

Figure 4.27. 500 MHz ^{1}H HRMAS NMR spectra of MG-63 cells with increasing times of storage, ranging from 1 week to 27 months. 5.2-8.5 ppm region is shown. (Arrow indicates His resonance).

Peak integration was performed to identify small quantitative changes as a consequence of storage. Regarding lipids (Figure 4.28a), CH_3 is the most stable resonance during the tested period of storage at -80˚C. $(CH_2)_n$ of lipids registered increases of around 10% and -CH=CH- changed very considerably, with a percentage of variation at the end of the 27 months of around 50%. However, during the 2 months of storage all the three lipid resonances (CH_3, $(CH_2)_n$ and CH=CH) suffer only a negligible variation. For choline-compounds (Figure 4.28b) fluctuations around -10 to 10% were measured.

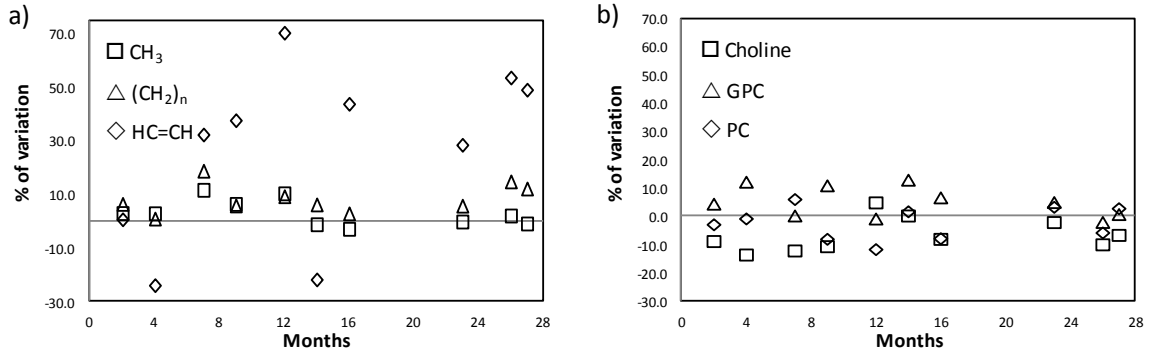

Figure 4.28. Time course (in %) of a) lipids and b) choline compounds during storage at -80˚C.

The analysis of the time course of amino acids (Figure 4.29) shows maximum negative fluctuations of around 20% for most amino acids and a slightly higher variation (around 30% negative) for Tyr, while Glu and Lys presented variations that were less than 10%.

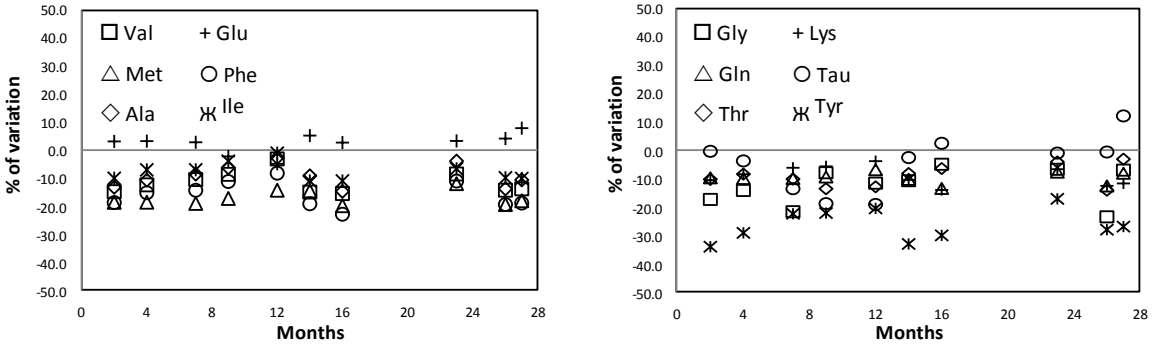

Figure 4.29. Time course (in %) of amino acids during storage at -80˚C.

Negligible changes were detected for Ino/Ado but uridine changed of around 40% (negative) after 26 months of storage (Figure 4.30a). GSH, *m*- and *s*-Inositol (Figure 4.30b) and creatine levels oscillated during the period of the test of around 10%.

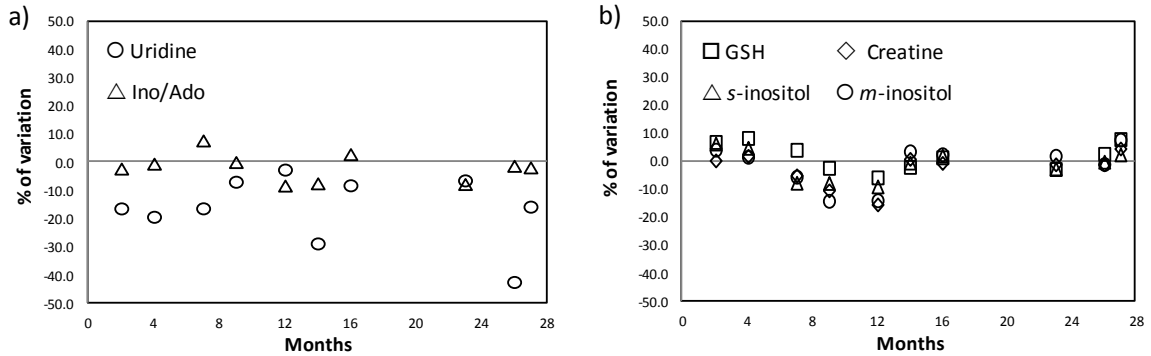

Figure 4.30. Time course (in %) of a) nucleotides and derivatives and b) other compounds during storage at -80˚C.

The low magnitude variations in the majority of metabolites found in these results, seem to suggest that lysed MG-63 cell samples have a high stability to storage at -80˚C for long periods of time, although these results do not enable the establishment of a window time during which spectra can be recorded with an acceptable stability of the metabolites in the sample. Further studies with replicates would be necessary to infer on the magnitude of the error associated with these measurements. Nevertheless, since most variations were around 10% (both positive or negative), this was tentatively assumed as the uncertainty dimension of the fluctuations here shown. Although some of the metabolites achieve slightly high percentages of variation over time (in relation to the first recorded spectrum), such variations were quite random in time and do not enable a clear tendency (of increase or decrease) to be established. Additionally, and recalling the value of these type of samples, studies of freeze-thaw cycles would also retrieve valuable information on the number of times that these samples can be analysed without significantly altering their global metabolic profile.

Variations in more intense resonances are assumed to be more reliable than those of low intensity peaks (with low S/N). Thus, variations in more reliable signals as choline compounds and lipids (exception for CH=CH, with low S/N) show increased stability over the entire period, what strongly suggests a high stability of lysed cell samples over the 27 months of storage at -80˚C.

5. Metabolic Impact of Conventional Drugs on Osteosarcoma MG-63 Cells

Administration of cisplatin (cDDP), doxorubicin (DOX) and methotrexate (MTX), often together with ifosfamide, constitute one of the most frequently adopted preoperative chemotherapy protocol for the treatment of osteosarcoma (Ta *et al*., 2009). Despite the already existing knowledge on the mechanism of action of these drugs, there is still little understanding on the metabolic adaptations that tumour cells undergo when exposed to them. Such knowledge may pave the way to the identification of possible metabolic markers of therapeutic efficacy. Accordingly, this chapter deals with the metabolic effects of cDDP, DOX and MTX, in sole administration, on the human osteosarcoma MG-63 cell line.

5.1. Cytotoxicity Assay Results

Dealing with different drugs, with distinct cytotoxic activities, requires preliminary assays to determine, for each drug, the concentration capable of inducing a certain extension of cell damage, either cell death (cytotoxic activity) or growth inhibition (cytostatic effect). These studies enable to determine the so called inhibitory concentration (IC), namely the IC_{50} values, that represent the drug dosage that results in 50 % of cell death (for a certain period of drug exposure). In the present work, IC_{50} at 24 hours was the concentration used for each drug in the cell culture experiments, in order to follow the metabolic consequences of treatment as a function of time, for a total of 48 hours.

Figure 5.1 shows the results of the Trypan blue tests performed for the human osteosarcoma cells that were harvested for HRMAS NMR analysis. This test was performed in order to assess the number of intact cells in each sample and ensuring that a suitable number of cells (5 to 10 million) is obtained for NMR analysis. For cDDP in the MG-63 cells, the IC_{50} value at 24 hours was found to be 30 μM. As shown in Figure 5.1a, the cytotoxic effect of cisplatin is already visible at 12 hours, becoming more pronounced, as expected, for increasing exposure times, with a clear reduction in the number of living cells up to 48 hours. Moreover, 30 and 50 μM of the drug have very similar effects on drug-induced cell death. Regarding DOX, the IC_{50} value at 24 hours was determined to be 3 μM and a clear decrease in the number of living cells occurs for increasing incubation periods with the drug (Figure 5.1b). As for MTX, the IC_{50} value is 3 μM at 24

hours but, interestingly, no clear decrease on the number of living cells is detected for higher periods of drug exposure, as opposed to the results obtained for cDDP and DOX (Figure 5.1c). This result indicates that the mechanism of action of MTX is somehow less effective in the longer term on MG-63 cells than cDDP or DOX.

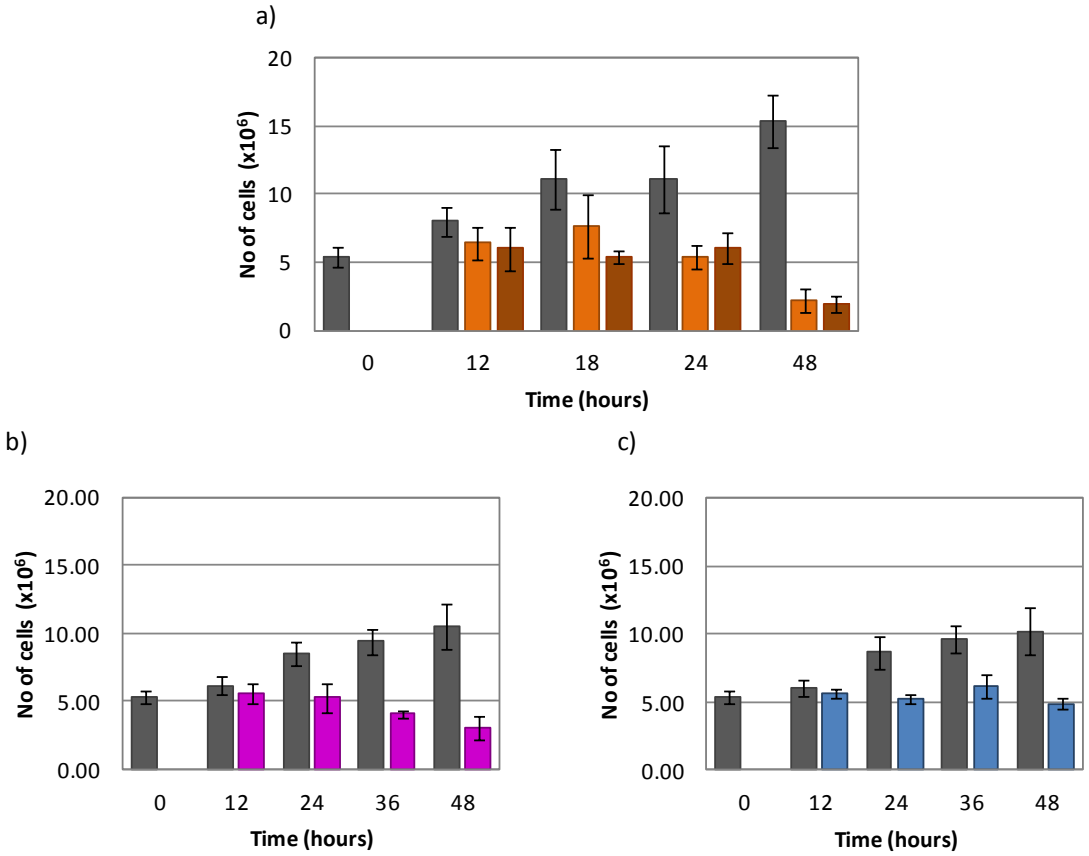

Figure 5.1. Dose- and time-response plots of the cytotoxic effect of a) cDDP, b) DOX and c) MTX, in sole administration, to MG-63 cells. Cell proliferation was evaluated by Trypan blue assay (as described in Chapter 3). Control (■); a) 30 µM (■) and 50 µM (■) cDDP; b) 3 µM DOX (■); c) 3 µM MTX (■). The data represent the average ± mean standard deviation from n=3 experiments, carried out in duplicate (n=6).

Hence, the IC_{50} concentration determined for cDDP is ten times higher than that obtained for DOX and MTX (30 *vs* 3 µM). Additionally, this concentration was found to induce an increased cell death over time (up to 48 hours) for both cDDP and DOX, while for MTX no significant cytotoxic effect was observed beyond 24 hours of drug exposure (Figure 5.1).

The IC_{50} values determined for cDDP and DOX are in agreement with those obtained in MG-63 cells, at 24 hours of drug-exposure, by Naruse and coworkers (Naruse *et al*., 2007), of 28.6 and 3.4 µM, respectively. In relation to MTX, the determined IC_{50} value (3 µM) is more than fifteen times higher than that obtained by Diddens (Diddens *et al*., 1983): 0.17 µM in MG-63 cells at 24

hours of MTX-treatment. Other three references refer quite distinct IC_{50} values for 72 hours of MG-63 treatment with MTX: 0.03 µM (Palmero *et al*., 2006; Bodmer *et al*., 2007) and 3.8 nM (Cole *et al*., 2002). In the present work, the results obtained were considered reliable since they were reproduced for all three independent experiments, each carried out in duplicate (section 3.1.3.1).

5.2. ^{1}H HRMAS NMR Analysis

In order to assess and interpret the metabolic changes induced by each of the above refered three drugs in sole administration, ^{1}H HRMAS NMR experiments were carried out as discussed below.

5.2.1. Cisplatin (cDDP)

The metabolic changes that occur in MG-63 cells exposed to cDDP are hereby analysed by ^{1}H HRMAS. These results were reported for the first time by us in Duarte *et al*., 2010 and are here presented with improved reprocessing of the NMR data, as described in a recent publication of our own (Lamego *et al*., 2014). At the time of the first report, the NMR spectra had been normalised to total area in order to account for differences in sample quantities, which became particularly significant when comparing controls with drug-treated samples (the latter containing much fewer cell numbers). However, with this type of data normalization, important variation in very intense and/or broad resonances markedly determine the normalization factor, eventually hiding changes in low intensity resonances. By defining one or a set of reference spectra, probabilistic quotient normalization (PQN) normalization finds the most probable normalisation factor for each sample spectrum (see Chapter 2) this better accommodating alterations of low intensity signals. Together with peak alignment, this data reprocessing should result in a more accurate assessment of spectral changes.

In order to compare the mean behavior of the drug-treated samples, visual inspection was performed by comparing the average ^{1}H HRMAS NMR spectra of the three samples collected at each condition (time point and drug concentration). Prior to the analysis of the cDDP-induced effects, it is important to evaluate how the metabolic profile of MG-63 cells changes with time, as a consequence of cell basal metabolism (controls). As depicted in Figure 5.2, 48 hours of cell growth result in a slight decrease of the unsaturation degree of lipids (δ 5.33) and of creatine, Glu, GSH and UXP compounds, suggesting a certain degree of stress affecting the cells, probably due

to their increased confluence in culture. Increases in *m*-Inositol levels may relate to the osmoregulatory function of this metabolite.

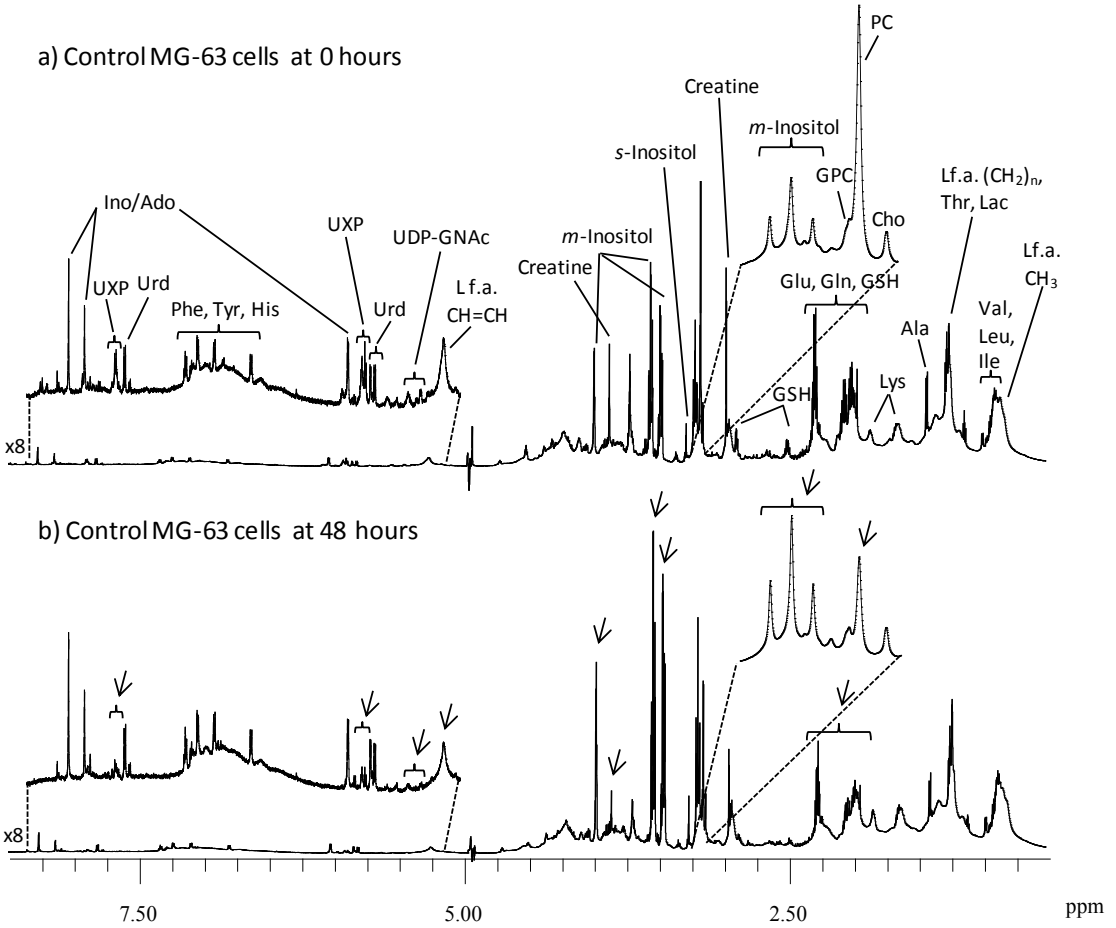

Figure 5.2. Average 700 MHz ^{1}H HRMAS NMR spectra of control MG-63 cells at: a) 0 hours and b) 48 hours. Insets show expansions of choline compounds (3.2-3.3 ppm) and aromatic (5.2-8.5 ppm) regions. Main assignments are noted and visible spectral changes due to time course are marked by arrows.

Visual inspection of the ^{1}H HRMAS NMR spectra of MG-63 cells exposed to cDDP, showed that, in general, drug-induced metabolic changes become more relevant as exposure time increases (not shown) as will be discussed further ahead in this section. Firstly, the metabolic impact of different concentrations of cDDP (30 and 50 μM) on MG-63 cells after 48 hours of treatment (Figure 5.3) is discussed.

As it is shown by the arrows in Figure 5.3b and 5.3c, the metabolic alterations induced by a 48 hours treatment with 30 and 50 μM of cDDP are essentially the same, generally more pronounced in the latter case. These changes comprise a marked increase of all detectable lipid resonances, together with increased choline (δ 3.21) and GPC (δ 3.24) levels, increased UXP (δ 5.99 and δ 7.98) and UDP-GNAc (δ 5.52) derivatives and decreased Ino/Ado (δ 8.36) contents. In

order to confirm visual findings and unveil the most relevant drug-induced metabolic changes, multivariate analysis was applied to the ^{1}H HRMAS spectra of controls and cDDP-treated cells.

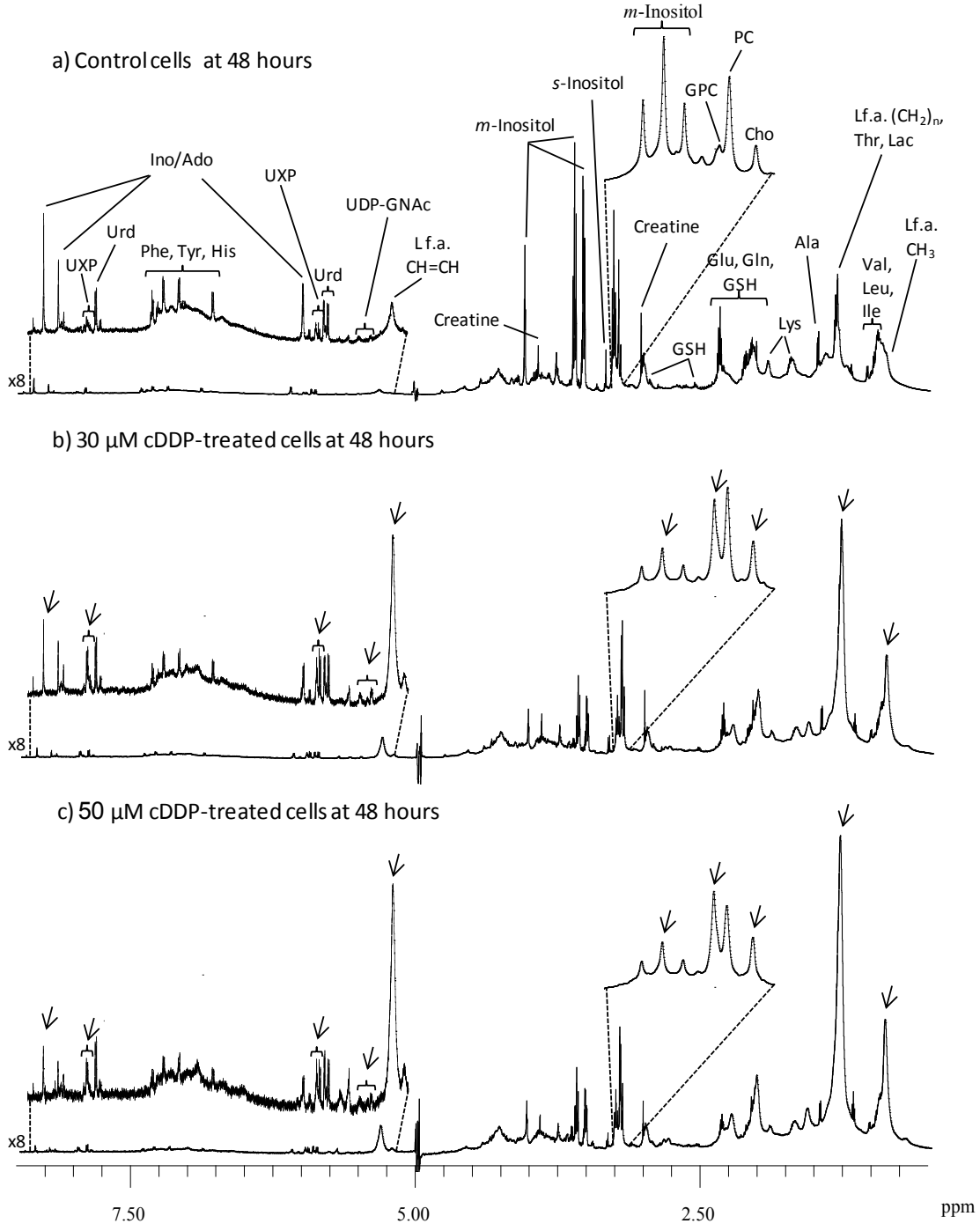

Figure 5.3. Average 700 MHz ^{1}H HRMAS NMR spectra of MG-63 cells, at 48 hours: a) under control conditions, b) exposed to 30 µM cDDP and c) exposed to 50 µM cDDP. Insets show expansions of choline compounds (3.2-3.3 ppm) and aromatic (5.2-8.5 ppm) regions. Main assignments are noted and visible spectral changes due to drug exposure are marked with arrows.

Due to the similarity between the results of the two tested cDDP concentrations, for the sake of simplicity, only the results from 30 µM treatment (IC_{50} concentration) are shown here (Figure 5.4).

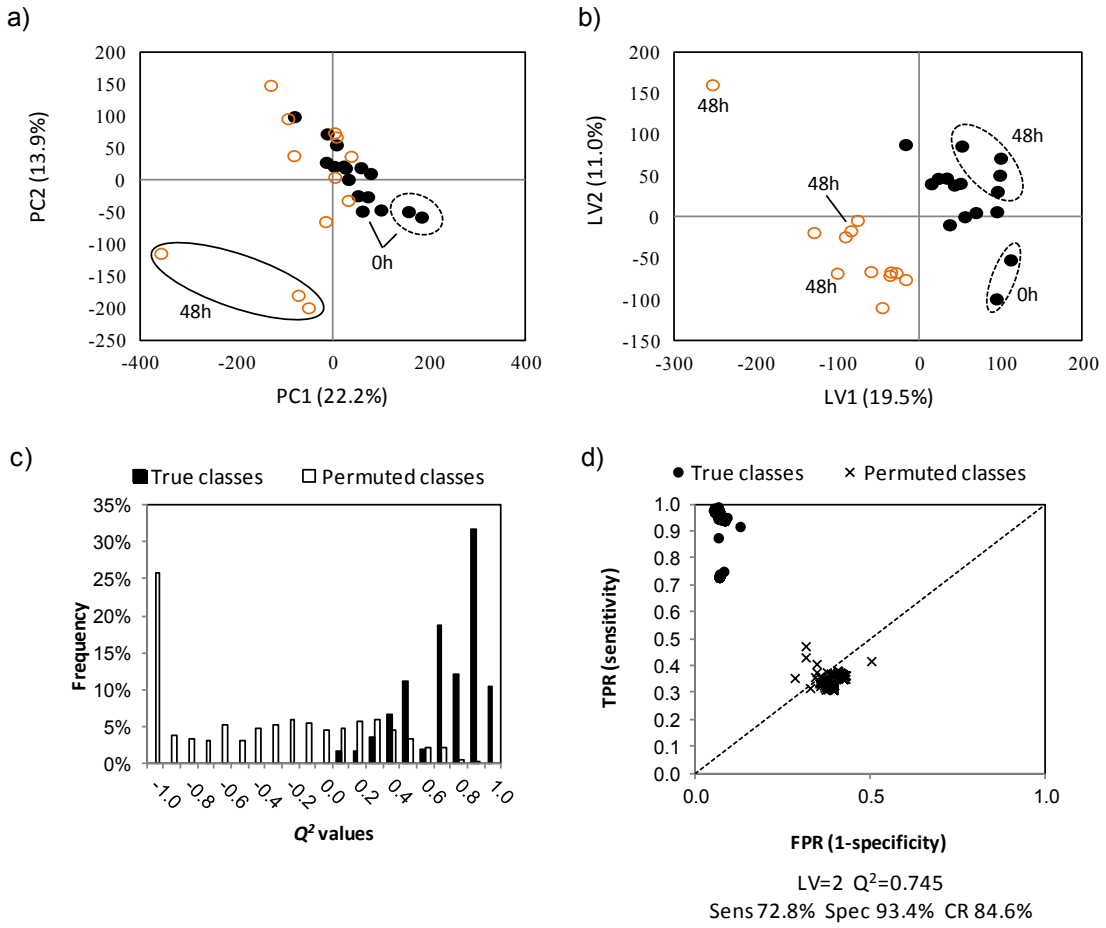

Figure 5.4. Multivariate analysis of controls (●) and 30 µM cDDP-treated (○) cells: (a) PCA scores plot, UV scaled data (b) PLS-DA scores plot, UV scaled model with 2 components calculated with R^2X = 0.306, R^2Y = 0.888 and Q^2 = 0.745. MCCV results of PLS-DA model in b): c) Q^2 distributions and d) ROC plots of true and permuted models. TPR: true positive rate, FPR: false positive rate, Sens.: sensitivity, Spec.: specificity, CR: classification rate.

PCA analysis (Figure 5.4a) shows that no significant discrimination occurs between controls and cDDP-treated cells along PC1 until 24 hours of treatment, but a clear discrimination is observed for cells treated for 48 hours (negative PC1 and PC2). No evident time course tendency can be seen for either control or treated samples. The corresponding PLS-DA scores plot (Figure 5.4b) shows good separation (Q^2 0.745) between controls and cDDP-treated samples along LV1, although time course tendencies are again not completely consistent, while a progression tendency is suggested from negative to positive LV2 for controls and for lower negative LV1 in the case of treated samples. The robustness of group discrimination is reflected in a very low Q^2

distribution overlap (Figure 5.4c) and reasonable MCCV results: 72.8% sensitivity, 93.4% specificity and 84.6% classification rate (Figure 5.4d).

The loadings plot coloured according to Variable Importance for Projection (VIP) values is a valuable tool to identify the signals that underlie class separation in PLS-DA models. The colour scale reflects the statistical relevance of the signals variation, with hot colours indicating more relevant changes. Accordingly, signals in the positive side of the VIP loadings plot for LV1 correspond to signals increased in samples located in the LV1 positive of the corresponding scores plot, a similar reasoning applying to negative peaks and samples located in negative LV1 quadrants in the scores plot. Figure 5.5 presents the VIP loadings plot of the model shown in Figure 5.4b. Variations in some metabolites are pin pointed as responsible for group separation upon cDDP exposure: increased lipid signals as well as of choline (δ 3.21) and GPC (δ 3.24), increased UXP (δ 5.99 and δ 7.98) and UDP-GlcNAc (δ 5.52) derivative, along with marked decreased *m*- and *s*-Inositol (δ 4.05 and δ 3.34), inosine/adenosine (δ 8.36) and phenylalanine (δ 7.32). Hence, visual observations were confirmed and complemented by this analysis.

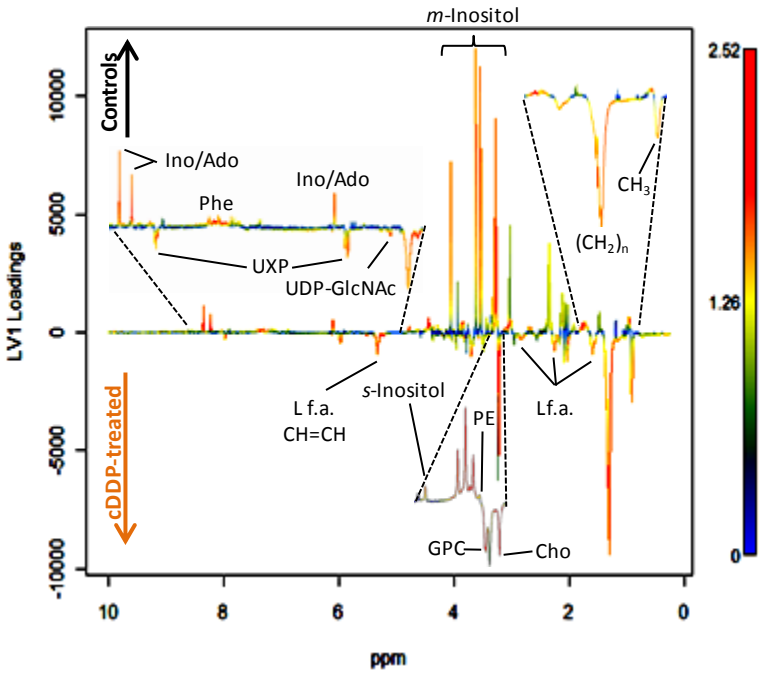

Figure 5.5. Loadings plot coloured according to VIP values of UV scaled PLD-DA model of controls and 30 µM cDDP-treated cells.

Following this analysis, signal integration and univariate statistical evaluation of the changes identified the relevant metabolites variations at 48 hours were computed (Table 5.1) and are shown as time course plots in Figure 5.6.

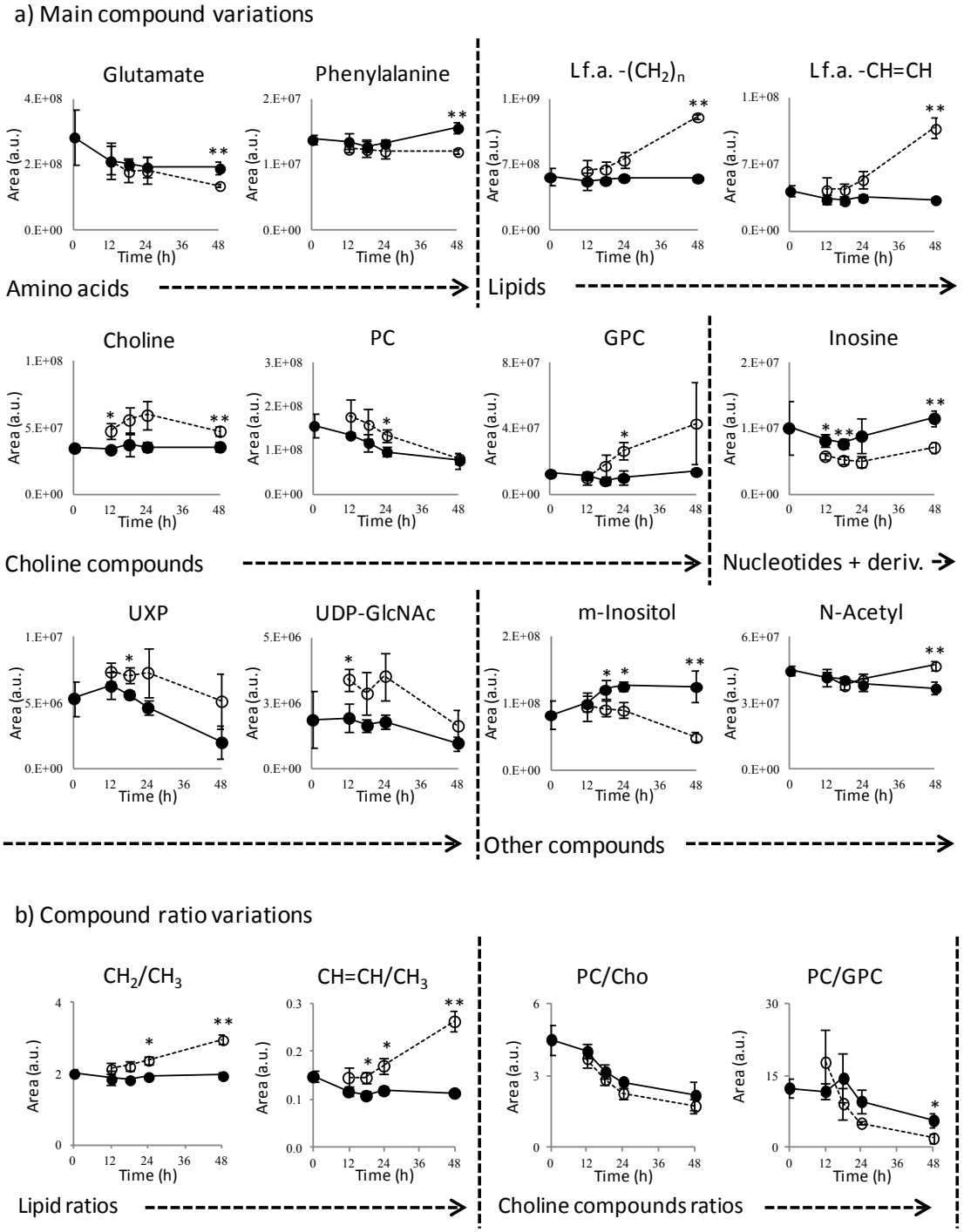

Figure 5.6. Time course changes of metabolites varying with cDDP (30 μM) treatment (dashed -○-) in relation to control (full –●–): a) main compound variations and b) compound ratio variations. **p* < 0.05 and **p* < 0.01.

As mentioned in the beginning of this section, the cDDP exposure results presently considered (and published in Lamego *et al*., 2014) were obtained through an improved processing of the data (peak alignment and PQN normalization), as compared to an initial report (Duarte *et al*., 2010). In spite some of the changes then reported having been shown presently to be not

significantly, namely regarding creatine, PC, succinate and taurine, most changes reported earlier were confirmed, while some were newly unveiled, namely for Pro, Thr, PE, UDP-GlcNAc and UXP (marked with § in Table 5.1). These correspond to low intensity resonances with a significant interference of noise and/or signals in which a considerable dispersion between replicates occurs, thereby more susceptible to be improved by the PQN normalization procedure used.

The cDDP-induced adaptations of the MG-63 cells metabolome comprise: marked increases in all detected lipids resonances, reflected in increased $(CH_2)_n/CH_3$ and $–CH=CH-/CH_3$ ratios which respectively represent average chain length and unsaturation degree (Blankerberg *et al*., 1997) (Figure 5.6 and Table 5.1 and 5.2); increases in choline and GPC and no change in PC, leading to decreased PC/Cho and PC/GPC ratios (Figure 5.5 and Table 5.2), while PE decreases; large number of treatment-sensitive amino acids show a general decreasing tendency (exception for Val and Ile); changes in UXP and glucosylated derivatives (UDP-GNAc); strong decreases in *m*- and *s*-Inositols in addition to an increase in acetate(s) (Figure 5.6 and Table 5.1).

Table 5.1. Metabolite variations in MG-63 cells exposed to 30 μM cisplatin (cDDP), 3 μM doxorubicin (DOX) or 3 μM methotrexate (MTX) for 48 hours, compared to control cells.

Metabolite	Signal (δ/ ppm)[a]	cDDP		DOX		MTX	
		% var.[b]	Effect size[c]	%var.[b]	Effect size[c]	% var.[b]	Effect size[c]
Lipids							
-C<u>H</u>$_3$	0.91	42.2±3.0**	8.88±2.46	_	_	_	_
-(C<u>H</u>$_2$)$_n$	1.30	115.6±2.4**	20.0±5.40	_	_	_	_
-C<u>H</u>$_2$CH$_2$CO	1.60	47.1±4.1**	7.24±2.04	_	_	_	_
-C<u>H</u>$_2$COO	2.25	41.8±3.4**	6.98±1.97	_	_	_	_
=CHC<u>H</u>$_2$CH=	2.83	61.1±12.6	2.88±1.00	53.4±10.5*	2.63±1.00	8.20±3.30	1.59±0.83
-C<u>H</u>=C<u>H</u>-	5.33	228.1±9.6**	9.14±2.52	(+)	(+)	_	_
Choline and phospholipids							
Choline	3.21, s	32.7±6.4**	2.88±1.00	178±15.4*	3.94±1.31	41.1±16.0	1.26±0.78
GPC	3.24, s	213±55.3	1.55±0.76	266±39.0	1.91 ± 0.86	(+)	(+)
PC	3.23, s	_	_	-28.6±12.3	-1.77±0.83	-56.4±17.2	-3.91±1.40
PE	3.25, s	-19.0±5.5*	-2.67±0.96§	(+)	(+)	(+)	(+)
Amino acids							
Alanine	1.40, d	-8.40±1.90**	-2.91±1.01	_	_	_	_
Glutamate	2.34, m	-27.7±6.2**	-2.79±0.98	_	_	-21.6±9.8	-1.54±0.82
Glycine	3.56, s	-35.6±9.0**	-2.73±0.97	-28.0±13.6	-1.57±0.80	24.4±6.9	1.60±0.84
Histidine	8.18, s	(+)	(+)	_	_	(+)	(+)

Table 5.1 (cont.). Metabolite variations in MG-63 cells exposed to 30 μM cisplatin (cDDP), 3 μM doxorubicin (DOX) or 3 μM methotrexate (MTX) for 48 hours, compared to control cells.

Metabolite	Signal (δ/ ppm)[a]	cDDP		DOX		MTX	
		% var.[b]	Effect size[c]	% var.[b]	Effect size[c]	% var.[b]	Effect size[c]
Isoleucine	1.02, d	12.3±5.1	1.75±0.80	_	_	_	_
Leucine		-10.0±2.9*	-2.10±0.85	_	_	_	_
Lysine	1.72, m	-12.6± 3.9*	-2.04±0.84	(-)	(-)	_	_
Phenylalanine	7.32, d	-23.0±4.1**	-3.91±1.23	_	_	17.6±4.2*	2.05±0.93
Proline	4.12, t	-10.1±5.8	-1.12±0.71[§]	_	_	_	_
Taurine	3.42, t	(-)	(-)	(-)	(-)	-12.5±4.1	-1.76±0.87
Threonine	3.58, d	(-)	(-)[§]	(-)	(-)	_	_
Tyrosine	6.89, d	-19.9±7.1*	-1.99±0.83	27.2±8.8	1.78±0.83	26.6±5.7	2.06±0.93
Valine	1.05, d	12.0±5.3	1.59±0.77	_	_	(+)	(+)
Nucleotides and derivatives							
Ado/Ino	8.36, s	-38.2±8.1**	-3.41±1.12	_	_	_	_
UDP-GlcNAc	5.52, m	66.4±28.9	1.13±0.73[§]	166±32.6	1.36±0.80	_	_
UXP	5.99, m	155±40.1	1.63±0.78[§]	_	_	(-)	(-)
	7.98, m	77.3±21.3*	1.72±0.79	(+)	(+)	_	_
Uridine	5.89, d	_	_	(+)	(+)	165.4±54.5	0.94±0.73
Other compounds							
Acetate (s)	2.02, s	27.5±4.7**	3.17±1.06	_	_	_	_
Creatine	3.93, s	_	_	13.7±6.1	1.37±0.76	-10.7±3.7	-2.28±0.98
GSH	2.56, m	_	_	-20.3±7.6	-1.94±0.86	(-)	(-)
m-Inositol	4.05, t	-60.7±13.9**	-3.30±1.09	-53.0±10.9*	-4.34±1.41	_	_
s-Inositol	3.34, s	-37.8±8.9**	-2.84±1.00	-22.1±8.3*	-1.96±0.86	_	_

[a] Resonance chosen for signal integration, [b] % variation and [c] effect size in relation to control cells. * $p < 0.05$, ** $p < 0.01$, $^{-}$: no significant variation. (+) and (-) indicate consistent positive and negative variations, respectively, without statistical meaning.

In the analysis of the values listed in Tables 5.1 and 5.2, variations were generally accepted as relevant when the corresponding errors did not exceed 50% of the variation (or ES) value. In some cases, however, variations affected by larger errors were also considered when carrying a known biochemical meaning. This is the case, for example, of UDP-GlcNAc variations (Table 5.1), noted before in other similar studies (Duarte *et al*., 2013; Pan *et al*., 2011).

The information listed in Table 5.1 and the plots in Figure 5.6 show that treatment with cDDP for 48 hours induces severe changes in the metabolome of MG-63 cells, for instance note the dramatic increases of lipid moieties with statistical relevant variation (except for polyunsaturated fatty acid, PUFA) ranging from *ca.* 40% (-CH_2COO- at 48 h) to around 230% (-

CH=CH- at 48 h), together with high ES, ranging from almost 3 to 20. Furthermore, than 19% variations are noted in choline and phospholipids with corresponding ES values in the 1.5-2.9 range and several amino acids statistically vary with cDDP-treatment (Ala, Glu, Gly, Leu, Lys, Phe and Tyr) with ES values ranging from 2 to almost 3 in relation to control conditions. Some nucleotides and derivatives (Ino/Ado and UXP) also show statistical relevant percentages of variation of 40-77% and ES values ranging from 1.7 to 3.34 (in magnitude) and variations in other compounds (acetate(s), *m*- and *s*-Ino) were also statistical relevant with significant ES values of *ca.* 3. Table 5.2 and Figure 5.6b show that the above refered cDDP-induced alterations in lipids, choline and phospholipids are also reflected in statistical relevant alterations in some compound ratios, namely CH_2/CH_3, $CH=CH/CH_3$ and PC/GPC.

Table 5.2. Mean ratios for lipids and choline compounds in MG-63 cells exposed to 30 µM cisplatin (cDDP), 3 µM doxorubicin (DOX) or 3 µM methotrexate (MTX) for 48 hours, compared to control cells.

Ratio	cDDP		DOX		MTX	
	Controls	cDDP	Controls	DOX	Controls	MTX
Lipid ratios						
$C\underline{H_2}/C\underline{H_3}$	1.96 ± 0.08	2.97 ± 0.12**	2.59±0.24	2.36±0.12	2.58±0.28	2.05 ± 0.21
$C\underline{H}=C\underline{H}/C\underline{H_3}$	0.11 ± 0.01	0.26 ± 0.02**	0.19±0.02	0.29±0.04*	0.20±0.04	0.16 ± 0.02
$=CHC\underline{H_2}CH=/\ C\underline{H_3}$	0.20 ± 0.01	0.22 ± 0.02	0.20±0.06	0.31±0.01	0.18 ± 0.04	0.25 ± 0.02
Choline compound ratios						
PC/Cho	2.17±0.60	1.72±0.29	2.18±0.64	0.56±0.15	2.68±0.46	0.83±0.08
GPC/Cho	0.38±0.04	0.91±0.44	1.17±0.22	1.55±0.42	0.92±0.02	0.86±0.19
PC/GPC	5.63±1.45	1.90±0.99*	1.86±0.52	0.36±0.18*	2.92±0.56	0.97±0.16

Abbreviations as defined in Table 5.1. * $p < 0.05$, ** $p < 0.01$.

Accordingly, significant increases in the mean chain length (given by CH_2/CH_3) and unsaturation degree ($CH=CH/CH_3$) of lipid fatty acids are depicted upon 48 hours treatment with cDDP. Additionally, a significant decrease in PC/GPC registered in MG-63 cells treated with cDDP for 48 hours suggest a drug-induced alteration in choline compounds, namely concerning its breakdown and storage pathways.

5.2.2. Doxorubicin (DOX)

The average ^{1}H HRMAS spectra of control and DOX-treated MG-63 cells, at 48 hours, are shown in Figure 5.7a and b, respectively. Visual inspection highlights relevant changes in the

choline-compounds region (relative increases in choline and GPC), a relative decrease in *m*-Inositol and some changes above 5 ppm, namely in UXP (δ 5.99 and δ 7.98) and UDP-GNAc derivatives (δ 5.52).

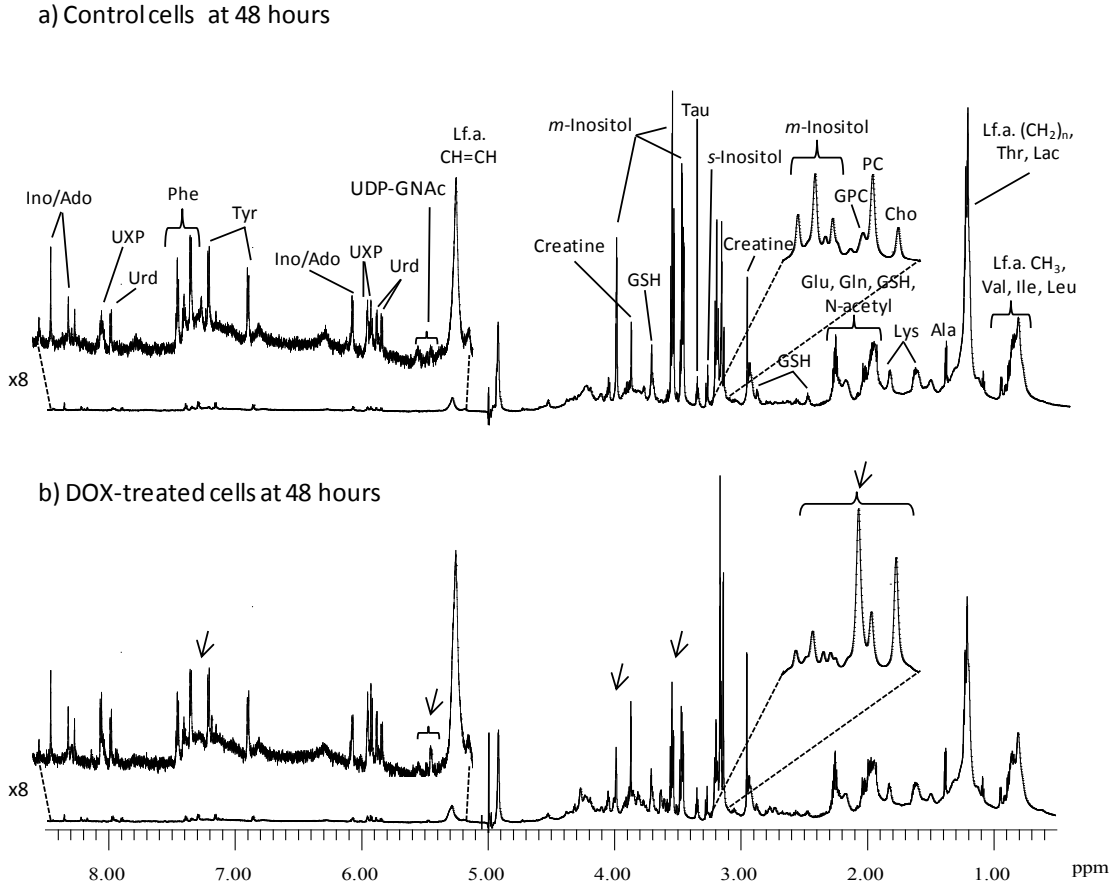

Figure 5.7. Average 800 MHz ^{1}H HRMAS NMR spectra of MG-63 cells, at 48 hours: a) under control conditions and b) exposed to 3 μM DOX. Insets show expansions of choline compounds (3.2-3.3 ppm) and aromatic (5.2-8.5 ppm) regions. Main assignments are noted and visible spectral changes due to drug exposure are marked with arrows.

PCA of the ^{1}H HRMAS spectra resulted in a clear separation between DOX-treated samples and controls, towards negative PC1 and positive PC2 (Figure 5.8a). Despite the suggestion of a time course tendency for control samples in PCA, such was only faintly observed for DOX-treated cells. The corresponding PLS-DA scores plot (Figure 5.8b) showed good separation between groups (Q^2 0.665), although time course trajectories were again unclear. The robustness of group discrimination was reflected in a low Q^2 distribution overlap and reasonable MCCV results (82.7% sensitivity, 90.2% specificity and 86.9% classification rate, Figure 5.8c and d). Despite these

results, some dispersion within the *true classes* samples is seen in Figure 5.8d, but it is noted that only 5 samples are dispersed from the whole rest of samples that cluster together.

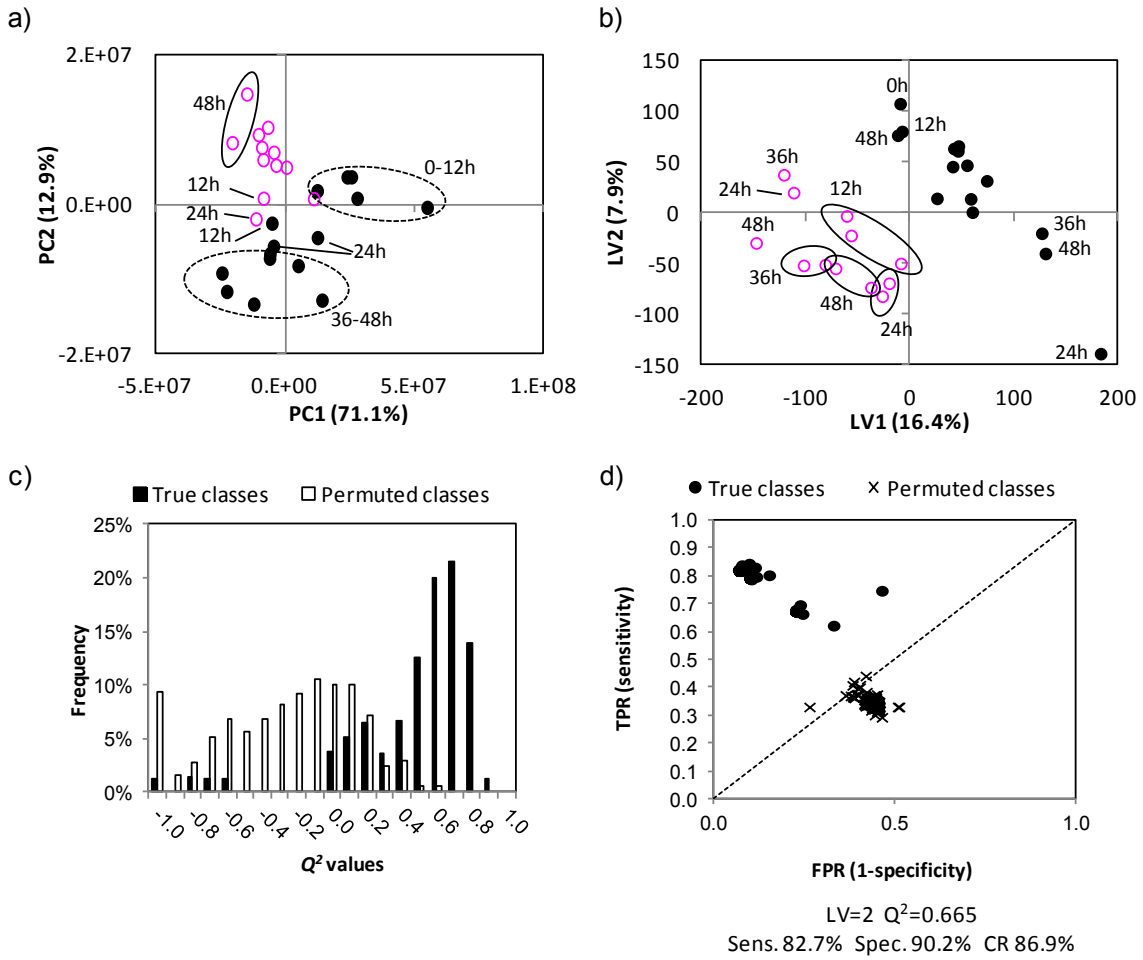

Figure 5.8. Multivariate analysis of controls (●) and DOX-treated (○) cells: (a) PCA scores plot, centered scaled data (b) PLS-DA scores plot , UV scaled model with 2 components calculated with R^2X = 0.243, R^2Y = 0.918 and Q^2 = 0.665. MCCV results of PLS-DA model obtained in b): c) Q^2 distributions and d) ROC plots of true and permuted models. TPR: true positive rate, FPR: false positive rate, Sens.: sensitivity, Spec.: specificity, CR: classification rate.

The VIP-coloured loadings (Figure 5.9) indicates decreases of *m*-Inositol (δ 4.05) and N-acetyl (δ 2.01) moieties in contrast with increases of Ala (δ 1.48), creatine (δ 3.03), choline (δ 3.21), GPC (δ 3.24) as well as of UXP (δ 5.99 and δ 7.98) and UDP-GlcNAc (δ 5.52).

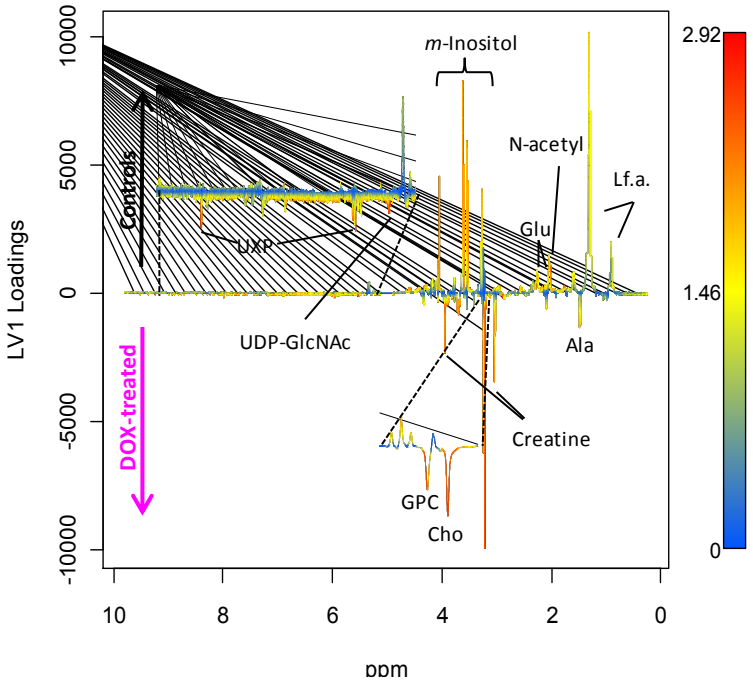

Figure 5.9. Loadings plot coloured according to VIP values of UV scaled PLD-DA model of controls and 3 µM DOX-treated cells.

Subsequently to signal integration, statistical calculations identified the most relevant compound variations (Table 5.1) and some compound ratios (Table 5.2) for 48 hours and shown as time course plots in Figure 5.10. These results show that the metabolic response of MG-63 cells to DOX exposure is described by residual changes in lipids with small increases in $=CHCH_2CH=$ and $–CH=CH-$ resonances at 48 hours (around 53% with an ES value of 2.6), also expressed by modest changes in $=CHCH_2CH=/CH_3$ and $–CH=CH-/CH_3$ lipid ratios (Figure 5.10b and Table 5.2). A marked increase in choline and GPC (of 178% and 266%, corresponding to ES values of around 4 and 2, respectively, at 48 hours), in tandem with PC decrease (negative variations of 29%, with ES value of -1.8) is seen, resulting in significant decreases in PC/Cho and PC/GPC ratios (Figure 5.10b and Table 5.2). Moreover, strong decreases in Gly (-28% with an ES value of -1.6) and Tyr increase (which, despite being positive, is identical in % and ES value to that of Gly) is detected, together with slight decreasing tendencies in other amino acids (Table 5.1). A large increase in UDP-GlcNAc at 24 and 48 hours (of around 166% and ES of 1.4) is observed, as well as small increases in UXP and uridine (Table 5.1). Creatine significantly increases (14% with an ES value of 1.4) whereas a decrease in seen for GSH (-20% and -1.9) and *m*- and *s*-Inositols (with -53% to -22% variation, to which correspond ES values ranging from -4.3 to -2).

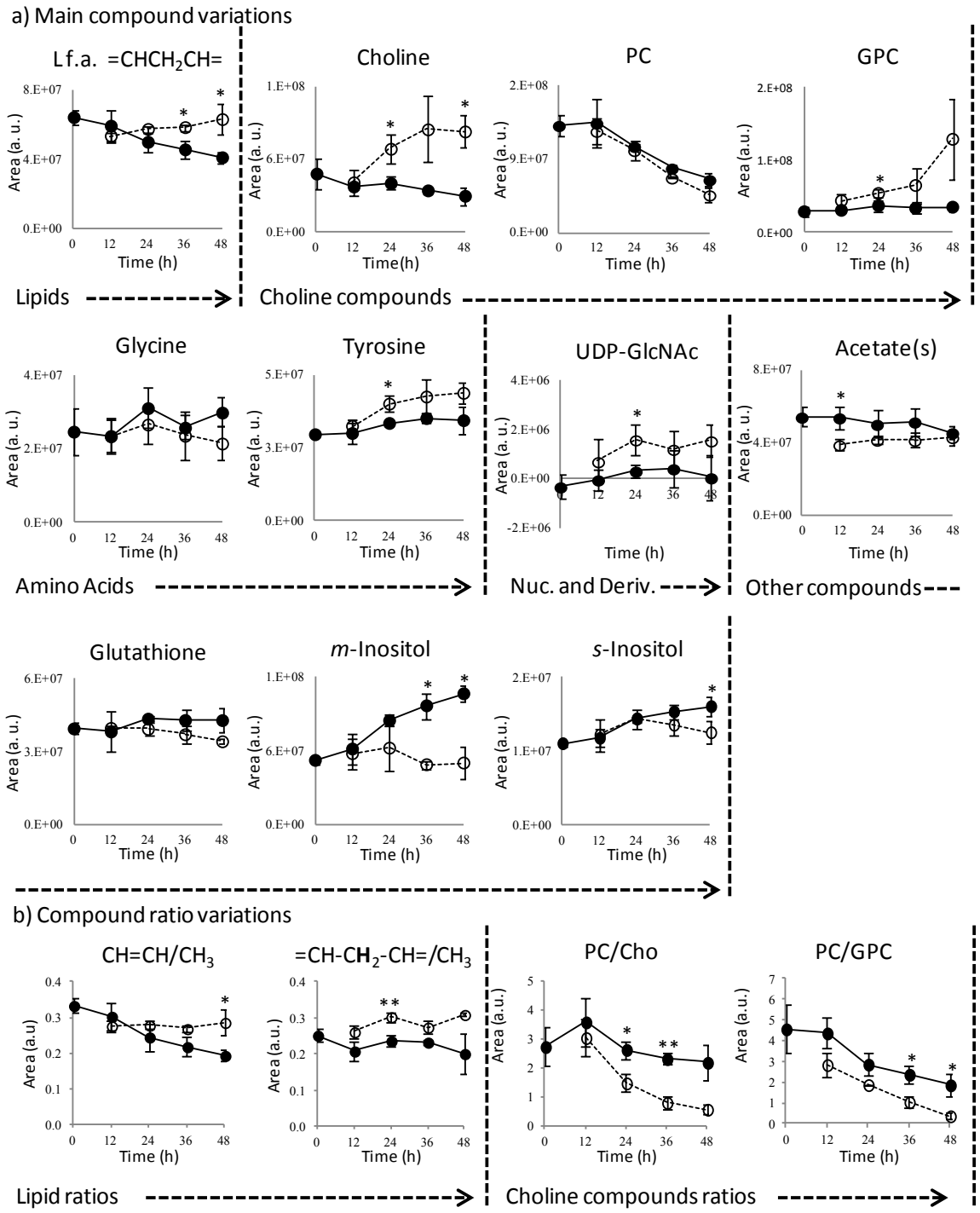

Figure 5.10. Time course of metabolites varying with DOX treatment (dashed -○-) in relation to control (full ⁻●⁻): a) main compound variations and b) compound ratio variations. *$p < 0.05$ and *$p < 0.01$.

In general, the above refered DOX-induced changes in the metabolome of MG-63 cells were both reduced in number and magnitude when compared to those induced by cDDP. Interestingly, the only observed change in lipids occurs in PUFA moieties (δ 5.33), and its 53% of variation was found to be statistically relevant, corresponding to a significant ES value of 2.6, this being similar

to that obtained by cDDP-treatment (which in turn, did not correspond to a significant percentage of variation). This result shows that the two drugs display different modes of action, despite their common target (DNA), leading to markedly different metabolism of lipids. Similarly to cDDP, DOX-treatment also triggers statistically relevant changes in choline, to which a significantly high value of ES of almost 4 was calculated, i.e. even more marked than the change observed with cDDP. In relation to amino acids, no statistically relevant changes were found, despite the relatively high ES values (around 1.6 and 1.8 in magnitude). A marked but not statistically significant increase of UDP-GlcNAc (δ 5.52) of 166% was noted, contrasting with the significant 53% and 22% decreases in *m*- and *s*-Inositol, for which ES values ranging from 2 to more than 4, similarly to that measured in cDDP-treatment).

5.2.3. Methotrexate (MTX)

The average ^{1}H HRMAS spectra of control and 48 hours MTX-treated MG-63 cells are shown in Figure 5.11a and b, respectively.

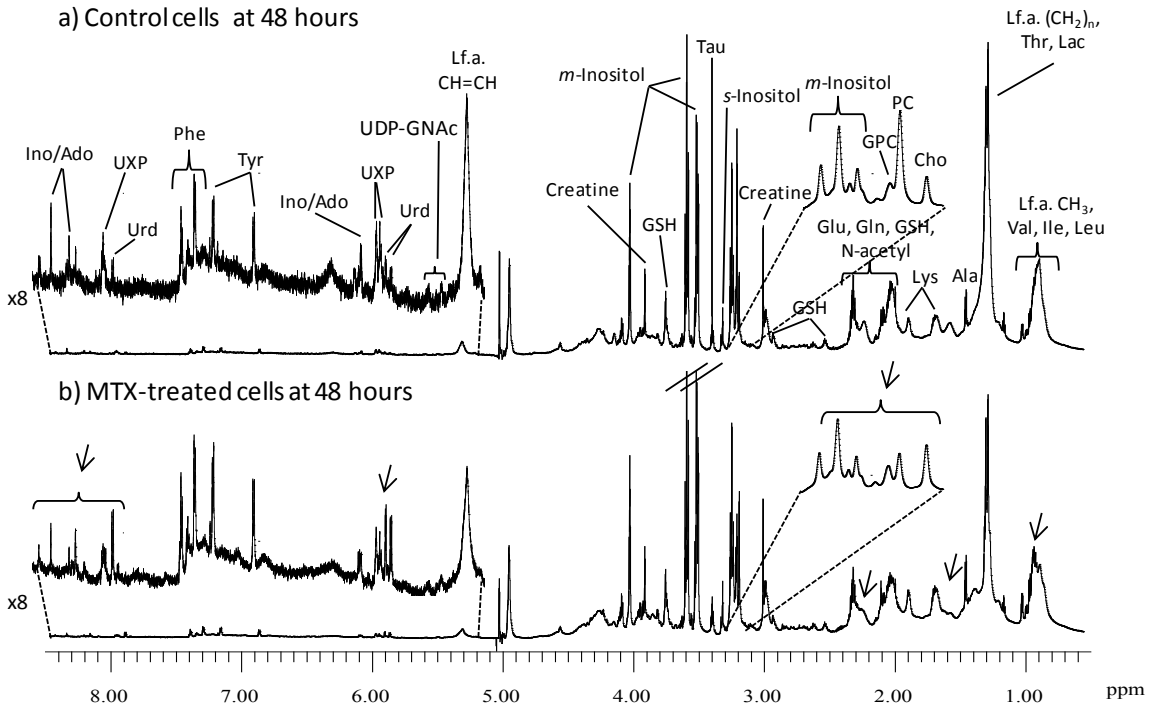

Figure 5.11. Average 800 MHz ^{1}H HRMAS NMR spectra of MG-63 cells, at 48 hours: a) under control conditions and b) exposed to 3 μM MTX. Insets show expansions of choline compounds (3.2-3.3 ppm) and aromatic (5.2-8.5 ppm) regions. Main assignments are noted and visible spectral changes due to drug exposure are marked with arrows.

Visual inspection suggests that the treatment with MTX slightly affects lipid contents, alters the relative proportion of choline compounds (decrease in PC, δ 3.23, and possible increase in choline, δ 3.21), changes levels of UXP (either UDP/UTP at δ 5.99 and δ 7.98 and UDP-GNAc species, δ 5.52), uridine (δ 5.89) and Ino/Ado (δ 8.36).

Multivariate analysis of the spectra of controls and MTX-treated samples show that group separation is not clear in the PCA scores plot (Figure 5.12a) but becomes obvious in the corresponding PLS-DA scores plot (Figure 5.12b).

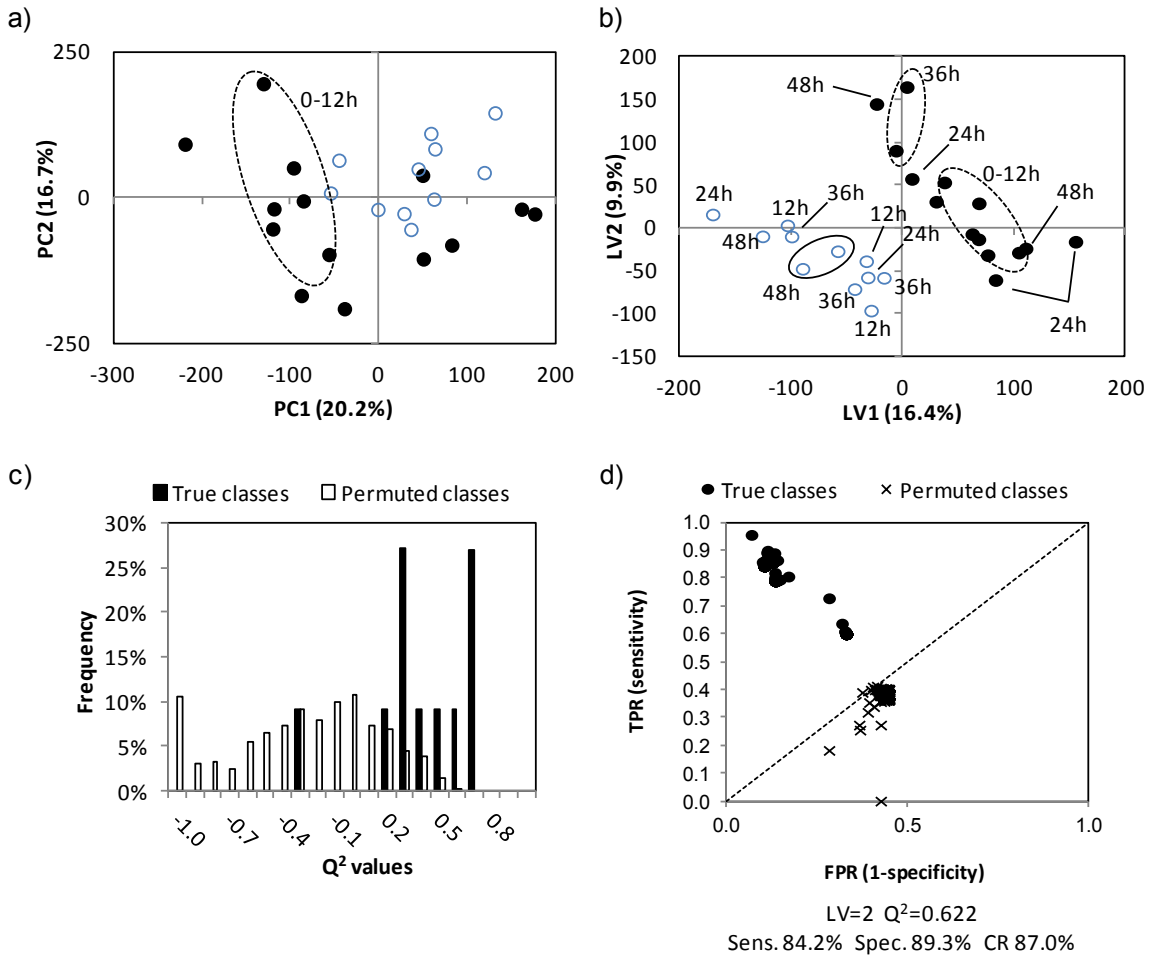

Figure 5.12. Multivariate analysis of controls (●) and MTX-treated (○) cells: (a) PCA scores plot, UV scaled data (b) PLS-DA scores plot , UV scaled model with 2 components calculated with R^2X = 0.262, R^2Y = 0.902 and Q^2 = 0.622. MCCV results of PLS-DA model in b): c) Q^2 distributions and d) ROC plots of true and permuted models. TPR: true positive rate, FPR: false positive rate, Sens.: sensitivity, Spec.: specificity, CR: classification rate.

MCCV results (Figure 5.12c and d) reflect a slightly lowered performance of the model (Q^2 0.622, 84.2% sensitivity, 89.3% specificity and 87.0% classification rate) when compared to cDDP exposure, suggesting an overall lesser impact of MTX on the cell metabolome compared to this

drug. Similarly to what was seen for DOX, MCCV results seem to be affected by a reduction in sensitivity and specificity of a few samples, evidenced in Figure 5.12d by their slight dispersion in relation to the remaining samples.

The VIP-coloured loadings plot (Figure 5.13) point to a distinct drug response profile, namely in choline compounds and nucleotide bases regions. Changes in lipids also seem to account for relevant differences between control and MTX-treated samples with decreases being suggested for CH_3 (δ 0.91) and $(CH_2)_n$ (δ 1.30) in treated samples. Decreases in PC (δ 3.23), N-acetyl moiety (δ 2.02), GSH (δ 2.56), Glu (δ 2.34) and Ino/Ado (δ 8.36) as well as an increase of uridine (δ 5.89) were also pointed by PLS-DA as metabolic consequences of MTX-exposure.

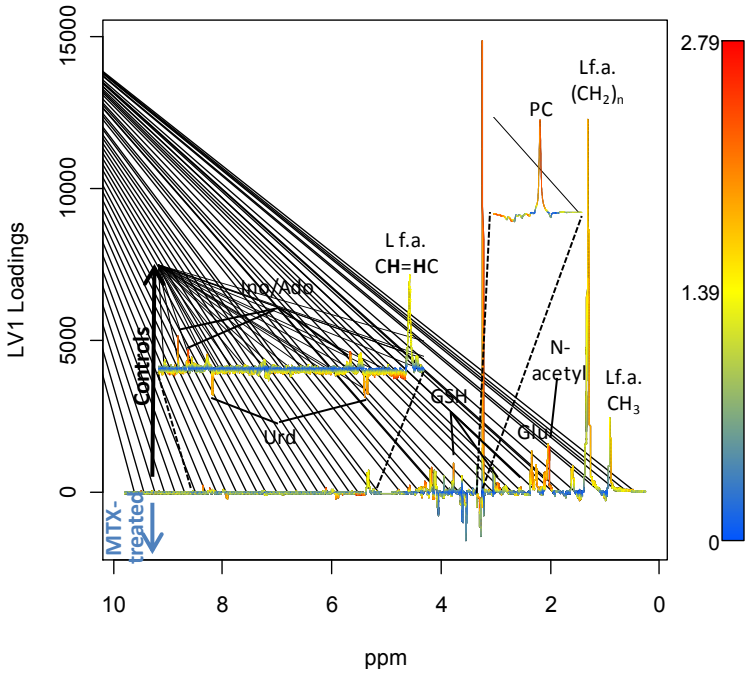

Figure 5.13. Loadings plot coloured according to VIP values of UV scaled PLD-DA model of controls and 3 μM MTX-treated cells.

Following the previously established procedure of data analysis, signal integration and statistical evaluation of changes were performed and are shown as time course graphs for each measured metabolite and listed in Table 5.1 (for 48 hours only). This confirms the following adaptations as induced by MTX: nearly absent lipid changes (Figure 5.14 and Table 5.1 and 5.2), showing that the VIP-loadings results were strongly influenced by the considerable dispersion between replicates in what concerns lipid signals. Additionally, almost no changes in choline and GPC (exception for small increases at 48 hours) and a marked increase in PC are detected (Figure 5.14a and Table 5.1), thus resulting in a strongly decreased PC/Cho and PC/GPC ratios (Figure

5.14b and Table 5.2). Furthermore, the amino acids Gly, Phe and Tyr increase and decreases in Glu and Tau are seen (Figure 14a and Table 5.1). MTX-treatment also seems to induce important increases in uridine (although with a large uncertainty in effect size value) and small decreases in creatine, as well as a modest decrease of GSH. For the first time (considering metabolic responses to cDDP and DOX) no changes in inositols are observed.

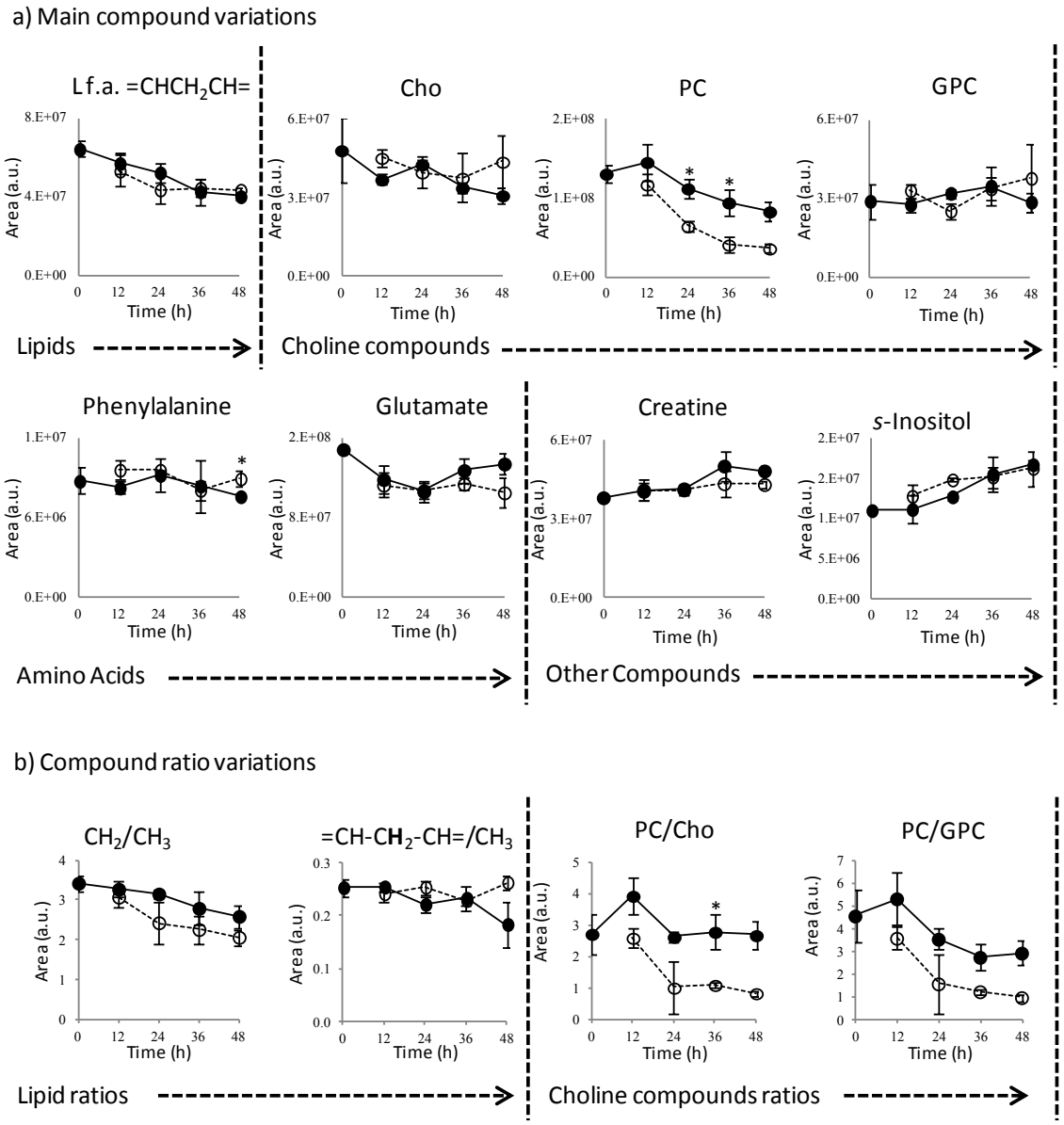

Figure 5.14. Time course of metabolites varying with MTX treatment (dashed -○-) in relation to control (full ⁻●⁻): a) main compound variations and b) compound ratio variations. **p* < 0.05.

The number of statistically relevant changes in MG-63 cells induced by MTX-treatment is lower than that determined for both DOX and cDDP (even more pronounced), reflecting the modest metabolic impact of this antifolate agent on these cells.

5.3. ^{1}H NMR Analysis of TCA Extracts of cDDP-, DOX- and MTX-Treated Cells

Acidic extraction with trichloroacetic acid (TCA) denatures and precipitates proteins and other macromolecules, and enables elimination of the volatile TCA by lyophilisation (McQueen, 2010). TCA extracts of mammalian cells have succeeded in revealing several nucleotide derivatives (AXP, UTP and NAD^+) signals (Lane *et al*., 2007; Fan *et al*., 2008). In this section, TCA extracts from controls and drug-treated samples at 48 hours (previously analysed by HRMAS) are compared. Since some of the tested drugs target DNA (cDDP and DOX), the analysis of TCA extracts aimed at extracting information on possible drug-induced changes in nucleotides and their derivatives. Below, a first comparison between the information retrieved by HRMAS and TCA extracts spectra is presented.

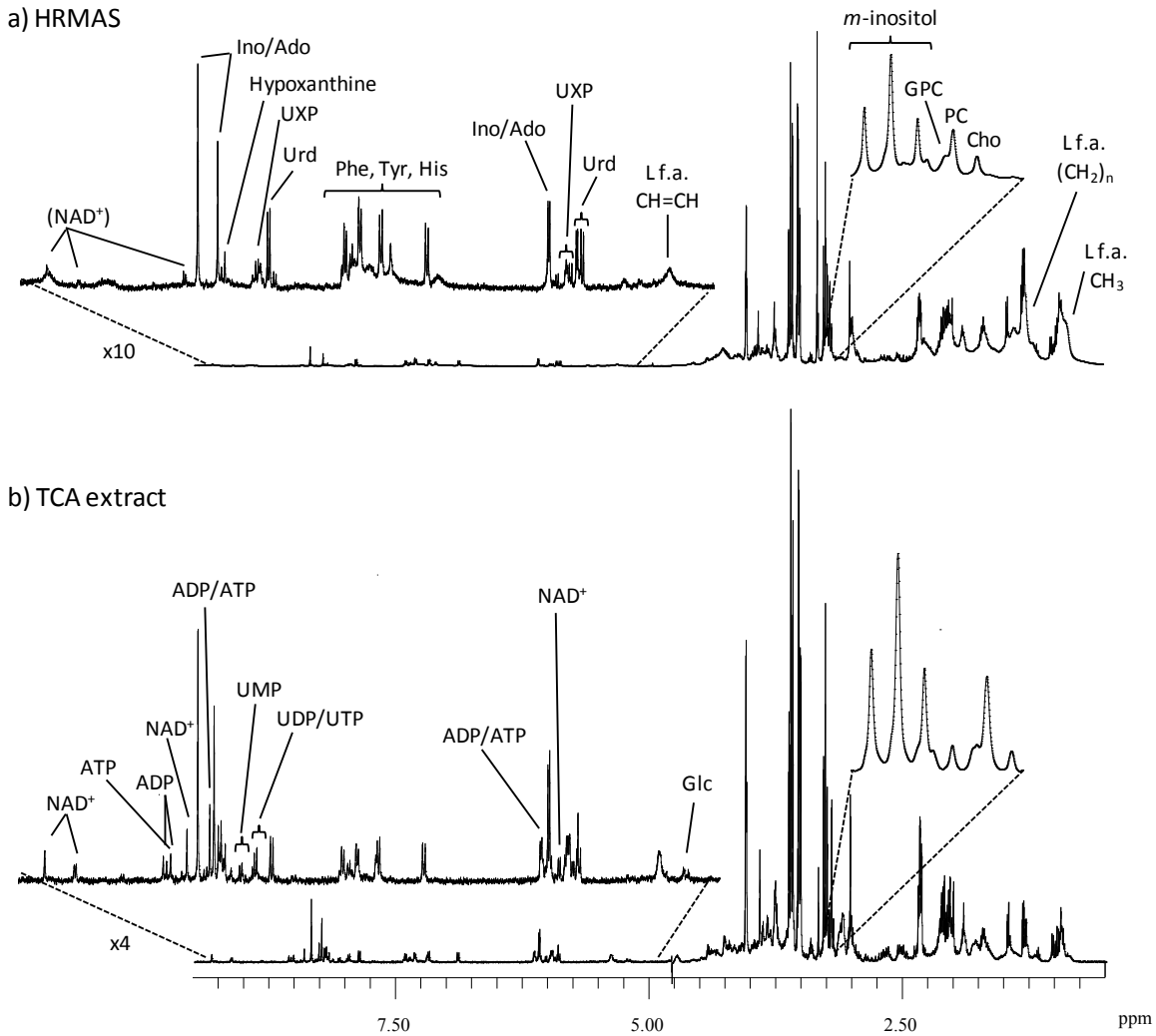

Figure 5.15. Average 500 MHz ^{1}H NMR spectra of MG-63 cells, at 48 hours: a) HRMAS and b) TCA extract. Expansion of the aromatic (5.0-9.5 ppm) region is shown. Main assignments are noted and those indicated in b) reflect those newly detected through analysis of extracts.

Figure 5.15 compares the metabolic profile of control cells at 48 hours when analysed by HRMAS (Figure 5.15a) and their respective TCA extracts (Figure 5.15b). Both HRMAS and TCA extracts yielded ^{1}H NMR spectra with very similar resolutions (width at half height, $\nu_{½}$, of 1.8 Hz for inosine at δ8.36 for the two spectra). Additionally, the NMR spectra of TCA extracts improve the information on nucleotide derivatives since ADP, ATP, UMP, UDP and ATP signals are only visible upon TCA extraction of samples. Moreover, the resonances of NAD^+, only slightly visible in the HRMAS spectra, are clearly identified in the spectra of TCA extracts. Glucose, which is also not visible in the HRMAS spectra of cells, probably due to low intracellular amounts and binding to other molecules, is clearly detected in the spectra of TCA extracts. On the other hand, resonances from lipids (δ 0.90, δ 1.31) and from other macromolecules that show broad signals in the HRMAS spectra (e.g. δ 7.37) are lost in the spectra of TCA extracts as expected. The 2D TOCSY spectrum of a control extract sample (not shown) also indicates that oxidation of glutathione takes place during TCA extraction: when assigning the glutathione spin system, the typical GSH resonance at δ 4.58 (present in the spectra of samples analysed by HRMAS) disappears and the GSSG typical resonance at δ 4.78 clearly emerges. This highlights the additional issue of oxidation arising from this type of sample manipulation, which must be taken into consideration when choosing between the two types of sample analysis.

Cell exposure to chemotherapy drugs may induce metabolic changes in nucleotides and derivatives, especially when considering metal-based agents that target DNA (as cDDP). Therefore, in order to detect more detailed alterations in these compounds, analysis of the aromatic region of TCA extracts of cell samples exposed to cDDP, DOX or MTX was performed (Figure 5.16). The average spectra of TCA extracts of cDDP-treated cells (Figure 5.16b) shows that treatment with this metal-based agent induces the disappearance of ADP/ATP and NAD^+ signals relative to the control (Figure 5.16a). Additional changes in the metabolic profile of the aromatic region of cDDP-treated cells are detected: Ino/Ado decreases in relation to uridine and UXP, which also seem to increase with treatment. When looking at the average spectrum of TCA extracts of DOX-treated cells (Figure 5.16c), resonances from ADP/ATP and NAD^+ (as with cDDP) and UXP, clearly disappear. Moreover, Ino/Ado signal clearly decreases in comparison to uridine (that seems to increase in relation to controls) and hypoxanthine increases. Similar alterations are seen in TCA extracts of MTX-treated cells (Figure 5.16d). The unassigned resonance (Un.) also disappears after treatment with any of the three drugs. These results suggest that DOX and MTX

treatments induce similar changes in nucleotide derivatives, these differing dramatically from the effects of cDDP exposure.

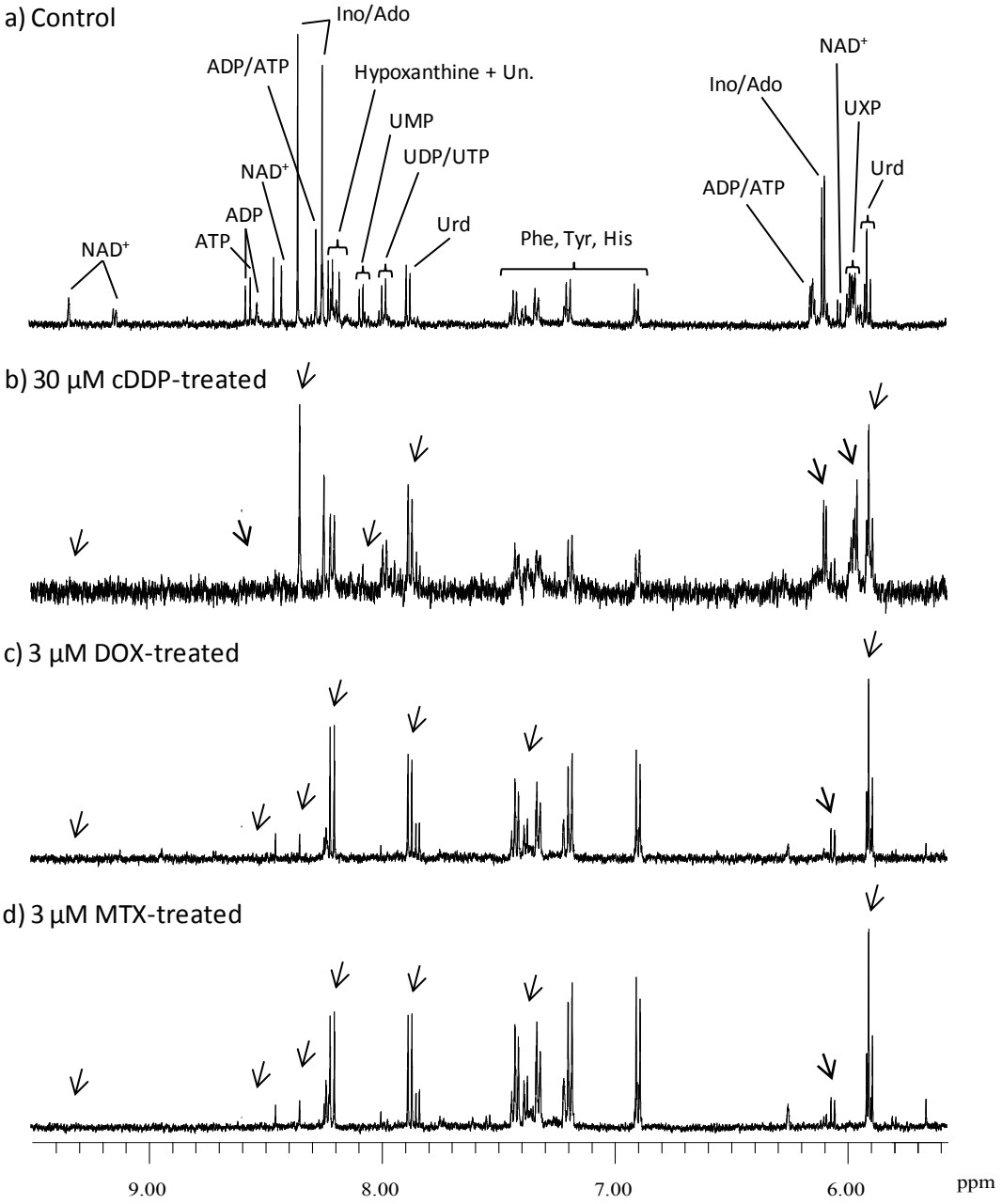

Figure 5.16. Average 500 MHz ^{1}H NMR spectra of TCA extracts of MG-63 cells, at 48 hours: a) under control conditions, b) exposed to 30 µM cDDP, c) exposed to 3 µM DOX and d) exposed to 3 µM MTX. Expansion of the aromatic (5.0-9.5 ppm) region is shown. Main assignments are noted and visible spectral changes due to drug exposure are marked by arrows.

These observations are somewhat surprising when considering the different mechanisms of action of each drug. In fact, it would be expected that DOX-induced changes would more closely

resemble those induced by cDDP, since both drugs target DNA (although through a different mechanism). In addition, since MTX is an antifolate drug, not directly targeting DNA, no pronounced changes in nucleotides would be expected. Therefore, it may be concluded that the relation of the nucleotide profile (as viewed through TCA extracts) and the drug mechanism is not a straightforward one, requiring more detailed investigation.

In terms of comparison between the information provided by HRMAS and TCA extracts, the information retrieved by HRMAS analysis of the same samples only revealed significant decreases in Ino/Ado upon cDDP treatment, while TCA extracts showed a decrease in Ino/Ado contents for the three treatments. HRMAS analysis showed similar variation trends in UXP levels with cDDP and MTX (increase and decrease, respectively) in relation to TCA extracts, but slight increases of UXP were suggested to occur upon DOX treatment while in TCA extracts UXP signal is not detected. Uridine, suggested to increase upon treatment with each of the three drugs according to the information contained in the spectra of the respective TCA extracts, was also increased in DOX- and MTX-treated samples analysed by HRMAS, whereas no significant changes were measured upon cDDP-exposure. These differences identified between HRMAS and TCA extracts in what regards to drug-induced changes in nucleotides and derivatives may relate to the high concentration of these compounds in extracts, possibly leading to a more accurate determination of compound fluctuations.

5.4. Comparison of the Metabolic Impact of cDDP, DOX and MTX

The heatmap of the effect size values shown in Figure 5.17a illustrates the most relevant drug-induced time course changes, hot and cold colors expressing, respectively, increased and decreased metabolite levels in the drug-treated samples as compared to controls. Clearly, the numerous yellow/orange patches seen in lipid resonances are a clear signature of cDDP response, whereas smaller and fewer changes in this region are noted for DOX and MTX. The increase in PUFA is a common feature to the three tested drugs, although more marked for DOX (even though total visible lipids do not increase). Regarding phospholipid related compounds, drug-specific changes include a PE decrease for cDDP, a marked PC decrease for MTX and a mixed behaviour for DOX (PC reduction and rise in both Cho and GPC). The heatmap of the compound ratios (Figure 5.17b), in turn, clearly evidences the time course increase in lipid chain length and unsaturation degree due to cDDP treatment, along with a suggestion of chain length shortening

for DOX and MTX, which, for the former is possibly accompanied by a some increase in lipid unsaturation degree, including in PUFA. Moreover, the distinct choline signatures detected in Figure 5.17a are highlighted when considering PC/Cho and PC/GPC ratios: cDDP affects these ratios to a much lesser extent than DOX or MTX, the latter leading to a clear gradual time-dependent response in both cases. These findings allow choline ratios to be identified as particularly sensitive markers of MG-63 cells metabolic response to DOX and MTX.

Regarding amino acids, a quite distinct colour distribution is obtained for the three drugs: for cDDP, a decrease in amino acid content (blue patches) is predominant, especially upon 48 hours of drug effect, whereas increases (yellow patches) dominate for DOX and MTX. The nucleotide bases profiles also seem distinct, with some pronounced changes detected for cDDP (Ino/Ado decrease and an increase in UXP species), whereas DOX and MTX induce, respectively, small increases (yellow) and decreases (blue) in these compounds. Special emphasis should be paid to the uridine variation at 48 hours with MTX, which is not reflected in the heatmap due to the high associated effect of size uncertainty.

a)

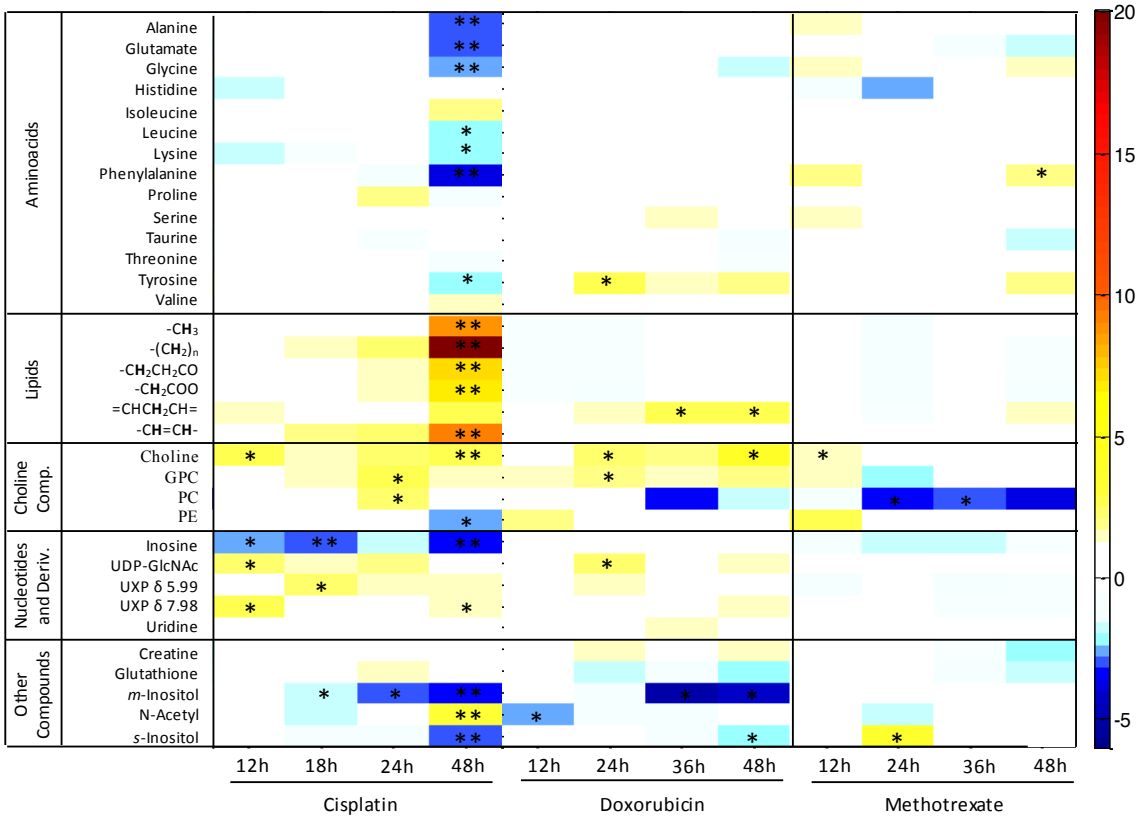

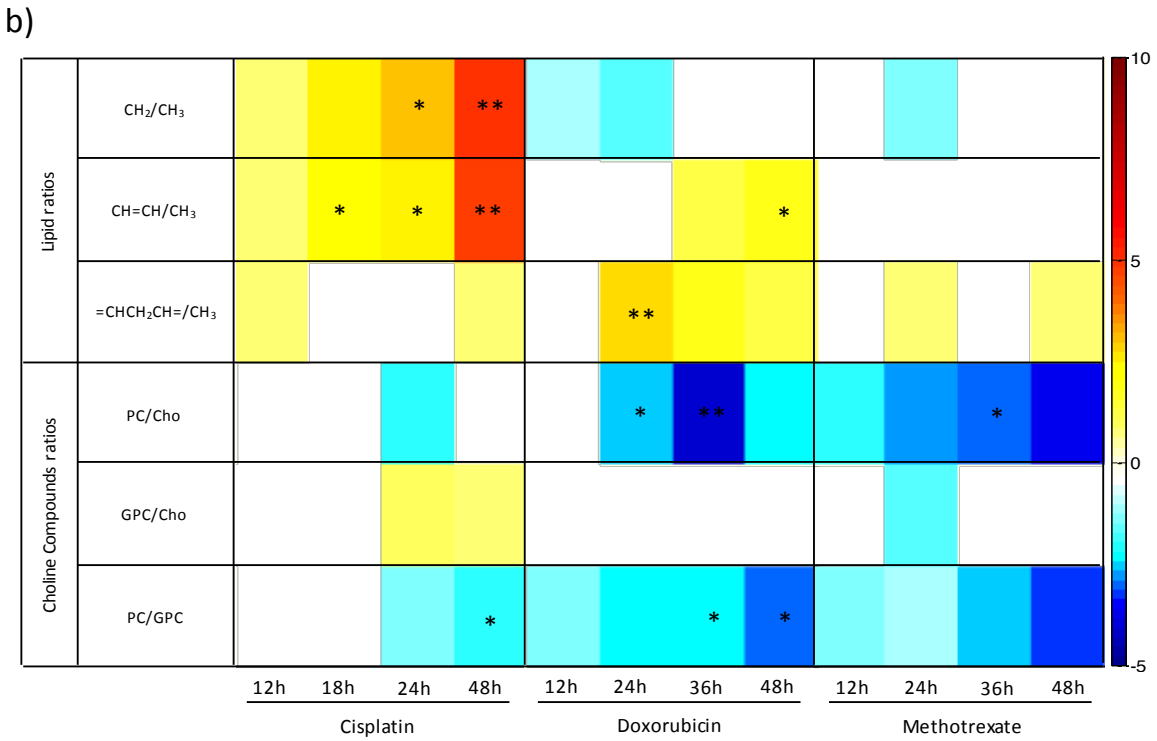

Figure 5.17. Heatmaps of effect size values of the time course response for a) several metabolites and b) compound ratios in MG-63 cells exposed to DOX, MTX or cDDP. The effect size values are shown in a colour scale from minimum (dark blue) to maximum (dark red) values. * $p < 0.05$ and ** $p < 0.01$ refer to the results of significance tests with integrals.

Concerning other compounds, a concomitant decrease in *m*- and *s*-Inositols, characteristic of cDDP and DOX responses, is shown to be absent in MTX treatment, and distinct trends are seen for acetate(s), creatine and GSH (with minor increases in the presence of cDDP at 24 hours and also minor decreases for DOX and MTX).

It is now clear that exposure to cDDP induces a much stronger metabolic response in MG-63 cells than incubation with either DOX or MTX. The following integrated discussion about the results obtained for these three drugs considers the cells metabolic response to cDDP as a reference and compares it to the other two drugs (one anticancer antibiotic and one antimetabolite), discussing the impact on the metabolic pathways associated with lipids and choline compounds, amino acids and nucleotides, among others (such as GSH and inositols). This work has been recently published in Lamego *et al.* 2014.

Biochemical interpretation of the results

Lipids and choline compounds

Some of the main differences between MG-63 cell responses to the three tested drugs relate to lipids and choline compounds. The significant lipids increase observed in the presence of cDDP was expected from previously reported studies, not only on OS cells (Duarte 2010) but also on different tumour lines (Pan *et al*., 2011; Pan *et al*., 2013; Duarte *et al*., 2013; Huang *et al*., 2003; Lindskog *et al*., 2004). NMR-visible lipid signals are believed to arise mainly from cytosolic lipid droplets (composed of mobile neutral lipids), rather than membrane components (Hakumaki and Kauppinen, 2000; Delikatny *et al*., 2011), but additional contributions have been suggested from membrane lipid microdomains or lipid rafts (Santini *et al*., 2001; Mannechez *et al*., 2005). An increase in neutral lipids have been associated with cell apoptosis (Huang *et al*., 2003; Rainaldi *et al*., 2008; Boren and Brindle, 2012), although some authors propose that they may also be due to other (still unspecified) causes (Milkevitch *et al*., 2005; Santini *et al*., 2006; Mirbahai *et al*., 2012). Specifically, it has been anticipated that apoptosis involves inhibition of mitochondrial fatty acid β-oxidation and divertion of fatty acids to an enhanced *de novo* lipid synthesis (Boren and Brindle, 2012), thus leading to an intensification of the corresponding NMR-visible signals. Also, increased lipid chain length and unsaturation degree, as clearly observed in this work for MG-63 cells exposed to cDDP, have also been suggested as indicative of apoptosis (Huang *et al*., 2003; Zietkowski *et al*., 2012). The PUFA structures, detected here for the first time in cDDP-treated OS cells through the $=CHCH_2CH=$ resonance (60% increased upon cDDP treatment for 48 hours), have been specifically suggested as pre-apoptotic functional lipid mediators in the cell death pathway (Pan *et al*., 2013). Remarkably, MG-63 cells exposed to DOX or MTX failed to exhibit an increase in neutral lipids (resonances assigned to CH_3 and $(CH_2)_n$), faint decreases having even been suggested (Figure 5.17a). In turn, particularly for DOX, increases in the PUFA resonance were observed. Up-regulation of the levels of neutral lipids (usually taken as apoptosis signs) was absent in previous studies with DOX-treated melanoma (Triba *et al*., 2010), leukemia (Rainaldi *et al*., 2008) and breast and colon carcinomas (Santini *et al*., 2001)**,** suggesting that no significant apoptosis is taking place in cells exposed to DOX or MTX, under the present experimental conditions. However, the increase in PUFA moieties (for both DOX and to a lesser extent for MTX) and the knowledge that both these drugs are known to ultimately induce apoptotic cell death (Minotti *et al*., 2004; Schmiegelow *et al*., 2009), suggests that apoptosis is perhaps at a very early stage at the time of sampling (contrary to cDDP-treated cells).

Regarding phospholipid-related compounds, the changes in choline metabolites previously reported for cDDP (Duarte *et al*., 2010) have been confirmed through the data reprocessing procedure presently carried out, and a relevant decrease in PE was now observed for the first time. cDDP is believed to induce membrane breakdown in MG-63 cells, leading to large and mild increases in GPC and Cho, respectively, the latter being also affected by an involvement in enhanced phospholipid biosynthesis through PC formation and/or PTC-cycle regulation (Duarte *et al*., 2010). The GPC peak at δ 3.24 correlated positively with the PUFA resonance (Figure 5.18), through STOCSY experiments, suggesting a close metabolic link to phosphatidylcholine (PTC) hydrolysis, which possibly releases PUFAs into the cytosol thus contributing to the NMR spectrum. It is important to note that STOCSY correlations between different compounds may indeed reflect metabolic links, but may also be simply casual, ultimate confirmation of metabolic relationships thus requiring additional evaluation, namely through specific pathway analysis. Regarding the elevated PC levels in cDDP-treated cells, as compared to controls (Figure 5.6), are proposed to be due to an intracellular overexpression of PE to PC conversion in order to sustain PTC synthesis, probably as an attempt to compensate for the concomitant membrane breakdown. Actually, these elevated PC levels seem specific of cDDP action (except at 48 hours), since relatively large PC decreases are observed for both DOX (Table 5.1, Figure 5.10) and MTX (Table 5.2, Figure 5.14), with no enhanced use of PE being noted (PE even experiences a slight increase, Table 5.1).

For DOX, the variations in choline compounds differ from the reported data on other DOX-treated cells (Sterin *et al*., 2001; Rainaldi *et al*., 2008; Triba *et al*., 2010), once more highlighting the strong dependence of drug effects on the cell type. Lower PC levels were accompanied by a large increase in GPC and Cho, the latter reflecting an extensive membrane breakdown through phospholipases action. Lowered PC levels are usually associated with reduced PTC biosynthesis, accompanying cell growth arrest and apoptosis (Knijn *et al*., 2005), but may also arise from enhanced catabolism to Cho (probably more active in the presence of DOX as compared to cDDP, given the much larger observed Cho increase for DOX). Low PC levels have also been proposed to evidence inhibition of *de novo* biosynthesis of cytosolic lipids (Ross *et al*., 2008), an effect possibly responsible for the lack of lipids increase in the DOX-treated cells. Furthermore, STOCSY analysis identified strong positive correlations between both GPC and Cho and the PUFA resonance (results not shown), once more establishing a clear relationship between membrane degradation and an increased polyunsaturation degree, clearly reflected in the NMR-visible lipids. Since no concomitant increase in lipids occurs, the proportion of cytosolic PUFA lipids should be increasing,

while keeping the total lipids amount unchanged, through a mechanism that still remains unclear at this stage.

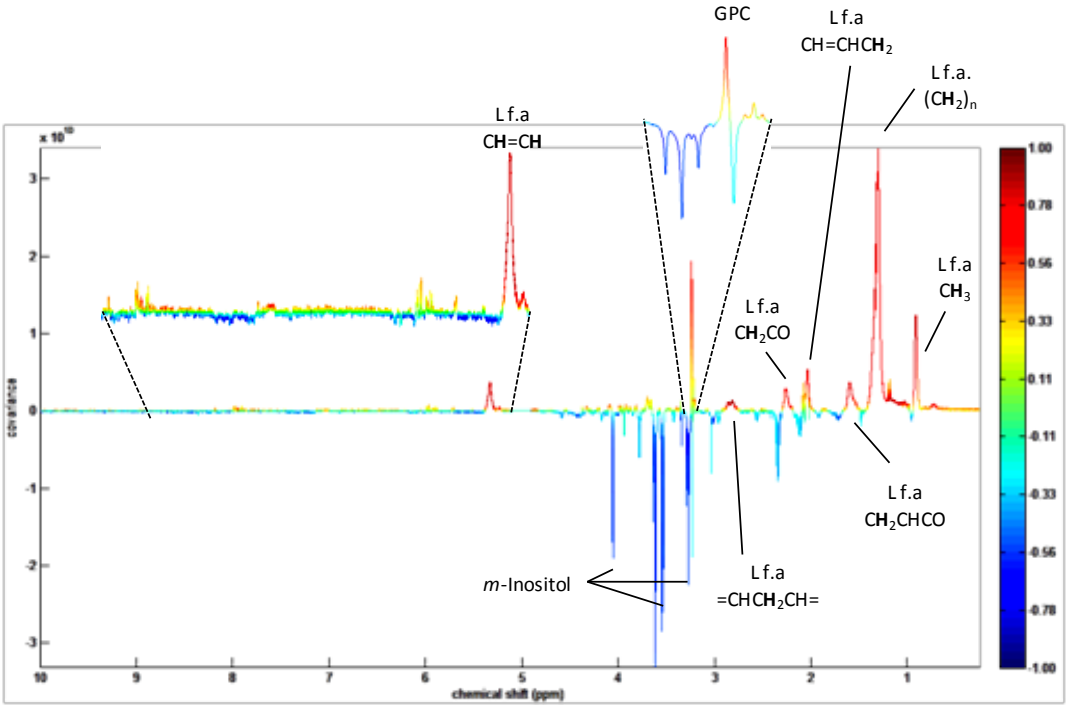

Figure 5.18. STOCSY results obtained for PUFA resonance at δ2.83, obtained for cDDP-treated cells.

The above described changes translate into a clear decrease in the PC/GPC and PC/Cho ratios (Figure 5.17b), the former having been related to cell growth arrest prior to apoptosis (Mirbahai *et al*., 2011). The distinctly different signature observed for MTX comprises a more marked decrease in PC than for DOX, reflecting a further decrease in PTC synthesis, and no meaningful changes in GPC or Cho (no significant membrane breakdown) were detected, in accordance with reports on MTX-treated breast cancer cells (Sterin *et al*., 2001) and imatinib-treated leukemia cells (Klawitter *et al*., 2009). These changes originate steadier decreases for PC/GPC and PC/Cho, which establish a clear signature for MTX reflecting, as for DOX, lower PTC synthesis not leading to the expected lipids accumulation.

Amino acids

The previously reported large impact of cDDP on the amino acid metabolism in MG-63 cells (Duarte *et al*., 2010) was confirmed after the present data reprocessing, with much less significant effects observed for DOX- and MTX-treated cells. For cDDP, the residually lower Tau levels (and the absence of measurable GSH changes) suggested a low level of oxidative stress (similarly to cDDP-treated lung cancer cells (Duarte *et al*., 2013), which probably justifies the efficiently

levelled GSH contents. Since Glu and Gly are GSH precursors (through the γ-glutamyl cycle (Macnicol *et al*., 1987), the concomitant decreases in both amino acids could also evidence some degree of activation of antioxidant protection mechanisms, which are often associated with cell cycle arrest and apoptosis (Santini *et al*., 2006; Garcia-Alvarez *et al*., 2011; Mirbahai *et al*., 2011; Santini *et al*., 2001; Triba *et al*., 2010). However, together with an Ala decrease (also observed in this work, for cDDP-treated cells), Gln/Glu reduction may also be indicative of enhanced Krebs cycle and oxidative phosphorylation activities, in order to produce more ATP to sustain apoptosis (Triba *et al*., 2010). In the OS cell line currently tested, this was not corroborated by variations in lactate or Krebs cycle intermediates (Mirbahai *et al*., 2011; Klawitter *et al*., 2009), but the decrease in Gly, Leu, Lys, Phe, Pro and Tyr may arise from their enhanced catabolism *via* an activated Krebs cycle, while acetate(s) may indicate a higher mithochondrial lipids β-oxidation activity. Finally, Val and Ile, not previously evaluated in cDDP-treated MG-63 cells, evolve against the general trend of amino acids decrease. STOCSY analysis (data not shown) revealed positive correlations of these branched chain amino acids with a typical lipidic profile, possibly due to the fact their catabolism crosses with the biosynthesis of branched chain fatty acids.

In DOX-treated cells, no relevant amino acid indicators of oxidative stress (decrease in Gln/Glu or Tau) were noted, although DOX induces a relevant decrease in intracellular GSH (reported by Cao *et al*., 2013 and Rainaldi *et al*., 2008). The absence of a consistent depletion of cellular amino acids (with even a positive variation detected for Tyr), suggests no Krebs cycle activation, although some kind of bioenergetic disturbance is noted through the increase in creatine, also reported to change in MG-63 spheroids exposed to radiation (Santini *et al*., 2006). On the other hand, in MTX-treated cells, Tau and Glu are clearly diminished, while GSH is slightly decreased, thus suggesting an oxidative stress enhancement. Furthermore, the observed increase in Gly, Tyr and Phe (in contrast to cDDP) may stem from their underuse as anaplerotic agents in the TCA cycle, possibly indicating a slowing down of the energy metabolism, in agreement with the observed creatine depletion (opposite to DOX-treated cells).

Nucleotide bases and other compounds

The nucleotide base signatures are quite distinct between the three tested drugs, showing an increase in UXP and UDP-GlcNAc species having been observed for cDDP- and DOX-treated cells, and a marked Ado/Ino decrease for cDDP (apparently specific for this drug). The rise in UXP and UDP-GlcNAc may relate to the fact that both cDDP and DOX exert their activity through

interaction with DNA (covalent binding or intercalation, respectively) and subsequent DNA conformational changes, and the distinct overall nucleotide profiles may relate to the different specific mechanisms (pharmacodynamics) involved. For MTX, the general absence of relevant changes (including for uridine, despite the apparent increase at 48 hours) or the decreasing tendencies for Ado/Ino and UXP are consistent with MTX (an antifolate) being known to hamper *de novo* purine synthesis, probably keeping nucleotide levels low or unchanged, including those of pyrimidine bases (such as uridine and UXP).

Specifically regarding UDP-GlcNAc, a donor in the glycosylation processes of post-translational proteins (Pan *et al*., 2011; Grande *et al*., 2011) its increase was newly noted in this work in cDDP- and DOX-treated OS cells (remaining unchanged for MTX). This compound was previously seen to increase, along with UDP-GalNAc, in cDDP-treated brain tumour (Pan *et al*., 2011) and lung cancer cells (Duarte *et al*., 2013), having been correlated to mobile lipids associated to apoptotic cell death. However, STOCSY analysis of the data (Figure 5.19a) failed to reveal any correlation to lipid resonances in cDDP-treated OS cells, showing positive correlations with GPC, Cho and PC (membrane degradation metabolism), and creatine and GSH (antioxidative process), with negative correlations with Lys, uridine and Ado/Ino (the latter proposed to vary relative to cDDP-induced DNA damage).

a)

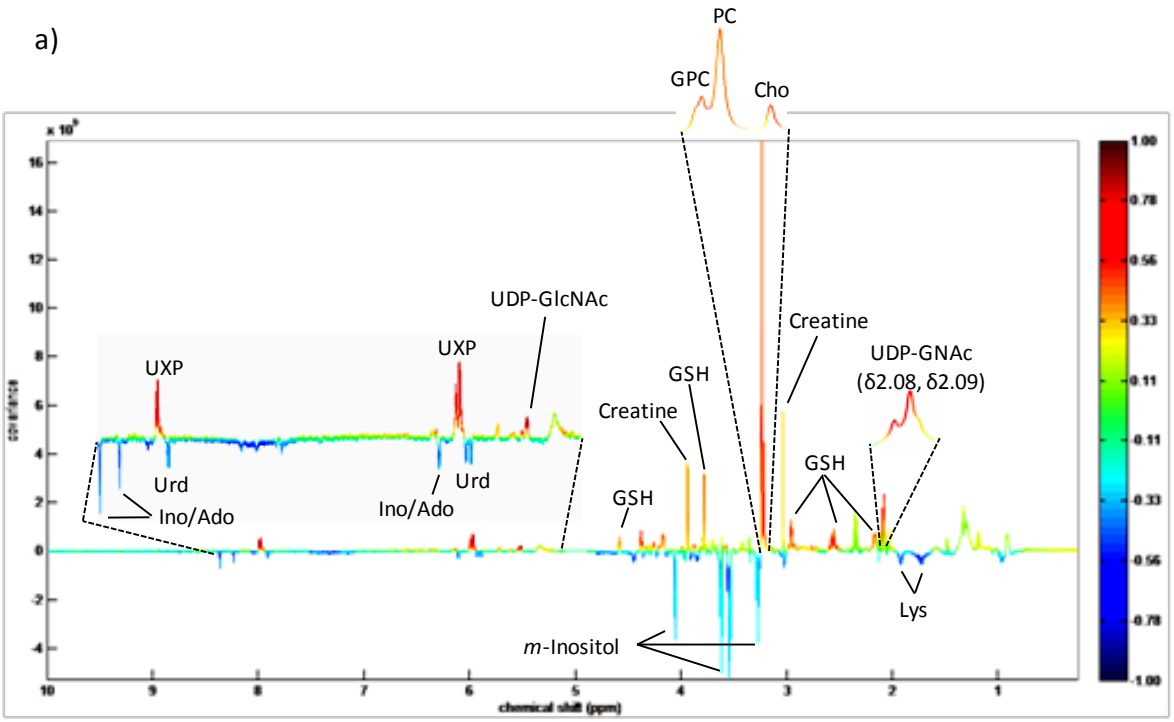

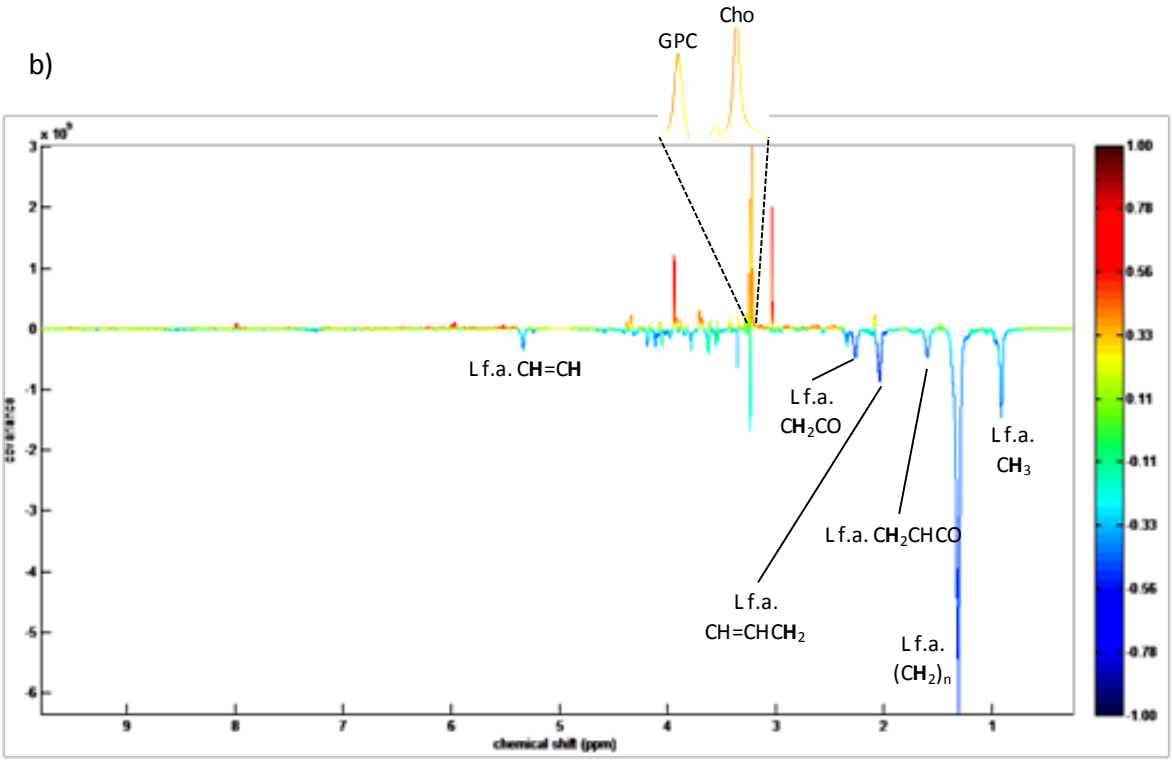

Figure 5.19. STOCSY results obtained for UDP-GlcNAc resonance at δ5.52, obtained for a) cDDP-treated and b) DOX-treated cells.

In DOX-treated cells (Figure 5.19b), UDP-GlcNAc (much increased relatively to cDDP) again correlates positively with the main membrane degradation products (GPC and Cho) and creatine but notably, not to GSH thus suggesting that in DOX-treated cells, the main metabolic origin of UDP-GlcNAc does not relate to antioxidative mechanisms as opposed to cDDP-incubated cells. In addition, for DOX, UDP-GlcNAc actually correlates negatively with lipids, in agreement with the slight decrease seen for CH_3 and $(CH_2)_n$ resonances (Figure 5.17) once more contradicting a direct relationship with a neutral lipids increase. Overall, the above observations suggest a general connection of UDP-GlcNAc with the active and preferential pathways of membrane degradation and energy metabolism (through creatine), while in cDDP an additional link to cellular oxidative state seems to exist.

Finally, some considerations are due regarding the marked decrease in *m*- and *s*-inositols (mainly for the former), detected for both cDDP- and DOX-treated cells. In turn, these compounds were unchanged in MTX-treated cells. Depletion in *m*-inositol has been previously reported (Griffin *et al*., 2003; Knijn *et al*., 2005; Triba *et al*., 2010) several explanations having been put forward: disturbance in its osmolytic function through drug-induced partial inhibition of the Na^+/*m*-inositol co-transporter (SMIT) (Knijn *et al*., 2005); diminished inhibition of the mitogen-

activated protein kinase (MAPK) signal transduction pathway, thus leading to stimulation of cells into apoptosis (Knijn *et al*., 2005); effect on the biosynthesis and turnover of some phospholipids (Ferreti *et al*., 2002); or activation of cell detoxification processes.

With a view to clarify the role of inositols in treated MG-63 cells (particularly with cDDP and DOX), STOCSY analysis of the inositol resonances (not shown) revealed that in the presence of cDDP *m*-inositol decreases concomitantly with Tau, Glu/Gln and creatine (besides *s*-inositol), whereas in DOX-treated cells *m*-inositol is reduced together with Glu/Gln and GSH (and *s*-inositol). These observations allowed a significant inositol decrease to be identified as preferentially related with an ongoing antioxidative mechanism, although the corresponding metabolite signatures seem distinct: i) for cDDP, it is apparent that Tau, Glu/Gln, inositols and (possibly) creatine help to regulate GSH levels efficiently (since such levels are unchanged upon drug treatment); ii) for DOX, Glu/Gln and inositols alone seem to be insufficient to avoid a concomitant GSH use in the cellular response to oxidative stress (negative variation, Table 5.1). For MTX, the resonances due to inositols, although unchanged upon drug treatment, were found to also correlate weakly to Glu/Gln, GSH and, possibly, creatine, confirming the proposed link to an antioxidative response.

6. Metabolic Impact of Pd_2Spm on Osteosarcoma MG-63 Cells and Comparison with Osteoblast HOb Cells

This chapter describes the application of the methodology used in the previous chapter to a similar study regarding a palladium complex with the biogenic polyamine spermine (Spm), Pd_2Spm, which has been reported to display significant antineoplastic activity (Fiuza *et al*., 2011).

Platinum and palladium belong to the same group (X, ten) of the periodic table, thus presenting similar coordination chemistry. Palladium (II) has lately attracted considerable interest as a potential metal ion center in drug formulations capable of effectively interacting with DNA while circumventing undesired toxicity and resistance phenomena usually associated with platinum agents (e.g. cDDP) (Marques, 2013; Silva *et al*., 2014; Silva *et al*., 2013; Fiuza *et al*., 2011; Tummala *et al*., 2010; Corduneanu *et al*., 2010). Pd_2Spm in particular, has shown very promising results towards a human breast cancer cell line, MDA-MB-231 (Fiuza *et al*., 2011), showing improved cytotoxic action coupled to less deleterious side-effects (damages in DNA and impact over cytoskeleton) when compared to cDDP. This chapter evaluates the metabolic response of MG-63 cells to Pd_2Spm, compared to that of cDDP. Moreover, a human osteoblast cell line (HOb) was analysed by HRMAS NMR in the presence of either cDDP or Pd_2Spm, this constituting the first reported study of the metabolic consequences of treatment in healthy cells, to our knowledge. Besides providing a more comprehensive knowledge of the impact of chemotherapy in both tumour and healthy cells, these results can help understand which of the two drugs is preferable by considering their potential to induce death in cancer cells and the least possible damage to healthy cells. Although this type of approach would have been extremely valuable as a complement of the drug exposure assays presented in Chapter 5, it was not possible to pursue it, due to time and economical constraints (mainly associated with HOb cells' very slow growth and expensive culture conditions).

6.1. Antiproliferative Activity and Cytotoxic Assay Results

Since no IC_{50} value was available in the literature for the Pd_2Spm complex towards MG-63 cells, the drug concentrations to be tested were chosen in the light of the experiments previously

reported for this Pd(II) agent in other cell lines, namely breast (Fiuza *et al*., 2011), tongue (Soares *et al*., 2007) and ovarian (Tummala *et al*., 2010) cancer cell lines (Table 6.1).

Table 6.1. Cell line studies of IC_{50} determination with the Pd_2Spm complex.

Cell Line	IC_{50} at 24 hours	Reference
MCF-7 (breast cancer)	10.9 µM	Fiuza *et al*., 2011
MDA-MB-231 (breast cancer)	4.7 µM	Fiuza *et al*., 2011
HSC-3 (tongue cancer)	19 µM	Soares *et al*., 2007
	IC_{50} at 72 hours	
A2780 (ovarian cancer)	1.25 µM	Tummala *et al*., 2010

Figure 6.1 shows the results of the first evaluation of antiproliferative activity of Pd_2Spm in MG-63 cells, using the SRB assay. In this preliminary study, a concentration of 12.06 µM of Pd_2Spm was found to inhibit 50 % of MG-63 cell growth (as shown in inset of Figure 6.1). Two additional determinations were performed and yielded the IC_{50} values of 9.32 and 9.01 µM (not shown), hence indicating an average IC_{50} value of 10.13 µM. However, due to timings of NMR spectrometer availability, all NMR experiments were performed using the first value measured (12 µM). This value is in broad agreement with those reported in literature for breast and tongue cancer cell lines (Table 6.1).

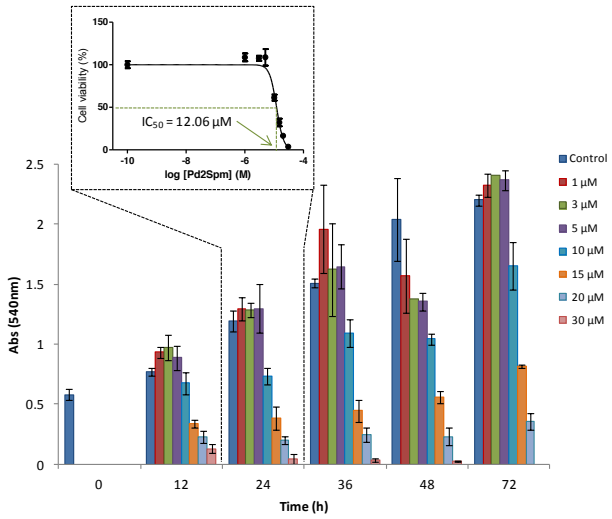

Figure 6.1. SRB evaluation of antiproliferative activity of Pd_2Spm against MG-63 cells. Inset shows the logaritmic determination of IC_{50} concentration upon 24 hours drug exposure.

Figure 6.2 represents the time- and dose-response plot of the cytotoxicity assays (using the Trypan blue assay) of the two considered assays for HRMAS NMR analysis. The results validated the previously value of IC_{50} of 12 µM determined by SRB.

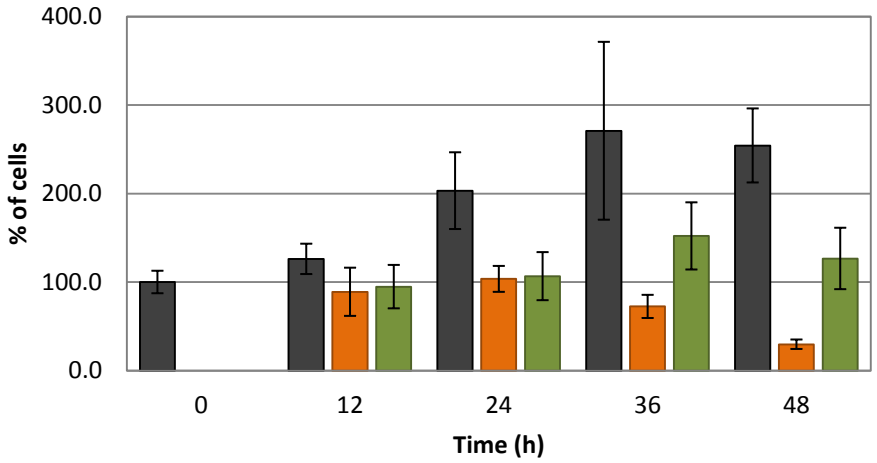

Figure 6.2. Time-dependent plot of the cytotoxic effect of cDDP and Pd_2Spm, in sole administration, towards the MG-63 cell line. Cell proliferation was evaluated by the Trypan blue assay (as described in the Experimental Procedures, Chapter 3). Control (■), 30 μM cDDP (■) and 12 μM Pd_2Spm (■). The data represent the average ± mean standard deviation from n=2 experiments, carried out in duplicate.

As previously determined for a 24 hours drug exposure, *ca.* 50% of MG-63 cells death is achieved for 30 and 12 μM concentrations of cDDP and Pd_2Spm, respectively. This indicates, therefore, that at this time point Pd_2Spm displays a growth-inhibiting effect about twice as high as that of cDDP. However, the results are less promising for higher exposure periods (36 and 48 hours), when cDDP-treated cells show a steady decrease in cell proliferation while some recovery is observed for Pd_2Spm-treated cultures. Recalling the results obtained for DOX and MTX (presented in Chapter 5), the former showed a long term effect on cell survival similar to that of cDDP, while the cytotoxic effect of MTX that resulted in the absence of a clear decrease on living cells from 24 hours more closely resembles that here obtained for Pd_2Spm.

Only two studies are to be found in the literature comparing the antineoplastic activity of cDDP and Pd_2Spm: one in human ovarian carcinoma cells (Tummala *et al.*, 2010) and another in two different breast cancer cell lines, estrogen-dependent (ER(+)) and estrogen-independent (ER(-)) (Fiuza *et al.*, 2011). The studies from Tummala *et al.*, 2010 showed that cDDP has a higher cytotoxic potency than Pd_2Spm towards ovarian carcinoma, although against the homologous cDDP-resistant cell line the degree of resistance was found to be much lower for Pd_2Spm. According to the same study, the most important mechanistic difference between these two compounds appears to be their potential to affect the biogenic polyamine pathway, this being much more pronounced for the spermine complex. According to Fiuza (Fiuza *et al.*, 2011), Pd_2Spm is more effective against the ER(-) breast cancer cells, while cDDP displays a higher efficacy towards the ER(+) line. Also, the Pd(II) complex was verified to trigger phosphorylation of H2AX, a

human histone (similarly to cDDP but to a higher extent), evidencing that it induces DNA conformational changes and cytoskeleton damage, with a greater impact on cell morphology than cDDP.

Another study (Soares *et al*., 2007), assessed the effect of the metal center (either Pt(II) or Pd(II)) in two analogous dinuclear spermine chelates on their anticancer activity towards human tongue epithelioma (HSC-3 cells). The results evidenced an improved cytotoxicity for the Pd(II) complex as compared to its Pt(II) counterpart. A similar test performed by Tummala *et al*., 2010, allowed to unveil an identical behaviour, as a Pd(II) complex also showed an increased cytotoxic capacity than its Pt(II) analogue against human ovarian carcinoma cells. Furthermore, Fiuza and co-workers (Fiuza *et al*., 2006) evaluated the antiproliferative effect of two homologous Pd(II) and Pt(II) complexes with a different polyamine ligand – the biogenic triamine spermidine (Spd) as opposed to the tetramine spermine (Spm). Once again, the Pd(II) agent displayed a higher effect towards the tested cancer cells (HSC-3) than its Pt(II) analogue.

Within the work of this thesis, a Pd(II) complex with Spd (Pd_3Spd_2) was assessed towards the MG-63 cells for a 24 hours exposure time (using the SRB method) and an IC_{50} value of 10.6 μM was obtained, which is identical to the one obtained for the spermine chelate Pd_2Spm. In the light of these similar results, experiments for the metabolic profiling proceeded with the Spm agent, due to its highly promising results towards human ER(-) breast cancer cells (Fiuza *et al*., 2011).

6.2. ^{1}H HRMAS NMR Analysis of Pd_2Spm-Induced Metabolic Changes in MG-63 Cells and Comparison to cDDP

The metabolic alterations that underlie the cytotoxic effect of Pd_2Spm over the MG-63 cells are hereby investigated and compared with those induced by cDDP-treatment. The results hereby presented were obtained from only two independent assays (see Experimental Section, Chapter 3), and for this reason they are affected by some degree of uncertainty, when compared to the rest of the data, based on three independent assays.

Visual inspection of the average spectra of controls *vs* Pd_2Spm-treated MG-63 cells (Figure 6.3) shows that, after 24 hours treatment with Pd_2Spm (Figure 6.3c), MG-63 cells exhibit slight increases in Val, Leu, Ile and Tyr and decreases in Glu, Tau and Pro resonances. Additional observations comprise decreased $(CH_2)_n$ of lipids and GPC and increased PC. Moreover, N-acetyl,

creatine, *m*- and *s*-Inositol, UXP and hypoxanthine signals also decreased with treatment and an increase of GSH was detected.

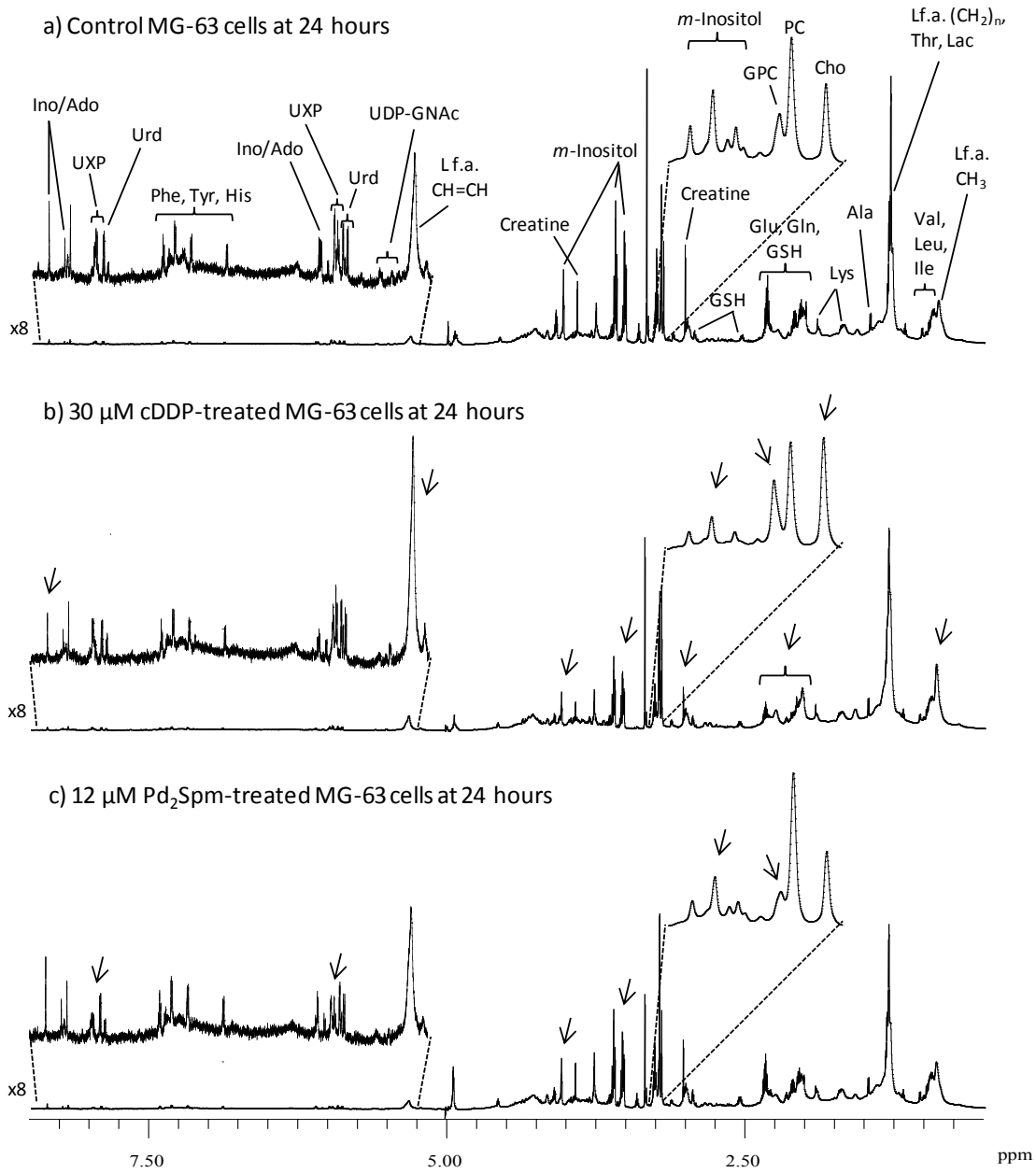

Figure 6.3. Average 800 MHz ^{1}H HRMAS NMR spectra of MG-63 cells, at 24 hours: a) under control conditions, b) exposed to 30 µM cDDP and c) exposed to 12 µM Pd_2Spm. Insets show expansions of choline compounds (3.2-3.3 ppm) and aromatic (5.2-8.5 ppm) regions. Main assignments are noted and visible spectral changes due to drug exposure are marked by arrows.

When compared to the global metabolic alterations induced by cDDP-treatment, Pd_2Spm clearly behaves differently in what concerns lipids and choline compounds biochemistry. The typical cDDP pattern of increased lipid resonances is not observed upon Pd_2Spm-treatment, instead, a slight decrease of the $(CH_2)_n$ peaks (δ 1.30) is suggested by visual inspection (Figure

6.3c). Moreover, upon 24 hours treatment, the alterations seen in choline compounds upon Pd_2Spm-exposure are less dramatic than those induced by cDDP, for instance, Pd_2Spm does not alter the profile of the three main choline compounds, with PC (δ 3.23) remaining the most abundant and GPC (δ 3.24) the less abundant choline compound. The different modes of action of the two drugs are also suggested by differences in the levels of Ino/Ado, since a decrease is detected already at 24 hours treatment with cDDP while no considerable alterations to this nucleoside are detected upon Pd_2Spm exposure. Nevertheless, the two drugs share a common decreasing effect over *m*-Inositol.

Following the established data analysis workflow, multivariate analysis was applied to the ^{1}H HRMAS NMR spectra in order to confirm visual findings and unveil the most relevant drug-induced metabolic changes. Multivariate analysis (Figure 6.4) suggested that changes compared to controls are much more pronounced upon cDDP than Pd_2Spm treatment. As shown by the PCA analysis (Figure 6.4a), controls and Pd_2Spm-treated cell cluster together, while cDDP-treated cells are clearly separated from the other two groups in the scores plot, in a time-dependent trajectory (in negative PC1). The corresponding PLS-DA scores plot (Figure 6.4b) shows good separation between the 3 groups of samples (Q^2 0.815): cDDP from Pd_2Spm and controls along LV1 and Pd_2Spm from controls along LV2 (positive and negative, respectively). In these results, a time-dependent disposition of samples in scores space is only clearly identified for cDDP-treated samples, since samples exposed to the drug for higher periods move to lower LV1. PLS-DA of controls *vs* cDDP-treated samples (Figure 6.4c) shows a clustering of the control samples while cDDP-treated ones dispose themselves in the scores plot in a time dependent manner (in agreement to what was suggested by PCA, Figure 6.4a), suggesting that metabolic changes that account for time course adaptations in controls are less marked than those induced by treatment with cDDP (in agreement to what is reported in Chapter 5 for cDDP-induced effects). In line to what is reported in Chapter 5 for cDDP, the robustness of the group discrimination is reflected in a very low Q^2 distribution overlap (Figure 6.5a) and good MCCV results: 79.9% sensitivity, 100% specificity and 91.1% classification rate (Figure 6.5b). PLS-DA of controls *vs* Pd_2Spm (Figure 6.4d) enables the discrimination of the two groups of samples along LV1, but no evident time course tendency can be drawn for neither control or treated samples, with the 48 hour samples differing considerably in lipids and *m*-inositol contents. In fact, in addition to the satisfactory Q^2 value (0.607) obtained for the model, some overlap of Q^2 distributions is visible (Figure 6.5c) along with poor MCCV results: 77.0% sensitivity, 60.8% specificity and 68.0% classification rate (Figure 6.5d).

This indicates that the metabolic impact of Pd_2Spm, at IC_{50}, is much weaker than that of cDDP. The increase of the number of samples per condition (time point) might probably improve the quality of this particular model by lowering the level of uncertainty, since, as has been suggested by results, Pd_2Spm-induced changes are globally tenuous thus being more affected by variation within duplicates.

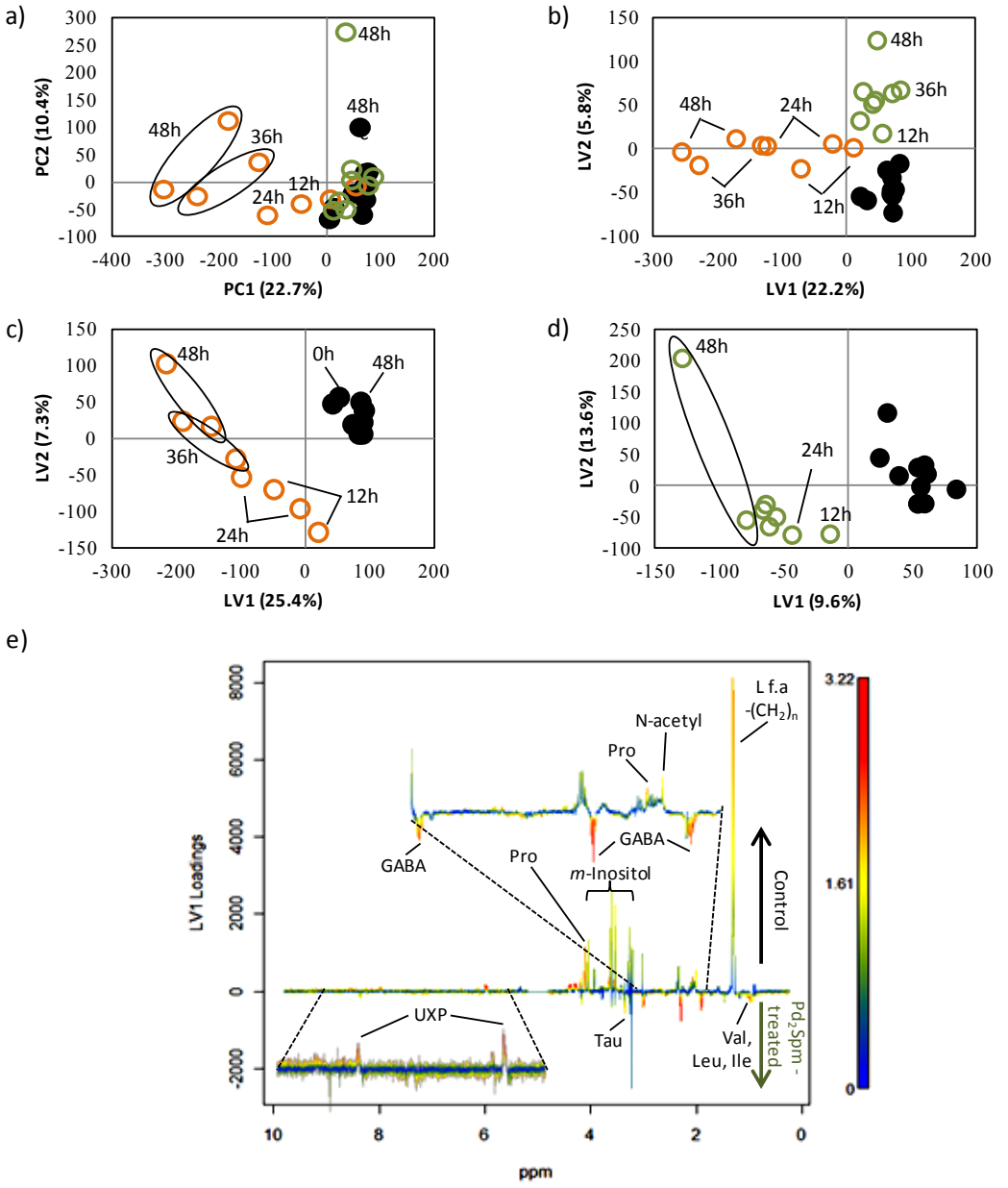

Figure 6.4. Multivariate analysis of controls (●), 30 µM cDDP- (○) and 12 µM Pd_2Spm-treated (○) cells: a) PCA scores plot for all samples, UV, 4 components, $R^2X = 0.462$ and $Q^2 = 0.087$, b) PLS-DA scores plot for all samples, UV, 6 components, $R^2X = 0.502$, $R^2Y = 0.993$ and $Q^2 = 0.815$, c) PLS-DA scores plot for cDDP assay, UV, 2 components, $R^2X = 0.327$, $R^2Y = 0.977$ and $Q^2 = 0.822$, d) PLS-DA scores plot for Pd_2Spm assay, UV, 3 components, $R^2X = 0.329$, $R^2Y = 0.991$ and $Q^2 = 0.607$ and e) loadings plot of the PLS-DA model shown in d).

The loadings plot corresponding to the PLS-DA model of controls *vs* Pd_2Spm-treated samples (Figure 6.4d) is shown in Figure 6.4e, helping to unveil the signals that underlie class separation. Amino acids Val (δ 1.05), Leu (δ 0.97) and Ile (δ 1.02) are suggested to be increased in Pd_2Spm-treated samples as well as γ-aminobutyric acid (GABA, δ 1.91, δ 2.30, δ 3.00). Important decreases of UXP (δ 5.99 and δ 7.98) and less marked decreases of *m*-inositol, Pro and N-acetyl moieties (δ 2.02) also seem to account for metabolic alterations induced by cells treatment with the Pd agent. Figure 6.4e also suggests that Pd_2Spm-treatment may induce a decrease of $(CH_2)_n$ resonances of lipids but, as stated above, the intensity of this particular resonance is considerable different within 48 hours replica, fact that can be erroneously influencing this result.

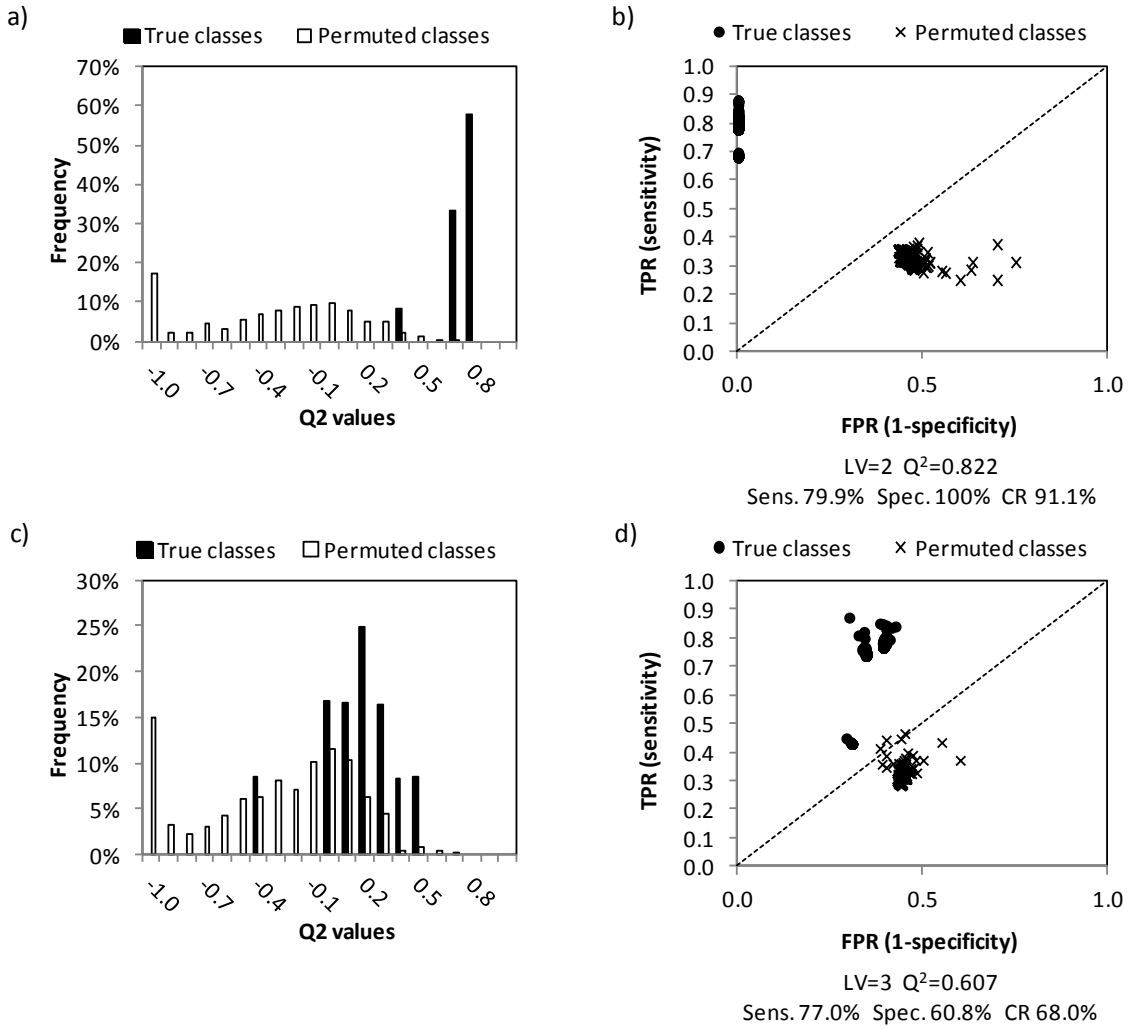

Figure 6.5. Monte Carlo Cross-Validation (MCCV) results of PLS-DA model obtained for MG-63 cells exposed to 30 μM cDDP (a and b) or 12 μM Pd_2Spm (c and d) , *vs* control cells: a) and c) Q^2 distributions, c) and d) ROC plots of true and permuted models. TPR: true positive rate, FPR: false positive rate, Sens.: sensitivity, Spec.: specificity, CR: classification rate.

Subsequent signal integration and univariate statistical analysis identified the relevant variations in metabolites over time and their time course plots are shown in Figures 6.6 and 6.7 and compiled in Tables 6.2 and 6.3 for 24 and 48 hours.

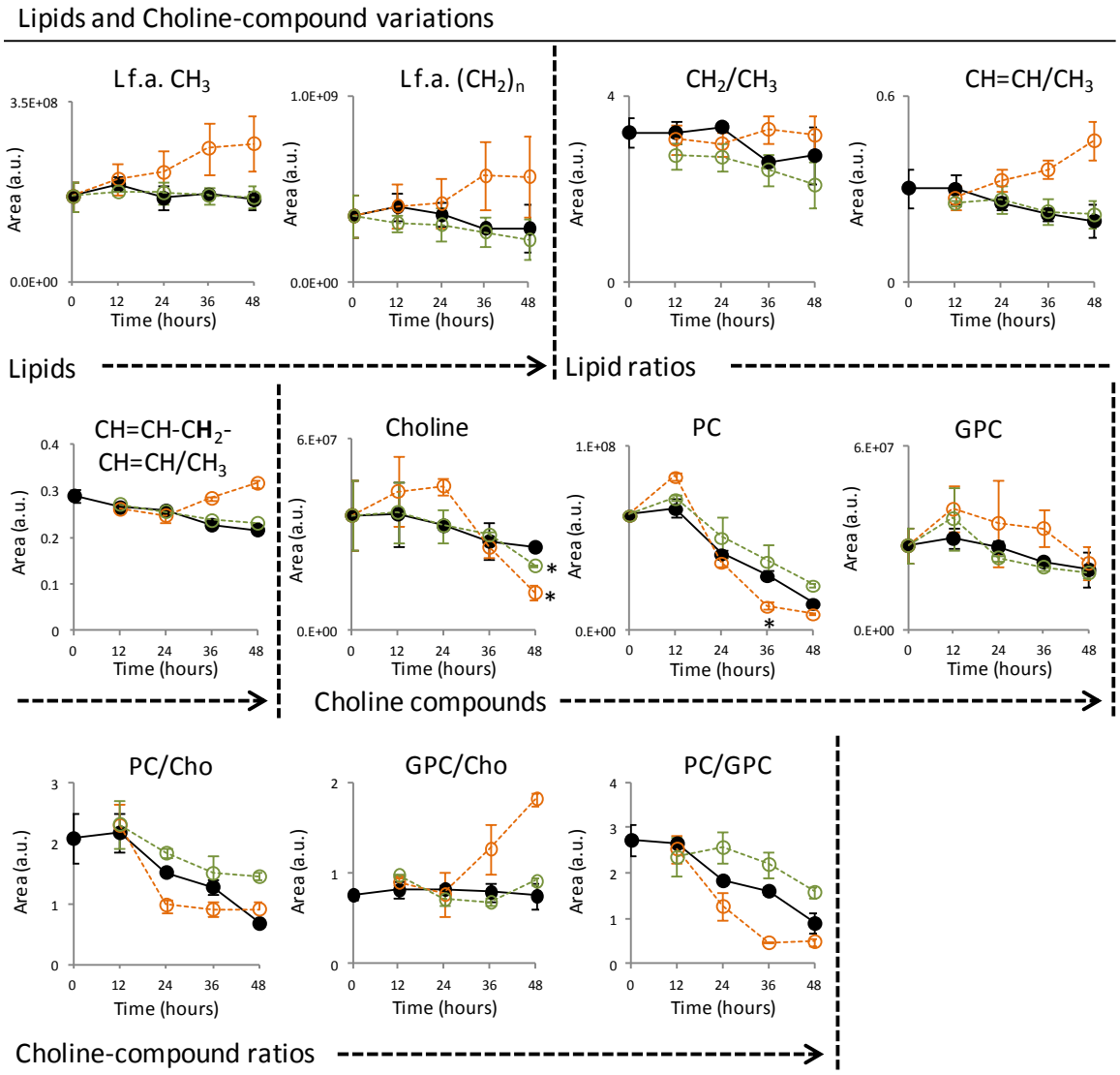

Figure 6.6. Time course variation of lipids (L f.a.) and choline compounds with cDDP (30 µM) and Pd_2Spm (12 µM) treatment. Controls (●), cDDP-treated (○) and Pd_2Spm (○) (controls are indicated with full lines and drug-treated with dashed lines).*$p < 0.05$.

Results show that the metabolic adaptations experienced by MG-63 cells upon exposure to Pd_2Spm comprise decreases in the amino acids Pro, Gly and Thr (with % of variation in the range -20 to -30 and ES of -1.4 to -3.5) and slight increases in Ser, Tyr and Phe (mainly detected at early periods of exposure). Moreover, decreases in Cho and increases in PC are detected, leading to slight increased PC/Cho and PC/GPC ratios. Pd_2Spm treatment also resulted in fluctuations in UDP-GlcNAc, slight increased Ino/Ado (only at 48 hours, with around 73% variation in relation

controls) and important decreases in UXP (with around -29 to -35% variation in relation to controls, to which ES values range from -2.4 to -1.5. Decreases in N-acetyl moieties, GSH (only at 12 hours) and *m*-Inositol (24 and 36 hours) are also seen in Pd_2Spm-treated MG-63 cells.

In what concerns to cDDP-treatment, the marked increases detected in L f.a. and respective ratios as well as global variations in choline compounds and choline compounds ratios (Figure 6.6) are generally in agreement with previous findings reported in Chapter 5. The compound variations shown in Figure 6.7, also confirm previous findings reported in Chapter 5, for cDDP-treated cells: decreased Glu and Phe, decreased Ino/Ado and *m*-Ino and slight increased UDP-GlcNAc. The error associated with variations in UXP ad N-acetyl moieties difficult similar comparisons. The variations in GABA, here detected for the first time, were also absent in previous assays of MG-63 cells exposure to cDDP.

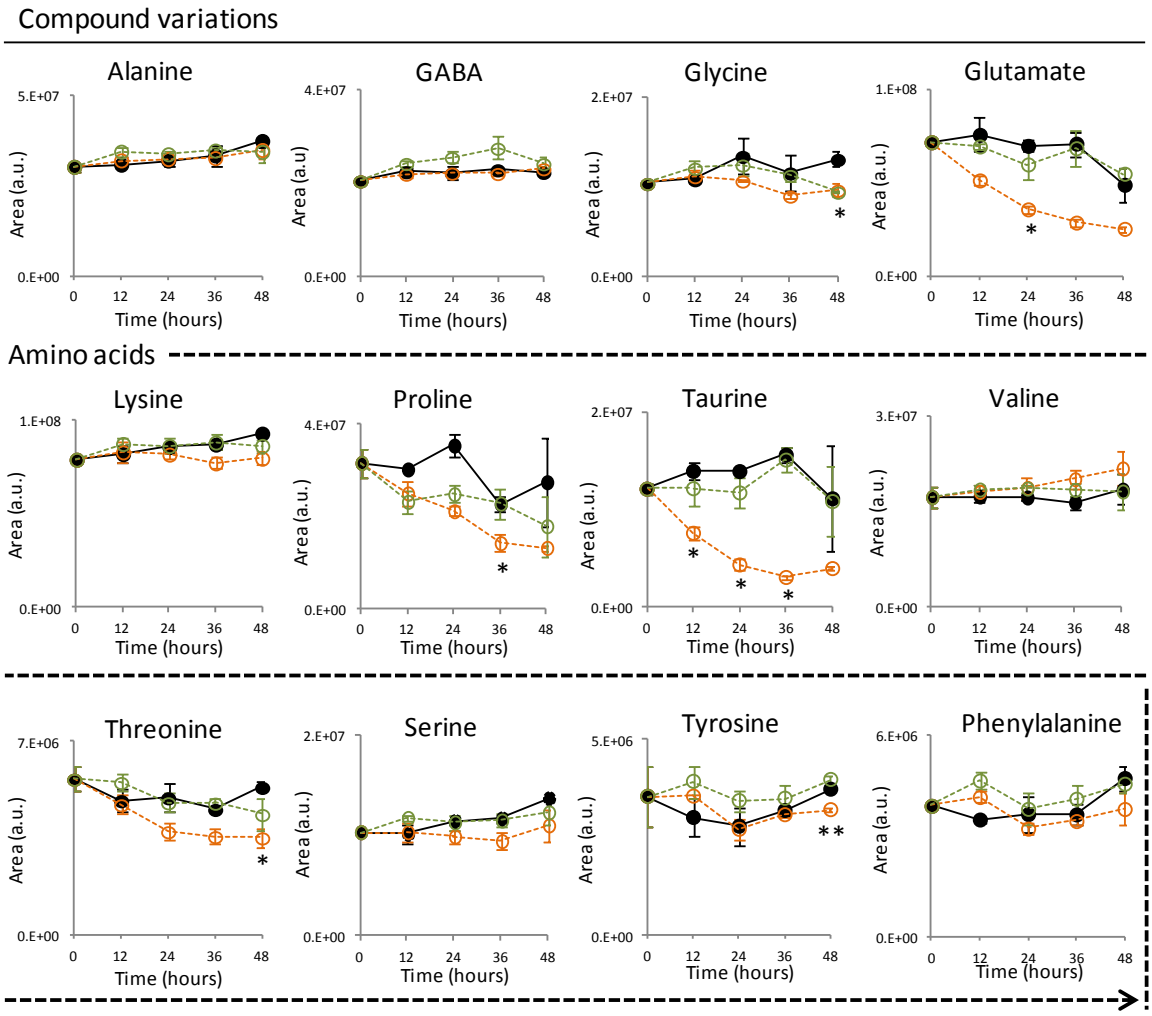

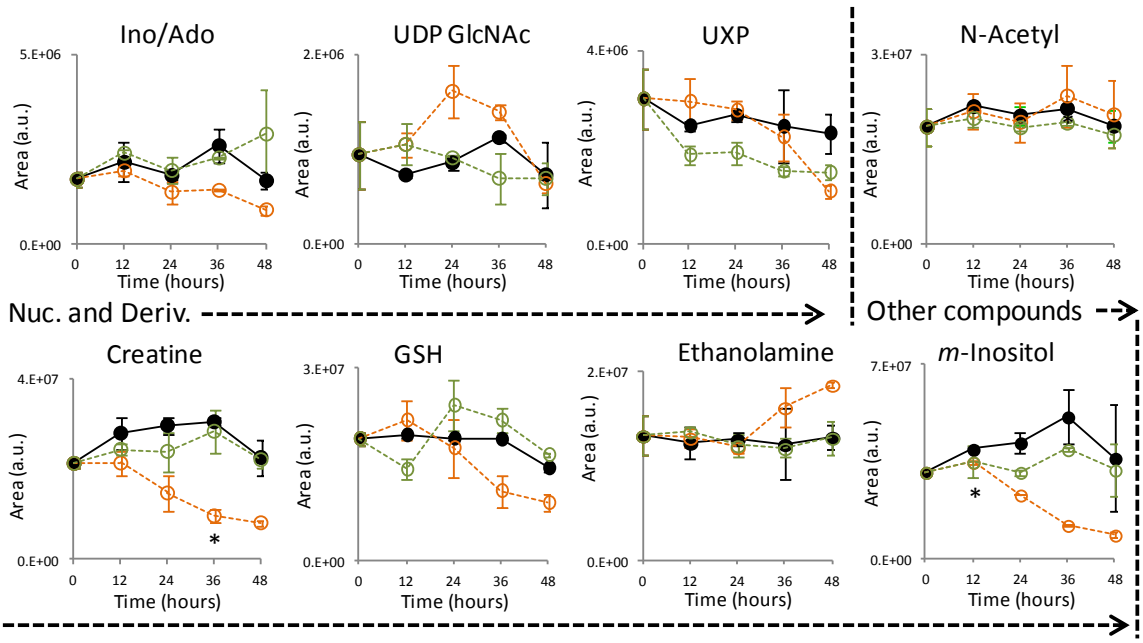

Figure 6.7. Time course variation of several compounds with cDDP (30 µM) and Pd_2Spm (12 µM) treatment. Controls (●), cDDP-treated (○) and Pd_2Spm (○) (controls are indicated with full lines and drug-treated with dashed lines).*$p < 0.05$, *$p < 0.01$.

The heatmap of the effect size values shown is Figure 6.8a highlights the most relevant time course changes induced by each of the two tested drugs. Pd_2Spm-induced alterations in amino acids occur mostly at initial times of exposure and are mainly positive, while for cDDP treatment most changes are negative and occur from 24 hours onwards, suggesting that Pd_2Spm has a slight higher and mostly transitory impact at initial periods of exposure while cDDP has a more sustained effect over time. Some similarities were found between cDDP and Pd_2Spm treated cells namely regarding increases in Phe and Val and the drug-induced decreases in Pro.

One of the most relevant differences between the two drugs concerns lipids, since no significant changes were noted with Pd_2Spm treatment while clear increases were confirmed again in cells treated with cDDP (consistently with Chapter 5). Regarding lipid ratios, a global increase in all calculated ratios was detected upon cDDP exposure, pointing to a drug-induced increase in mean chain length ($(CH_2)_n/CH_3$), mono ($CH{=}CH/CH_3$) and polyunsaturation degrees ($=CHCH_2CH=/CH_3$). On the other hand, Pd_2Spm, which induced no alterations in lipids, was found to promote a decrease in mean chain length of lipid fatty acids at 24 hours (cancelled at higher exposure periods) and an increase in the polyunsaturation degree after 48 hours treatment.

Table 6.2. Metabolite variations in MG-63 cells exposed to 30 µM cDDP or 12 µM Pd_2Spm for 24 and 48 hours and after the 3 days reversibility period, compared to control cells

Metabolite	Signal (δ,ppm)[a]	cDDP (30 µM)						Pd_2Spm (12 µM)					
		24h		48h		Reversibility		24h		48h		Reversibility	
		% var[b]	Effect size[c]	% var[b]	Effect size[c]	% var[b]	Effect size[c]	% var[b]	Effect size[c]	% var[b]	Effect size[c]	% var[b]	Effect size[c]
Amino acids													
Alanine	1.48, d	-	-	-	-	-	-	-	-	-	-	-	-
Glutamate	2.34, m	-49.0±4.8*	-7.76±2.80	-48.5±17.2	-2.13±0.94	-70.1±7.60*	-8.09±2.92	-	-	-	-	-	-
Glycine	3.56, s	(-)	(-)	-26.2±6.8*	-2.52±1.06	-58.6±10.1	-4.68±1.75	-	-	-27.9±5.3	-3.46±1.35	-	-
Isoleucine	1.02, d	nv	nv	(+)	(+)	-	-	7.00±3.20	(+)	-	-	-	-
Lysine	1.72, m	-4.70±2.20	(-)	-14.4±2.9	-3.02±1.21	-33.7±10.6	2.19±0.96	-	-	-7.1±2.7	-1.56±0.80	-	-
Phenylalanine	7.32, d	-	-	-19.5±9.7	(-)	-35.1±17.0	-1.43±0.76	-	-	-	-	-	-
Proline	4.12, t	-40.2±6.90	-4.15±1.58	(-)	(-)	-58.1±18.6	-2.52±1.06	-29.8±7.60	-2.64±1.09	-	-	-	-
Serine	3.84, d	-13.6±4.8	-1.72±0.83	-19.8±9.4	(-)	-49.4±11.1	-3.38±1.32	-	-	-	-	-	-
Taurine	3.42, t	-68.6±4.7*	-12.59±4.49	(-)	(-)	-68.4±10.2**	-5.82±2.14	(-)	(-)	-	-	-	-
Threonine	3.58, d	-24.8±10.0	-1.61±0.81	-34.3±6.2*	-3.82±1.47	-41.8±17.1	-1.76±0.85	-	-	-18.4±8.6	-1.35±0.74	-	-
Tyrosine	6.89, d	-	-	-14±1.3**	-6.62±2.41	-33.2±15.0	-1.52±0.78	-	-	6.7±2.5	1.51±0.78	-	-
Valine	1.05, d	-	-	-	-	-	-	8.20±3.10	1.42±0.76	-	-	-	-
Lipids													
-C<u>H</u>$_3$	0.91	(+)	-	68.5±18.7	1.56±0.79	83.2±27.3	(+)	-	-	-	-	-	-
-(C<u>H</u>$_2$)$_n$	1.30	-	-	95.4±41.0	-	135.8±38.0	(+)	-	-	-	-	-	-
-C<u>H</u>$_2$CH$_2$CO	1.60	-	-	87.2±23.1	1.50±0.78	91.1±30.4	(+)	-	-	-	-	-	-
-C<u>H</u>$_2$COO	2.25	-	-	73.0±22.4	1.37±0.75	68.8±30.3	(+)	-	-	-	-	-	-
=CHC<u>H</u>$_2$CH=	2.83	25.8±11.6	(+)	146.8±24.2	2.00±0.91	170.8±30.2	(+)	-	-	-	-	-	-
-C<u>H</u>=C<u>H</u>-	5.33	68.4±33.2	-	287.7±46.6	1.45±0.77	364.6±34.8	(+)	-	-	-	-	-	-

Table 6.2 (cont.). Metabolite variations in MG-63 cells exposed to 30 µM cDDP or 12 µM Pd_2Spm for 24 and 48 hours and after the 3 days reversibility period, compared to control cells.

Metabolite	Signal (δ,ppm)[a]	cDDP (30 µM)						Pd_2Spm (12 µM)					
		24h		48h		Reversibility		24h		48h		Reversibility	
		% var[b]	Effect size[c]	% var[b]	Effect size[c]	% var[b]	Effect size[c]	% var[b]	Effect size[c]	% var[b]	Effect size[c]	% var[b]	Effect size[c]
Choline compounds													
Choline	3.21, s	37.9±4.90	3.70±1.43	-54.4±8.9*	-4.81±1.79	-70.2±34.5	-1.79±0.85	-	-	-22.3±3.0*	-4.76±1.78	-	-
GPC	3.24, s	-	-	-	-	-34.4±8.10	-2.94±1.18	-13.3±6.20	(-)	-	-	-	-
PC	3.23, s	-10.9±5.00	(-)	-38.4±4.70	-5.76±2.12	-65.3±7.80*	-7.12±2.58	-	-	67.1±4.2**	6.87±2.50	-	-
PE	3.25, s	-	-	-	-	-43.0±15.6	-2.01±0.91	-	-	-	-	-	-
Nucleotides and Derivatives													
Inosine	8.36, s	-	(-)	-45.6±14.2	-2.37±1.01	-	-	-	-	73.4±36.4	-	12.7±4.90	1.39±0.75
UDP-GlcNAc	5.52, m	87.9±16.5	2.12±0.94	-	-	-	-	-	-	-	-	-	-
UXP	5.99, d	-	-	-52.1±17.7	-2.27±0.98	-	-	-28.6±8.00	-2.38±1.02	-35.3±16.3	-1.51±0.78	-	-
Uridine	5.89, d	-	-	90.8±26.3	(+)	-	-	-	-	-	-	-	-
Other Compounds													
Creatine	3.93, s	-50.6±13.5	-2.87±1.16	-64.3±18.1	-3.00±1.20	-74.6±5.5**	-12.3±4.40	-	-	-	-	-	-
Ethanolamine		-	-	42.3±5.60	3.55±1.38	80.3±8.20	3.99±1.52	-	-	-	-	14.7±5.40	(+)
GSH	2.56, m	-	-	-37.6±8.4	-3.14±1.25	-61.4±2.2**	-23.52±8.33	27.0±12.7	(+)	14.3±2.80	2.75±1.13	-	-
Hypoxanthine	8.18, s	-26.6±13.0	(-)	(-)	(-)	-	-	-	-	-	-	-	-
m-Inositol	4.05, t	-45.0±8.00	-4.16±1.58	(-)	(-)	-81.8±0.90**	-92.8±32.8	-25.4±7.40	-2.26±0.98	-	-	-	-
s-Inositol	3.34, s	-36.4±5.50	-4.61±1.73	-66.5±37.9	-1.50±0.78	-	-	-18.2±4.80	-2.37±1.01	-	-	-	-
N-acetyl	2.02, s	-	-	-	-	-	-	-	-	-	-	-	-

[a] Resonance chosen for signal integration, [b] % variation and [c] effect size in relation to control cells. * $p < 0.05$, ** $p < 0.01$, $^-$: no significant variation. (+) and (-) indicate consistent positive and negative variations, respectively, without statistical meaning.

Table 6.3. Mean ratios for lipids and choline compounds in MG-63 cells exposed to either 30 µM cDDP or 12 µM Pd_2Spm, for 24 and 48 hours and after a 3 days reversibility period.

Metabolite	cDDP (30 µM)						Pd_2Spm (12 µM)					
	24h		48h		Reversibility		24h		48h		Reversibility	
	Controls	cDDP	Controls	cDDP	Controls	cDDP	Controls	Pd_2Spm	Controls	Pd_2Spm	Controls	Pd_2Spm
Lipid ratios												
$(CH_2)_n/CH_3$	3.34±0.09	2.98±0.26	2.73±0.61	3.16±0.40	2.73±0.29	3.52±0.19	3.34±0.09	2.69±0.29	2.73±0.61	2.10±0.50	2.73±0.29	2.64±0.36
$CH=CH/CH_3$	0.26±0.02	0.33±0.03	0.20±0.05	0.46±0.06	0.23±0.20	0.59±0.00*	0.26±0.02	0.27±0.05	0.20±0.05	0.22±0.04	0.23±0.20	0.22±0.02
$=CHCH_2CH=/CH_3$	0.26±0.01	0.25±0.01	0.22±0.00	0.32±0.01*	0.23±0.01	0.34±0.00*	0.26±0.01	0.26±0.00	0.22±0.00	0.23±0.00	0.23±0.01	0.22±0.01
Choline compound ratios												
PC/Cho	1.52±0.04	0.98±0.08	0.68±0.04	0.91±0.11	0.98±0.21	1.15±0.09	1.52±0.04	1.84±0.08	0.68±0.04	1.45±0.06*	0.98±0.21	1.03±0.32
GPC/Cho	0.82±0.04	0.77±0.25	0.75±0.14	1.82±0.07*	0.61±0.10	1.34±0.02	0.82±0.04	0.71±0.06	0.75±0.14	0.91±0.04	0.61±0.10	0.71±0.15
PC/GPC	1.84±0.04	1.28±0.31	0.90±0.22	0.50±0.08	1.62±0.07	0.86±0.08*	1.84±0.04	2.57±0.33	0.90±0.22	1.59±0.13	1.62±0.07	1.47±0.15

* $p < 0.05$, ** $p < 0.01$.

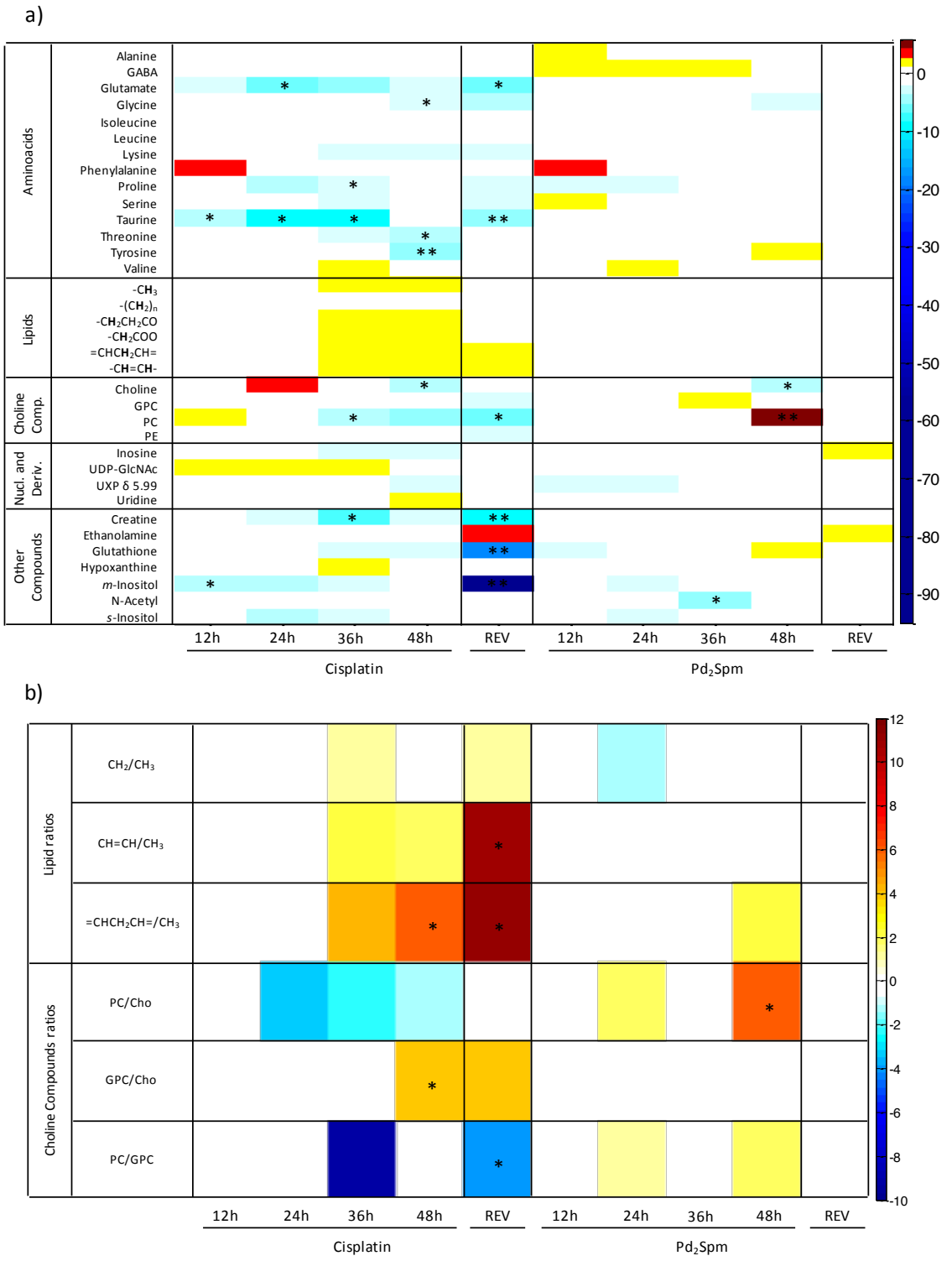

Figure 6.8. Heatmaps of effect size values of the time course response for a) several metabolites and b) compound ratios in MG-63 cells exposed to cDDP or Pd_2Spm. The effect size values are shown in a colour scale from minimum (dark blue) to maximum (dark red) values. * $p < 0.05$ and ** $p < 0.01$ refer to the results of significance tests with integrals. Column indicated as *REV*, refers to cells exposed to the drug for 24 hours, followed by a recovery period of 3 days in drug free medium.

In what concerns to choline compounds, significant choline decreases are measured at 48 hours for both drugs, a transitory increase in GPC (36 hours) is induced by Pd_2Spm drug and opposite variations are seen in PC at 48 hours (decreases with cDDP and a marked increase of around 67% with Pd_2Spm, to which correspond an ES value close to 7). The results of choline compound ratios were also found to be drug-specific: cDDP induced a decrease of PC/Cho while Pd_2Spm promoted its increase; significant increases in GPC/Cho were detected upon 48 hours exposure to cDDP, while no alterations were detected with Pd_2Spm treatment; changes in PC/GPC were opposite (down-regulated upon cDDP exposure and up-regulated upon treatment with Pd_2Spm) and specific in time.

Concerning the impact on nucleotides and their derivatives, Pd_2Spm only influences the levels of UXP (which decrease at initial times of exposure) while the same tendency is only achieved upon 48 hours exposure to cDDP. In what refers to changes in other metabolites, alterations in creatine (decrease) are exclusive from cDDP treatment, while none of the drugs altered the levels of ethanolamine along the 48 hours exposure period. Interestingly, cDDP and Pd_2Spm differently affect the time course of GSH: upon 48 hours treatment, Pd_2Spm induces its increase (upon a slight decrease at 12 hours) while a decrease is registered in cDDP-treated samples. Hypoxanthine, also seems to be affected only by cDDP treatment, since exposure to the Pt(II) drug induced its increase at 36 hours. *M*- and *s*-Ino decrease upon exposure to each of the two drugs, but effects are slightly more pronounced with cDDP. Negative variation of N-acetyl moiety was only detected in Pd_2Spm-treated cells.

Some of these Pd_2Spm-induced alterations may be a consequence of the known effect of this complex on histone H2AX, the cytoskeleton and the expression of genes in the polyamine pathway, as already suggested in literature as being a consequence of Pd_2Spm treatment (Tummala *et al*., 2010; Fiuza *et al*., 2011). However, this hypothesis would need further investigations, namely beginning by a targeted search for DNA and cytoskeleton alterations in Pd_2Spm-treated MG-63 cells. Despite the novelty of the use of Pd_2Spm in metabolomic studies, interpretation of some of its drug-induced effects could be tentatively advanced by comparison with the cDDP-induced effects, most widely explored. One of the most marked differences between Pd_2Spm and cDDP treatments, was the absence of changes in lipids in the former, while marked increases were found to be characteristic of cDDP treatment in osteosarcoma (Duarte *et al*., 2010; Lamego *et al*., 2014) and other cancer cell lines (Huang *et al*., 2003; Lindskog *et al*., 2004; Pan *et al*., 2011; Pan *et al*., 2013; Duarte *et al*., 2013). Since the increase in lipids has been

associated with cell apoptosis (Rainaldi *et al*., 2008; Boren and Brindle *et al*., 2012), the absence of changes with Pd_2Spm suggests that the decreases in the number of living MG-63 cells are not due to cell death.

Regarding the variations in choline compounds, similar variations were found in choline while opposite changes were detected in PC levels upon treatment with either cDDP or Pd_2Spm, what may point to distinct PTC-cycle regulation (Knijn *et al*., 2005; Duarte *et al*., 2010) by the two drugs. These differences translated into increases in the PC/GPC and PC/Cho for Pd_2Spm-treated cells, while decreases in both ratios were detected in cDDP-treated cells. This result once again reinforces the idea that Pd_2Spm-treated MG-63 cells are not undergoing apoptosis (differently from cDDP-treated ones), since cell growth arrest prior apoptosis has been associated with variations in PC/GPC opposite from those now observed with the Pd(II) agent (Mirbahai *et al*., 2011).

Quite distinct amino acid signatures characterise the MG-63 cells response to either of the two drugs, suggesting that cDDP and Pd_2Spm differently affect the Krebs cycle. Additionally, and although non significant, distinct nucleotide variations are registered for cDDP and Pd_2Spm, strongly suggesting that, despite their interaction with DNA, different downstream effects account for the mode of action of each drug.

6.3. ^{1}H NMR Analysis of TCA Extracts of cDDP- and Pd_2Spm-Treated MG-63 Cells

By measuring the drug-induced alterations in nucleotides and derivatives, the extent to which cDDP and Pd_2Spm affect DNA can be indirectly assessed. TCA extraction was applied to the samples analysed by HRMAS, with the aim of assessing such alterations in nucleotides and derivatives, namely AXP and UXP derivatives, Ino/Ado and NAD^+. Comparison between the average spectra of controls and cDDP- and Pd_2Spm-treated cells (Figure 6.9) shows considerable drug-induced changes in the aromatic region. Treatment with cDDP (Figure 6.9b) induces increases in uridine, UXP, UDP/UTP and hypoxanthine, while decreases occur for ADP/ATP and NAD^+. Upon exposure to Pd_2Spm (Figure 6.9c), cells experience slight increases in uridine and hypoxanthine (like cDDP) while UXP, Ino/Ado, ADP/ATP (like cDDP) and NAD^+ (like cDDP) levels decrease. Pd_2Spm-induced changes in UXP and Ino/Ado resemble those induced by DOX and MTX treatment, eventually pinpointing similar influences of these drugs over pathways involving these compounds.

Beyond the metabolites newly detected in extracts compared to HRMAS (ADP/ATP, UDP/UTP and NAD^+), alterations in some metabolites already detected by HRMAS slightly differ from TCA analysis. Regarding cDDP-treatment, slight increases in uridine were also measured by HRMAS but the hypoxanthine, which showed no alteration with this drug, now reveals to be increased and opposite variations were detected for UXP. The HRMAS results from Pd_2Spm-treated cells also pointed for decreases (slight) in UXP but uridine and hypoxanthine showed no variations and opposite variations in relation to TCA analysis were detected in Ino/Ado contents, upon cells' treatment with Pd_2Spm.

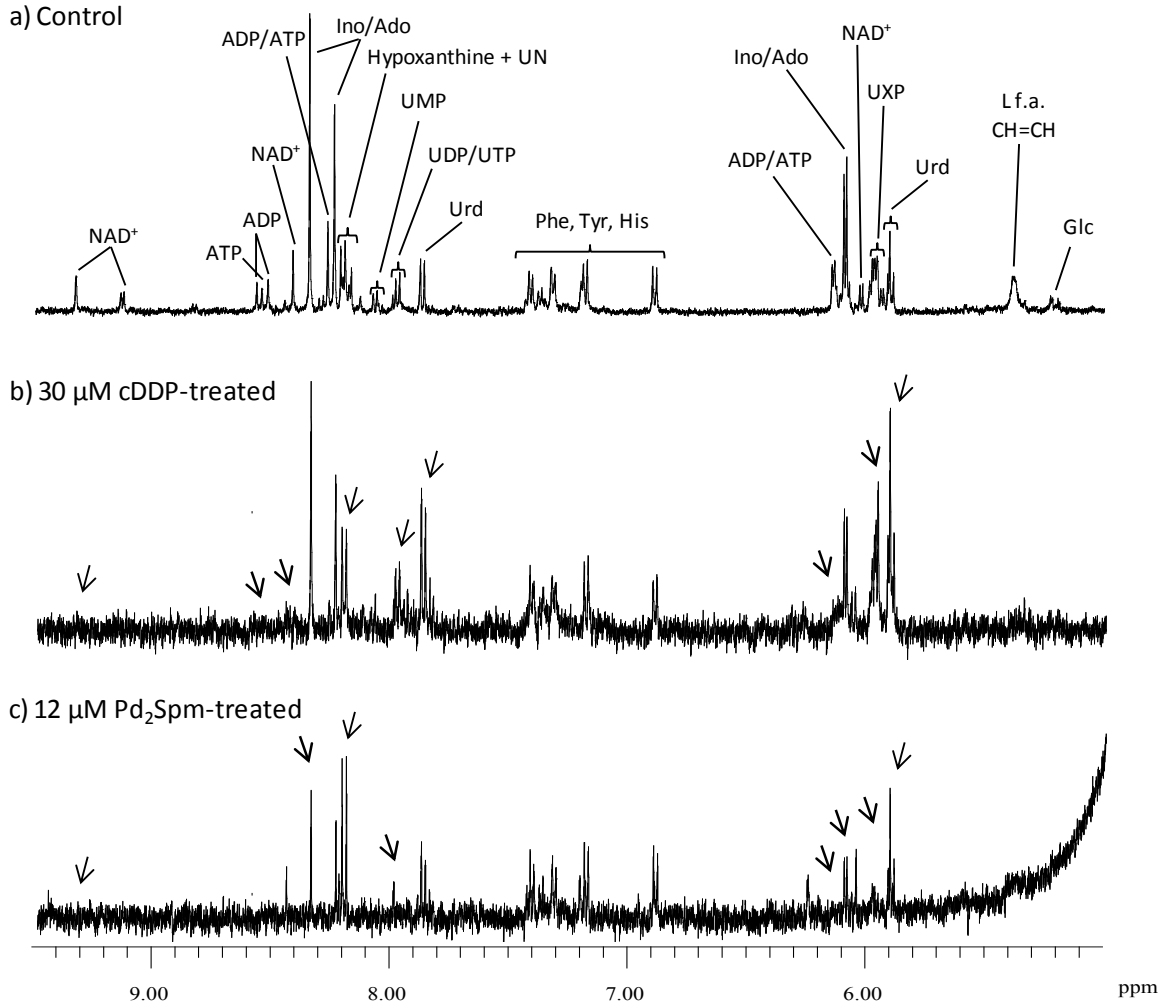

Figure 6.9. Expansion of aromatic (5.0-9.5 ppm) regions of average 500 MHz ^{1}H NMR spectra of TCA extracts of MG-63 cells, at 48 hours: a) under control conditions, b) exposed to 30 µM cDDP and c) exposed to 12 µM Pd_2Spm. Main assignments are noted and visible spectral changes due to drug exposure are marked by arrows.

6.4. ^{1}H HRMAS NMR Analysis of Pd_2Spm-Induced Metabolic Changes in HOb Cells and Comparison to cDDP

In this section, the metabolic alterations in HOb cells induced by exposure to either Pd_2Spm or cDDP are presented. Since the HRMAS NMR analysis of HOb cells is performed for the first time, a general characterization of the metabolic profile of these non-neoplastic cells is presented and a comparison with the metabolic profile of MG-63 cells is discussed.

6.4.1. Metabolic Profile of Osteoblast HOb Cells: Comparison to MG-63 Cells

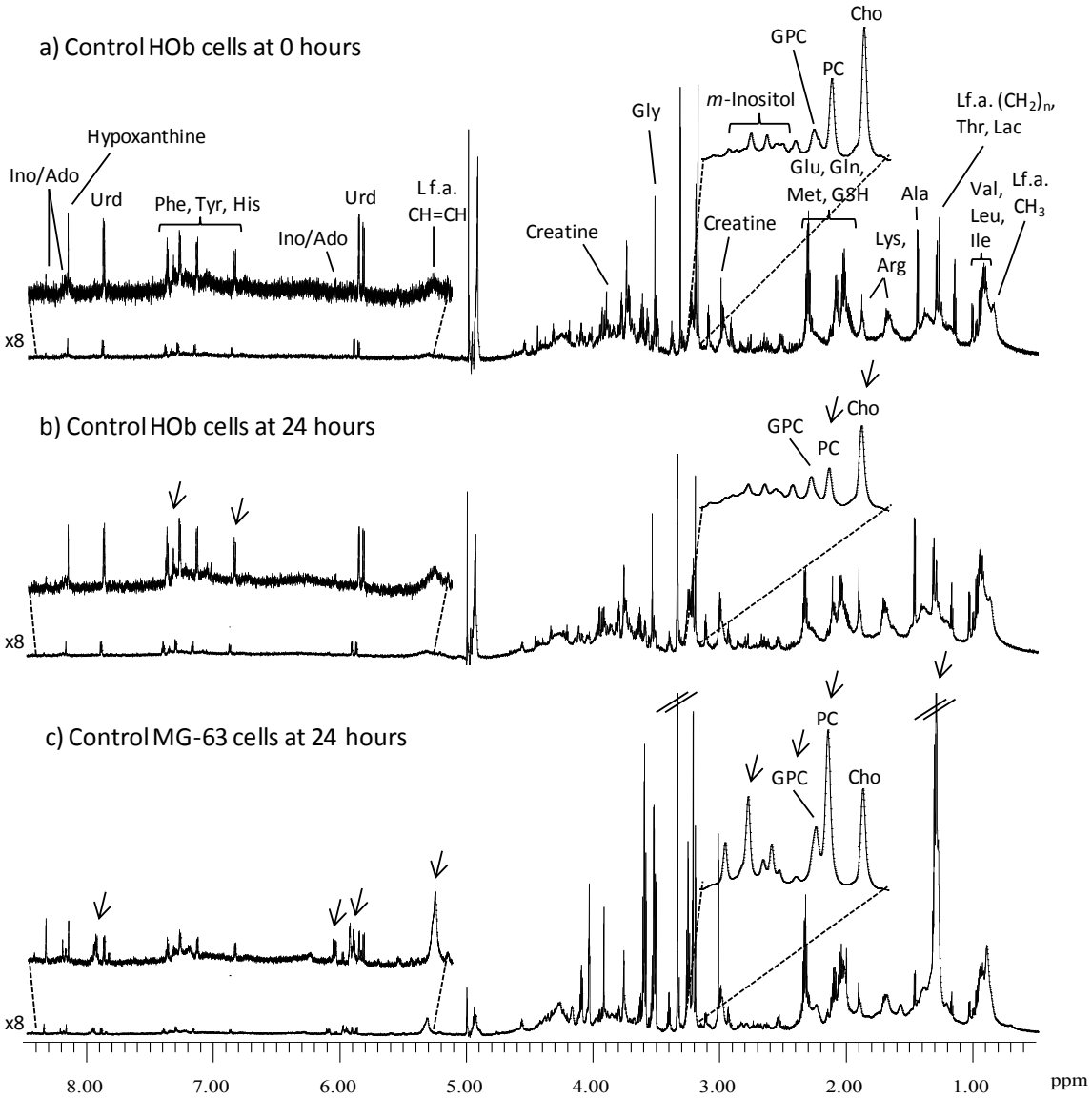

Figure 6.10. Average 800 MHz ^{1}H HRMAS NMR spectra of HOb cells at a) 0 and b) 24 hours and of c) MG-63 cells at 24 hours, in control conditions. Insets show expansions of choline compounds (3.2-3.3 ppm) and aromatic (5.2-8.5) regions. Arrows in b) indicate main changes from a); arrows in c) indicate main changes from b).

The 1D ^{1}H HRMAS NMR metabolic profile of HOb cells is presented in Figure 6.10 (a, b) and 2D HRMAS NMR spectra are shown in Figure 6.11. A total of 43 metabolites were assigned in the spectrum of lysed HOb cells and other 3 remain unassigned, as compiled in Table 6.4. To our knowledge, there are no reports in the literature about metabolomic studies, either by HRMAS NMR or MS, on osteoblasts (either using whole cells or cell extracts). This may be explained by the high costs involved in HOb cells culture, their long doubling time compared to OS cells (around 3 days, as compared to 24 hours for MG-63 cells) and the high number of cells needed for metabolomic studies.

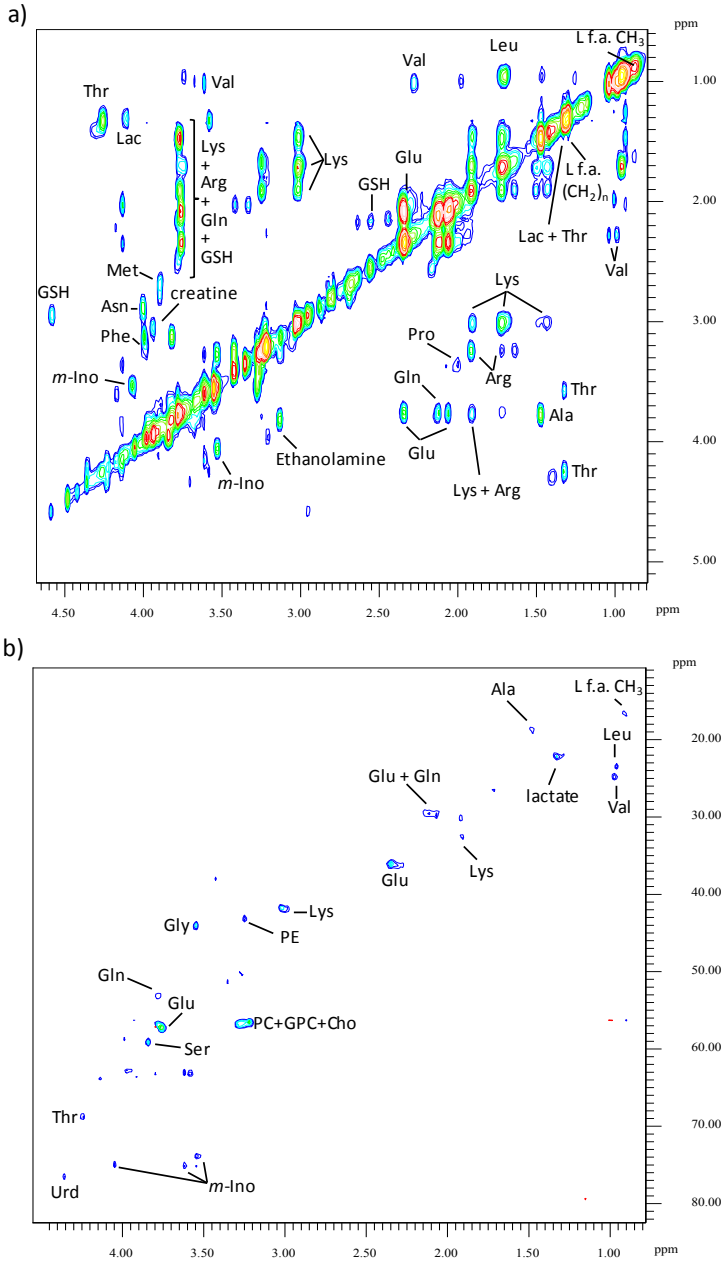

Figure 6.11. Expansions of 0.5-4.5 ppm region of the 800 MHz 2D HRMAS NMR spectra of HOb cells: a) TOCSY and b) HSQC.

Table 6.4: List of metabolite assignments in HRMAS NMR spectra of lysed HOb cells. Legend: *s* singlet, *d* doublet, *t* triplet, *q* quartet, *dd* double of doublets, *m* multiplet.

Compound	Assignment	δ ^{1}H ppm (multiplicity)/ δ ^{13}C ppm
Acetate	βCH_3	1.92 (s)
Alanine	βCH_3	1.48 (d)/ 18.79
	αCH	3.78 (q)
Arginine	γCH_2	1.69 (m)
	βCH_2	1.92 (m)/ 30.20
	δCH_2	3.25 (t)
	αCH	3.77 (t)
Asparagine	βCH_3	2.87 (dd)
	$\beta' CH_3$	2.95 (dd)
	αCH	4.01 (dd)
Aspartate	βCH_3	2.69 (dd)
	$\beta' CH_3$	2.82 (dd)
	αCH	3.90 (dd)
Choline	$N(CH_3)_3$	3.22 (s)/ 56.49
	$CH_2(NH)$	3.54/ 75.10
	$CH_2(OH)$	4.07
Creatine	CH_3	3.03 (s)
	CH_2	3.94 (s)
Dihydroxyacetone	αCH_2	4.42 (s)
Ethanol	βCH_3	1.19 (t)
	αCH_2	3.65 (q)
Ethanolamine	$CH_2(NH_2)$	3.13 (t)
	$CH_2(OH)$	3.82 (t)
Fatty acyl (L f.a.) chain	CH_3	0.88/16.50
	$(CH_2)_n$	1.31
	CH_2CO	2.28
	CH=CH	5.33
β-Glucose	C1H	4.65 (d)
Glutamate	$\beta\beta' CH_3$	2.09/29.70
	γCH_2	2.35/36.03
	αCH	3.75 (dd)/ 57.18
Glutamine	βCH_2	2.13/29.66
	γCH_2	2.45/33.70
	αCH	3.78/53.02
GSH[a]	βCH_2 Glu	2.17
	γCH Glu	2.56
	αCH_2 Cys	2.95
	αCH Glu	3.77
	γCH_2 Cys	4.17
	βCH_2 Cys	4.58
Glycerol	$C1H_2$	3.57
	$C3H_2$	3.64
	C2H	3.78
Glycerol (in lipids)	$C3H_2$	4.30
	C2H	5.23
Glycerophosphocholine (GPC)	$N(CH_3)_3$	3.24 (s)/ 56.50
	γCH_2	3.65
	$\beta CH/\beta' CH_2(N)$	3.87/3.91
	αCH_2	3.94
	$\alpha CH_2(P)$	4.33

Table 6.4 (cont.): List of metabolite assignments in HRMAS NMR spectra of lysed HOb cells. Legend: *s* singlet, *d* doublet, *t* triplet, *q* quartet, *dd* double of doublets, *m* multiplet.

Compound	Assignment	δ ^{1}H ppm (multiplicity)/ δ ^{13}C ppm
Glycine	αCH_2	3.56 (s)/ 43.97
Histidine	C4H, ring	7.10 (s)
Hypotaurine	βCH_2	2.67 (t)
	αCH_2	3.34 (t)
Hypoxanthine	C2H	8.19 (s)
	C8H	8.21 (s)
Inosine / Adenosine	C2'H, ribose	4.78 (t)
	C1'H, ribose	6.11 (d)/ 94.30
	C2H, ring	8.24 (s)
	C8H, ring	8.36 (s)
Isoleucine	δCH_3	0.94 (t)
	$\beta' CH_3$	1.01 (d)
	βCH	1.99
	αCH	3.65
Lactate	βCH_3	1.33 (d)/ 22.70
	αCH	4.14 (q)
Leucine	δCH_3	0.96 (d)
	$\delta' CH_3$	0.97 (d)/ 23.49
	$\gamma CH/\beta CH_2$	1.71
	αCH	3.76 (t)
Lysine	γCH_2	1.47
	δCH_2	1.73/26.40
	βCH_2	1.92/32.50
	εCH_2	3.02 (t)/ 41.73
	αCH	3.76 (t)
Methanol	CH_3	3.35 (s)/51.22
Methionine	$\varepsilon CH_3/ \beta CH_2$	2.14 (s)
	γCH_2	2.64 (t)
	αCH	3.88 (t)
m-Inositol[a]	C5H	3.27 (t)
	C1H, C3H	3.54 (dd)/ 73.86
	C4H, C6H	3.62 (t)/ 75.03
	C2H	4.05 (t)/ 74.97
NMN^+		8.99 (d)
		9.32
		9.62
Phenylalanine	βCH	3.12
	β'CH	3.29
	αCH	3.99 (dd)/ 58.66
	C2H, C6H, ring	7.32/127.20
	C4H, ring	7.37
	C3H, C5H, ring	7.42
Phosphatidylcholines (PTC)	$N(CH_3)_3$	3.26 (s)/ 56.68
Phosphocholine (PC)	$N(CH_3)_3$	3.23 (s)/ 56.50
	$N\text{-}CH_2$	3.61 (s)
Phosphoethanolamine (PE)	$N\text{-}CH_2$	3.25/43.04
	$PO_3\text{-}CH_2$	3.97

Table 6.4 (cont.): List of metabolite assignments in HRMAS NMR spectra of lysed HOb cells. Legend: *s* singlet, *d* doublet, *t* triplet, *q* quartet, *dd* double of doublets, *m* multiplet.

Compound	Assignment	δ ^{1}H ppm (multiplicity)/ δ ^{13}C ppm
Proline	γCH_2	2.01
	βCH	2.07
	β'CH	2.35
	δCH	3.33 (t)
	δ'CH	3.41 (t)
	αCH	4.12 (t)/ 63.75
s-Inositol	CH	3.34 (s)
Serine	αCH	3.84/59.10
	ββ'CH	3.97 (dd)/ 62.82
Taurine	S-CH_2	3.28 (t)
	N-CH_2	3.42 (t)/ 37.95
Threonine	γCH_3	1.32 (d)/ 22.70
	αCH	3.58 (d)/ 63.07
	βCH	4.26/68.71
Tyrosine	ββ'CH	3.05/3.18
	αCH	3.95
	C3H, C5H, ring	6.89 (d)/ 118.8
	C2H, C6H, ring	7.19 (d)
UN 1		4.46 (s)
UN 2		4.48 (s)
UN 3		4.68 (d)
Uridine	C4'H, ribose	3.81 (dd)
		3.92 (dd)
	C3'H, ribose	4.23 (t)
	C2'H, ribose	4.36 (t)/ 76.40
	C1'H, ribose	5.89 (d)/ 104.9
	C5H, ring	5.93 (d)/ 92.00
	C6H, ring	7.91 (d)
Valine	γCH_3	0.99 (d)/ 24.78
	γ'CH_3	1.05 (d)
	βCH	2.28
	αCH	3.61 (d)/ 63.00

[a] Metabolites assigned through STOCSY.

Comparison between the average spectra corresponding to 0 and 24 hours growth (Figure 6.10a and 6.10b, respectively) shows that during their basal growth, HOb cells exhibit a slight decrease in several amino acids (Val, Leu, Ile, Glu, Gln and Met) and discrete increases in Phe and Tyr. Additionally, decreases of Cho (δ 3.21) and PC (δ 3.23) are seen at 24 hours growth, as well as a slight decrease in *m*-Inositol (δ 3.27).

Comparison between the metabolic profiles of HOb and MG-63 cells in comparable conditions of 24 hours growth (Figure 6.10b and 6.10c), enables the identification of relevant differences. One of the most evident differences relates to lipid resonances, much more intense in MG-63 cells with only CH_3, $(CH_2)_n$ and CH=CH being unequivocally identified in the spectra of HOb cells, due to their low intensity. This could, at least in part, be due to the longer size of the non-

neoplastic cells in relation to cancer ones (6500 μm^2 and 1200 μm^2 respectively, a difference of about 6 times according to Pautke *et al*., 2004), resulting in a decreased proportion of membrane lipids in relation to the rest of the detected metabolites. Examples of compounds significantly more abundant in MG-63 cells, compared to HOb cells, comprise *m*-Ino, Ino/Ado and UXP derivatives (δ 5.99 and δ 7.98, absent in the spectra of HOb cells).

Through comparison of the relative intensities of choline compounds in HOb cells spectra, it can be advanced that free choline (δ 3.21) is the most abundant choline compound followed by PC; on the other hand, PC is the dominant choline-compound resonance in MG-63 cells. In both cell lines, GPC and PE are the less abundant choline-compounds. It is interesting to note the different ratios of Ala/lactate in the spectra of MG-63 and HOb cells. The HOb cells spectra also show a decrease in the relative proportion of creatine (δ 3.03 and δ 3.93) (for example in relation to lysine) and increased glycine intensity (δ 3.56).

6.4.2. Pd_2Spm- *vs* cDDP-Induced Metabolic Changes in HOb Cells

In order to understand how Pd_2Spm compares with cDDP in affecting non-malignant cells, the effects of these drugs were also tested in non-neoplastic HOb cells. The drugs were administered at concentrations corresponding to their IC_{50} values to the MG-63 cell line. Only two time points (0 and 24 hours) were considered due to cell culture constrains associated with HOb cells). It was found that the integrity of the cellular membrane is not significantly compromised upon 24 hours treatment with either cDDP or Pd_2Spm (Figure 6.12).

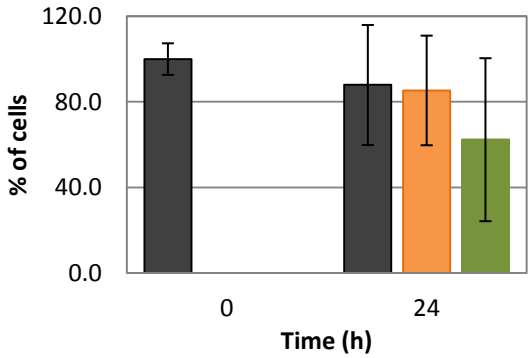

Figure 6.12. Plot of the cytotoxic effect of cDDP and Pd_2Spm, in sole administration, towards the HOb cell line. Cell proliferation was evaluated by Trypan blue assay (as described in the Experimental Procedures, Chapter 3). Control (■), 30 μM cDDP (■) and 12 μM Pd_2Spm (■). The data represent the average ± mean standard deviation from n=2 experiments, carried out in duplicate.

Nevertheless, it is suggested that the Pd complex induces a slightly higher damage to the HOb cellular membrane than cDDP. However, this absence of a significant influence of these two drugs on the HOb cellular membrane may be partly due to the much larger doubling time of these cells (*ca.* three days, Chapter 3) relative to MG-63 (24 hours) and the drug concentrations used in the experiments (equal to their IC_{50} values towards MG-63 cell at 24 hours). The drug-induced effects in HOb cells may thus be underestimated. It is also worth noting the large error bars in HOb measurements, which is probably associated with the extra care that is needed at the time of cells recovery, since non-neoplastic cells are more sensitive to trypsin exposure, possibly leading to considerable differences in efficiency of cells recovery between replicas.

Comparison between the cytotoxic effects of Pd_2Spm and cDDP in human fibrobasts (BJ cell line) was performed by Fiuza *et al*. (Fiuza *et al*., 2011). In this study both compounds behaved similarly and BJ cells showed to be more resistant to both Pd_2Spm and cDDP than the two tested breast cancer cell lines. These are very promising results, since they reflect a certain degree of tissue-selectivity of the Pd_2Spm complex, a very important feature for an anticancer agent.

The average ^{1}H HRMAS spectra of HOb cells under control conditions and upon 24 hours treatment with either cDDP (30 μM) or Pd_2Spm (12 μM) are shown in Figure 6.13. Visual inspection suggests that cDDP-treatment (Figure 6.12b) induces a considerable increase in acetate(s) (δ 1.92), increases the Cho (δ 3.21) and GPC (δ 3.24) levels as well as the uridine contents and possibly alters the levels of *m*-inositol (δ 3.27). Pd_2Spm-treatment seems to induce a slight decrease of several amino acids (Val, Ala, Lys, Arg and Gly) and increase of acetate(s) (δ 1.92), altering the relative proportion of choline compounds (decreases Cho, δ 3.21, and increases GPC, δ 3.24) and possibly changing *m*-inositol (δ 3.27) and CH=CH of L f.a. (δ 5.33) contents.

Next, signal integration and statistical evaluation of changes were performed and are compiled in Table 6.5. As refered previously for MG-63 results, the statistical evaluation was performed with just two replicas per condition, meaning that the determined degree of statistical meaning is low. For this reason, particular attention was paid to the determined effect size values. The only amino acid affected by 24 hours treatment of HOb cells with cDDP was Glu, which levels decreased (-14.2% and an ES of -2.4). cDDP treatment didn't induce any considerable alteration in lipids or choline compounds in HOb cells. Uridine and GSH were found to increase with cDDP

exposure (26.4% and 10.9% and ES of 1.5 and 2.1, respectively) together with a decrease in *m*-Ino contents (-17.7% and ES of -1.8) in HOb cells.

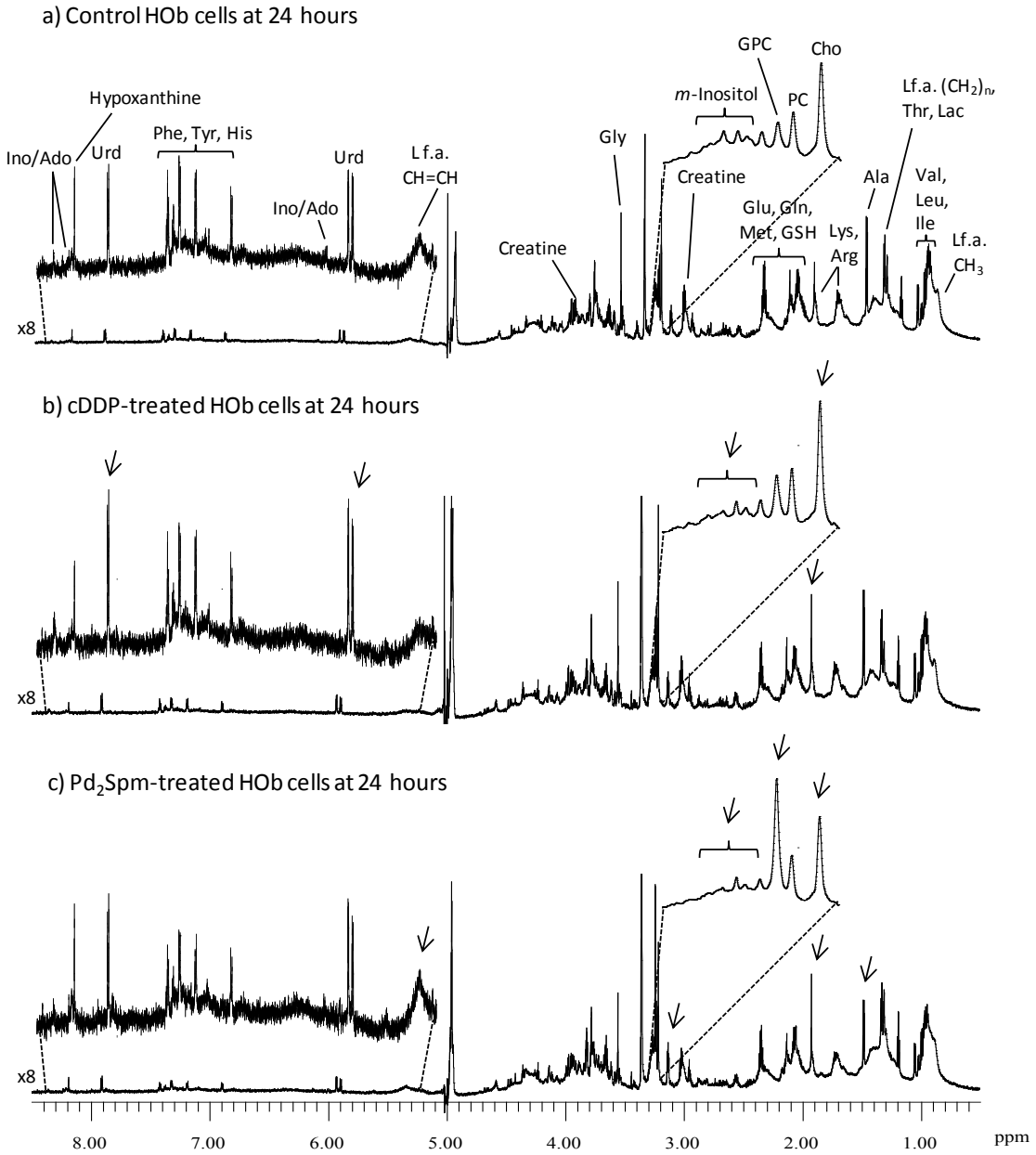

Figure 6.13. Average 800 MHz ^{1}H HRMAS NMR spectra of HOb cells, at 24 hours: a) under control conditions, b) exposed to 30 µM cDDP and c) exposed to 12 µM Pd_2Spm. Insets show expansions of choline compounds (3.2-3.3 ppm) and aromatic (5.2-8.5 ppm) regions. Main assignments are noted and visible spectral changes due to drug exposure are marked by arrows.

Table 6.5 Metabolite and choline compounds variations in HOb cells exposed to 30 µM cDDP or 12 µM Pd_2Spm, for 24 hours and after a 3 days reversibility period.

Metabolite	Signal (δ,ppm)[a]	cDDP (30 µM)				Pd_2Spm (12 µM)			
		24h		Reversibility		24h		Reversibility	
		% var.[b]	Effect size[c]	% var.[b]	Effect size[c]	% var.[b]	Effect size[c]	% var.[b]	Effect size[c]
Amino acids									
Alanine	1.48, d	-	-	-	-	-21.2±5.30	-2.57±1.07	-37.8±17.7	-1.51±0.78
Arginine	1.65, m	-	-	-	-	-4.40±1.20	-2.09±0.93	-	-
Glutamate	2.34, m	-14.2±3.60	-2.43±1.03	-30.5±11.0	-1.87±0.87	-22.5±4.70	-3.06±1.22	-53.2±12.2	-3.38±1.33
Glutamine	2.45, m	-	-	-	-	-	-	-	-
Glycine	3.56, s	-	-	-23.2±4.60	-3.24±1.28	-18.8±4.30	-2.78±1.14	-35.3±12.0	-2.04±0.92
Isoleucine	1.02, d	-	-	-	-	-5.40±2.10	-1.51±0.78	-	-
Lysine	1.72, m	-	-	-	-	-14.0±3.50	-2.48±1.05	-	-
Methionine	2.64, s	-	-	9.40±4.50	(+)	-9.40±4.00	-1.41±0.76	-	-
Phenylalanine	7.32, d	-	-	-6.70±2.70	-1.47±0.77	-	-	-	-
Proline	4.12, t	-	-	-8.60±4.1	(-)	-9.50±3.60	-1.57±0.80	-28.3±13.0	-1.44±0.77
Serine	3.98, d	-	-	19.8±1.4*	7.25±2.63	-	(-)	-17.7±4.50	-2.46±1.04
Threonine	3.58, d	-	-	-2.1±0.5	-2.19±0.96	-	-	-	-
Tyrosine	6.89, d	-	-	-	-	-	-	-	-
Valine	1.05, d	-	-	-	-	-13.8±4.50	-1.88±0.88	-	-
Lipids									
$-(C\underline{H}_2)_n$	1.30	-	-	-	-	24.1±10.1	(+)	-	-
Choline and phospholipids									
Choline	3.21, s	-	-	-	-	-	-	-49.6±7.60*	-4.93±1.84
GPC	3.24, s	-	-	15.3±4.70	1.75±0.84	99.8±31.4	(+)	-	-
PC	3.23, s	-	-	57.0±2.50**	10.29±3.68	-	-	-	-

Table 6.5 (cont.). Metabolite and choline compounds variations in HOb cells exposed to either 30 µM cDDP or 12 µM Pd_2Spm, for 24 hours and after a 3 days reversibility period.

Metabolite	Signal (δ,ppm)[a]	cDDP (30 µM)				Pd_2Spm (12 µM)			
		24h		Reversibility		24h		Reversibility	
		% var.[b]	Effect size[c]	% var.[b]	Effect size[c]	% var.[b]	Effect size[c]	% var.[b]	Effect size[c]
PE	3.25, s	-	-	-	-	-	-	-	-
Nucleotides and Derivatives									
Inosine	8.36, s	-	-	-	-	-	-	41.1±5.2*	3.72±1.43
Uridine	5.89, d	26.4±8.7	1.54±0.79	-	-	(+)	(+)	8.3±1.6	2.88±1.17
Other Compounds									
Creatine	3.93, s	-	-	-	-	-	-	-34.2±9.70	-2.44±1.04
Dihydroxyacetone	4.42, s	-	-	-	-	-	-	-24.9±8.40	-1.94±0.89
Ethanolamine	3.13, t	-	-	-	-	-	-	49.4±18.3	(+)
GSH	2.56, m	10.9±2.80	2.12±0.94	21.3±5.50	2.00±0.91	-	-	-	-
Hypoxanthine	8.18, s	-	-	-19.0±8.30	-1.45±0.77	-	-	-	-
Lactate	1.33, d	-	-	-	-	-	-	-	-
m-Inositol	4.05, t	-17.7±6.10	-1.83±0.86	-41.5±13.6	-2.21±0.97	-28.6±5.90	-3.25±1.28	-50.4±14.6	-2.64±1.09
s-Inositol	3.34, s	-	-	-	-	-	-	-	-
Ratios		**Controls**	**cDDP**	**Controls**	**cDDP**	**Controls**	**Pd_2Spm**	**Controls**	**Pd_2Spm**
Choline compound ratios									
PC/Cho		0.89±0.01	0.56±0.07	0.56±0.02	0.93±0.02**	0.89±0.01	0.68±0.28	0.56±0.02	1.03±0.14
GPC/Cho		0.98±013	0.64±0.21	0.58±0.03	0.71±0.03	0.98±013	1.44±0.67	0.58±0.03	1.48±0.12
PC/GPC		0.92±0.17	0.89±0.17	0.96±0.01	1.31±0.03*	0.92±0.17	0.47±0.03	0.96±0.01	0.70±0.15

[a] Resonance chosen for signal integration, [b] % variation and [c] effect size in relation to control cells. * $p < 0.05$, ** $p < 0.01$, $^{-}$: no significant variation. (+) and (-) indicate consistent positive and negative variations, respectively, without statistical meaning.

The drug-response profile of HOb cells treated with Pd_2Spm for 24 hours is globally distinct from that of cDDP-treated cells. Several amino acids were found to decrease after Pd_2Spm, from which Ala, Glu (similarly to what was seen for cDDP) and Gly registered the most marked changes (with % of variation of around -20 and ES values around -3). Pd_2Spm was also suggested to induced a slight increase of L f.a. $(CH_2)_n$ and GPC. Similarly to what was seen for cDDP treatment, a decrease in *m*-Ino (-28.6% and ES of -3.2) was also measured as consequence of HOb cells exposure to Pd_2Spm. With the exception of PC/GPC, for which a *ca*. 50% decrease was determined in HOb cells treated with Pd_2Spm for 24 hours, no relevant changes were measured for choline compound ratios upon a 24 hours treatment with either cDDP or Pd_2Spm.

Graphical comparison between the metabolic impact of cDDP and Pd_2Spm on the HOb cell line is shown in Figure 6.13. Upon 24 hours of treatment, Pd_2Spm was found to induce a more significant change in their metabolic profile than cDDP. Regarding amino acids, negative variations were detected for Ala, Arg, Gly, Lys, Pro and Val, in Pd_2Spm-treated HOb cells compared to the controls, Glu being decreased for both drugs. Recent results from cDDP administration to rats (Ozaki *et al*., 2013) indicated that the drug caused a marked decrease in the activity of the mitochondrial enzyme aspartate aminotransferase, by binding to it. Since this enzyme catalyses the conversion of Asp and α-ketoglutarate to oxaloacetate and Glu, its reduced activity may underlie the observed decrease in Glu upon cDDP exposure.

Regarding lipid signatures, and despite the reduced expression of these compounds in the metabolic profile of HOb cells, there are no evidences of disturbance upon 24 hours administration of any of the two compounds, eventually proving that a reduced cell death rate is taking place at this time, as suggested in Figure 6.12. Likewise, no variations were detected in the choline compounds upon either cDDP or Pd_2Spm treatment. Since several studies (Ridgway *et al*., 2013; Blankenberg *et al*., 2013; Wright *et al*., 2004) refer to alterations in lipids and choline compounds as fingerprints of programmed cell death, the absence of such changes may indicate that for this period of drug exposure (24 hours) there are still no clear metabolic evidences of apoptosis. In relation to compound ratios, due to the low intensity of the lipid resonances only the $(CH_2)_n$ moiety was integrated, thus not disabling the determination of lipid ratios. Still, the choline compound ratios (Figure 6.14b) show that, despite showing no relevant change in each of the two compounds when considered separately (Figure 6.14a), the ratio between PC and GPC was found to be decreased in HOb cells treated with Pd_2Spm for 24 hours, evidencing that, in opposition to cDDP, Pd_2Spm appears to affect the dynamics of the choline compounds.

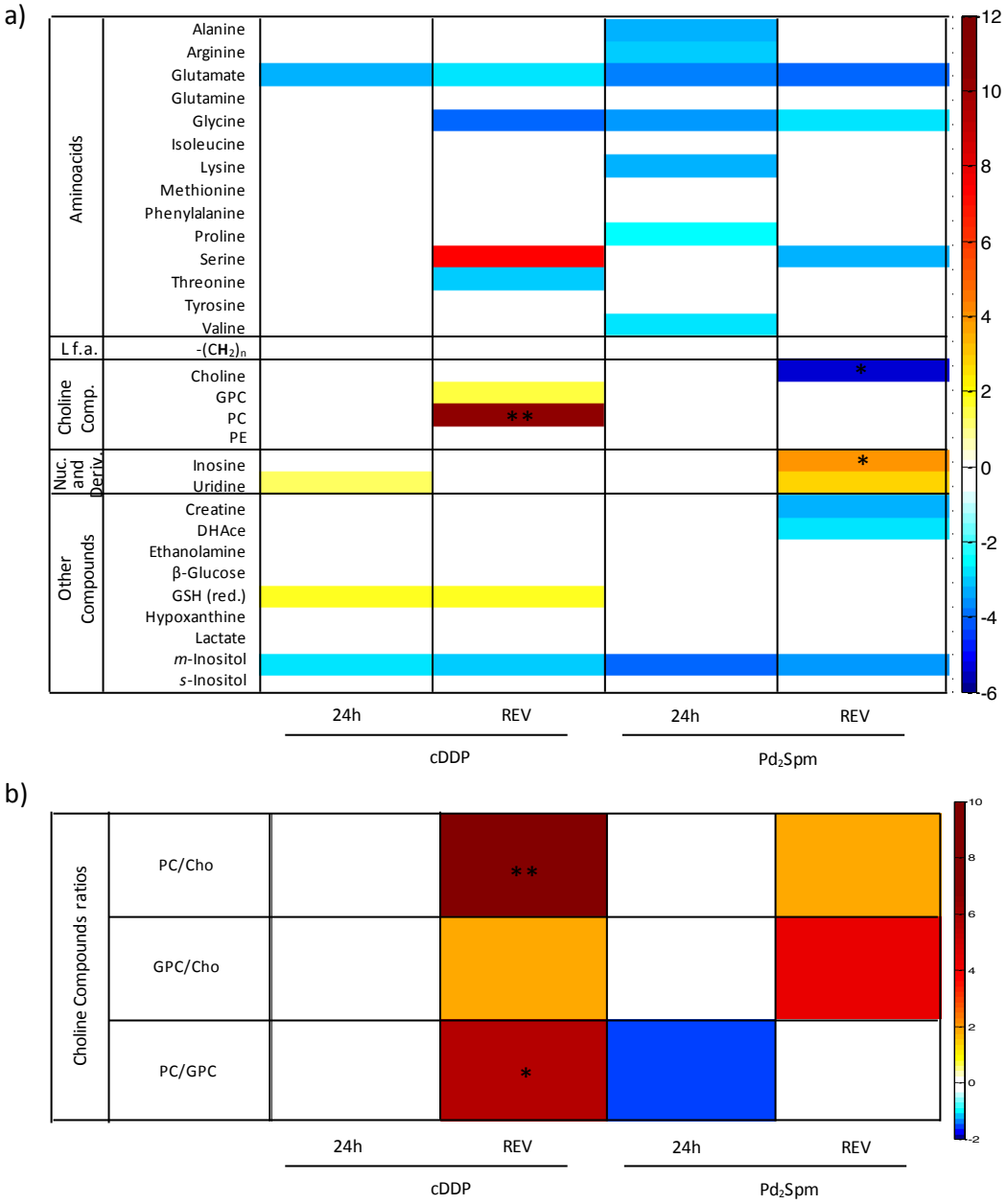

Figure 6.14. Heatmaps of effect size values of the time course response for a) several metabolites and b) choline compound ratios in HOb cells exposed to cDDP or Pd_2Spm. The effect size values are shown in a colour scale from minimum (dark blue) to maximum (dark red) values. * $p < 0.05$ and ** $p < 0.01$ refer to the results of significance tests with integrals. Column indicated as *REV*, refers to cells exposed to the drug for 24 hours, followed by a recovery period of 3 days in drug free medium.

Uridine, the most abundant nucleotide derivative found in the metabolic NMR profile of osteoblasts, was the only compound showing changes at 24 hours incubation with cDDP. Accumulation of uridine, one of the basic components of RNA, may suggest altered RNA synthesis as a consequence of treatment.

Regarding drug-induced changes in other metabolites, GSH was found to be upregulated in HOb cells exposed to cDDP while no alterations were detected upon Pd_2Spm treatment. Interestingly, exactly the opposite was found in MG-63 cells, where Pd_2Spm induced an increase of GSH at 24 hours while no alterations were measured upon the same period of treatment with cDDP. These results suggest that each one of these drugs display a particular influence on the redox system of either non-neoplastic or cancer cells, which can be an advantage in a treatment regimen where these two agents are administered in combination.

The levels of *m*-Inositol are decreased in HOb cells exposed to both cDDP and Pd_2Spm, what, together with the drug-induced decreased Glu, may be indicative that both drugs share, in their mechanism of action, common metabolic pathways at least with respect to those involving these two metabolites. This hypothesis could not be confirmed through STOCSY analysis, since strong correlations with the chosen signals were found even for noise regions, probably as a consequence of the reduced number of samples per group. The decreases in *m*-Inositol registered for both drugs, may reflect perturbations in the metabolism of phospholipids and/or inositol phosphate as well as in the osmotic homeostasis, since *m*-Inositol is implicated in all of these biofunctions. The decreased *m*-Inositol levels in both the cDDP- and Pd_2Spm-treated HOb cells is similar to that measured for the MG-63 cell line upon the same drug-exposure conditions. Apart from their osmolytic functions, inositol and other polyols are known to play an important role in cellular detoxification processes, and its decrease due to chemotherapy treatment may reflect a lower turnover of phosphoinositides, a class of signaling phospholipids implicated in the control of cell proliferation (Triba *et al*., 2010) Thus, inositol can act as an indicator of membrane phospholipid turnover, and its reduction suggests an inhibition of cell proliferation.

6.5. Assessment of Biological and Metabolic Reversibility of Effects of cDDP and Pd_2Spm

After assessing the metabolic consequences of a continuous cell exposure to either cDDP or Pd_2Spm, the reversibility of the drug-induced alterations are were measured. As explained in the Experimental Section (Chapter 3), reversibility assays involved the analysis of cells that were exposed to IC_{50} concentrations of either cDDP or Pd_2Spm for 24 hours and then allowed to grow in drug-free medium for 3 additional days.

6.5.1. Osteosarcoma MG-63 Cells

As previously shown (Figure 6.2), no considerable changes in cell growth inhibition were detected at 36 and 48 hours of Pd_2Spm-exposure relative to the 24 hours levels. A different behavior, however, was observed upon cDDP-treatment, since increasing treatment periods always led to a decreased cell proliferation. Figure 6.15 shows the time-dependent effect of cDDP and Pd_2Spm on the MG-63 cells, for a 24 hours drug-exposure followed by a recovery period of 3 days. It is clearly seen that in the presence of 30 µM cDDP the MG-63 cells are already committed to death since, even after a recovery period of 3 days (in the absence of the drug), the percentage of living cells is close to zero. On the contrary, for Pd_2Spm drug removal for 3 days ensures a partial recovery of MG-63 cell growth, up to 65%, proving that, contrary to cDDP, Pd_2Spm action can be reverted by cells when drug is removed from the growth medium.

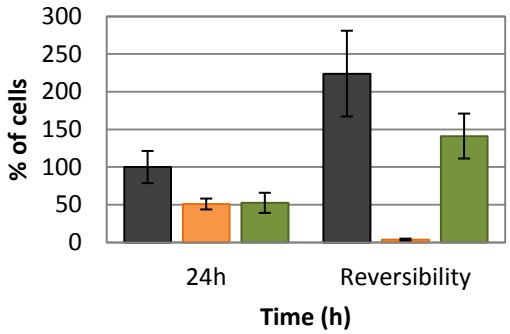

Figure 6.15. Cytotoxic effect of cDDP and Pd_2Spm, in sole administration, towards the MG-63 cell line, upon 24 hours and a 3 days recovery period. Cell proliferation was evaluated by Trypan blue assay (as described in the Experimental Procedures, Chapter 3). Control (■), 30 µM cDDP (■) and 12 µM Pd_2Spm (■). The data represent the average ± mean standard deviation from n=2 experiments, carried out in duplicate.

Figure 6.14 reveals that the metabolism of MG-63 cells reacts differently to the removal of cDDP or Pd_2Spm. For cDDP, the alterations detected in nine metabolites at 24 hours increased to fifteen after the 3 days growth in drug-free medium with a higher number of alterations being detected in amino acids, lipids, choline compounds and other miscellaneous metabolites, most of them being new ones or resulting from the intensification of the alteration measured at 24 hours, showing that cDDP-induced effects are not reversible. Interestingly enough, since DNA is one of the preferred targets of cDDP, no changes are detected in nucleotides and derivatives upon the recovery period, and even the slight increase of UDP-GlcNAc (δ 5.52) registered at 24 hours disappears. On the other hand, the reduced number of changes, five, detected upon 24 hours exposure to Pd_2Spm are all reverted upon the reversibility period, with only two new increases in

Ino/Ado and ethanolamine. Increases of Ino/Ado probably reflect perturbations at the DNA level and changes of ethanolamine, a component of glycerophospholipids metabolism, point to altered phospholipid dynamics despite the absence of changes in choline compounds.

Regarding reversibility to either cDDP- or Pd_2Spm-treatment, no such studies have been found for MG-63 cells. The reversibility of the drug effect is highly dependent on the type of cancer cell line, which is confirmed by the results reported by Soares *et al* (Soares *et al*., 2007) on the Pd_2Spm activity towards human tongue epitelioma HSC-3 cells, which showed to be almost irreversible upon a 3 days recovery period without the drug, as opposed to the results obtained here for the MG-63 cell line.

6.5.2. Osteoblast HOb Cells

Figure 6.16 shows the time-dependent effect of cDDP and Pd_2Spm on the HOb cells, for a 24 hours drug-exposure followed by a recovery period of 3 days. As it can be seen, the negligible alterations in the percentage of living cells (cells with intact cell membrane) upon 24 hours exposure to each of the two drugs gain relevance after 3 days of growth in drug-free medium: a reduced percentage of Trypan blue excluding cells was determined for both treatments with cell density being *ca* 50% or 30% relative to the control for cDDP and Pd_2Spm, respectively. Moreover, and despite the considerable dimension of both error bars, these results suggest that, even after a 3 days growth in drug-free medium, Pd_2Spm possess a higher cytotoxic power over HOb cells than cDDP.

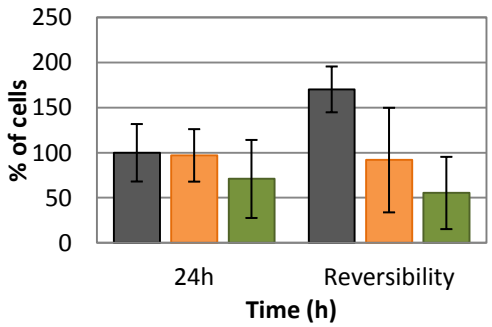

Figure 6.16. Cytotoxic effect of cDDP and Pd_2Spm, in sole administration, towards the HOb cell line, upon 24 hours and a 3 days recovery period. Cell proliferation was evaluated by Trypan blue assay (as described in the Experimental Procedures, Chapter 3). Control (■), 30 µM cDDP (■) and 12 µM Pd_2Spm (■). The data represent the average ± mean standard deviation from n=2 experiments, carried out in duplicate.

In fact, PCA analysis (Figure 6.17a) also reveals that control and cDDP-treated HOb cells are much closer in the scores plot than control and Pd_2Spm-treated cells, meaning that HOb cells are less affected by cDDP than by Pd_2Spm. The PLS-DA analysis of the three groups (Figure 6.17b) shows a clear separation between the three sample groups but, interestingly, while all cDDP-treated samples (24 hours and reversibility) remain globally equidistant in the scores space from controls, the Pd_2Spm-reversibility samples become more distant in LV1 from both controls and samples treated with Pd_2Spm for 24 hours, once again suggesting that a larger set of differences distinguishes controls from Pd_2Spm-treated samples. PLS-DA analysis of both control *vs* cDDP-treated (Figure 6.17c) and control *vs* Pd_2Spm-treated samples (Figure 6.17d) show a clear discrimination between control and drug-treated groups, however more consistent/pronounced differences between groups probably underlie the higher Q^2 value obtained for the Pd_2Spm model in relation to cDDP (0.787 and 0.509, respectively).

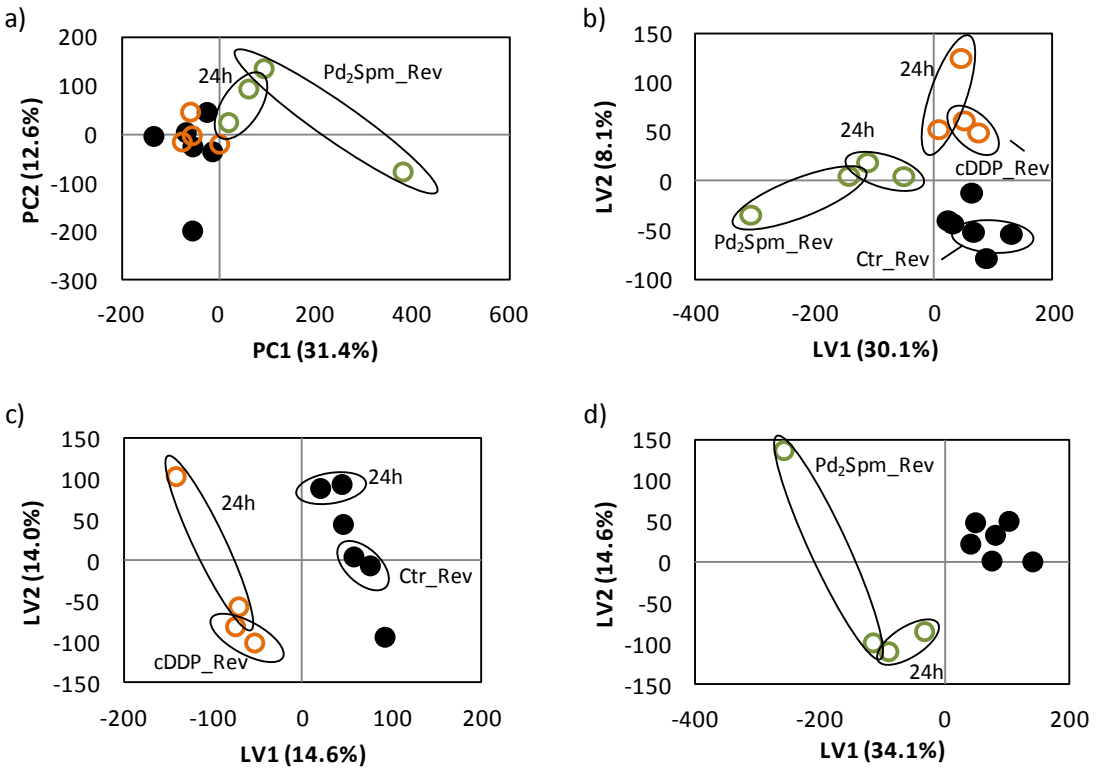

Figure 6.17. Multivariate analysis of controls (●), 30 µM cDDP- (○) and 12 µM Pd_2Spm-treated (○) HOb cells. a) PCA scores plot for all samples, UV, 3 components, R^2X = 0.552 and Q^2 = -0.129, b) PLS-DA scores plot for all samples, UV, 2 components, R^2X = 0.382, R^2Y = 0.780 and Q^2 = 0.298, c) PLS-DA scores plot for cDDP assay, UV, 2 components, R^2X = 0.286, R^2Y = 0.990 and Q^2 = 0.509 and d) PLS-DA scores plot for Pd_2Spm assay, UV, 3 components, R^2X = 0.572, R^2Y = 0.993 and Q^2 = 0.787.

The loading plots of the models presented in Figures 6.17c and 6.17d, resulted in representations in which noise was significantly coloured, thus eventually masking real and

important metabolic changes. For this reason, this information was not considered relevant and data analysis proceeded with the integration of as many signals as possible, based on observations made by visual inspection. The results from signal integration are summarised in Table 6.5 and the information contained therein is expressed as heatmap in Figure 6.14.

As shown in Figure 6.14a, the low number of alterations induced by 24 hours treatment with cDDP (Glu, Urd, GSH and *m*-inositol) are still present upon the recovery period (with exception of Urd, which level seems to normalise), in addition to five new amino acid changes (Gly, Ser and Thr) and choline compounds (GPC and PC). This shows that cDDP has a long term effect over HOb cells. The higher number of metabolic alterations induced upon 24 hours treatment with Pd_2Spm (mainly in amino acids) are globally reverted upon cells growth for 3 days in drug-free medium, excluding changes in Glu and Gln that persist. Reversibility results from Pd_2Spm-treatment reveal alterations in Ser levels as well as in choline, Ino/Ado and Urd (both increase), creatine and dihydroxyacetone (DHA, δ 4.42). The long term decrease of choline induced by Pd_2Spm immediately suggests a perturbation of the metabolism of membrane phospholipids (as most choline is found in phospholipids). However, and since this alteration is not accompanied by a change of either GPC or PC, other pathways involving the use of choline may underlie this variation, namely its oxidation to form betaine which may be used as an antioxidant. Nevertheless, the typical resonances of betaine, at δ 3.25 and δ 3.89, could not be identified in either 1D or 2D spectra, eventually due to the its low concentration. Changes in Ino/Ado and Urd probably reflect perturbations in DNA synthesis and metabolism, induced by Pd_2Spm-treatment. DHA is a component of glycerophospholipid and inositol metabolism and can also be used as energy source. Thus, its decrease in HOb cells once again reinforce the idea of altered phospholipid metabolism as a consequence of cells treatment with Pd_2Spm. Decreases in *m*-inositol and Glu persist upon the recovery period, similarly to what was seen for cDDP, eventually pointing to a common metabolic pathway shared by the two drugs. In relation to choline compound ratios, all registered increases upon the recovery period with exception for PC/GPC in Pd_2Spm which recovered after the decrease upon treatment for 24 hours. Despite the similar trends observed for the two drugs, statistically significant increases were only registered in PC/Cho and PC/GPC of HOb cells treated with cDDP.

In the light of these results, it becomes apparent that Pd_2Spm induces more dramatic alterations in HOb cells than cDDP, such alterations being also more pronounced compared to those noted in osteosarcoma MG-63 cells.

6.6. Evaluation of Apoptosis in MG-63 Cells Exposed to cDDP or Pd_2Spm: FITC Annexin V/PI Assays

The above discussed results showed that, despite the established IC_{50} concentration determined at 24 hours for the drugs under study, the consequences in terms of cell survival and metabolic profile that result from cDDP or Pd_2Spm exposure are clearly distinct. Regarding MG-63 cells, cDDP treatment induced the highest decrease in the number of living cells (even after drug removal) and their metabolic profile revealed a marked increase of the lipid content, an important marker of apoptosis.

As to Pd_2Spm-treated MG-63 cells, the number of living cells after 24 hours of exposure was kept stable and the metabolic profile did not reveal a perturbation of the lipid moieties which raised the question of whether these cells are indeed dying or if drug is somehow only inducing a time lag in their normal growth and division processes. Accordingly, a FITC Annexin V/PI apoptosis detection experiment was performed with a view to determine and compare apoptosis in MG-63 cells treated with either cDDP or Pd_2Spm (at IC_{50} concentrations - 30 and 12 µM, respectively) over a period of 48 hours (Figure 6.18).

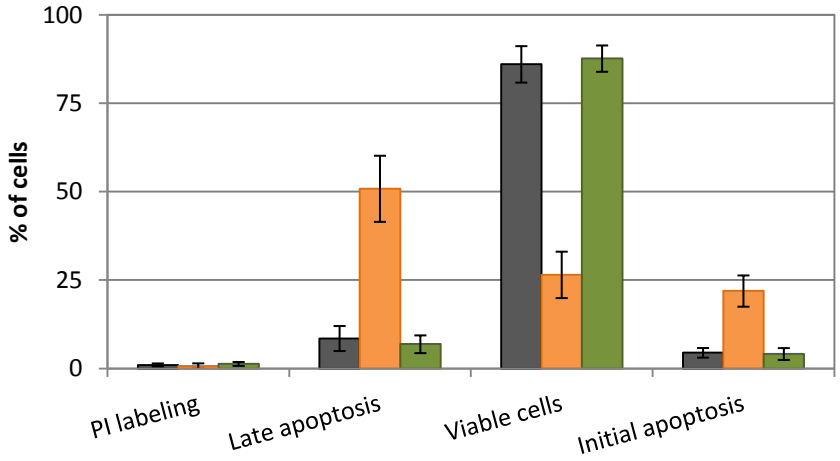

Figure 6.18. Global results of FITC Annexin V/PI assays of control (■), 30 µM cDDP- (■) and 12 µM Pd_2Spm-treated (■) MG-63 cells. The data represent the average ± mean standard deviation from n=3 experiments, carried out in duplicate.

The results presented in Figure 6.18 show that at 48 hours, and as expected, the great majority of the control cells are viable (around 86%) and only a small percentage is undergoing apoptosis, as can be seen in more detail in Figure 6.19a. On the other hand, after 48 hours of exposure to cDDP, only 26% of the cells remain viable, while around 22% are undergoing initial apoptosis and 51% are already in late stage apoptosis (Figure 6.19b). Interestingly enough,

analysis of the results for the Pd_2Spm-treated samples (Figure 6.19c) revealed a significant similarity to controls, both for viable and apoptotic cells, which means that Pd_2Spm-treatment does not compromise their overall viability.

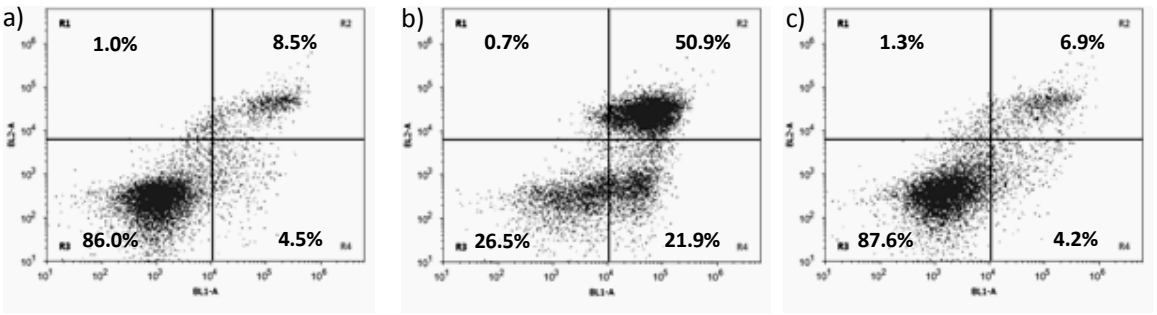

Figure 6.19. Global results of FITC Annexin V/PI assays, at 48 hours, of a) control, b) cDDP- and c) Pd_2Spm-treated MG-63 cells. Values represent the average from n=3 experiments, carried out in duplicate.

These assays were accompanied by a parallel Trypan blue assay that ensured that for each of the two drug treatments, at 24 hours, only 50% of cells remain alive, i.e. the drug concentration to which cells were exposed was in agreement with the previously determined IC_{50}.

According to these results it becomes clear that cDDP-exposed MG-63 cells were undergoing extensive apoptosis, in agreement with reported studies for this drug (Kinoshita *et al*., 2000; Koyama *et al*., 2004; Tsai *et al*., 2014). Regarding Pd_2Spm, the results suggest that the reduction in the number of cells when treated with this agent might be due to a lag effect of the drug over their normal growth and division times, instead of relating to a cell death induced mechanism, since neither apoptosis nor necrosis were found to take place.

The data by Fiuza (Fiuza *et al*., 2011) for human breast cancer cells have shown that the activity of Pd_2Spm on the cytoskeleton, and its expected impact on cell morphology, is much greater than for cDDP, although no experiments on apoptosis detection were reported at that time. Taken together, these results suggest that both Pd_2Spm and cDDP impair cell proliferation *via* distinct cellular targets.

6.7. Glutathione Competition Assays

Due to the high affinity of soft metals such as Pt(II) and Pd(II) for the sulphur atom (a soft ligand), glutathione is a key component in the pharmacokinetic pathway of Pt- and Pd-containing

agents, being known to affect their intracellular bioavailability and to be responsible for mechanisms associated to acquired resistance to Pt(II) agents such as cDDP (Marques, 2013; Wang *et al*., 2007; Zhang *et al*., 1998). Glutathione, a tripeptide comprising Gly, Glu and Cys, is the most abundant non-protein thiol in the cell and acts as a fundamental antioxidant preventing the oxidative damage of intracellular components (mainly by reactive oxygen species, ROS, such as peroxides and free radicals). Glutathione exists predominantly in the reduced form (GSH), at intracellular concentrations in the range of 0.5-10 mM and can be readily oxidised to the stable disulfide species (GSSG) (Lushchak *et al*., 2012). The liquid state ^{1}H NMR spectra of both reduced and oxidised glutathione solutions are shown in Figures 6.20a and 6.20b, respectively.

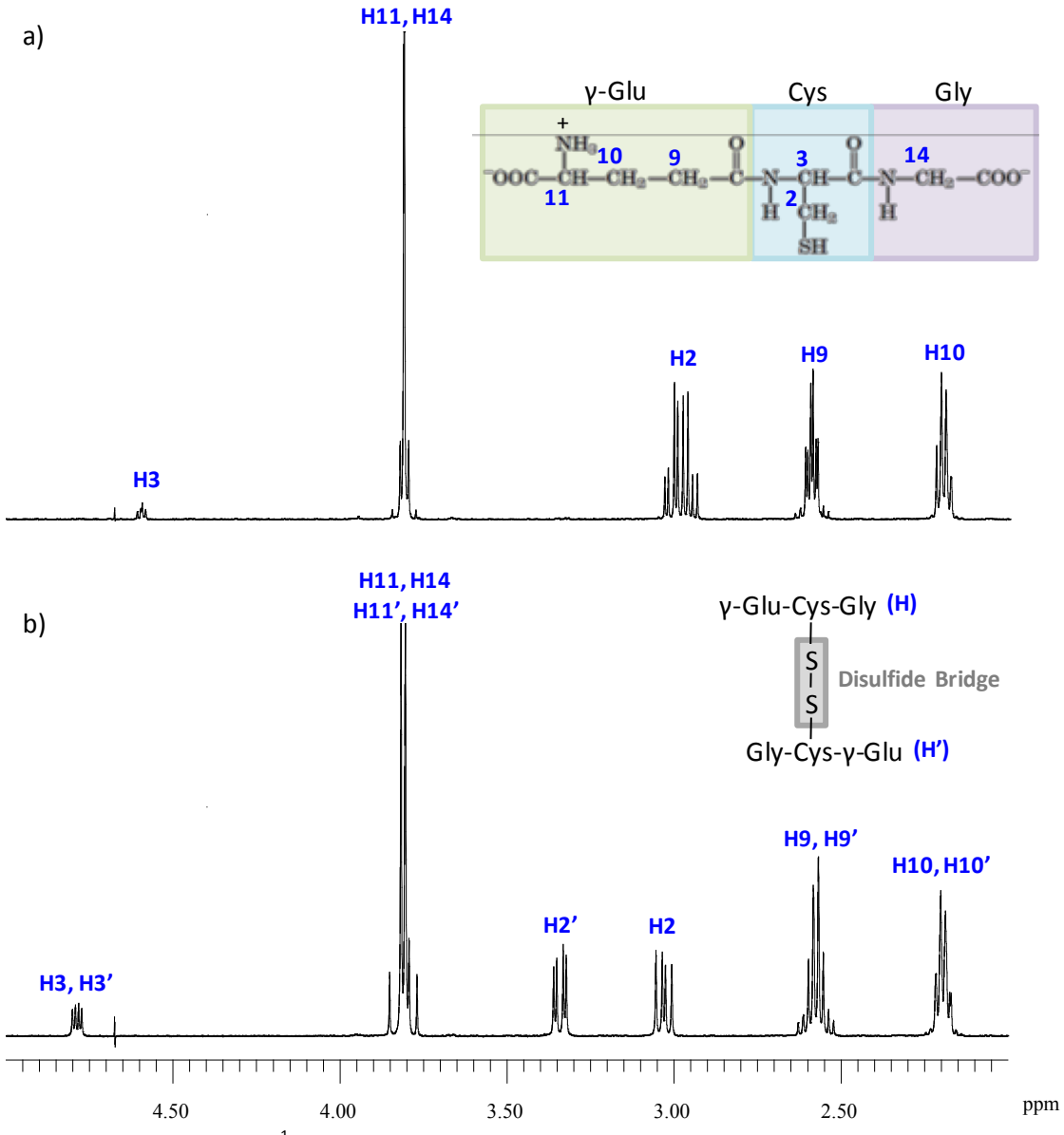

Figure 6.20. 500 MHz ^{1}H NMR spectra of aqueous solutions of a) 1 mM GSH and b) 1 mM GSSG, at 310K.

As shown in Figure 6.19, spectra from GSH and GSSG possess identical resonances for H10 (δ 2.17), H9 (δ 2.56) and H11 and H14 (δ 3.79). However, an additional resonance appears for H2' (δ 3.34) from GSSG and the H3 and H3' from GSSG resonate at δ 4.78, while for GSH, H3 resonance appears at δ 4.58. In fact, H2 or H2' and H3 or H3' refer to the protons that are closest to the disulfide bridge that is established when GSH is oxidised to GSSG, and thus are those for which chemical shift is more prone to be affected as consequence of the oxidation process.

Since the drugs hereby tested, cDDP and Pd_2Spm, contain the metal ions Pt(II) and Pd(II) (with a high affinity for glutathione's sulphur), it is worth investigating whether the GSH signal chosen for integration in the cell studies (H9, at δ 2.56) can be affected by the presence of such agents. This will help understanding whether the measured variations in cell metabolites refer indeed to alterations in GSH levels or if, on the other hand, competition by GSH coordination with Pt(II) or Pd(II) ions are erroneously influencing the results. Therefore, competition assays of GSH towards cDDP or Pd_2Spm were performed, in solution, with a view to assign the resonances of the drug-GSH adducts, for each of the two drugs. The results from these experiments are presented below.

6.7.1. Pt (II) Drug: cDDP

cDDP (through is Pt(II) centre) is known to display a higher affinity for sulphur donors like cysteines and methionines than for nitrogen donors such as the purine bases of DNA (Pearson *et al*., 1968). Nevertheless, the drug's mode of action is known to primarily involve the establishment of intra- and interstrand crosslinks with DNA (mostly with guanine and adenine), triggering a series of conformational rearrangements and biochemical changes that ultimately lead to apoptosis (Basu and Krishnamurthy, 2010). Hence, in spite of ongoing debate around this matter, it is generally assumed that GSH is closely associated to drug-resistance mechanisms of Pt-based chemotherapeutic agents.

Up to this date, numerous studies have unequivocally correlated partial cDDP inactivation in several human cancer cell lines with increased GSH intracellular levels (Mistry *et al*., 1991; Komiya *et al*., 1998; Godwin *et al*., 1992). Chen and co-workers (Chen *et al*., 2008) concluded that cells with increased GSH levels become more sensitive to cDDP by up-regulation of the copper transporter hCtr1 (involved in transporting cDDP into cells), while other authors have suggested that the high affinity of the Pt(II) drugs for the glutathione's thiol group favours the formation of

stable Pt-glutathione adducts thus lowering the amount of drug available for DNA binding (Reedijk *et al*., 1999). Kasherman and collaborators (Kasherman *et al*., 2009) determined such a decrease in active drug concentration to be around 20% in human ovarian cancer cells. A review from Chen and Kuo (Chen and Kuo, 2010) summarises the three mechanisms that have been proposed for the role of GSH in the regulation of cDDP sensitivities that ultimately influence its ability to induce cell death: 1) GSH can act as a cofactor that facilitates the efflux of cDDP in mammalian cell by multidrug resistance protein 2 (MDR2); 2) GSH can act as a redox-regulating cytoprotector; 3) GSH can act as a copper chelator.

Due to the conflicting nature of results regarding this issue, the kinetics of the GSH:cDDP competition reaction was presently followed by liquid state ^{1}H NMR (carrying out signals integration), in order to understand if our determinations of GSH in the spectra of the cell samples may have been miscalculated by a possible interference from Pt-GSH adducts.

Figure 6.21 compares the spectra of fresh solutions of glutathione, both reduced (Figure 6.20a) and oxidised (Figure 6.20b) with that of a GSH:cDDP solution (2:1 in PBS/D_2O). The kinetics of the reaction between GSH and cDDP was followed by the continuous acquisition of one spectrum of the GSH:cDDP solution every 15 minutes, starting with the fresh solution (Figure 6.21c) up to a total of 3 hours reaction time (Figure 6.21d). One last spectrum was registered 18 days after the preparation of the solution (Figure 6.21e). Considering the minor changes observed when analysing the spectra, only the initial (15 minutes) and final (3 hours) spectra were chosen for comparison, and are represented in Figure 6.21. For increasing reaction times, the initial GSH:cDDP sample evidences a higher degree of glutathione oxidation, reflected by the strong GSSG resonances at δ 3.34 and δ 4.78. As expected, at day 18, all glutathione was in the oxidised form - the GSH typical resonance at δ 4.58 from H3 being absent and only one multiplet being detected at δ 4.78 attributed to the typical resonance of H3' protons of GSSG. As highlighted in grey in Figure 6.21, the increasing GSH oxidation is accompanied by the appearance of broad signals at δ 2.25, δ 2.65 and δ 3.86 (more evident at day 18) which were attributed to the formation of the cDDP-glutathione adduct. Also, already after 3 hours upon adding cDDP and GSH, a signal appears at δ 2.75, possibly corresponding to an intermediate species.

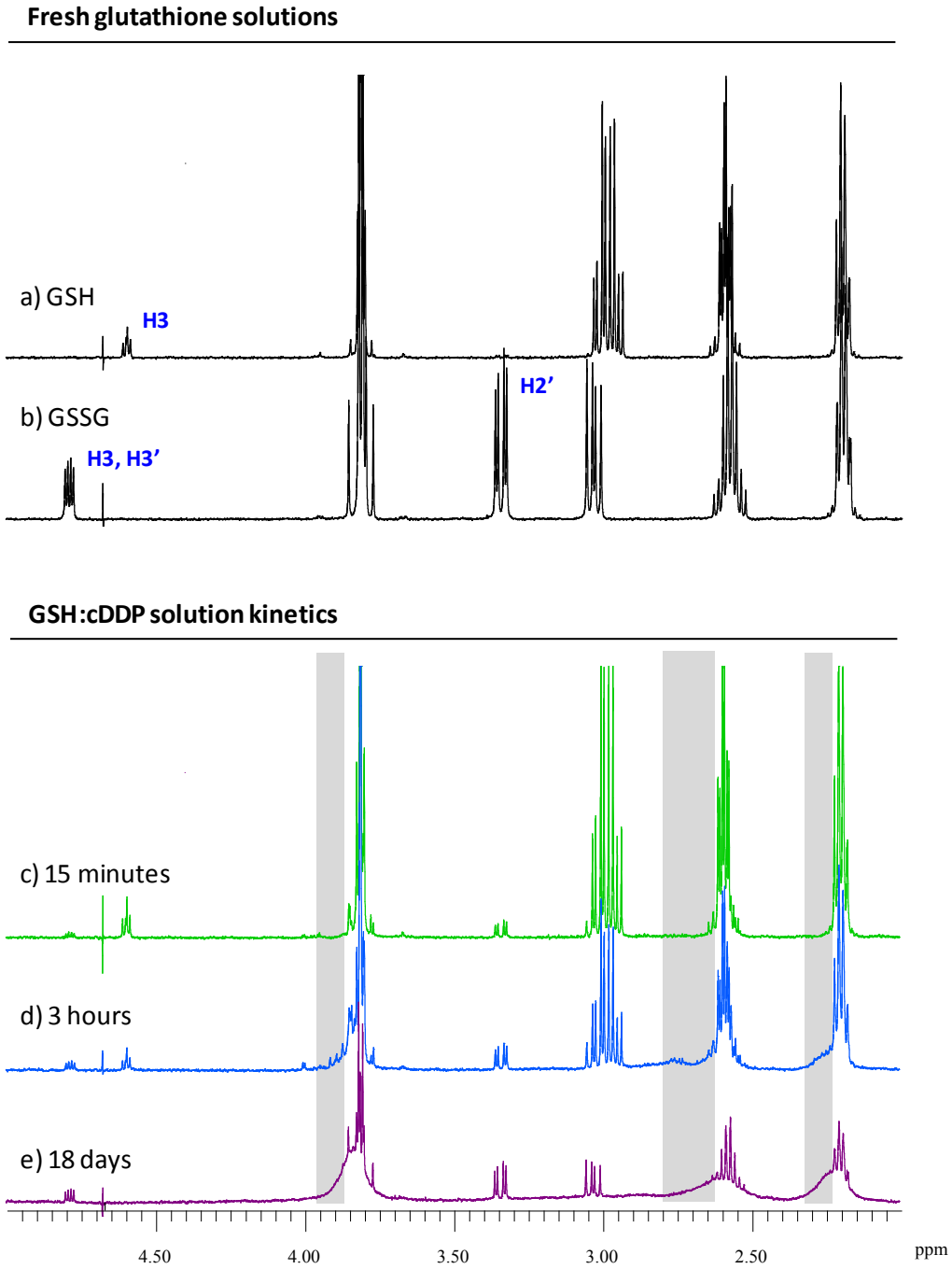

Figure 6.21. 500 MHz ^{1}H NMR spectra of a) GSH and b) GSSG solutions and GSH:cDDP kinetics at c) 15 minutes, d) 3 hours and d) 18days after solution preparation, at 310 K. Grey areas highlight broad resonances attributed to the cDDP-glutathione adduct formation.

Kinetic studies reported by Hagrman (Hagrman *et al.*, 2004) evaluated the formation of Pt(II)-glutathione species for several platinum-based drugs (oxaplatin, carboplatin and cDDP). Reactions were performed at 37˚C and concentrations were selected to mimic those of GSH in cells in organism (6.75 mM, according to Souid *et al.*, 2001) and those that mimic the passage of clinical concentrations of the drugs (4.62, 6.63 and 7.82 mM) through the cytosol (135 µM) (Oguri

et al., 1988; Grolleau *et al*., 2001; Souid *et al*., 2003). Regarding cDDP, formation of the metal-glutathione adduct was monitored for a 40 hours period, almost total depletion of the free drug having been observed during the first 5 hours, with a $t_{1/2}$ value (time necessary for a 50% concentration decrease) for free cDDP equal to 1.03-1.06 hours. This $t_{1/2}$ value was considered in the present experiments when establishing the 3 hours periods to follow the reaction cDDP:GSH to cDDP-glutathione by NMR.

In an attempt to quantify the extension of glutathione oxidation, as well as the formation of the cDDP-glutathione adduct, the following analysis was carried out: the ratios between the areas of the typical resonances from GSH (δ 4.58) or GSSG (δ 4.78) and the total area of the spectrum of each form of glutathione in fresh solutions (prepared in equal concentrations) were assumed as reflecting 100% of each form of glutathione. Then, using these values as a reference, the percentages of GSH and GSSG in the cDDP:GSH solutions were calculated over periods of 3 hours and 18 days, the residual percentage being attributed to cDDP-glutathione adduct formation (Table 6.6).

Table 6.6. Quantification of GSH, GSSG and cDDP-glutathione in a solution containing 0.5mM cDDP and 1 mM GSH, upon increasing reaction times.

Spectra	Time	Total Area	% of GSH[1]	% of GSSG[2]	% of cDDP-glutathione adduct[3]
cDDP-glutathione_1	0h15	4.88E+08	90.9	6.10	3.00
cDDP-glutathione _2	0h30	4.90E+08	89.1	8.40	2.50
cDDP-glutathione _3	0h45	4.90E+08	85.8	7.40	6.80
cDDP-glutathione _4	1h00	4.86E+08	81.0	8.40	10.6
cDDP-glutathione _5	1h15	4.83E+08	75.7	8.20	16.1
cDDP-glutathione _6	1h30	4.84E+08	72.7	11.0	16.2
cDDP-glutathione _7	1h45	4.81E+08	69.1	10.3	20.6
cDDP-glutathione _8	2h00	4.83E+08	70.6	12.0	17.4
cDDP-glutathione _9	2h15	4.83E+08	64.4	13.1	22.5
cDDP-glutathione _10	2h30	4.82E+08	63.5	13.0	23.5
cDDP-glutathione _11	2h45	4.81E+08	61.0	12.3	26.6
cDDP-glutathione _12	3h00	4.79E+08	53.5	13.9	32.6
cDDP-glutathione _18days	18 days	4.55E+08	-1.60	22.4	79.2

[1] δ 4.58 signal integration – extrapolation based on the assumption that GSH/Total Area of fresh GSH solution is 100%; [2] δ 4.78 signal integration – extrapolation based on the assumption that GSSG/Total Area of fresh GSSG solution is 100%; [3] % (cDDP-glutathione adduct) = 100 - (%GSH + %GSSG), assuming that no other species are formed/altered during the experiment.

According to these calculations, after a 3 hours kinetics, only 53.5% of GSH is present in solution, the percentage of GSSG increasing up to near 14%, thus yielding a 32.6% formation of cDDP-glutathione adduct during this time (assuming that no other chemical species is formed). After 18 days, around 20% of glutathione was oxidised to GSSG and the other 80% seems to be complexed with cDDP.

Due to the complexity of the ^{1}H HRMAS NMR spectra obtained for the cells treated with cDDP, coupled to the low intensity of the glutathione signals detected, it was impossible to infer about the presence of the base-broadened patterns here suggested to be associated to the presence of the cDDP-glutathione adducts. Nevertheless, the formation of such adducts should account for a minor fraction of the measured GSH signal once its time course (Figure 6.22) shows either maintenance (until 24 hours) or decrease (24 hours onwards) relative to the control. If the peak assumed as GSH was instead mainly assigned to the cDDP-glutathione adduct, it would be expected that for treated cells, after an initial increase (cDDP addition is performed at the very beginning of the experiment), the levels of this signal would remain quite stable along the rest of the experiment (assuming the high stability of the adduct, since no other competing species are present in solution).

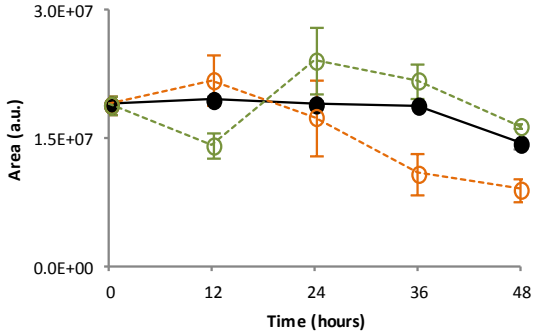

Figure 6.22. Time course variation of GSH (δ2.56) in controls (●), 30 µM cDDP- (○) and 12µM Pd_2Spm-treated (○) MG-63 cells (controls are indicated with full lines and drug-treated with dashed lines).

Besides reacting with free cDDP, a second GSH molecule can also react with the drug-glutathione adduct. This process was well described by Singh and collaborators (Singh *et al*., 2005), who proposed the reaction scheme depicted in Figure 6.23. The binding of cisplatin to a second GSH molecule may be explained by the *trans*-ammine labilisation effect of the first coordination of Pt(II) to glutathione's sulphur atom, which facilitates the substitution of cDDP's NH_3 groups by GSH.

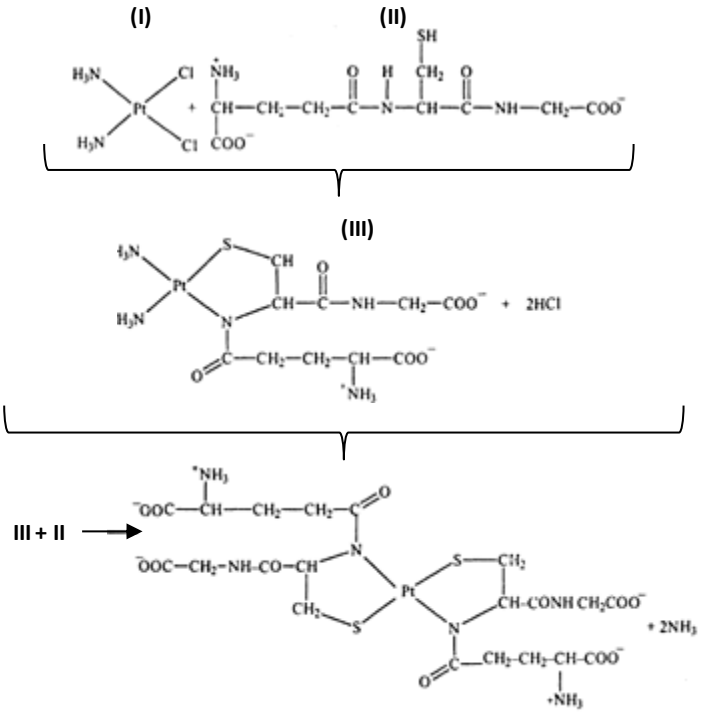

Figure 6.23. Reaction scheme proposed for the formation of Pt(glutathione)$_2$ species (adapted from Singh *et al*., 2005).

The maximum GSH:cDDP ratio of 2 considered in the present competition assay is far lower than that occurring intracellularly, which once more reinforces the proposed hypothesis of a minor contribution of the drug-glutathione adduct for the NMR signal of GSH considered for integration in cell samples, meaning that a decrease of GSH integral is most probably attributed to its increased degradation (probably by oxidation).

6.7.2. Pd (II) Drug: Pd_2Spm

Due to the chemical similarity between the Pt(II) and the Pd(II) ions, the Pd_2Spm complex is also expected to react with intracellular GSH in cell cultures. The following set of experiments aimed at understanding whether this reaction occurs and to what extent, through the analysis of the GSH NMR resonance at δ 2.56, chosen for signal integration.

Figure 6.24 compares the spectra of fresh solutions of glutathione (both reduced and oxidised forms) with the spectra of GSH:Pd_2Spm solution (1 mM: 0.5 mM in PBS/D_2O) analysed fresh and 3 hours after the preparation of the solution (one spectrum was registered each 15

minutes). Due to the very small magnitude of the observed changes, only the initial and final spectra are shown, for simplicity sake.

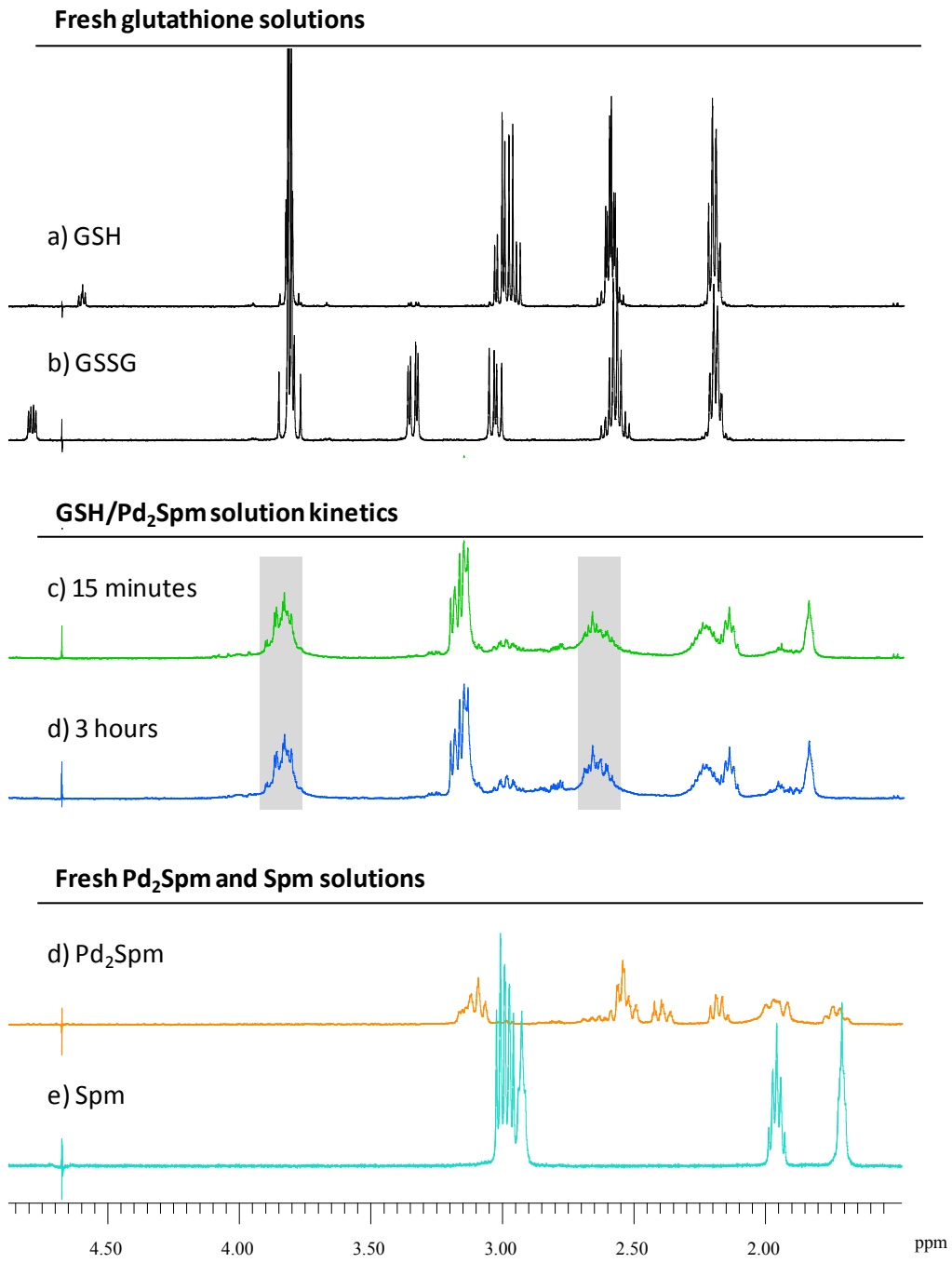

Figure 6.24. 500 MHz ^{1}H NMR spectra of a) GSH and b) GSSG solutions and GSH:Pd_2Spm kinetics at c) 15 minutes and d) 3 hours after solution preparation, e) Pd_2Spm and f) Spm, at 310 K. Grey areas highlight broad resonances attributed to Pd_2Spm-glutathione adduct formation.

As shown in Figure 6.24c, 15 minutes of reaction (time needed for spectral acquisition) are enough to remove all typical resonances from GSH and GSSG (δ 4.58 and δ 4.78, respectively),

showing that the great majority, if not all, of the free GSH reacted with Pd_2Spm during this time and did not undergo oxidation to GSSG. In fact, when GSH and Pd_2Spm solutions were mixed together, an exothermic reaction took place and the solution immediately turned yellow-orange (characteristic of the formation of a Pt-S or Pd-S bond).

As expected, there are some similarities between the signals yielded by the Pd_2Spm-glutathione solution and those from Pd_2Spm and Spm solutions. Resonances from GSH also seem to contribute to the NMR signals that appear in the spectrum of the adduct, but due to the considerable changes in chemical shift in relation to the reference samples, it was not possible to unequivocally assign the peaks from the Pd_2Spm-glutathione solution. Despite this fact, it seems quite reasonable to conclude that no GSH oxidation to GSSG occurred and that reduced Pd(II) coordination with glutathione took place. The broadening of the glutathione signals, clearly depicted in Figure 6.24c and Figure 6.24d, can thus be attributed to the larger dimension and lower mobility of this adduct, this effect being particularly clear at δ 3.78, where neither Pd_2Spm nor Spm display any signals.

Studies by Sovago and Martin (Sovago and Martin, 1981) showed that, in an equimolar solution of Pd(II) and GSH, broadening of the NMR signal arising from $–CH_2CH$ part of the γ-glutamate residue at δ 2.56 occurs as a consequence of metal chelation at the α-amino terminus, in addition to thiol coordination. In this study, Pd(II) and GSH are in equimolar conditions (2 Pd(II) ions are present per molecule of Pd_2Spm) and a broad signal is detected at δ 2.56, immediately at 15 minutes of reaction, suggesting that the refered chelation may have take place.

As for cDDP, the ^{1}H HRMAS NMR spectra of Pd_2Spm-treated cells have a low intensity GSH signal which makes it impossible to infer about broadening effects coming from adduct formation, that may account for an erroneous interpretation of the results of GSH peak integration (δ 2.56). However, taking into consideration the above refered results that seem to indicate a significant chemical shift change of the peak of GSH at δ 2.56 when coordinated with Pd(II), and once HRMAS spectra of treated cells do show a GSH peak at this chemical shift comparable in magnitude to that of control cells, it seem plausible to assume that the formation of the Pd_2Spm-glutathione adduct would account for a small peak at slight higher chemical shifts. Thus, the GSH peak at δ 2.56 chosen for integration does seem to reflect free GSH variation, either in the presence or absence of the drug.

These drug:GSH competition assays showed that both drugs chelate glutathione but, according to the alterations observed in the spectra, the most dramatic ones are seen in Pd_2Spm:GSH solution. Together with the release of heat when mixing Pd_2Spm with GSH solution (pointing to chelation of metal ion to sulfur of GSH), NMR spectral analysis showed that Pd more easily and strongly coordinates with GSH. Regarding the differences in GSH time course in the ^{1}H HRMAS NMR spectra of cDDP- and Pd_2Spm-treated MG-63 cells (Figure 6.22), the drug:GSH kinetic assays strongly suggested that the signal that is integrated is, in fact, mainly attributed to GSH (and not the GSH-drug complex). Therefore, the presented time course can not be interpreted as reflecting higher or lower coordination power of the metal ions (Pt(II) or Pd(II)) of the drugs to GSH, instead it seems to reflect the consequence of drug action in the metabolism of GSH.

7. Metabolic Impact of Drug Combination on Osteosarcoma MG-63 Cells

This chapter intends to go a step further in the understanding of the metabolic impact of drugs currently used for osteosarcoma treatment, through experiments that aim to closely mimic the combination regiment in which these agents are administered in the clinic. By comparing these with the data previously described for single drug administration, synergistic effects may be identified. Moreover, the possible benefits of replacing cDDP by the Pd(II) agent Pd_2Spm in combination regimens are discussed, by comparing nature and magnitude of the metabolic alterations induced by cDDP- and Pd_2Spm-cocktails in MG-63 cells.

7.1. Antiproliferative Activity and Cytotoxic Results

The EURAMOS protocol (http://212.219.75.232/euramos/euramos_i_trial.asp) defines that the first cycle of chemotherapy for an OS patient consists of a five week treatment protocol, in which cDDP and DOX are administered simultaneously in the first week and then MTX is given twice at weeks 4 and 5. A second cycle of this regimen is repeated prior to surgery and, at that time, a histological evaluation of treatment response is performed, in order to decide on a possible new cycle of treatment that includes ifosfamide and etoposide administration.

In an attempt to translate the first cycle of treatment performed in the clinic to cell culture assays, we reduced the timescale from weeks to days and performed preliminary tests to determine the concentrations of drugs (cDDP, DOX and MTX) that were in agreement with the proportion in which they are used in the clinic (120 mg: 75 mg: 12 g), while ensuring that at the end of the experiment the number of cells still enabled the analysis by NMR, i.e. a minimum of around 5 million cells (obtained, if necessary, by replica samples). According to this and considering the lowest determined IC_{50} concentration of 3 μM for DOX, the cDDP and MTX concentrations should be of 4.8 and 480 μM, respectively. Our preliminary cytotoxicity tests (not shown), showed that the time needed for a second dose of MTX induces an even higher reduction in the number of cells and, on the other hand, control groups would be under an additional 24 hours period of stress induced by extremely high cell densities and for these reasons we decided to stop the experiments after just one dose of MTX. Additionally, our cytotoxicity results (not shown) also showed that, interestingly, 4.8, 48 or 480 μM of MTX resulted in similar decreases in

MG-63 cells survival and for this reason, the lowest MTX concentration (4.8 µM) was chosen, despite it not respecting the proportion in relation to the other 2 drugs in clinics. A schematic representation of the experimental procedure adopted is presented in Figure 7.1, showing the time points of addition of drug-cocktails and of sample collection.

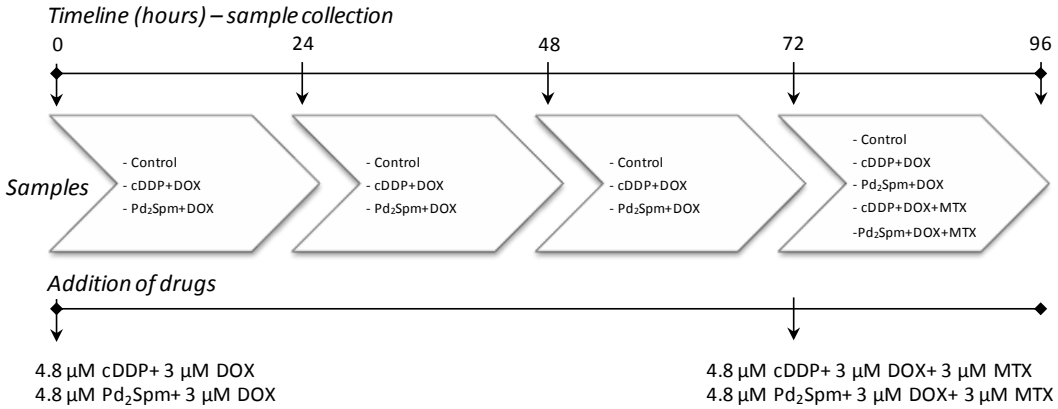

Figure 7.1. Schematic representation of the experimental procedure followed in drug combination metabolic assays, showing the time points of sample collection and addition of drug-cocktails.

Figure 7.2 shows the cytotoxic results reflecting the impact of treatment with 4.8 µM cDDP + 3 µM DOX and 4.8 µM Pd_2Spm + 3 µM DOX cocktails in both MG-63 (Figure 7.2a) and HOb (Figure 7.2b) cells' survival after 24, 48, 72 and 96 hours of treatment. Moreover, the impact of the addition of 4.8 µM MTX during the last 24 hours of the total 96 hours period of continuous exposure to either cDDP- or Pd_2Spm-combination treatments is also shown.

The cytotoxic results of the MG-63 cells exposed to either cDDP- or Pd_2Spm-combination treatments (Figure 7.2a) yielded similar results in terms of cell survival: after 24 hours of treatment with either cDDP or Pd_2Spm, in combination with DOX, an inhibition of cell growth of about 50% was achieved. Larger exposure times resulted in a slight decrease in cell survival, without significant differences being detected for the regimens based on either cDDP or Pd_2Spm. When compared to the results previously obtained for MG-63 cells exposed to DOX, for only 48 hours (Figure 5.1b, Chapter 5), a similar decreasing tendency in cells survival was detected. Interestingly enough, administration of MTX for the last 24 hours (of a total drug incubation period of 96 hours), at a concentration higher than the corresponding IC_{50} for these cells (4.8 µM as opposed to the IC_{50} value of 3 µM) does not induce a detectable change in cells' survival relative to cDDP+DOX or Pd_2Spm+DOX. From this first experiment, two interesting conclusions can be drawn: 1) despite the considerable differences in the IC_{50} values for cDDP and Pd_2Spm (the

latter being about half of the first), the combination of each of these drugs with DOX (at its IC_{50} dosage) induces identical levels of cell death; 2) MTX addition, at a concentration higher than its IC_{50}, does not seem to cause additional cell death.

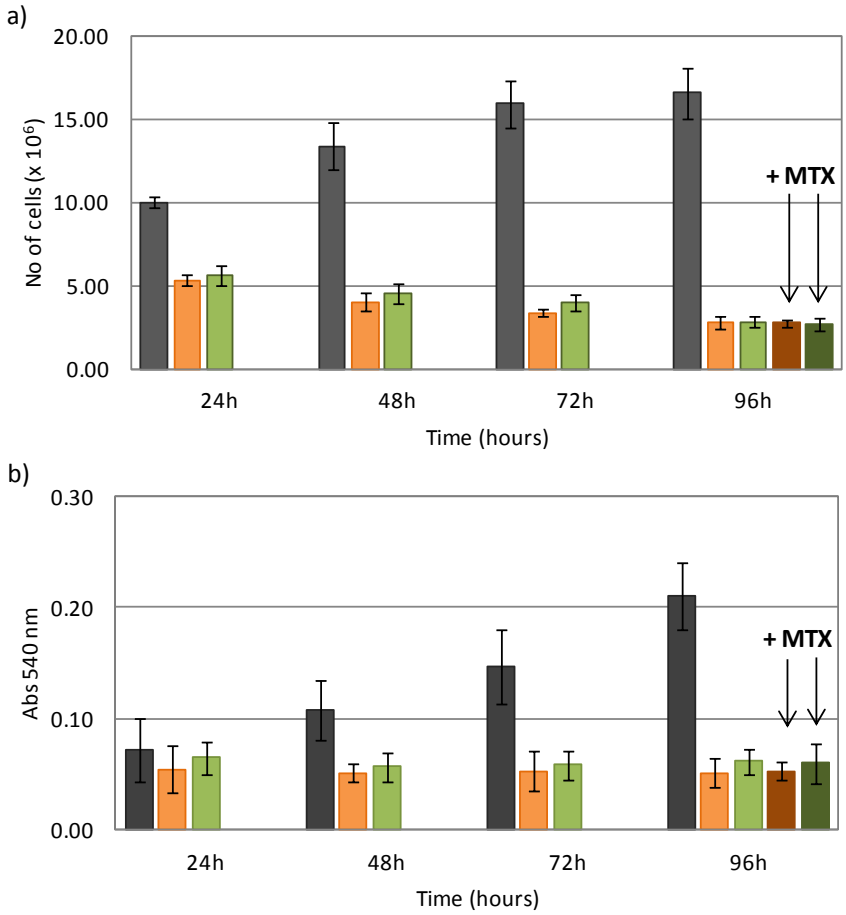

Figure 7.2. Cytotoxic results and antiproliferative activity of several drug combinations towards the MG-63 and HOb cell lines: a) MG-63 cells (Trypan blue assay); b) HOb cells (SRB assay). The cells were exposed to cDDP- or Pd_2Spm-cocktails. Control (■), 4.8 µM cDDP+3 µM DOX (■), 4.8 µM Pd_2Spm+3 µM DOX (■), 4.8 µM cDDP+3 µM DOX+3 µM MTX (■), 4.8 µM Pd_2Spm+3 µM DOX+3 µM MTX (■). The data represent the average ± mean standard deviation from a) n=3 experiments, carried out in duplicate and b) n=3 experiments, carried out in triplicate.

The evaluation of the impact of these drug-cocktails on the non neoplastic HOb cells was carried out only through the SRB colorimetric assay, due to the already mentioned difficulties in achieving the large number of cells needed for the NMR experiments. For both cDDP+DOX and Pd_2Spm+DOX combination regimens, a significant decrease in cells' survival was achieved after 48 hours of drug exposure (Figure 7.2b). This inhibition of cell proliferation seems to be maintained throughout the whole duration of the experiment (96 hours), whereas the number of osteoblasts

kept the increasing tendency in the controls. Again, addition of the antimetabolite MTX was not found to enhance the effects of either the cDDP- or Pd_2Spm-cocktails.

Comparison of cell survival data obtained for the neoplastic (MG-63) and non-neoplastic (HOb) cells seems to indicate that: 1) the two combination schemes induce very similar cell survival rates for each of the two cell lines; 2) the measured growth-inhibition effect is detected for shorter drug incubation times for the MG-63 cells than for the osteoblasts, meaning that drug cocktails seem to be more effective in cancer cells than in healthy ones; 3) administration of MTX does not seem to induce a synergistic effect for either cDDP- or Pd_2Spm-combination regimens.

7.2. ^{1}H HRMAS NMR Analysis

7.2.1. cDDP-Cocktail

Based on the results of Trypan blue assays that show a marked decrease of MG-63 cells survival as a consequence of cells treatment with the cDDP-cocktail, the next step was to understand which metabolic changes underlie this decreased number of living cells and whether they are in agreement with those identified in single drug treatment assays (both cDDP, DOX or MTX) or if new changes emerge, reflecting a synergistic action of these drugs when administered in combination. Once again, HRMAS NMR metabolomics was the chosen approach to perform this evaluation, in which only MG-63 cells were studied due to the already mentioned difficulties to obtain large numbers of HOb cells for NMR analysis.

The metabolic impact of simultaneous administration of cDDP (4.8 μM) and DOX (3 μM) to the MG-63 cells was evaluated over 96 hours, with samples being collected every 24 hours. Visual inspection of cDDP+DOX-treated spectra compared to the control spectra (Figure 7.3) reveals relevant drug-induced changes already at 24 hours of treatment: strong increases in choline, GPC, UXP and glucosylated derivatives, increased alanine and clear changes in other metabolites (namely higher amounts of acetates and creatine and a marked decrease of *m*-Inositol). For longer exposure periods (72 and 96 hours), the metabolic changes are intensified relative to the 48 hours time-point: increase of lipid resonances, choline and GPC levels, as well as of uridine, UXP and UDP-GNAc derivatives, global decrease of amino acids (Ala, Lys, Glu, Gln, Thr, Gly, Tyr, Phe and His), decreased *m*-Inositol and increased hypoxanthine (δ 8.19 and δ 8.21) and Un. at δ 7.86 (d).

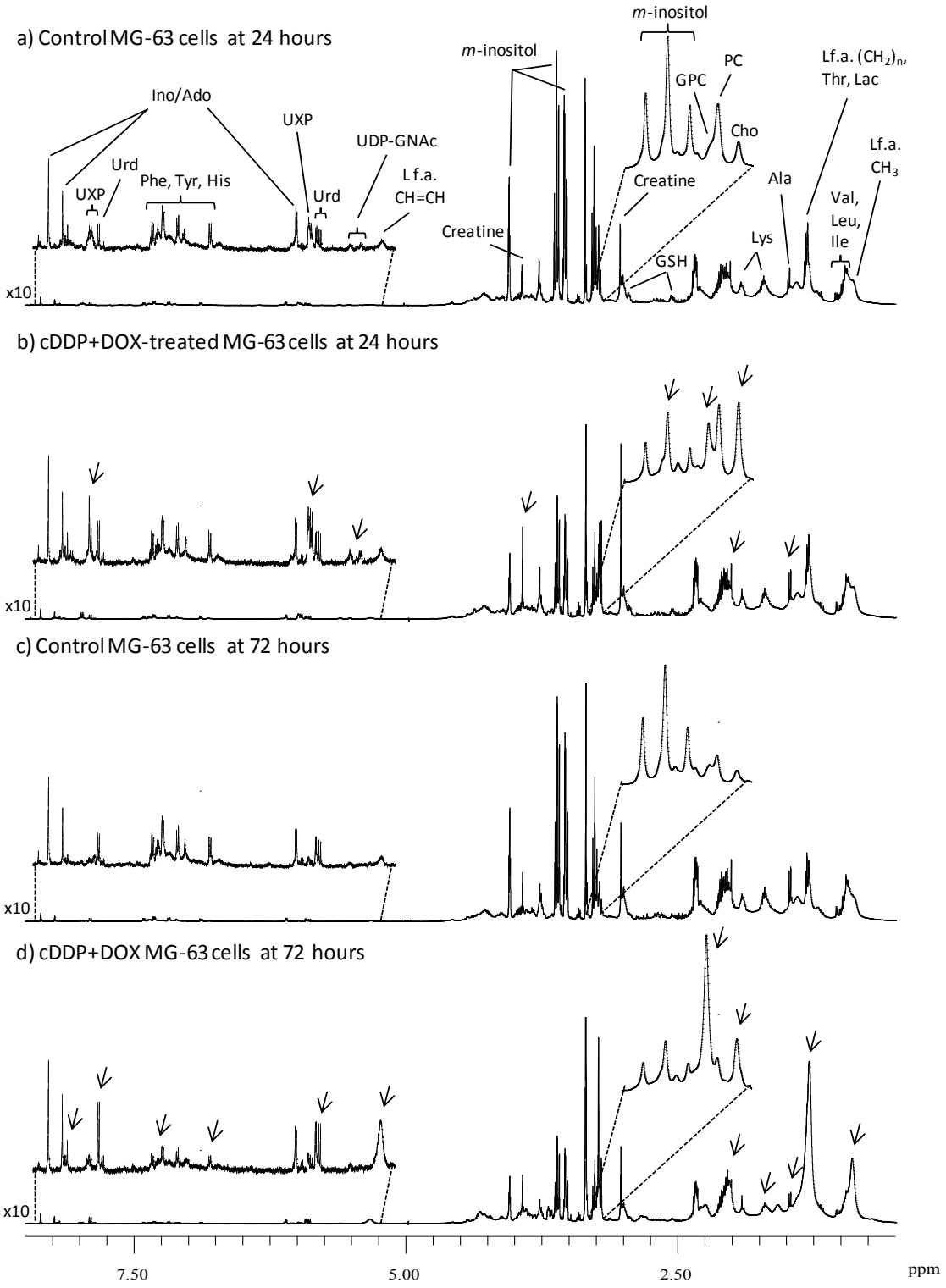

Figure 7.3. Average 500 MHz ^{1}H HRMAS NMR spectra of MG-63 cells: a) control and b) exposed to cDDP+DOX, at 24 hours; c) control and d) exposed to cDDP+DOX, at 72 hours. Insets show expansions of choline compounds (3.2-3.3 ppm) and aromatic (5.2-8.5 ppm) regions. Main assignments are noted and visible spectral changes due to drug exposure are marked by arrows.

Changes in acetates (δ 1.92 and δ 2.02) show some fluctuations over time, with frequent dispersion between samples. At 96 hours there are some variations that deserve special attention: all choline compounds (Cho, PC and GPC) are increased relative to the control (including PC) and a new signal (a shoulder of the choline peak) appears at δ 3.21; increases in UDP-GNAc are detectable just for UDP-GalNAc (δ 5.62) since the resonances of these glucosylated metabolites decrease already at 72 hours. No clear changes in GSH were detected between control and treated cells over the 96 hours of the experiment.

According to the cytotoxic results (by the Trypan blue assay), addition of MTX subsequently to the cDDP+DOX cocktail does not induce considerable alterations in MG-63 cells survival. Nevertheless, it is worth investigating if this antimetabolite has indeed no effect on the metabolic profile of MG-63 cells. A comparison with the metabolic changes induced by exposure to MTX alone should be performed. Figure 7.4 compares the average metabolic profile of control, cDDP+DOX- and cDDP+DOX+MTX-treated cells for a total period of 96 hours.

In general, the addition of MTX for 24 hours does not alter the metabolic profile of MG-63 cells treated with only cDDP+DOX for 96 hours. Visual inspection of the results reveals an increase in the NMR signal at δ 7.86 (d) only when MTX is added to the drug cocktail, as well as the absence of the unassigned shoulder of the choline peak (at δ 3.21) with cDDP+DOX treatment. Additionally, the increase in lipids, choline compounds (choline and PC) and uridine seem to be enhanced by MTX administration (Figure 7.4c).

Further investigations on the most relevant metabolic alterations that underlie drug-induced effects were performed by multivariate analysis of the ^{1}H HRMAS spectra of both controls and drug-treated cells with cDDP+DOX and cDDP+DOX+MTX (Figure 7.5). PCA analysis (Figure 7.5a) led to a clear separation between controls and drug-treated cells mostly along PC1. A time course tendency from negative PC1 and PC2 to positive PC1 and PC2 can be clearly assigned for treated samples, whereas no such temporal tendency can be addressed for control samples. Moreover, a clear separation between treated samples is achieved when MTX is added to the 96 hours treatment with cDDP+DOX, strongly suggesting that, despite the absence of considerable changes in Trypan blue results, changes in metabolism do occur as consequence of MTX addition to the cocktail.

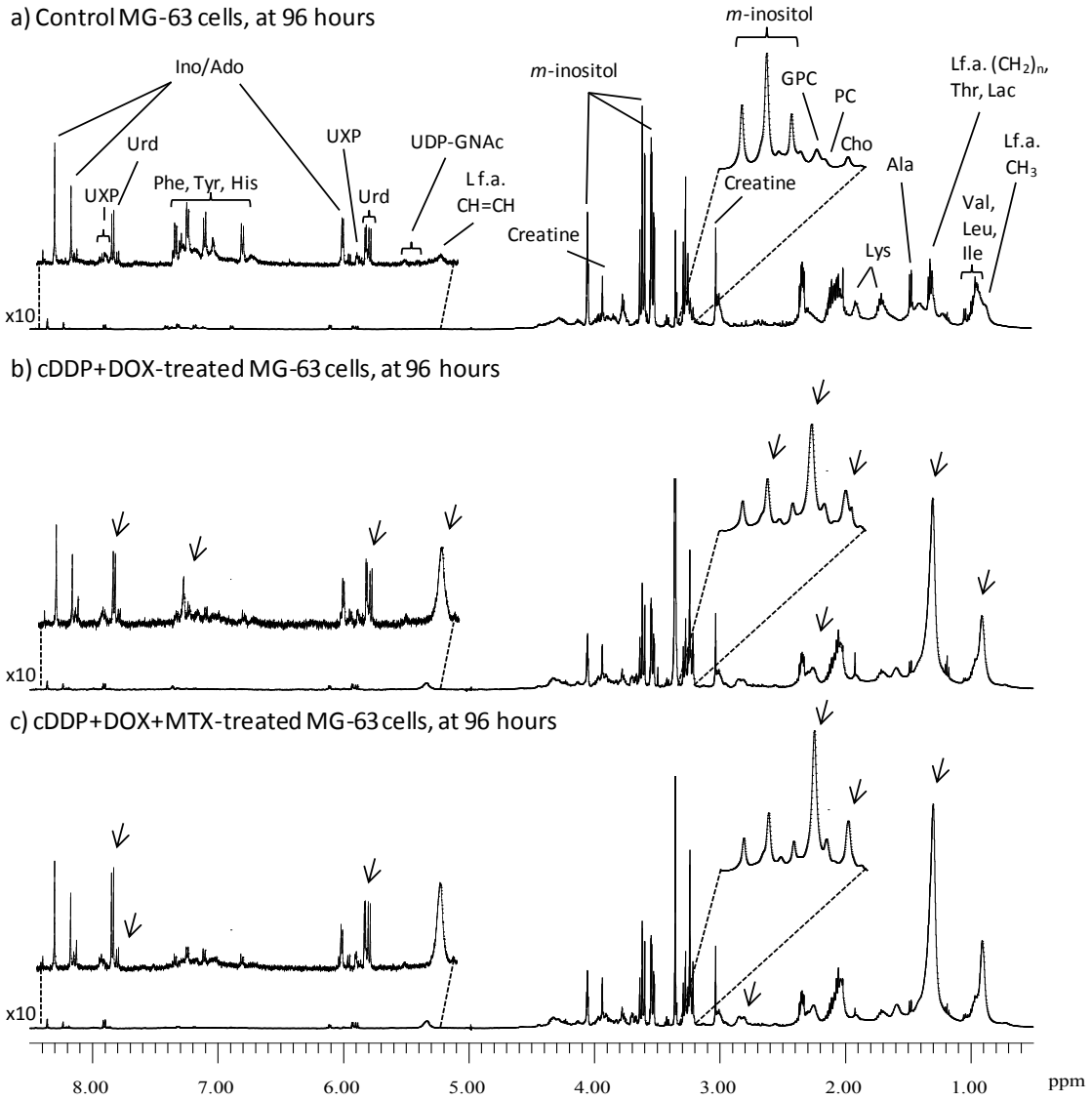

Figure 7.4. Average 500 MHz ^{1}H HRMAS NMR spectra of MG-63 cells, at 96 hours: a) under control conditions, b) exposed to cDDP+DOX and c) exposed to cDDP+DOX+MTX. Insets show expansions of choline compounds (3.2-3.3 ppm) and aromatic (5.2-8.5 ppm) regions. Main assignments are noted and visible spectral changes due to drug exposure are marked by arrows.

For PLS-DA analysis, UV scaled data were chosen since time course tendency of samples in scores plot is similar to that of Ctr scaling, with increased ability to identify variations of lower magnitude. PLS-DA scores plot (Figure 7.5b) showed very good separation between groups (Q^2 0.838, considering only two classes: control and drug-treated) with the maintenance of the time course tendency for treated samples. The robustness of group discrimination achieved was reflected in a very low Q^2 distribution overlap and good MCCV results (97.5% sensitivity, 99.3% specificity and 98.3% classification rate) shown in Figure 7.5c and 7.5d.

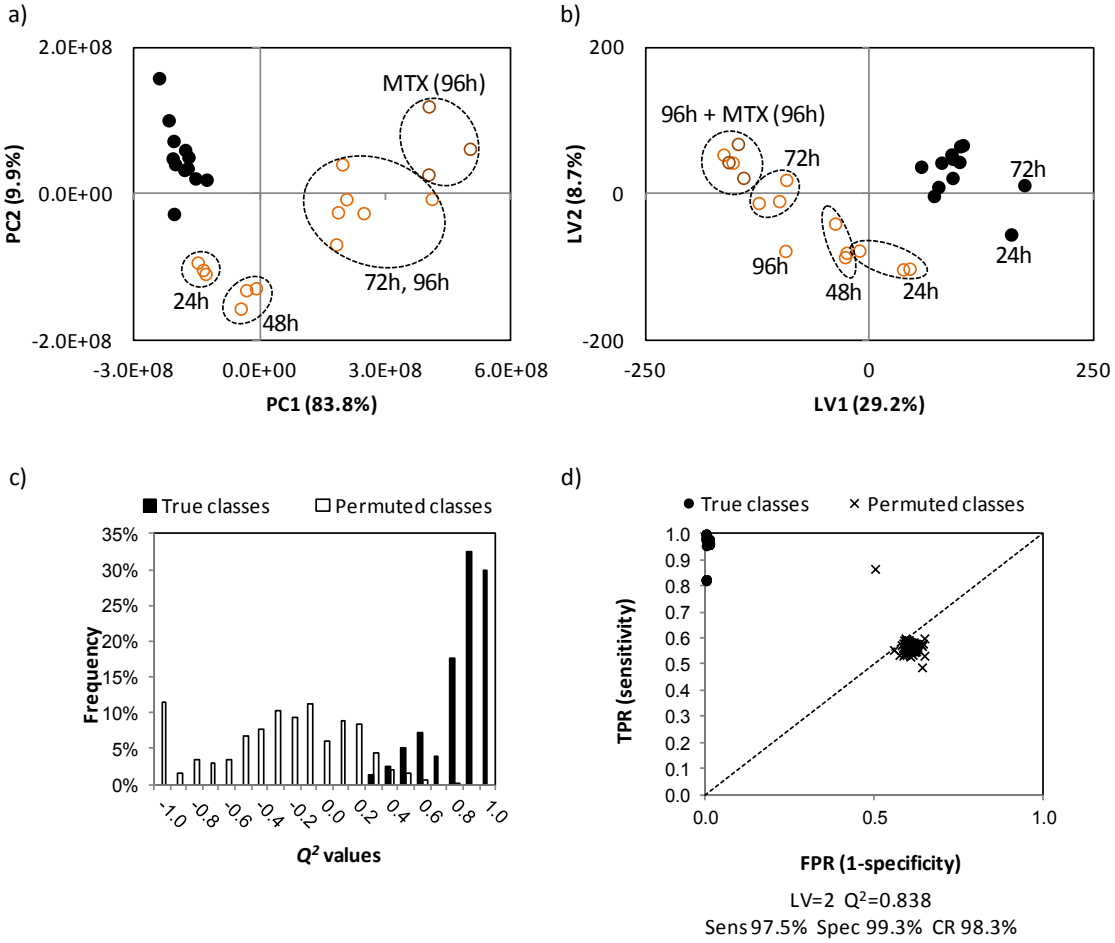

Figure 7.5. Multivariate analysis of controls (●) and cDDP-cocktail treated (○/○) cells: (a) PCA scores plot, Ctr scaled data (b) PLS-DA scores plot , UV scaled model with 2 components calculated with R^2X = 0.379, R^2Y = 0.930 and Q^2 = 0.838. MCCV results of PLS-DA model obtained for MG-63 cells exposed to cDDP-cocktail *vs* control: c) Q^2 distributions and d) ROC plots of true and permuted models. TPR: true positive rate, FPR: false positive rate, Sens.: sensitivity, Spec.: specificity, CR: classification rate.

The identification of the most relevant changes underlying this group separation is assisted by VIP-colored loadings (Figure 7.6). According to this analysis, increased lipid contents, choline compounds, uridine and UDP-GNAc metabolites coupled to significantly decreased *m*-inositol and amino acids contents (namely Ala, Lys, Met, Tyr and Phe) are the most relevant variations induced by cDDP-cocktail treatment in this type of cancer cells. These cDDP-cocktail-induced changes pointed out by MVA, confirm those previously suggested by visual inspection.

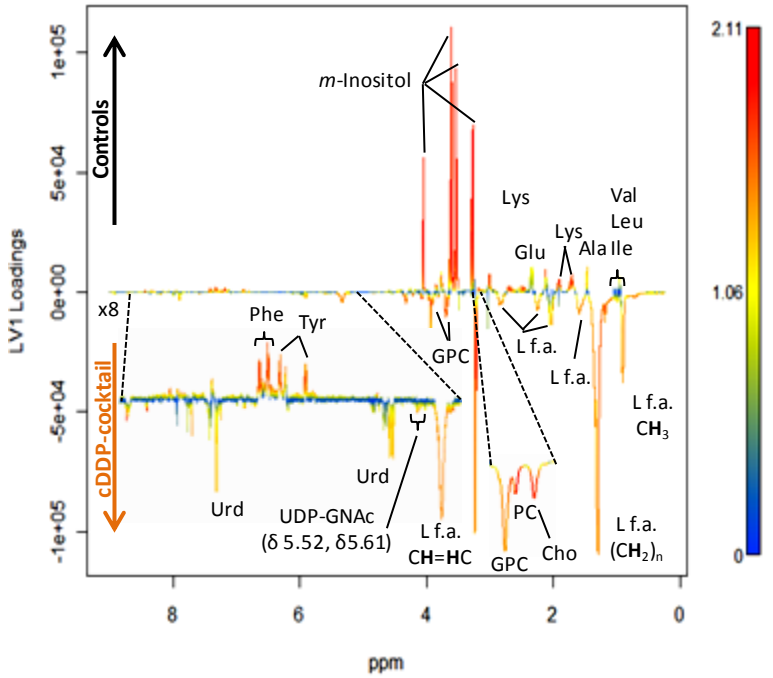

Figure 7.6. Multivariate analysis of controls and cDDP-cocktail-treated cells, using the full spectral range: UV scaled PLS-DA LV1 loadings plot, colored as function of VIP values.

In order to obtain further information on the time course of metabolites in response to cDDP-cocktail treatment, signal integration was performed and time course plots for several metabolites were constructed (Figures 7.7, 7.8 and 7.9).

The time course response of lipids and lipid ratios to cells exposure to cDDP-cocktail is shown in Figure 7.7. The cocktail cDDP+DOX induces a clear increase of all measured resonances which get more pronounced for longer periods of exposure with lipid ratios increasing in the same way. This effect over lipids resembles that of cDDP in sole administration (Figure 5.6, Chapter 5) while for DOX, in the same conditions, only slight increases were registered for PUFA and lipids ratios. Thus, even in combination regimens, cDDP seems to exert a dominant effect in the metabolism of lipids. Remarkably, and despite the absence of this behaviour in sole administration, the addition of MTX to the cDDP-cocktail potentiates this increasing tendency, as observed by the relative increases in CH_3, $(CH_2)_n$, HC=CH and $=CHCH_2CH=$ resonances (the latter is not shown). Although with a reduction in magnitude, this effect of MTX addition over lipids also resulted in a slight increased CH_2/CH_3 ratio (suggesting increased mean chain length of fatty acid chains) and a slight reduction in $HC=CH/CH_3$ (degree of unsaturation) when compared to the

results obtained for cDDP+DOX. This suggests that, in combination regimens, MTX enhances the lipidic response to chemotherapy by the metabolome of cells.

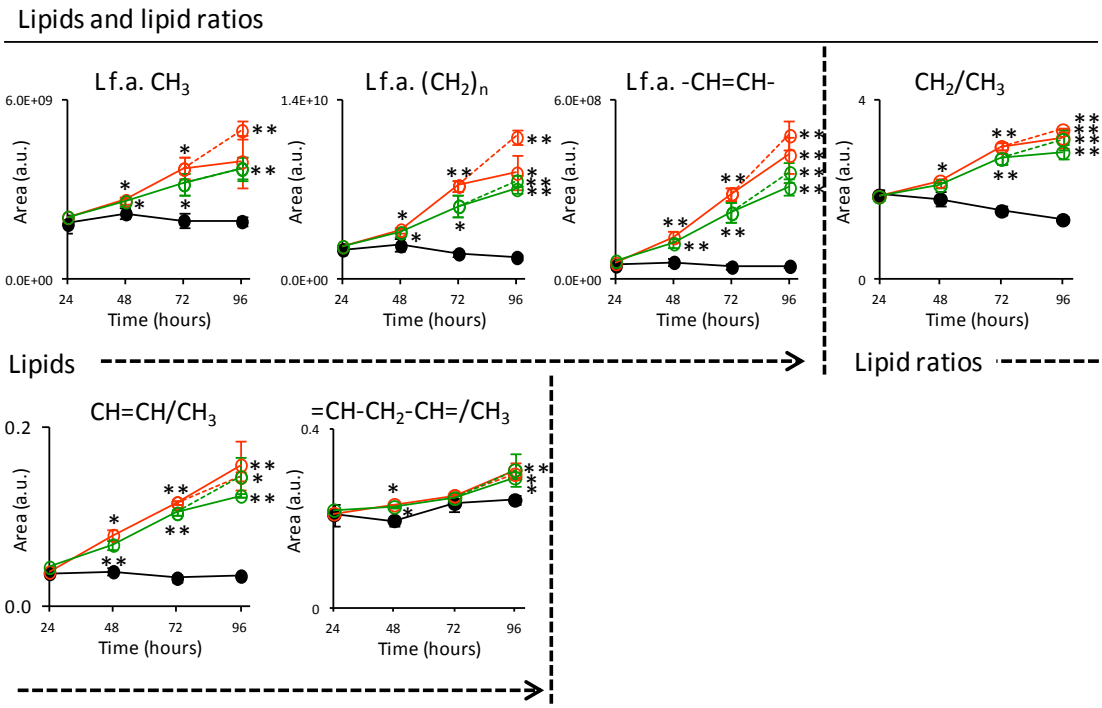

Figure 7.7. Time course of lipids and lipid ratios varying with cDDP- (orange) or Pd_2Spm-cocktail (green) treatments. Dashed lines represent the effect of the addition of MTX to drug-cocktail). *$p < 0.05$ and **$p < 0.01$.

In relation to choline compounds (Figure 7.8), increases in choline and GPC had already been seen as a consequence of cDDP or DOX in sole administration, thus suggesting a synergistic effect of these two drugs over these compounds. However, slight decreases in PC and the absence of variations in PE upon combined treatment are coincident to DOX-treatment (Figure 5.10, Chapter 5), pointing to a slight dominant effect of DOX over choline compounds when used in combination with cDDP. Choline compound ratios (Figure 7.8) behave similarly to when the two drugs are administered alone (Figures 5.6 and 5.10, Chapter 5). When MTX is added to the cDDP-based cocktail, only the PC levels seem to be slightly enhanced, but no significant influence is observed on choline compound ratios.

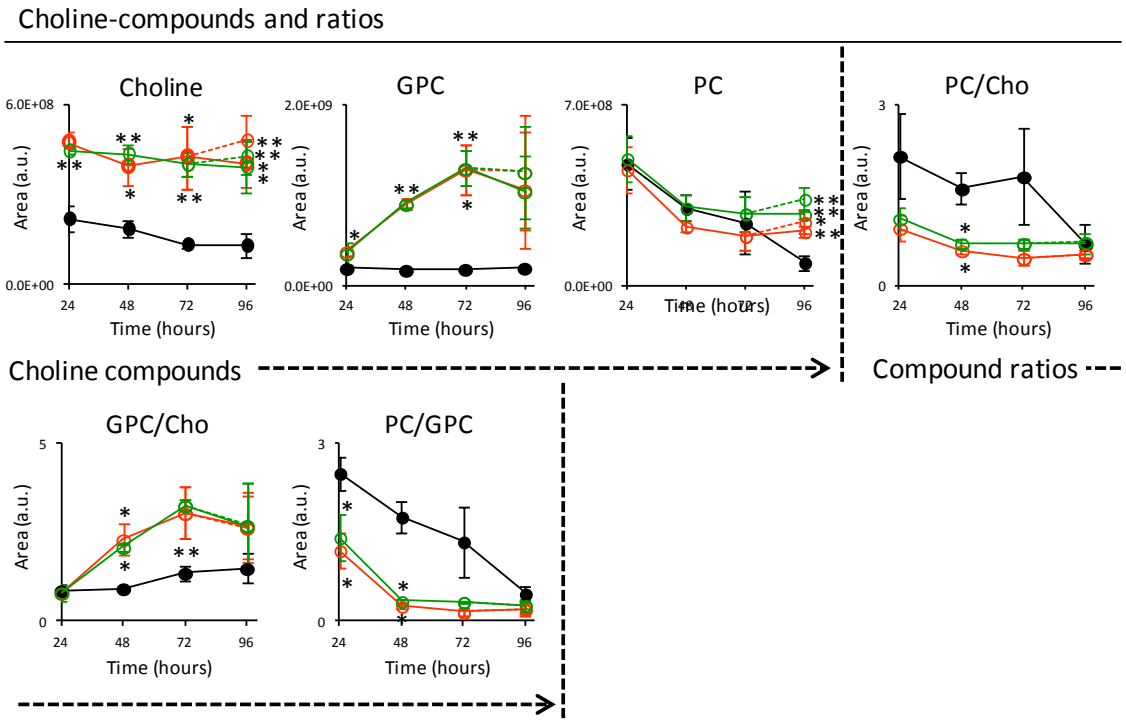

Figure 7.8. Time course of choline-compounds and ratios varying with cDDP- (orange) or Pd_2Spm-cocktail (green) treatments. Dashed lines represent the effect of the addition of MTX to drug-cocktail. *p < 0.05 and **p < 0.01.

In general, a time-dependent decrease of amino acids is observed upon cells' exposure to cDDP+DOX (with the exception of Ile, for which increases are seen at 72 and 96 hours) (Figure 7.9). The alterations induced by this cDDP-based cocktail at 48 hours more closely reflect those resulting from single exposure to DOX (Figure 5.10, Chapter 5), but the measured decreases in Gly, Lys and Thr were also detected upon cells' treatment with 30 µM cDDP (Figure 5.6, Chapter 5). On the other hand, the absence of variations in Tyr and the decrease in Val upon cDDP+DOX were not coincident with those registered for single drug administration (with either cDDP or DOX). Interestingly, the majority of the variations detected in amino acids upon addition of MTX to the cocktail, although small, seem to reduce the differences between treated and control cells. Exception for the branched amino acids Val and Ile, for which MTX addition potentiate the difference between treated and control cells, in relation to what happens upon treatment with cDDP+DOX. Nevertheless, single administration of MTX (section 5.2.3, Chapter 5) did not result in any significant change of Val or Ile levels, thus suggesting some degree of synergism of cDDP+DOX+MTX combination over amino acids variation upon treatment.

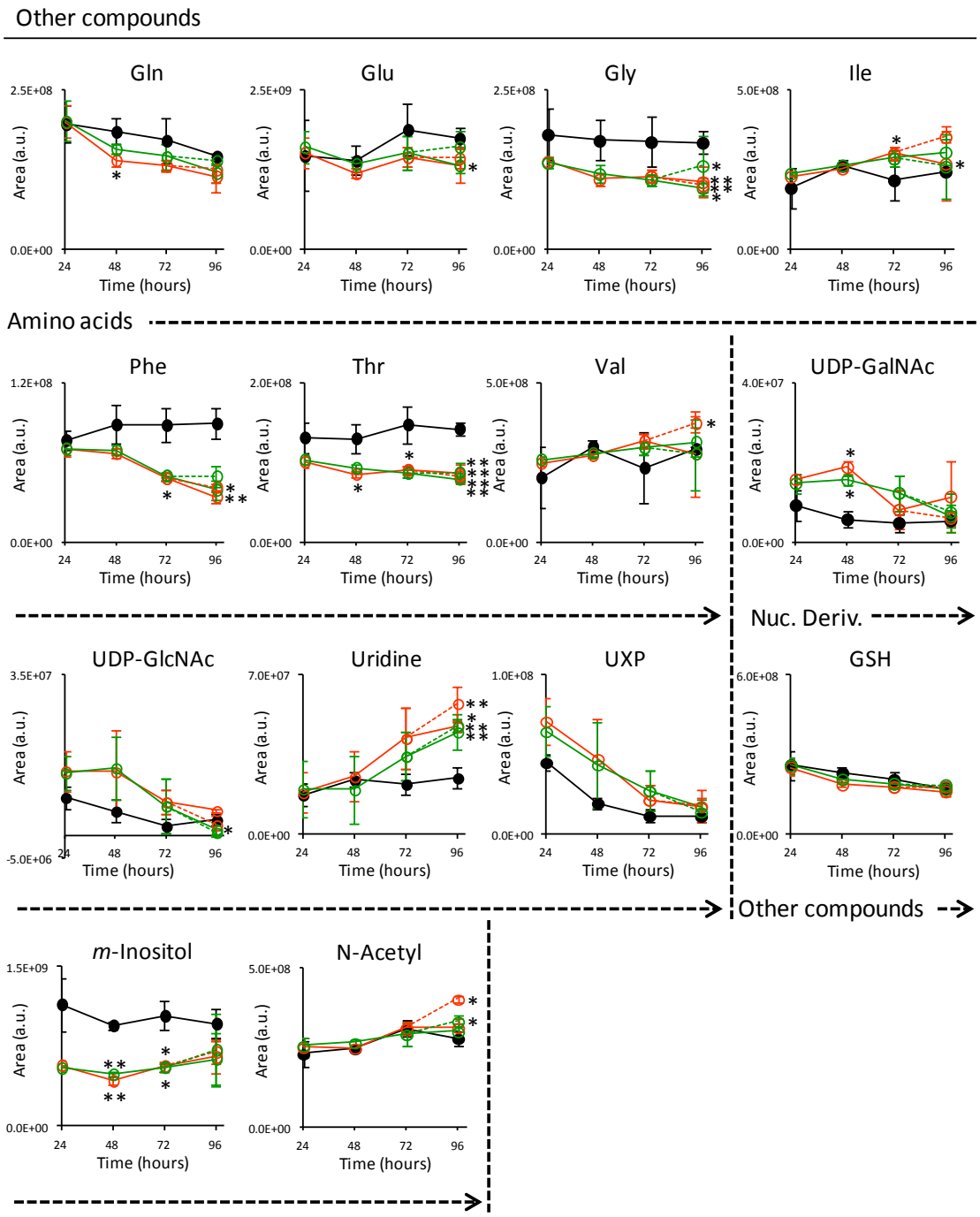

Figure 7.9. Time course of other compounds varying with cDDP- (orange) or Pd_2Spm-cocktail (green) treatments. Dashed lines represent the effect of the addition of MTX to drug-cocktail. *p < 0.05 and **p < 0.01.

7.2.2. Pd_2Spm-Cocktail

As mentioned before, and similarly to what was observed for cDDP-cocktail experiments, a marked decrease of MG-63 cells survival was determined by the Trypan blue assay after administration of the Pd_2Spm-cocktail. The following results describe the metabolic changes that accompany the corresponding drug-induced growth inhibition of MG-63 cells.

The metabolic impact of the Pd_2Spm-based cocktail was studied following the same experimental setup and sample collection scheme as that referred for cDDP-cocktail studies. Visual inspection of drug-treated *vs* control samples at 24 hours (Figure 7.10a and 7.10b) revealed significant drug-induced alterations: marked increases of choline, GPC, uridine, UXP and glucosylated derivatives (both at δ 5.52 and δ 5.62), increased alanine and significant changes in other metabolites (namely increased creatine and decreased *m*-inositol). When comparing the metabolic profile of Pd_2Spm+DOX-treated cells with that of controls, for increasing periods of drug-exposure, it becomes clear that the metabolic changes observed at 72 and 96 hours are the same to those detected at 48 hours of treatment, but with an increased magnitude. In general, an increase in all lipid signals, choline, GPC, hypoxanthine and UN (δ 7.86, d), as well as in nucleotides and its derivatives (Ino/Ado, UXP, UDP-GNAc and uridine), and a global decrease in amino acids (Ala, Lys, Glu, Gln, Thr, Gly, Tyr, Phe and His). Despite the maintenance of increased UDP-glucosylated metabolites in treated cells, at 72 and 96 hours the intensity of these resonances were found to undergo a marked decrease such as that at 96 hours only UDP-GalNAc (δ 5.62) was detected. Resonances assigned to acetates (δ 1.92 and δ 2.02) suffer some fluctuations upon chemotherapy administration, but the dispersion between samples makes it difficult to address the direction of the change. These described changes for MG-63 cells upon Pd_2Spm+DOX-treatment are coincident with those detected upon cDDP+DOX-treatment, evidencing that Pd_2Spm may be an interesting alternative to cDDP, namely in combination with DOX. In other words, Pd_2Spm seems to substitute cDDP efficiently when combined with DOX, as viewed by HRMAS metabolomics of treated MG-63 cells.

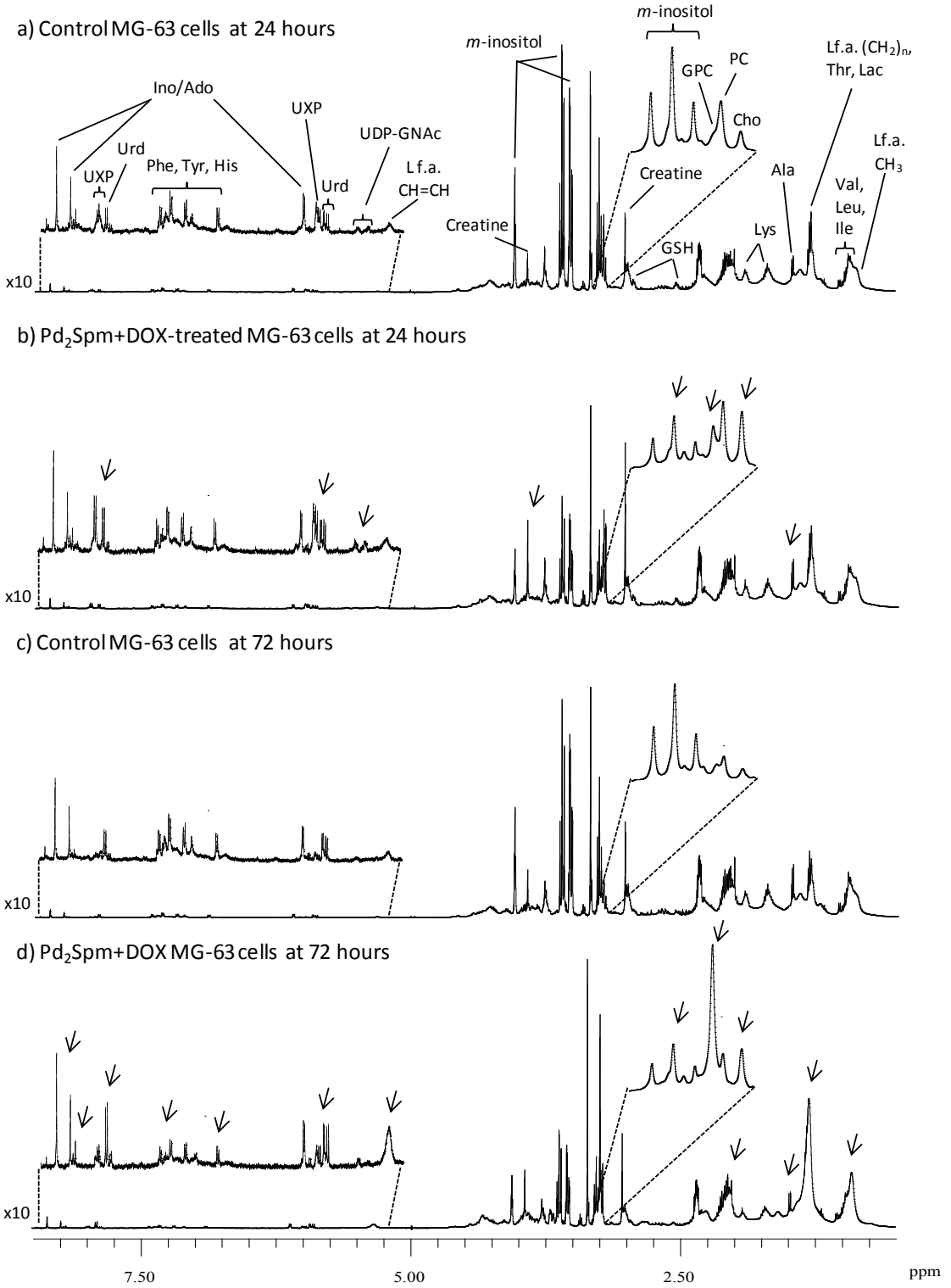

Figure 7.10. Average 500 MHz ^{1}H HRMAS NMR spectra of MG-63 cells: a) control and b) exposed to Pd_2Spm+DOX, at 24 hours; c) control and d) exposed to Pd_2Spm+DOX, at 72 hours. Insets show expansions of choline compounds (3.2-3.3 ppm) and aromatic (5.2-8.5 ppm) regions. Main assignments are noted and visible spectral changes due to drug exposure are marked by arrows.

Similarly to what was observed for the cDDP+DOX cocktail, addition of MTX to the Pd_2Spm+DOX cocktail does not seem to alter the survival of MG-63 cells (Figure 7.2a). Even so, the metabolic profile of these cells exposed to either Pd_2Spm+DOX or Pd_2Spm+DOX+MTX may unveil eventually (if any) specific metabolic changes associated with MTX addition to the drug cocktail. Figure 7.11 compares the average metabolic profile of the control, Pd_2Spm +DOX and Pd_2Spm+DOX+MTX-treated cells, at 96 hours.

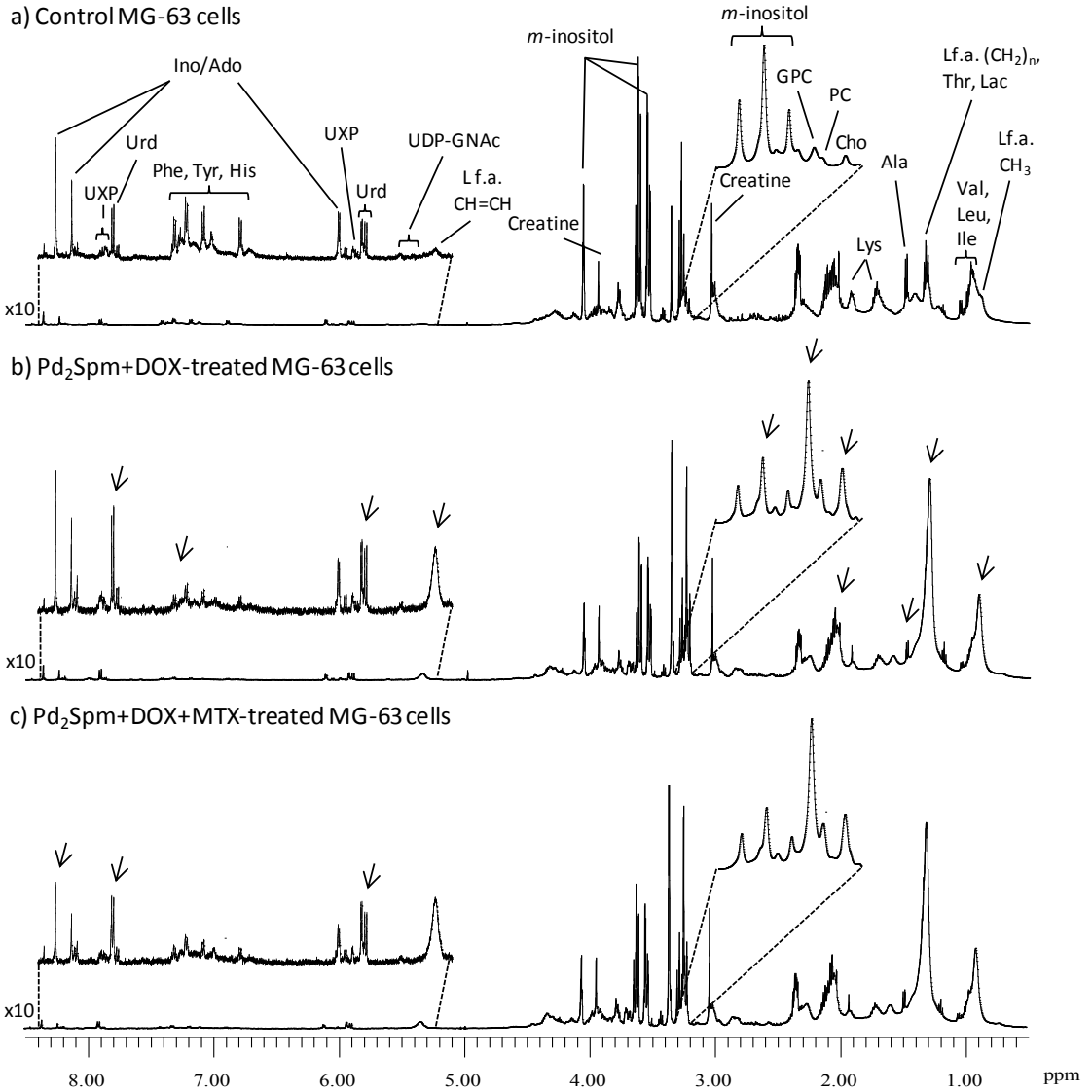

Figure 7.11. Average 500 MHz ^{1}H HRMAS NMR spectra of MG-63 cells, at 96 hours: a) under control conditions, b) exposed to Pd_2Spm+DOX and c) exposed to Pd_2Spm+DOX+MTX. Insets show expansions of choline compounds (3.2-3.3 ppm) and aromatic (5.2-8.5 ppm) regions. Main assignments are noted and visible spectral changes due to drug exposure are marked by arrows.

The addition of MTX to the Pd_2Spm+DOX-cocktail globally preserves the metabolic changes attributed to the treatment with Pd_2Spm+DOX: an increase in lipids and choline compounds, slight

increase in uridine, UXP and UDP-GNAc, and a global decrease in amino acids and *m*-Inositol. However, a decrease in Ino/Ado was observed only after treatment with the MTX-containing cocktail (Figure 7.11c), which seems to be a marker for this particular drug combination (as it did not occur for cDDP+DOX+MTX-treated cells, Figure 7.4c).

The results from multivariate analysis of the ^{1}H HRMAS spectra of controls and drug-treated cells, both with Pd_2Spm+DOX and Pd_2Spm+DOX+MTX are presented in Figure 7.12.

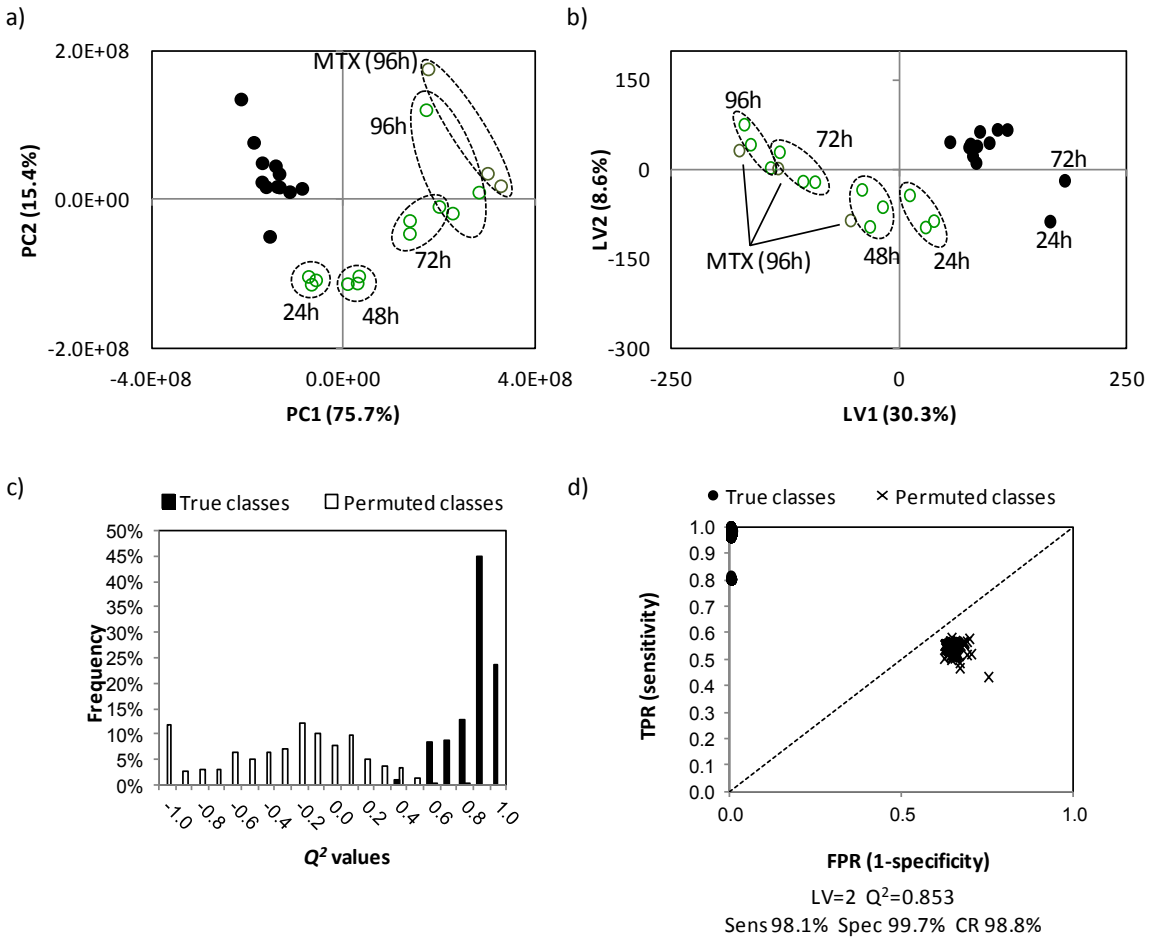

Figure 7.12. Multivariate analysis of controls (●) and Pd_2Spm-cocktail treated (○/○) cells, using the full spectral range. (a) PCA scores plot, Ctr scaled,(b) PLS-DA scores plot, UV scaled, 2 components, R^2X = 0.389, R^2Y = 0.925 and Q^2 = 0.853. Monte Carlo Cross-Validation (MCCV) results of PLS-DA model obtained for MG-63 cells exposed to Pd_2Spm-cocktail *vs* control: c) Q^2 distributions and d) ROC plots of true and permuted models. TPR: true positive rate, FPR: false positive rate, Sens.: sensitivity, Spec.: specificity, CR: classification rate.

PCA analysis (Figure 7.12a) resulted in a clear separation between controls and drug-treated cells mostly along PC1. A time course tendency can be clearly assigned for treated samples from negative PC1 and PC2 to positive PC1 and PC2, whereas no such temporal tendency

can be addressed for control samples. Moreover, similarly to what was seen for the cDDP-cocktail, MTX addition to the Pd_2Spm+DOX-treatment induces a separation between samples treated for 96 hours, suggesting metabolic alterations that specifically emerge upon addition of this agent. PLS-DA scores plot (Figure 7.12b) showed a very good separation between control and drug-exposed groups (Q^2 0.853) with the maintenance of the time course tendency for treated samples. The robustness of achieved group discrimination was reflected in a very low Q^2 distribution overlap and good MCCV results (98.1% sensitivity, 99.7% specificity and 98.8% classification rate) shown in Figure 7.12c and 7.12d. These results are once again very similar to those obtained for the multivariate analysis of the data of cDDP-cocktail treated samples.

The loadings analysis (Figure 7.13) yields qualitative information on the metabolic alterations underlying this class separation upon treatment with Pd_2Spm-cocktails: increased lipid contents and choline compounds (Cho, PC and GPC) as well as slight increased uridine and UDP-GNAc (especially the Gal derivative at δ 5.62). Additionally, significantly decreases in amino acids (Ala, Lys, Met, Tyr and Phe) coupled to marked decreases in *m*-inositol seem also to be associated with Pd_2Spm-cocktail treatment.

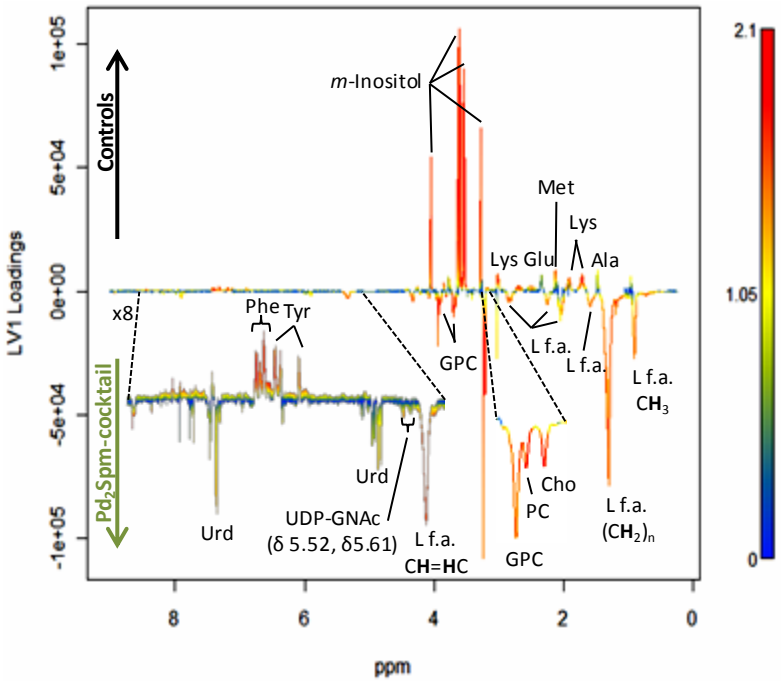

Figure 7.13. Multivariate analysis of controls and Pd_2Spm-cocktail-treated cells, using the full spectral range: UV scaled PLS-DA LV1 loadings plot, colored as function of VIP values.

The plots of the time course variation of several compounds with Pd_2Spm-cocktail treatment were shown in Figures 7.7, 7.8 and 7.9. Concerning lipids (Figure 7.7), Pd_2Spm-cocktail induced a pronounced increase in all measured resonances as well as an increase in all calculated lipid ratios in relation to control conditions. In sole administration Pd_2Spm did not cause lipids increase (Figure 6.6, Chapter 6) but, interestingly, in combination regimen it induces their marked increase, resembling one of the most determinant effects of cDDP, indicating that in combination to DOX, Pd_2Spm might be possibly used in substitution of cDDP. Moreover, MTX addition to the Pd_2Spm-based cocktail also slightly potentiates this increase, resembling once more, the effect of cDDP-based cocktail over these tumour cells.

The time course of choline compounds (Figure 7.8) also show identical time course fluctuations for Pd_2Spm- and cDDP-based cocktails: marked increases in choline and GPC levels and also pronounced increases in PC (although only at 96 hours). Generally, the direction of variation suggests a central role of DOX in the regulation of choline compounds levels, since, in sole administration, Pd_2Spm was found to slightly affect only the PC levels. The addition of MTX to the Pd_2Spm+DOX cocktail seems to slight potentiate the change in PC contents, an interesting result reminding that PC was the only choline compound significantly affected (decrease) by single administration of MTX (Figure 5.14, Chapter 5). Concerning choline compounds ratios (Figure 7.8), marked decreases of PC/Cho and PC/GPC and increased GPC/Cho emerge upon cells exposure to Pd_2Spm+DOX with no further alteration in their levels when MTX is added to the drug cocktail. These alterations in choline compounds ratios are opposite from those found upon single exposure to Pd_2Spm, and thus they arise as consequence of combination with DOX.

In relation to the variation of amino acids (Figure 7.9) in response to Pd_2Spm+DOX treatment, a global decreasing tendency with treatment is seen for Ala, Glu, Gln, Gly, Lys, Phe, Met, Thr and Tyr, while slight increases are only detected for Ile. The time course plots of Gly and Phe, suggest that MTX addition to the Pd_2Spm-based cocktail slightly reduce the magnitude of variation of these amino acids relative to controls, eventually pointing to a special interference of MTX in the pathways in which these metabolites participate.

In response to Pd_2Spm+DOX, concomitant increases in uridine are measured together with a time course decrease of UXP (Figure 7.9). Additionally, Pd_2Spm+DOX-treated cells show increased levels of UDP-GalNAc and UDP-GlcNAc. Interestingly, while a very slight increase in Ino/Ado occurs upon 96 hours treatment with Pd_2Spm+DOX, a slight decrease relative to control

is measured when MTX is added to the cocktail, as already suggested by visual inspection (Figure 7.11c). *M*- and *s*-Inositol markedly decrease with Pd_2Spm+DOX treatment but MTX addition does not interfere with the levels of these compounds. GSH does not seem to be significantly altered by treatment with Pd_2Spm-based cocktail.

7.3. ^{1}H NMR Analysis of TCA Extracts of cDDP- and Pd_2Spm-Cocktail-Treated MG-63 Cells

After HRMAS analysis, samples of both control and treated MG-63 cells with either cDDP+DOX or Pd_2Spm+DOX cocktails for 48 hours were recovered and extracted with TCA, for ^{1}H NMR analysis. This time point was chosen to enable a comparison with the results from single drug exposure. The average spectra of triplicates for each of the three conditions are shown in Figure 7.14. Since TCA extraction was performed with the objective of revealing additional information on nucleic acids and derivatives, the analysis focused on the aromatic region of the spectra.

As indicated in Figure 7.14b (arrows), upon 48 hours treatment with cDDP+DOX a considerable number of alterations is detected in the aromatic region of the spectra: increases in UXP, ADP/ATP and UDP/UTP and decreases in NAD^+. UXP was also found to increase in MG-63 cells exposed to cDDP alone but decreased upon DOX exposure. On the other hand, ADP/ATP dramatically decrease upon single exposure to either cDDP or DOX, revealing a synergistic effect of these two agents when combined. UDP/UTP levels remained essentially stable upon cDDP exposure but markedly decrease upon DOX treatment, once again suggesting a synergistic effect of drug combination. In agreement with the results from cDDP-cocktail, NAD^+ levels decreased in cells exposed to cDDP as well as to DOX.

Regarding Pd_2Spm+DOX-treated cells (Figure 7.14c), the analysis of the extracts reveal the following changes: increases in UXP, ADP/ATP, UDP/UTP and UMP and decreases in uridine, Ino/Ado and NAD^+. In Pd_2Spm-based cocktails, a synergistic effect with DOX seems to account for the increases in ADP/ATP, since these signals are absent from spectra of cells treated with each of the two drugs in sole administration. Increases in UXP in Pd_2Spm+DOX-treated cells, point to drug synergism (as such change is absent in sole administration of these drugs). Decreases in NAD^+ follow those registered in drugs' sole administration.

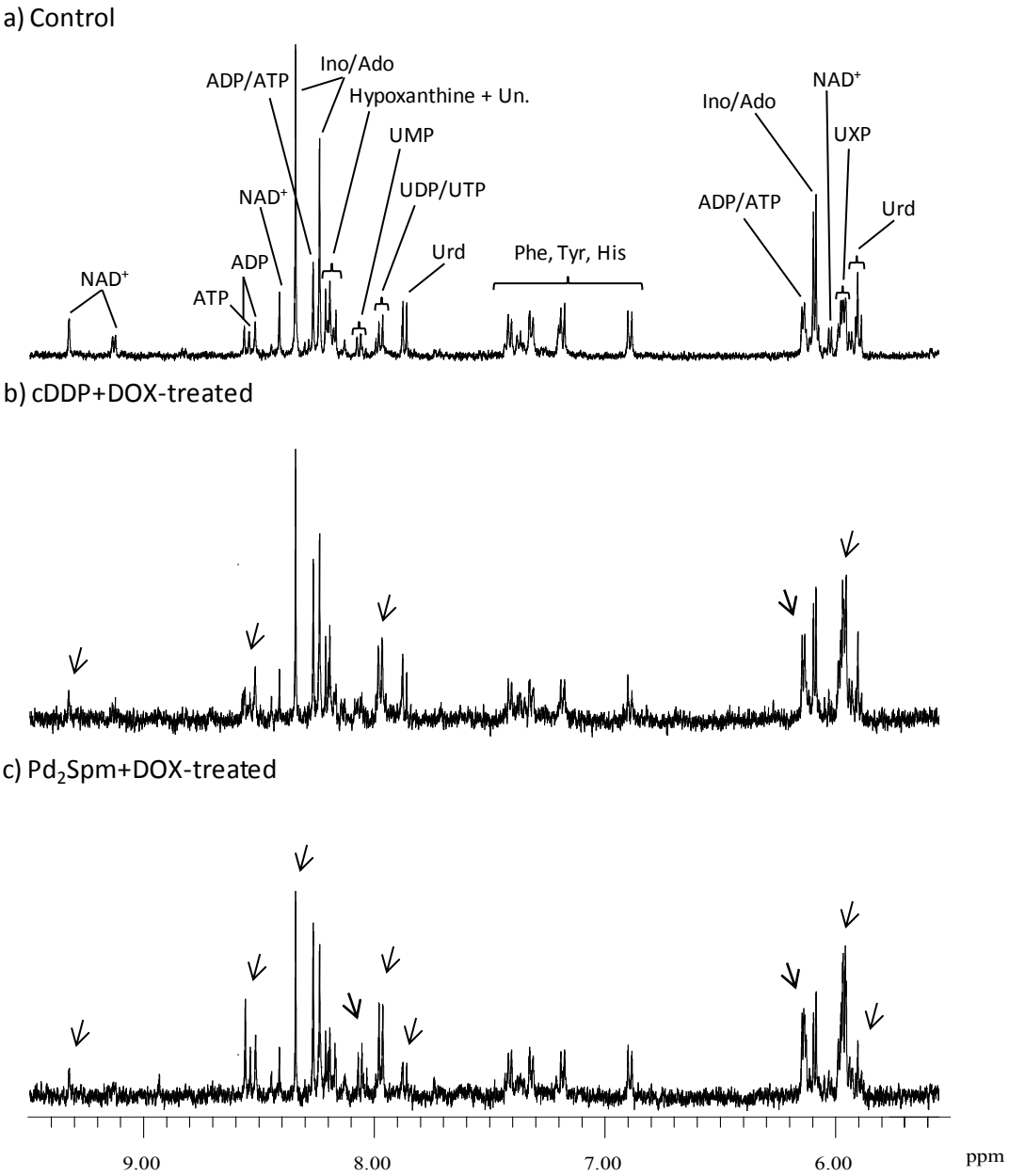

Figure 7.14. Average 500 MHz ^{1}H NMR spectra of TCA extracts of MG-63 cells, at 48 hours: a) under control conditions, b) exposed to cDDP+DOX and c) exposed to Pd_2Spm+DOX. Expansion of aromatic (5.0-9.5 ppm) region is shown. Main assignments are noted and visible spectral changes due to drug exposure are marked by arrows.

The spectra of TCA extracts also show increases in glucose (not detected in the ^{1}H HRMAS NMR spectra of the same cells) in cDDP+DOX treated cells. This may reflect its reduced utilisation by these cells, eventually suggesting a reduction in their energetic demands. This possibility is also supported by the detected accumulation of ADP/ATP, since glucose is needed for the formation of ATP: since both accumulate in cDDP+DOX treated cells, it seems plausible to assume that treated cells are lowering their energetic demands. A similar deduction can help explain the increased

levels of UXP, especially due to increased UDP/UTP (as no relevant changes in UMP are detected). In addition, ATP production requires reduction of NAD^+ to NADH what may explain its decrease upon treatment.

Regarding Pd_2Spm+DOX treatment, similar increases in glucose, UXP, ADP/ATP and UDP/UTP as well as identical NAD^+ decreases were found in relation to cDDP+DOX treatment. However, additional decreases in uridine and Ino/Ado and increases in UMP were detected when cells were treated with the Pd_2Spm-based cocktail. Both uridine and inosine can be used to produce UMP and AMP compounds, respectively, which in turn can generate UDP/UTP and ADP/ATP. Together with the slightly increased accumulation of glucose in relation to that observed in cDDP+DOX and the increased UMP levels (registered for Pd_2Spm+DOX), the decreases in uridine and Ino/Ado possibly point to preferences for distinct pathways involving the synthesis of UXP/AXP compounds according to the metal (Pt or Pd) used in the drug cocktail.

Apart from the compounds that are newly detected by analysis of sample extracts (glucose, ADP/ATP, UMP/UDP/UTP and NAD^+) changes detected for UXP are coincident with those revealed by HRMAS for the treatment with both cDDP- and Pd_2Spm-based cocktails, but no relevant changes were detected in Ino/Ado upon 48 hours treatment with Pd_2Spm+DOX.

7.4. Comparison of the Metabolic Impact of cDDP- and Pd_2Spm-Cocktails

Signal integration results were used to construct two summary tables in which all variations of metabolites and compound ratios (both in % and ES values) are compared, including with those from single drug assays, in order to more easily identify eventual synergistic or antagonistic effects of drug combination.

As already refered, a marked change in lipid levels was measured during the metabolic response of MG-63 cells to both cDDP- and Pd_2Spm-cocktails. In the case of cDDP+DOX combination, this increase seems to result from cDDP action, since a marked increase of lipids was already recognized in Chapter 5, as a characteristic metabolic response of MG-63 cells to cDDP in single administration while no significant variations were detected upon single exposure to DOX. The percentages of variation of lipid resonances at 96 hours exposure to cDDP+DOX are in the range 73-826%, to which correspond ES values of 3.1-6.9. Interestingly, both percentages of variation (106-972%) and ES values (8.4-19.5) suffer very significant increases when MTX is added

to the cDDP+DOX cocktail, although the results in Chapter 5 have shown that, in single administration, MTX does not alter the lipids profile. Nevertheless, when comparing the lipid ratios at 96 hours with and without MTX, identical values are seen. Pd_2Spm+DOX also increase the lipids levels, with maximum increases being registered at 96 hours, ranging from 53-584% and ES values in the range 4.1-18 ES. When MTX is added to the cocktail, no additional variations are detected and both percentage of variation (67-695%) and ES values (4.6-13).

Regarding choline compounds, for cDDP+DOX no significant variations are detected in PE while increases in choline, GPC and PC occur. However, when MTX is added, the positive variations are kept but a negative variation appears in PE (-30.4% and ES value of -1.7). When the analysing the Pd_2Spm+DOX, this negative variation in PE already emerges at 96 hours (-45% and ES of -3.4) and the tendency is preserved when MTX is added.

In terms of amino acids, upon 96 hours of treatment, cDDP+DOX induces decreases is several amino acids (Ala, Glu, Gly, Lys, Met, Phe, Ser, Thr and Tyr) and increases in Ile and Val, all maintained when MTX is added to the drug cocktail. For Pd_2Spm+DOX, at 96 hours, all the previously described decreases in amino acids are seen and an additional negative variation is registered for Gln (-18% and ES value of -1.8), while positive variations are only addressed to Ile. All amino acids variations are kept when MTX is added, with exception of the newly observed variation in Gln, which disappears.

Furthermore, in relation to nucleotides, 96 hours of exposure to cDDP+DOX induces non significant increases of UDP-GlcNAc (59% and ES of 1.6) which disappear upon addition of MTX, giving rise to the new and non significant increase of UXP resonances (58.2%), which is particularly interesting considering that MTX alone did not change it levels. The Pd_2Spm+DOX treatment induces a slight increase of Ino/Ado and UXP at 96 hours (of around 13 and 52%). When MTX is added to this Pd_2Spm-based cocktail, a significant decrease in the former is detected (-16% and ES of -2.8) and, although previous variation in UXP disappears, a newly detected decrease in UDP-GlcNAc (-81% and ES of -2) was significant. This suggests that MTX displays a slightly different influence over nucleotides and derivatives levels, depending on the use of cDDP or Pd_2Spm in the drug cocktail.

Table 7.1: Metabolite and compound ratio variations in MG-63 cells exposed to cDDP-based cocktail for 24, 48, 72 and 96 hours, compared to control cells. * $p < 0.05$, ** $p < 0.01$. Symbols ✓ and ✖ show variations that are in agreement or different, respectively, from those seen in single drugs (**cDDP**, **DOX** and **MTX**).

Metabolite	Signal (δ,ppm)[a]	cDDP+DOX									
		24h		48h		72h		96h		96h+MTX	
		% var.[b]	Effect size[c]	% var.[b]	Effect size[c]	% var.[b]	Effect size[c]	% var.[b]	Effect size[c]	% var.[b]	Effect size[c]
Lipids											
-C<u>H</u>$_3$	0.91	nv	nv	19.7±5.4*✓✖	2.2±0.9	87.8±9.1*	4.40±1.43	102.5±17.5	2.5±1.0	156.2±5.8**✖	10.0±2.9
-(C<u>H</u>$_2$)$_n$	1.30	nv	nv	46.2±9.2*✓✖	2.6±1.0	262.4±6.3**	11.7±3.45	378.2±15.7*	5.4±1.7	538.8±4.9**✖	19.5±5.7
-C<u>H</u>$_2$CH$_2$CO	1.60	nv	nv	16.6±4.3*✓✖	2.3±0.9	78.8±6.8**	5.41±1.69	99.8±14.0*	3.1±1.1	140.4±6.4**✖	8.4±2.5
-C<u>H</u>$_2$COO	2.25	nv	nv	7.3±3.0✓✖	(+)	44.1±5.8*	4.10±1.35	72.7±9.5*	3.7±1.2	105.6±4.5**✖	10.0±3.0
=CHC<u>H</u>$_2$CH=	2.83	13.5±2.5*	3.29±1.15	41.5±3.0**✓✓	7.5±2.2	101.2±8.4*	5.22±1.64	159.4±12.6*	4.6±1.5	217.4±7.5**✓	9.1±2.7
-C<u>H</u>=C<u>H</u>-	5.33	nv	nv	142.3±13.1**✓✖	4.2±1.4	577.3±8.2**	11.9±3.50	826.1±15.2**	6.9±2.1	972.1±11.1**✖	9.8±2.9
Choline and Phospholipids											
Choline	3.21, s	115.0±9.0**	5.30±1.66	110.9±12.9*✓✓	3.6±1.2	216.1±21.5*	3.15±1.12	207.0±19.0*	3.5±1.2	267.2±17.9**✓	4.2±1.4
GPC	3.24, s	98.7±10.3*	4.20±1.38	427.6±7.3**✓✓	12.1±3.6	608.4±21.7*	4.53±1.46	449.6±59.1	(+)	548.6±50.2✓	1.9±0.8
PC	3.23, s	nv	nv	-24.0±11.6✖✓	(-)	nv	nv	133.9±13.6**	3.8±1.3	175.6±19.4*✖	3.2±1.1
PE	3.25, s	nv	nv	nv✖✓	nv	nv	nv	nv	(-)	-30.4±13.8✖	-1.7±0.8
Amino acids											
Alanine	1.48, d	12.6±3.2*	2.42±0.96	nv✖✓	nv	-18.3±8.0	-1.65±0.81	-23.0±8.2	-2.1±0.9	-15.6±5.9✖	-1.9±0.8
Glutamate	2.34, m	31.8±12.7	nv	nv✖✓	nv	-12.1±6.3	(-)	-33.0±5.8*	-1.6±0.8	-17.9±7.8✓	-1.6±0.8
Glutamine	2.45, m	nv	nv	-24.2±7.9*	-2.3±0.9	nv	nv	nv	nv	nv	nv
Glycine	3.56, s	-12.2±5.4	(-)	-35.4±13.7✓✓	-2.1±0.9	nv	nv	-45.1±8.4**	-2.3±0.9	-39.8±9.3**✖	-3.5±1.2
Isoleucine	1.02, d	nv	nv	nv✓	nv	18.5±4.3*	2.05±0.93	36.6±7.7	3.6±1.3	44.3±3.9**✖	6.0±1.8
Lysine	1.72, m	nv	nv	-15.8±2.5*✓✓	-4.4±1.4	-22.0±5.0*	-2.24±0.92	-19.7±6.4	-2.2±0.9	-15.1±3.1*✖	-3.4±1.2
Methionine	2.13, s	nv	nv	-23.7±8.6	-2.0±0.9	-26.5±9.2*	-2.16±0.90	-32.8±4.7**	-5.4±1.7	-26.4±5.1**	-3.9±1.3

Table 7.1 (cont.): Metabolite and compound ratio variations in MG-63 cells exposed to cDDP-based cocktail for 24, 48, 72 and 96 hours, compared to control cells. * $p < 0.05$, ** $p < 0.01$. Symbols ✓ and ✖ show variations that are in agreement or different, respectively, from those seen in single drugs (**cDDP**, **DOX** and **MTX**).

Metabolite	Signal (δ,ppm)[a]	cDDP+DOX									
		24h		48h		72h		96h		96h+MTX	
		% var.[b]	Effect size[c]	% var.[b]	Effect size[c]	% var.[b]	Effect size[c]	% var.[b]	Effect size[c]	% var.[b]	Effect size[c]
Phenylalanine	7.32, d	nv	nv	-24.5±11.2✓✖	-1.6±0.8	-45.6±11.0*	-3.51±1.21	-62.0±11.6**	-5.1±1.6	-53.7±10.4*✖	-4.6±1.5
Serine	3.84, d	nv	nv	-14.3±5.8	-1.7±0.8	-21.8±6.3*	-2.53±0.98	-23.9±7.5	-2.4±0.9	-23.9±4.6*	-3.8±1.3
Taurine	3.42, t	nv	nv	nv✓	nv	nv	nv	nv	nv	nv✖	nv
Threonine	3.58, d	-23.3±10.2	-1.69±0.82	-34.5±10.3*✓✓	-2.6±1.0	-38.7±11.4*	-2.75±1.03	-39.9±7.7**	-4.2±1.4	-41.8±5.1**✖	-6.7±2.1
Tyrosine	6.89, d	nv	nv	nv✖✖	(-)	-45.3±19.6	-1.95±0.86	-65.6±26.1	-2.4±1.0	-61.8±25.4✖	-2.3±0.9
Valine	1.05, d	-3.9±1.9	nv	-9.3±4.6✖✖	(-)	nv	nv	20.6±10.1	1.6±0.8	27.7±4.6*✓	3.5±1.2
Nucleotides and derivatives											
Inosine	8.36, s	nv	nv	nv✖✓	nv	nv	nv	nv	nv	nv✓	nv
UDP-GalNAc	5.62, m	71.0±18.4	1.86±0.85	233.3±12.7*	5.5±1.7	nv	nv	nv	nv	nv	nv
UDP-GlcNAc	5.52, m	70.1±25.8	(+)	161.6±56.3✓✓	nv	263.8±51.5	1.92±0.90	59.0±16.0	1.6±0.8	nv✓	nv
UXP	5.99, d	68.5±14.5	1.86±0.84	142.5±44.2✓✓	(+)	121.0±38.5	(+)	nv	nv	58.2±25.9✖	(+)
Uridine	5.89, d	nv	nv	nv✓✓	nv	91.8±25.5	1.61±0.80	91.2±8.4**	4.9±1.6	132.4±12.5**✓	4.2±1.4
Other compounds											
Acetate	1.92, s	nv	nv	nv	nv	nv	nv	nv	nv	-18.5±7.8	-1.7±0.8
Creatine	3.93, s	79.3±9.0*	3.18±1.21	nv✓✖	nv	nv	nv	-19.9±5.6*	-2.5±1.0	nv✖	nv
Formate	8.46, s	nv	nv	47.9±17.4	(+)	nv	nv	nv	nv	nv	(-)
GSH	2.56, m	nv	nv	-18.9±6.5✖✓	-2.1±0.9	nv	nv	nv	nv	nv✓	nv
Hypoxanthine	8.18, s	nv	nv✓	nv✓✓	nv	125.8±16.7*	3.02±1.09	78.8±28.5	(+)	102.9±20.5✓	nv
m-Inositol	4.05, t	-50.0±17.2	-2.53±0.98	-55.0±4.5**✓✓	-10.2±3.0	-45.6±10.3*	-3.74±1.26	-32.5±15.0	-1.7±0.8	-27.7±12.2✖	-1.7±0.8
s-Inositol	3.34, s	-17.1±6.8	(-)	-41.0±12.2✓✓	-2.5±1.0	-71.9±11.9*	(-)	-66.9±27.0	(-)	-49.4±15.8✖	-1.6±0.8

Table 7.1 (cont.): Metabolite and compound ratio variations in MG-63 cells exposed to cDDP-based cocktail for 24, 48, 72 and 96 hours, compared to control cells. * p < 0.05, ** p < 0.01. Symbols ✓ and ✖ show variations that are in agreement or different, respectively, from those seen in single drugs (**cDDP**, **DOX** and **MTX**).

Metabolite	Signal (δ,ppm)[a]	cDDP+DOX									
		24h		48h		72h		96h		96h+MTX	
		% var.[b]	Effect size[c]	% var.[b]	Effect size[c]	% var.[b]	% var.[b]	Effect size[c]	% var.[b]	Effect size[c]	% var.[b]
N-acetyl	2.02, s	nv	nv	nv✖✓	nv	nv	nv	nv	(+)	44.0±4.1**✖	5.8±1.8
		Controls	**Drug**	**Controls**	**Drug**	**Controls**	**Drug**	**Controls**	**Drug**	**Controls**	**Drug**
Lipid ratios											
CH_2/CH_3		1.88±0.10	1.86±0.04	1.80±0.15	2.20±0.05*✓✖	1.54±0.12	2.96±0.09**	1.34±0.05	3.16±0.22**	1.34±0.05	3.34±0.05**✖
$CH{=}CH/CH_3$		0.04±0.00	0.04±0.00	0.04±0.01	0.08±0.01**✓✓	0.03±0.00	0.12±0.00**	0.04±0.00	0.16±0.03*	0.04±0.00	0.14±0.01**✖
$=CHCH_2CH=/\ CH_3$		0.21±0.03	0.21±0.01	0.19±0.01	0.23±0.00*✓✓	0.23±0.02	0.25±0.01	0.24±0.01	0.31±0.02*	0.24±0.01	0.30±0.01**✓
Choline compounds ratios											
PC/Cho		2.15±0.69	0.95±0.21	1.61±0.26	0.58±0.04*✓✓	1.81±0.80	0.45±0.12	0.68±0.32	0.52±0.07	0.68±0.32	0.51±0.07✓
GPC/Cho		0.86±0.18	0.80±0.05	0.92±0.07	2.29±0.42*✓✓	1.35±0.21	3.03±0.73	1.48±0.41	2.65±0.99	1.48±0.41	2.61±0.89✖
PC/GPC		2.49±0.28	1.19±0.31*	1.75±0.26	0.25±0.26*✓✓	1.34±0.60	0.15±0.06	0.46±0.12	0.20±0.10	0.46±0.12	0.20±0.09✓

[a] resonance chosen for signal integration, [b] % of variation and [c] effect size in relation to control cells.

Table 7.2: Metabolite and compound ratio variations in MG-63 cells exposed to Pd_2Spm-based cocktail for 24, 48, 72 and 96 hours, compared to control cells. * $p < 0.05$, ** $p < 0.01$. Symbols ✓ and ✖ show variations that are in agreement or different, respectively, from those seen in single drugs (**Pd_2Spm**, **DOX** and **MTX**).

Metabolite	Signal (δ,ppm)[a]	Pd_2Spm+DOX									
		24h		48h		72h		96h		96h+MTX	
		% var.[b]	Effect size[c]	% var.[b]	Effect size[c]	% var.[b]	Effect size[c]	% var.[b]	Effect size[c]	% var.[b]	Effect size[c]
Lipids											
-C<u>H</u>$_3$	0.91	nv	nv	18.1±5.2*✖✖	2.1±0.9	61.5±10.2*	3.02±1.09	91.0±7.8**	5.2±1.6	89.7±8.8**✖	4.6±1.5
-(C<u>H</u>$_2$)$_n$	1.30	nv	nv	38.1±10.0*✖✖	2.1±0.9	183.4±12.5*	5.01±1.59	305.3±4.4**	18.0±5.2	342.7±6.2**✖	13.2±3.9
-C<u>H</u>$_2$CH$_2$CO	1.60	nv	nv	13.4±4.0✖✖	2.0±0.9	53.5±8.3*	3.32±1.16	79.9±8.5*	4.4±1.4	86.7±4.3**✖	9.2±2.7
-C<u>H</u>$_2$COO	2.25	nv	nv	6.0±2.6✖✖	(+)	26.1±6.6	2.29±0.93	52.9±6.6**	4.1±1.4	67.1±4.2**✖	7.8±2.4
=CHC<u>H</u>$_2$CH=	2.83	18.1±1.2**	9.13±2.71	36.6±2.8**✓✖	7.2±2.2	69.4±11.0*	3.07±1.01	130.7±8.4**	6.2±1.9	142.5±4.3**✓	12.6±3.7
-C<u>H</u>=C<u>H</u>-	5.33	33.3±8.7	2.15±0.90	107.0±13.0**✖✖	3.5±1.2	423.6±15.1**	5.88±1.82	583.8±8.7**	11.2±3.3	695.3±9.0**✖	11.3±3.3
Choline and Phospholipids											
Choline	3.21, s	102.5±7.5**	5.92±1.83	133.8±9.5*✓✖	6.5±2.2	198.3±8.9**	7.32±2.21	199.6±21.2*	3.1±1.1	256.5±17.0**✓	4.3±1.4
GPC	3.24, s	84.6±26.1	(+)	429.3±3.5**✓✖	25.7±7.4	616.0±15.4**	6.40±1.96	437.3±37.8	2.4±1.0	548.9±40.5✓	2.4±0.9
PC	3.23, s	nv	nv	nv✖✖	nv	nv	nv	209.2±11.2**	6.0±1.8	275.6±14.8**✖	5.1±1.6
PE	3.25, s	nv	nv	nv✓✓	(-)	nv	nv	-44.9±11.2*	-3.4±1.2	-26.3±12.8✖	(-)
Amino acids											
Alanine	1.48, d	16.4±4.9	2.03±0.88	nv✓✓	nv	-18.3±7.0	-1.89±0.85	-22.7±9.6	-1.7±0.8	-18.4±6.4✖	-2.1±0.9
Glutamate	2.34, m	39.0±12.5	nv	nv✓✓	nv	nv	nv	-24.2±7.3*	-2.4±1.0	-15.2±6.6✓	nv
Glutamine	2.45, m	nv	nv	nv	(-)	nv	nv	-17.7±7.1	-1.8±0.8	nv	nv
Glycine	3.56, s	-13.4±6.2	(-)	-30.4±13.8✓✓	-1.7±0.8	nv	-1.68±0.81	-42.3±8.5*	-4.1±1.4	-37.1±9.4*✖	-2.8±1.1
Isoleucine	1.02, d	3.7±1.5	(+)	nv✓	nv	12.6±5.9	(+)	24.7±9.0	1.6±0.8	29.8±8.6✖	2.7±1.1
Lysine	1.72, m	nv	nv	-14.0±2.8*✓✓	-3.6±1.2	-23.3±4.0**	-4.30±1.40	-20.8±8.1	-1.9±0.8	-17.0±4.3**✖	-2.8±1.1
Methionine	2.13, s	nv	nv	-17.8±8.7	-1.5±0.8	-24.3±9.1	-1.99±0.87	-32.1±5.3**	-4.7±1.5	-21.6±5.3*	-3.0±1.1

Table 7.2 (cont.): Metabolite and compound ratio variations in MG-63 cells exposed to Pd_2Spm-based cocktail for 24, 48, 72 and 96 hours, compared to control cells. * $p < 0.05$, ** $p < 0.01$. Symbols ✓ and ✖ show variations that are in agreement or different, respectively, from those seen in single drugs (Pd_2Spm, DOX and MTX).

Metabolite	Signal (δ,ppm)[a]	Pd_2Spm+DOX									
		24h		48h		72h	96h			96h+MTX	
		% var.[b]	Effect size[c]	% var.[b]	Effect size[c]	% var.[b]	% var.[b]	Effect size[c]	% var.[b]	Effect size[c]	% var.[b]
Phenylalanine	7.32, d	nv	nv	nv✓✓	(-)	-43.3±11.1*	-3.26±1.15	-56.2±12.1*	-4.2±1.4	-44.7±11.8✖	-3.2±1.1
Serine	3.84, d	nv	nv	-11.1±5.4✖	(-)	-21.4±4.6*	-3.36±1.17	-26.4±6.6*	-3.0±1.1	-21.9±3.3*	-4.9±1.6
Taurine	3.42, t	nv	nv	nv✓✓	nv	nv	nv	nv	nv	nv✖	nv
Threonine	3.58, d	-21.0±10.0	(-)	-28.5±10.1✓✓	-2.2±0.9	-41.4±11.6*	-2.94±1.07	-44.4±4.9**	-7.6±2.3	-38.6±7.2**✖	-4.3±1.4
Tyrosine	6.89, d	nv	nv	nv✖✖	(-)	-41.6±19.1	-1.79±0.83	-67.7±26.2	-2.6±1.0	-57.7±27.4✖	-1.9±0.9
Valine	1.05, d	nv	nv	nv✓✓	nv	nv	nv	nv	nv	nv✓	(+)
Nucleotides and derivatives											
Inosine	8.36, s	nv	nv	nv✓✖	nv	nv	nv	13.4±5.7	(+)	-15.5±4.0*✖	-2.8±1.0
UDP-GalNAc	5.62, m	60.2±21.5	(+)	177.0±12.7*	4.8±1.5	160.8±35.0	1.66±0.81	nv	nv	nv	nv
UDP-GlcNAc	5.52, m	64.3±23.1	(+)	178.3±41.3✓✖	(+)	219.5±83.1	(+)	nv	(-)	-81.0±4.0*✖	-2.0±0.9
UXP	5.99, d	53.3±16.5	(+)	122.7±49.2✓✖	nv	182.6±39.8	(+)	52.1±25.4	nv	nv✓	nv
Uridine	5.89, d	nv	nv	nv✓✓	nv	55.9±23.5	(+)	81.7±15.2*	2.5±15.2	93.2±8.9**✓	4.7±1.5
Other compounds											
Acetate	1.92, s	nv	nv	nv✓	nv	-27.2±7.1*	-2.91±1.06	nv	nv	nv✓	nv
Creatine	3.93, s	82.6±9.0*	3.26±1.23	18.4±8.7✓✖	(+)	nv	nv	nv	nv	8.10±3.50✖	(+)
Formate	8.46, s	nv	nv	nv	nv	-61.4±26.3*	-2.20±0.91	nv	(-)	nv	nv
GSH	2.56, m	nv	nv	nv✖✖	nv	nv	nv	nv	nv	nv✓	nv
Hypoxanthine	8.18, s	nv	nv	33.9±15.4	(+)	59.1±11.1*	2.69±1.01	86.6±22.2	1.8±0.8	nv	nv
m-Inositol	4.05, t	-52.3±17.3	-2.68±1.01	-48.4±3.7**✓✖	-11.2±3.3	-46.4±10.2*	-3.86±1.29	nv	(-)	nv✓	nv
s-Inositol	3.34, s	nv	nv	-49.6±13.3✓✖	(-)	-39.9±12.2*	-1.78±0.83	-62.9±12.2*	(-)	-61.5±14.6✖	-1.7±0.8

Table 7.2 (cont.): Metabolite and compound ratio variations in MG-63 cells exposed to Pd_2Spm-based cocktail for 24, 48, 72 and 96 hours, compared to control cells. * $p < 0.05$, ** $p < 0.01$. Symbols ✓ and ✖ show variations that are in agreement or different, respectively, from those seen in single drugs (Pd_2Spm, DOX and MTX).

Metabolite	Signal (δ,ppm)[a]	Pd_2Spm+DOX									
		24h		48h		72h		96h		96h+MTX	
		% var.[b]	Effect size[c]	% var.[b]	Effect size[c]	% var.[b]	% var.[b]	Effect size[c]	% var.[b]	Effect size[c]	% var.[b]
N-acetyl	2.02, s	nv	nv	7.6±3.0✖	1.6±0.8	nv	nv	nv	nv	19.2±5.7*	2.0±0.9
		Controls	**Drug**	**Controls**	**Drug**	**Controls**	**Drug**	**Controls**	**Drug**	**Controls**	**Drug**
Lipid ratios											
$C\underline{H}_2/C\underline{H}_3$		1.88±0.10	1.85±0.03	1.80±0.15	2.11±0.05✖✖	1.54±0.12	2.70±0.12**	1.34±0.05	2.84±0.16**	1.34±0.05	3.13±0.23**✖
$C\underline{H}$=$C\underline{H}/C\underline{H}_3$		0.04±0.00	0.04±0.00	0.04±0.01	0.07±0.01**✓✖	0.03±0.00	0.11±0.00**	0.04±0.00	0.12±0.00**	0.04±0.00	0.14±0.02*✖
=$CHC\underline{H}_2CH$=/ $C\underline{H}_3$		0.21±0.03	0.22±0.00	0.19±0.01	0.22±0.00*✓✓	0.23±0.00	0.24±0.01	0.24±0.01	0.29±0.00*	0.24±0.01	0.31±0.04✓
Choline compounds ratios											
PC/Cho		2.15±0.69	1.11±0.18	1.61±0.26	0.69±0.09*✓✖	1.81±0.80	0.70±0.08	0.68±0.32	0.71±0.16	0.68±0.32	0.72±0.02✖
GPC/Cho		0.86±0.18	0.79±0.22	0.92±0.07	2.07±0.11*✓✖	1.35±0.21	3.24±0.16**	1.48±0.41	2.65±1.20	1.48±0.41	2.69±1.21✖
PC/GPC		2.49±0.28	1.41±0.39*	1.75±0.26	0.33±0.03*✓✖	1.34±0.60	0.22±0.02	0.46±0.12	0.27±0.07	0.46±0.12	0.27±0.11✓

[a] resonance chosen for signal integration, [b] % of variation and [c] effect size in relation to control cells.

Regarding other compounds, acetate (δ 1.92) and N-acetyl (δ 2.02) resonances remain unchanged upon 96 hours of exposure to cDDP+DOX, but are altered when MTX is added, particularly N-acetyl (44% and ES value of 5.8). MTX action also leads to the disappearance of the significant variation in creatine at 96 hours of treatment with cDDP+DOX (-20% and ES value of -2.5). Pd_2Spm+DOX+MTX induces a similar effect over N-acetyl (increase of 19%, ES of 2) but opposite change in creatine (8%) in relation to Pd_2Spm+DOX at 96 hours.

The effect size values from drug-cocktail variations in relation to control conditions were also calculated from signal integrals, and were used to construct heatmaps of time course response for metabolites and compound ratios (Figure 7.15).

a)

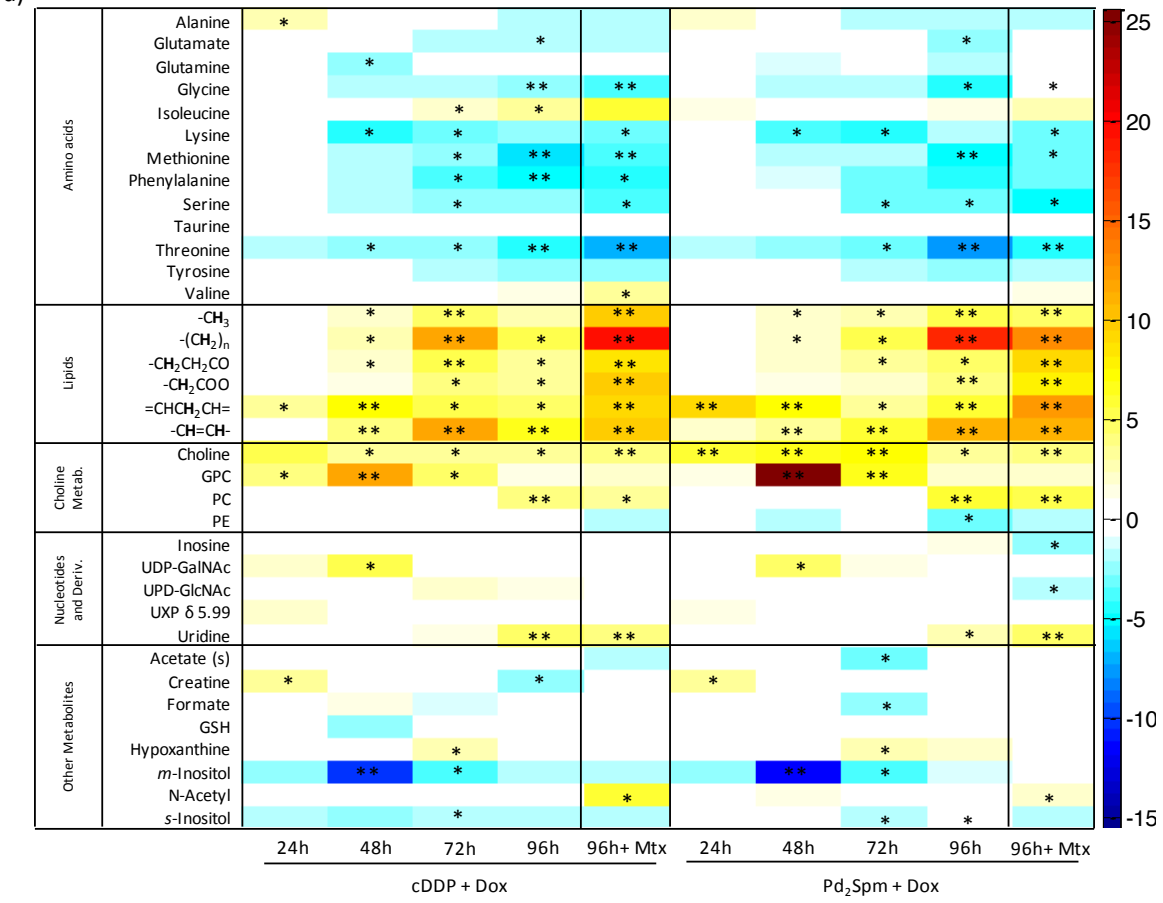

b)

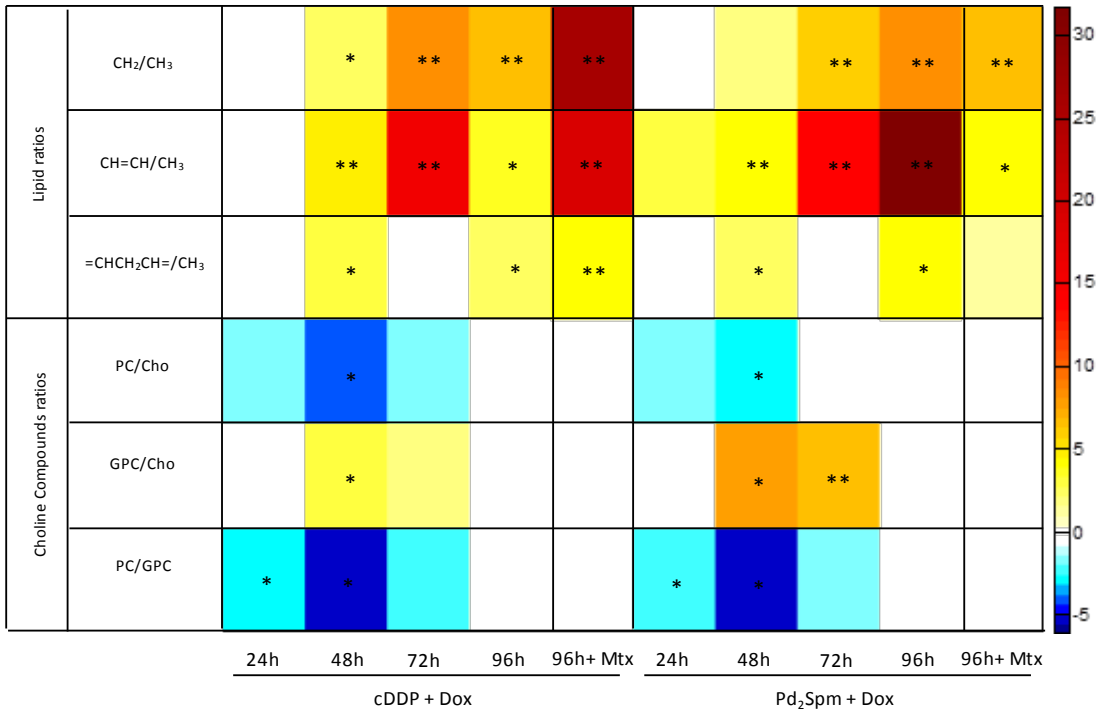

Figure 7.15. Heatmaps of effect size values of the time course response for a) several metabolites and b) compound ratios in MG-63 cells exposed to cDDP- and Pd_2Spm-based cocktails. The effect size values are shown in a colour scale from minimum (dark blue) to maximum (dark red) values. * $p < 0.05$ and ** $p < 0.01$ refer to the results of significance tests with integrals.

This global analysis of drug-induced metabolic changes (Figure 7.15a) corroborates the findings pointed out by both visual inspection and multivariate analysis: cells undergo very similar alterations with both drug cocktails, globally described by a marked increase in lipids content and choline compounds (with slight decreased PE), a decreasing tendency for the majority of amino acids (exception for alanine at initial stages and isoleucine) and changes in other compounds as decreased *m*- and *s*-inositol. Also worth noting are the changes in the creatine, hypoxanthine and N-acetyl levels which show slight fluctuations over time that seem to be characteristic of either cDDP- or Pd_2Spm-based cocktails. Regarding the compound ratios (Figure 7.15b), changes are once again common to cDDP- and Pd_2Spm-based cocktails. In what concerns the lipid ratios, a global increase occurs reflecting enlargement of the corresponding chain length (CH_2/CH_3), as well as higher unsaturation ($CH{=}CH/CH_3$) and polyunsaturation ($=CHCH_2CH{=}/CH_3$) degrees. Choline ratios show a quite opposite variation, with marked changes in PC/Cho and PC/GPC at initial times of drug exposure, while an increase in GPC/Cho is observed at intermediate times. Remarkably, such changes in lipid and choline compounds ratios seem to take place at different stages of treatment: for choline compounds until 72 hours and for lipids essentially from 48 hours onwards.

The clear decreasing tendency observed for the majority of the amino acids for both cDDP+DOX and Pd_2Spm+DOX, was also a mark associated with cDDP treatment (single exposure, section 5.2.1) and probably reflect their enhanced catabolism *via* de Krebs cycle. For Val and Ile a slightly different trend is found (for both cocktails), consistent with that found for single exposure to cDDP, and their catabolism were associated with the biosynthesis of branched chain fatty acids. Finally, the absence of significant changes in Tau and GSH levels suggest a low level of oxidative stress (Duarte *et al*., 2013) in cells exposed to either cDDP+DOX or Pd_2Spm+DOX. However, the decreases in both Glu and Gly (GSH precursors) possibly indicate the activation of antioxidant protection mechanisms by the cells (associated with cell cycle arrest and apoptosis) (Santini *et al*., 2006; Garcia-Alvarez *et al*., 2011; Mirbahai *et al*., 2011; Santini *et al*., 2001; Triba *et al*., 2010). In fact, STOCSY analysis revealed strong positive correlations between GSH and the two referred amino acid precursors (not shown), suggesting that Glu and Gly usage to form GSH occurs in such an efficient rate that (despite being used for antioxidant protection purposes) GSH levels are kept around control levels.

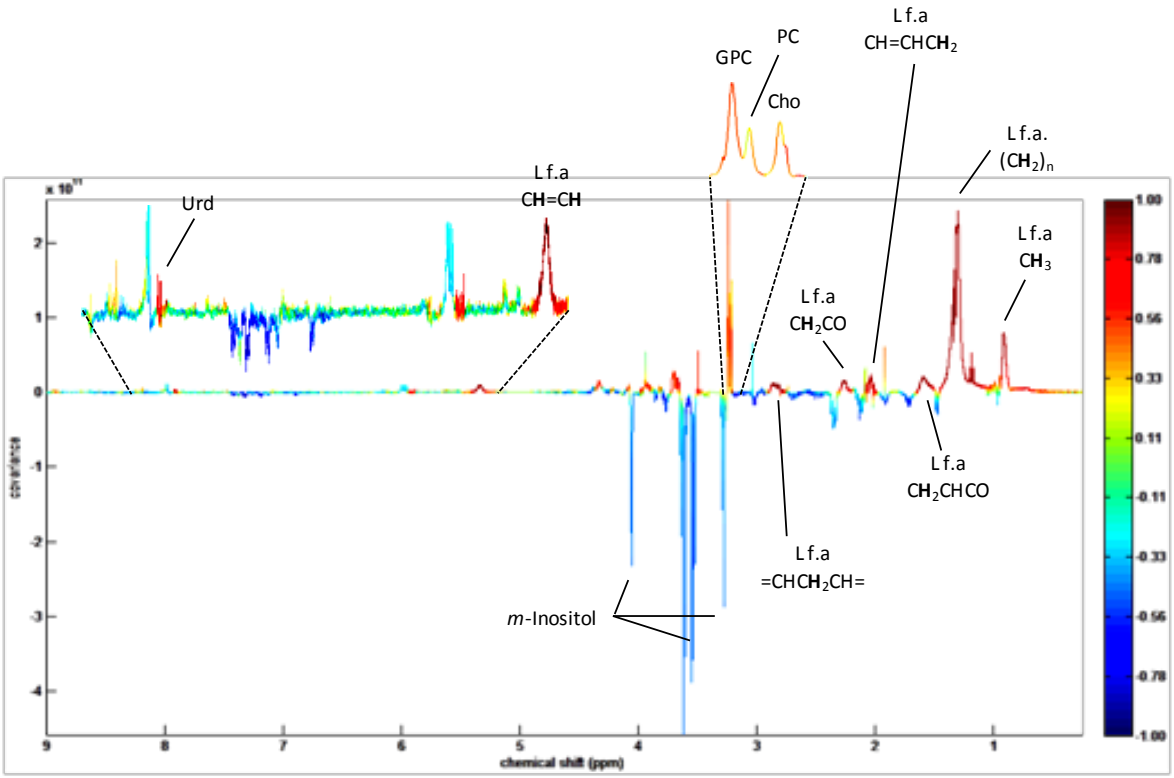

Figure 7.16. STOCSY results obtained for PUFA resonance at δ 2.83 for cDDP+DOX-treated MG-63 cells.

STOCSY results obtained for the PUFA resonance (Figure 7.16) yielded similar results for the two cocktails: strong positive correlations between lipids resonances and the GPC and uridine

peaks. A positive correlation between GPC and PUFA resonance was already detected in MG-63 cells exposed to cDDP (sole administration, Chapter 5), which was interpreted as revealing a close metabolic link to PTC hydrolysis. With regard to PUFA and GPC, this interpretation might possible apply for the similar results obtained for cDDP+DOX and Pd_2Spm+DOX, however, differently from single exposure conditions, positive correlations were also assigned with uridine and PC, eventually pointing to specific PTC pathway adaptations when cells are treated with the drug cocktails.

Figure 7.15a, shows significant increases of UDP-GalNAc, at 48 hours, for MG-63 cells treated with either cDDP+DOX or Pd_2Spm+DOX. This compound was previously found to increase, along with UDP-GlcNAc in cDDP-treated brain tumour (Pan *et al*., 2011) and lung cancer cells (Duarte *et al*., 2013) and was correlated to mobile lipids associated with apoptotic cells death. In fact, STOCSY results obtained for UDP-GalNAc show a positive correlation with lipid resonances for cDDP+DOX-treated cells (Figure 7.17) but fail to reveal any correlation to lipid resonances for Pd_2Spm+DOX-treated cells (not shown), pointing to different pathways of this nucleotide derivative.

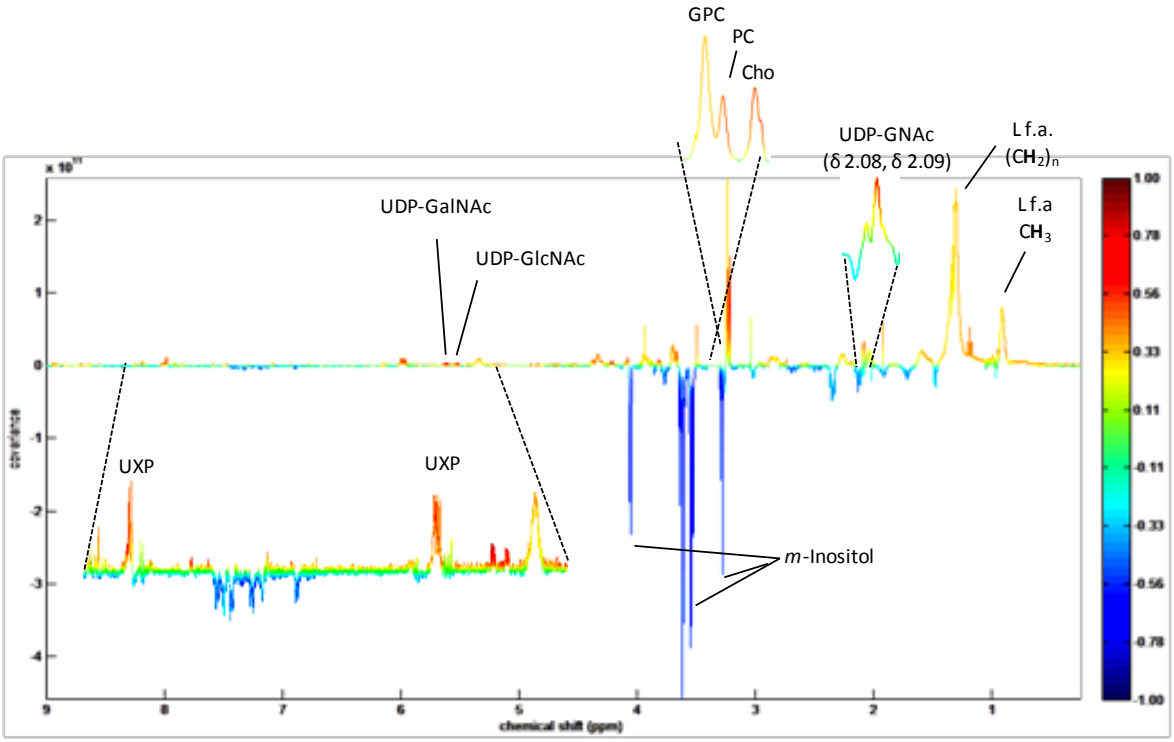

Figure 7.17. STOCSY results obtained for UDP-GalNAc resonance at δ 5.62, in cDDP+DOX-treated MG-63 cells.

However, for both cocktails, positive correlations were found between UDP-GalNAc and membrane degradation products (GPC and Cho). Although not significant, increases of UXP levels are seen in Figure 7.15a, and its resonances also strongly correlate with UDP-GalNAc, possibly arising from the drugs interaction with DNA. On its turn UDP-GlcNAc, which show just very tenuous increases in cDDP+DOX-treated cells, shows strong positive correlations with UXP and negative correlations with lipid resonances for both cocktails (shown in Figure 7.18 for cDDP+DOX). Additional positive correlations were found with GSH peaks (stronger for Pd_2Spm+DOX combination) as seen previously for cDDP in sole administration (but not for DOX), suggesting a relation between UDP-GlcNAc and antioxidative mechanisms.

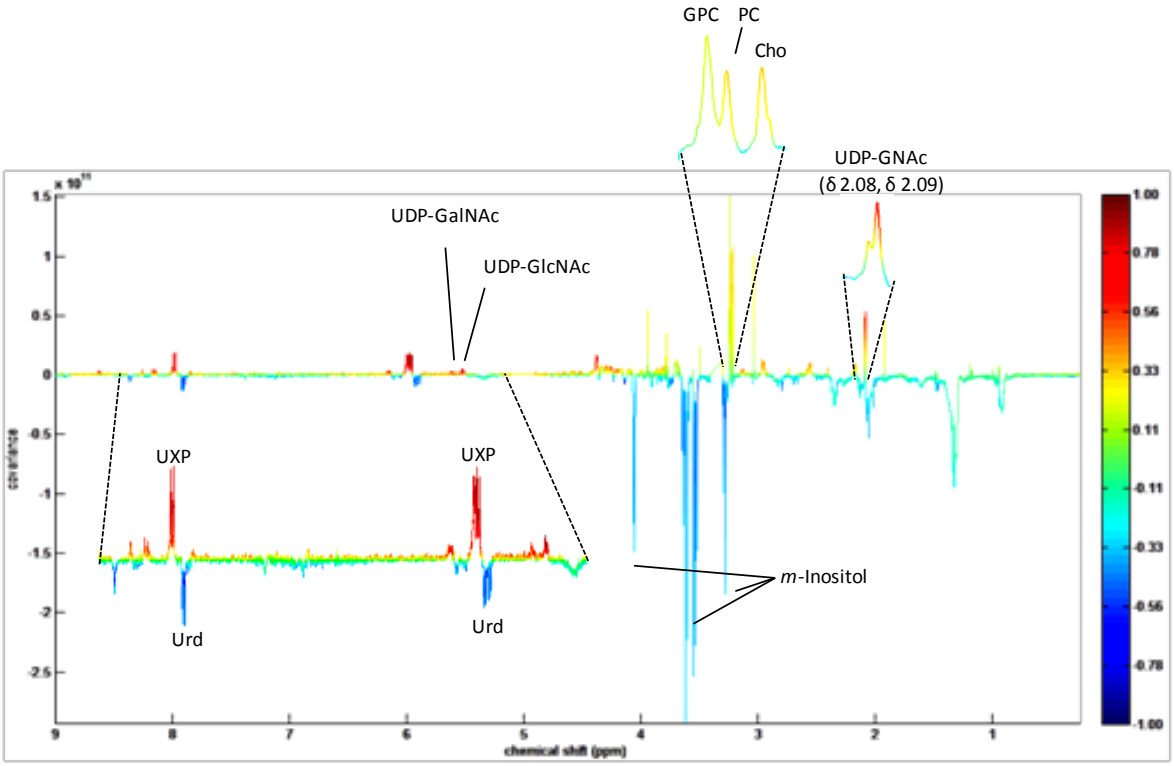

Figure 7.18. STOCSY results obtained for UDP-GlcNAc resonance at δ 5.52, in cDDP+DOX-treated MG-63 cells.

Another interesting finding is the effect of MTX when administered after these drug combinations. The analysis of the NMR spectra for MTX-induced metabolic changes in osteosarcoma cells exposed to cDDP- or Pd_2Spm-based cocktails, suggests very scarce modifications due to the addition of this antimetabolite to the drug-cocktails. However, the heatmap of lipid ratios (Figure 7.15b) reflects a different role for MTX: in cDDP-cocktail, MTX clearly increased lipid ratios CH_2/CH_3 and $CH{=}CH/CH_3$ in comparison to cDDP+DOX exposure while in Pd_2Spm-cocktail exposure MTX is responsible for a decrease of the lipid ratios. Figure 7.15a also

shows that marked increases of PUFA levels (=$CHCH_2CH$=) are induced by MTX addition. Regarding the choline compounds ratios, MTX does not seem to influence their mobilisation (no considerable changes in choline compounds contents after MTX administration are seen in Figure 7.15a, with just a non statistically relevant decrease of PE in cDDP-based cocktail exposure). Furthermore, MTX addition does not seem to significantly interfere with amino acids dynamics, but seems to considerable alter N-acetyl moieties (δ 2.02) (in both drug-based formulations) and induce important decreases in Ino/Ado contents when added to the Pd_2Spm-cocktail (Figure 7.15a).

8. Conclusions and Future Perspectives

The work described in this thesis employed NMR metabolomics to evaluate the response of osteosarcoma cells to conventional (cDDP, DOX and MTX) and a new possible anticancer drug (Pd_2Spm), as well as to drug-combination treatments. The metabolic impact of cDDP and Pd_2Spm was also investigated in normal osteoblast cells. Following an introduction to the subject (Chapter 1) and to the methods employed (Chapter 2) and the description of the experimental procedures followed in this work (Chapter 3), an initial study carried out to select the acquisition parameters that yielded the best high resolution ^{1}H HRMAS NMR spectral profile was described, as well as the influence of handling and storage conditions on the obtained spectra evaluated (Chapter 4). The results obtained from the drug-cell assays are presented in Chapters 5 to 7 of this thesis, and the main conclusions are hereby summarised.

The study described in Chapter 4 aimed at defining the acquisition parameters that give the best ^{1}H HRMAS NMR spectra of cells, understand the impact of different sample handling and storage conditions on the cell spectral profile and evaluate the reproducibility of the entire experimental protocol. The HRMAS NMR analysis of MG-63 cells enabled the simultaneous identification of hydrophilic and lipophilic compounds and results showed that the analysis of mechanically lysed cells increase the information recovery by improving the detection of choline compounds and sharp peaks arising from metabolites released from the intracellular shell. Regarding sample spinning rate (SR), the most significant improvements in spectral resolution were achieved until 4 kHz. The choice of 4 kHz as the best SR value was also motivated by the slight increases in lipids resonances and deviations in chemical shift for some compounds at higher SR, which were associated with sample heating phenomena and/or sample degradation. An increase in the temperature of the sample during acquisition (4 to 25˚C range) entailed identical consequences in the spectra: lightly increased visibility of lipid moieties and considerable changes in the chemical shift without a substantial increase of signal intensities. For long periods of acquisition, the temperature of sample revealed to be determinant for the profile obtained over time: at 4˚C, lipids, choline compounds and amino acids vary from around 10 % while at room temperature (22˚C) some of the variations reach the 100%. T_2 measurements enabled the evaluation of the relative overall molecular mobility of different metabolites in the sample and T_1

measurements revealed that the relaxation delay time (D1) chosen of 4 s ensures quantitative analysis of PC, lactate, Ala, Glu, Ser and Val, while for other compounds (such as Cho, Gly, Phe and Ino/Ado) measurements are only semi-quantitative. Reproducibility assays showed that choline compounds (particularly GPC and PC), the amino acids Gly, Phe and Pro as well as *m*- and *s*-inositols showed statistically significant variations between assays. These variations then will have to be taken into account when studying the metabolites drug-induced changes. Despite their exploratory nature, the results of different number of passages suggested that the profile of cells that differ in about 20 passages are very similar, although slight variations namely in choline compounds, creatine, *m*-inositol, Tau, Glu and Thr were detected when cells were treated with cDDP. Finally, and despite some considerable variations in signals with low S/N (experimental error), the high stability of lipids and choline compounds suggested that sample stability is high during at least 27 months of storage at -80˚C.

MG-63 cells exposed to cDDP were assumed to undergo extensive membrane degradation accompanied by a marked increase of lipids, while DOX- and MTX-treated cells showed no significant lipid variations and different phospholipid signatures. DOX-induced changes in metabolites in MG-63 were associated with membrane degradation, decreased membrane synthesis and (apparent) inhibition of *de novo* lipids synthesis. MTX-induced alterations were described by decreased membrane synthesis, without any signs of membrane disruption or *de novo* synthesis of lipids. Amino acids and nucleotide metabolisms as well as oxidative state of cells treated with each of the three drugs were also distinct. Changes in nucleotides seem to reflect different mechanisms of action, a link having been advanced for cDDP and DOX (both targeting DNA), between UDP-GlcNAc and the metabolically active pathways of membrane degradation and energetics. NMR analysis of TCA extracts added information on ADP/ATP, UMP/UDP/UTP and NAD^+ variations. The results suggested similar variations of nucleotides and derivatives upon DOX- and MTX-treatment, both different from those appearing upon cDDP-treatment particularly in what regards to UXP and Ino/Ado. Furthermore, a relation between oxidative state and DNA degradation was suggested upon cDDP-treatment. Moreover, specific antioxidative metabolite signatures were unveil by correlation studies for each drug, suggesting a decisive influence of *m*- and *s*-inositols, Tau, Glu/Gln and possibly creatine in GSH metabolism.

A new Pd(II) agent (Pd_2Spm) was investigated as potentially active against osteosarcoma by comparing its impact on MG-63 and non-neoplastic (HOb) cells, compared to that of cDDP. Trypan blue results showed that, at 24 hours, Pd_2Spm has an increased cytotoxic potential over MG-63

cells than cDDP (expressed by the much lower IC_{50} value, 12 μM, than half of that of cDDP, 30 μM). However, this effect remains essentially constant for longer exposure periods (36 and 48 hours) while for cDDP, cytotoxicity increases with the time of exposure to the drug.

The metabolic alterations that accompanyed these cytotoxic differences were clear from HRMAS NMR metabolomics: these comprised no changes in lipids, contrary to cDDP exposure, and lesser alterations in other metabolites. The results of TCA extracts NMR analysis showed that the metabolic consequences upon their administration are different in what relates to nucleotides and derivatives, namely in regard to UXP and ADP/ATP. This reinforces the idea that the two drugs act through different mechanisms of action. Interestingly, in this respect, the metabolic profile of MG-63 cells treated with Pd_2Spm more closely resembles that of DOX or MTX treated, than that of cDDP. The results from Annexin assays, revealed that the reduction in the number of living cells upon Pd_2Spm-exposure was not due to apoptotic cell death (proven to take place as a response to cDDP) or necrosis (since no significant PI labelling was detected). Additionally, the reversibility assays performed by HRMAS NMR showed that after the recovery period (three days in drug-free medium) the metabolic alterations that persist upon Pd_2Spm-treatment are globally reverted or attenuated, while, for cDDP, a considerable number of drug-induced changes persist or emerge *de novo*, suggesting that cells are able to overcome the Pd_2Spm-induced toxicity. Considering now the drug-induced effects in HOb cells, and although no significant differences regarding the number of living cells (Trypan blue assay) have been detected, a higher number of alterations in the metabolic profile of cells were detected in response to Pd_2Spm, relative to cDDP exposure. The reversibility assays showed that, even in the absence of the drug, new additional changes appeared in HOb cells in response to cDDP-treatment and the marked alterations due to Pd_2Spm-exposure were maintained, suggesting an increased and sustained cytotoxic power of Pd_2Spm in healthy cells. Together, the above results showed that Pd_2Spm induces more tenuous metabolic changes in cancer cells than cDDP, whereas the opposite trend was noted for osteoblasts. This suggests that Pd_2Spm may not be a good option for cDDP substitution in osteosarcoma treatment, at least in sole administration.

Since no important alterations in the GSH levels were detected through HRMAS NMR of cells treated with either cDDP or Pd_2Spm, studies were performed in order to understand whether drug-glutathione competition phenomena could have masked real GSH changes as response to drug exposure. The results from ^1H NMR, suggested the formation of adducts with both Pt(II) and Pd(II), reflected in the broadening of particular resonances. Nevertheless, in none

of the cases the formation of these adducts seemed to interfere with the integral of the measured GSH integral in the ^{1}H HRMAS NMR spectra.

Combination assays intended to unveil the metabolic alterations induced by exposure to the drug-cocktail used nowadays in osteosarcoma treatment. Additionally, the metabolic effects of the substitution of cDDP by Pd_2Spm in the drug-cocktail were investigated. Cytotoxic results showed that exposure to cDDP-based and Pd_2Spm-based cocktails induce similar decreases in the number of MG-63 and HOb cells. ^{1}H HRMAS NMR results demonstrated that the metabolic consequences that follow this drug-induced decrease in the number of MG-63 cells are similar for both cDDP+DOX and Pd_2Spm+DOX combination treatments. Observed alterations encompassed dramatic increases in lipid contents and altered levels of choline compounds, pointing to cell death by apoptosis. Several amino acids decreased upon treatment with each of the two tested cocktails and identical changes were also measured for the both cDDP- and Pd_2Spm-based cocktails in nucleotides and derivatives and other compounds as m- and s-inositol. Results of NMR analysis of TCA extracts showed identical response profiles in the aromatic region of cDDP+DOX- and Pd_2Spm+DOX-treated MG-63 cells, which resembled those seen in cDDP for UXP levels. The accumulation of energetic compounds (AXP and UXP) may suggest that the carcinogenicity of the cells is being reverted in some way, revealing the success of the treatment. Moreover, the addition of MTX to each of the two cocktails was not translated into an alteration in the number of living cells, when compared to the effect induced by both cocktails without MTX. Regarding its influence over cell metabolism, it was shown that when MTX is added to the cocktails, a slight but consistent potentiation of the effect of the cocktail over lipids (augment) was detected, suggesting that MTX somehow sensitises cells for the exposure to cocktails. In Pd_2Spm-cocktail, MTX addition induced important decreases in Ino/Ado levels, thus suggesting a different influence over DNA in relation to cDDP-based cocktail. In conclusion, these results showed that, differently from when used in sole administration, when combined to DOX, Pd_2Spm induces metabolic changes that resemble those resulting from cDDP+DOX exposure.

The work presented in this thesis demonstrated the potential of HRMAS NMR metabolomics to understand the metabolic consequences of drugs already used in the clinic, thus helping to unveil their metabolic impact and potentially defining markers of action and efficacy. HRMAS NMR was also proven to be a very useful approach to investigate the effect of potentially

active drugs alone or in combination. Despite the time-consuming task of cell culture procedures, the amount of information revealed by metabolomics together with the ease of sample preparation for NMR experiments strongly encourage the use of HRMAS NMR metabolomics in drug-testing assays.

As future work, additional cell metabolomic studies could be performed to understand how does Pd_2Spm works in cells with acquired resistance to treatment (namely to cDDP), especially in cocktail formulations. Furthermore, and since in this work HOb cells were analysed upon 24 hours treatment (far from their doubling time), assays that evaluate the drug-induced metabolic changes upon an exposure period closer to their doubling time (around 72 hours) would reveal additional long term treatment-induced consequences. In order to get a broader knowledge on the metabolic consequences or drug-combination treatment, it would be interesting to understand the metabolic consequences of osteoblasts treatment with cDDP- and Pd_2Spm-based cocktails. Future work would also necessarily entail enzymatic studies and metabolic pathway network analysis, to follow in a more target way the metabolism of lipids and choline compounds upon drug-treatments. In this line, ^{31}P NMR experiments and assays using hyperpolarised ^{13}C substrates would also certainly be of crucial relevance to unveil more clues on the metabolic pathways in which these compounds are involved. Further insights into Pd_2Spm mode of action would necessarily entail cell cycle analysis of treated cells, since annexin assays already showed that this Pd(II) drug does not induce cell death (either by apoptosis or necrosis). Finally, *in cell* Raman techniques would certainly offer additional information on the status of different cellular organelles upon drug-exposure.

References

Airley, R. Cancer Chemotherapy: Basic Science to the Clinic. *John Wiley & Sons. Ltd.: West Sussex*. **2009**.

Abu-Surrah, A. S.; Al-Sa'doni, H. H.; Abdalla, M. Y. Palladium-based chemotherapeutic agents: Routes toward complexes with good antitumor activity. *Cancer Therapy*. **2008**, 6, 1-10.

Akoka, S.; Barantin, L.; Trierweiler, M. Concentration Measurement by Proton NMR Using the ERETIC Method. *Analytical Chemistry*. **1999**, 71 (13), 2554-2557.

Albers, M. J.; Butler, T. N.; Rahwal, I.; Bao, N.; Keshari, K. R.; Swanson, M. G.; Kurhanewicz, J. Evaluation of the ERETIC method as an improved quantitative reference for 1H HR-MAS spectroscopy of prostate tissue. *Magnetic Resonance in Medicine*. **2009**, 61(3), 525-532.

Alberts, B.; Johnson, A.; Lewis, J.; Raff, M.; Roberts, K; Walter, P. Molecular Biology of the Cell. *Garland Science: New York.* **2002**, 4th Ed.

Annibaldi, A. and Widmann, C. Glucose metabolism in cancer cells. *Current Opinion in Clinical Nutrition and Metabolic Care*. **2010**, 13 (4), 466-470.

Antone, P. D. Energy metabolism in cancer cells: How to explain the Warburg and Crabtree effects? *Medical Hypotheses*. **2012**, 79, 388-392.

Alm, E.; Torgrip, R. J. O.; Aberg, K. M.; Schuppe-Koistinen, I.; Lindberg, J. A solution to the 1D NMR alignment problem using an extended generalized fuzzy Hough transform and mode support. *Analytical and Bioanalytical Chemistry*. **2009**, 395(1), 213-223.

Al-Saffar, N. M. S.; Troy, H.; de Molina, A. R.; Jackson, L. E.; Madhu, B.; Griffiths, J. R.; Leach, M. O.; Workman, P.; Lacal, J. C.; Judson, I. R.; Chung, Y.-L. Noninvasive Magnetic Resonance Spectroscopic Pharmacodynamic Markers of the Choline Kinase Inhibitor MN58b in Human Carcinoma Models. *Cancer Research*. **2006,** 66 (1), 427-434.

Amaravadi, R. K.; Thompson, C. B. The roles of therapy-induced autophagy and necrosis in cancer treatment. *Clinical Cancer Research*. **2007**, 13, 7271-7279.

Amoêdo, N. D.; Rodrigues, M. F.; Pezzuto, P.; Galina, A.; Madeiro da Costa, R.; de Almeida, F. C. L.; El-Bacha, T.; Rumjanek, F. D. Energy Metabolism in H460 Lung Cancer Cells: Effects of Histone Deacetylase Inhibitors. *PLoS One*. **2011**, 6 (7), e22264.

Apel, A.; Zentgraft, H.; Büchler, M. W.; Herr, I. Autophagy - A double-edged sword in oncology. *International Journal of Cancer*. **2009**, 125, 991-995.

Assaraf, Y. G. Molecular basis of antifolate resistance. *Molecular Metastasis Reviews*. **2007**, 26 (1), 153-181.

Astashkina, A.; Mann, B.; Grainger, D. W. A critical evaluation of in vitro cell culture models for high-throughput drug screening and toxicity. *Pharmacology and Therapeutics*. **2012**, 134, 82-106.

Atadja, P. W. HDAC inhibitors and cancer therapy. *Progress in Drug Research*. **2011**, 67, 175-1795.

Baines, A. T.; Xu, D.; Der, C. J. Inhibition of Ras for cancer treatment: the search continues. *Future Medicinal Chemistry*. **2011**, 3 (14), 1787-1808.

Barantin, L.; Le Pape, A.; Akoka, S. A new method for absolute quantitation of MRS metabolites. *Magnetic Resonance in Medicine*. **1997**, 38 (2), 179-182.

Bardos, T. J. Antimetabolites: Molecular design and mode of action. *Medicinal Chemistry*. **1974**, 52, 63-98.

Basu, A.; Krishnamurthy, S. Cellular Responses to Cisplatin-Induced DNA Damage. *Journal of Nucleic Acids*. **2010**, 201367.

Bayet-Robert, M. and Morvan, D. Metabolomics Reveals Metabolic Targets and Biphasic Responses in Breast Cancer Cells Treated by Curcumin Alone and in Association with Docetaxel. *PLOS One*. **2013**, 8 (3), e57971.

Bayet-Robert, M.; Loiseau, D.; Rio, P.; Demidem, A.; Barthomeuf, C.; Stepien, G.; Morvan, D. Quantitative Two-Dimensional HRMAS ^{1}H-NMR Spectroscopy-Based Metabolite Profiling of Human Cancer Cell Lines and Response to Chemotherapy. *Magnetic Resonance in Medicine*. **2010**, 63, 1172-1183.

Becker, E. D. A brief history of nuclear magnetic resonance. *Analytical Chemistry*. **1993**, 65 (6), 295A-302A.

Beloueche-Babari, M.; Jackson, L. E.; Al-Saffar, N. M. S.; Eccles, S. A.; Raynaud, F. I.; Workman, P.; Leach, M. O.; Ronen, S. M. Identification of magnetic resonance detectable metabolic changes associated with inhibition of phosphoinositide 3-kinase signaling in human breast cancer cells. *Molecular Cancer Therapy*. **2006**, 5 (1), 187-196.

Beloueche-Babari, M.; Jackson, L. E.; Al-Saffar, N. M. S.; Workman, P.; Leach, M. O.; Ronen, S. M. Magnetic Resonance Spectrsocopy Monitoring of Mitogen-Activated Protein Kinase Signaling Inhibition. *Cancer Research*. **2005**, 65 (8), 3356-3363.

Berben, L.; Sereika, S. M.; Engberg, S. Effect Size Estimation: Methods and Examples. *International Journal of Nursing Studies*. **2012**, 49, 1039-1047.

Bergers, G. and Song, S. The role of pericytes in blood-vessel formation and maintenance. *Neuro-Oncology*. **2005**, 7 (4), 452-464.

Berridge, M. V.; Tan, A. S. Characterization of the Cellular Reduction of 3-(4,5-Dimethylthiazol-2-yl)-2,5-Diphenyltetrazolium Bromide (MTT): Subcellular Localization, Substrate Dependence, and Involvement of Mitochondrial Electron Transport in MTT Reduction. *Archives of Biochemistry and Biophysics*. **1993**, 303, 474-482.

Billiau, A.; Edy, V. G.; Heremans, H.; Van Damme, J.; Desmyter, J.; Georgiades, J. A.; De Somer, P. Human interferon: mass production in a newly established cell line, MG-63. *Antimicrobial Agents and Chemotherapy*. **1977**, 12, 11-15.

Blankenberg, F. G.; Katsikis, P. D.; Storrs, R. W.; Beaulieu, C.; Spielman, D.; Chen, J. Y.; Naumovski, L.; Tait, J. F. Quantitative Analysis of Apoptotic Cell Death Using Proton Nuclear Magnetic Resonance Spectrosocpy. *Blood*. **1997**, 89, 3778-3786.

Blasco, M. A. Telomeres and human disease: ageing, cancer and beyond. *Nature Reviews|Genetics*. **2005**, 6, 611-622.

Bollard, M. E.; Garrod, S.; Holmes, E.; Lindon, J. C.; Humpfer, E.; Spraul, M.; Nicholson, J. K. High-resolution (1)H and (1)H-(13)C magic angle spinning NMR spectroscopy of rat liver. *Magnetic Resonance in Medicine*. **2000**, 44(2), 201-207.

Borel, M.; Degoul, F.; Communal, Y.; Mounetou, E.; Bouchon, B.; Gaudreault, R. C-.; Madelmont, J. C.; Miot-Noirault, E. N-(4-iodophenyl)-N'-(2-chloroethyl)urea as microtubule disrupter: *in vitro* and *in vivo* profiling of antitumoral activity on CT-26 murine colon carcinoma cell line cultured and grafted to mice. *Brithish Journal of Cancer*. **2007**, 96, 1684-1691.

Boren, J.; Brindle, K. M. Apoptosis-Induced Mitochondrial Dysfunction Causes Cytoplasmic Lipid Droplet Formation. *Cell Death Differentiation*. **2012**, 19, 1561-1570.

Boros, L. G.; Lee, P. W. N.; Brandes, J. L.; Cascante, M.; Muscarella, P.; Schirmer, W. J.; Melvin, W. S.; Ellison, E. C. Nonoxidative pentose phosphate pathways and their direct role in ribose synthesis in tumors: is cancer a disease of cellular glucose metabolism? *Medical Hypotheses*. **1998**, 50, 55-59.

Brisdelli, F.; Iorio, E.; Knijn, A.; Ferreti, A.; Marcheggiani, D.; Lenti, L.; Strom, R.; Podo, F.; Bozzi, A. Two-step formation of ^{1}H NMR visible lipids during apoptosis of paclitaxel-treated K562 cells. *Biochemical Pharmacology*. **2003**, 65, 1271-1280.

Bruker Avance 1D/2D Manual. *Bruker*. **2003**.

Buck, A. and Walch, A. In situ drug and metabolite analyzes in biological and clinical research by MALDI MS imaging. *Bioanalysis*. **2014**, 6 (9), 1241-1253.

Burkhart, D. L. and Sage, J. Cellular mechanisms of tumour suppression by the retinoblastoma gene. *Nature Reviews|Cancer*. **2008**, 8, 671-682.

Butour, J. L.; Wimmer, S.; Wimmer, F.; Castan, P. Palladium (II) compounds with potential antitumor properties and their platinum analogues: a comparative study of the reaction of some orotic acid derivatives with DNA in vitro. *Chemico-Biological Interactions*. **1997**, 104 (2-3), 165-178.

Buzatto, A. Z.; de Sousa, A. C.; Guedes, S. F.; Cieslarová, Z.; Simionato, A. V. Metabolomic investigation of human diseases biomarkers by CE and LC coupled to MS. *Electrophoresis*. **2014**, 35 (9), 1285-1307.

Cantor, J. R. and Sabatini, D. M. Cancer cell metabolism: one hallmark, many faces. *Cancer Discovery*. **2012**, 2 (10), 881-898.

Cao, B.; Li, M.; Zha, W.; Zhao, Q.; Gu, R.; Liu, L.; Shi, J.; Zhou, J.; Zhou, F.; Wu, X.; Wu, Z.; Wang, G.; Aa, J. Metabolic approach to evaluating adriamycin pharmacodynamics and resistance in breast cancer cells. *Metabolomics*. **2013**, 9, 960-973.

Chen, H. H. W.; Kuo, M. T. Role of Glutathione in the Regulation of Cisplatin Resistance iin Cancer Chemotherapy. *Metal-Based Drugs*. **2010**, 430939.

Chen, H. H.; Song, I. S.; Hossain, a.; Choi, M. K.; Yamane, Y.; Liang, Z. D.; Lu, J.; Siddik, Z. H.; Klomp, L. W.; Savaraj, N.; Kuo, M. T. Elevated glutathione levels confer cellular sensitization to cisplatin toxicity by up-regulation of copper transporter hCtr1. *Molecular Pharmacology*. **2008**, 74 (3), 697-704.

Chen, J.-H.; Enloe, B. M.; Weybright, P.; Campbell, N.; Dorfman, D.; Fletcher, C. D.; Cory, D. G.; Singer, S. Biochemical Correlates of Thiazolidinedione-Induced Adipocyte Differentiation by High-Resolution Magic Angle Spinning NMR Spectroscopy. *Magnetic Resonance in Medicine*. **2002**, 48, 602-610.

Cheng, M. –L.; Shiao, M. –S.; Chiu, D. T. –Y.; Weng, S. –F.; Tang, H. –Y.; Ho, H. –Y. Biochemical disorders associated with antiproliferative effect of dehydroepiandrosterone in hepatoma cells as revealed by LC-based metabolomics. *Biochemical Pharmacology*. **2011**, 82, 1549-1561.

Chiaradonna, F.; Moresco, R. M.; Airoldi, C.; Gaglio, D.; Palorini, R.; Nicotra, F.; Messa, C.; Alberghina, L. From cancer metabolism to new biomarkers and drug targets. *Biotechnology Advances*. **2012**, 30, 30-51.

Chung, Y. –L.; Troy, H.; Kristeleit, R.; Aheme, W.; Jackson, L. E.; Atadja, P.; Griffiths, J. R.; Judson, I. R.; Workman, P.; Leach, M. O.; Beloueche-Babari, M. Noninvasive Magnetic Resonance

Spectroscopy Pharmacodynamic Markers of a Novel Histone Deacetylase Inhibitor, LAQ824, in Human Colon Carcinoma Cells and Xenografts. *Neoplasia*. **2008**, 10 (4), 303-313.

Chung, Y.-L.; Troy, H.; Banerji, U.; Jackson, L. E.; Walton, M. I.; Stubbs, M.; Griffiths, J. R.; Judson, I. R.; Leach, M. O.; Workman, P.; Ronen, S. M. Magnetic Resonance Spectroscopy Pharmacodynamic Markers of the Heat Shock Protein 90 Inhibitor 17-Allylamino, 17-Demethoxygeldanamycin (17AAG) in Human Colon Cancer Models. *Journal of the National Cancer Institute*. **2003**, 95 (21), 1624-1633.

Claridge, T.D.W. High-resolution NMR techniques in organic chemistry. *Elsevier: Oxford*. **1999**.

Cloarec, O.; Dumas, M. E.; Craig, A.; Barton, R. H.; Trygg, J.; Hudson, J.; Blancher, C.; Gauguier, D.; Lindon, J. C.; Holmes, E.; Nicholson, J. Statistical Total Correlation Spectroscopy: An Exploratory Approach for Latent Biomarker Identification from Metabolomic ^{1}H NMR Data Sets. *Analytical Chemistry*. **2005**, 77 (5), 1282-1289.

Cole, P. D.; Smith, A. K.; Kamen, B. A. Osteosarcoma cells, resistant to methotrexate due to nucleoside and nucleobase salvage, are sensitive to nucleoside analogs. *Cancer Chemotherapy and Pharmacology*. **2002**, 50, 111-116.

Cooper, W. A.; Bartier, W. A.; Rideout, D. C.; Delikatny, E. J. ^{1}H NMR Visible Lipids Are Induced by Phosphonium Salts and 5-Fluorouracil in Human Breast Cancer Cells. *Magnetic Resonance in Medicine*. **2001**, 45, 1001-1010.

Corduneanu, O.; Chiorcea-Paquim, A. M.; Diculescu, V.; Fiuza, S. M.; Marques, M. P. M.; Oliveira-Brett, A. M. DNA Interaction with Palladium Chelates of Biogenic Polyamines Using Atomic Force Microscopy and Voltammetric Characterization. *Analytical Chemistry*. **2010**, 82 (4), 1245-1252.

Corominas-Faja, B.; Quirantes-Piné, R.; Oliveras-Ferraros, C.; Vazquez-Martin, A.; Cufí, S.; Martin-Castillo, B.; Micol, V.; Joven, J.; Segura-Carretero, A.; Menendez, J. A. Metabolomic fingerprint reveals that metformin impairs one-carbon metabolism in a manner similar to the antifolate class of chemotherapy drugs. *Aging*. **2012**, 4 (7), 480-498.

Craig, A.; Cloarec, O.; Holmes, E.; Nicholson, J. K.; Lindon, J. C. Scaling and normalization effects in NMR spectroscopic metabonomic data sets. *Analytical Chemistry*. **2006**, 78 (7), 2262-2267.

Cuperlovic-Culf, M.; Barnett, D. A.; Culf, A. S.; Chute, I. Cell culture metabolomics: applications and future directions. *Drug Discovery Today*. **2010**, 15 (15/16), 610-621.

Dai, X.; Ma, W.; He, X.; Jha, R. K. Review of therapeutic strategies for osteosarcoma, chondrosarcomas, and Ewing's sarcoma. *Medical Science Monitor*. **2011**, 17 (8), 177-190.

D'Alessandro, A.; D'Amici, G. M.; Timperio, A. M.; Merendino, N.; Zolla, L. Docohaexanoic acid-supplemented PACA44 cell lines and over-activation of Krebs cycle: An integrated proteomic, metabolomic and interactomic overview. *Journal of Proteomics*. **2011**, 74, 2138-2158.

Dang, C. V. Links between metabolism and cancer. *Genes and Development*. **2012**, 26, 877-890.

Dang, C. V. MYC, Metabolism, Cell Growth, and Tumorigenesis. *Cold Spring Harbor Perspectives in Medicine*. **2013**, 3 (8), pii: a014217.

Davies, M.A. and Samuels, Y. Analysis of the genome to personalize therapy for melanoma. *Oncogene*. **2010**, 29, 5545-5555.

Daye, D. and Wellen, K. E. Metabolic reprogramming in cancer: unraveling the role of glutamine in tumorigenesis. *Seminars in Cell and Developmental Biology*. **2012**, 23 (4), 362-369.

De Berardinis, R. J.; Lum, J. J.; Hatzivassiliou, G.; Thompson, C. B. The biology of cancer: metabolic reprogramming fuels cell growth and proliferation. *Cell Metabolism*. **2008**, 7 (1), 11-20.

DeFeo, E. M. and Cheng, L. L. Characterizing human cancer metabolomics with ex vivo 1H HRMAS MRS. *Technology in Cancer Research and Treatment*. **2010**, 9 (4), 381-391.

Delikatny, E. J.; Chawla, S.; Leung, D.-J.; Poptani, H. MR-Visible Lipids and the Tumor Microenvironment. *NMR in Biomedicine*. **2011**, 24, 592-611.

Dewar, B. J.; Keshari, K.; Jeffries, R.; Dzeja, P.; Graves, L. M.; Macdonald, J. M. Metabolic assessment of a novel chronic myelogenous leukemic cell line and an imatinib resistance subline by H NMR spectroscopy. *Metabolomics*. **2010**, 6 (3), 439-450.

Diaz, S. O. Pregnancy and newborns disorders followed by urine metabolomics. *PhD Thesis presented to University of Aveiro, Portugal*. **2014**.

Dieterle, F.; Ross, A.; Schlotterbeck, G.; Senn, H. Probabilistic quotient normalization as robust method to account for dilution of complex biological mixtures. Application in ^{1}H NMR metabonomics. *Analytical Chemistry*. **2006**, 78(13), 4281-4290.

Drexler, D. M.; Reily, M. D.; Shipkova, P. A. Advances in mass spectrometry applied to pharmaceutical metabolomics. *Analytical and Bioanalytical Chemistry*. **2011**, 399 (8), 2645-2353.

Duarte, I. F.; Diaz, S. O.; Gil, A. M. NMR metabolomics of human blood and urine in disease research. *Journal of Pharmaceutical and Biomedical Analysis*. **2014**, 93, 17-26.

Duarte, I. F.; Ladeirinha, A. F.; Lamego, I.; Gil, A. M.; Carvalho, L.; Carreira, I. M.; Melo, J. B. Potential markers of cisplatin treatment response unveiled by NMR metabolomics of human lung cells. *Molecular Pharmaceutics*. **2013**, 10 (11), 4242-4251.

Duarte, I. F.; Lamego, I.; Marques, J.; Marques, M. P. M.; Blaise, B. J.; Gil, A. M. Nuclear Magnetic Resonance (NMR) Study of the Effect of Cisplatin on the Metabolic Profile of MG-63 Osteosarcoma Cells. *Journal of Proteome Research*. **2010**, 9 (11), 5877-5886.

Duarte, I. F.; Marques, J.; Ladeirinha, A. F.; Rocha, C.; Lamego, I.; Calheiros, R.; Silva, T. M.; Marques, M. P. m.; Melo, J. B.; Carreira, I. M.; Gil, A. M. Analytical Approaches toward Successful Human Cell Metabolome Studies by NMR Spectroscopy. *Analytical Chemistry*. **2009**, 81, 5023-5032.

Ebbels, T. M.; Lindon, J. C.; Coen, M. Processing and modeling of nuclear magnetic resonance (NMR) metabolic profiles. *Methods in Molecular Biology*. **2011**, 708, 365-388.

Edwards, J. C. Principles of NMR. (accessed on 15th May)

El-Deredy, W.; Ashmore, S. M.; Branston, N. M.; Darling, J. L.; Williams, S. R.; Thomas, D. G. T. Pretreatment Prediction of the Chemotherapeutic Response of Human Glioma Cell Cultures Using Nuclear Magnetic Resonance Spectroscopy and Artificial Neural Networks. *Cancer Research*. **1997**, 57, 4196-4199.

Ellis, J. K.; Chan, P. H.; Doktorova, T.; Athersuch, T. J.; Cavill, R.; Vanhaecke, T.; Rogiers, V.; Vinken, M.; Nicholson, J. K.; Ebbels, T. M. D.; Keun, H. C. Effect of the Histone Deacetylase Inhibitor Trichostatin A on the Metabolome of Cultured Primary Hepatocytes. *Journal of Proteome Research*. **2010**, 9, 413-419.

Emwas, A. –H. M.; Salek, R. M.; Griffin, J. L.; Merzaban, J. NMR-based metabolomics in human disease diagnosis: applications, limitations, and recommendations. *Metabolomics*. **2013**, 9, 1048-1072.

Esmaeili, M.; Bathen, T. F.; Engebraten, O.; Maelandsmo, G. M.; Gribbestad, I. S.; Moestue, S. A. Quantitative ^{31}P HR-MAS MR Spectroscopy for Detection of Response to PI3K/mTOR Inhibition in Breast Cancer Xenografts. *Magnetic resonance in Medicine*. **2014**, 71, 1973-1981.

Fan, T. W. –M. Metabolite profiling by one- and two-dimensional NMR analysis of complex mixtures. *Progress in Nuclear Magnetic Resonance Spectroscopy*. **1996**, 28, 161-219.

Fan, T. W. –M.; Kucia, M.; Jankowski, K.; Higashi, R. M.; Ratajczak, J.; Ratajczak M. Z.; Lane, A. N. Rhabdomyosarcoma cells show an energy producing anabolic metabolic phenotype compared with primary myocytes. *Molecular Cancer*. **2008**, 7, 79.

Fan, T. W.-M.; Bandura, L. L.; Higashi, R. M.; Lane, A. N. Metabolomics-edited transcriptomics analysis of Se anticancer action in human lung cancer cells. *Metabolomics*. **2005**, 1(4), 325-339.

Fernandis, A. Z. and Wenk, M. R. Lipid-based biomarkers for cancer. *Journal of Chromatography B*. **2009**, 877, 2830-2835.

Feng, J.; Li, J.; Wu, H.; Chen, Z. Metabolic responses of HeLa cells to silica nanoparticles by NMR-based metabolomic analyses. *Metabolomics*. **2013**, 9, 874-886.

Fernández-Arroyo, S.; Gómez-Martínez, A.; Rocamora-Reverte, L.; Quirantes-Piné, R.; Segura-Carretero, A.; Fernández-Gutiérrez, A.; Ferragut, J. A. Application of nanoLC-ESI-TOF-MS for the metabolomic analysis of phenolic compounds from extra-virgin olive oil in treated colon-cancer cells. *Journal of Pharmaceutical and Biomedical Analysis*. **2012**, 63, 128-134.

Ferreira, L. M. R. Cancer metabolism: The Warburg effect today. *Experimental and Molecular Pathology*. **2010**, 89, 372-380.

Ferretti, A.; D'Ascenzo, S.; Knijn, A.; Iorio, E.; Dolo, V.; Pavan, A.; Podo, F. Detection of Polyol Accumulation in a New Ovarian Carcinoma Cell Line, CABA I: a ^{1}H NMR study. *British Journal of Cancer*. **2002**, 86, 1180-1187.

Fiachi, T. and Chiarugi, P. Oxidative Stress, Tumor Microenvironment, and Metabolic Reprogramming: A Diabolic Liaison. *International Journal of Cell Biology*. **2012**, 762825.

Fiuza, S. M..; Holy, J.; Batista de Carvalho, L. A.; Marques, M. P. Biologic activity of a dinuclear Pd(II)-spermine complex toward human breast cancer. *Chemical Biology & Drug Design*. **2011**, 77 (6), 477-488.

Fiuza, S. M.; Amado, A. M.; Oliveira, P. J.; Sardao, V. A.; de Carvalho, L. A. E. B.; Marques, M. P. M. Pt(II) vs Pd(II) polyamine complexes as new anticancer drugs: A structure-activity study. *Letters in Drug Design & Discovery*. **2006**, 3 (3), 149-151.

Fyfe, C. A. Solid State NMR for Chemists. *CFC Press: Guelph, Ontario*. **1983**.

Gao, D.; Jin, F.; Liu, H.; Wang, Y.; Jiang, Y. Metabonomic study on the antitumor effect of flavonoid derivative 3d in HepG2 cells and its action mechanism. *Talanta*. **2014**, 118, 382-388.

García-Álvarez, I.; Fernández-Mayoralas, A.; Garrido, L. Effect of Drugs in Cells and Tissues by NMR Spectrsocopy. *Current Topics in Medicinal Chemistry*. **2011**, 11, 27-42.

Gaude, E. and Frezza, C. Defects in mitochondrial metabolism and cancer. *Cancer and Metabolism*. **2014**, 2, 10

Gebregiworgis, T. and Powers, R. Application of NMR metabolomics to search for human disease biomarkers. *Combinatorial Chemistry and High Throughput Screening*. **2012**, 15 (8), 595-610.

Gibson, D. The mechanism of action of platinum anticancer agents – what do we really know about it? *Dalton Transactions*. **2009**, 48, 10681-10689.

Godwin, A. K.; Meister, A.; O'Dwyer, P. J.; Huang, C. S.; Hamilton, T. C.; Anderson, M. E. High Resistance to Cisplatin in Human Ovarian Cancer Cell Lines is Associated with Marked Increase of Glutathione Synthesis. *Proceedings of the National Academy of Sciences USA*. **1992**, 89 (7), 3070-3074.

Goel, H. L. and Mercurio, A. M. VEGF targets the tumour cell. *Nature Reviews|Cancer*. **2013**, 13, 871-882.

Gomez-Monterrey, I.; Sala, M.; Musella, S.; Campiglia, P. Heat shock protein 90 inhibitors as therapeutic agents. *Recent Patents on Anticancer Drug Discovery*. **2012**, 7(3), 313-336.

Goodacre, R. Metabolomics – The way forward. *Metabolomics*. **2005**, 1(1), 1-2.

Gottschalk, S.; Anderson, N.; Hainz, C.; Eckhardt, S. G.; Serkova, N. Imatinib (STI571)-Mediated Changes in Glucose Metabolism in Human Leukemia BCR-ABL-Positive Cells. *Clinical Cancer Research*. **2004**, 10, 6661-6668.

Gowda, G. A.; Zhang, S.; Gu, H.; Asiago, V.; Shanaiah, N.; Raftery, D. Metabolomics-based methods for early disease diagnosis. *Expert Review of Molecular Diagnostics*. **2008**, 8 (5), 617-633.

Grande, S.; Palma, A.; Luciani, A. M.; Rosi, A.; Guidoni, L.; Viti, V. Glycosidic Intermediates Identified in H-1 MR Spectra of Intact Tumour Cells May Contribute to the Clarification of Aspects of Glycosylation Pathways. *NMR in Biomedicine*. **2011**, 24, 68-79.

Griffin, J. L.; Pole, J. C. M.; Nicholson, J. K.; Carmichael, P. L. Cellular Environment of Metabolites and a Metabonomic Study of Tamoxifen in Endometrial Cells Using Gradient High Resolution Magic Angle Spinning ^{1}H NMR Spectroscopy. *Biochimica et Biophysica Acta*. **2003**, 1619, 151-158.

Grivennikov, S. I.; Greten, F. R.; Karin, M. Immunity, inflammation, and cancer. *Cell*. **2010**. 140, 883-899.

Hagrman, D.; Goodisman, J.; Souid, A.-K. Kinetic Study on the Reactions of Platinum Drugs with Glutathione. *Pharmacology and Experimental Therapeutics* **2004**, 308 (2), 658-666.

Hakumäki, J. M.; Kauppinen, R. A. ^{1}H NMR Visible Lipids in the Life and Death of Cells. *Trends in Biochemical Sciences*. **2000**, 25, 357-362.

Halama, A. Metabolomics in cell culture – A strategy to study crucial metabolic pathways in cancer development and the response to treatment. *Archives of Biochemistry and Biophysics*. **2014**, 564C, 100, 109.

Halama, A.; Riesen, N.; Möller, G.; de Andelis, M. H.; Adamski, J. Identification of biomarkers for apoptosis in cancer cells lines using metabolomics: tools for individualized medicine. *Journal of International Medicine*. **2013**, 274, 425-439.

Hanahan, D. and Weinberg, R. A. Hallmarks of Cancer: The Next Generation. *Cell*. **2011**, 144, 646-674.

Harrigan, G. G.; Colca, J.; Szalma, S.; Boros, L. G. PNU-91325 increases fatty acid synthesis from glucose and mitochondrial long chain fatty acid degradation: a comparative tracer-based metabolomics study with rosiglitazone and pioglitazone in HepG2 cells. *Metabolomics*. **2006**, 2 (1), 21-29.

Harris, R. K. Nuclear Magnetic Resonance Spectroscopy. *John Wiley & Sons: New York*. **1987**, 3rd Ed.

Heiden, M. G. V.; Cantley, L. C.; Thompson, C. B. Understanding the Warburg Effect: The Metabolic Requirements of Cell Proliferation. *Science*. **2009**, 324, 1029-1033.

Hensley, C. T.; Wasti, A. T.; DeBerardinis, R. J. Glutamine and cancer: cell biology, physiology, and clinical opportunities. *The Journal of Clinical Investigation*. **2013**, 123 (9), 3678-3684.

Heremans, H.; Billiau, A.; Cassiman, J. J.; Mulier, J. C.; de Somer, P. In vitro cultivation of human tumor tissues. II. Morphological and virological characterization of three cell lines. *Oncology*. **1978**, 35, 246-252.

Holzgrabe, U. Quantitative NMR spectroscopy in pharmaceutical applications. *Progress in Nuclear Magnetic Resonance Spectroscopy*. **2010**, 57, 229-240.

Hortobágyi, G. N. Anthracyclines in the Treatment of Cancer. *Drugs*. **1997**, 54 (Suppl 4), 1-7.

Hu, Y.; Qi, Y.; Liu, H.; Fan, G.; Chai, Y. Effects of celasterol on human cervical cancer cells as revealed by ion-trap gas chromatography-mass spectrometry based metabolic profiling. *Biochimica et Biophysica Acta*. **2013**, 1830, 2779-2789.

Huang, D.; Zhang, Y.; Chen, X. Analysis of the intracellular nucleoside triphosphate levels in normal and tumor cell lines by high-performance liquid chromatography. Journal of Chromatography B. **2003**, *784*, 101-109.

Huang, Z.; Tong, Y.; Wang, J.; Huang, Y. NMR Studies of the Relationship Between the Changes of the Membrane Lipids and the Cisplatin-Resistance of A549/DDP Cells. *Cancer Cell International*. **2003**, 3, 5.

Ibáñez, C.; Simó, C.; Garcia-Cañas, V.; Gómez-Martínez, Á.; Ferragut, J. A.; Cifuentes, A. CE/LC-MS multiplatform for broad metabolomic analysis of dietary polyphenols effect on colon cancer cells proliferation. *Electrophoresis*. **2012**, 33, 2328-2396.

Jacobsen, N.E. NMR spectroscopy explained. *John Wiley & Sons: New Jersey*. **2007**.

Jain, R. K. Tumor angiogenesis and accessibility: role of vascular endothelial growth factor. *Seminars in Oncology*. **2002**, 29 (6 Suppl 16), 3-9.

Jennen, D.; Ruiz-Aracama, A.; Magkoufopoulou, C.; Peijnenburg, A.; Lommen, A.; van Delft, J.; Kleinjans, J. Integrating transcriptomics and metabonomics to unravel mode-of-action of 2,3,7,8-tetrachlorodibenzo-p-dioxin (TCDD) in HepG2 cells. *BMC Systems Biology*. **2011**, 5, 139.

Jobard, E.; Trédan, O.; Elena, B.; Blaise, B. J.; Bachelot, T. Metabolomics: a novel tool for translation research in oncology. *Oncologie*. **2010**, 409-415.

Johnson, C. H. and Gonzalez, F. J. Challenges and opportunities of metabolomics. *Journal of Cellular Physiology*. **2012**, 227 (8), 2975-2981.

Jones, N. P. and Schulze, A. Targeting cancer metabolism – aiming at a tumour's sweet-spot. *Drug Discovery Today*. **2012**, 17 (5/6), 232-241.

Jones, R. G. and Thompson, C. B. Tumor suppresors and cell metabolism: a recipe for cancer growth. *Genes and Development*. **2009**, 23 (5), 537-548.

Jordan, B. F.; Black, K.; Robey, I. F.; Runquist, M.; Powis, G.; Gillies, R. J. Metabolite changes in HT-29 xenograft tumors following HIF-1a inhibition with PX-478 as studied by MR spectroscopy in vivo and ex vivo. *NMR in Biomedicine*. **2005**, 18, 430-439.

Kaplan, O.; Jaroszewski, J. W.; Clarke, R.; Fairchild, C. R.; Schoenlein, P.; Goldenberg, S.; Gottesman, M. M.; Cohen, J. S. The Multidrug Resistance Phenotype: ^{31}P Nuclear Magnetic Resonance Characterization and 2-Deoxyglucose Toxicity. *Cancer Research*. **1991**, 51, 1638-1644.

Kasherman, Y.; Sturup, S.; Gibson, D. Is Glutathione the Major Cellular Target of Cisplatin? A Study of the Interaction of Cisplatin with Cancer Cell Extract. *Journal of Medicinal Chemistry*. **2009**, 52, 4319-4328.

Keeler, J. Understanding NMR Spectroscopy. *John Wiley & Sons, Ltd: Cambridge*. **2002**.

Keepers, Y. P.; Pizao, P. E.; Peters, G. J.; van Ark-Otte, J.; Winograd, B.; Pinedo, H. M. Comparison of the Sulforhodamine B Protein and Tetrazolium (MTT) Assays for *in vitro* Chemosensitivity Testing. *European Journal of Cancer*. **1991**, 7, 897-900.

Kelland, L. The resurgence of platinum-based cancer chemotherapy. *Nature Reviews|Cancer*. **2007**, 7 (8), 573-584.

Keller, P. Basic Principles of MR Imaging. *Medical Systems, GE: Milwaukee*. **1988**.

Kepp, O.; Galluzzi, L.; Lipinski, M.; Yuan, J.; Kroemer, G. Cell Death Assays for Drug Discovery. *Nature Reviews|Drug Discovery*. **2011**, 10, 221-237.

Kerr, J. F.; Wyllie, A. H.; Currie, A. R. Apoptosis: a basic biological phenomenon with wide-ranging implications in tissue kinetics. *British Journal of Cancer*. **1972**, 26, 239-257.

Kim, D. W.; Kim, K. O.; Shin, M. J.; Ha, J. H.; Seo, S. W.; Yang, J.; Lee, F. Y. siRNA-based targeting of antiapoptotic genes can reverse chemoresistance in P-glycoprotein expressingchondrosarcoma cells. *Molecular Cancer*. **2009**, 8, 28.

Kim, D.-H.; Allwood, J. W.; Moore, R. E.; Marsden-Edwards, E.; Dunn, W. B.; Xu, Y.; Hampson, L.; Hampson, I. N.; Goodacre, R. A metabolomics investigation into effects of HIV protease inhibitors on HPV16 E6 expressing cervical carcinoma cells. *Molecular BioSystems*. **2014**, 10, 398-411.

Kinoshita, H.; Yoshikawa, H.; Shjikj, K.; Hamada, Y.; Nakajima, Y.; Tasaka, K. Cisplatin (CDDP) Sensitizes Human Osteosarcoma cell to Fas/CD95-Mediated Apoptosis by down-regulating FLIP-L Expression. *International Journal of Cancer*. **2000**, 88 (6), 986-991.

Kjeldahl, K. and Bro, R. Some common misunderstandings in chemometrics. *Journal of Chemometrics*. **2010**, 24 (7-8), 558-564.

Klawitter, J.; Anderson, N.; Klawitter, J.; Christians, U.; Leibfritz, D.; Eckhardt, S. G.; Serkova, N. J. Time-Dependent Effects of Imatinib in Human Leukaemia Cells: a Kinetic NMR-Profiling Study. *British Journal of Cancer*. **2009**, 100, 923-931.

Klawitter, J.; Shokati, T.; Moll, V.; Christians, U.; Klawitter, J. Effects of lovastatin on breast cancer cells: a proteo-metabonomic study. *Breast Cancer Research*. **2010**, 12, R16.

Klawitter, J.; Klawitter, J.; Gurshtein, J.; Corby, K.; Fong, S.; Tagliaferri, M.; Quattrochi, L.; Cohen, I.; Shtivelman, E.; Christians, U. Bezielle (BZL101)-induced oxidative stress damage followed by redistribution of metabolic fluxes in breast cancer cells: a combined proteomic and metabolomic study. *International Journal of Cancer*. **2011**, 129, 2945-2957.

Klymkowsky, M. W. and Savagner, P. Epithelial-mesenchymal transition: a cancer researcher's conceptual friend and foe. *The American Journal of Pathology*. **2009**, 174 (5), 1588-1593.

Knijn, A.; Brisdelli, F.; Ferretti, A.; Iorio, E.; Marcheggiani, D.; Bozzi, A. Metabolic alterations in K562 cells exposed to taxol and tyrphostin AG957: 1H NMR and biochemical studies. *Cell Biology International*. **2005,** 29, 890-897.

Kominsky, D. J.; Klawitter, J.; Brown, J. L.; Boros, L. G.; Melo, J. V.; Eckhardt, S. G.; Serkova, N. Abnormalities in Glucose Uptake and Metabolism in Imatinib-Resistant Human BCR-ABL–Positive Cells. *Clinical Cancer Research*. **2009,** 15 (10), 3442-3450.

Komiya, S.; Gebhardt, M. C.; Mangham, D. C.; Inoue, A. Role of glutathione in cisplatin resistance in osteosarcoma cell lines. *Journal of Orthopaedic Research*. **1998**, 16 (1), 15-22.

Kotze, H. L.; Armitage, E. G.; Fletcher, J. S.; Henderson, A.; Williams, K. J.; Lockyer. N. P.; Vickerman, J. C. ToF-SIMS as a tool for metabolic profiling small biomolecules in cancer systems. *Surface and Interface Analysis*. **2013**, 45, 277-281.

Koyama, T.; Suzuki, H.; Imakjire, A.; Yanase, H.; Hata, K.; Mizuquchi, J. Id3-Mediated Enhancement of Cisplatin-Induced Apoptosis in Sarcoma Cell Line MG-63. *Anticancer Research*. **2004**, 24 (3a), 1519-1524.

Lamego, I.; Duarte, I. F.; Marques, M. P. M.; Gil, A. M. Metabolic Markers of MG-63 Osteosarcoma Cell Line Response to Doxorubicin and Methotrexate Treatment: Comparison to Cisplatin. *Journal of Proteome Research*. **2014**, 13, 6033-6045.

Lane, A. N. and Fan, T. W. –M. Quantification and identification of isotopomer distributions of metabolites in crude cell extracts using ^{1}H TOCSY. *Metabolomics*. **2007**, 3 (2), 79-86.

Lefort, N.; Brown, A.; Lloyd, V.; Ouellette, R.; Touaibia, M.; Culf, A. S.; Cuperlovic-Culf, M. ^{1}H NMR metabolomic analysis of the effect of dichloroacetate and allopurinol on breast cancers. *Journal of Pharmaceutical and Biomedical Analysis*. **2014**, 93, 77-85.

Le Moyec, L.; Legrand, O.; Larue, V.; Kawakami, M.; Marie, J. P.; Calvo, F.; Hantz, E.; Taillandier, E. Magnetic Resonance Spectroscopy of Cellular Lipid Extracts from Sensitive, Resistant and Reverting K562 Cells and Flow Cytometry for Investigating the P-Glycoprotein Function in Resistance Reversion. *NMR in Biomedicine*. **2000**, 13, 92-101.

Le Moyec, L.; Tatoud, R.; Degeorges, A.; Calabresse, C.; Bauza, G.; Eugene, M.; Calvo, F. Proton Nuclear Magnetic Resonance Spectroscopy Reveals Cellular Lipids Involved in Resistance to Adriamycin and Taxol by the K562 Leukemia Cell Line. *Cancer Research.* **1996**, 56, 3461-3467.

Lei, Z.; Huhman, D. V.; Sumner, L. W. Mass spectrometry strategies in metabolomics. *The Journal of Biological Chemistry*. **2011**, 286 (29), 25435-25442.

Liesenfeld, D. B.; Hanermann, N.; Owen, R. W.; Scalbert, A.; Ulrich, C. M. Review of mass spectrometry-based metabolomics in cancer research. *Cancer Epidemiology, Biomarkers and Prevention*. **2013**, 22 (12), 2182-2201.

Lindon, J. C.; Beckonert, O. P.; Holmes, E.; Nicholson, J. High-resolution magic angle spinning NMR spectroscopy: Application to biomedical studies. *Progress in Nuclear Magnetic Resonance Spectroscopy*. **2009,** 55 (2), 79-100.

Lindon, J. C.; Holmes, E.; Bollard, M. E.; Stanley, E. G.; Nicholson, J. K., Metabonomics technologies and their applications in physiological monitoring, drug safety assessment and disease diagnosis. *Biomarkers*. **2004,** 9 (1), 1-31.

Lindon, J. C.; Holmes, E.; Nicholson, J. K. Metabonomics in pharmaceutical R & D. *FEBS Journal*. **2007,** 274, 1140-1151.

Lindon, J. C.; Nicholson, J. K.; Holmes, E. The handbook of metabonomics and metabolomics. *Elsevier: Oxford*. **2007**.

Lindskog, M.; Spenger, C.; Jarvet, J.; Graslund, A.; Kogner, P. Predicting Resistance or Response to Chemotherapy by Proton Magnetic Resonance Spectroscopy in Neuroblastoma. *Journal of the National Cancer Institute*. **2004**, 96, 1457-1466.

Liu, S.; Wang, W.; Zhou, X.; Gu, R.; Ding, Z. Dose Responsive Effects of Cisplatin in L02 Cells Using NMR-Based Metabolomics. *Environmental Toxicology and Pharmacology.* **2014**, 37, 150-157.

Liu, Y. and Deisseroth, A. Tumor vascular targeting therapy with viral vectors. *Blood*. **2006**, 107 (8), 3027-3033.

Locasale, J. and Cantley, L. C. Altered metabolism in cancer. *BMC Biology*. **2010**, 8, 88.

Lodi, A. and Ronen, S. M. Magnetic Resonance Spectroscopy Detectable Metabolomiv Fingerprint of Response to Antineoplastic Treatment. *PLOS One*. **2011**, 6 (10), e26155.

Loiseau, D.; Morvan, D.; Chevrollier, A.; Demidem, A.; Douay, O.; Reynier, P.; Stepien, G. Mitochondrial Bioenergetic Background Confers a Survival Advantage to HepG2 Cells in Response to Chemotherapy. *Molecular Carcinogenesis*. **2009**, 48, 733-741.

Luetke, A.; Meyers, P. A.; Lewis, I.; Juergens, H. Osteosarcoma treatment – Where do we stand? A state of the art. *Cancer Treatment Reviews*. **2014**, 40, 523-532.

Lutz, N. W.; Tome, M. E.; Aiken, N. R.; Briehl, M. M. Changes in phosphate metabolism in thymoma cells suggest mechanisms for resistance to dexamethasone-induced apoptosis. A ^{31}P NMR spectroscopy study of cell extracts. *NMR in Biomedicine*. **2002**, 15, 356-366.

Lutz, N. W.; Franks, S. E.; Frank, M. H.; Pomer, S.; Hull, W. E. Investigation of multidrug resistance in cultured human renal cell carcinoma cells by ^{31}P-NMR spectroscopy and treatment survival assays. *Magma*. **2005**, 18, 144-161.

Lushchak, V. I. Glutathione Homeostasis and Functions: Potential Targets for Medical Interventions. *J Amino Acids* **2012**, 736837.

Ma, D.; Tremblay, P.; Mahngar, K.; Collins, J.; Hudlick, T.; Pandey, S. Selective cytotoxicity against human osteosarcoma cells by a novel synthetic C-1 analogue of 7-deoxypancratistatin is potentiated by curcumin. PLoS One. **2011**, 6(12), e28780.

Mac Gabhann, F. and Popel, A. S. Systems biology of vascular endothelial growth factors. *Microcirculation*. **2008**, 15 (8), 715-738.

MacKinnon, N.; Khan, A. P.; Chinnaiyan, A. M.; Rajendiran, T. M.; Ramamoorthy, A. Androgen receptor activation results in metabolite signatures of an aggressive prostate cancer phenotype: an NMR-based metabonomics study. *Metabolomics*. **2012**, 8, 1026-1036.

Macnicol, P. K. Homoglutathione and Glutathione Synthetases of Legume Seedlings: Partial Purification and Substrate Specificity. *Plant Science*. **1987***,* 53, 229-235.

Madsen, R.; Lundtedt, T.; Trygg, J. Chemometrics in metabonomics - A review in human disease diagnosis. *Analytica Chimica Acta*. **2010**, 659, 23-33.

Mancuso, A.; Zhu, A.; Beardsley, N. J.; Glickson, J. D.; Wehrli, S.; Pickup, S. Artificial Tumor Model Suitable for Monitoring ^{31}P and ^{13}C NMR Spectroscopic Changes During Chemotherapy-Induced Apoptosis in Human Glioma Cells. *Magnetic Resonance in Medicine*. **2005**, 54, 67-78.

Mannechez, A.; Reungpatthanaphong, P.; de Certaines, J. D.; Leray, G.; Le Moyec, L. Proton NMR Visible Mobile Signals in Sensitive and Multidrug-Resistant K562 Cells Are Modulated by Lipid Rafts. *Cancer Cell International*. **2005**, 5, 2.

Mardor, Y.; Kaplan, O.; Sterin, M.; Ruiz-Cabello, J.; Ash, E.; Roth, Y.; Ringel, I.; Cohen, J. S. Noninvasive Real-Time Monitoring of Intracellular Cancer Cell Metabolism and Response to Lonidamine Treatment Using Diffusion Weighted Proton Magnetic Resonance Spectroscopy. *Cancer Research*. **2000**, 60, 5179-5186.

Marques, M. P. M. Platinum and Palladium Polyamine Complexes as Anticancer Agents: The Structural Factor. *ISNR Spectroscopy* **2013**, 287353.

Massimi, M.; Tomassini, A.; Sciubba, F.; Sobolev, A. P.; Devirgiliis, L. C.; Miccheli, A. Effetcs of resveratrol on HepG2 cells as revealed by ^{1}H-NMR based metabolic profiling. *Biochimica et Biophysica Acta*. **2012**, 1820, 1-8.

Mathew, R.; Karantza-Wadsworth, V.; White, E. Role of autophagy in cancer. *Nature Reviews|Cancer*. **2007**. 7, 961-967.

McQueen, C. Comprehensive Toxicology. *Elsevier* Science. **2010**, 2nd Ed.

Meiboom, S. and Gill, D.; Modified spin-echo method for measuring nuclear relaxation times. *Review of Scientific Instruments*. **1958**, 29(8), 688-691.

Merz, A. L. and Serkova, N. J. Use of nuclear magnetic resonance-based matabolomics in detecting drug resistance in cancer. *Biomarkers in Medicine*. **2009,** 3 (3), 289-306.

Miao, X. –S.; Zhong, C.; Wang, Y.; Savage, R. E.; Yang, R. –Y.; Kizer, D.; Volckova, E.; Ashwell, M. A.; Chan, T. C. K. *In vitro* metabolism of β-lapachone (ARQ 501) in mammalian hepatocytes and cultured human cells. *Rapid Communications in Mass Spectrometry*. **2009**. 23, 12-22.

Milkevitch, M.; Shim, H.; Pilatus, U.; Pickup, S.; Wehrle, J. P.; Samid, D.; Poptani, H.; Glickson, J. D.; Delikatny, E. J. Increases in NMR-Visible Lipid and Glycerophosphocholine During Phenylbutyrate-Induced Apoptosis in Human Prostate Cancer Cells. *Biochimica et Biophysica. Acta*. **2005**, 1734, 1-12.

Milkevitch, M.; Jeitner, T. M.; Beardsley, N. J.; Delikatny, E. J. Lovastatin enhances phenylbutyrate-induced MR-visible glycerophosphocholine but not apoptosis in DU145 prostate cells. *Biochimica et Biophysica Acta*. **2007**, 1771, 1166-1176.

Minotti, G.; Menna, P.; Salvatorelli, E.; Cairo, G.; Gianni, L. Anthracyclines: Molecular Advances and Pharmacologic Developments in Antitumor Activity and Cardiotoxicity. *Pharmacological Reviews.* **2004**, 56, 185-229.

Mirbahai, L.; Wilson, M.; Shaw, C. S.; McConville, C.; Malcomson, R. D. G.; Kauppinen, R. A.; Peet, A. C. Lipid Biomarkers of Glioma Cell Growth Arrest and Cell Death Detected by ^{1}H Magic Angle Spinning MRS. *NMR in Biomedicine*. **2012**, 25, 1253-1262.

Mirbahai, L.; Wilson, M.; Shaw, C. S.; McConville, C.; Malcomson, R. D.; Griffin, J. L.; Kauppinen, R. A.; Peet, A. C. ^{1}H Magnetic Resonance Spectroscopy Metabolites as Biomarkers for Cell Cycle Arrest and Cell Death in Rat Glioma Cells. *Int. J. Biochem. Cell Biology*. **2011**, 43, 990-1001.

Mistry, P.; Kelland, L. R.; Abel, G.; Sidhar, S. The relationship between glutathione, glutathione-S-transferase and cytotoxicity of platinum drugs and melphalan in eight human ovarian carcinoma cell lines. *British Journal of Cancer*. **1991**, 64 (2), 215-220.

Miura, D.; Fujimura, Y.; Tachibana, H.; Wariishi, H. Highly Sensitive Matrix-Assisted Laser Desorption Ionization-Mass Spectrometry for High-Throughput Metabolic Profiling. *Analytical Chemistry.* **2010**, 82, 498-504.

Moestue, S.; Sitter, B.; Bathen, T. F.; Tessem, M. –B.; Gribbestad, S. HR MAS MR Spectroscopy in Metabolic Characterization of Cancer. *Current Topics in Medicinal Chemistry*. **2011**, 11, 2-26.

Morin, P. Jr.; Ferguson, D.; LeBlank, L. M.; Hébert, M. J. G.; Paré, A. F.; Jean-François, J.; Surette, M. E.; Touaibia, M.; Cuerlovic-Culf, M. NMR Metabolomics Analysis of the Effects of 5-Lipoxygenase Inhibitors on Metabolism in Gliobastomas. *Journal of Proteome Research*. **2013**, 12, 2165-2176.

Morse, D. L.; Raghunand, N.; Sadarangani, P.; Murthi, S.; Job, C.; Day, S.; Howison, C.; Gillies, R. J. Response of Choline Metabolites to Docetaxel Therapy Is Quantified In Vivo by Localized ^{31}P

MRS of Human Breast Cancer Xenografts and In Vitro by High-Resolution ^{31}P NMR Spectroscopy of Cells Extracts. *Magnetic Resonance in Medicine*. **2007**, 58, 270-280.

Morvan, D.; Demidem, A.; Papon, J.; Madelmont, J. C. Quantitative HRMAS Proton Total Correlation Spectroscopy Applied to Cultured Melanoma Cells Treated by Chloroethyl Nitrosourea: Demonstration of Phospholipid Metabolism Alterations. *Magnetic Resonance in Medicine*. **2003**, 49, 214-248.

Morvan, D. and Demidem, A. Metabolomics by Proton Nuclear Magnetic Resonance Spectroscopy of the Response to Chlroethylnitrosourea Reveals Drug Efficacy and Tumor Adaptive Metabolic Pathways. *Cancer Research*. **2007**, 67 (5), 2150-2159.

Morvan, D. Functional Metabolomics Uncovers Metabolic Alterations Associated to Severe Oxidative Stress in MCF7 Breast Cancer Cells Exposed to Ascididemin. *Marine Drugs*. **2013**, 11, 3846-3860.

Mosmann, T. Rapid Colorimetric Assay for Cellular Growth and Survival: Application to Proliferation and Cytotoxicity Assays. *Journal of Immunological Methods*. **1983**, 65, 55-63.

Muhammad, N. and Guo, Z. Metal-based anticancer chemotherapeutic agents. *Current Opinion in Chemical Biology*. **2014**, 19, 144-153.

Musacchio, T.; Tomiutti, M.; Kautz, R.; Torchilin, V. P. ^{1}H NMR Detection of Mobile Lipids as a Marker for Apoptosis: The Case of Anticancer Drug-Loaded Liposomes and Polymeric Micelles. *Molecular Pharmaceutics*. **2009**, 6 (6), 1876-1882.

Myint, K. T.; Uehara, T.; Aoshima, K.; Oda, Y. Polar Anionic Metabolome Analysis by Nano-LC/MS with a Metal Chelating Agent. *Analytical Chemistry*. **2009**, 81, 7766-7772.

Nagy, Z. B.; Csanád, M.; Tóth, K.; Börzsönyi, B.; Demendi, C.; Rigó, J. Jr.; Joó, J. G. Current Concepts in the Genetic Diagnosis of Rheumatoid Arthritis. *Expert Review of Molecular Diagnosis*. **2010**, 10 (5), 603-618.

Naruse, T.; Nishida, Y.; Ishiguro, N. Synergistic effects of meloxicam and conventional cytotoxic drugs in human MG-63 osteosarcoma cells. *Biomedicine and Pharmacotherapy*. **2007**, 61, 338-346.

Navarro-Ranninger, C.; Pérez, J. M.; Zamora, F.; González, V. M.; Masaquer, J. R.; Alonso, C. Palladium (II) compounds of putrescine and spermine. Synthesis, characterization, and DNA-binding and antitumor properties. *Journal of Inorganic Biochemistry*. **1993**, 52 (1), 37-49.

Negrini, S.; Gorgoulis, V. G.; Halazonetis, T. D. Genomic instability – an evolving Hallmark of cancer. *Nature Reviews|Molecular Cell Biology*. **2010**, 11, 220-228.

Nelson, D. L and Cox, M. M. Lehninger Principles of Biochemistry. **2005**, 4th Ed.

Nicholson, J. K.; Connelly, J.; Lindon, J. C.; Holmes, E. Metabonomics: a platform for studying drug toxicity and gene function. *Nature Reviews|Drug Discovery*. **2002**, 1, 153-161.

Nicholson, J. K.; Lindon, J. C.; Holmes, E., "Metabonomics": understanding the metabolic responses of living systems to pathophysiological stimuli via multivariate statistical analysis of biological NMR spectroscopic data. *Xenobiotica*. **1999,** 29 (11), 1181-1189.

O'Day, K. and Gorlick, R. Novel therapeutic agents for osteosarcoma. *Expert Reviews|Anticancer Therapy*. **2009**, 9(4), 511-523.

Ohmine, K.; Kawaguchi, K.; Ohtsuki, S.; Motoi, F.; Egawa, S.; Unno, M.; Teraki, T. Attenuation of Phosphorylation by Deoxycytidine Kinase is Key to Acquired Gemcitabine Resistance in a Pancreatic Cancer Cell Line: Targeted Proteomic and Metabolomic Analyses in PK9 Cells. *Pharmaceutical Research*. **2012**, 29, 2006-2016.

Olivier, M.; Hollstein, M.; Hainaut, P. TP53 mutations in human cancers: origins, consequences, and clinical use. *Cold Spring Harbor perspectives in biology*. **2010**, 2 (1), a001008.

Ozaki, T.; Ishiguro, S.; Itoh, H.; Furuhama, K.; Nakazawa, M.; Yamashita, T. Cisplatin Binding and Inactivation of Mitochondrial Glutamate Oxaloacetate Transaminase in Cisplatin-Induced Rat Nephrotoxicity. *Bioscience, Biotechnology, and Biochemistry*. **2013**, 77 (8), 1645-1649.

Palmero, A.; Berger, M.; Venturi, C.; Ferrero, I.; Rustichelli, D.; Berta, L.; Frairia, R.; Madon, E.; Fagioli, F. High energy shock waves enhance the cytotoxic effect of doxorubicin and methotrexate to human osteosarcoma cell lines. *Oncology Reports*. **2006**, 15, 267-273.

Pan, X.; Wilson, M.; McConville, C.; Arvanitis, T. N.; Griffin, J. L.; Kauppinen, R. A.; Peet, A. C. Increased Unsaturation of Lipids in Cytoplasmic Lipid Droplets in DAOY Cancer Cells in Response to Cisplatin Treatment. *Metabolomics*. **2013**, 9, 722-729.

Pan, X.; Wilson, M.; Mirbahai, L.; McConville, C.; Arvanitis, T. N.; Griffin, J. L.; Kauppinen, R. A.; Peet, A. C. In Vitro Metabonomic Study Detects Increases in UDP-GlcNAc and UDP-GalNAc, as Early Phase Markers of Cisplatin Treatment Response in Brain Tumor Cells. *Journal of Proteome Research*. **2011**, 10, 3493-3500.

Pan, Z. and Raftery, D. Comparing and combining NMR spectroscopy and mass spectrometry in metabolomics. *Analytical and Bioanalytical Chemistry*. **2007**, 387 (2), 525-527.

Pandher, R.; Ducruix, C.; Eccles, S. A.; Raynaud, F. I. Cross-platform Q-TOF validation of global exo-metabolomic analysis: Application to human gliobastoma cells treated with the standard PI 3-Kinase inhibitor LY294002. *Journal of Chromatography B*. **2009**, 877, 1352-1358.

Pautke, C.; Schieker, M.; Tischer, T.; Kolk, A.; Neth, P.; Mutschler, W.; Milz, S. Characterization of Osteosarcoma Cell lines MG-63, Saos-2 and U-2 OS in Comparison to Human Osteoblasts. *Anticancer Research*. **2004**, 24, 3743-3748.

Pearson, R. G. Hard and Soft Acids and Bases HSAB 0.1. Underlying Theories. *Journal of Chemical Education* **1968**, 45 (9), 581-587.

Pearson, R. G. Hard and Soft Acids and Bases HSAB 0.2. Underlying Theories. *Journal of Chemical Education* **1968**, 45 (10), 643-648.

Peng, S.; Yan, L.; Zhang, J.; Wang, Z.; Tian, M.; Shen, H. An integrated metabonomics and transcriptomics approach to understand metabolic pathway disturbance induced by perfluorooctanoic acid. *Journal of Pharmaceutical and Biomedical Analysis*. **2013**, 86, 56-64.

Petrie, A. and Sabin, C. Medical Statistic at a Glance. *Blackwell Science, Ltd.: Oxford*. **2009**.

Phan, L. M.; Yeung, S. –C. J.; Lee, M. –H. Cancer metabolic reprogramming: importance, main features, and potentials for precise targeted anti-cancer therapies. *Cancer Biology and Medicine*. **2014**, 11, 1-19.

Piccioni, F.; Borioni, A.; Delfini, M.; Giudice, M. R. D.; Mustazza, C.; Rodomonte, A.; Risuleo, G. Metabolic alterations in cultured mouse fibroblasts induced by an inhibitor of the tyrosine kinase Fibroblast Growth Factor Receptor 1. *Analytical Biochemistry*. **2007**, 367, 111-121.

Pirman, D. A.; Efuet, E.; Ding, X. –P.; Pan, Y.; Tan, L.; Fischer, S. M.; DuBois, R. N.; Yang, P. Changes in Cancer Cell Metabolism Revealed by Direct Sample Analysis with MALDI Mass Spectrometry. *PLOS One*. **2013**, 8 (4), e61379.

Piva, R.; Manferdini, C.; Lambertini, E.; Torreggiani, E.; Penolazzi, L.; Gambari, R.; Pastore, A.; Pelucchi. S.; Gabusi, E.; Piacentini, A.; Filardo, G.; Facchini, A.; Lisignoli, G. Slug contributes to regulation of CXCL12 expression in human osteoblasts. *Experimental Cell Research*. **2011**, 317(8), 1159-1168.

Pizarro, A. M. and Sadler, P. J. Unusual DNA binding modes for metal anticancer complexes. *Biochimie*. **2009**, 91, 1198-1211.

Podo, F. Tumour phospholipid metabolism. *NMR in Biomedicine*. **1999**, 12, 413-439.

Polyak, K. and Weinberg, R. A. Transitions between epithelial and mesenchymal states: acquisition of malignant and stem cell traits. *Nature Reviews|Cancer*. **2009**, 9 (4), 265-273.

Powers, R. NMR metabolomics and drug discovery. *Magnetic Resonance in Chemistry*. **2009,** 47, S2-S11.

Putluri, N.; Shojaie, A.; Vasu, V. T.; Nalluri, S.; Vareed, S. K.; Putluri, V.; Vivekanandan-Giri, A.; Byun, J.; Pennathur, S.; Sana, T. R.; Fischer, S. M.; Palapattu, G. S.; Creighton, C. J.; Michailidis, G.; Sreekumar, A. Metabolic Profiling Reveals a Role for Androgen in Activating Amino Acid Metabolism and Methylation in Prostate Cancer Cells. *PLOS One*. **2011**, 6 (7), e214117.

Rainaldi, G.; Romano, R.; Indovina, P.; Ferrante, A.; Motta, A.; Indovina, P. L.; Santini, M. T. Metabolomics Using 1H-NMR of Apoptosis and Necrosis in HL60 Leukemia Cells: Differences Between the Two Types of Cell Death and Independence from the Stimulus of Apoptosis Used. *Radiation Research.* **2008**, 169, 170-180.

Ray, S.; Mohan, R.; Singh, J. K.; Samantaray, M. K.; Shaikh, M. M.; Panda, D.; Ghosh, P. Anticancer and Antimicrobial Metallopharmaceutical Agents Based on Palladium, Gold, and Silver N-Heterocyclic Carbene Complexes. *Journal of American Chemical Society*. **2007**, 129 (48), 15042-15053.

Raza, A.; Franklin, M. J.; Dudek, A. Z. Pericytes and vessel maturation during tumor angiogenesis and metastasis. *American Journal of Hematology*. **2010**, 85 (8), 593-598.

Reynolds, W. F. NMR pulse sequences. Encyclopedia of spectroscopy and spectrometry. Lindon, J. C.; Tranter, G. E.; Holmes, J. L. *Academic Press: London*. **2000**, 2, 1554-1567.

Ritter, J. and Bielack, S. S. Osteosarcoma. *Annals of Oncology*. **2010**, 21 (Suppl 7), vii320-325.

Rodríguez, I.; Pérez-Rial, S.; González-Jimenez, J.; Pérez-Sánchez, J.; Herranz, F.; Beckmann, N.; Ruíz-Cabello, J. Magnetic resonance methods and applications in pharmaceutical research. *Journal of Pharmaceutical Sciences*. **2008**, 97 (9), 3637-36-65.

Ronen, S. M.; DiStefano, F.; McCoy, C. L.; Robertson, D.; Smith, T. A. D.; Al-Saffar, N. M.; Titley, J.; Cunningham, D. C.; Griffiths, J. R.; Leach, M. O.; Clarke, P. A. Magnetic Resonance Detects Metabolic Changes Associated with Chemotherapy-Induced Apoptosis. *British Journal of Cancer*. **1999**, 80, 1035-1041.

Rosi, A.; Grande, S.; Luciani, A. M.; Barone, P.; Mlynarik, V.; Viti, V.; Guidoni, L. ^{1}H MRS studies of signals from mobile lipids and from lipid metabolites: comparison of the behavior in cultured tumoe cells and in spheroids. *NMR in Biomedicine*. **2004**, 17, 76-91.

Ross, J.; Najjar, A. M.; Sankaranarayanapillai, M.; Tong, W. P.; Kaluarachchi, K.; Ronen, S. M. Fatty Acid Synthase Inhibition Results in a Magnetic Resonance-Detectable Drop in Phosphocholine. *Molecular Cancer Therapy*. **2008**, 7, 2556-2565.

Ruiz-Aracama, A.; Peijnenburg, A.; Kleinjans, J.; Jennen, D.; van Delft, J.; Hellfrisch, C.; Lommen, A. An untargeted multi-technique metabolomics approach to studying intracellular metabolites in HepG2 cells exposed to 2,3,7,8-tetrachlorodibenzo-p-dioxin. *BMC Genomics*. **2011**, 12, 251.

Saccenti, E.; Hoefsloot, H. C. J.; Smilde, A. K.; Westerhuis, J. A.; Hendriks, M. M. W. B. Reflection on univariate and multivariate analysis of metabolomics data. *Metabolomics*. **2014**, 10, 361-374.

Santini, M. T.; Rainaldi, G.; Romano, R.; Ferrante, A.; Clemente, S.; Motta, A.; Indovina, P. L. MG-63 human osteosarcoma cells grown in monolayer and as three-dimentional tumor spheroids present a different metabolic profile: a ^{1}H NMR study. *FEBS Letters*. **2004,** 557, 148-154.

Santini, M. T.; Romano, R.; Rainaldi, G.; Ferrante, A.; Indovina, P.; Motta, A.; Indovina, P. L. 1H-NMR evidence for a different response to the same dose (2 Gy) of ionizing radiation of MG-63 human osteosarcoma cells and three-dimensional spheroids. *Anticancer Research*. **2006,** 26 (1A), 267-281.

Santini, M. T.; Romano, R.; Rainaldi, G.; Ferrante, A.; Motta, A.; indovina, P. L. Increases in ^{1}H-NMR Mobile Lipids Are Not Always Associated with Overt Apoptosis: Evidence from MG-63 Human Osteosarcoma Three-Dimensional Spheroids Exposed to a Low Dose (2 Gy) of Ionizing Radiation. *Radiation Research.* **2006,** 165, 131-141.

Santini, M. T.; Romano, R.; Rainaldi, G.; Filippini, P.; Bravo, E.; Porcu, L.; Motta, A.; Calcabrini, A.; Meschini, S.; Indovina, P. L.; Arancia, G. The Relationship Between ^{1}H-NMR Mobile Lipid Intensity and Cholesterol in Two Human Tumor Multidrug Resistant Cell Lines (MCF-7 and LoVo). *Biochimica et Biophysica Acta*. **2001**, 1531, 111-131.

Santini, M. T.; Romano, R.; Rainaldi, G.; Indovina, P.; Ferrante, A.; Motta, A.; Indovina, P. L. Temporal Dynamics of ^{1}H-NMR-Visible Metabolites During Radiation-Induced Apoptosis in MG-63 Human Osteosarcoma Spheroids. *Radiation Research*. **2006,** 166, 734-745.

Santos, C. R. and Schulze, A. Lipid Metabolism in cancer. *FEBS Journal*. **2012**, 279 (15), 2610-2623.

Sasada, S.; Miyata, Y.; Tsutani, Y.; Tsuyama, N.; Masujima, T.; Hihara, J.; Okada, M. Metabolomic analysis of dynamic response and drug resistance of gastric cancer cells to 5-fluorouracil. *Oncology Reports*. **2013**, 29, 925-931.

Savorani, F.; Tomasi, G.; Engelsen, S. B.; icoshift: A versatile tool for the rapid alignment of 1D NMR spectra. *Journal of Magnetic Resonance.* **2010**, 202(2), 190-202.

Schmiegelow, K. Advances in Individual Prediction of Methotrexate Toxicity: a Review. *British Journal of Haematology.* **2009**, 146, 489-503.

Schulze, A. and Harris, A. L. How cancer metabolism is tuned for proliferation and vulnerable to disruption. *Nature*. **2012**, 491 (7424), 364-373.

Schwab, J. H.; Springfield, D. S.; Raskin, K. A.; Mankin, H. J.; Hornicek, F. J. What's new in primary bone tumors. *The Journal of Bone and Joint Surgery*. **2012**, 94 (20), 1913-1919.

Semenza, G. L. Targeting HIF-1 for cancer therapy. *Nature Reviews|Cancer*. **2003**, 3 (10), 721-732.

Senese, S.; Lo, Y. C.; Huang, D.; Zangle, T. A.; Gholkar, A. A.; Robert, L.; Homet, B.; Ribas, A.; Summers, M. K.; Teitell, M. A.; Damoiseaux, R.; Torres, J. Z. Chemical dissection of the cell cycle: probes for cell biology and anticancer drug development. *Cell Death and Disease*. **2014**, 5, e1462.

Serkova, N. and Boros, L. G. Detection of Resistance to Imatinib by Metabolic Profiling. Clinical and Drug Development Implications. *American Journal of Pharmacogenomics*. **2005**, 5 (5), 293-302.

Serkova, N. J. and Glunde, K. Metabolomics and Cancer. *Methods in Molecular Biology*. **2009**, 520, 273-295.

Shay, J. W. and Wright, W. E.; Hayflick, his limit, and cellular ageing. *Nature Reviews|Molecular Cell Biology.* **2000**, 1, 72-76.

Silva, T. M.; Andersson, S.; Kumar, S.; Marques, M. P. M.; Persson, L.; Oredsson, S. Norspermidine and Novel Pd(II) and Pt(II) Polynuclear Complexes of Norspermidine as Potential Antineoplastic Agents Against Breast Cancer. *PLOS One* **2013**, 8(2), e55651.

Silva, T. M.; Fiuza S. M.; Marques, M. P. M.; Persson, L.; Oredsson, S. Increased Breast Cancer cell Toxicity by Palladination of the Polyamine Analogue N1, N11-bis(ethyl)Norspermine. *Amino Acids*. **2014**, 46, 339-352.

Singh, B. K. Complexation Behaviour of Glutathione with Metal Ions. *Asian Journal of Chemistry*, **2005**, 17 (1), 1-32.

Sitter, B.; Bathen, T. F.; Tessem, M. –B.; Gribbestad, I. S. High-resolution magic angle spinning (HR MAS) MR spectroscopy in metabolic characterization of human cancer. *Progress in Nuclear Magnetic Resonance Spectroscopy*. **2009**.

Skeel, R. T. Handbook of Cancer Chemotherapy. *Lippincott Williams & Wilkins: Philadelphia*. **2007**, 7th Ed.

Skehan, P.; Storeng, R.; Scudiero, D.; Monks, A.; McMahon, J.; Vistica, D.; Warren, J, T.; Bokesch, H.; Kenney, S.; Boyd, M. R. New Colorimetric Cytotoxicity Assay Screening. *Journal of the National Cancer Institute*. **1989**, 82, 1107-1102.

Smolinska, A.; Blanchet, L.; Buydens, L. M. C.; Wijmenga, S. S. NMR and patterns recognition methods in metabolomics: From data acquisition to biomarker discovery: A review. *Analytica Chimica Acta*. **2012**, 750, 82-97.

Soares, A. S.; Fiuza, S. M.; Gonçalves, M. J.; Batista de Carvalho, L. A. E.; Marques, M. P. M.; Urbano, A. M. Effect of the Metal Center on the Antitumor Activity of the Analogous Dinuclear Spermine Chelates $(PdCl_2)_2$(Spermine) and $(PtCl_2)_2$(Spermine). *Letters in Drug Design and Discovery*. **2007**, 4 (7), 460-463.

Souid, A. –K.; Fahey, R. C.; Aktas, M. K.; Sayin, O. A.; Karjoo, S.; Newton, G. L.; Sadowitz, P. D.; Dubowy, R. L.; Bernstein, M. L. Blood thiols following amifostine and mesna infusions, a Pediatric Oncology Group study. *Drug Metabolism and Disposition*. **2001**, 29, 1–7.

Sovago, I.; Martin, R. B. Transition Metal ion Induced Deprotonation of Amide Hydrogens in Sulfhydryl Containing Compounds. *J Inorganic Nuclear Chemistry* **1981**, 43 (2), 425-429.

Spratlin, J. L.; Serkova, N. J.; Eckhardt, S. G. Clinical Applications of Metabolomics in Oncology: A Review. *Clinical Cancer Research*. **2009**, 15, 431-440.

von Stechow, L.; Ruiz-Aracama, A.; van de Water, B.; Peijnenburg, A.; Danen, E.; Lommen, A. Identification of Cisplatin-Regulated Metabolic Pathways in Pluripotent Stem Cells. *PLOS One*. **2013**, 8 (10), e76476.

Sterin, M.; Cohen, J. S.; Mardor, Y.; Berman, E.; Ringel, I. Levels of Phospholipid Metabolites in Breast Cancer Cells Treated with Antimitotic Drugs: a ^{31}P-Magnetic Resonance Spectroscopy Study. *Cancer Research.* **2001**, 61, 7536-7543.

Strober, W. Trypan blue exclusion test of cell viability. *Current Protocols in Immunology*. **2001**, Appendix 3.

Ta, H. T.; Dass, C. R.; Choong, P. F. M.; Dunstan, D. E. Osteosarcoma treatment: state of the art. *Cancer Metastasis Reviews*. **2009**, 28, 247-263

Tacar, O.; Sriamornsak, P.; Dass, C. R. Doxorubicin: an update on anticancer molecular action, toxicity and novel drug delivery systems. *The Journal of Pharmacy and Pharmacology*. **2013**, 65 (2), 157-170.

Teng, Q.; Huang, W.; Collette, T. W.; Ekman, D. R.; Tan, C. A direct cell quenching method for cell-culture based metabolomics. *Metabolomics*. **2009**, 5, 199-208.

Tian, H. and Cronstein, B. N. Understanding the Mechanisms of Action of Methotrexate. *Bulletin of the NYU Hospital for Joint Diseases*. **2007**, 65 (3), 168-173.

Tiziani, S.; Lodi, A.; Khanim, F. L.; Viant, M. R.; Bunce, C. M.; Günther, U. L. Metabolomic Profiling of Drug Responses in Acute Myeloid Leukaemia Cell Lines. *PLOS One*. **2009**, 4 (1), e4251.

Tiziani, S.; Kang, Y.; Choi, J. S.; Roberts W.; Paternostro, G. Metabolomic high-content nuclear magnetic resonance-based drug screening of a kinase inhibitor library. *Nature Communications*. **2011**, 2, 545.

Tong, X.; Zhao, F.; Thompson, C. B. The molecular determinants of de novo nucleotide biosynthesis in cancer cells. *Current Opinion in Genetics and Development.* **2009**, 19, 32-37.

Triba, M. N.; Starzec, A.; Bouchemal, N.; Guenin, E.; Perret, G. Y.; Le Moyec, L. Metabolomic Profiling with NMR Discriminates Between Biphosphonate and Doxorubicin Effects on B16 Melanoma Cells. *NMR in Biomedicine*. **2010**, 23, 1009-1016.

Trygg, J.; Holmes, E.; Lundstedt, T. Chemometrics in Metabonomics. *Journal of Proteome Research*. **2007,** 6, 469-479.

Tsai, H. C.; Huang, C. Y.; Su, H. L.; Tsang, C. H. CCN2 Enhances Resistance to Cisplatin-Mediating Cell Apoptosis in Human Osteosarcoma. *PLOS One* **2014**, 9 (3), e90159.

Tsang, R. Y.; Al-Fayea, T.; Au, H.-J. Cisplatin Overdose: Toxicities and Management. *Drug Safety Journal*. **2009,** 32 (12), 1109-1122.

Tummala, R.; Diegelman, P.; Fiuza, S. M.; Batista de Carvalho, L. A.; Marques, M. P.; Kramer, D. L.; Clark, K.; Vujcic, S.; Porter, C. W.; Pendyala, L. Characterization of Pt-, Pd-spermine complexes for their effect on polyamine pathway and cisplatin resistance in A2780 ovarian carcinoma cells. *Oncology Reports* **2010**, 24 (1), 15-24.

Uehara, T.; Yokoi, A.; Aoshima, K.; Tanaka, S.; Kadowaki, T.; Tanaka, M.; Oda, Y. Quantitative Phosphorus Metabolomics Using Nanoflow Liquid Chromatography-Tandem Mass Spectrometry and Culture-Derived Comprehensive Global Internal Standards. *Analytical Chemistry*. **2009,** 81 (10), 3836-3842.

Ulrich, E. L.; Akutsu, H.; Doreleijers, J. F.; Harano, Y.; Ioannidis, Y. E.; Lin, J.; Livny, M.; Mading, S.; Maziuk, D.; Miller, Z.; Nakatani, E.; Schulte, C. F.; Tolmie, D. E.; Kent Wenger, R.; Yao, H. and Markley, J. L.; BioMagResBank. *Nucleic Acids Research*. **2008**, 36 (suppl 1), D402-D408.

Valdés, A.; Simó, C.; Ibáñez, C.; Rocamora-Reverte, L.; Ferragut, J. A.; García-Cañas, J.; Cifuentes, A. Effect of dietary polyphenols on K652 leukemia cells: A Foodomics approach. *Electrophoresis*. **2012**, 33, 2314-2327.

van den Berg, R. A.; Hoefsloot, H. C. J.; Westerhuis, J. A.; Smilde, A. K.; van der Werf, M.J. Centering, scaling, and transformations: improving the biological information content of metabolomics data. *BMC Genomics*. **2006**, 7(1), 142.

Van Driel, M. and van Leeuwen, J. P. Cancer and bone: a complex complex. *Archives of Biochemistry and Biophysics*. **2014**, 561, 159-166.

Vermes, I.; Haanen, C.; Steffens-Nakken, H.; Reutelingsperger, C. A novel assay for apoptosis. Flow cytometric detection of phosphatidylserine expression on early apoptotic cells using fluorescein labeled Annexin V. *Journal of Immunological Methods*. **1995**, 185 (1), 39-51.

Veselkov, K. A.; Lindon, J. C.; Ebbels, T. M. D.; Crockford, D.; Volynkin, V. V.; Holmes, E.; Davies, D. B.; Nicholson, J. K. Recursive segment-wise peak alignment of biological ^{1}H NMR spectra for improved metabolic biomarker recovery. *Analytical Chemistry*. **2009**, 81 (1), 56-66.

Veselkov, K. A.; Vingara, L. K.; Masson, P.; Robinette, S. L.; Want, E.; Li, J. V.; Barton, R. H.; Boursier-Neyret, C.; Walther, B.; Ebbels, T. M.; Pelczer, I.; Holmes, E.; Lindon, J. C.; Nicholson, J. K. Optimized preprocessing of ultra-performance liquid chromatography/mass spectrometry urinary metabolic profiles for improved information recovery. *Analytical Chemistry*. **2011**, 83 (15), 5864-5872.

Voigt, W. Sulforhodamine B Assay and Chemosensitivity. *Methods in Molecular Medicine*. **2005**, 110, 39-48.

Vu, T. N.; Valkenborg, D.; Smets, K.; Verwaest, K. A.; Dommisse, R.; Lemiere, F.; Verschoren, A.; Goethals, B.; Laukens, K. An integrated workflow for robust alignment and simplified quantitative analysis of NMR spectrometry data. *BMC Bioinformatics*. **2011**, 12,405.

Wang, T. N.; Qian, X.; Granick, M. S.; Solomon, M. P.; Rothman, V. L.; Berger, D. H.; Tuszynski, G. P. Thrombospondin-1 (TSP-1) promotes the invasive properties of human breast cancer. *The Journal of Surgical Research*. **1996**, 63 (1), 39-43.

Wang, X.; Guo, Z. The role of sulfur in platinum anticancer chemotherapy. *Anti-Cancer Agents in Medicinal Chemistry*. **2007**, 7 (1), 19–34.

Wang, J.; Jin, L.; Li, X.; Deng, H.; Chen, Y.; Lian, Q.; Ge, R.; Deng, H. Gossypol induces apoptosis in ovarian cancer cells through oxidative stress. *Molecular BioSystems*. **2013**, 9, 1489-1498.

Warburg, O.; Posener, K.; Negelein, E. Uber den Stoffwechsel der Karzinomzellen. *Biochemische Zeitschrift*. **1924**, 152, 309-344

Warburg; O. On origin of cancer cells. *Science*. **1956,** 123, 309-314.

Ward, P. S. and Thompson, C. B. Metabolic reprogramming: a cancer hallmark even Warburg did not anticipate. *Cancer Cell*. **2012**, 21 (3), 297-308.

Warwick, G. P. The Mechanism of Action of Alkylating Agents. *Cancer Research*. **1963**, 23, 1315-1333.

Weljie, A. and Jirik, F. R. Hypoxia-induced metabolic shifts in cancer cells: Moving beyond the Warburg effect. *The International Journal of Biochemistry & Cell Biology*. **2011**, 43, 981-989.

Wellen, K. E.; Lu, C.; Mancuso, A.; Lemons, J. M.; Ryczko, M.; Dennis, J. W.; Rabinowitz, J. D.; Coller, H. A.; Thompson, C. B. The hexosamine biosynthetic pathway couples growth factor-induced glutamine uptake to glucose metabolism. *Genes and Development*. **2010**, 24, 2784-99.

Westerhuis, J.; Hoefsloot, H.; Smit, S.; Vis, D.; Smilde, A.; van Velzen, E.; van Duijnhoven, J.; van Dorsten, F. Assessment of PLSDA cross validation. *Metabolomics*. **2008**, 4 (1), 81-89.

White, E.; DiPaola, R. S. The double-edged sword of autophagy modulation in cancer. *Clinical Cancer Research*. **2009**, 15, 5308-5316.

Wider, G. and Dreier, L. Measuring protein concentrations by NMR spectroscopy. *Journal of the American Chemical Society*. **2006**, 128 (8), 2571-2576.

Wise, D. R. and Thompson, C. B. Glutamine addiction: a new therapeutic target in cancer. *Trends in Biochemical Sciences*. **2010**, 35 (8), 427-433.

Wiklund, S.; Johansson, E.; Sjöström, L.; Mellerowicz, E. J.; Edlund, U.; Shockcor, J. P.; Gottfries, J.; Moritz, T.; Trygg, J. Visualization of GC/TOF-MS-Based Metabolomics Data for Identification of Biochemically Interesting Compounds Using OPLS Class Models. *Analytical Chemistry*. **2008**, 80, 115-122.

Wishart, D. S.; Jewison, T.; Guo, A. C.; Wilson, M.; Knox, C.; Liu, Y.; Djoumbou, Y.; Mandal, R.; Aziat, F.; Dong, E.; Douatra, S.; Sinelnikov, I.; Arndt, D.; Xia, J.; Liu, P.; Yallou, F.; Bjorndahl, T.; Perez-Pineiro, R.; Eisner, R.; Allen, F.; Neveu, V.; Greiner, R.; Scalbert, A. HMDB 3.0 – The Human Metabolome Database in 2013. *Nucleic Acid Research*. **2013**, 41, D801-807.

World Cancer Report, 2014

Worley, B. and Powers, R. Multivariate Analysis in Metabolomics. *Current Metabolomics*. **2013**, 1, 92-107.

Wu, D. H., Chen, A. D. and Johnson, C. S.; An Improved Diffusion-Ordered Spectroscopy Experiment Incorporating Bipolar-Gradient Pulses. *Journal of Magnetic Resonance, Series A* **1995**, 115(2), 260-264.

Wu, W. and Zhao, S. Metabolic changes in cancer: beyond the Warburg effect. *Acta Biochimica et Biophysica Sinica (Shanghai)*. **2013**, 45 (1), 18-26.

Xia, J. G.; Broadhurst, D. I.; Wilson, M.; Wishart, D. S. Translational biomarker discovery in clinical metabolomics: an introductory tutorial. *Metabolomics*. **2013**, 9(2), 280-299.

Xu, Q. -S. and Liang, Y. -Z. Monte Carlo cross validation. *Chemometrics and Intelligent Laboratory Systems*. **2001**, 56(1), 1-11.

Yang, F.; Teves, S. S.; Kemp, C. J.; Henikoff, S. Doxorubicin, DNA torsion and chromatin dynamics. *Biochimica et Biophysica Acta*. **2014**, 1845 (1), 84-89.

Yip, K. W. and Reed, J. C. Bcl-2 family proteins and cancer. *Oncogene*. **2008**, 27, 6398-6406.

Zhang, Q.; Zhong, W.; Xing, B.; Tang, W.; Chen, Y. Binding properties and stoichiometries of a palladium(II) complex to metallothioneins in vivo and in vitro. *Journal of Inorganic Biochemistry*. **1998**, 72 (3-4), 195–200.

Zhang, L.; Wang, L.; Hu, Y.; Liu, Z.; Tian, Y.; Wu, X.; Zhao, Y.; Tang, H.; Chen, C.; Wang, Y. Selective metabolic effects of gold nanorods on normal and cancer cells and their application in anticancer drug screening. *Biomaterials*. **2013**, 34, 7117-7126.

Zietkowski, D.; Payne, G. S.; Nagy, E.; Mobberley, M. A.; Ryder, T. A.; De Souza, N. M. Comparison of NMR Lipid Profiles in Mitotic Arrest and Apoptosis as Indicators of Paclitaxel Resistance in Cervical Cell Lines. *Magnetic Resonance in Medicine*. **2012**, 68, 369-377.